

Xiao-Su Yi · Shanyi Du
Litong Zhang *Editors*

Composite Materials Engineering, Volume 2

Different Types of Composite Materials



Chemical Industry Press



Springer

Composite Materials Engineering, Volume 2

Xiao-Su Yi · Shanyi Du · Litong Zhang
Editors

Composite Materials Engineering, Volume 2

Different Types of Composite Materials



Chemical Industry Press



Springer

Editors

Xiao-Su Yi
Beijing Institute of Aeronautical Materials
(BIAM)
Beijing, Hebei
China

Litong Zhang
Northwestern Polytechnical University
Xi'an, Shaanxi
China

Shanyi Du
Center for Composite Materials
Harbin Institute of Technology
Harbin, Heilongjiang
China

ISBN 978-981-10-5689-5 ISBN 978-981-10-5690-1 (eBook)
<https://doi.org/10.1007/978-981-10-5690-1>

Jointly published with Chemical Industry Press, Beijing, China

The print edition is not for sale in China Mainland. Customers from China Mainland please order the print book from: Chemical Industry Press, Beijing. ISBN of the China Mainland edition: 978-7-122-06372-4.

Library of Congress Control Number: 2017947741

Translation from the Chinese language edition: 中国材料工程大典 第10卷 复合材料工程. © Chemical Industry Press 2006. All Rights Reserved.

© Springer Nature Singapore Pte Ltd and Chemical Industry Press, Beijing 2018

This work is subject to copyright. All rights are reserved by the Publishers, whether the whole or part of the material is concerned, specifically the rights of translation, reprinting, reuse of illustrations, recitation, broadcasting, reproduction on microfilms or in any other physical way, and transmission or information storage and retrieval, electronic adaptation, computer software, or by similar or dissimilar methodology now known or hereafter developed.

The use of general descriptive names, registered names, trademarks, service marks, etc. in this publication does not imply, even in the absence of a specific statement, that such names are exempt from the relevant protective laws and regulations and therefore free for general use.

The publishers, the authors and the editors are safe to assume that the advice and information in this book are believed to be true and accurate at the date of publication. Neither the publishers nor the authors or the editors give a warranty, express or implied, with respect to the material contained herein or for any errors or omissions that may have been made. The publishers remains neutral with regard to jurisdictional claims in published maps and institutional affiliations.

Printed on acid-free paper

This Springer imprint is published by Springer Nature
The registered company is Springer Nature Singapore Pte Ltd.
The registered company address is: 152 Beach Road, #21-01/04 Gateway East, Singapore 189721, Singapore

Preface

The concept of composites is well illustrated by biological materials such as wood, bone, teeth, and hides; these are all composites with complex internal structures that provide mechanical properties well suited to the performance requirements. In general, heterogeneous materials combining the best aspects of dissimilar constituents have been used by nature for millions of years. These could be considered the first composite materials. In modern materials engineering, the term ‘composite’ has become a broad and important class of engineering materials, typically referring to a matrix material that is reinforced with fibers. For instance, GFRP is a thermosetting polyester matrix containing glass fibers, and this particular composite has the lion’s share of today’s commercial composite market.

Nowadays, composite materials are found in a wide variety of situations, and they play important supporting roles in economic development and defense applications. Many composites used today are at the cutting edge of materials technology, with performance and costs appropriate to ultra-demanding applications such as spacecraft. Composite materials are undoubtedly a pillar of the materials family, parallel to metallic, polymeric and nonmetallic inorganic materials, in terms of the worldwide demand and production. Composite materials are so fundamental and so critical that their importance is hard to overemphasize.

The main objective of this book is to provide a comprehensive overview of current composite materials that have considerable influence on technical and economic development in China. Many achievements presented in this book result from individual research groups and research and development projects financially supported by Chinese government. Hence, one aim of this book is to bring state-of-the-art knowledge and accomplishments on composite materials together in a single book of two volumes. Of course, this book also provides an understanding of the physical structure–properties relationship of composites for postgraduate students and researchers, scientists and engineers alike. This understanding forms a basis for the application and improvement of the properties, manufacturing processes, characterization and testing, selection methods, and design of products made from composites. This knowledge has evolved from many disciplines and is common to all composite materials.

This book is a part of a large-scale publishing project, *China Materials Engineering Canon*, initiated and supported by the Chinese Mechanical Engineering Society and the Chinese Materials Research Society, co-sponsored by many governmental ministries and national institutions, including the Chinese Academy of Sciences and the Chinese Academy of Engineering. We would like to acknowledge the support and contribution of many colleagues in different universities, institutes, and national research establishments, many of whom are well known in the composite materials community in China. They were kindly agreed to provide their particular expertise for individual chapters. We are also grateful to many other scientists who made their contribution by taking part in the extensive reviewing process, particularly in the translation process from Chinese to English. Finally, we would like to thank the organizer of this book, Chemical Industry Press, for its management.

Beijing, China
Harbin, China
Xi'an, China

Xiao-Su Yi
Shanyi Du
Litong Zhang

Contents

1	Advanced Polymer Matrix Composites	1
	Naibin Yang	
2	Industrial Polymer Matrix Composites and Fiber-Glass-Reinforced Plastics	165
	Qixian Liu, Zhongmin Xue, Zaiyang Liu, Hongmei Gao, Rongqi Zhang, Weizhong Li, Zhihua Du and Dexu Yang	
3	Metal Matrix Composites	305
	Lin Geng and Kun Wu	
4	Cement-Based Composite Materials	489
	Keru Wu and Dong Zhang	
5	Carbon Composites	531
	Shouyang Zhang, Yulei Zhang, Aijun Li, Qiang Chen, Xiaohong Shi, Jianfeng Huang and Zhibiao Hu	

Editors and Contributors

About the Editors



Prof. Xiao-Su Yi is the director of the National Key Laboratory of Advanced Composites at Beijing Institution of Aeronautical Materials. His major research fields include high-performance structural composite materials, functional composite materials, materials process and engineering, and polymeric materials. Prof. Yi is the author or editor of more than 10 academic books and over 300 academic papers. He is a member of the ACCM Council; IOC member of WRCAP; standing member of the Chinese Material Research Society and Chinese Society for Composite Materials; chief editor of *Acta Materiae Compositae Sinica*, *Aviation Journal*, and the *Journal of Aeronautical Materials*, among others.



Prof. Shanyi Du is a member of the Chinese Academy of Engineering and works at the Center for Composite Materials and Structures of Harbin Institution of Technology (HIT), where he is involved in education and research courses in mechanics and composite materials. His achievements include theories and methods for performance characterization and safety evaluation of composite materials. Prof. Du has authored or co-authored over 260 academic papers, as well as 10 monographs on mechanics and composite materials. Prof. Du is president of the Chinese Society for Composite Materials and executive councilor of the International Committee on Composite Materials (ICCM) and member of the editorial committees of several

international journals, such as *Composite Science and Technology*, *ACTA MACHANICA SOLIDA SINICA*, and the *International Journal of Computational Methods*.



Prof. Litong Zhang a member of the Chinese Academy of Engineering, works in Northwestern Polytechnical University. She was engaged in research on aerospace ceramic and composites in the last 20 years and completed a series of innovative research projects. She and her research group innovated manufacturing techniques in the field of continuous fiber-reinforced silicon carbide ceramic matrix composites and established equipment systems with independent intellectual property rights. She received 26 national invention patents and the First Class Award for Technological Inventions of People's Republic of China in 2004. Prof. Zhang has published more than 260 scientific papers and several books. She is the director of academic board at the National Key Laboratory of Thermostructure Composite Materials and vice-president of Chinese Society for Composite Materials.

Contributors

Qiang Chen Northwestern Polytechnical University, Xi'an, Shaanxi, China

Zhibiao Du Beijing FRP Institute, Beijing, China

Hongmei Gao Beijing FRP Institute, Beijing, China

Lin Geng Harbin Institute of Technology, Harbin, Heilongjiang, China

Zhibiao Hu Northwestern Polytechnical University, Xi'an, Shaanxi, China

Jianfeng Huang Northwestern Polytechnical University, Xi'an, Shaanxi, China

Aijun Li Northwestern Polytechnical University, Xi'an, Shaanxi, China

Weizhong Li Beijing FRP Institute, Beijing, China

Qixian Liu Harbin FRP Institute, Harbin, Heilongjiang, China

Zaiyang Liu Harbin FRP Institute, Harbin, Heilongjiang, China

Xiaohong Shi Northwestern Polytechnical University, Xi'an, Shaanxi, China

Keru Wu Tongji University, Shanghai, China

Kun Wu Harbin Institute of Technology, Harbin, Heilongjiang, China

Zhongmin Xue Beijing FRP Institute, Beijing, China

Dexu Yang Beijing FRP Institute, Beijing, China

Naibin Yang Beihang University, Beijing, China

Dong Zhang Tongji University, Shanghai, China

Rongqi Zhang Beijing FRP Institute, Beijing, China

Shouyang Zhang Northwestern Polytechnical University, Xi'an, Shaanxi, China

Yulei Zhang Northwestern Polytechnical University, Xi'an, Shaanxi, China

Abbreviations

2D	Two-dimensional
2E4MZ	2-vinyl-4-methyl imidazole
3D	Three-dimensional
6FDE	Hexafluoro-trimethylene di-o-phenyl dimethyl ester
ABS resins	Polyacrylonitrile-butadiene-styrene resins
AC	Dielectric
ACEE	Aircraft energy efficiency
ACE-MRL	Advanced Civil Engineering Materials Research Laboratory
ACI	American Concrete Institute
ACM	Advanced composite materials
ACT	Advanced composite technology
ACT plan	A NASA's plan to improve textile composites in civil aircraft
AE	Allyl phenol-oxidant resin
AEC	French Atomic Energy Commission
AFM	Atomic force microscopy
AFML	Air Force Material Laboratory
AFP	Automated fiber placement
AGA	Agile combat aircraft
AlN	Aluminum nitride
AMC	Aerospace Metal Matrix Composites Company
ANN	Artificial neural networks
ANOVA	Analysis of variance
APA	1,3-di-(3-amine phenoxy) phenyl
APB	3-acetylene phenol amine
AR coating	Anti-reflection coating
ARALL	Aramid fiber-reinforced Al laminate
ARPA	Advanced Research Projects Agency
AS	Average stress criterion
ASTM	American Society for Testing and Materials
ATF	Advanced fighter plane

ATL	Automated tape-laying
ATP	Automated tow placement; automated tape placing
ATS	Applications Technology Satellite
BA	Butyl acrylate
BAS	$\text{BaO-Al}_2\text{O}_3\text{-SiO}_2$
BBA	Building block approach
BDAF	Bietherdisphenylamine-6F-bisphenyl-A
BDAO	Bietherdiphenylamine oxide
BDAP	Biether disphenyl amine bisphenyl-a
BDAS	Bietherdisphenylaminesulfone
BEM	Boundary element method
BG	2,4-biamine-6-phenol- 1,3,5 triazine
BIAM	Beijing Institute of Aeronautical Materials
BM	Bridging model
BMAS	$\text{BaO-MgO-Al}_2\text{O}_3\text{-SiO}_2$
BMC	Bulk molding compounds
BMI	Bismaleimide
BN	Boron nitride
BPACy	Cyanate ester
BPTA	Benaophenonel-tetra-dianhydride
BSAS	$\text{BaO-SrO-Al}_2\text{O}_3\text{-SiO}_2$
BSU	Basic structural unit
BTDE	Bisphenyl ketone tetraanhydride dimethyl ester
BUE	Build-up edge
BVID	Barely visible impact damage, low-energy impact damage
C/C	Carbon/Carbon
CAA	Chromic acid anodization
CAD	Computer-aided design
CAE	Computer assisted engineering
CAI	Composite affordability initiative; compression after impacting
CAM	Computer-aided manufacturing
CAS	Calcium aluminosilicate, $\text{CaO-Al}_2\text{O}_3\text{-SiO}_2$
CB	Carbon black
CBCC	CB-filled cement-based composites
CBT™	Cyclobutanone terephthalate
CDF	Cumulative density function
CE	Cyanate ester
CEC	Cation exchange capacity
CF	Carbon fiber
CFA	Composite Factor of American
CFCC	Continuous fiber-reinforced ceramic matrix composite
CFRC	Carbon fiber-reinforced concrete
CFRCMC	Continuous fiber-reinforced ceramic matrix composite
CFRP	Carbon fiber-reinforced plastic
CIMS	Computer-integrated manufacturing system

CIRTM	Co-injection RTM
CL	Central line
CLT	Classical laminate theory
CLVI	Chemical liquid-vaporized infiltration
CM	Crimp model
CMC	Ceramic matrix composites
CME	Coefficient of moisture expansion
CMR	Creep mismatch ratio
CNT	Carbon nanotube
CPCy	Single functional degree cyanate ester model compound
CRADA	Cooperation research and developing agreement
CRC	Compact-reinforced concrete
CRTM	Continuous RTM
CTA	Cold temperature ambient
CTBN	Carboxylic-terminal butadiene-nitride
CTE	Coefficient of thermal expansion
CTNN	Carboxyl NBR
CVD	Chemical vapor deposition
CVI	Chemical vapor infiltration
D/MI	Design/manufacturing integration
DABDT	2,5-diamino- 1,4-benzenedithiol salt
DABPA	O,O'-diallyl-bisphenol A
DABPS	Diallyl bisphenol S
DBDPO	Decabromodiphenyl oxide
DCC	Dicyclohexylcarbodiimide
DCP	Peroxidate diisopropyl phenol
DDA	Dynamic dielectric analysis
DDAC	Dimethyl di-dodecyl ammonium salt
DDS	Data damage structure; diaminedipheylsulfone
DETA	Dielectric thermal analysis
DFM	Design for manufacture
DGEBA	Diglycidyl ether bisphenyl-A, bisphenol A epoxy
DGEBF	Fluorine epoxy; 9,9-bi (4-hydroxyl-benzol)-p-fluorine-diglycidyl ether
DGEBS	Bisphenyl-S diglycidyl ether
DGEIB	Bi-(4-hydroxyl-benzol)-p-diisopropyl benzene-diglycidyl ether
DGEPP	Phenolphthalein epoxy resins
DI	Damage influence criterion XX
DMA	Dynamic mechanical analysis
DMC	Dough molding compounds
DMP	Dimethyl polyamide
DMTA	Dynamic mechanical thermal analysis
DOS	Directionally oriented structures
DSC	Differential scanning calorimetry
DSP	Densified system with ultra-fine particles

DTA	Differential thermal analysis
DTMA	Dynamic thermal mechanical analysis
DUL	Design ultimate loads
EAR	Earth antenna reflector
EB	Electronic beam
EBED	Electron beam evaporation deposition
ECC	Engineered cementitious composite
EELS	Electronic energy loss spectroscopy
EFG	Edge-defined film-fed growth
EL	Electro-luminescent
EMC	Electromagnetic compatibility
EMI	Electromagnet interference
EP	Thermosetting epoxy resin
EPDM	Ethylene propylene diene rubber
EPMA	Electron probe microscope analysis
EP-PUR	An epoxy modified by hydrothermally decomposed polyurethane
ER	Electrorheological
ETW	Elevated temperature wet
EVA	Ethylene-vinyl acetate
EVID	Evident visible impact damage
EW	Explosive welding
F/I	Fiber/interphase interface
FBG	Fiber Bragg gratings
FCC	Face-centered cubic
FCVI	Forced chemical vapor infiltration, forced convection CVI; forced-flow CVI
FD	Fiber breakage damage failure criterion
FDN	A water-reducing agent
FEA	Finite element analysis
FEM	Finite element analysis
FGM	Functionally gradient materials
FHC	Filled hole compression
FHT	Filled hole tensile
FIM	Fiber inclination model
FIT	Fluid impact technology
FML	Fiber-metal Laminates
FMS	Flexible manufacturing system
FPF	First ply failure
FPI	Fast probability integrator; fiber optic interferometer
FPL	Forest Products Laboratory
FPZ	Fracture process zone
FRDSP	DSP mortar + steel fiber, $V_f = 6\%$
FRP	Fiber-reinforced plastic
FRS	Fine Rahmen surface
FRTM	Flexible RTM

FT-IR	Infrared spectroscopy
FTIR	Fourier transform infrared spectrometry
FW	Filament winding
GC	Chromatography
GEM	General effective medium equation
GFRP	Glass fiber-thermosetting matrix composites; glass fiber-reinforced polymer
GLARE	Glass fiber-reinforced Al
GM	General Motors Corporation
GP	Graphite
GP zone	Guinier-Preston
GPC	Gel penetration chromatography
GRC	Glass fiber-reinforced cement-based composites
GrF	Graphite fibers
HCL	Hard contact lens
HCVI	Heaterless chemical vapor infiltration
HDPE	High-density polyethylene
HDT	Heat distortion temperature; heat deflection temperature; heat deformation temperature
HEMA	Hydroxyethyl methacrylate
HIP	Hot isostatic pressing
HIPN	Half-interpenetrating networks
HIT	Harbin Institution of Technology
HM	High modulus type
HMDS	Chlorosilane and hexamethyldisilazane
HMEPE	High molecular weight polyethylene
HMW	High molecular weight
HOLZ	High-order Laue zone
HPC60	High-performance concrete
HPLC	High-pressure liquid chromatograph
HRR	Heat release rate
HSRS	High-strain-rate superplasticity
HT	High tenacity type
H.T.	High temperature
H/W	Hot/Wet
ICCAS	Institute of Chemistry of Chinese Academy of Sciences
ICCM	International Committee on Composite Materials
ICVI	Isothermal CVI; isobaric CVI
IF	Infrared light
IHPTET	Integrated high-performance turbine engine technology
ILSS	Inter-laminar shear strength
IMU	Inertial measurement unit
IPACS	Integrated probabilistic assessment of composite structures
IR	Infrared spectrometer
ISC	Inter-system conversion

ISO	Isotropic
LACVD	Laser-assisted CVD
LAS	$\text{Li}_2\text{O}-\text{Al}_2\text{O}_3-\text{SiO}_2$; lithium aluminosilicate
LC	Superduralumin alloy
LCL	Low control limit
LCM	Liquid composite molding
LCMC	Laminated ceramic matrix composite
LCP	Liquid crystal polymers
LD	Forged aluminum alloy
LDPE	Low-density polyethylene
LEC	Linear expansion coefficient
LED	Light-emitting diodes
LMO	Local molecular orientation
LMW	Low molecular weight
LOI	Limit oxygen index
LROM	Linear rule of mixtures
LSS	Laminating stacking sequence
LTCVI	Limited temperature forced-flow CVI
LTM	Low-temperature molding
LVDT	Linear voltage differential transducer
LWA	Lower boundary predictions
LWC	Upper boundary predictions
LY	Duralumin alloy
MI	Matrix/interphase interface
M5	Polypyridobisimidazole
MA	Mechanical alloying; maleic anhydride; methyl acrylate
MAO	Methylaluminoxane
MAS	$\text{MgO}-\text{Al}_2\text{O}_3-\text{SiO}_2$
MBMI	Bi-phenyl methyl bismaleimide
MC	Methyl cellulose
MCM	Plasma spray coating method
MD	Machine direction
MDA	Bimethyl diphenyl amine
MDF	Macro-defect-free
MDI	4,4'-Diphenylmethane Diisocyanate
MEL	Magnesium Elektron Ltd.
MM	Mosaic model
MMA	Methyl methacrylate
MMC	Metal matrix composite
MMW	Medium molecular weight
MNR	Maximum normed residual
MOL	Material Operation Limit
MOR	Modulus of rupture
MS	Magnetron sputtering
MTS	Material testing system; methyltrichlorosilane

MTT	Montmorillonite
MWCNT	Multiwalled carbon nanotube
MWK	Multiaxial warp-knitted
nano-TPO	Thermoplastic polypropylene nanocomposites
NASA	The National Aeronautics and Space Administration
NASP	National Aeronautics and Space Shuttle
NBR	Nitrile-butadiene rubber
NC30	Normal concrete
NCF	Non-crimp fabric
NCH	Nylon-clay hybrids
NDI	Non-destructive inspection
NE	Nadic acid methyl ester
NEC	Nano-engineered concrete
NEMC	Nano-Enabled Multifunctional Concrete
NGC	Northrop Grumman Corp.
NGCAD	Northrop Grumman Commercial Aircraft Division
NMP	N-methyl ketopyrrolidine
NMR	Nuclear magnetic resonance
NOL	Noel ring, ring specimen firstly used by Naval Ordnance Laboratory of American
N-PNMI	N-phenyl maleimide
NPU	Northwestern Polytechnical University
NSF	American National Science Foundation
NTC	Negative temperature coefficient of resistance
OC	Owens Corning
OCF	Owens Corning Fiberglass
ODA	Diamine phenylate
OHC	Open hole compression
OHT	Open hole tensile
OMMT	Organic modified montmorillonite
O-phase	Orthorhombic structure phase
ORNL	Oak Ridge National Laboratory
P3AT	Poly(3-alkylthiophene)
PA	Polyamide
PAA	Polyarylacetylene; phosphoric acid anodization
PAAM	Polyacrylamide
PAE	Polyacrylic ester
PAI	Polyamide-imide
PAN	Polyacrylonitrile; polyphenylamine
PANI	Polyaniline
PAR	Polyarylate
PAVCD	Plasma-assisted CVD
PBI	Poly(p-phenylene benzimidazole); polybenzimidazole
PBO	poly(p-phenylene benzobisoxazole); polybenzoxazole; poly-p-phenylene benzo-bis; polybutadiene

PBOX	Phenylene bioxazoline
PBS	4-tert-butylstyrene-SBR
PBT	Poly(p-phenylene benzobisthiazole); polybenzothiazoles; polybutylene terephthalate
PC	Phenolic resin polymer matrix composites; polycarbonate
PCC	Polymer cement concrete
PCL	Polycaprolactone
PCN	Polymer/clay nanocomposites
PCP	Propinyl-substituted cyclopentadiene
PCS	Polycarbosilane
PCT	Polyethylenecyclodimethyl terephthalate
PCVI	Pulsed CVI
PDA	Phenyl diamine
PDF	Probability density function
PDFCE	Polydifluorochloroethylene
PE	Polyethylene
PECVD	Plasma-enhanced chemical vapor deposition
PEEK	Polyether ether ketone
PEG	Polyethylene glycol
PEI	Polyether imide
PEK	Polyetherketone
PEK-C	Modified polyetherketone
PEO	Polyoxyethylene
PES	Polyethersulfone
PES-C	Modified polyethersulfone
PET	Polyester; polyethylene glycol terephthalate
PFE	Polyfluoroethylene
PGLA	Polyglycolide-co-L-lactide
PH	Polyhydantoin
PI	Thermosetting polyimide; polyimide
PIC	Polymer-impregnated concrete
PIP	Polymer impregnation and pyrolysis
PIPD	Polypyridobisimidazole
PL	Photoluminescent
PLA	Polylactic acid
PLC	Polymer matrix nanocomposite
PM	Powder metallurgy
PMC	Resin matrix composites
PMMA	Polymethyl methacrylate; polymethyl methacrylate
PMR	Polyimide resin
POF	Plastic optic fiber
POM	Polyoxymethylene
PP	Polypropylene
PPD	p-phenylenediamine; pre-ceramic polymer-derived
PPE	Polyphenylether

PPP	Poly-p-phenylene
PPS	Polyphenylsulfureter; polyphenylene sulfide
PPTA	poly p-phenylene p-phenylene diamine terephthalamide; p-phenylene terephthalamide
PPV	poly-phenylene vinylene
PS	parallel-series; polysulfone; point stress criterion; polystyrene
PSU	Polysulfone
PSZ	Partially stabilized zirconia; polysilazane
PT	Phenol-triazine
PTBPCN	Tert-butyl phenyl cyanate ester
PTC	Positive temperature coefficient
PTFCE	Polytrifluorinechloroethylene
PTFE	Polytetrafluoroethylene
PTMC	Particle-reinforced titanium matrix composite
PU	Polyurethane
PVA	Polyvinyl alcohol; polyvinyl acetate
PVC	Polyvinyl chloride
PVD	Physical vapor deposition
PVDF	Polyvinylidene fluoride
PVK	Polyvinyl karbazol
PyC	Pyrolytic carbon
QA	Quiacrodone
QI	α components
RA	Rheological analysis
RAM	Resonate energy absorption
RARTM	Rubber-aided RTM
RBSN	Reactive-sintered Si_3N
RC	Enhanced layer
RCS	Cross section
RE	Rare earth
RFI	Resin film infusion
RICRTM	Resin injection circulating RTM
RIM	Reaction injection molding
RIMP	Variable infusion molding process
RIRM	Resin Injection Re-circulating Molding
RL	Rough laminar
RMI	Reactive melt infiltration
RPC	Reactive powder concrete
RPMP	Glass fiber-reinforced plastic mortar
RQL	Rich-Quench-Lean
RRIM	Reinforced reaction injection molding
RT	Room temperature
RTA	Room temperature ambient,
RTL	Ratios of transverse strain to the longitudinal strain
RTM	Resin transfer mold; resin transfer molding

RVE	Radius of a composite volume element; representative volume element
SAN	Styrene-acrylonitrile copolymer
SARTM	solution-aided RTM
SAW	Surface acoustic wave
SAXC	Small angle X-ray scattering
SAXS	Small angle X-ray scattering
SBR	Styrene-butadiene rubber
SBS	Short beam shear
SCF	Short carbon fiber
SCL	Soft contact lens
SCRIMP	Seaman's composite resin infusion molding process
SCS-6	CVD SiC fibers on carbon cores
SEA	Specific extinction area
SEM	Scanning electron microscopy
SFRP	Short fiber-reinforced polymer
SGL	A transnational corporation situated in Germany
Carbon	
SHS	Self-propagating high-temperature synthesis
SIFCON	A fiber-reinforced cement-based composite
SL	Smooth laminar
SM	Surface of mat
SMA	Styrene-malei anhydride; shape memory alloy
SMC	Sheet molding compounds
SOC	Spiro ortho carbonates
SP	Series-parallel
SPC	Statistical processing control
SPM	Scanning probe microscopy
SRIM	Structure reaction injection molding
SRM	Short-range missiles
SS	Stainless steel
SThM	Scanning thermal microscopy
STM	Scanning tunneling microscope
SVF	Silicone vacuum fluid
SWCNT	Single-walled carbon nanotube
TA	Terephthalic acid; thermal analysis; α titanium alloys
TANGO	Technology application to the near-term business goals and objectives
TB	β titanium alloys
TBA	Thermal braiding analysis; torsion braid analysis
TC	α + β titanium alloys
TCRDL	Toyota Central Research and Development Laboratories, Inc.
TEC	Thermal expansion coefficient
TEM	Transmission electron microscope; transverse electromagnetic waves

TEMPEST	Transient electromagnetic pulse emanation standards
TEOS	Tetraethoxysilane
TERTM	Thermal expansion RTM
TFAA	Trifluoroacetic anhydride
TG	Thermogravimetry
TGA	Thermal gravimetric analysis
TGAP	Tri-glycidyl p-aminophenol amines
TGBAP	bi-(4-hydroxyl-benzol)-p-diisopropyl benzene-N,N, N' N'-tetra-glycidyl ether
TGDDM	4,4-tetraglycidyl-amine-diaminodiphenylmethane; Cured 4-functional epoxy resins
TGIL	Tri-glycidyl ether
TGMBAP	Bi-(3,5-dimethyl-4-amine-l-benzol)-p-diisopropyl benzene-N,N,N', N'-tetra-glycidyl ether
THF	Tetrahydrofuran
TLC	Thermotropic liquid crystal
TLCP	Thermal liquid crystal polymer
TLP	Tension leg platform
TMA	Thermal mechanical analysis
TMC	Titanium matrix composites
TNK	Toa Nenryo Kogyo K. K.
TOS	Thermal oxidative stability
TP	Thermoplastics
TPU	Thermoplastic polyurethane
TS	Triode sputtering
TsAGI	The Central Aero-Hydrodynamic Institute
TTA	Thenoyl trichloroacetone
TZP	Tetragonal zirconia polycrystals
UCL	Up control limit
UD	Unidirectional
UHM	Ultra-high modulus type
UHMWPE	Ultra-high molecular weight polyethylene
UHT	Ultra-high tenacity type
UP	Unsaturated polyester resin
UV	Ultraviolet
UVRTM	Ultraviolet (cure) RTM
VA/VeoVa	Poly vinyl acetate-vinyl versatate
VAATE	Versatile affordable advanced turbine engines
VAFI	Vacuum-assisted resin infusion
VARI	Vacuum-aided resin injection
VARTM	Vacuum-assisted resin transfer molding; vacuum-assisted RTM
VB	Vacuum bag
VE	Virtual enterprise
VGCF	Vapor-grown carbon fiber
VHP	Vacuum hot pressing

VID	Visible impact damage
VIP	Vacuum injection process; vacuum infusion process
VLS	Vapor-Liquid-Solid
VLSI	Very-large-scale integration
VM	Virtual manufacturing
VR	Virtual reality
VRTM	Vacuum RTM
VS	Vapor-Solid
VTP	Virtual-type project
WAXD	Wide angle X-ray diffraction
WBL	Weak boundary layer
WCMC	Whisker-reinforced ceramic matrix composite
WFM	Woven meso-mechanical analysis program
W/C ratio	Water/Cement ratio
XD	Exothermic dispersion; a trademark of the Martin Marietta Corporation
XRD	X-ray diffraction
ZL	Cast aluminum alloy
ZTA	Zirconia-toughened alumina
ZTC	Zirconia-toughened ceramics

Chapter 1

Advanced Polymer Matrix Composites

Naibin Yang

In this chapter, high-performance continuous fiber-reinforcing thermosetting resin matrix composites for aerospace structural applications are introduced. Highlights about processing and manufacturing technologies of advanced resin matrix composites and composite material performances will be presented.

After more than 40 years of research and development and engineering application, advanced resin matrix composites are currently used to generate a wide variety of material systems and their processing and manufacturing technologies are available for different aerospace vehicle structures as they meet the requirements of different engineering applications.

Generally, the advantages of advanced resin matrix composites can be realized by placing high-performance fibers in resin matrixes with different orientations. Based on this approach, composite properties can be designed and optimized to a large extent. However, because of the particular hot-compressing curing process for advanced resin matrix composites, the integrated molding process used to fabricate structural components with a composite material needs to be simultaneous. The structural performance requires complicated fiber orientation and placement and a higher fiber volume fraction, and thus, all these aspects make the manufacturing processes very important in composite part production feasibility. Product quality is important, and these factors directly influence production costs. Furthermore, many good design concepts are not realized because of the limitations of processing and manufacturing technologies or because the production costs are too high. Therefore, searching for and developing innovative processing and manufacturing technologies and reducing production costs are the main research targets in many countries at present [1–3].

N. Yang (✉)
Beihang University, Beijing 100191, China

1.1 An Overview of Aerospace Composites

1.1.1 *Research and Development of Advanced Resin Matrix Composites*

To increase and improve military aircraft performance, since the mid-1950s, the US Air Force Material Laboratory (AFML) has developed new materials that have higher specific strength and modulus than conventional aluminum alloys and titanium alloys that are used in airplanes. As a result, light and high-performance materials such as advanced resin matrix composites and Al-Li alloys have been exploited. Advanced resin matrix composites have been very successfully used in aerospace vehicle applications and are currently an important aircraft structural material together with aluminum alloys, titanium alloys, and steels.

The development of advanced resin composites was inspired by an understanding of and experiences derived from glass fiber-reinforced plastics (GFRP). Glass fiber gives a lower modulus even though its strength and modulus are relatively high, and its density is low. Recent attention has been given to high-modulus and low-density reinforcing fibers. Boron fibers were initially investigated and produced because boron (B) has a smaller molecular mass than silicon (Si). Si is the main chemical constituent of glass fibers. In 1960, small batches of boron fibers containing a tungsten filament core were produced. Boron fiber has a diameter of about 100 μm and can give a tensile modulus and strength of 400 GPa and 3800 MPa, respectively. Boron fiber-reinforced epoxy composites (60% fiber volume fraction) can give a tensile modulus up to 200 GPa (relative density 2.0), which is more than 5 times that of GFRP with a 40 GPa modulus (relative density 1.8), and its modulus is 3 times higher than that of aluminum alloy at 70 GPa (relative density 2.7). Accordingly, the Air Force Material Laboratory is referred to boron fiber-reinforced epoxy as advanced composite materials (ACM) (briefly referred to as composites) to distinguish it from traditional glass fiber-reinforced plastics. Applications in aircraft structures had thus begun. By the end of the 1960s, some boron fiber composite aircraft structural parts such as horizontal tails and vertical stabilizer boxes were created. However, boron fibers have a very complicated production process and are expensive. Boron fiber in itself is too thick and too rigid, which limits the wide application of boron fibers for aerospace structural purposes.

Subsequently, a new type of fiber, carbon fiber, was developed because carbon comes after boron in the periodic table. In 1971, high-strength carbon fibers such as T300 and AS4 were produced in small quantities and they were cost-effective. Carbon/epoxy composites such as T330/5208 and AS4/3501-6 have good hygrothermal properties and processing performance and, therefore, have gained wide application in aerospace vehicles.

Resin matrix is another main constituent material in composites. During composite parts, curing the resin matrix will undergo physical and chemical reactions and can be cured into a final structural shape. The resin matrix curing process

determines the real composite's structural manufacturing method as well as the production cost. Different resin systems require different processing parameters, while different manufacturing methods require different resin systems. The function of resin matrixes is to bind reinforcing fibers together and transfer load to fibers, and also to provide support and protection to reinforcing fibers. Resin performance can play a very important role in some fundamental properties of composites such as service temperature, compression, transverse (90°), longitudinal and transverse shear properties (including interlaminar shear strength), as well as hygrothermal behavior, which impacts damage resistance. The more widely applied composites in aircraft structures have the stricter requirements in terms of resin matrixes.

As mentioned above, for high-performance applications, the research and development of advanced resin matrix composites should include fibers and resins, as these two are the main constituent materials in composites, and also their related curing processing technologies.

Investigations into advanced composites have been carried out together with their engineering application. In December of 1975, the US Air Force issued a new specification for aircraft structure design, an outline on structural integrity—aircraft requirement—in which composite structures were covered. The clauses described in the specification were suitable for composite structures in principle, but no particular requirements were specified for composites in this document. To expand advanced composite applications to primary load-bearing structures such as wings and front fuselages, in 1975 the research and development department of the US Air Force studied and examined technological conditions for advanced composites used in planes and established a Structural Composite Integrity Roadmap (1976–1992). The objective was to use carbon/epoxy composites to make wings for the production of jet F/A-18s, as well as wings and front fuselages for AV-8Bs.

To meet the composite performance for military fighter usage and to lead investigations into resin matrix composites, in 1983 NASA cooperated with Boeing, Douglas, and Lockheed to develop the standard testing method on Resin Toughness Evaluation (revised version)—NASA RP 1092. The testing methods included open-hole tension (OHT), open-hole compressing (OHC), compression strength after impacting (CAI), and edge delamination G_c . Afterward, the specification on carbon fiber/toughened thermosetting resin matrix composites—NASA 1142—was compiled in 1985. This was the first authorized specification on advanced resin matrix composites (standardized samples on material specification).

T300/5208 carbon/epoxy composites have been widely used in manufacturing airplane secondary structures since their launch in 1973. Their prepregs satisfied Boeing Material Specification (BMS) 8-256, and they give good hygrothermal performances. However, its fracture elongation is low, its toughness is poor, and its CAI tested at 67 J/cm only gave 110 MPa. Therefore, impact damage could only be mitigated by limiting the designed strain levels in aircraft. The designed allowable strains were limited to 0.3–0.4%, and this strain level limiting design method results in a decrease in weight-saving efficiency. NASA defined T300/5208 as a baseline for carbon/epoxy composites. Following T300/5208s introduction, T300/BP907 carbon/highly toughened epoxy composite is a structural material system with

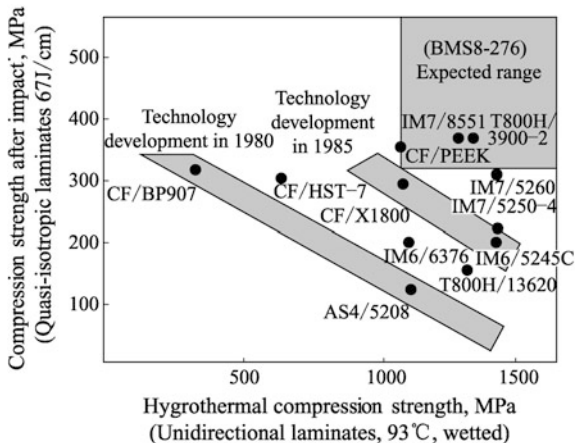
greater fracture elongation and good toughness. Its CAI result at 67 J/cm was up to 320 MPa. It basically meets the requirements for an allowable design strain range of 0.5–0.6% and a weight saving of 30%. However, its thermal resistance is poor, and it is not suitable for structural purposes. T300/BP907 showed great promise and gave direction toward the improvement of composite toughness. Therefore, NASA selected T300/BP907 as a baseline material for the development of carbon fiber/toughened resin matrix composites. Taking the hot/wet compression strength as an abscissa and CAI values as ordinate, a figure showing a combined evaluation of the hot/wet resistance and impact toughness of resin matrix composites was obtained, as shown in Fig. 1.1. This figure provides a basis for the performance targets in the development of new hot/wet resistance and highly tough composites (Boeing BMS 8-276 specification, in 1989). This target has guided research and development into advanced resin matrix composites since the 1980s.

Based on the requirements of carbon fibers, the tensile strength and modulus should increase by 30–40% and the fracture elongation by 20%. High tensile strength fibers with a relatively medium modulus such as IM6, IM7, and T800H were the first to be developed.

For resin matrixes, development has been carried out mainly for three types of vehicles: commercial and military transport planes, jet fighters, and helicopters. Epoxy resins have been improved and toughened and have already been used to produce a matrix system series with different service temperatures and compression strength after impacting (CAI). Because primary composite structures like jet fighter wings have service temperatures exceeding the temperature resistance of improved epoxy resins, and the performance requirements in hot/wet environments have also increased, the development of bismaleimide (BMI) resin systems such as 5245C and 5250-4 has been undertaken.

High-strength carbon fiber with an intermediate modulus together with toughened epoxy or BMI is used in principal composite material systems in aerospace structural applications. These include 120 °C curing epoxy resin systems, 180 °C

Fig. 1.1 Schematic for the combined evaluation of hot/wet resistance and anti-impact damage (historic advanced resin matrix composite development)



curing epoxy resin systems with varied service temperatures and toughness, high-temperature curing, and post-treatment BMI systems, as shown in Fig. 1.1.

Over the last 10 years, the highlight of resin matrix development has been the production of new resin systems that meet innovative processing technology. One category is automated manufacturing technologies with a large production requirement, for example, resin systems used in the resin transferring molding (RTM) process and in the resin film injection (RFI) process.

The other category is low-cost processing technologies using small batch composite structure production such as resin systems for low-temperature (below 80 °C), low-pressure (less than vacuum pressure), and non-autoclave curing processing. These are thus resin matrixes used for low-temperature molding (LTM). In addition, the resin systems used for new manufacturing processes such as electronic beam curing and light curing are also of interest.

1.1.2 Processing and Manufacturing Characteristics of Advanced Resin Matrix Composites and Low-Cost Technologies

Metal components and parts are usually made by the following manufacturing methods: mechanical machining, press extension, forging, and casting. This is because of the metallic material's inherent ductile performance, which allows cutting, forging, press extension, and melting.

The processing and manufacturing of advanced resin matrix composites utilizes different principles. Resins and fibers are subjected to a certain temperature, pressure, and time. Resins undergo complicated physical and chemical reaction processes and are then cured and bonded to fibers. At the same time, the desired end shapes of composite parts can be obtained using molding tools. Therefore, composite structural parts are generally made by hot-compression molding, and end product fabrication can be completed simultaneously with composite material processing.

Structural design has critical requirements for processing and manufacturing technologies such as a guarantee of composite part quality and performance. Processing techniques for composite part manufacture should have the following features:

- 1) To exactly control and achieve fiber orientation and ply layup sequences for a composite part in structural design.
- 2) To give a higher fiber volume content ($V_f \approx 60\%$).
- 3) Uniform resin distribution (no resin-rich or resin-poor areas) and a lower void content ($<2\%$).
- 4) Accurate part dimensions and good production repeatability.

Guided by these requirements, prepreg autoclave processing techniques have become the first choice for composite part production. Other available technologies include the prepreg vacuum bag process, the pressure tape process, and the hot-press molding process. Prepregs are regarded as an intermediate-phase composite material with a desired fiber volume content (or resin content). Prepregs can be tailored and laid up to achieve accurate fiber placing orientations and ply layup sequences, as specified in the composite structural design. They potentially guarantee smooth autoclave processing or pressure tape processing. The end composite products made using prepregs should be of high quality and give good performance including a higher fiber volume fraction ($V_f \approx 60\%$), outstanding mechanical properties, accurate dimensions, and good production repeatability. The composite co-curing manufacturing process can be used to make large integrated structural components. Using this technique, mechanically assembled and joining counts could be extensively reduced. Most composite airplane structures have been produced using this manufacturing method. However, the preparation and storage of prepregs together with the very expensive autoclave equipment requires much capital investment, and it has high energy consumption. Additionally, the handy layup process is still the main approach in composite part making so the production costs using this technique are relatively very high.

Advanced resin matrix composites are technologically advanced with high performance, but with a high input cost, outstanding structural weight reduction should be forthcoming. Cost problems can play a very important role in delaying or in promoting the development of composite technologies.

Low-cost composite technologies are a global priority at present, and the most important criterion is the performance to cost ratio. Any technical approach used needs to deliver low-cost production without degrading the high-performance of composites. The goals for low-cost production should include a comparison with aluminum alloys in equivalent coats, a performance comparison and a weight reduction of 20–30%.

The main technical approaches that should be considered and used to reduce advanced composite curing processing costs are as follows [4–6]:

- 1) To eliminate intermediate prepreg material preparation, to develop liquid composite molding (LCM) technologies such as preform/resin transfer molding (RTM), preform/resin film infusion (RFI), as well as the development of exclusive resin systems.
- 2) To replace handy cutting and layup procedures by highly automated prepreg cutting, and the use of prepreg tape or fiber placement to achieve high processing quality and production efficiency. Automated fiber placement equipment will be very expensive and will only be used in high-volume production where a cost reduction can be realized.
- 3) To develop innovative curing techniques such as low-temperature curing, electronic beam curing, and light curing processes. This will lead to the development of exclusive resin systems such as the resin systems for LTM techniques that can be cured at low temperature (below 80 °C) and then heated

to a higher temperature for post-treatment (180 °C). The properties of these resins can achieve the desired level required for airplane structural applications. These techniques can greatly reduce the manufacturing costs in molds and tools production and eliminate autoclave operations.

- 4) To computerize the digital simulation of curing processing and save processing testing costs.

If a life cycle cost of composite structures is required, low-cost technique development should incorporate the following issues:

- 1) To innovate in composite structural design including design/manufacture integration, design for manufacture (DFM), large structure integrated fabrication (extensively reduce assembly and joining), structural/functional integration.
- 2) To improve composite structure maintenance and repair techniques to achieve design/manufacture/maintenance integration (guaranteed design) and low-cost repairing techniques.

In Table 1.1, the milestones of advanced resin matrix composite technique development is listed.

Table 1.1 Development of advanced resin matrix composite technologies

Years	1965–1980	1985 present
Program goal (compared with Al alloy structures)	Weight-saving 15–20% (high cost paid)	Weight-saving 20–30% (cost competitively reduced)
Highlights	<ul style="list-style-type: none"> 1) Structure application development 2) High-performance resin matrix and fiber investigations 	<ul style="list-style-type: none"> 1) Enhance structural application level and quantity 2) Design/material/fabricating/maintenance technique development for cost reduction
Technical features	<ul style="list-style-type: none"> 1) Classical laminate theory 2) Air dynamic elastic tailor optimized design 3) Mainly prepreg/autoclave curing processing (including co-curing) 4) Intensive manual operation 	<ul style="list-style-type: none"> 1) Design/manufacturing integration (D/MI) 2) Structures enlarged and integrated 3) Simplified and digitized processing (also curing process) to reduce material and mold costs as well as energy consumption 4) Automated manufacturing technologies to reduce manual labor 5) Improved maintenance and repair
Measures for increasing material and structure performance	Focus on resin modification and toughening (in-plane fiber 2D reinforcing)	Fiber preforms for 3D reinforcing

1.1.3 Special Features of Advanced Resin Matrix Composites and Their Characterization

The improvement of material properties is promising for material development and application. After the introduction of advanced composites, a unified material specification and property data bank was established in the late 1960s by the USA government, its military, and other industries. This was a cooperative organization for polymer matrix composites, and a military handbook, MIL-HDBK-17A, was produced and published in Jan. 1971. This handbook standardized and unified the characterization and standard testing methods for resin matrix composite properties, providing formalized material property data and acting as a guideline for composite development and engineering applications.

Because of the special features of advanced composites such as multiconstituent material systems and their related curing processes, sensitivity toward service environmental conditions (wet/hot, impact), multiple failure modes, no regularity of damage growth, and scattered data distribution, composites require many unique property characterization methods and parameters. Because constituent materials, resin matrixes, and reinforcing fibers have been already presented in other sections, they will not be included in this section.

1.1.3.1 Property Characterization and Data Expression Criterion of Structural Composites

(1) The property characterization of structural composites

The property characterization of structural composites relates to raw materials or composite products in different stages such as constituent materials (fibers and matrixes), intermediate-phase materials (prepregs), laminars, laminates, and structural components. Additionally, property characterization should also involve fundamental material properties in chemistry, physics, and mechanics as well as properties related to processing techniques (including quality control) and applications, as shown in Fig. 1.2. However, recent interest in structural design has been focused on laminar properties and laminate properties.

Physical property parameters—fiber content (volume fraction, $V_f \approx 55\text{--}60\%$), void content ($<2\%$), glass transition temperature (dry or wet), linear thermal expansion coefficients/ $10^{-6} \text{ }^\circ\text{C}^{-1}$ (0° and 90° directions).

- 1) Fundamental mechanical properties have 9 parameters: engineering constants used in design (if the tensile modulus and the compressing modulus are not equal, they are then added to give 11 parameters), longitudinal tensile and compressing modulus/GPa, transverse tensile and compressing modulus/GPa and strength/MPa, principal Poisson's ratio, longitudinal and transverse shear modulus/GPa and strength/MPa.

laminar → fibers —(interface) matrices orthotropic $E_1 E_2 V_{12} G_{12}$ $X X' Y Y'$ $\alpha_1 \alpha_2$ $\beta_1 \beta_2$	laminates → ply angle θ ply ratio lay-up sequence design feasibility $\begin{bmatrix} A & B \\ B & D \end{bmatrix}$ $\begin{bmatrix} \alpha & \beta \\ \beta^T & \delta \end{bmatrix}$ symmetry, anti-symmetry, unsymmetry balance, unbalance	laminated structures configuration open hole and machining joining unique failure models wet/hot effect -strength and modulus decreased impact damage, delamination -strength and modulus dramatically decreased fatigue ($R=-10, -1, -0.1$) - varied fatigue damage models, no growing regularity stiffness dropped
matrices T_g wet absorption	interlaminar performance -Short beam interlaminar shear strength -Interlaminar shear strength -Model-I interlaminar fracture toughness -Model-II interlaminar fracture toughness	properties related to structures -Open Hole Tension (OHT) -Open Hole Compressing (OHP) -Filled Hole Tensile -Filled Hole Compressing -Extrusion strength -Compression after impact(CAI) -Quasi-static indentation force (damage resistance)

Fig. 1.2 Schematic of laminar, laminate, and laminated structure performance

- 2) Environmental effects (hot/wet) on fundamental mechanical properties (property retention is a big concern in structural design).
- 3) Fatigue performance ($R = -10, -1, -0.1$) S-N curve.
- 4) Interlaminar performance: short-beam interlaminar shear strength, interlaminar shear strength, model-I and model-II interlaminar fracture toughness.
- 5) Properties related to composite structures. open-hole tension/MPa (OHT), open-hole compression/MPa (OHP), filled hole tensile, filled hole compression, extrusion strength compression after impact/MPa (CAI), quasi-static indentation force (damage resistance).

The CAI values determined at an impact energy of 67 J/mm are mostly used to evaluate composite impact damage resistance.

CAI values below 193 MPa indicate low toughness, 193–255 MPa indicates toughened composites, and higher than 255 MPa indicates a high degree of toughness. In Boeing’s specification BMS8-276 and CAI values determined at an impact energy of 67 J/mm are expected to be higher than 320 MPa for commercial airplane structures.

Short-beam interlaminar strength in laminate design is a processing and quality monitoring property. The flexural modulus/GPa and strength/MPa are currently used in material investigations for raw material selection, medium resistance evaluations, and process monitoring batch sample tests. This is because the flexural testing specimens are simple geometric shapes, easy to fabricate, and their test results can be compared.

(2) Data expressing criteria of composite properties

Material properties should be characterized by material behavior parameters under certain outer conditions. The data obtained in property tests should reflect a material's performance and should be presented by digital expressions.

Material property data collected from tests should have the following functions.

- ① To indicate material performance levels. Superior or inferior material performance will depend on the higher or lower test data.
- ② To make a connection between material investigations and applications.

The requirements of material applications will be expressed by property test data; on the other hand, the data will reflect achievements in material studies and development, and therefore, material property data are a link between investigation and application.

- ③ To provide records or indications about material research and developing advances.
- ④ To support material selection and structural design.

In composite structure design, the allowable material property data are required and the allowable values should include A-allowable, B-allowable, classical allowable, and S-allowable values.

Composites' strength data use B-allowable values and typical allowable values in part design.

For modulus, fatigue, fracture, durability, creep, and physical properties, classical allowable values are generally used for design.

1.1.3.2 Mechanical Properties of Composites

For structural applications, the mechanical properties of composites have the following features compared with metals.

- ① Fundamental composite properties show orientational and linear elastic characteristics. Metals are mostly isotropic materials with yielding or conditional yielding behavior. However, their laminar properties apparently show direction-dependent behavior. Mechanical performances in the fiber direction are much higher than those in the fiber vertical direction (transverse) and also than the shear properties in both the longitudinal and transverse (exceeding about first or second orders of magnitude) directions. The stress-strain behavior shows a linear correlation until the fracture accrues. Mechanical properties in the off-fiber directions indicate a regular change between longitudinal and transverse directions and a particular tensile may be generated such as shear coupling. Other physical properties, like wet/hot expansion coefficients, are also direction-dependent.

- ② The stiffness and strength of composite laminates can be tailored, but the interlaminar strength is quite low and will be very sensitive to the loads applied vertically to the laminate plane. Based on laminate theory, by selecting each single ply angle, ply ratio, and ply layup sequence the desired stiffness and strength of laminates can be achieved. This method is similar to a tailor making a cloth and is referred to as tailoring design. By laminate tailoring design, in-plane stiffness and bending-twisting modulus as well as unique modulus coupling between in-plane (tensile, compression, shear) and out-plane (bending, twisting) can be offered. This is a specialized coupling effect in composites and serves as the basis for wing surface air dynamic elastic tailoring.

The strength between layers in a laminate, that is, the strength in the vertical direction to the laminate plane, will strongly depend on the resin's strength and the interfacial strength, and therefore, the interlaminar tensile and shear strength in composite laminates will be extremely low. They are usually lower than the in-plane strength by 1–2 orders of magnitude, and therefore, they will be very sensitive to loads applied vertically to the laminate plane.

- ③ Sensitive to wet/hot environment: Under wet/hot conditions, resin matrixes may absorb a small amount of moisture (only aramid can absorb water among reinforcing fibers). This will cause the dimension of the composite structure to change (wet expansion) and the glass transition temperature T_g to decrease (decrease in maximum operating temperature), and it also influences the compression and shear performance of the resin matrix and the interface between matrixes and fibers. Therefore, the compression performance of composites under wet/hot conditions is a critical standard in resin matrix selection.
- ④ Major defects/damage pattern delamination and impact damage: Cracks are the main damage phenomenon in metal materials, and from investigations into crack formation, growth and fracturing processes, requirements relating to the durability, and damage tolerance of metal structures have been specified. Related design analysis approaches have been developed. In composite part making processes or in composite applications, many kinds of defects/damage patterns may exist. For example, a void content beyond the standard, delamination, surface scratches, unacceptable (machined) holes, and impact damage is caused by external objects. Delamination caused by the separation between layers within laminates is invisible from the surface. Delamination can cause a decrease in laminate performance, especially its compression strength. The impact damage caused by external objects as determined by visual inspection (or impact energy) can be divided into barely visible impact damage (BVID) (low-energy impact damage), visible impact damage (VID) or evident visible impact damage (EVID) (intermediate-energy impact damage), and penetrated damage (high-energy impact damage). Once impact damages occur, the compression load-bearing ability of laminated composite parts will

suddenly decrease. Therefore, delamination and impact damage are the major defect/damage pattern of composite structures.

Allowable (dimension) delamination and BVID in quality control are used in structural durability studies. Delamination beyond the allowable dimension, VID/EVID, and penetrated damage are the subject of structure damage toleration studies. Currently, compression strength after impacting (CAI) is another important standard for resin matrix selection.

Damage growth or extension in composites results from several failures such as cracks in matrixes, interfacial debonding, delamination, and fiber ruptures. These failures show irregular growth and accumulation in composites. These irregularities cause major difficulties in structure durability analysis and damage tolerance investigations.

- ⑤ Outstanding fatigue performance: Composite testing results indicate that S-N curves are relatively flat and smooth, and the ratio of conditional fatigue limits to static strength can reach 0.6 or even higher.
- ⑥ The scattering coefficient of property data is larger than that of metals.

1.1.3.3 Characterization of Physical Properties of Composite Laminates

The characterization of physical properties of laminar or composite laminates involves fiber volume content, resin volume content, density, laminar thickness, void content, glass transition temperature, water absorption rate, linear thermal expansion coefficient, and moisture expansion coefficient.

- ① Fiber volume content: The fiber volume content in composite laminates is a principal performance-dependent parameter. Taking a cross section from a unidirectional laminate specimen vertical to the fiber axis, the fiber accompanied areas are accumulated and the ratio to the total cross-sectional area under a microscope is calculated. This ratio represents the fiber volume content of the specimen. Test methods include GB/T 3366—1982, Testing Method for Determining Fiber Volume Content in Carbon Fiber-Reinforced Plastics (Microscopy). The fiber volume content in structural laminates should be in the range of 60–65%.
- ② Resin volume content: The resin volume content in laminates is of interest. Because the void content in laminates should be limited to about 1% (<2%), the sum of the resin volume content V_m plus the fiber volume content will be almost 1. Therefore, the value of the resin volume content also represents the fiber volume content in the same specimen. It is a parameter that indicates laminate performance. The resin content in composites is usually determined by acid extraction or burning, and the principles are the same as those in prepreg resin content determinations. The related testing standards include GB/T 3855—1983, Testing

Method for Determining Resin Content in Carbon Fiber-Reinforced Plastics. GB/T 2577—1981, Testing Method for Determining Resin Content in Glass Fiber-Reinforced Plastics. $V_m \approx 1 - V_f = 35\text{--}40\%$ (cured).

- ③ Void content: The impurity or inclusion content in a laminate is the sum of entrapped air, gas, or cavities, and this is used as a composite quality control parameter. It can be determined by observing the surface view of a cross section under a microscope or by converting the constituent material mass to volume. Testing methods are GB/T 3365—1982, Testing Method for Determining Void Content in Carbon Fiber-Reinforced Plastics (microscopy), or JC/T 287—81, Testing Method for Determining Void Content in Glass Fiber-Reinforced Plastics. The void content should be limited to about 1% (less than 2%).
- ④ Glass transition temperature: When polymer matrixes in laminates are heated to a specific temperature at a given rate, there will be a dramatic turndown point on the temperature-modulus curve. At this temperature, the polymer matrix will undergo a transition from a solid glassy state to a flexible elastic state, and a series of changes will occur in its physical parameters. This phenomenon is referred to as the glass transition, the corresponding temperatures are referred to as the glass transition temperatures, and these are the maximum operating temperatures of polymer matrix composites (T_g , °C). Different resin systems have different glass transition temperatures; see the Resin Systems section for details.
- ⑤ Water or moisture absorption: The laminate weight will increase by about 1–1.2% after saturation by moisture absorption.
- ⑥ Linear expansion coefficient: The linear expansion coefficients of laminates are orthotropic. For carbon/epoxy, $\alpha_1 \approx 0$, $\alpha_2 \approx 22$.
- ⑦ Moisture expansion coefficient: The moisture expansion coefficients of laminates are also orthotropic. For carbon/epoxy, $\beta_1 \approx 0$, $\beta_2 \approx 0.6$.

1.2 Processing and Manufacturing Technologies for Advanced Resin Matrix Composites

1.2.1 Processing and Manufacturing Technologies for Advanced Resin Matrix Composites and Their Classification

- (1) The characteristics of processing and manufacturing technologies in advanced composites

The principal technological characteristics of processing and manufacturing in advanced resin matrix composites can be summarized as follows:

- ① To guarantee desired fiber orientations and ply layup sequences as specified by the structural design.
- ② To yield a higher fiber volume content ($V_f \approx 60\%$).
- ③ To provide a uniform resin distribution without resin-rich or resin-starved phenomena.
- ④ To satisfy the exact control part dimension and thickness requirements.
- ⑤ To establish authorized processing specifications and quality assurance systems.

For resin matrix composite curing processes, the temperature, pressure, and time are three essential factors in which a number of processing parameters will be involved such as the heating rate, the dwell or debulk time, the pressure application point, the maintained time, and the cooling rate. These parameters should be exactly specified and controlled for different parts production. Simultaneously, reliable and effective quality assurance measures should be available during the entire curing process to guarantee part quality.

(2) Classification of processing and manufacturing technologies in advanced resin matrix composites

The processing and manufacturing methods for advanced resin matrix composites are basically grouped into two types: resin-impregnated fiber methods and fiber preform/liquid processing methods, as shown in Fig. 1.3.

- 1) Resin-impregnated processing methods: The features of these techniques are that the resin pre-impregnated reinforcing fibers are bound and placed in molds to yield the desired shapes. They are then cured into final parts. Resin pre-impregnated fibers can be transformed into intermediate materials referred

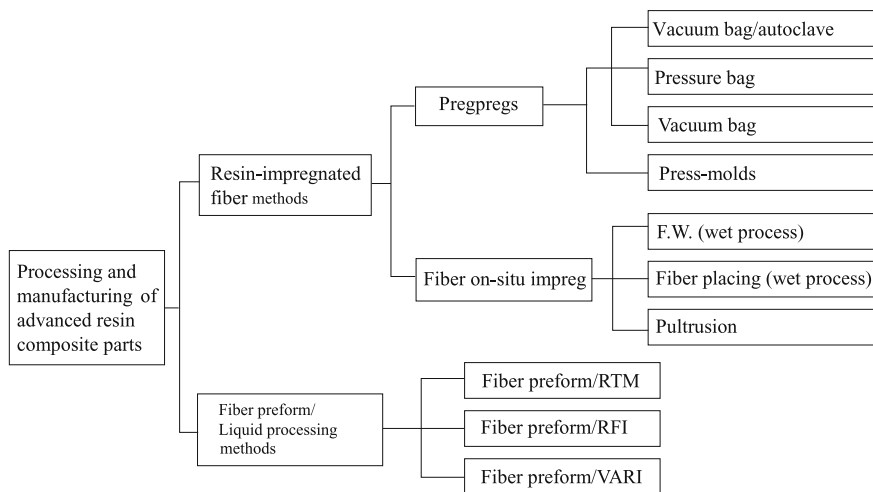


Fig. 1.3 Schematic showing the classification of processing and manufacturing technologies

to as prepregs and stored in a freezer for later use. Fiber pre-impregnation processes can also be carried out in situ in a fiber production line and can immediately be placed in molds after that. The final part shape is then imparted in the molds after curing.

Prepreg/vacuum bag–autoclave processes, pressure bag processes, and vacuum bag processes are essentially included in compression bag/half-mold (male or female only) processing techniques. The main differences among them are the different operating pressures and temperatures used in the curing processes.

In the prepreg press molding processing method, a pair of matched molds (assembled molds) is used and the closed molds containing the composite parts are heated or put into an oven for elevated temperature applications. Pressure is applied either by mold body interference or by expandable rubber and airbags attached within the part. In this way, the prepregs are finally cured into composite parts.

Fiber in situ impregnation processes can be divided into filament winding (FW) processes, in which the fibers are resin-impregnated in situ in a fiber production line and subsequently wound onto a part mandrel, and fiber placing processes, in which the impregnated fibers are immediately placed on a mold surface. The difference between these two methods is that fiber tension control is required during the winding operation in the FW process but not necessary for fiber placement processes. The composite parts fabricated by these two processes can be put into a chamber or autoclave for heating and curing.

Pultrusion is another alternative in situ fiber impregnation process, and the impregnated fibers pass through a heated die and yield the desired product profiles. They are then cured into end products.

- 2) Preform/liquid molding processes: The features of this type of process could be described as follows: The reinforcing fibers are initially made into part preforms and then placed in assembled mold cavities. The resin systems are pumped or injected into preforms with the aid of molds, and resin-impregnated prepregs are assigned an end part shape and cured under applied heat and pressure.

RTM process. In this process, resins are injected and flowed into preforms along the part plane. Generally, this method gives a lower fiber volume content ($V_f = 20\text{--}45\%$). In the RFI process, resin films are heated and melted and subsequently flowed into preforms along the direction vertical to the part plane. Both RTM and RFI need assembled molds.

Vacuum Assisted Resin Infusion (VARI) is an improvement to RTM in which a half-mold and a vacuum bag are required. With the aid of applied vacuum pressure, the resins are injected and flow into the preforms along the part plane. In this method, composite parts with higher fiber volume content and a lower void content are obtained.

Preform/liquid molding processes are quickly gaining popularity in composite part fabrication.

Processes derived from RTM include variable infusion molding process (RIMP), thermal expansion RTM (TERTM), rubber-assisted RTM (RARTM), resin

injection recirculating molding (RIRM), continuous RTM (CRTM), and co-injection RTM (CIRTM).

The alternatives to VARI include vacuum-assisted resin injection (VARI), vacuum-assisted RTM (VARTM), vacuum RTM (VRTM), vacuum injection process (VIP) as well as the similar patterned technique called Seeman's composite resin injection molding process (SCRIMP), and ultraviolet (cure) RTM (UVRTM).

1.2.2 Prepreg Preparation Processes

Composite prepregs are mixtures of resin matrixes and reinforcements prepared by resin impregnating continuous fibers or fabrics under precisely controlled conditions. As intermediate-phase materials, prepregs can be used to make various composite structures. Whether the prepreg quality is superior or not will strongly affect the composite quality and performance. Therefore, prepregs have great significance in composite development and application.

Prepreg preparations are a professional processing technique in which automated and specialized prepreg production processes can be offered to guarantee consistent product quality. Furthermore, a wide range of prepreg products are available to meet various processing and manufacturing needs. Commercial prepreg products of different types, performances, and specifications are available.

(1) The basic requirements and operating features of prepregs

1) The basic requirements: Prepregs play an important role in composite performance. The processing properties and mechanical performance of composites strongly depend on prepregs. The basic requirements of prepregs are as follows:

- ① Good compatibility between resin matrix and reinforcement: The reinforcement, after surface treatment, should be very compatible with the resin matrix to provide outstanding interlaminar strength.
- ② Proper tack and drape: The prepreg tack and drape together should have the ability to take the shape of a contoured surface. The tack in prepregs should not be too high so that plies can be easily separated if a layup error occurs, and relaying should be easy too. On the other hand, the tack should not be too low either so that firmly bonded adjacent plies can be guaranteed without any debonding. For complex and large curved surface parts, prepregs should be able to be laid down over the molds without any rebound from molds, even if the applied force action is removed.
- ③ Resin content deviation in different batches of prepregs should be as small as possible and be at least controlled to within $\pm 3\%$, which will assure consistent composite fiber volume content and mechanical performance. This is more important in non-resin impregnating prepregs in which resin content deviations should be $\pm 1\%$.

- ④ The volatile content in prepregs should be minimized to reduce the void content in composites and enhance mechanical performance. Generally, the volatile content should be less than 2% and within 0.8% in prepregs that are to be used to make primary structures.
 - ⑤ For a longer shelf life: The tacky shelf life at room temperature should be longer than one month and more than 6 months below $-18\text{ }^{\circ}\text{C}$ so that composite layup processing and mechanical performance needs are satisfied.
 - ⑥ To have a broaden pressure application zone during the curing process: The cure pressure should be able to be applied over a broaden temperature range to yield good quality composite parts without any performance loss.
 - ⑦ To have appropriate flow ability: The resin's flow ability should be fairly high so that a uniform resin distribution and full reinforcement impregnation can occur in prepregs. Resin systems in prepregs for sandwich structure skins should have a relatively low flow ability so that the skins and cores can be firmly bound.
- 2) Prepreg service features

The prepregs used in composites should have the following features:

- ① Exact control of reinforcement content and layup orientations. Because of precise resin content control in prepreg production, very little resin should flow out during curing. The desired reinforcement arrangement should be assured by designing an appropriate layup sequence. The part should be locally strengthened, and a composite part with varied thickness should be generated by changing the number of prepreg layers.
- ② Most prepregs available in a dry state are easily laid up.
- ③ A high-quality part surface should be expected because prepregs are fully resin-saturated and bubble-free.
- ④ As an intermediate-phase material, prepregs can offer benefits to production safety and management.
- ⑤ More production procedures will lead to a higher price.

(2) Raw materials

The raw materials in prepregs include resin matrixes and reinforcements. The other main auxiliary materials are backing papers and different colored and pattern-rolled polyethylene films.

- 1) Reinforcement requirements: The reinforcements for prepregs are basically carbon, glass, and aramid fibers or their fabrics. Other fibers such as boron fibers, ultra-molecular weight polyethylene fibers, and silicon-carbonized fibers are rarely used in structural composites at present.

For use in prepregs, the reinforcements should satisfy the following requirements:

- ① High strength and modulus, large fracture elongation, and the variation in performance should be as low as possible.

- ② Fiber linear density and fabric plane density should be consistent.
- ③ Fibers should accept surface treatments and be able to be perfectly bonded by resins and contribute good interfacial performance to the composites.
- ④ Fibers should be subjected to sizing processes. The sizing agents should have good compatibility with resin matrixes. The sizing agent content should generally be limited to about 1% without affecting other properties, which will be helpful in resin impregnation.
- ⑤ The fibers used for unidirectional prepregs should be untwisted or detwisted for good dispersion during resin impregnation.
- ⑥ Hairball-free, no broken yarns, and minimal yarn waste.

As reinforcements, a variety of fibers are candidates for prepreg preparation and fiber selection should be carried out by comparison and by considering various aspects. Table 1.2 shows such a comparison between fibers currently available for prepregs, as a reference for fiber selection.

2) Basic requirements of resin matrixes

A variety of requirements may exist for a resin matrix, but a narrow selection exists for prepreg applications. Resin systems are usually in half-solid or solid states at room temperature, and for low-tack resins, tack addition may be required. Resins used for resin solution prepreg preparation can be dissolved in low-boiling point solvents.

Different resin systems require different prepreg preparation procedures. Prepreg preparation requirements for resins are listed in Table 1.3.

The production of large composite structures requires a longer operating period. The layup and other operations require more time under the prepreg uncuring state. The shelf life of prepregs should be one month at room temperature and more than 12 months at temperatures below $-18\text{ }^{\circ}\text{C}$ without any property loss. This will strongly depend on the performance of the selected resin system.

The volatile content and flow ability of the resin systems will result in a void content in composites because the higher volatile content may leave entrapped residual solvents in the parts. A higher viscosity can affect the resin's flow ability and is not desired for fiber impregnation as it will result in a resin-starved phenomenon in the corners of the cured parts. This will subsequently yield more voids in the composites and cause a dramatic loss of mechanical properties.

Table 1.2 Comparison between reinforcing fibers

Fibers	Cost	Density	Modulus	Strength	Toughness	Thermal resistance	Anti-impact
E-glass	Superior	Poor	Poor	Medium	Good	Good	Good
S-glass	Good	Medium	Medium	Good	Good	Superior	Good
Aramid	Medium	Superior	Good	Good	Superior	Poor	Superior
Carbon	Poor	Good	Superior	Superior	Poor	Medium	Poor
Boron	Poor	Poor	Superior	Superior		Superior	

Table 1.3 Prepreg requirements for resins

Performance	Requirements
Mechanical	High modulus and strength, good toughness
Processing	Lower processing temperature and pressure, short curing time
	Broad pressure application zone, good for co-curing and zero-resin-sucking process
	Medium tack, good drape ability
	Low volatile content, no hazard to personnel
Thermal resistance	Relatively higher T _g , good thermal resistance
Environmental issues	Good resistance to water, oil, and chemicals
Flaming	Low smoke, low toxicity, low heat release rate
Storage	Long shelf life

The cure temperature is expected to be low and the cure time to be short, but in practice, the cure temperature will increase as the resin's thermal resistance increases. A higher cure temperature will give a shorter cure time. Currently, around 180 °C is the most accepted cure temperature.

The resin systems and solvents used should not be harmful to the working environment or to the operation personnel.

As discussed above, many aspects need to be considered for resin system selection. A comprehensive evaluation and analysis of the resin's performance will be needed to make a right choice to meet composite structural application needs, as shown in Table 1.4.

- 3) Requirements of backing papers: Backing papers are auxiliary materials used in prepreg preparation and composite processing. Although backing papers are not in the composite parts, they are very important in prepreg performance. The backing papers used in prepreps are a kind of craft paper as they are strong and of high quality with tacky-resistant coatings on both surfaces. The basic requirements of backing papers are as follows:

- ① Sufficient tensile and peel strength. No easy rupturing upon application.
- ② Easily separated from prepreg sheets without any residual waste.

Table 1.4 Comparison of the fundamental properties of different resin systems

Resins	Cure temp./°C	Operating temp./°C	Processing performance	Flow ability	Wet/hot mechanical	Fracture toughness	Flaming retardant
Epoxy	120–177	80–177	Superior	Low-high	Poor	Good	Poor
Phenolic	~ 170	~ 200	Superior	Medium-high	Poor	Poor	Superior
Cyanate	~ 177	~ 200	Superior	Low-high	Poor	Poor	Superior
BMI	~ 230	~ 260	Good	Low-high	Good	Poor	Superior
Polyimide	~ 316	~ 371	Good	Low-high	Good	Poor	Superior

- ③ Strong binding ability to prepregs. No removal during lamination and no dissolution in low-boiling point solvents.
- ④ Good dimensional stability without any changes as the environmental temperature and humidity change. Uniform and consistent thickness with minimal deviation. This is expected for the automated controlling resin content in closed-loop production.
- ⑤ Different release abilities for the two sides in double-sided tape backing paper. Release ability on the prepreg-binding surface should be lower than in a non-binding surface.

To meet all the needs mentioned above, the main backing paper producers, Dauber and Akrosil in the USA use different base papers and have developed a number of coating application techniques. Backing papers with different functions are now available for different applications.

(3) Prepreg preparation processes

Prepreg preparation refers to the fiber or fabric resin impregnating process. Corresponding techniques will depend on different resins. For thermosetting resin matrix prepregs, many well-developed processing techniques are available.

The preparation techniques for thermosetting resin matrix prepregs can be divided into two types: resin solution impregnation methods and resin hot melting methods.

- 1) Resin solution impregnation methods: In these methods, the constituents in a resin matrix will be set to a proper proportion and dissolved in a low-boiling point solvent to obtain a resin solution with a certain concentration. Fiber bundles or fabrics are then guided and pulled to pass through the solution at a specific rate to yield the desired resin impregnation. These processes must include a solvent-removal procedure, and the prepregs need to be heated during production to form a B-stage with appropriate viscosity.

Resin solution impregnation methods can be further divided into drum winding processes and multiple fiber bundles or fabrics continuous impregnation processes.

- ① Drum winding processes: In these processes, fiber bundles are guided and pulled to pass through a resin solution bath and then to pass over a group of guiding rolls for extra resin removal. The next step is to pull the impregnated fibers and wind them on the drum. Finally, they are cut in the drum axis direction to obtain the prepregs. This is a low-efficiency technique and is suitable for new product investigations and development. It is possible to use a bundle of fibers and a small amount of resin to prepare prepregs for the evaluation of resin and fiber performance, and even composite performance.
- ② Multiple fiber bundles or fabric continuous impregnation processes: In these techniques, the fiber bundles are guided and pulled out from a filament shelf. The tension forces are adjusted for each bundle to obtain a balanced state. After warp streaming, unbundling, and flattening steps, the fibers are guided into

Fig. 1.4 Schematic of horizontal-type solution resin impregnation procedures

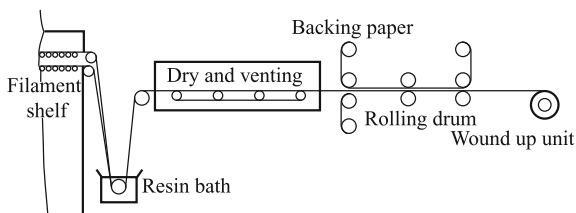
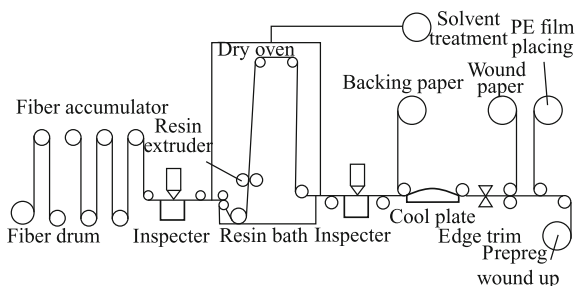


Fig. 1.5 Schematic of stand-type solution resin impregnation procedures



a resin bath for impregnation and are then extruded to remove extra resin. The impregnated fibers are then guided into a dry chamber to release volatiles, while the resin content and quality are inspected by an attached monitoring device. Finally, the prepregs are covered by backing paper or pattern-rolled PE films and wound into drums. In multiple fiber bundles or the fabric continuous impregnation process, either horizontal-type prepreg machines or stand-type machines can be used since the former needs a larger floor area and a long heating channel. The actual operations are difficult, and the end product quality is not easily controlled. Therefore, the current widely used processes are stand-type machines and related preparation techniques. Figure 1.4 shows a schematic of horizontal-type solution resin impregnation procedures, and the stand-types are given in Fig. 1.5.

In resin solution impregnation processes, the resin content in the prepregs will depend on the resin solution concentration in the resin bath, the reinforcing fiber feeding speed, and the distance between extruding rolls. As impregnation proceeds, the solvents continually evaporate and the resin concentration will continually increase resulting in a higher resin content in the prepregs. Therefore, in the production lines, a large resin solution tank should be included for continuous solution circulation between tank and bath. To maintain a consistent solution concentration in the resin bath, the storage tank should be equipped with a solution concentration monitoring device as well as solvent addition facilities. The linear feeding speed and the distance between extruding rolls can be adjusted easily. By these necessary measures, the deviation in resin content in prepregs can be limited to $\pm 3\%$ and even to $\pm 2\%$ with more precise control.

The advantages of resin solution impregnation processes are as follows: full resin impregnation in reinforcement, produce thinner or thicker prepregs, and a relatively low equipment cost. The drawbacks are as follows: drying oven required for solvent removal or recycling, and this may cause a fire or environmental problems with incorrect operation; residual solvent in prepregs results in more voids during part curing; and this affects composite performance.

- 2) Resin hot melting methods: These methods are based on resin solution impregnation methods, and the many problems caused by solvents can be eliminated. These methods are considered a big achievement in prepreg preparation processes and have been rapidly extended to a wide range of applications. Many professional prepreg manufacturers in developed countries are currently using resin hot melting procedures to make prepregs, especially for primary structural purposes.

Based on their different processing steps, resin hot melting methods can be further divided into two types: direct hot melting methods (one-step process) or resin film roll-extending methods (two-step process). In the former, resin systems are put into a resin bath, heated to a certain temperature, and melted, and then, the fiber bundles are guided in turn to pass through an unbundled device, a resin bath, a set of extruding rolls, a rearrange machine and are finally wound up on drums. The typical process is illustrated in Fig. 1.6. In these processes, the resin systems should have good flow ability and remain in a flow state at medium temperature as this is helpful for fiber impregnation. This type of process is mainly used to make rove prepregs or narrow prepreg tapes for the winding process. The resin content in prepregs is generally lower and can be controlled exactly. For example, the resin content in the unidirectional rove prepregs used to make clam plates for a helicopter spinner system can be controlled to 23% and controlled to a precision of $\pm 1\%$. The latter is currently widely used and has become the method of choice in prepreg production. This method consists of two steps, as shown in Fig. 1.7. First, resins are placed in a mixing pot for full mixing and are heated to an optimum film-forming temperature. They are then sent to coating rolls by a motor-driven metering pump or by pressure. Resin films of varied thicknesses can be produced by adjusting the distance between the rolls and the backing paper feed speed. The resin film thickness and the plane density can be inspected and monitored by a β -ray instrument, and the resin films should be cooled by cooling plates to minimize the cure degree. They are then wound up, packed, and stored in a freezer for later use.

Fig. 1.6 Schematic showing the direct melting impregnation processes

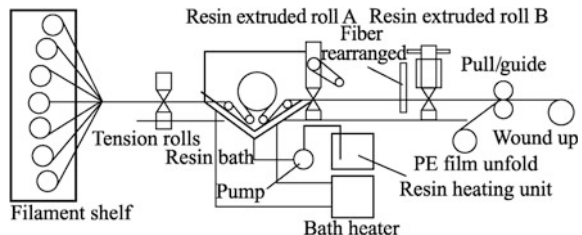


Fig. 1.7 Schematic showing resin film preparation

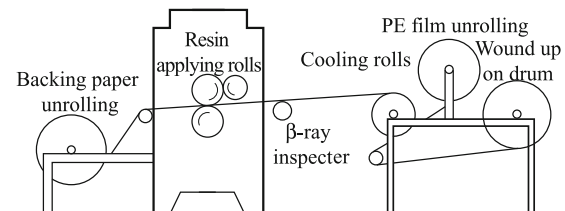


Fig. 1.8 Schematic showing resin film impregnation

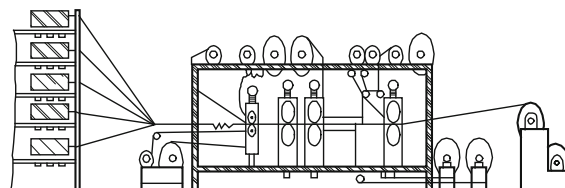


Figure 1.8 shows an illustration of the resin film impregnation processes. The fibers are guided and pulled from a shelf, the tension is adjusted, and they are then bundle-accumulated by a comb and flattened to a desired width. The preformed resin films are stretched between the upper and lower rolls to trap fibers and form a sandwich construction. The sandwich construction, in turn, is guided to pass through a set of heat-pressing rolls to allow the resin systems to melt and embed fibers. After cooling, trimming, and winding up, the end prepreg products are obtained.

The advantages of resin hot melting methods are as follows:

- Higher processing speed for a high production rate.
- Easy to control resin content and no solvents used.
- Less volatile in prepregs.
- Safe operation, no drying ovens needed, pollution eliminated.
- Resin film preparation and impregnation can be separately carried out. Material waste, especially high price reinforcement waste, can be reduced.
- Prepreg products have perfect surface qualities.

The main drawbacks of these methods are the difficulties in fully impregnating thicker reinforcements, especially fabrics, and resins with high viscosity are not suitable for this impregnation method while backing papers and PE films will be consumed.

Solution impregnation and hot melting impregnation have different features, but they are complementary and have coexisted for a long time and suit different applications. However, recent trends indicate that hot melting methods are being used more. In foreign countries, hot melting prepreg preparation processes are carried out using automated process monitoring. The computerized control of resin film thickness assures a uniform resin content in the products. Precise control can limit resin content deviations to $\pm 2\%$.

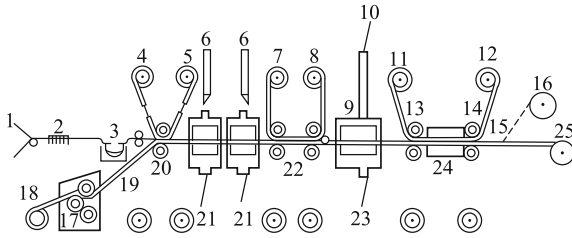


Fig. 1.9 Illustration of the multifunctional prepreg machine. 1 Fiber shelf; 2 comb; 3 resin bath; 4 top backing paper unrolled; 5 top backing paper wound up; 6 air and solvents exiting or recycling; 7 top backing paper unrolled; 8 top backing paper wound up; 9 drying oven; 10 air and solvents exiting or recycling; 11 top backing paper unrolled; 12 top backing paper wound up; 13 rolling; 14 guiding and pulling rolls; 15 cutting knives; 16 cutting knives; 17 reverse coating rolls; 18 bottom backing paper unrolled; 19 coated resin films; 20 pressing and rolling; 21 air or inert gas; 22 pressing roll set; 23 air or inert gas; 24 cooling facilities; 25 end products

To incorporate the functions and advantages of solution methods and hot melting methods, the Langley Research Center at NASA developed a multifunctional prepreg machine. This equipment can be used to make prepreps for resin solution impregnation and for resin melt processing, as illustrated in Fig. 1.9.

- 3) Prepreg quality control: In thermal setting resin prepreps, some chemical reactions can take place during production, delivery, and storage and prepreg quality should thus be seriously controlled. In foreign countries, comprehensive quality assurance techniques have been established. Standard testing methods and specifications for various preparation steps are also available to guarantee prepreg quality. Basic procedures for prepreg development and quality control are presented in Fig. 1.10.

Quality control in prepreg production lines mainly involves resin content control, and the resin content should have a homogeneous distribution and be consistent with minimal deviation.

In solution impregnation procedures, the prepreg machine is equipped with a soft X-ray instrument to measure and monitor the resin content. Resin content control can be achieved by adjusting the extruding roll's position and distance, or by changing the prepreg roll wrap angles.

In hot melting techniques, a β -ray instrument is attached to prepreg machine, and by repeatedly scanning the resin film along the width direction, the instrument will exactly monitor the resin content by measuring the ray penetration abilities to give a different film thickness.

In prepreg preparations, all the raw materials such as fibers, resins, curing agents, modifiers, and backing papers have to be inspected and only after qualification by some standards or specifications should they be accepted for prepreg production.

Environmental controls for prepreps should cover environmental controls in operation, storage, and applications. The main issues will include temperature, humidity, and media. The environmental temperature in prepreg preparation and

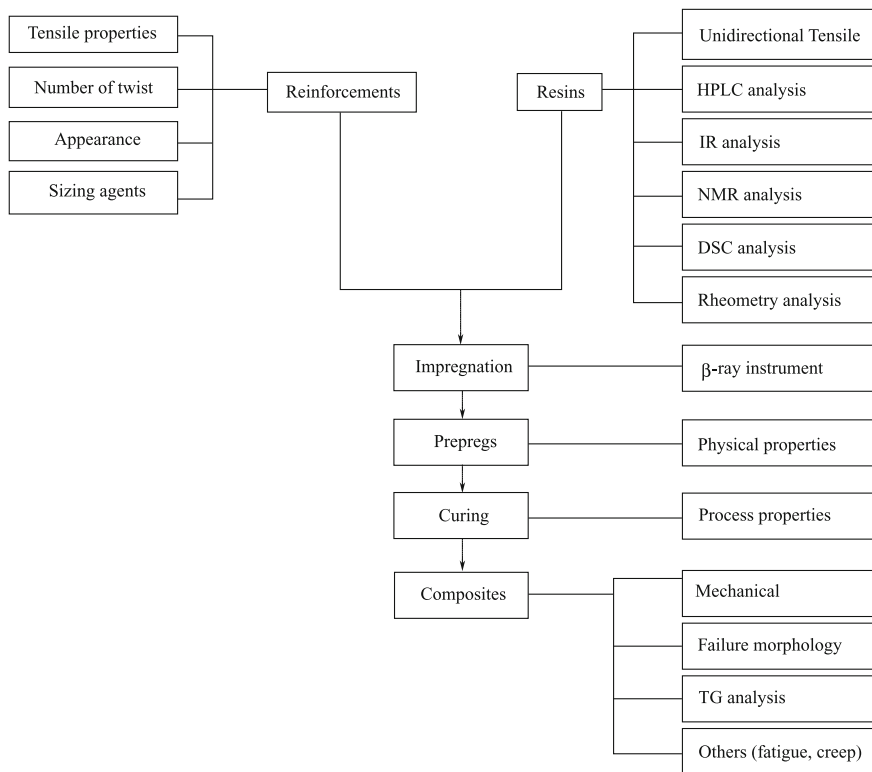


Fig. 1.10 Basic procedures for prepreg development and quality control

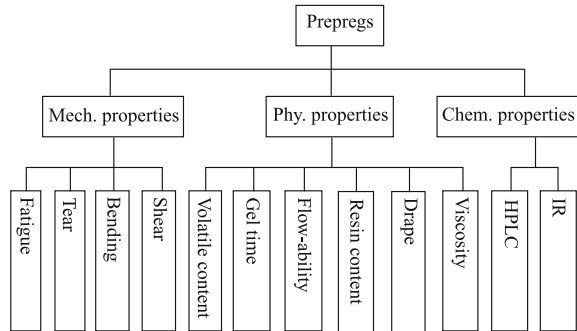
application should be set to about 20 °C. The storage temperature will usually be -18 °C to guarantee a longer shelf life.

Humidity may be a more important issue in prepreg preparation. In aramid prepreg preparations and applications, the humidity should be strictly controlled to within 45–50%.

For the quality control of end prepreg product, inspection and testing should be conducted on chemical compositions, physical properties, processing properties, as well as a segment of the mechanical properties of composite parts, as shown in Fig. 1.11.

- 4) Prepreg products: Based on their physical states, prepregs can be divided into unidirectional fiber tape, unidirectional fabric prepregs, and fabric prepregs. For resin matrixes, thermosetting and thermoplastic prepregs should be used; for reinforcing materials, carbon fiber or fabric prepregs should be used, and glass fiber or fabric prepregs should be used for aramid fiber or fabric prepregs. For fiber length, there is chopped fiber prepregs (<4.76 mm), long fiber prepregs (12.7 mm), and continuous fiber prepregs. For curing temperature,

Fig. 1.11 Main inspection procedure for end prepreg products



there are medium-temperature curing (120 °C), high-temperature curing (180 °C), and ultra-temperature curing (above 200 °C).

Unidirectional prepregs are those where fibers are placed and orientated along the fiber longitudinal direction with a proportion greater than 90% and only a little in the transverse direction. These types of prepregs are mostly used in Russia. Another alternative is to use a very thin glass fabric on the prepreg top surface to prevent fiber scattering. In Japan, Korea, and Europe, some of these prepregs are used for the production of sport goods.

Narrow prepreg tapes are those prepregs with a width of several millimeters or tens of millimeters, and they are primarily used in fiber automated placement or in filament winding processes, but they are not suitable for laminating.

(4) Prepreg performance

Prepreg performance usually covers resin or prepreg physical properties, chemical properties, defects and dimensional specifications, processing properties, laminate or sandwich structure physical properties, laminate or sandwich structure mechanical properties, laminate or sandwich structure flaming performances, electric properties, and shelf life.

Since prepregs are available in different types, grades, specifications and are prepared using different resins and reinforcements or used in different environmental conditions, there will be many different requirements for prepreg performances.

1) Resin and prepreg physical properties

Resin content: The resin content is expressed as resin mass fraction, and control precision is $\pm 3\%$ in resin solution impregnation prepregs; $\pm 2\%$ in hot melting prepregs; and $\pm 1\%$ in narrow prepreg tapes prepared by direct hot melting methods.

Volatile content: The volatile content should be within 2% in solution prepared prepregs, less than 1% in hot melting prepregs, but can be up to 5–10% in polyimide resin matrix prepregs.

Resin flow ability is generally 5–25%. Gel time vs temperature-gel time curves. Resin viscosity vs temperature-gel time curves.

Fiber mass in a unit area should be $\pm 5\%$ in unidirectional prepreg tapes and $\pm 10\%$ in fabric prepregs.

Viscosity: Viscosity should not to be too high and not tack-free either. They are good for manual work under ambient temperature and are easily layed up. If a laminating error occurs, ply separation is possible and relaying can be done without a performance loss; that is, it has a self-binding ability.

Drape ability: It is very flexible and suitable for complex structure lamination.

2) Chemical properties

Infrared spectroscopy: These are standard spectra given in prepreg specifications, and they indicate the chemical composition of uncured resin systems. They are also used to inspect pollution and changes in resin matrixes.

High-pressure liquid chromatography (HPLC): It is mostly used in prepreg quality control and can be used to determine the chemical composition of resin matrixes and to measure resin concentrations quantitatively.

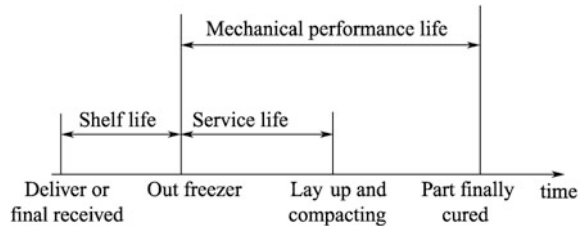
Gel penetration chromatography (GPC): It can be used to determine the relative molecular weight of resins and their distribution.

Differential scanning calorimeter (DSC): It is very useful for composite processing quality control and to study resin curing parameters. DSC curves can give much valuable data about resin or prepreg composition such as their T_g , the curing reaction heat, the resin B-stage content, and curing processing parameters such as the curing onset temperature, the peak and terminal temperatures, the curing degree, and the residual curing degree.

3) Processing properties

- ① Curing processing suitability: The suitability of various prepreg processing techniques such as hot-press molding, autoclave processing, vacuum bag processing, and automated tape placement.
 - ② Curing parameters: To guarantee composite performance, the curing temperature should be as low as possible, the curing pressure as low as possible, and the curing time as short as possible, while the pressure application zone should be as broad as possible.
 - ③ Good laminating ability: Proper tack and good drape ability.
 - ④ Suitability for honeycomb sandwich structure manufacturing: Resin drops can form in sandwich structure processing and high peel strength.
 - ⑤ Shelf life, service life, and mechanical performance life: The shelf life, service life, and mechanical performance life of prepregs will depend on the resin matrix, and different resin systems will yield different prepreg performances. For example, the 177 °C cured epoxy resin system is shown in Fig. 1.12.
- a) Shelf life: Prepregs stored at -12 °C or lower should have a one-year shelf life from the prepreg delivery date.

Fig. 1.12 Shelf life, service life, and mechanical performance life of a 177 °C cured prepreg



- b) If the shelf life exceeds one year, before use, the prepregs should be rechecked for flow ability, gel time, viscosity, and compression strength by following the same acceptance standards within one month after the shelf life has expired. The shelf life can be extended to 6 months for accepted prepregs, but beyond 1.5 years, the prepregs should be discarded.
 - c) At room temperature ($21 \pm 3 \text{ }^\circ\text{C}$), the service life of prepregs is about 240 h, and beyond this period, the prepregs cannot be used any more.
 - d) At room temperature ($21 \pm 3 \text{ }^\circ\text{C}$), the mechanical performance life of prepregs is about 1008 h, and if exceeded, the prepregs are to be rejected.
- 4) Laminate-level performance: Laminate performance can be used to evaluate a prepreg's physical and mechanical properties after the prepreg is transformed into a laminate.
- ① Laminate physical properties;
 - a) Single-layer cured thickness;
 - b) Density;
 - c) Fiber volume content;
 - d) Resin mass content;
 - e) Void content;
 - f) Glass transition temperature.
 - ② Laminate mechanical properties
 - a) Tensile properties: 0° tensile strength and modulus;
 0° tensile failure;
 90° tensile strength and modulus;
 90° tensile failure.
 - b) Bending properties: 0° bending strength and modulus;
 90° bending strength.
 - 5) Other performances
 - a) Flaming performance: 60-s vertical burning;
Average self-extinguishing time;
Horizontal burning scorch length;

Average self-extinguishing time of a dripped substance.

- b) Dielectric performance: Dielectric constants and loss factor.
 - c) Wave penetration.
 - d) Wave absorption.
 - e) Thermal performance: Linear expansion coefficient and thermal conductivity.
- (5) Global sources of prepreg supply and their performance

In 1999, the USA published a prepreg guideline and introduced nearly 30 prepreg manufacturers in the world as well as their products and performances, including 22 companies in the USA and companies in Germany, England, France, Canada, and Italy. The resin systems used in prepreps consist of two types: thermosetting and thermoplastic, and the reinforcing fibers are carbon fibers including standard-modulus carbon fibers AS-4, T300, G30-500 (207–276 GPa); medium-modulus fibers IM6, IM7 (276–344 GPa); high-modulus fibers M55 J, XN70A and also aramid Kevlar, Twaron; S-2 glass fibers; supermolecular weight PE fibers; quartz fibers; and boron/carbon hybrid fibers. As shown in Tables 1.5 and 1.6, Many prepreg suppliers and their products listed in these tables are comparable, and the data shown in these tables were collected from each company and can be used as a reference for prepreg selection. In these tables, different general-purpose prepreps and improved prepreps are provided together with the following properties: toughness, dielectric behavior, hot/oxidation strength, curing suitability at room temperature or low temperature, high flow ability, quick curing ability, high modulus, high-temperature resistance, flame-retardant ability, and suitability for RTM and FW processes.

In China, prepreps are basically prepared for self-use purposes or imported. Many current prepreg preparation techniques including resin solution methods, direct hot melting methods, hot melting resin film methods, static-electric resin powder methods, and their corresponding products are available for various applications. The prepreg products include various thermosetting resin prepreps and thermoplastic prepreps, unidirectional prepreps, and fabric prepreps. Nearly 30 different types of resin systems have been developed including epoxy, phenolic, BMI, cyanate ester, and thermoplastic PEEK. About 50 classes of prepreps prepared by different resin matrixes and reinforcements can be supplied to satisfy a wide range of applications including different service temperatures, different curing processes, different functions (flame retardant, dielectric, damping, wave penetration), different structure types (primary, secondary, non-load bearing, laminates, and sandwiches), as well as different processing techniques. Typical prepreps produced in China are presented in Table 1.7. Most of these products are technically mature, they have strict quality control systems, consistent batch productions are guaranteed, and these should be qualified to increase their application scope.

Table 1.5 Characteristics of unidirectional prepregs available outside China

Prepregs	Processing temp./°C	Service temp./°C	Fiber V.C./% %	Resin cont./% %	Tensile strength/MPa	Tensile modulus/GPa	Bending strength/MPa	Bending modulus/GPa	Comp. strength/MPa	Comp. modulus/GPa	Shelf life (-18°C)/month	Stand-by time RT/d
Epoxy/standard M. CF (T-300, AS4, G30-500, T-700)	121-154	82-127	57-63	32-45	1240-2200	103-152	1100-1860	96-138	1100-1720	103-131	6-12	14-30, 365
Epoxy/medium. M. CF (IM6, IM7)	121	121	57-60	38-42	2200-3030	138-171	1130-1670	138-151	1170-1630	127-138	12	30
Epoxy/standard M. CF (T-300, AS4, G30-500)	177	149-232	57-63	32-45	1310-2200	112-143	1580-193	100-155	8820-1720	117-138	6-12	10-21
Epoxy/medium. M. CF (IM6, IM7)	177	121-177	60-62	29-45	2340-2720	158-172	-	-	1520-1720	145-158	6-12	10-21
Epoxy/aramid	121-140	82	55-60	34-55	965	68.9	661-716	69	227	62	6	10-30
Epoxy/S-2 G.F	121-177	-	55-63	25-55	806-1580	-	1070-1630	44-56	689-1100	41-56	6	10-30
Epoxy/B and C hybrid (AS4, IM7)	121-177	121-177	77	15-20	1620-2200	220-269	2440-2960	234-255	2890-3440	220-269	6	12
BMI/standard M. CF (T-300, AS4)	177-246	232-315	55-59	33-37	1580-1720	186-200	1790-2070	118-193	1680	207	6-12	7
BMI/medium. M. CF (IM6, IM7)	177-227	232-115	60-67	26-33	2620-2740	165	1790-1860	145-156	1620-1740	151-158	6-12	28
Cyanate/standard M. CF (T-700)	121-315	249	-	-	-	-	1240	69	-	-	12	30
Cyanate/medium M. CF (MR-40, IM7)	121-232	232	57-63	32-43	689-2720	32-172	1350-1760	-	1420-1580	127-158	-	-
Cyanate/S-2 GF	121-177	204	-	32	1240	48	1580	58	896	62	6	10
Cyanate/pitch H. M. CF (XXN70A)	121-154	149	60	36	2160	413	572	344	344	400	-	-
Cyanate/pan H. M. CF (M55 J)	121-177	165	56.2	32	2050	336	1190	283	824	276	12	14

Post-treatment temperature is included in the processing temperature

Table 1.6 Characteristics of fabric prepregs available outside China

Prepregs	Processing temp./°C	Service temp./°C	Fiber V.C./%	Resin cont./%	Tensile strength/MPa	Tensile modulus/GPa	Bending strength/MPa	Bending modulus/GPa	Comp. strength/MPa	Comp. modulus/GPa	Shelf life (-18°C)/month	Stand-by time (RT)/d
Epoxy/standard M. CF (AS4,G30-500, T-300)	121-154	93-121	57-63	38-45	517-854	55-63	758-834	42-48	448-654	48-64	-	365
Epoxy/standard M. CF (T-300, AS4, Fortafil3C)	132-154	93	50-65	27-40	1378	124	-	-	-	-	-	365
Epoxy/standard M. CF (T-300, AS4,G30-500)	177	171	57-63	32-45	634-1030	55-83	840-965	68-76	606-965	48-83	6-12	10-21
Epoxy/spectra PE fibers	93-121	-	58	42	468	14	1560	14	14	-	-	365
Epoxy/Kevlar	113-177	82-177	50-60	40-63	331-558	21-36	316-716	10-62	172-241	21-36	6	10-21 365
Epoxy/S-2 GF	121-154	-	60	40	448-620	21-34	882-1030	69-124	138-241	21-34	-	365
Cyanate/medium M. CF (MR-40)	121	-55-82	55	-	551	34	413	34	379	31	6	10 365
Cyanate/high M. CF (XN50)	121-204	-	-	-	690	32	1760	173	1480	127	-	-
Cyanate/spectra PE fibers	121-177	177	60	36	909	186	592	131	234	138	-	-
Cyanate/kevlar	121	107	-	50	482	22	186	25	69	14	6	10
Cyanate/quarts	121-177	204	-	40	558	33	-	-	165	30	6	10
BMI/standard M. CF (T-33, G30-500)	121-177	93-177	-	33-42	351-696	25-26	517-792	20-27	406-524	23-29	-	-
BMI/medium M. CF (IM7)	163-204	-59-232	60	-	627-792	65-69	896-923	63-69	730-896	65	6	21
Polyimide/quarts	190-227	232	60	-	999	76	1030	76	896	72	12	28
Polyimide/quarts	288-343	316	55	-	586	26	551	24	482	24	6	10

Processing temperature includes post-treating temperature
 Fabrics are plain woven cloth (other fabrics can be used)

Table 1.7 Fabric prepregs and their performances

No.	Prepregs	Resin type	Prepreg features	Curing temp./°C	Max. service temp.		Processing method ¹	Gel time/min	Toughness ²	Shelf life		Prepreg type	Applications
					Dry	Wet				R. M./d	-18°C/month		
1	3231/CF	Modified epoxy	Good tack, long shelf life, good for processing	125	100	70	A.P., VB	2-4 ^b	6	120	18	Unid.	General structures
2	3232/H.S. GF	Modified epoxy	Narrow tape, direct melting made, good flow	125	100	70	A.P., FW	6-16 ^b	3	30	12	Unid. narrow	FW composite parts in helicopter
3	3233/C cloth	Modified epoxy	Self-extinguishable, good for processing, good toughness	125	100	70	A.P.	5-15 ^b	7	30	6	Fabric	Load-bearing structures
4	3233/G cloth	Modified epoxy	Self-extinguishable, good for processing, good toughness, suitable for sandwich	120	100	70	A.P.	5-15 ^b	7	30	6	Fabric	Sandwich in helicopter
5	3234/C cloth	Modified epoxy	Good for processing, good H/W resis	125	100	70	A.P.	6-14 ^b	4	45	12	Fabric	Load-bearing structures
6	3234/Kevlar 49	Modified epoxy	Good for processing, good H/W resis.	125	100	70	A.P.	6-14 ^b	4	45	12	Unid. narrow	FW composite parts
7	3235/C cloth	Modified epoxy	Good for processing	125	100	70	A.FW	2-6 ^b	4	30	12	Unid. Fabric	Horizontal tail and side vertical tail in helicopter
8	3236/CF	Modified epoxy	Super high toughness, good for structural applications	120	80	60	A.P.	6-16 ^a	9	>7	6	Unid.	Load-bearing parts in helicopter
9	3236/CF	Modified epoxy	Low dielectric loss, good for processing and H/W resis	120	80	60	A.P.	6-16 ^a	9	>7	6	Fabric	Load-bearing parts in helicopter
10	3242/Kevlar cloth	Modified epoxy	Self-extinguishable, good for processing, suitable for sandwich	125	85	70	A.P.	5-15 ^b	8	30	6	Fabric	Radar dome, seat, horizontal tail in helicopter
11	4211/CF	Modified epoxy	Good toughness, long shelf life, brittle	170	150	100	A.P.	4-10 ^f	1	>60	12	Unid.	Structural materials, Plane vertical stabilizer
12	5222/CF	Modified epoxy	Good for processing	180	160	120	A.P.	3-5 ^f	3	23	6	Unid.	Load-bearing structures

(continued)

Table 1.7 (continued)

No.	Prepregs	Resin type	Prepreg features	Curing temp./°C	Max. service temp.		Processing method ¹	Gel time/min	Toughness ²	Shelf life		Prepreg type	Applications
					Dry	Wet				R. M./d	-18°C/month		
13	5224/C cloth	Modified epoxy	Good toughness, outstanding for processing	180	160	130	A, P	5-25 ^g	4	30	12	Fabric	Primary parts, vertical tail, bypass
14	5228/CF	Modified epoxy	Good toughness and resistant to wet/hot conditions, good processing and H.T. resistant	180	170	130	A, P	17-27 ^g	6	21	12	Unid.	Primary structures
15	5231/G cloth	Modified epoxy	Good fire retardancy, suitable for sandwich	160	130	100	A, P	1-10 ^d	5	30	6	Fabric	Engine shell
16	5232/H.S.GF	Modified epoxy	Narrow tape, direct melting made, good flow	180	170	120	A, FW	2-20 ^g	3	10	6	Unid./narrow	FW for helicopter
17	5288/CF	Modified epoxy	Super toughness and resistant to wet/hot conditions, good combined performance	180	130	130	A, P	13-23 ^g	8	21	12	Unid.	Primary structures
18	5405/CF	Modified BMI	Good toughness and resistant to wet/hot conditions, high T resistance	180	180	150	A, P	27-29 ^g	5	15	12	Unid.	Primary structures
19	5429/CF	Modified BMI	Super toughness, resistant to wet/hot conditions, good for processing	200	180	150	A, P	-	8	30	12	Unid.	Primary structures
20	QY8911/CF	Modified BMI	Good toughness and resistant to wet/hot conditions	185	180	150	A	10-25 ^c	5	30	12	Unid.	Primary structures
21	QY9511/CF	Modified BMI	High CAI and resistant to wet/hot conditions	185	177	150	A	15-30 ^c	5	14	3	Unid.	Primary structures
22	QY8911-II/CF	Modified BMI	High T and resistant to wet/hot conditions	185	230	150	A	10-40 ^c	5	14	3	Unid.	Primary structures
23	LP-15/CF	Polyimide	Stable to high-temperature and hot oxidizing conditions, good for processing	320	280	-	A, P	25-35 ^h	3	15	-	Unid.	Engine parts

^a 120°C, ^b 125°C, ^c 150°C, ^d 160°C, ^e 170°C, ^f 175°C, ^g 180°C, ^h 280°C
¹A-Autoclave, P-Press molding, V-B-Vacuum Bag, FW-Filament Winding

²Toughness: Larger values indicate better toughness

1.2.3 Processing Molds and Tools

(1) The basic features of processing molds and tools

Processing molds and tools with different constructions and shapes are basic requirements in composite production. Molds can be divided into stiff molds or soft molds depending on the tooling materials. Stiff molds usually refer to the processing molds made using stiffer materials (most common metals). Soft molds are mainly made using rubbers or elastic materials for pressure applications. Soft molds must be incorporated in stiff mold processing techniques. For different applications, composite molds have the following features.



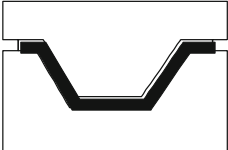
- 1) The machined mold end dimensions should differ from the dimensions of the end composite parts that are to be made. Tolerance selection will depend on mold types and the tooling material's linear expansion coefficients.
- 2) The end part dimensions should be the part dimensions obtained after the resin matrixes are fully cured under the desired curing temperature.

Based on different applications, processing molds can be classified as male molds, female molds, and assembled molds and each of these has the features shown in Table 1.8.

Idealized composite processing molds should have the following features:

- 1) The same linear expansion coefficients as the composite part to be processed.
- 2) No deformation or damage under a certain applied temperature and pressure.
- 3) Good dimensional stability.
- 4) Lower costs.

Table 1.8 Basic features of composite processing molds

Types	Features
Male molds 	<ul style="list-style-type: none"> • Lower costs, wide uses • Good part internal surfaces, external surfaces are lower quality • Easy to apply to vacuum bag
Female molds 	<ul style="list-style-type: none"> • Corner angles on curved surface limits application • Good part external surface, internal surface of lower quality • Possible to form a vacuum bag bridge
Assembled molds 	<ul style="list-style-type: none"> • High production costs • Good quality internal and external surfaces • Easy to control part thickness • High match precision for male and female molds and partial inner quality defects • Larger heat capacity, slower heating rate

- 5) Good sustainability.
- 6) Repeated use.

All the requirements mentioned above are not easily satisfied in composite processing mold designs. Metal materials almost meet these requirements except for the different linear expansion coefficients compared with carbon and glass fibers. In addition, metals are easily machined and can be well gratified if required by the application. Metals are the best candidates for mold material selection to achieve a lower production cost and a longer service life.

(2) Mold material requirements and selection

- 1) Mold material requirements: For mold material selection, the curing temperature of a part should be made and the processing techniques as well as costs should be seriously taken into account. In terms of curing temperature, a smaller linear expansion coefficient and high-temperature resistance are required for mold materials when undergoing high-temperature curing. For the processing techniques to be used, the mold materials should meet all the technical requirements. If costs are to be considered, lower material and manufacturing costs are better. The requirements for mold materials and general mold materials are listed in Tables 1.9 and 1.10, respectively.
- 2) Mold material selection: Currently, a variety of mold materials are available for composite processing, and any selection should consider the requirements of different applications. Costs should be taken into account when other requirements are satisfied. Criteria for mold material selection are as follows:
 - ① Consistent thermal expansion between part and molds.
 - ② Thermal conductivity.
 - ③ Dimensional accuracy.

Table 1.9 Requirements for mold materials

No.	Conditions		Requirements
1	Cure Temp.	R.T.–80 °C	No need to consider the thermal expansion of materials
		80–145 °C	Prefer materials with smaller linear expansion coefficients for large mold making
		145–220 °C	Materials with small linear expansion coefficients and heat resistance, composite tooling materials recommended
		Above 220 °C	Prefer materials with smaller linear expansion and heat resistance. Also, thermal expansion effects on part shape surface taken into account; necessary compensation measures needed
2	Processing to be used		Sanding and buffing free in materials located near the vacuum system or leakage can occur and cause part rejection
			Sometimes rubbers or pretreated rubbers required for processing techniques, for example, in a fixed location curing process or in a co-curing integrated process, soft rubber molds are often used together with metal molds (except for particular requirements)
3	Production costs		Easily machined at lower cost

Table 1.10 Some currently used mold materials

No.	Materials	Remarks
1	Aluminum	Good thermal conductivity and processing ability, light mass; larger linear expansion, service temp. below 180 °C and easily deformed, poor dimensional stability, often used to make panels or single curvature parts/structures where dimensional accuracy and consistency are not absolute
2	Steel	Linear expansion coefficient only half that of aluminum, high stiffness and service temp. long service life, relatively poor thermal conductivity/processing ability and heavier compared with aluminum; 20 [#] and 45 [#] super carbon steels and invar steel are widely used as mold materials for making structural molds with high dimension accuracy. However, thermal expansion should be of concern for large part production under high-temperature curing, and may require compensation
3	Cast irons or cast steels	Low costs, easily machined, large mold stiffness; thicker molds, larger thermal capacity, non-uniform temperature distribution in molds, heavy mold, microholes possible on mold surface, often used for digitalized machining of mold surface
4	Rubbers	Vulcanized rubber soft molds have advantages such as good shape compatibility, easily fits parts/structure, and reliable pressure transfer. Prepregs can be placed inside unvulcanized rubbers and cured simultaneously with rubber vulcanization to obtain higher rubber stiffness and stable dimensions. These soft molds have the desired stiffness and good compatibility with molds or parts. However, costs are higher, and they have poor dimensional stability. Widely used in integrated co-curing processes
5	Silicon rubbers	Give pressure by thermal expansion, suitable for various part shapes, low costs, service temperature below 300 °C, easily worn out, limited service life
6	Carbon/epoxy composites	Have the same linear expansion as composite parts, light mass, high material modulus and high mold stiffness, stable dimensions, but poor durability, service temperatures limited by the epoxy, material costs are high. Suitable for large structural parts with high accuracy
7	Woods	Light mass, low price, easily machined, short service life and disposable, poor part dimensional accuracy, limited use in processing test specimen preparations

- ④ Strength and stiffness.
- ⑤ Ability for mold making.
- ⑥ Part costs.
- ⑦ Durability.
- ⑧ Ability retention.
- ⑨ Mold service life.
- ⑩ Mold storage requirements.

In Table 1.11, the basic properties of current mold materials are provided.

Table 1.11 Basic properties of mold materials

Material property	Molds core molds	GFRP	CFRP	Electric cast Ni shell molds	Aluminum	Steel	Cast iron
Density/g · cm ⁻³	0.4–0.6	1.5–2	1.5	8.9	2.7	7.9	7.2
Strength/MPa	20	150–400	500	300	50	300	100–200
Modulus/GPa	1	7–20	35–50	200	71	210	100
LEC/10 ⁻⁶ K ⁻¹	Equivalent to plastics	15–20	4	13	23	15	11
Specific thermal capacity/ J · (kg · K) ⁻¹	Equivalent to plastics	1000	1000	460	913	420	500
Thermal conductivity/W · (m · K) ⁻¹	–	1	1	50	200	60	70
Max. service temp.	–	≤ 150 °C	≤ 180 °C	Suitable for all resins	≤ 180 °C	Suitable for all resins	Suitable for all resins

(3) Mold construction in autoclave processing

- 1) Requirements for mold construction in autoclave processing: The requirements for mold construction in autoclave processing are listed in Table 1.12.
- 2) Processing mold construction: Processing mold construction depends on the individual structure patterns. Different individual structures will give different processing mold constructions.

Figure 1.13 shows a schematic of a frame-like mold construction currently used in autoclave processing.

(4) Composite molds

Composite molds refer to a kind of composite structure fabricated using carbon fiber prepreps or glass fiber prepreps laid up on a master model and then cured and post-cured.

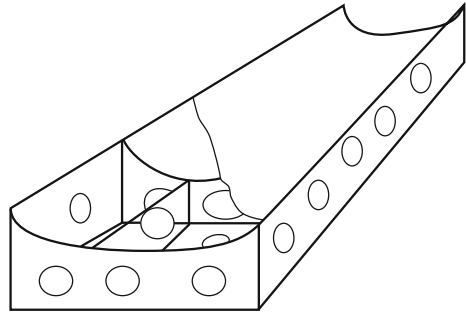
- 1) Composite mold features: Compared with metal molds, composite molds have a number of advantages including a light structural mass, a high specific strength, an equivalent linear expansion to composite products, small thermal deformation, high-quality surface finishing, a repairable mold, and the possible use of the same master model set for repeated composite mold production, which removes deviations in series mold products. The main drawbacks are limitations in mold construction, high initial capital costs, easy damage, and a high manufacturing cost.

Composite molds are mostly used to produce composite structures with large outer dimensions and high location accuracy requirements.

Table 1.12 Requirements of mold construction in autoclave processing

No.	Items	Requirements
1	Mold surfaces	The whole mold surface must be smooth, flat, dense, crack-free and show no penetration and can guarantee no leakage in vacuum system consisting of molds and vacuum bag. There should be a wide enough margin on the mold boundary for vacuum bag edge sealing; mold surface should be marked with partial outer edge lines, margin lines, partial location set lines, fiber oriented lines, and other mating spars, rib and rod axis lines, selected area for batch samples on the non-operation surfaces, there should be several vacuum nozzle locations that are properly arranged
2	Mating, coordinating and location	Usually, skin-type single parts are simpler for positioning and are not necessarily taken into account. However, in co-cured or adhering integrated parts, it is necessary to check whether the positions of the cured components meet design requirements because the very high-temperatures in autoclaves will make component location difficult. The coordination or consistency of applied pressure among the components in a co-cured or adhering integrated part should be also considered
3	Temperature distribution	The molds used in autoclave processes have preferred thin-walled constructions, and to open vents on support frames, it is helpful to reduce the mold weight to achieve a uniform temperature distribution in the composite parts; in skin-type part production, frame-like molds are selected because they have advantages of uniform thickness, good ventilation, fast heating and cooling and a uniform temperature distribution in different mold areas. Therefore, it is possible to avoid the mold deformation caused by inhomogeneous mold temperature during heating or cooling procedures. This phenomenon should also be taken into account for mold integrated processing
4	Mold stiffness	Since no support platforms are available in autoclaves, it is necessary to pay attention to mold stiffness in mold design as a lack of stiffness will result in mold deformation, especially during integrated processing under high temperature
5	Mold release	Mold release should receive significant attention during mold design. Although cured composite parts can be released from molds using release materials, uncertainty in part release can occur because the high processing pressure applied to the part will cause it to be laid firmly onto the mold surface and it may be difficult to remove after curing. A simple release method should be targeted in mold construction design. Some parts such as spars, ribs, frames, and beams with a dent or a closed angle are usually released with difficulty from a mold in single part production or in integrated processing. It is necessary to take this into account when designing a removable mold assembly so that the cured part can be easily removed after mold disassembly

Fig. 1.13 Schematic of a frame-like mold construction used in autoclave processing



- 2) Tooling materials for composite molds: A variety of material systems are available for composite mold making. In China, the main mold materials are the “TOOLMASTER” product systems imported from the USA and the “LTM” mold material systems developed by the ACG company in the UK.
- ① Mold material selection criteria: Many mold materials are available with various property specifications such as service temperature, linear expansion, strength, modulus. Mold material selection should incorporate several factors including composite part performance requirements, linear expansion coefficients, and curing parameters. The following points should be adopted in composite mold material selection:
 - a) Carbon fiber mold materials should be selected for carbon fiber composite part making.
 - b) Candidate mold materials for glass fiber or aramid composite production can be selected from carbon fibers or glass fibers and hybrid carbon and glass fibers depending on part needs.
 - c) The thermal deformation temperature must exceed the part curing temperature by up to more than 20 °C.
 - d) The curing temperature of mold materials must satisfy the thermal resistance requirements of the master models.
 - e) The post-curing temperature of the mold materials should take into account the ability of the curing equipment to be used.
 - f) The mold materials should have appropriate viscosity, good drape ability, and proper service periods at ambient temperatures.
- ② Mold material types: The main mold materials available for composite molds consist of tooling preregs, mold surface adhesives, and master model materials, as listed in Tables 1.13, 1.14, 1.15, 1.16, 1.17, 1.18, and 1.19.
- 3) Typical composite mold constructions: Vacuum bag molding processes and hot-press molding processes are widely applied in composite part making, and the corresponding composite molds used in these processes are vacuum processing molds and hot-press processing molds. Because of the limitations in

Table 1.13 Tooling prepregs supplied by the AIRTECH company in the USA

Prepregs	TMFP3100	TMFP3200	TMGP4000	TMGP4100	TMGP4200
Mass/g · m ⁻²	325	617	190	340	644
Resin content/%	45 ± 3	37 ± 3	47 ± 3	42 ± 3	47 ± 3
Single-layer thickness/mm	0.28	0.48	0.28	0.36	0.66
Shrinkage/%	0.08	0.08	0.02	0.02	0.02
L.E.C/10 ⁻⁶ K ⁻¹	12.6	12.6	2.7	2.7	2.7
Tensile modulus (22/177 °C)/GPa	23/19	23/19	64/50	64/50	64/50
Bending modulus (22/177 °C)/GPa	26/25	26/25	51/44	51/44	51/44
Compre. strength (22 °C/177 °C)/MPa	379/289	379/289	427/283	427/283	427/283
Initial curable temp./°C	121	121	121	121	121
Post-cure temp./°C	196	196	196	196	196
Max. service temp./°C	202	202	202	202	202
Pot life (25 °C)/d	40	40	40	40	40
Shelf life (-17 °C)/m	12	12	12	12	12
Prepregs	LTCG1400	LTCG1600	LTCF5500	LTCG56	
Mass/g · m ⁻²	193	644	325	617	
Resin content/%	55 ± 3	40 ± 3	45 ± 3	37 ± 3	
Single layer thickness/mm	0.30	0.66	0.28	0.48	
Shrinkage/%	0.02	0.02	0.08	0.08	
L.E.C/10 ⁻⁶ K ⁻¹	2.7	2.7	12.6	12.6	
Tensile modulus (22/177 °C)/GPa	52/47	52/47	21/19	21/19	
Bending modulus (22 °C/177 °C)/GPa	59/31	49/31	25/20	25/20	
Compre. strength (22/177 °C)/MPa	400/221	400/221	372/228	372/228	
Initial curable temp./°C	60	60	60	60	
Post-cure temp./°C	196	196	196	196	
Max. service temp./°C	202	202	202	202	
Pot life (25 °C)/d	5-7	5-7	5-7	5-7	
Shelf life (-17 °C)/m	12	12	12	12	

composite mold construction, the best candidates are large or medium vacuum processing molds. Typical mold constructions are shown in Fig. 1.14.

- ① Rules for selecting composite mold constructions: The concepts given below should be taken into account when selecting composite mold constructions.
- a) Sufficient strength and stiffness can meet all the needs of composite products' manufacturing.
 - b) Good part shape consistency and the thermal deformation should be limited to within the allowable shape tolerance of composite parts.

Table 1.14 Tooling prepregs from the LTM 210 series supplied by the ACG company in the UK

Prepregs	LTM210	LTM211	LTM212	LTM213	LTM215
Initial curable temp./°C	30	35	37	40	45
Initial curable time/h					
45 °C	12	16	20	24	48
60 °C	4	6	10	12	14
70 °C	2.5	3	4	6	7
Post-cure temp./°C	200	200	200	200	200
Max. service temp./°C	200	200	200	200	200
Pot life. (21 °C)/d	1–2	2–3	3–4	4–6	8–10
Shelf life (–18°C)/m	12	12	12	12	12
Prepregs	LTM217	LTM217EL	LTM218RC	LTM218	LTM219
Initial curable temp./°C	55	60	60	70	60
Initial curable time/h					
45 °C	–	–	–	–	–
60 °C	16	24	24	–	24
70 °C	8	12	12	48	12
Post-cure temp./°C	200	200	200	200	200
Max. service temp./°C	200	200	200	200	160
Pot life (21 °C)/d	10–14	15–20	20–30	>120	100
Shelf life (–18 °C)/m	12	12	12	12	12

Table 1.15 Tooling prepregs in the LTM 10 series supplied by the ACG company in the UK

Prepregs	LTM10	LTM12	LTM13	LTM16	LTM17	LTM18
Initial curable temp./°C	20	30	30	40	50	70
Initial curable time/h (temp./°C)	14(40)	13(45)	16(50)	10(60)	16(160)	15(75)
Post-cure temp./°C	200	200	200	200	200	200
Max. service temp./°C	210	210	160	210	160	210
Pot life. (21 °C)/d	2–3	4–5	2–3	7–8	8–10	30
Shelf life (–18 °C)/m	12	6	12	12	12	12

- ② Typical mold constructions: In foreign countries, various stiffened components, supporting rods, and tube joints are available in product series for typical composite mold constructions. The right choice should be based on different mold constructions and dimension requirements.
- a) Spiral-type flexible strengthening components: The spiral-type flexible strengthening components shown in Fig. 1.15 easily bend to a required shape to fit a mold curvature, and they can be used to stiffen shell-type molds for rigidity by reinforcing and backing up the mold with tooling prepregs. The result is a permanent mold construction.

Table 1.16 The machine-workable MASTER series from the AIRTECH company in the USA

Performances	MODELMASTER A160	MODELMASTER A250
L.E.C (22–71 °C)/ 10^{-6} K^{-1}	73.8	39.6
Hardness (sharpe D)	61 ± 2	68 ± 2
Tg/°C	72	126
Color	Brown	Light gray
Density/ $\text{g} \cdot \text{cm}^{-3}$	0.5206	0.5382
Tensile strength/ MPa	19	15.2
Bending strength (25 °C)/MPa	24.5	24.1
Bending modulus (25 °C)/MPa	1100.4	1689.2
Compre. Strength/ MPa	24.8	32.4
Compre. modulus (25 °C)/MPa	1083.2	1068.7
Specification/mm	1524 × 610 × 50.8 1524 × 610 × 101.6 1524 × 610 × 152.4	1524 × 610 × 50.8 1524 × 610 × 101.6 1524 × 610 × 152.4
Application	Used to make master models with consistent dimensions and with ease for machining, jointly used at 60 °C with curing tooling prepregs	Used to make master models with consistent dimensions and with ease for machining, jointly used with low temp. curing tooling prepregs

- b) Square-section tubes, angle shapes, and I-beams: The products shown in Fig. 1.16 are used to make mold supporting structural components.
- c) Tube joints: Various tube joints and their couplings for support structure connections are shown in Fig. 1.17.
- 4) Typical processing specifications
- ① Master model fabrication: Before making composite molds, a master model should be made and used to make duplicate composite molds. The master model should be made by digital control machining.
- a) Master model materials: The best materials for master model making are the machinable MASTER panels that are auxiliary to tooling prepregs. These reduce costs, and convenient epoxy or plaster can be selected. For any tooling materials used for master model making, the following factors should be taken into account:

Table 1.17 Machinable MASTER series from the ACG Company in the UK

Performance	TB650	TB620	TB560	TB320	UB450
L.E.C (22-71 °C)/10 ⁻⁶ K ⁻¹	38	39	73	40	55
T _g /°C	110	110	58	72	50
Specification/ mm	2000 × 1000 × 123 1000 × 1000 × 123 1000 × 500 × 123 1000 × 1000 × 49 1000 × 500 × 49	2000 × 1000 × 123 1000 × 1000 × 123 1000 × 500 × 123 1000 × 1000 × 49 1000 × 500 × 49	1000 × 1000 × 49 1000 × 500 × 49	2000 × 1000 × 123 1000 × 1000 × 123 1000 × 500 × 123 1000 × 1000 × 49 1000 × 500 × 49	1500 × 400 × 100
Application	Used to make master models with consistent dimensions and with ease for machining, jointly used below 110 °C with curing tooling prepregs	Used to make master models with consistent dimensions and with ease for machining, jointly used below 110 °C with curing tooling prepregs	Used to make the master models, jointly used with low temp. curing tooling prepregs	Used to make master models, with consistent dimensions and with ease for machining, jointly used with medium temp. curing tooling prepregs	Used to make master models, jointly used with low temp. curing tooling prepregs

Table 1.18 MASTER panel adhesives from the AIRTECH company in the USA

Performance	MASTERBOND16 A/B	MASTERBOND25 A/B
Mix ration A:B	1:1	3:1
Curing time at room temp./h	18–24	18–24
Pot life (normal temp. 100 g)/min	90	120
Density/g · cm ⁻³	0.72	0.62
Compre. Strength/MPa	22.1	24.8
Max. service temp./°C	71	149
Shelf life (below 22 °C)/m	12	12
Color	Brown	Light blue

- i) Sufficient strength and modulus can withstand the processing pressure of composite part fabrication.
 - ii) Good thermal resistance to ensure composite molds without cracks or deformation during curing processes.
 - iii) Easy machining or manual polishing.
 - iv) Lower linear expansion coefficients.
- b) Master model surface preparation: The aim of surface preparation (surface treatment) is to achieve a smooth and finished model surface. The ready composite mold should be released easily, and a high-quality mold surface should be guaranteed. Current surface preparation methods are listed below.
- i) Spray: In this method, a thin layer of resin coating is applied to the model surface. This resin coating is bright and heat resistant and can protect and fill the model surface.
 - ii) Polishing and waxing: In these methods, the model surface is carefully grounded by fine abrasive paper and a thin layer of wax is applied; it is then polished using silk cloth.
 - iii) Using release film: In this method, the model surface is carefully grounded by fine abrasive paper, cleaned, and then placed on release film.
- ② Composite mold laminating design: The following factors should be considered in mold ply design:
- a) Sufficient strength and modulus to meet the composite part's processing requirements.
 - b) Guarantee long-term shape stability after composite mold fabrication.
 - c) Mold service life to be long.
 - d) Provide an acceptable mold surface.

Table 1.19 Surface resins from the AIRTECH company in the USA

Performance	TMSFR5100A/TMSFHR5100B	LTCSEFR520A/LTCSFHR520B	MASTERSEAL TK27
Mix ratio A: B	100:12	100:12	100:28
Max. service temp./°C	202	202	182
Application	Mold surface coating, jointly used with TMFP 3000/3100, and TMGP 4000/4100 to eliminate tiny spots on mold surfaces and forms a protective coating	Mold surface coating, jointly used with LTC-F5500/5600 and LTC-G1400/1600 to eliminate tiny spots on mold surfaces and forms a protective coating	Used to seal machined MODELMASTER and other porous surfaces and also for rebuilding the vacuum sealing of composite molds

Fig. 1.14 Typical mold construction

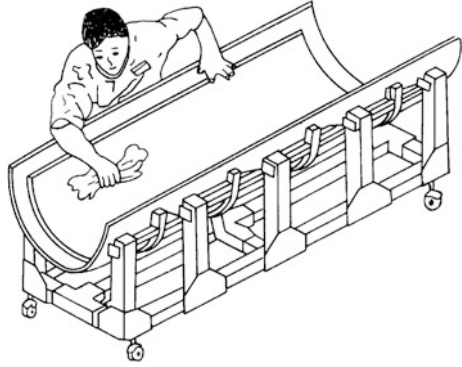


Fig. 1.15 Spiral-type flexible strengthened components

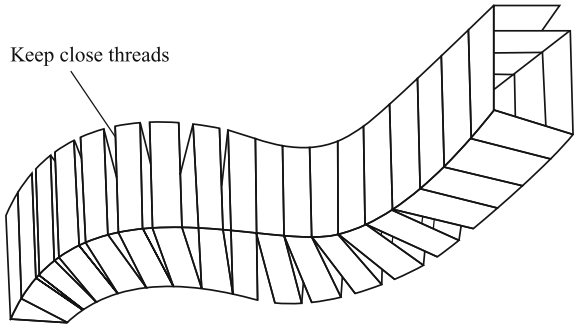
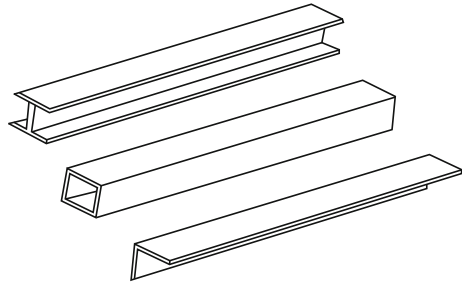
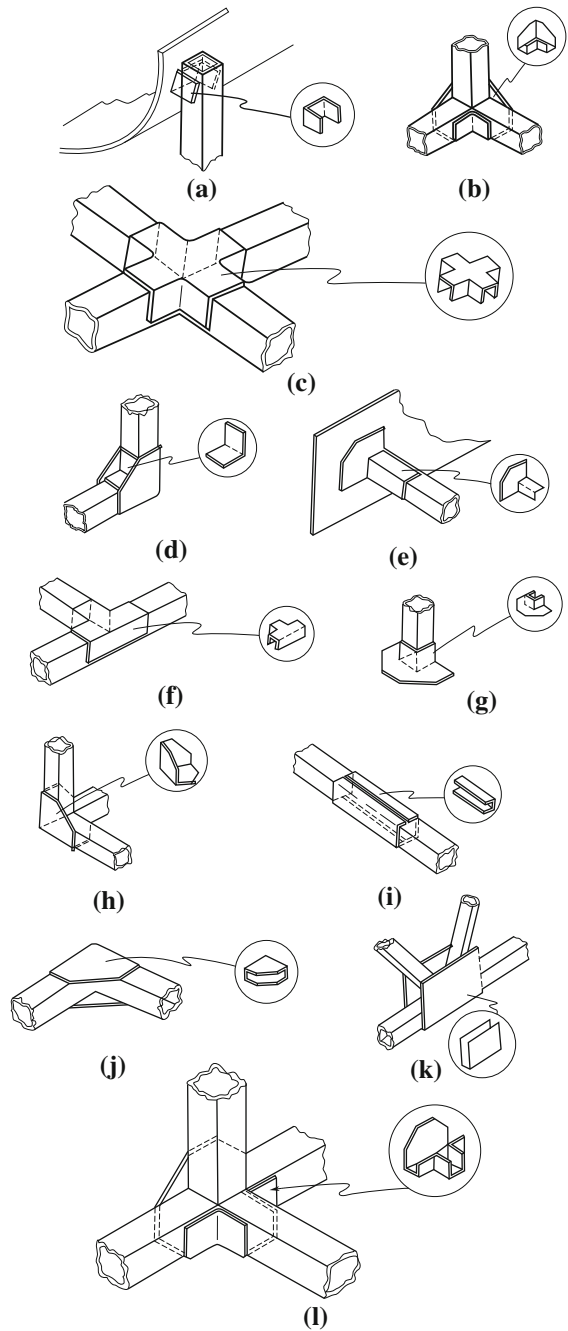


Fig. 1.16 Square tubes, angle shapes, and I-beams for structural purposes



After the laminate thickness is determined, one or two layers of light cloth prepreg with high resin content are required on both the inner and outer mold surfaces to ensure mold surface quality and an airtight seal. A layer of TEDLAR film will be also needed on the mold's top surface as a damp-proof layer. The ply orientations are basically $0^\circ/90^\circ$ cross-plyes and depend on mold shape and dimensions. For large surface plane molds, some additional $\pm 45^\circ$ cross-plyes may be needed for mold stiffening.

Fig. 1.17 Various tube joints and their couplings



- ③ Mold laminating principles: Environmental requirements: temperature 18–24 °C, relative humidity 40–65%, and workplace to be dust-free and air-conditioned.

Laminating should follow the designed ply orientation and sequence.

After each of two or three layers of lamination, a vacuum is used to remove entrapped air and compact the laminated plies.

Prepreg ply alignments or overlaps should be dislocated during lamination. The selection of ply alignments or overlaps will depend on mold shape and the prepreg types used.

④ Composite mold fabrication

- a) Master model surface preparation: The master surface is cleaned with an acetone-dipped sponge or a hair-free cotton cloth. It is checked for an airtight seal in the duplicated molds. The residual release agents left on the surface are removed and cleaned, and new release agents are applied.
- b) Mold surface gel coat resin preparation and application: The resin-block strips or ribbons are placed and fixed along the composite mold's outer edge marked lines as resin flow barriers. Glue tape or wax paper is then applied for protection.

The surface gel coat resins are prepared proportionally and are fully stirred before obtaining a uniform mixture.

A hair-chopping brush is then used to apply the surface resin onto the master model surface along one direction repeatedly. The brush should be vertical to the master surface, and the applied resin should be thick and cover the master surface until it is invisible.

A new brush without hair is then used to wipe the applied resin vertically in the applied direction repeatedly to remove bubbles entrapped in the resin coatings. A small angle should be maintained between the brush and the mold surface so that a homogeneous resin coating is formed, as shown in Fig. 1.18.

The master model with the applied surface resin should be shelved for a period at a specified temperature to allow resin drying and tack loss. The resin should not be sticky to hands.

- c) Cloth prepreg lamination (Fig. 1.19): The fully thawed prepregs are unpacked and cut to the desired shapes and dimensions.

Fig. 1.18 Schematic showing mold surface gel resin application

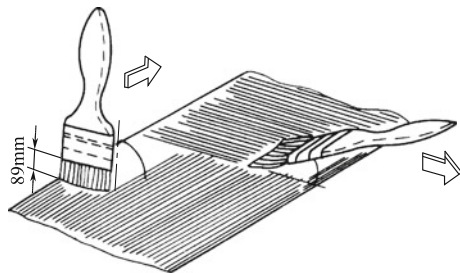
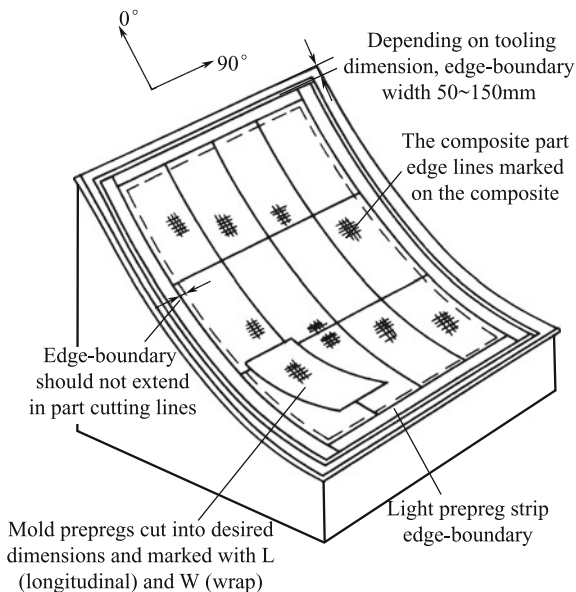


Fig. 1.19 Schematic showing cloth prepreg lamination



Light prepreg strips are used to make an edge boundary on the master model surface with the designed dimensions. The edge boundary should be laid outward from the mold edges, and the width of the edge boundary should be 50–150 mm depending on mold size. The function of the edge boundary is to eliminate continuous fiber bridges between the mold edges and the part making area.

By following the designed orientation, the first layer of prepreg is placed on the mold surface within the edge boundary and a vacuum is applied for at least one hour until a full vacuum is generated.

To trace the back ply orientation, a layup code table containing each prepreg layer's marked orientation is required during lamination. Once a prepreg layer is laid on a model, a corresponding mark should be made on the code table to avoid possible laminating errors.

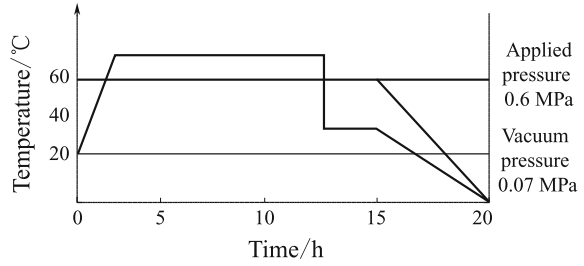
When laminating at an angle on a female mold, the prepregs should not cross the angle, and the fibers in the prepregs should be removed from the angle point. An aligned or slightly overlapped lamination should be carried out.

Lamination and compacting should continue until all ply laminations are complete. Edge boundary lamination should end by the sixth ply. From the seventh ply, the lamination can extend to resin-block strips or ribbons.

- d) Initial curing (autoclave curing): The mold with the vacuum bag should remain in a full vacuum state.

A specific positive pressure should be applied, usually in the range of 0.4–0.7 MPa, depending on mold panel thickness.

Fig. 1.20 Typical initial curing time, temperature, and pressure curve



Initial curing should continue by following the specified curing parameters. A typical curing parameter curve is shown in Fig. 1.20.

- e) Integrated strengthened constructions: Spiral-type flexible strengthening components can be attached to a mold panel after the last mold prepreg layer has been laid down and rolled. It is then co-cured with the mold panel for the second lamination operation. In terms of production costs, the co-curing process should be the right choice.

If strengthening components are to be attached to the mold’s back, two or three layers of prepreg cloth or resin pre-impregnated cloth can be attached and the cloth should be cut to the desired width, which is the same as the strengthening components. The strengthening components are cut to the desired length and put into a vacuum bag where the release film has already been enveloped. It is then placed on the mold’s back where the prepreg layers or the resin pre-impregnated cloth has already been laminated. The application of a slight pressure forces the strengthening components to bind to the prepregs. After prepreg curing, an integrated mold construction with the strengthening components attached is finally constructed. A typical lamination process is shown in Fig. 1.21. The prepreg stacking thickness

Fig. 1.21 Typical lamination in an integrated strengthening construction

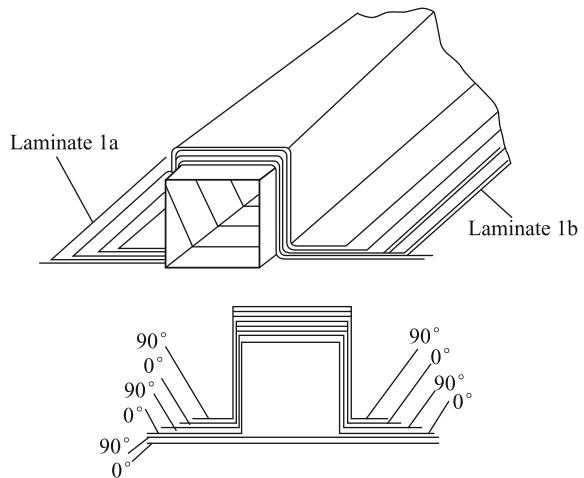
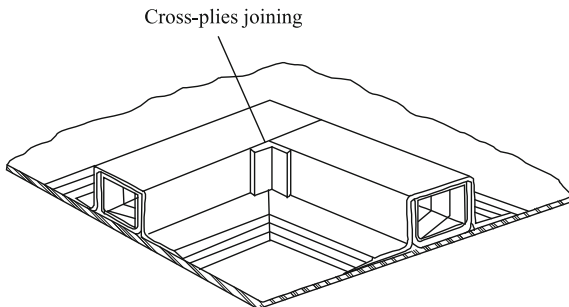


Fig. 1.22 Cross-ply joining for a strengthening construction

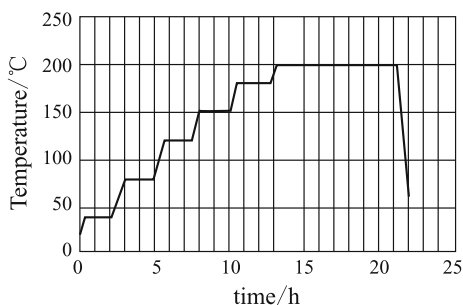


will depend on the mold shape and dimensions and is usually 4–6 layers. If a cross-strengthening concept is adopted, as shown in Fig. 1.22, the joint should be wrapped and connected by prepreps or resin pre-impregnated cloth.

- f) Mold support structures: The support structures for composite molds can be selected and assembled from the components shown in Figs. 1.17 and 1.18 or from metal support structural components. A non-fixed joining between a metal supporting structure and a mold panel should be adopted to avoid possible stresses caused by a linear expansion difference between the metal support structure and the mold panel.
- g) Post-curing: Post-curing should be carried out after mold release, and it is usually not necessary for support.

A typical post-curing cycle is shown in Fig. 1.23. In post-curing processes, heating and cooling should be carefully controlled based on the used prepreps. Generally, a rate of 1–2 °C/min for heating or cooling should be acceptable. The post-cured mold can be put into production after the necessary fixing.

Fig. 1.23 A typical post-curing cycle



1.2.4 Prepreg/Vacuum Bag–Autoclave Process

(1) Basic concepts in the prepreg/vacuum bag–autoclave process

In terms of resin matrix composite processing techniques, the prepreg/vacuum bag–autoclave process and the vacuum bag/pressure bag process are of the same type. Both require the negative pressure created by an applied vacuum between the processing bag and the mold, and the outer applied pressure (only the outer pressure in the pressure bag process) to force the composite part prototype firmly onto mold. It is then cured into an end part, and the final fabricated parts should have the same shapes as the processing molds. The best advantage of these processing techniques is that only a half-mold (male or female) is used, and large composite parts with complex shapes and high quality can thus be produced. It can also be used to make sandwich structures.

In prepreg/vacuum bag processes, the desired pressure can be applied to parts by the vacuum bag under vacuum conditions. The vacuum bag can only provide a low pressure between 0.05 and 0.07 MPa. These methods are most commonly used in cavity-type mold processing for part making, as illustrated in Fig. 1.24.

In prepreg/pressure bag processes, pressure is created by applying condensed air to the bag and to the parts to be made. The pressure can reach 0.25–0.5 MPa, and the desired heat is usually supplied by electric-heating metal wires inserted into the metal molds, and this can be adopted for use in plug-type and cavity-type molds, as shown in Fig. 1.25.

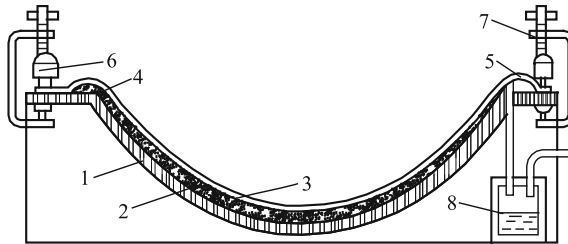


Fig. 1.24 Diagram showing prepreg/vacuum bag and cavity-type mold processing. 1 Molds; 2 part prototype; 3 rubber mat; 4 air collector; 5 washer; 6 bolts; 7 C-clamps; 8 resin collection bath

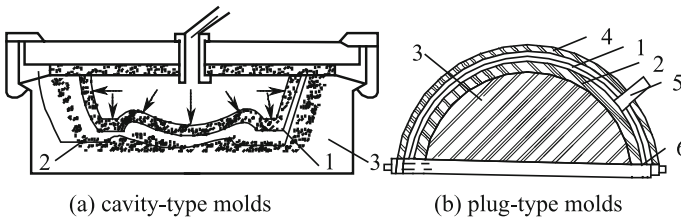


Fig. 1.25 Diagram showing prepreg/pressure bag processing. 1 Rubber bag; 2 part prototype; 3 molds; 4 outer shell cover(steel); 5 nozzle; 6 bottom plate

Fig. 1.26 Diagram showing autoclave equipment. 1 Rubber bag; 2 processing gloves; 3 molds; 4 part prototype; 5 C-clams; 6 autoclave; 7 bottom plates

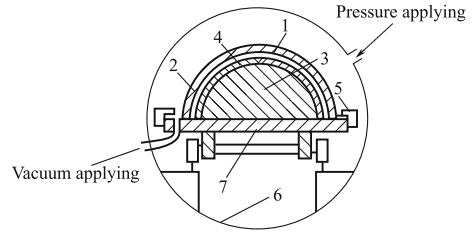
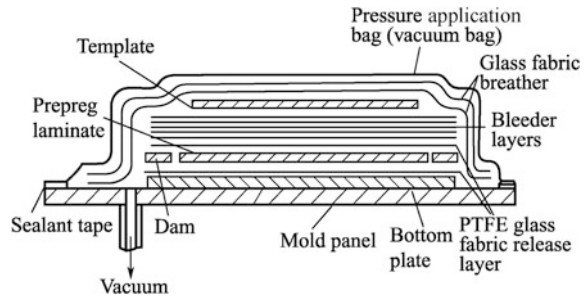


Fig. 1.27 Schematic showing prepreg/autoclave part making process assembly



An autoclave is a barrel-type metal pressure vessel to which a required temperature and pressure can be applied in its cavity. It is usually operated horizontally. The pressure needed for part curing is supplied by applying compressed air and is generally limited to 1.5–2.5 MPa. The desired cure temperatures come from heated air, steam, or heating elements installed in the molds. The parts are cured inside the autoclave under applied temperature and pressure. The autoclave configuration is shown in Fig. 1.26, and a schematic showing prepreg/autoclave part making process assembly is presented in Fig. 1.27.

(2) Technique features and major applications of prepreg/vacuum bag–autoclave processes

Autoclave processes are the techniques of choice for the manufacture of advanced composite structures, honeycomb sandwich structures, and metal/composite adhesive structures. The parts fabricated using this technique can be applied in the aerospace area as primary or secondary structures. The features of this process are summarized in Table 1.20. The applicable range of autoclave processes is summarized in Table 1.21.

(3) Operating procedures in autoclave processes

- 1) Composite part fabrication procedures: A flowchart showing composite part fabrication procedures is given in Fig. 1.28. Detailed information is listed in Table 1.22.
- 2) Adhering structure fabrication procedures are given in the chapter “Advanced composite adhering techniques”.

Table 1.20 Features of an autoclave process

No.	Features		Remarks
1	Advantages	Homogeneous pressure inside	Because of the pressure supplied by the input compressed air or inert gases (N ₂ , CO ₂) or the mixture of air and inert gases, the pressure applied vertically to a vacuum bag will have a uniform distribution so that the part inside the vacuum bag can be cured into an end shape under homogeneously applied pressure
2		Uniform air temperature inside	Because the autoclave's interior area is equipped with a high-power fan or wind-flow guide sleeves, the heated (cooled) air can circulate at high-speed. The inner temperature distribution can be consistent with the aid of a perfect mold construction. It is possible to guarantee a smaller temperature deviation inside the part (sealed on mold top) during heating or cooling. Generally, the wind-facing direction and the front section inside the autoclave will undergo a higher heating (or cooling) rate than the wind-backing direction and the rear section
3		Wide application range	Simple mold construction, high efficiency, applicable to large area and complex skins, wall panels and shell processing. Can process or adhere to different airplane parts. For large autoclaves, multiple-stack molds can be placed once, and different parts with complex structures or different sizes can be fabricated by curing or adhering. The temperature and pressure supplied in the autoclave process almost meets all the requirements for polymer-based composite processing. Can be used for low-temperature processing of polyester-based composites or high-temperature (300–400 °C) and high-pressure (>10 MPa) processing of PMR-15 or PEEK composites. Can also be used in knitting fabric/ RFI processes
4		Stability and consistency in processing	Since a homogeneous temperature and pressure exist inside the autoclave, the fabricated or adhered part quality is consistent and can be guaranteed. Generally, parts made in an autoclave process have a lower void content and a uniform resin content compared with other processes. Autoclaves create parts with consistent and reliable mechanical properties that meet the requirements of aerospace applications. To date, most composite structures requiring a high load-bearing ability are manufactured by autoclave techniques
5	Drawbacks	Big investment/high costs	Compared with other processes, the autoclave is a kind of pressure vessel and is a huge system with a complex construction. To build a set of autoclaves requires a large financial investment, and since each curing cycle needs a vacuum-sealant system, too many expensive accessory materials will be consumed. The energy consumption is also very high for each processing cycle

Table 1.21 The applicable range of autoclave processes

No.	Applicable ranges	Remarks	
1	Adaptable for many types of structures	Laminated structures	Composite panels, beams, frames, skins, wall panels, and co-curing integrated structures
		Sandwich structures	Metal honeycomb sandwich panels, composite honeycomb sandwiches, and other sandwiches
		Adhesive structures	Metals to metals, metals to composites, composites to composites
		Knitting structures	Knitting/RFI spar-stiffened wall panels
2	Suitable for different size parts	Airplanes	Small or large airplane structures or parts (autoclave should be large enough)
		Astronautics	Large barrel-type parts
3	Limitations	Not suitable for particular complex structures or cost-sensitive parts. Other options include RTM and other low-cost processing methods	

Fig. 1.28 Flowchart of composite part fabrication procedures

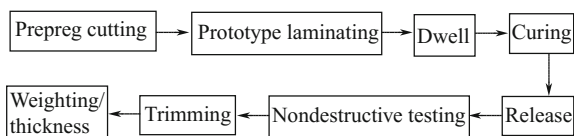


Fig. 1.29 Schematic showing unidirectional tape and fabrics splicing

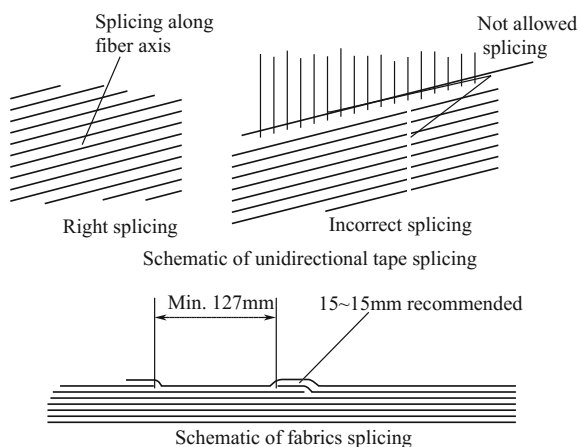


Fig. 1.30 Co-curing process (skin and angle strip co-curing)

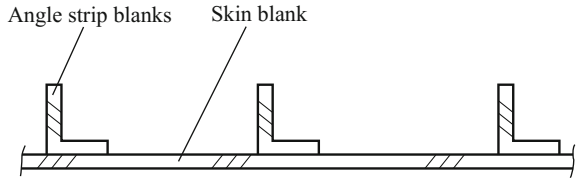


Fig. 1.31 Secondary adhering process (cured skin and angle strip adhered to integrated part)

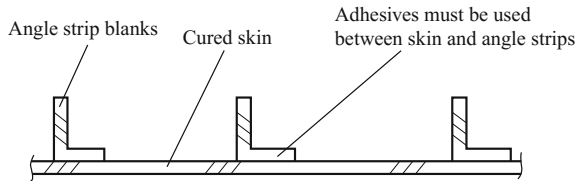
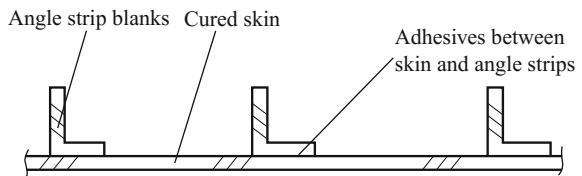


Fig. 1.32 Co-curing and adhering process (skin cured first, then angle strips attached by co-curing)



(4) Integrated techniques and basic requirements of autoclave processes

The integrated techniques and the basic requirements of autoclave processes are described in Table 1.23

(5) Choice of processing scheme in autoclave processes

The choice of processing scheme should follow the steps given in Fig. 1.33.

For large composite parts, the processing scheme should be chosen only after the processing acceptance tests and cabinet section tests. Reliable conclusions are required.

1.2.5 Prepreg/Press Molding Process

Based on the different resin matrixes and reinforcement resin impregnation in press molding compounds, prepreg/press molding processes can be divided into two principal types: Wet processes, in which resin matrixes together with reinforcements are placed into a mold cavity almost simultaneously, include manual layup and prototype press molding. Dry or half-dry processes, in which resins and reinforcements are fully mixed into press compounds before molding and the mixtures are then directly put into a mold cavity during processing.

Table 1.22 Composite part fabrication procedures

No.	Steps	Remarks
1	Prepreg cutting	<p>① Inspect prepregs by following the corresponding specifications; measure and record the resin content for later use in the resin-attracting system</p> <p>② Plies or interpolating plies expandable or near-expandable into planes can be cut using a template or by an automated cutting machine. Manual cutting or automatic cutting is the most popular methods. Manual cutting is more convenient and cheap but slower. It is only suitable for single part or low-volume production. Automatic cutting is faster and more accurate but needs a large investment. It is suitable for high-volume production</p> <p>③ Plies or interpolating plies that are impossible to expand or to near-expand into planes can be cut into prepreg strips with a desired width</p> <p>④ In manual layup, workers should wear gloves as bare hand handling of prepregs is not allowed. Care should be taken for fiber orientation during cutting as a direction deviation less than $\pm 1^\circ$ is required. The cut prepregs should be laid down flat, and folding should be strictly controlled</p> <p>⑤ The cut plies should be numbered and the prepreg batch number recorded</p>
2	Laminating	<p>① Skin-type parts expandable or near-expandable into planes can be laminated on platforms or on molds. Skin-type parts do not expand or near-expand into planes and should be laminated only on molds</p> <p>② Beams, ribs, frames, and spars are only laminated on molds</p> <p>③ Lamination should follow the template or the position line on the mold surface</p> <p>④ Each layer should be expanded and flattened using a rubber roller or a blade to remove entrapped bubbles in plies and, if necessary, an electric air blower or an electric iron can be used to assist lamination</p> <p>⑤ Ply splicing will often be encountered during lamination, and splicing should be along the fiber direction. A slight overlap on the splicing location may be necessary, and the overlap joint should be dislocated. Generally, in unidirectional prepreg splicing, only a 1 mm seam is allowed. In fabric prepreg lamination, only overlap rather than splicing is allowed and the overlapping width should be limited to 10–15 mm, as shown in Fig. 1.29</p> <p>⑥ The plies on a dent, corner, or curved surface should be flat and compact; attention should be given to a possible bridge in the dent area</p> <p>⑦ Lamination records should be kept including series number, stacking number, angles, prepreg type, and batch number</p>
3	Vacuum precompacting	For thick prototypes, the vacuum should be applied after each 10 layers of lamination, and the aim is to remove entrapped air and volatiles in the prepreg during lamination and to ensure part quality
	Dwell	<p>① The amount of resin to be used should be calculated based on the individual unit area of the prototype, and the correspond resin-attracting system should be set up</p> <p>② The resin-attracting system should be set up</p> <p>③ Resin-attracting specifications should be established for the different prepregs</p>
4	Assembly	The individual parts that are subjected to resin attraction are assembled on the mold and packed
5	Curing	Curing specifications are compiled based on the gel time test results and the partial temperature fields measured using the related prepreg standards

(continued)

Table 1.22 (continued)

No.	Steps	Remarks
6	Release	After curing, the parts are removed from the molds. Care should be taken to avoid part damage. The ease of part release will depend on mold design. Generally, for a perfect mold design, the cured parts should be released easily
7	Nondestructive testing	The cured parts should be subjected to ultrasonic C-scanning or soft X-ray inspection for quality according to the related specifications and design. Test reports should be compiled
8	Thick. measure	The part thickness should be measured ultrasonically, especially for critical parts
	Trim/grinding	Trim and grind along the part's outer edges Trimming methods include ① sand wheel blade cutting. This is convenient, practical, and easy to adjust. ② Ultrasonic cutting High cutting rates up to 3 m/s. If computerized control and a sharp knife used, a high cutting precision can be guaranteed. Total investment not too high. ③ High-pressure water cutting. Suitable for carbon fiber composites, especially aramid composite cutting, but in the case of thick panel cutting, a horn mouth is required. Delamination on cutting edges can occur if incorrect cutting parameters are used. ④ Laser cutting: Very expensive and limited to thin panel cutting. Currently, diamond-sand wheel blades, and high-pressure water are the most widely used cutting methods. Ultrasonic cutting can also be included as an option Grinding: In terms of composites, grinding should involve in-plane and edge grinding. In-plane grinding is a finishing for any resin lumps left on the part surface. Edge grinding is a finishing for edge burrs and gross cuttings
	Weighing	Generally, aerospace parts need weighing, and the precision is determined by part mass

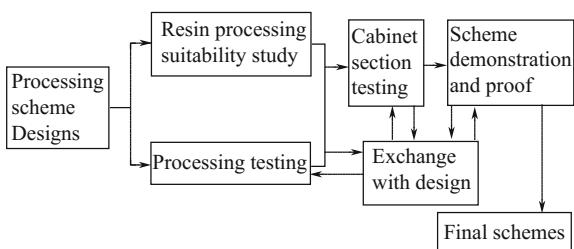
Based on different reinforcement patterns and different grades of molding compounds, press molding processes can be further divided into the following classes:

- 1) Lamination press molding: In this method, prepreg cloths or impregnated mats are cut into desired shapes and then laminated and placed in a pair of matched metal molds and cured into final parts under an applied temperature and pressure. This is suitable for making thin-walled parts with a simple construction and a small mold depth, and it is mostly used in shape simple thermal-resistant or corrosion-resistant product manufacturing. The advantage of this method is that the reinforcements do not move during processing.
- 2) Winding press molding: In this method, the resin pre-impregnated fibers or fabrics will be wound into mandrels and then placed in a pair of matched metal molds and cured into final parts under an applied temperature and pressure.

Table 1.23 Basic requirements for integrated techniques in autoclave processes

No.	Integrated tech.	Remarks	Basic requirements
1	Co-curing	All the components are co-cured into a final shape simultaneously. These include skins, vertical tail skins plus spar panels, the top and bottom wall panels for the front fuselage, and the middle fuselage, as shown in Fig. 1.30	Metals with a high linear expansion should not be used in integrated co-curing with composites at high temperature (180 °C)
2	Secondary adhering	Parts are made first and adhered onto integrated constructions such as the outer or inner lift ailerons and rudders, as shown in Fig. 1.31	
3	Co-curing/ adhering	Some parts are made first, and then, other parts are adhered or attached to them. For example, a skin is made first, and then, spars are attached by co-curing. The bottom skin is made first, and a Nomex honeycomb is attached. At the time of co-curing the top skin, a honeycomb sandwich structural cap or frame is produced, as shown in Fig. 1.32	

Fig. 1.33 Steps to choose an autoclave processing scheme



This is suitable for making parts with a particular requirement as well as pipes or rotary-section parts. As autoclave and hydraulic pot processes are widely applied in composite part production, this method is currently less used.

- 3) Directional placing molding: In this method, the unidirectional prepreg tape (fiber or nonwoven fabric) is placed along the part’s principal stress direction and a prototype is fabricated. It is then put into a mold and cured at a certain

temperature and pressure. This method can be used to make higher fiber content parts in which the fiber orientation and distribution can be designed according to loading direction. This is suitable for making parts where directional strength is important.

1.2.6 Filament Winding Process

The filament winding process has advanced remarkably and is being used in more applications and breakthrough technologies. This is reflected in the following three fields: equipment development, raw material development, and winding technique development [7–10].

(1) Development of winding equipment

The basis of filament winding equipment is the winding machine. Previously, mechanically driven or chain transmission winding machines were reserved, but now they are in service in some applications. However, with the widespread use of microcomputers, winding machines have been developed into the fourth generation. The number of mandrels used has increased from one to two, and even up to four. Compared with mechanical drive types, the computer-controlled machines can offer incomparable advantages such as a more scientific winding operation to optimize and combine processing parameters, rather than conventional processing test procedures wherein the desired parameters are finally determined by experiments and data analysis. In computerized machines, parameter determinations can be done directly with the aid of a computer. This will possibly allow all the factors that influence part quality to be included in parameter determination. The parameters can be optimized and combined by computer aided analysis and then input to computer control system to be implemented. This eliminates complicated testing, data gathering, and analysis and also expands wound part applications. Robotic operation winding machines are available and greatly reduce labor as they develop toward high-end automated, mechanized, and robotic machines.

(2) Development of raw materials

Reinforcements of glass fibers, carbon fibers, aramid, silicon-carbonized fibers, boron fibers, and ceramic fibers as well as various fiber hybrids have been developed to make wound structural parts with higher specific strength, specific modulus, low shrinkage, fatigue resistance, corrosion resistance, and low linear expansions. For resin matrixes, many modified resin systems are also available.

(3) Development of winding techniques

- 1) The development of thermosetting composite winding techniques: Thermosetting composite winding techniques include raw material selection, mandrel construction and manufacturing, winding machines and accessory

devices, fiber impregnation, winding processing, and curing techniques. The development of winding techniques includes the following aspects:

- ① **Wet/pre-impregnation processes:** These processing techniques were developed to combine the advantages of wet and dry winding processes. The winding procedures used in these techniques are almost the same as those used in wet processes. The only exception is that no resin bath is installed on the winding machines, and resin impregnation is eliminated. Fiber impregnation is completed in a separated impregnation production line before winding. From the impregnated yarns in the dry winding process, the resin statues remain unchanged throughout the whole impregnation and the resins will not have increased viscosity. No B-stage exists in the freezer. A comparison between dry, wet, and wet/pre-impregnation is given in Table 1.24.

Table 1.24 Comparison between the three winding processes

Items	Dry process	Wet process	Wet/ pre-impregnation process
Clean state in working site	Best	Worst	Equal to dry process
Reinforcement Specifications	More series, limiting to some specifications	Any specifications	Any specifications
Possible problems in using carbon fibers (CF)	No problems	Possible problems caused by fly CF hair	No problems
Resin content control	Best	Most difficult	Not best, some change in resin viscosity
Material storage	Must be in freezer and storage records required	No storage problems	Similar to dry process, nut shorter storage life
Fiber damage	Relay on impregnating devices, more possibilities	Least possibilities	Less possibilities
Product quality assurance	Good in some respects	Need series quality control procedures	Similar to dry process
Production costs	Highest	Lowest	Slightly higher than dry process
Possibility for room temperature curing	Impossible	Possible	Possible
Applications	Aerospace	Wide application	Similar to dry process

Table 1.25 Comparison between tape winding and filament winding

Mechanical performance (comparison values)	0° tensile		In-plane shear		Compression strength
	Strength	Modulus	Strength	Modulus	
Tape winding	100	100	100	100	100
Filament winding	83	93	72	97	82

- ② Prepreg tape winding process: This process meets the high structure-effect requirements of aerospace parts and was developed based on filament winding techniques. The principle of and the raw materials used in this process are a perfect combinations of wet/spiral winding and prepreg tape/plane winding processes. In this process, the raw materials used are prepreg tapes with backing papers, and spiral winding or circular winding is carried out to give parts made under very strictly controlled conditions to give specific geometric shapes and dimensions. It only suits a narrow range of applications. In the prepreg tape winding process, a unique tape guiding system and winding head are used to achieve a unidirectional tape that is perfectly wound on the mandrel surface and that satisfies processing requirements such as being fold-free, densely compacted, and with a uniform distribution. The tape width, thickness, fiber placement collimation (quasi-straight), and resin quantity can be controlled to a very precise level. As a result, tape winding-made parts apparently have a much better mechanical performances compared with those made by filament winding. A comparison between them is given in Table 1.25.
- ③ Improvement in plane winding systems: In conventional plane winding, there are only two moving mechanisms. One is the fiber feeding mouth circular rotation movement around the mandrel (y -axis), and the other is a mandrel self-turning (x -axis). For each round of fiber feeding mouth rotation, the mandrel will self-turn across the tape width, and this is problematic. The problem is that after each tape layer is placed on the layer sides or on the areas between the layer sides and layer central part, different compacting statuses appear between the tapes and the mandrel surface. This results in composite performance problems. This problem can be mitigated by reducing the tape width or using multiple yarn bundles. However, this measure can cause non-uniform tension between fibers. In the “narrow layer and wide tape winding” technique, a device that moves back and forth periodically along its rotation axis is attached to the fiber feed mouth diving mechanics, and the non-uniform tension problem is thus resolved.
- ④ Particular plane winding process: To overcome difficulties in winding some conic parts with a consistent wall thickness requirement such as a missile head’s cone cap or a fighter’s radar dome, a unique plane winding technique has emerged. The filament wound composite radar dome is used in the US Bowmark missiles.
- ⑤ Curing technique studies: Curing techniques greatly influence the curing degree, the resin flow, and void formation in composite parts as well as

mechanical, physical, and electric properties. The study into curing techniques involves the following aspects: innovative curing techniques, in situ curing monitoring, optimistic curing settlement studies and experimental certification, curing progression and the effect of curing degree on composite performance, and curing degree characterization as well as related test procedures.

- 2) Fiber placement techniques: This technique is based on filament winding, robotics, and tape placement techniques. In fiber placement techniques, there are common points that are shared with tape placement winding. On the other hand, apparent differences also exist between these two techniques. In fiber placement processes, multiple impregnated fiber bundles are combined into quasi-straight tape sheets and placed on mandrels or mold surfaces. The general procedures used in the fiber placement technique are basically the same as those in filament winding or tape placement. The difference is that the part shape is not limited in the rotation patterns when compared with tape placement. The curvature in part shape can be varied over a larger range and is even suitable for dent surface part production.

Fiber placement techniques can be divided into one-step or two-step methods. For a two-step method, the fibers are carried out after winding and are post-processed into final composite structures. For example, in the manufacture of an I-section beam, a cylindrical prototype is wound and is then press-molded into sectional goods.

3) Breakthroughs in winding technologies

- ① Filament winding compartment: Considering production costs and operating expenses, the production of compartments by conventional materials such as steels and aluminum alloys has not been feasible. Composites have become the option of choice in material selection, while filament winding is the best processing technique. Compartment shells need to be considered to be large square-section pipes based on which winding processing schemes should be worked out. The specialized design and manufacture of winding machines have limits of 3.8 m maximum winding diameter, 25 m machine total length, and 15 m effective winding length. Procedures for compartment body manufacture range from inner surface to outer surface. A form layer is inserted between these surfaces to give a sandwich construction. Both inner and outer surfaces are fiber wound layers. To increase the compartment's structural stability, sound-proofing, and thermal isolation performances, it is also possible to use a two-layer form and three-layer winding surfaces to create a double-layer sandwich construction. Wire tubes and vent pipes are directly installed in compartment walls. The doors and windows are cut and produced at predetermined locations.
- ② The development of composite driving shafts by filament winding: Composite driving shafts were initially aimed at cars, but recently, their main applications include power station cooling towers, trucks, helicopters, marine ships,

submarines, and special lathes. According to news reports, hundreds of cooling tower driving shafts are in service and they are of 200–300 mm in diameter and 7–9 m in length. The annual increase is 20–25%.

- ③ Equipment rollers: Recently, composite processing equipment rollers are being more widely used in chemical industries, plastic film production, the paper industry, and the publication industry. The advantages are their versatility and durability without the need for frequent maintenance and replacement as for steel rollers.

Similar to filament winding, in the aviation industry, the production of plane back fuselages has been extensively investigated by winding processes. A square-section structure with network spars has been built but not been put into service.

Filament winding composites have immense potential in infrastructural applications including bridges, piers, highways, water margin structures, aeronautical exhibition halls, contaminated water treatment systems, and transportation facilities and their accessories. Studies and applications of composite technologies have focused on these fields recently. The combinations of composite features and winding technique advantages have attracted an increasing amount of attention, and achievements have been forthcoming.

1.2.7 Pultrusion Process

Pultrusion is a low-cost and high-quality processing technique that can be used to make composite parts with a desired fiber bundle orientation. It is most suitable for medium volume or higher commercial or military production. Early pultrusion products mainly consisted of various bars, rods, and angle shapes. As pultrusion techniques improved, they have been used to produce a wide range of products in the aviation, transport, sport, and medical fields. The raw materials used include S-glass, carbon and aramid fiber reinforcements as well as epoxies and thermoplastic resins.

- (1) The basic concepts and technical features in pultrusion processes

The basic concept of a pultrusion process is that fibers or fabrics are continuously guided and pulled through a resin bath for impregnation. A preprocessing die and a processing die are heated and cured into composite parts with fiber orientation and high-strength characteristics, as shown in Fig. 1.34. The entire pultrusion process is an ordered and continuous combination of each individual process. The first step is to form fiber bundles into properly oriented prepultrusion strips, and the second step is strip resin impregnation (sometimes, these two steps can be simultaneously carried out, preprocessing while impregnating). The third step is to lead the prepultrusion strips to pass the preprocessing die and the processing die (thermal setting die) completing the shape setting and then curing into final parts.

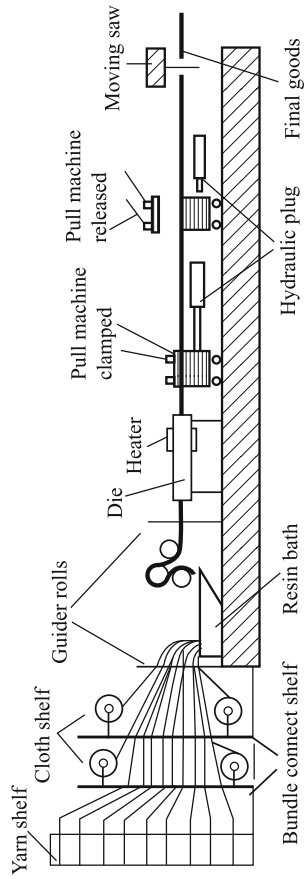


Fig. 1.34 Diagram showing the basic concept of the pultrusion process

The technical features in the pultrusion process are as the follows.

- 1) Continuous fibers or fabrics upon in situ resin impregnation.
- 2) The impregnated fibers or fabrics pass through the processing die and complete shape setting and curing follows.
- 3) The resins used should be low shrinkage and volatile-free and undergo rapid curing to guarantee part dimensions and consistency, a desired linear pulling speed, and the elimination of defects such as voids and bubbles during pultrusion.
- 4) Pultrusion linear speeds depend on resin curing characterization and geometric sectional shapes and sizes of the parts to be made.

Generally, processing dies are 0.5–2.0 m in length and have a double function of processing and curing. If the pultrusion of fiber bundles needs 3 min to pass through the die for part curing, the processing linear speeds should be 0.167–0.67 m/min.

The processing linear speeds are directly related to production rate, and an increase in linear speeds will depend on an increase in resin curing speed and in turn a decrease in the die passing time. To date, the pultrusion speeds have reached 4 m/min and have even been as high as 6 m/min. This allows a very short resin curing time.

The features of pultrusion processes are as follows:

- 1) Simple processing procedures, high efficiency, suitable for medium-volume production for high-performance fibers, and a high-volume content in composite parts.
 - 2) Pultrusion can fully extend and straighten the fibers in parts, and fiber reinforcement can mostly be carried out. End products have excellent unidirectional mechanical performance.
 - ③ Highly automated processing, less processing steps, consistent quality, and low deviations.
 - 4) High raw material usage and low waste.
 - 5) Difficult to use in non-straight or varied-section goods production and impossible to use with non-continuous fibers.
- (2) Advances in pultrusion processes

To extend their production applications, pultrusion processes have undergone constant improvement and innovation. The main technical advances are summarized below:

- 1) Combined with in situ textile, winding, and braiding equipment to achieve complex fiber preform for continuous fabrication and deliberate processing. Enables transverse or non-axis reinforcement by the addition of cloths, mats, or fabrics and can also meet particular performance requirements of hybrid fibers.

- 2) Improved and optimized resin temperature– pressure curves, radiation, or induction heating used.
- 3) Combined with RTM processes, conventional resin impregnation is eliminated and innovative resins can be directly injected by pultrusion techniques. Braided fiber preforms are directly led into pultrusion processing dies, while resin systems are pumped and injected directly into fiber preforms, heated, and cured into final pultrusion products. In this process, the resins can be mixed in situ and can also be heated under inert gas, which reduces the resin injection viscosity and increases impregnation effects. Because of the elimination of an open resin bath, resin pollution is reduced and the release of volatile substances is efficiently reduced, which is good for health and is an improvement in the operating environment.
- 4) Together with the press molding process, varied-section goods is possible in continuous production mode. Pultrusion preforms can be used for in situ deforming and processing, and the pultrusion dies only need to complete continuous processing on the resin-impregnated preforms (resins in B-stage). They can then undergo further press molding. The perfect combination of these two procedures can give varied-section parts in continuous pultrusion production; that is, the B-stage resin-impregnated preforms are guided and pulled between the two plates in a press. The press becomes a processing mold and a pulling clamp causing the preform to undergo reforming. Part curing is completed simultaneously, and the press will guide and pull the next pultrusion preform to give continuous pultrusion and press molding products.

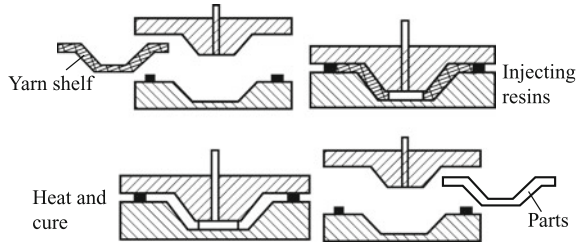
1.2.8 Liquid Composite Molding (LCM) Processes

Liquid composite molding (LCM) processes are a class of composite processing techniques and typically consist of RTM (resin transfer molding), RFI (resin film infusion), and SRTM (structural reaction injection molding). In these techniques, the reinforcement preforms with designed performance and structural requirements are firstly placed in a mold cavity. Specially prepared resin systems are then injected into the closed mold cavity by a pump, or the resin films previously placed in the mold cavity are heated and melted. The resins will flow into the cavity, and air is removed upon which the fibers are impregnated. The parts in the molds are then heated and cured, cooled, and released to give an end part. Figure 1.35 shows the principles of LCM processes.

LCM consists of the following steps.

- 1) Preform placement;
- 2) Closing molds;
- 3) Injecting resin;

Fig. 1.35 Principles of the LCM processes



- 4) Resin curing;
- 5) Part release.

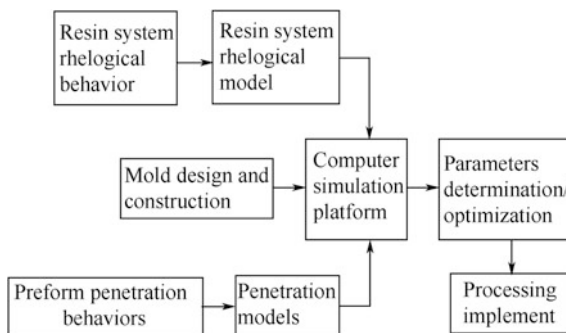
Each step depends on the mold shape, the fiber preform construction, and the mold design, and both mold shapes and preform construction depend on product design. The successful mold design should be based on a simulation of the entire LCM process.

LCM processes are one-step processing techniques with advantages compared with other traditional processes. Either can produce large and integrated composite structures or a variety of precise small composite parts. Either can shorten the part making cycle or guarantee part quality. LCM products have many advantages including highly reliable strength and performance, simplified processing, high production rate, superior quality of surface finishing, and environmental friendliness.

Because of the unique advantages of LCM processes, some technical difficulties arise; in LCM mold filling, the resins have to be fully injected into the mold cavity and adequately impregnate fiber preforms, and defects such as bubbles and dry spots should be minimized because defects can result in stress concentrations and influence part performance and service life. In LCM processes, all the procedures are carried out in a closed mold cavity and many parameters such as preform impregnation and resin chemical rheological characteristics, injection pressure, injection port, and drain port settings will affect resin flow and impregnation. In addition, LCM is often used for complex geometric shape part making resulting in poor control and predictable possibilities in resin/fiber flow and impregnation. Process design requires multiple experiments and tests to determine whether an optimized LCM process requires a higher input, limiting its applications.

Recently, since the requirements for LCM parts in aerospace, automobile, machine manufacturing, marine engineering, and infrastructure applications have continuously increased, a further reduction in LCM costs has become urgent. Computer simulations of LCM processing are an effective approach for this problem. By computer simulations and analogs, all the necessary data for LCM processing can be generated at a low calculation cost and in a shorter time, which plays a very important role in proper mold design and processing parameter optimization. The main goals of processing simulations should be a reduction in production costs and a shortening of product development cycles.

Fig. 1.36 Flowchart showing computer simulations in LCM processes



Computer simulations and analogous techniques for LCM processing are shown in Fig. 1.36. This figure shows how resin flow characteristics can be qualitatively predicted. If the correct and reliable parameter data are used as the input, the injection pressure, resin flow rate, and behavior can be perfectly predicted. The important issues in analog analysis and numerical modeling will be the generation and input of critical parameters such as penetration rate, resin rheological behavior, thermal diffusion, and boundary flow abilities. All these parameters are closely related to resin systems, reinforcing materials, molds, and processing techniques.

To generate the correct parameters for use in computer simulations, it is necessary to develop a good understanding of the physical and chemical changes that occur in resin systems during mold-filling procedures and to create theoretical numerical models.

1.2.8.1 RTM Process

(1) RTM principles and operating procedures

RTM is the abbreviation for resin transfer molding. The operating procedures include the following: First, the fiber preforms with designed performance and construction are placed into a mold cavity. Then, with the aid of vacuum or pump injection pressure, special resins are injected into the closed mold cavity until the preforms are fully impregnated in the cavity. The preforms are then finally cured and released. Figures 1.37 and 1.38 show the RTM process principle and the operation flowchart.

The important points to be considered in RTM are as follows:

- ① Before injecting into molds, RTM special resins should undergo bubble removal treatment.
- ② After placing into molds, the clearance between preform edges and the mold border should be limited.
- ③ Molds to be closed and airtight.

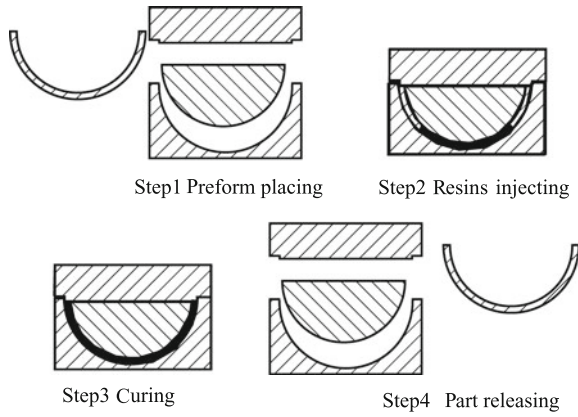


Fig. 1.37 Principles of the RTM processes

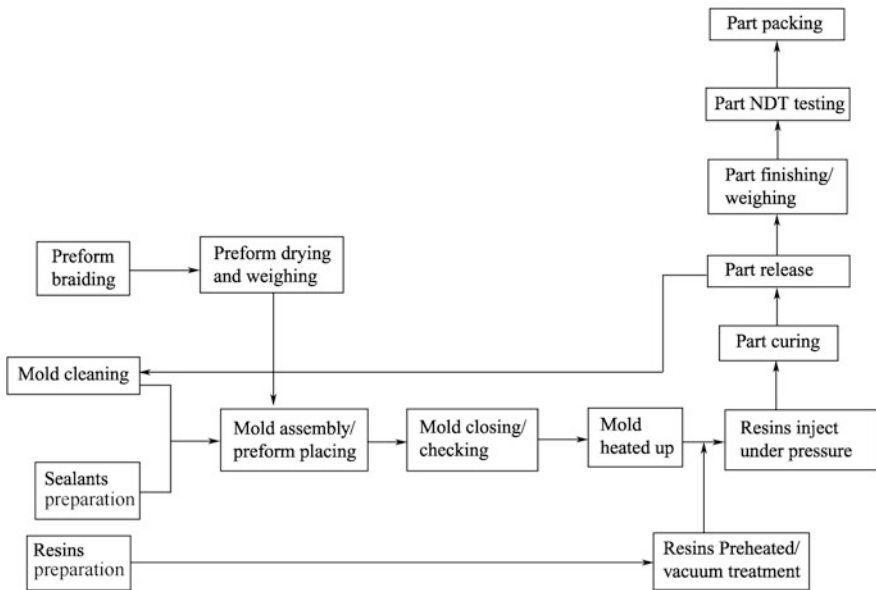


Fig. 1.38 Flowchart of RTM processes

- ④ Precise control of mold temperature and resin injection time.
- ⑤ Proper injection pressure selection.
- (2) RTM mold design.

For high-performance aerospace composite structures, the first priority in RTM mold material selection should be metals such as steel, aluminum and alloys, and fiber-reinforced composites with good comprehensive performance.

RTM mold design should include the following:

- ① Design of injection inlets and air exhaust outlets;
 - ② Design of mold clamps and be airtight;
 - ③ Design of mold strengthening schemes;
 - ④ Design of mold release mechanism;
 - ⑤ Design of various inserts and embodiments.
- 1) Design of injection inlets and air exhaust outlets: The proper selection of inlet and outlet positions has become an important matter in RTM mold design because it relates to the successful implementation of RTM processing and also the end RTM part quality. For RTM molds, the design of mold inlets and outlets should follow the principles given below: The perfect design of mold inlets and outlets should allow resins to distribute quickly and homogeneously in each layer of preform and to fully impregnate the fibers.

By accepting the above-mentioned principles, the mold inlets are usually arranged near the geometric shape core under the molds, while the outlets should be at the end of the mold's top surface or the dead points in the resin's flow. However, when carrying out a practical RTM mold design, much attention should be given to part particulars or features to optimize the number and locations of inlets and outlets. Figures 1.39, 1.40, and 1.41 show some options for typical injections.

- 2) Sealing of molds: The aim of mold sealing is to avoid resin leaks and air diffusion into molds. Many options for mold sealing are given in Fig. 1.42.

The selection of mold sealing strips should be determined by the individual RTM mold surface patterns. For flat and smooth surfaces, the strips with smaller diameters or cross sections should be used; for a poor surface, strips with a larger diameter or cross sections should be considered.

- 3) Clamps for molds: The particulars of RTM processes will dictate whether RTM molds need to be assembled or disassembled repeatedly in processing operations. Therefore, in RTM mold design, if mold sealing can be ensured, it

Fig. 1.39 Cup-pattern part injection

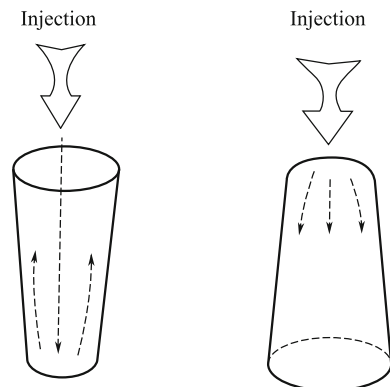


Fig. 1.40 Part injection with a form core

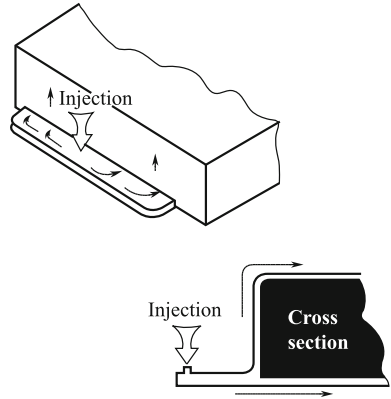


Fig. 1.41 Tube-type part injection

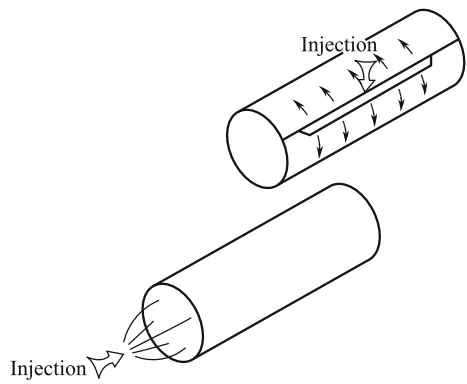


Fig. 1.42 Mold sealing schematics

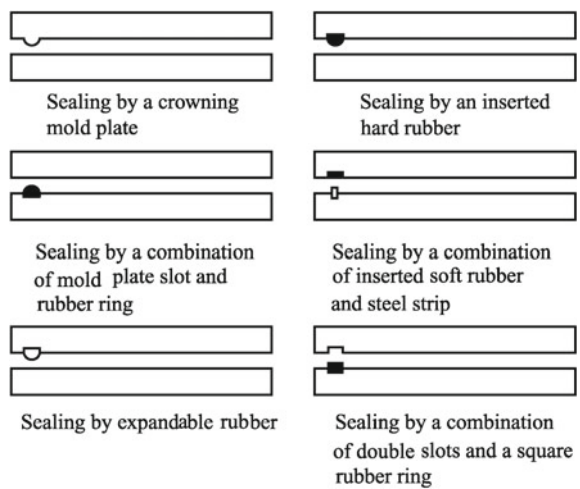
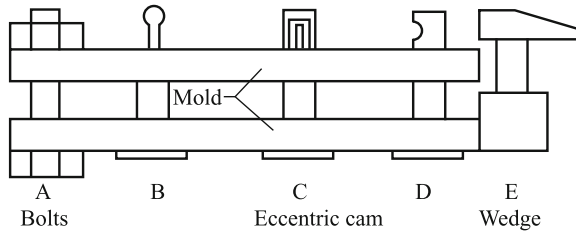


Fig. 1.43 Mold locking and clamping tools



is necessary to consider the convenience and ease of mold clamping and disassembly.

In Fig. 1.43, a number of RTM mold clamping methods are shown. Considering the clamping effectiveness and costs, high-strength bolts and nuts are recommended for RTM mold clamping. The bolt dimensions and numbers depend on the mold locking pressure and the mold inner pressure generated during resin injection. The mold locking pressures depend on the preform states, the fiber volume content, and the mold stiffness, while the mold inner pressure is related to resin viscosity and the injection pressure.

- 4) Mold strengthening: The injection pressure usually ranges from 0.1–0.6 MPa. When designing molds for smaller RTM parts, it is not necessary to consider the effects of mold stiffness on part dimensional accuracy, while for large RTM parts, the mold stiffness should be taken into account.

Inadequate mold stiffness can result in the following problems: The molds show a “balloon” phenomenon under injection pressure resulting in overtolerance and rejected parts; the other is mold surface cracking after repeated use resulting in abandoned parts. To guarantee part accuracy and extend the mold service life, mold strengthening should be taken into account in RTM mold design. Currently, RTM mold strengthening will be mostly achieved by square-section steel strips, steel shapes, or steel plate welding, as shown in Fig. 1.44.

- 5) Mold release: Mold release is the vital step in RTM processes. Generally, the release of small parts with a simple structure can be carried out by applying releasing agents to the mold surface; however, for large and complex parts, the release must be conducted with special release apparatus.

Fig. 1.44 Mold strengthening

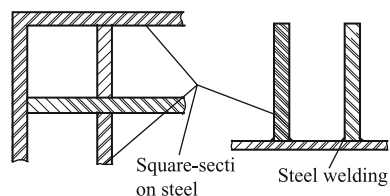
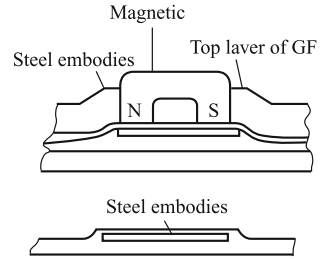


Fig. 1.45 Metal embodiments buried inside parts



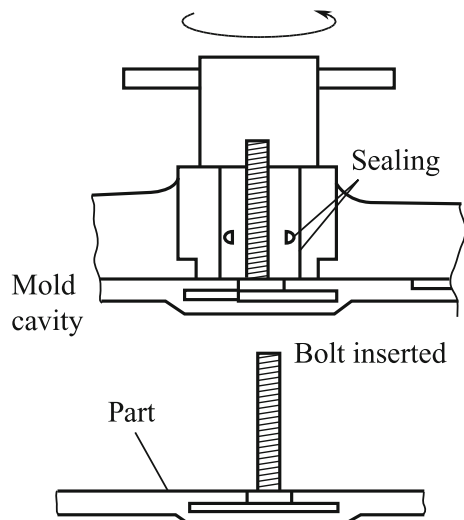
Built-in release agents do not have good release effectiveness in epoxy resin RTM molds. Separate release agents should be applied to the mold surfaces. When using outer release agents, it is necessary to use solvents or special detergents to clean and remove all the residual release agents or dirt left on the mold surfaces. Release agents are applied according to usage instructions.

- 6) Design of inserts and embodiments: To process RTM parts with particular insert constructions, some metal inserts or embodiments should be attached to the mold within the mold design. In Figs. 1.45 and 1.46, some commonly used metal inserts are presented.
- (3) RTM processing techniques

Injection temperature, pressure, and speed are three important parameters in RTM processes as follows:

- 1) Injection temperature: Injection temperature refers to the resin injection temperature during RTM processing. At this temperature, resins not only have lower viscosity but also a long enough operating period. The selection of

Fig. 1.46 Bolts inserted into parts



injection temperature is usually based on dynamic viscosity curves or isothermal viscosity curves for the resins to be injected. Generally, the resin injection temperature should be near the temperature of which resins have the lowest viscosity.

The incorrect selection of injection temperature will result in the two problems below.

- ① A too low injection temperature will result in an increase in resin viscosity resulting in insufficient impregnation of fiber inside preforms and also local dry spots or resin-starved areas.
 - ② A too high injection temperature can shorten the resin operating life and influence RTM processing although a higher injection temperature can improve the resin impregnation of fibers within preforms and this helps to remove entrapped air bubbles.
- 2) Injection pressure: Injection pressure refers to the applied pressure for resin injection. The selection of injection pressure should consider factors such as resin viscosity, mold stiffness, and part construction.

The incorrect selection of injection pressure can result in following problems:

- ① A too low injection pressure will result in the reduction of resin flow in fiber preforms, this affects operation rate, and it also causes inadequate fiber impregnation in large and complex preforms. Therefore, dry spots or resin-starved defects occur in parts.
 - ② A too high injection pressure increases mold deformation and influences part dimensional stability. It also causes the fibers in preforms to distort, especially the fibers near the injection inlets. A high pressure can increase resin flow ability in preforms and enhance the processing rate. For ordinary RTM parts, the injection pressure is usually 0.1–0.3 MPa.
- 3) Injection rates: The injection rate refers to the quantity of resin injected into the mold cavity per minute. The injection rate correlates to the preform penetration rate, the resin viscosity, mold stiffness, part dimensions, and fiber volume content.

Injection machines can be divided into two types: One is an air pressure injection machine, and the other is a metering pump injection machine. Both can be used for single-compound, double-compound, or triple-compound resin injection.

(4) Derived RTM techniques

After decades of development, modern RTM processes are being used in a number of innovative derivations of traditional RTM processes.

- 1) RTM for hollow construction processing: RTM processes are especially suitable for hollow composite structure fabrication, and processing depends on

the shapes and sizes of cores (or core models) to be used. The following are the most common cores in RTM processes.

- ① **Metal alloy cores:** In general, metal cores are preformed in separated molds and have advantages of good dimensional stability without deformation. However, metal cores require high temperature to remove core materials from the end parts (based on the metal alloy's melting point, core materials are recyclable).
- ② **Wax cores:** Compared with metal alloy cores, wax cores can provide a certain stiffness and separate molds are required for preforming. Wax cores are much cheaper than metal alloy cores, and they can be removed at lower temperature. Since wax cores have a lower stiffness than metals, care should be taken to avoid core damage in assembly (wax cores are also recyclable).
- ③ **“Washable” cores:** “Washable” cores are basically made using plaster and salts and have a desired stiffness. However, they can be washed away by pressurized water.

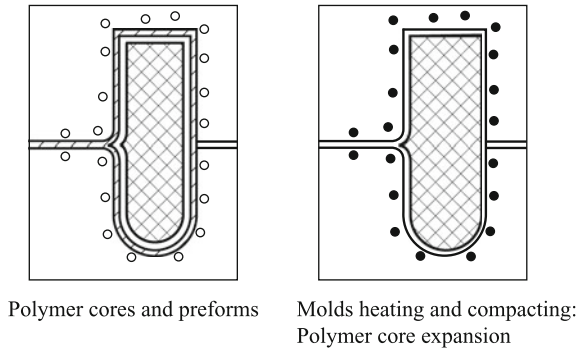
The drawbacks of the above-mentioned cores are that the preforms (including cores and reinforcements) can possibly be squeezed by the top and bottom molds during mold closure. This problem can be addressed by selecting a core that is slightly smaller than its real size.

- ④ **Expandable cores:** When special polymer cores (like thermoplastic resin) are used, negative dimension deviations should be used. In heated molds, the difference in linear expansion between mold materials and core materials can be used to guarantee that all preforms are easily placed into molds and good compaction is provided by core expansion during heat application. In Table 1.26, several polymer core materials with their linear expansion coefficients are listed. Figure 1.47 shows a schematic of thermoplastic core-aid hollow composite part processing.
- ⑤ **Filling and removable cores films:** Another option for hollow structure formation is to use films as removable core materials. These films contain free-flowing particles (sands or dusts) when used as inner fillings. Before use, the removable films are formed in separated molds and are prepared using special open holes with free-flowing particles like dust. They are then filled, and the extra air between the particles is removed by vacuum and seal holes. Because of the existing inner vacuum, the cores have a certain stiffness and can retain their desired shapes. One of the advantages of these cores is that the squeezing of reinforcements can be avoided during mold closure. After this kind of core is placed into the molding molds, core expansion can be

Table 1.26 Several core materials and their linear expansion coefficients (LECs)

Materials	LEC
Nylon	8.8×10^{-5} 1/K
Aluminum	2.35×10^{-5} 1/K
Iron	1.2×10^{-5} 1/K

Fig. 1.47 Schematic showing thermoplastic core-aid hollow composite part processing



generated by injecting water and giving inner pressure to the molds. This is the “smart core” technique developed by Plastech TT in the UK. The main drawback is the complex performance of the cores.

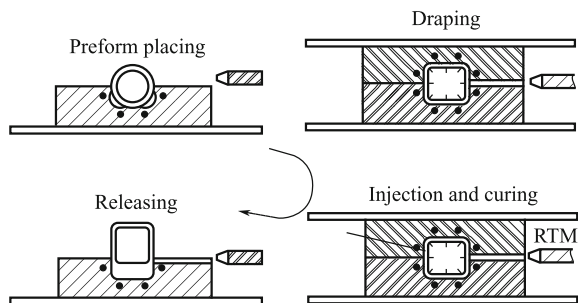
- ⑥ Air-chargeable expanding (bladder) cores: To overcome the drawbacks of the above-mentioned cores, an air-chargeable expanding core is widely used. This air-chargeable expanding core also referred to as the bladder is combined with RTM in RTM/bladder processes. Figure 1.48 shows a flowchart of the RTM/bladder process.

In the RTM/bladder process, dried fabrics, fiber mats, or braided tubes can be preprocessed on the expandable bladder and subsequently placed in heated molds. The molds are closed, the bladder is sealed, and pressure is applied to expand the bladder. The inner pressure produced in the bladder causes the dried fabrics to tightly contact the mold cavity surface. RTM is then used to inject resins and impregnate fibers, and the part is finally cured and released. Figure 1.49 shows a diagram showing the attachment of an expandable polyamide film to a preform placed in a square mold cavity.

The critical processing parameters in the RTM/bladder process is as follows:

- a) Resin injection temperature;
- b) Mold temperature;
- c) Injection pressure and relative volume flow rate;

Fig. 1.48 Use of RTM/bladder to make hollow composite parts



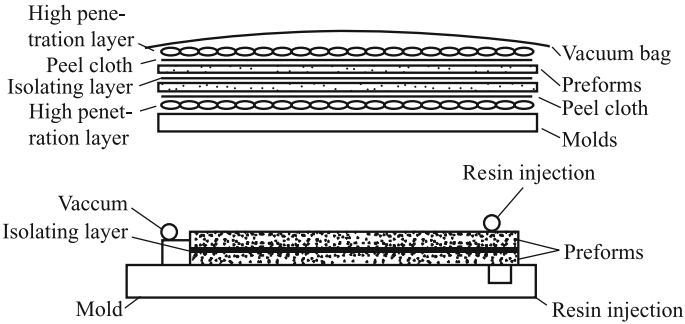


Fig. 1.49 Diagram of vacuum-aid co-injection processing

- d) The inner pressure of the bladder during injection;
- e) The inner pressure after injection and during the curing process.

Among all the above parameters, bladder pressure is the most important because it can affect the interlaminar and surface quality of the laminates, as well as the fiber volume content in the final parts.

The bladder's inner pressure should normally be $p_{\text{bladder}} - p_{\text{injection}} > 0.1\text{--}0.2$ MPa.

- 2) TERTM processes: TERTM (Thermal Expansion RTM) is a unique RTM process. In this process, polyurethane, PVC, and PU forms are used as core materials in preform prototypes. The resins simultaneously penetrate the core materials and preforms during injection. The core materials undergo expansion under applied temperature and further adhere to the fiber reinforcements. Presently, TERTM is used to make cabinet doors in small airplanes, for example, the cabinet doors in Cessna 206 airplanes.

The advantages of the TERTM process are a higher part strength, reduced weight, and production costs, and it is a good replacement for aluminum alloys.

- 3) Co-injection RTM processes: Although vacuum-aided RTM (VARTM) has become the most popular economic technique for the production of large composite parts, it mostly suits mono-resin systems. Multiple-layer composite requirements are becoming more stringent. These structures have different materials in each layer; for example, integrated armor multiple structures can simultaneously provide multiple functions such as structural, bulletproofing, flaming retardation, and wave absorption. Innovative processing techniques are also continuously being developed, and one of these is co-injection RTM. In co-injection RTM, a single process can deliver multiple functional composites so that production costs are reduced and secondary adhering or secondary co-curing is eliminated. The principle of co-injection RTM is shown in Fig. 1.49.

The function of an isolation layer is shown in this figure, and it is to isolate different resins. The selection of isolation materials should take the following factors into account:

- ① Lower penetration rate materials are selected as isolating layers. In this method, the isolating layers should have a large difference in penetration rate compared with fiber preforms.
 - ② The same materials as the preform should be selected. The pre-impregnation resin can serve as an isolating material. In this method, the two types of resin should have equivalent viscosities; the selection of this kind of isolating material is very helpful for perfect bonding between layers.
 - ③ Films should be selected as isolating materials. A film can fully separate two different resins before curing, and resins can penetrate films and increase interlaminar toughness.
- 4) AdvRTM™ processes: The AdvRTM™ process was developed by Dow-UT, and it involves colloidal chemistry, a braiding technique, preform automated placement, and mold design.

In Figs. 1.50 and 1.51, a flowchart of AdvRTM™ processes and the use of AdvRTM™ to make commercial plane engine blades are shown, respectively.

- 5) Flexible RTM (FRTM) processes: In flexible RTM process, the preforms are placed between two rubber membranes and the resins are injected to impregnate the preforms, and then, the entire membrane and the contained part are put into molds for curing. Since reinforcement lamination and impregnation are carried out in a flat manner, the lamination time and labor are substantially reduced. Additionally, the inlet and outlet configurations are simplified, which

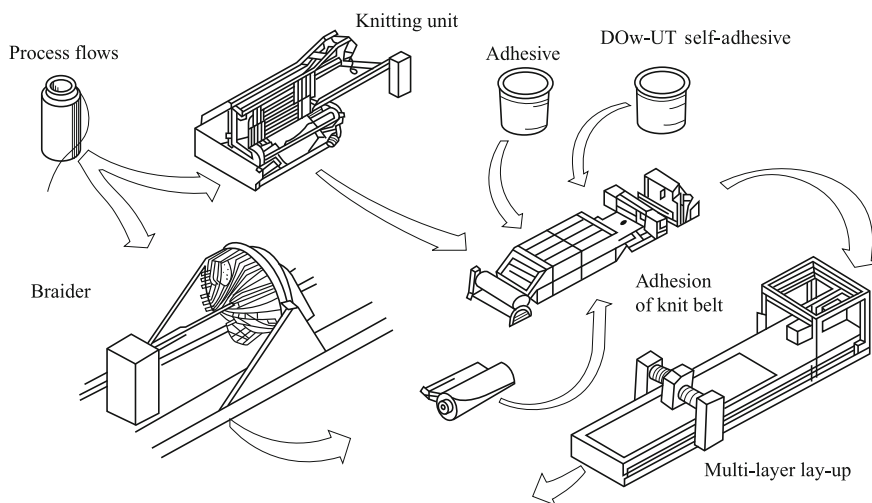


Fig. 1.50 Flowchart of AdvRTM™ processes

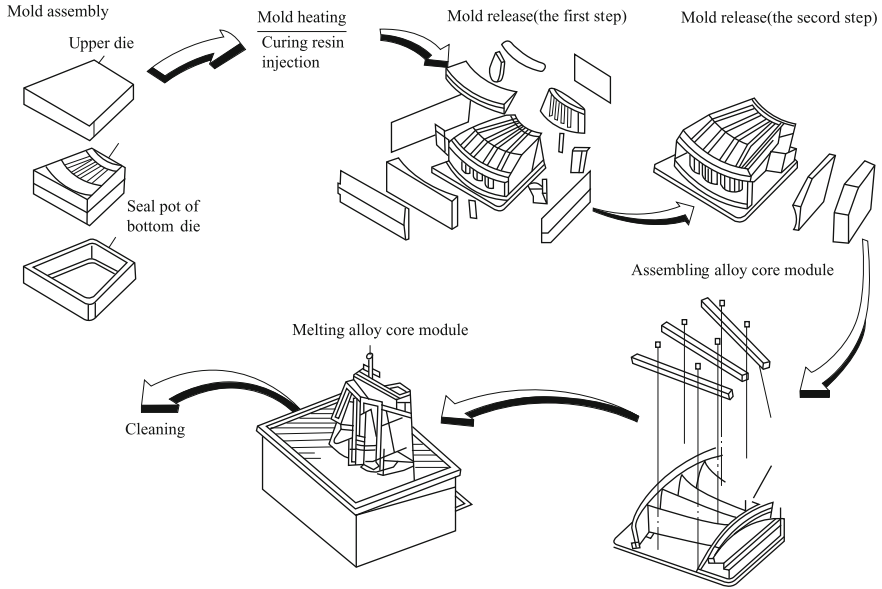


Fig. 1.51 Flowchart of engine blade formation

stabilizes processing quality. Part surface finishing depends on the rubber membrane’s surface finishing, which is independent of the mold surface so the mold cost is greatly reduced.

1.2.8.2 RFI Process

(1) RFI process principle

The RFI process is a composite LCM technique. The principle is that resins fully penetrate the fiber preforms with the aid of an applied vacuum or pressure and all the air trapped in the resins and the mold cavities are removed. The fibers are completely impregnated. Figure 1.52 shows a schematic of RFI processing assembly, and Fig. 1.53 shows a flowchart of RFI processes.

A substantial difference between RFI and traditional composite processing techniques can be described as follows: In RFI processes, resin/fiber impregnation is completed by low-viscosity resin penetration into the preform and the removal of trapped air in the preform and in the resin.

The RFI process involves the following theoretical fundamentals:

- 1) Resin flow and impregnation mechanism.
- 2) Fiber preform technique, penetration mechanism, and models.
- 3) Low-viscosity resins and their rheological characterization.

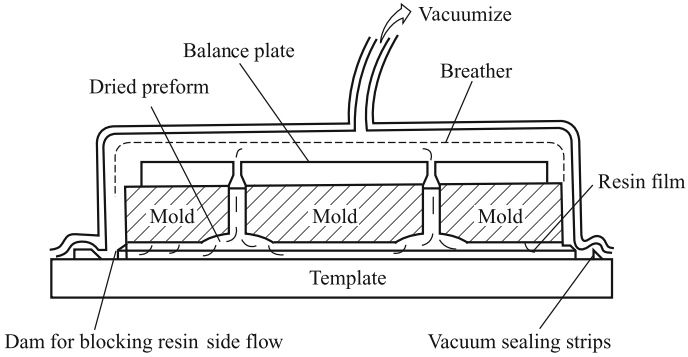


Fig. 1.52 RFI processing assembly

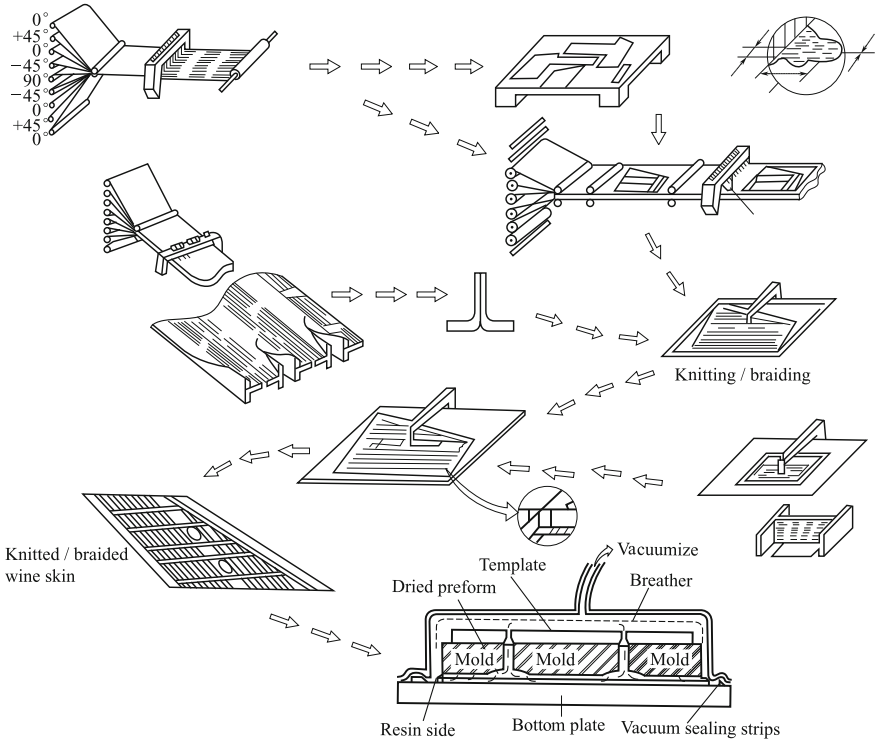
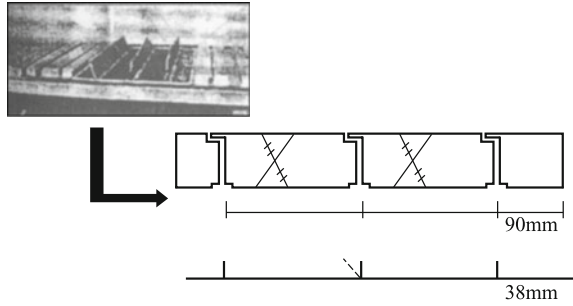


Fig. 1.53 Knitting braiding/RFI processing flowchart

(2) RFI mold design

Mold design and manufacture play very critical roles in RFI processing. Apart from the necessary consideration of mold structural stiffness, thermal capacity,

Fig. 1.54 Mold with a spar-attached construction



linear expansion, weight, and release requirements, the most important factor is to guarantee resin penetration into the preform from the bottom to the top under vacuum or under applied pressure. The full resin/fiber impregnation should then be completed. Figure 1.54 shows commonly used RFI molds with a spar-attached construction.

1.2.8.3 VAFI Processes

Vacuum-assisted resin infusion (VAFI) is an innovative low-cost processing technique for making large composite parts. In this process, the air trapped in fiber preforms is removed under an applied vacuum and this is followed by resin flow, penetration, and completion of preform impregnation. The preform is then cured into a final part with a desired resin/fiber ratio. This process should reduce composite costs to a large extent.

(1) VAFI process principle

There are some similarities between VAFI and RTM, for example, the use of fiber preforms and honeycomb sandwich structures. On the other hand, VAFI has some differences compared with RTM. VAFI does not require closed and pressure sustainable molds or processing pressure. For the production of composite parts, VAFI only needs a single face mold without any leakage under vacuum. The most commonly used molds in conventional composite processes are made by metal casting or machining, while in VAFI processes only a single face mold and a simple vacuum bag are required. This will allow the easy and moderate use of panels and core materials to fabricate large area (186 m²) sandwich structures. Even high-performance parts with 3D constructions and weights up to 1500 kg can be produced. The molds in VAFI processes do not have too many requirements except for a desired rigidity for fiber preform placement and the ability to guarantee a part's contour. This simplifies mold making procedures and reduces costs. A flexible vacuum bag film is the main accessory material that will be put onto the composite part surface in pressure applications, and this makes VAFI easier than RTM and reduces the costs significantly. Most resins for VAFI usually require an

operating temperature of around 80 °C. Only a few resins can be cured at room temperature wherein all the processing steps can be completed under ambient temperature without requiring additional heat. Vacuum pressure is sufficient for part curing, and it is not necessary to apply pressure.

Compared with other conventional composite processing techniques, VAFI is much more suited to thick and large part fabrication, especially for thick and large ship, automobile, and aircraft structures. VAFI is a very effective processing technique, and with the assistance of vacuum pressure, slow flowing resins, and the patented resin assignment system in VAFI, the resins will fully penetrate and impregnate the laminates. For two single face skin structures or sandwich structures, the entire laminate can be fully impregnated during resin penetration, which eliminates relatively weak secondary adhering as well as other problems caused by secondary adhering operations. For the conventional RTM used in large part fabrication, difficulties in mold material selection and production will be encountered and the corresponding costs are very high. If the production is divided into segments, more working procedures are required while assembly and coordination concerns should be considered. If manual layup is selected, a part with lower fiber content, higher void rate, and poor performance will be produced. According to a report, the Hdadcore Company produced a ship hull with an area of 186 m² and a thickness of 150 mm by VAFI. The hull uses glass fiber as reinforcement with a fiber mass fraction up to 75–85%. Compared with most other composite processes, VAFI gives very good part duplication. Once a balanced resin content (55–60% fiber volume content) is reached, the processing steps can be subsequently terminated. In aerospace composites, part quality is guaranteed by removing all entrapped air before resin injection and transforming the fiber preform into an effective resin-absorption layer. When the resins are absorbed, they flow along predesigned channels and fully impregnate the fiber preform, removing all the bubbles. The escape of volatiles is simultaneously prevented during resin curing cycles. In summary, parts made by VAFI have advantages such as low cost, less void content, and good performance as well as processing flexibility. Table 1.27 lists a comparison between several composite processes.

(2) Key issues in VAFI

In VAFI composite processes, resin flow control and white spot prevention depend on a consistent fiber/resin ratio and these are still important issues in high-quality part manufacturing and are problems to be further studied and investigated.

In liquid processes, fully impregnated resin fibers are required and the resin penetration rate is a critical factor which is closely related to fiber impregnation angles in fabrics, resin flow, bubble escape, and volume compaction. These factors change with time.

Strictly speaking, the resin viscosity is not constant and the laminated geometric shapes are usually not regular either. Therefore, for parts with a thickness more than 20 mm, an area larger than 0.5 m², and a fiber content higher than 50%, there can be problems, including:

Table 1.27 Comparison between composite processing techniques

Process Items	Autoclave	Wet layup	VAFI
Equipment input	High ($\times 1000000$ Yuan)	Low	Low ($\times 10000$ Yuan)
Equipment operation	High	Low	Low
Processing cycle	Long	Long	Short
Energy consumption	High	Low	Low
Part performance	Good	Normal	Better
Fiber content	High	Not high	Not high
Void content	Low	High	Low
Mold expenses	High	Low	Low
Labor costs	Higher	High	Low
Environmental pollution	Some pollution	Significant pollution	Pollution-free
Large part production	Limited by autoclave size	Suitable	Suitable

- ① Scattered white spots;
- ② Color not uniform;
- ③ Bubbles included;
- ④ Inconsistent thickness;
- ⑤ Delamination;
- ⑥ Z-axis not uniform;
- ⑦ Strength and modulus not acceptable.

To achieve higher resin flow rate, two conditions need to be met.

- ① Low resin viscosity;
- ② High pressure difference between layers.

In addition, resin flow visibility is also critical.

Important factors to achieve a successful VAFI are as follows:

- ① Resin systems with low-viscosity and good mechanical performance, curable at ambient temperature;
- ② Resin viscosity should be $0.1\text{--}0.3 \text{ Pa} \cdot \text{s}$;
- ③ Resin viscosity should not exceed $0.3 \text{ Pa} \cdot \text{s}$ such as over 2 h at high temperature;
- ④ Resin-to-fiber impregnation angle $< 8^\circ$;
- ⑤ Sufficient vacuum to achieve good laminar compacting;
- ⑥ Observe resin flow forward points from both sides and adjust if necessary;
- ⑦ Select a proper penetration layer;

- ⑧ Perfect packing will be helpful in removing bubbles and allowing them to escape;
- ⑨ Resin flow channel design is critical.

(3) VAFI processing scheme design

Compared with traditional processes, VAFI eliminates autoclaves and only needs vacuum pressure for processing. Heat is not required, and parts are curable at room temperature and can be serviced at higher temperatures after post-treatment. Parts made by VAFI have higher performance, higher fiber content, and lower void rates than parts made by manual layup.

1) Flow channel design in VAFI: Flow channel design covers resin flow channels and vacuum passages. Some options for flow channel design are given below:

- ① Machining slots on the mold surface: This configuration enables resin penetration from the bottom to the top surface. Proper slots can be cut as resin flow channels. The slot sizes and numbers should be determined experimentally on the basis of part shape, dimension, and resin viscosity. For complex profile molds, some difficulties will be encountered when cutting slots, and the costs will increase. In Fig. 1.55, basic patterns for flow channel design are given.
- ② Cut vacuum passages on mold surface: High penetration rate media are used as resin flow channels. High penetration rate media are usually braided cubic network constructions and are good for resin flow and penetration. In this arrangement, resins penetrate from the top to the bottom surface. Two layers of media are placed on both the preform top and bottom surfaces as resin flow channels, as shown in Fig. 1.56.
- ③ Open holes or cut slots on the foam core as resin flow channels: Foam cores are placed on the mold surface, and resin penetrates from the mold bottom surface to the top surface. The foam with open holes or cut slots (slots have many patterns, either in one direction or in crosswise) finally becomes a segment of the end product. Resin flow channels and vacuum passages are shown in Figs. 1.57 and 1.58, respectively.
- ④ Making a major flow slot and its joint use with high penetration rate media: In this arrangement, it is not necessary to cut too many slots. One or a few major slots may be required as resin input channels. It is also possible to use

Fig. 1.55 Machined flow slots on a mold surface

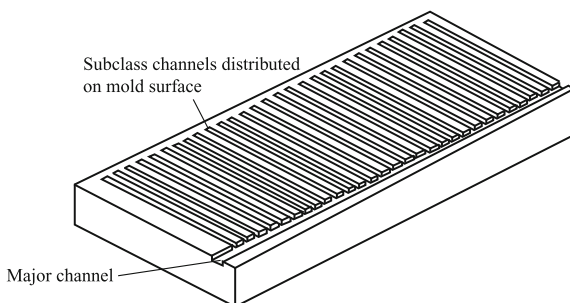


Fig. 1.56 Machined mold with vacuum passages

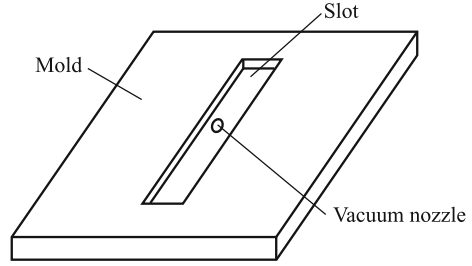


Fig. 1.57 Foam plate with cut resin flow slots on the surface

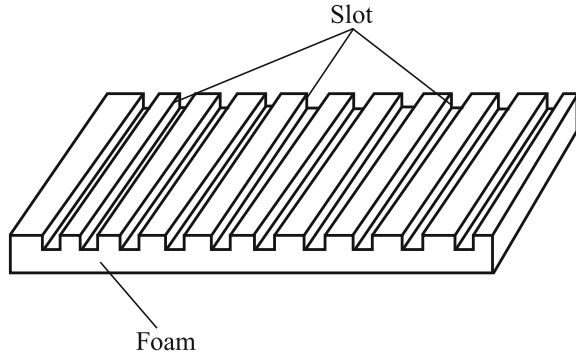
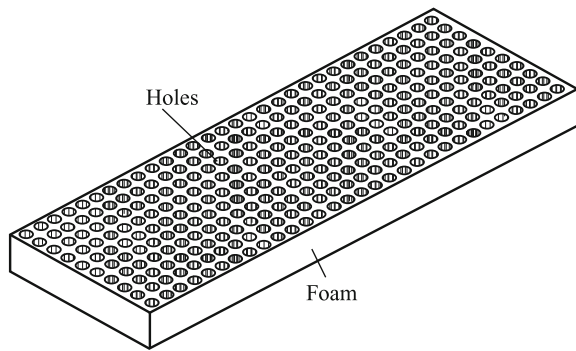


Fig. 1.58 Foam plate with open resin flow holes



tubes to replace slots. Eliminating mold surface machining also works. Resins penetrate from bottom to top, and the resins flow over the entire part surface and are carried out by high penetration rate media. A mold is shown in Fig. 1.59.

- ⑤ Metal plates with holes and slots can replace high penetration rate media as resin flow and vacuum passages. In this arrangement, resins penetrate from top to bottom and metal plates with holes and slots are placed on both the top and bottom side of the preform. Resin flow major channels are prepared as holes or slots on the mold as shown in Figs. 1.60 and 1.61.

Fig. 1.59 Machined mold with a major flow slot and a resin injection inlet

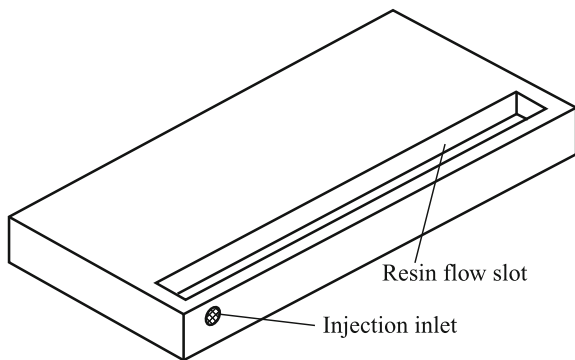


Fig. 1.60 Metal plate with holes and slots placed on the mold

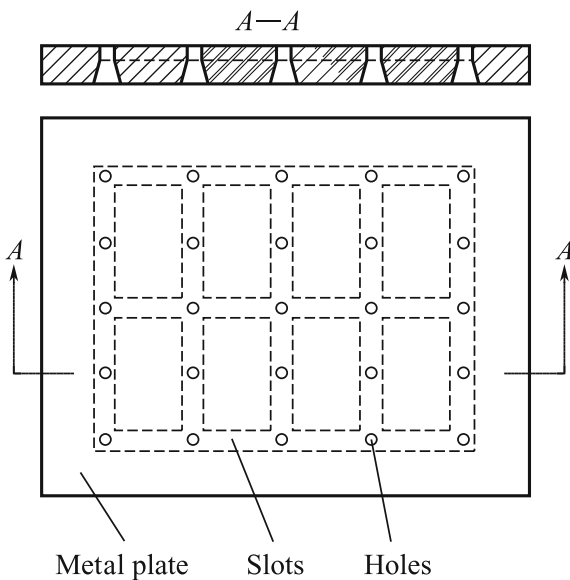


Fig. 1.61 Metal plate with holes on the mold

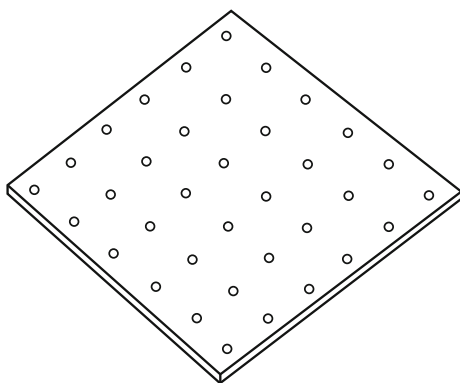
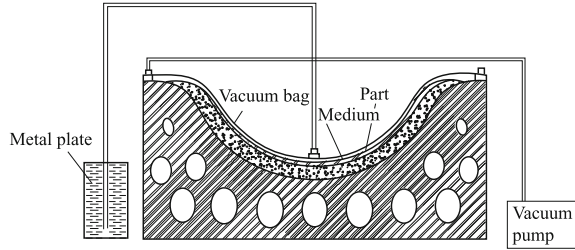


Fig. 1.62 Schematic of a typical VAFI packing



- 2) Cores in VAFI: Commonly available cores can be used except open-hole type cores like honeycores. The cores should be light and also have the desired strength to at least sustain the vacuum pressure. Most cores consist of foam or light mass honeycores.
- 3) VAFI packing: Typical VAFI packing is shown in Fig. 1.62.
- 4) VAFI process flowchart (Fig. 1.63)
- 5) VAFI processing procedures: VAFI processing procedures can be illustrated by the following example—a S-2 glass fiber twill unweaved fabric-reinforced composite panel with dimensions of 1300(L) mm × 600(w) mm × 30 (t) mm, and processing steps are given below:

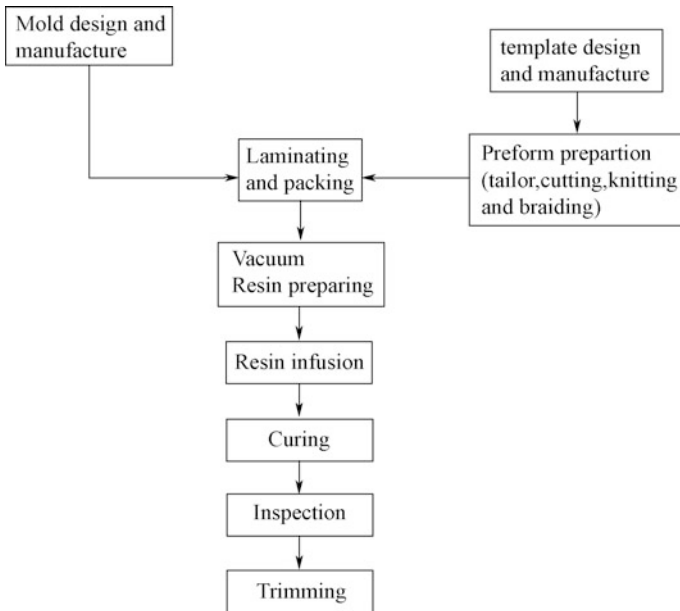


Fig. 1.63 VAFI processing flowchart

- ① Mold manufacture: To observe resin flow on the preform top and bottom surfaces for further processing study, a specially designed processing mold consisting of two transparent platforms as mold plates with each mold plate attached to a plane mirror with an adjustable angle between the mirror and mold plane can be used.
 - ② Template making: Design and make a template according to part size and shape.
 - ③ Cut glass cloth: Use a template to cut the S-2 glass fabric into desired sizes and shapes.
 - ④ Packing: Before packing, a layer of release film is required on the mold plates for easy release after part curing. Determine and arrange resin inlets and vacuum passages based on part size and shape.
 - ⑤ Vacuum: Apply vacuum after the packing is finished and simultaneously prepare the resin and determine the correct resin quantity and cure time by referring to part size and shape.
 - ⑥ Resin infusion: Make sure that the packed system is leak-free, apply a vacuum of up to -0.95 MPa for good resin infusion, and once the part is cured, stop the vacuum.
 - ⑦ Inspection: Carry out a NDT inspection on the final cured part.
 - ⑧ Acceptance: Edge trimming and finishing.
- 6) VAFI cost analysis (compare with autoclave process): The main procedures in an autoclave process are as follows:
- ① Prepare prepregs;
 - ② Prepregs stored in freezer;
 - ③ Prepreg cutting template;
 - ④ Cutting prepregs;
 - ⑤ Mold manufacture;
 - ⑥ Vacuum bag, dwell, breather, isolation sealing, and accessory material consumption;
 - ⑦ Apply vacuum;
 - ⑧ Apply heat for curing, much more energy consumed;
 - ⑨ Curing monitoring and process control;
 - ⑩ Inspection;
 - ⑪ Modification.

Comparing the labor and material expenses, energy consumption, equipment depreciation, etc., the production cost of the same part of $1300\text{ mm} \times 600\text{ mm} \times 30\text{ mm}$ in dimension using VAFI is only 25% that of autoclave processing.

1.2.9 Automated and Innovative Low-Cost Processing Techniques

(1) Fiber automated placement techniques

The challenges that composite industries have been encountering are costs and automation. Filament winding (FW) and prepreg automated tape placing (ATP) have become the most widely used automated technologies in composite production. In these processes, unidirectional composite materials are wound on mandrels or placed on molds. FW processes are more suitable for simple rotation parts such as cylinders, tanks, pipes, balls, and conic fabrication. They can also be used to manufacture non-rotation parts such as airplane fuselages, wings, and automobile bodies. By comparison with other composite processing techniques, FW has a number of advantages. Depending on the different load-bearing conditions of a part in different applications, fiber placements can be designed in different distributions to increase fiber strength sufficiently and to achieve a high specific strength. In FW processing, it is far easier to realize automated and mechanized production. The production cycles are short and rates are high. The part quality is high and consistent. Fiber reinforcements for FW parts do not need weaving, and thus, weaving procedures can be eliminated reducing production costs. The major drawback of FW is its unsuitability for dent surface part fabrication, and thus, applications are limited. Prepreg tape placing techniques are more suitable for the manufacture of large and flat parts with a constant curvature surface.

Pioneering work in fiber placement techniques was initiated in the 1980s in the USA. Investigation and development have been carried out on different equipment for filament winding and fiber placement. In the mid-1980s, the fiber placement equipment shown in Fig. 1.64 was developed. This equipment has 7 computer-controlled coordinates and an attached incline saddle base with a horizontal feed axis. The major advantage of this equipment is the fiber shelf installed on the horizontal feed slide base. This construction can reduce fiber bundle tension device requirements and simplify fiber shelf design.

In Fig. 1.65, the fiber feed head and the necessary processing functions are shown. The major features of the automated fiber placement machine developed by Cincinnati Milacron are as follows:

- ① 3-axis wrist-joint delivering fiber tapes;
- ② different bundle feed speeds;
- ③ fiber bundle cutting, clamping, and reset;
- ④ compacting.

- 1) Fiber delivery: During fiber placement, the fiber tapes are straightened from a yarn shelf and delivered to a feed head through a 3-axis wrist-joint. The fiber

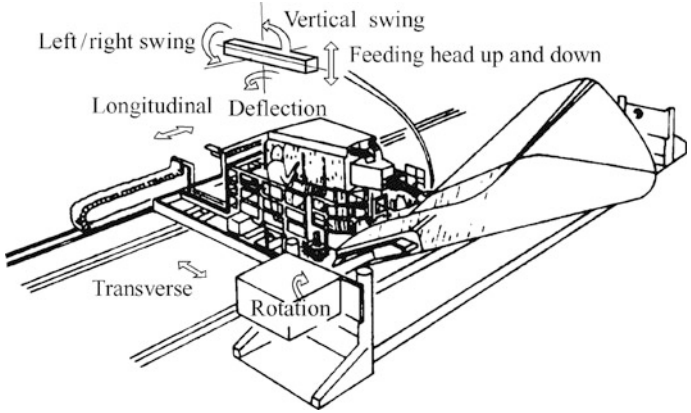
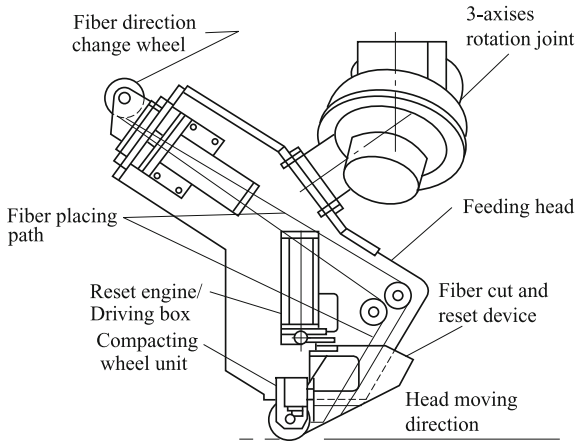


Fig. 1.64 Schematic of fiber bundle automated placement equipment

Fig. 1.65 Schematic of fiber placement head



tapes must be delivered through the above-mentioned path so that the movement range of the feed head will not be seriously restricted. For feed head operation, the head central line must be maintained to be consistent with the core axis or any specified point on the mold surface along the fiber feed path. The fiber shelf is closely related to the feed head movement to control and limit any directional changes to the fiber's delivery path. Using a rolling wheel device, which can change the feed direction and attaches to the fiber shelf and a feed head, to straighten the fiber bundles is the best method to pass the fiber bundles in this direction. These direction-changeable rolling wheels must be installed on the same pivot so that its position can be automatically adjusted and maintained to coordinate with the feed head movement.

- 2) Different fiber bundle feed speed: The second major feature in fiber automatic placement is that each individual fiber bundle has its own independent guiding and delivering system so that each bundle can have a different delivery speed for placement. Each individual fiber bundle has its own independent guiding wheel unit for fiber delivery from the fiber shelf until compacting. When the fibers are pulled from the shelf by the feed head and compacted on the part's surface, each fiber bundle will have a single corresponding linear length within the placement tape width. When the feed head is compacting a curved surface, the bundles on the fiber tape edges will be pulled out to a longer distance than those in the tape central area. Similarly, when the fibers are carried out for placement on the same part section, the later placed bundles should have a longer length than those previously placed so that each bundle has a different delivery speed during placement if necessary.
- 3) Fiber bundle cutting, clamping, and resetting: The third major feature, which is also the most challenging feature in fiber automatic placement, is the automatic fiber cutoff and resetting placement. This is certainly necessary for continuous feed head compacting movement as well as independent fiber cutoff/clamping and resetting placement. As a part of the off-line software, the orders for bundle cutting and fiber placement resetting should be programmed by following the part's geometric shape requirements. This feature allows all the bundles or any joined bundles to be eliminated or added to change fiber tape widths. The change in tape width should be equal to multiples of the individual bundle width. With this function, the fiber tape width can be reduced if necessary to avoid material waste. At the same time, all the bundles on part edges on the return surface can be cut to save materials.
- 4) Compacting: The last feature in fiber automatic placement is to use a mechanical compaction device to compress the pre-impregnated fiber bundles into molds or part surfaces. Compacting is carried out to remove air bubbles by compressing fiber bundles onto a mold or a part surface. This eliminates bundle gaps along the width. In the early stage of feed head development, the compacting device was a soft rolling wheel with a diameter of 76 mm (3.0 in). In most cases, the rolling wheel compressing area should be heated to decrease the resin's viscosity in bundles and viscosity strengthening in processing. The applied heat will cause the resin to flow, and the rolling wheel can easily eliminate the gaps between the fiber bundles. The increased viscosity also allows the placed fibers to quickly and firmly bond onto a mold or onto the previously placed fiber layer.

(2) Low-temperature molding (LTM) techniques

For fiber and fiber tape automated placement, or for part curing, very expensive molds and tools are required. The initial input is very high and only acceptable for high-volume production. For small-volume or multiple-phase production, the cost is too high and no value can be added. On the other hand, using prepregs to manufacture composites depends on the necessary molds. Prepregs require a high curing temperature, and processing molds are required to maintain structural

integrity under the same curing temperature. High-temperature sustainable mold materials are usually expensive, and in the case of high-volume composite production, the shared mold costs will not be too high. However, for newly designed parts or prototype parts in small quantity, the mold cost will be relatively higher. A cost evaluation of composite part production has indicated that the molds contribute 20% to the overall cost of each part at a 250 production scale. In prototype part production where only 2–3 pieces are produced, the molds will contribute about 70% to the overall cost of each part. Therefore, studies into LTM techniques, which are curing processing techniques carried out at 60–80 °C, have been carried out at the US Air Force Material Laboratory.

The important factor in LTM processes is to develop innovative resin systems curable at room temperature to 80 °C as well as develop correlated low-temperature curable prepregs. All low-temperature curable prepregs should use cheap molds such as plaster and wood and should be able to be cured in normal ovens.

The advantages of LTM are the use of cheap molds and tools as well as cheap auxiliary materials, the curing of parts in ovens, the elimination of expensive autoclave equipment, and the large reduction in manufacturing costs.

Prepregs prepared with resins curable from room temperature to 80 °C are referred to as low-temperature curable prepregs. All low-temperature curable prepregs should undergo the necessary post-curing in ovens. This can start at room temperature, increase to a desired temperature, and be maintained for entire part curing. For epoxy resins, 177 °C is required and the post-cured parts should have an increased glass transition temperature, T_g , which is higher than the post-curing temperature. Additionally, improved mechanical properties will result. Such prepregs are available in the UK from ACG and US Hexcel. The low-temperature curable prepreg series supplied by ACG and their typical properties are listed in Tables 1.28 and 1.29, respectively.

The inherent feature of low-temperature curable prepregs is a higher reaction activity, and this is the critical factor in cost savings. A higher reaction activity will result in a shorter operating period at room temperature. The limited shelf life at room temperature will cause difficulties if this kind of material is selected for large or complicated structures. Therefore, in developing innovative low-temperature curing structural prepregs, the initial curable temperature needs to be increased to 80–100 °C rather than 60 °C, and the aim is to increase the working life and to improve wet performance. Furthermore, comprehensive performance similar to 177 °C curing prepregs especially in terms of toughness and T_g is targeted.

(3) Electronic beam curing techniques

Most current advanced composites are basically cured and processed by heat such as in autoclave and hot-press molding processes. Since the thermal curing processes are long, usually several hours to tens of hours, composite production will be expensive. This is the main factor that limits the use of composites in the defense industry and in other civil fields. Additionally, the curing agents and organic solvents used in thermosetting composites are mostly toxic substances that can harm

Table 1.28 Typical properties of the L.T. curable prepregs supplied by ACG

Prepregs	LTM10 series	LTM20 series	LTM30 series	LTM40 series	LTM100 series
Resin type	Epoxy	Epoxy	Epoxy	Epoxy	Cyanate ester
Typical curing temperature	20–80	30–60	30–70	50–80	75
$T_g/^\circ\text{C}$	210	130	170	200	375
Mechanical performance	Good	Superior	Good	Superior	Good
Wet/mechanical performance at 120 °C	Superior	Poor	Superior	Superior	Most superior
Thermal stability, Long term/ $^\circ\text{C}$	210	120	170	200	250
Suitability for room temp. service and machining fabrication	Requires post-curing	No requirements	Requires post-curing	Requires post-curing	Requires post-curing
Post-processing time/d	2–30	2–30	2–10	3–10	3
Shelf life at $-18\ ^\circ\text{C}$	12	6	6	6	6
Toughness	Low	Excellent	Low	Good	low
Typical applications	High-temperature molds and parts	Medium-temperature molds and parts	Low-cost molds	High-temperature structures	Supertemperature molds and parts

Table 1.29 Low-temperature curable prepreg series supplied by ACG

Series No.	Remarks
LTM10 series	L.T. curable epoxy prepregs for high-temperature service molds and parts
LTM20 series	Toughened L.T. curable epoxy prepregs for medium-temperature service molds and parts
LTM30 series	Low-cost prepregs for medium-temperature service molds
LTM40 series	Toughened L.T. curable epoxy prepregs for medium-temperature service molds and parts
LTM100 series	L.T. curable prepregs for extremely high-temperature service molds and parts
LTM200 series	L.T. curable prepregs for high-temperature service molds

the environment as well as workers. Because of these disadvantages of thermal curing techniques and to comply with developing trends of cost reduction and public hazard avoidance, scientists and engineers are searching for technical approaches to improve thermal curing processing of composites by exploring innovative curing techniques. Electronic beam curing resin matrix composites is an innovative composite processing technology that has been developed for this reason.

In the late 1970s, investigations into electronic beam curing resin matrix composites were initially carried out in France. In 1990, this technique was used to make full-scale composite back linings for rocket engines. In the mid-1990s, two principle projects began in the USA: One was a development program funded by DARPA and the Air Force to determine the feasibility of electronic beam curing techniques and their low-cost potential in aerospace composite manufacturing; the other was the Co-operation Research and Developing Agreement (CRADA), which was co-sponsored and implemented by several companies and the State Laboratory of the US Energy Ministry, and its goal was to develop and enhance electronic beam curing processing techniques. The launch of these two projects as well as engagement with Italy and Canada led to a significant advancement of electronic beam curing resin techniques. Electronic beam curing equipment and processes have been successfully developed, and significant achievements were also forthcoming in the development of resin systems, especially epoxy resins. Hundreds of products became available for different applications and research into the electronic beam curing of the bismaleimide (BMI) series resins, which are critical to aerospace applications, also advanced significantly.

Electronic beam curing refers to techniques in which high-energy electronic beams are used to induce cross-linking reactions in prepreg resins and to make thermosetting composites with a high cross-linking density.

Electronic beam curing is a radiation curing technique, and with other radiation curing techniques, it involves processes in which light or ray plasma energies are

used to induce resin monomer polymerization, cross-linking, and finally curing. Among these, light curing research has been carried out for more than 50 years, while electronic beam curing techniques are relatively young.

Because of the unique features that are not available to thermal curing processes, electronic beam curing techniques have been given much more attention and have grown quickly recently.

In electronic beam curing techniques, curing can take place at room temperature or lower; curing agents and solvents can be highly reduced; it is possible to apply radiation to a local area to carry out local curing; electronic beam curing can be incorporated into filament winding, automated fiber placing, and RTM to fulfill continuous production; and the resins curable by electronic beams have good shelf consistency. Because of the characteristics mentioned above, electronic beam curing techniques are superior to thermal curing processes.

- 1) Lower costs: Since curing can be carried out at room temperature or lower, a series of advantages can be expected. The first is a lower shrinkage rate in cured parts, which is good for part dimensional accuracy and a high product acceptance rate. Second, a reduction in residual stresses in cured composite parts leads to a reduction in assembly difficulties. A reduction in residual stresses and an increase of dimensional precision will reduce assembly costs. A reduction in residual stresses increases the thermal fatigue performance of composites. Because of low-temperature curing, cheap materials such as foams, plasters, and wood can possibly be used as molds and thus replace expensive steels, invar steels, and composites. Furthermore, the energy consumed by electronic beam curing is only 1/20–1/10 that of thermal curing processes. Some research reports have indicated that the energy required for the electronic beam curing of a 1-kg composite is 0.1–0.72 kW, while 1.76–2.86 kW is required for thermal curing.
- 2) High production rate: Accelerated curing speeds and shortened processing cycles. For example, a 1.6 pJ and 50 kW electronic beam accelerator can cure 1800 kg of composite in one hour, which is many times a conventional autoclave's curing speed. At the Unipolis Company in France, the curing process of a single composite part can be completed by electronic beam in 8 h while 100 h is required with an autoclave. Electronic beam curing is feasible for continuous operating procedures, and it can be used with RTM, fiber braiding, filament winding, fiber placement, and pultrusion processes for further cost reduction.
- 3) Less pollution: The resins used for electronic beam curing generally contain little or no volatiles or toxic solvents limiting environmental and personnel hazards.
- 4) Possible for part local curing: In thermal curing processes, a spherical temperature field is supplied, while in electronic beam curing, a "sighting-line" curing zone is implemented. Therefore, in electronic beam curing processes, a local area on a part can be selected as the curing zone and be subjected to electronic radiation curing rather than entire part curing. This gives cost

reduction benefits. Therefore, electronic beam curing is much more suitable for composite part repair. In addition, portable electronic accelerators allow electronic beam curing techniques to be used for composite field repair. Because of lower shrinkage rates and smaller residual stresses of cured materials, electronic beam curing techniques can also be used for different material co-curing or co-adhering processes.

- 5) Suitability for large part fabrication: Because of the elimination of autoclaves, electronic beam curing can be used for huge composite part production if a perfect shield case on an electronic accelerator is available. The largest electronic beam curing equipment was built by Aerospatial in France, and it can be used to cure large composite parts up to $5\text{ m} \times 10\text{ m}$. Building an autoclave for such a large part for curing will be very difficult.
- 6) Good processing performance: In conventional thermal curing resin systems, the maximum shelf life at room temperature is several months, while in resin systems for electronic beam curing, the shelf life can be unlimited at room temperature and under dark storage conditions.

However, electronic beam curing techniques have some drawbacks such as an extra protection facility required for the electronic beam and X-ray shielding to eliminate hazards to personnel. Additionally, it is difficult to apply pressure during the curing process.

(4) Light curing techniques

Recently, composite resin matrix curing technologies have undergone fast development. Traditional heat application curing processes like autoclaves have encountered a series of challenges, including their low-energy utilization rates, long processing cycles, and environmental pollution. Innovative radiation curing techniques such as light curing and electronic beam curing have undergone very fast development because of their advantages of low curing temperature, high curing speed, small thermal shrinkage, small inner stresses, and less environmental pollution. Compared with radiation curing techniques, the advantages of electronic beam curing are higher energy utilization rate, stronger penetration ability, and the possibility of eliminating induction agents; however, the equipment is expensive, and the inputs and operating costs are high, which has seriously limited its application. As a result, light curing technologies currently occupy 95% of the total radiation curing market.

Optical curing refers to cure polymerization processes in which monomers or prepolymers are subjected to ultraviolet light or visible light to induce molecular cross-linking and curing into solid bulk polymers. Light polymerization refers to the chemical reactions in which chemical compounds absorb light energy and undergo molecular polymerization to increase their molecular weight.

Apart from optical condensation (local chemical polymerization), in terms of reaction mechanism, optical polymerization mostly refers to molecular chain reactions, that is, chain growth processes induced by a reactive species (free groups or ions), which is different from well-known free group-induced polymerizations or

ion polymerizations. The difference is reactive species generation in optical polymerizations as the reactive species are generated in optical–chemical reactions. Therefore, in optical polymerization, the optical energy required is absorbed in molecular chain inducing phases during polymerization.

Compared with chemically induced polymerizations, the advantages of optical–chemical reactions are lower reaction activation energies allowing optical polymerization to be carried out over a large temperature range. They especially allow easier low-temperature polymerizations. In research laboratories, optical polymerization can yield pure polymers without any residual inducing agents, and this is very helpful for further studies. Furthermore, in optical chemical chain reactions, only absorbed photons can induce monomer polymerization into large molecules. Therefore, in terms of reaction rates, optical polymerizations are highly efficient quantum chemical reactions and have great potential for different applications.

For optical polymerization, a chemical segment that can absorb optical energy of a certain wavelength is required for polymer systems and the optical energy absorption molecules can further decompose or react with other molecules to form primary reactive species. All the substantial molecular chemical bonds generated by polymerization can withstand the desired optical radiation; therefore, the proper selection of suitable radiation energies to generate the necessary reaction species is critical.

Since organic molecules require 7–12 eV of energy for ionization, the amount of energy in the near violet to visible light range cannot ionize a single organic molecule. Therefore, the public view has always been that optical polymerization can only be induced by free reactive species. However, with the introduction of aromatic onium salt inducing agents as well as extensive research into polymerizations induced by the ion reactive species generated by optical chemical reactions with electric charge interimmigration, the development of ion optical polymerization has been advanced. Ion optical polymerization has greatly increased the number of usable monomer species. Optical polymerization has now advanced far beyond chain growth reactions. Most monomers, low polymers, and prepolymers do not generate induction cores with enough quantum efficiency. In practice, low molecular weight organics should be added as light-inducing agents or light-sensitive agents to increase the medium light absorption rate and to generate polymers.

With the advancement of research and technology, a variety of innovative visible light curable prepolymers, monomers, reactive diluents and a variety of optical inducing agents and light-sensitive species such as expandable monomers, organic sulfur compounds, phosphor compounds, visible light-inducing agents/light-sensitive agents, water (amphiphiles), and light-inducing agents/light-sensitive agents are available.

Table 1.30 shows the optical curing techniques used in different applications.

Table 1.30 Different applications of optical curing techniques

Applications	Objectives
Coating and paints	Paper, wood, plastics, leathers, etc. Wire, cable, pipe, optical fiber, polyethylene floor paint, protection film, special glue sheet, shielding booth, high-class bridge coating, car repair paint, and packing film
Adhesives	Laminating adhesives, pressure-sensitive glue
Decorating materials	Backing ink, printing board, decorate paint
Photoengraving adhesives	IT techniques: printing circuit board or integral circuit
3D mold manufacture	
Dental materials	
Laser photoimaging	IT: large or superintegrated circuits, laser printing, and laser imaging

1.2.10 *Examples of Processing Scheme Selection and Implementation for Typical Composite Structures*

The following examples will show processing scheme selection and implementation in typical airplane composite structure fabrication.

Example 1: Front fuselage composite special cabin The front fuselage composite special cabin is the first large and complex composite assemble structure developed and manufactured for aircraft applications in China and has become a successful example showing Chinese composite technology milestones. In trial flights, all structural performances were verified, especially its good electric–magnetic compatibility and static electricity resistance.

The structural configuration of this composite airplane part is given in Fig. 1.66. The whole construction is a torsion-bearing I-type backbone structure consisting of top and bottom laminated cabin boxes as well as sandwich longitudinal walls between the cabin boxes. There are four laminated composite frames that guarantee a desired stiffness and operational ease when cabin hatches are to be opened for field maintenance. The material systems of choice are carbon/epoxy. Hatch frames are composed of longitudinal beams and partition frame bumps; the hatches are made using sandwich carbon/aramid hybrid surfaces and aramid paper honeycores; the hatch boundary connections consist of titanium fast-removing hinges. The main points of the front fuselage composite special cabins are given below:

- (1) Co-curing integrated processing of laminated cabin boxes

The top box construction shown in Fig. 1.67 contains three closed chambers. The laminated cabin boxes are processed by co-curing, which can increase

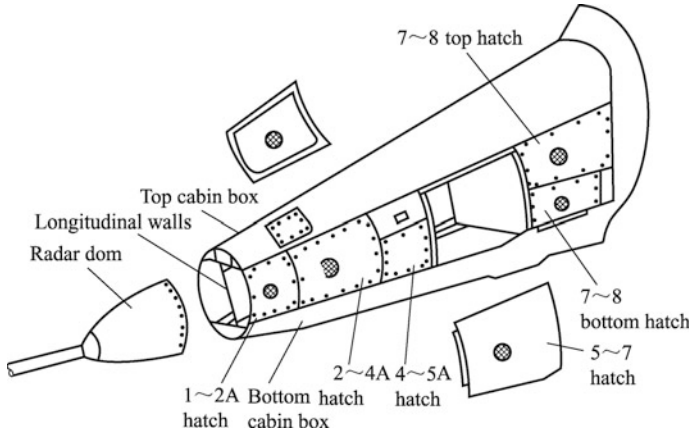


Fig. 1.66 Structural configuration of the front fuselage special cabin (type 1)

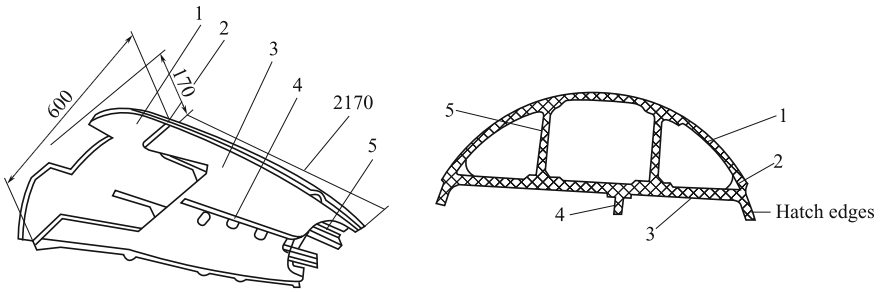


Fig. 1.67 Top cabin box construction. 1 Skin; 2 top beam; 3 top floor; 4 angle shapes; 5 walls

structural integrity and reduce part weight and joint counts. A comparison has been carried out to evaluate a number of processing schemes.

- a) Thermal expansion rubber core processing in which the mold strength and fabrication precision are important and where pressure application and uniformity are difficult to control.
- b) Autoclave processing in which laminated cores composed of multiple layers of high elastic Airpad rubbers and carbon prepregs are used in closed chamber processing. This causes localization difficulties or longitudinal wall dislocation and deformation.
- c) The last approach is autoclave processing using metal core wrapped Airpad rubbers, in which good part quality is obtained. The processing tool used for top cabin box fabrication is a steel female mold constructed using a 1.5-mm-thick steel shell welded to a steel frame. The steel shell is formed using a stretch forming machine; the cores are cast aluminum, as shown in Fig. 1.68.

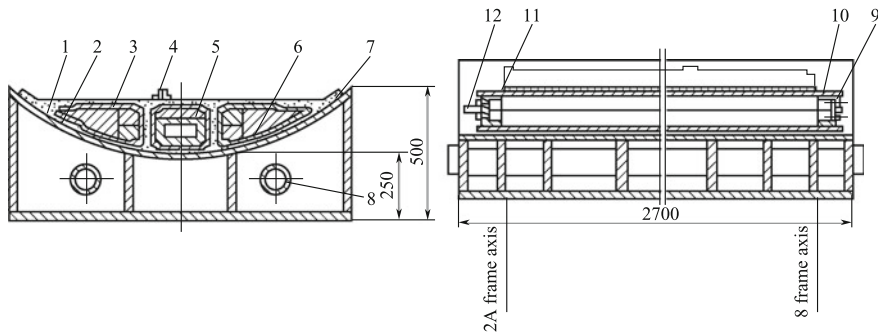


Fig. 1.68 Top cabin box processing molds. 1 Part; 2 female mold; 3 rubber; 4 angle sharp; 5 cores; 6 walls isolating layers; 7 back strip; 8 steel pipe; 9 bolts; 10 back cap; 11 front cap; 12 handle

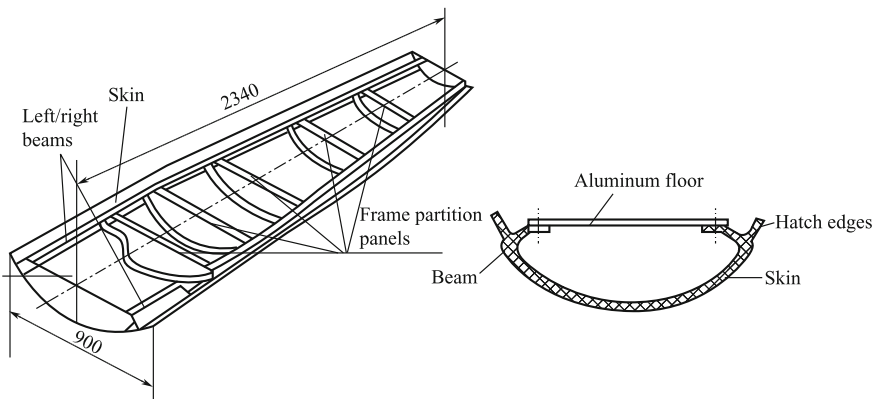


Fig. 1.69 Bottom cabin box construction

The bottom cabin box shown in Fig. 1.69 is a multiple frame construction consisting of a skin, beam, frame partition panels, and aluminum floors. Five frame partition panels share the space between the top and bottom cabin boxes and form six chambers. In this multiframe construction, if the skin, beam, and frame partition panels have been previously cured and joined by secondary adhering, difficulties in part quality control will be encountered such as part curing deformation, hyperbolic match precision, and firm adherence. Co-curing should thus be used. The important techniques are the processing of inner surfaces in box sections using an air-charged rubber bag attached to the removable metal cores to apply pressure and the separate removal of metal cores after part curing. The processing of the left and right edge surfaces on the bottom skin, the left and right bottom beam surfaces, and the five frame partition panels is carried out using top cap molds. The female molds for the bottom cabin box are made in the same way as those used in the top box.

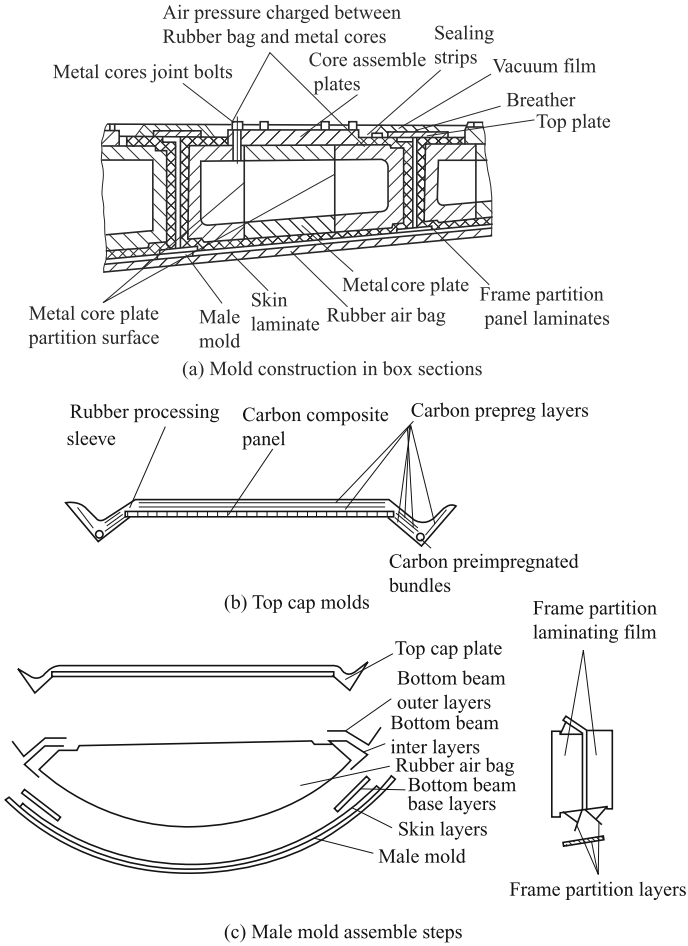


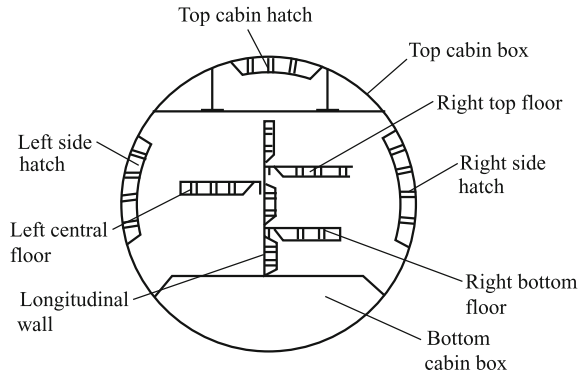
Fig. 1.70 Bottom cabin box processing molds

The processing assembly is shown in Fig. 1.70. In this processing, the laminated prepregs should be subjected to precompacting and compacting and then cured.

(2) Honeycomb sandwich construction Co-curing processing

For the composite front fuselage, the positions used for the honeycomb sandwich construction are shown in Fig. 1.71. In terms of shape surface features, the honeycomb sandwich parts used can be divided into two classes. One is the different hatches, which will require a desired surface contour to fit the front fuselage in a double-curvature surface; the other is the inner plane panels without contour requirements. The honeycomb sandwich construction has features such as the surface panels being section-varied and unsymmetrically ply stacked, but both the inner and outer panels should be symmetrical along the sandwich central plane;

Fig. 1.71 Positions of the honeycomb sandwich structures in composite front fuselages



most Nomex honeycomb edges are enclosed by surface panels. Because of the above features, co-curing processes are used for honeycomb sandwich production. In contrast, secondary adhering processes need high precision molds and high inputs and longer production cycles and unsymmetrical surface panels are not suitable for two-step co-curing processes.

Example 2: Helicopter propeller hub central system

The helicopter propeller hub central system is a dynamic assembly bearing high centrifugal loads and flapping, shimmying, and moment-varied alternative loads in service. Therefore, exploiting the advantages of superior performance in unidirectional fibers and/or fabrics is an important factor in the design and manufacture of the central assembly.

(1) Filament wound ring strap hub central structure

In Fig. 1.72, a Boeing 360 all-hinge type composite hub is shown. The central assembly consists of top/bottom core assemblies and inner/outer ring straps. The inner/outer ring straps are filament wound parts. This is the most optimized load transfer and bearing configuration as illustrated by the hub load transfer schematics.

In the EH101 propeller hub system, to increase reliability, the safety cycle, and damage safety, a double load transfer path consisting of five inner rings and one outer ring is used to form a “chrysanthemum-like” structural configuration. Inner rings and outer rings are the filament wound composite parts as shown in Fig. 1.73.

(2) Laminated and press-molded central hub flexible asterisk structure

The central hub flexible star structure in a “dolphin” helicopter is shown in Fig. 1.74.

The asterisk flexible structure is a laminated composite part. Unidirectional glass fiber cloth/epoxy and cross-glass cloth/epoxy composites were selected for this design. Unidirectional glass fibers are used to bear the longitudinal centrifugal loads, while cross-glass fibers are used to adjust the stiffness of the asterisk flexible

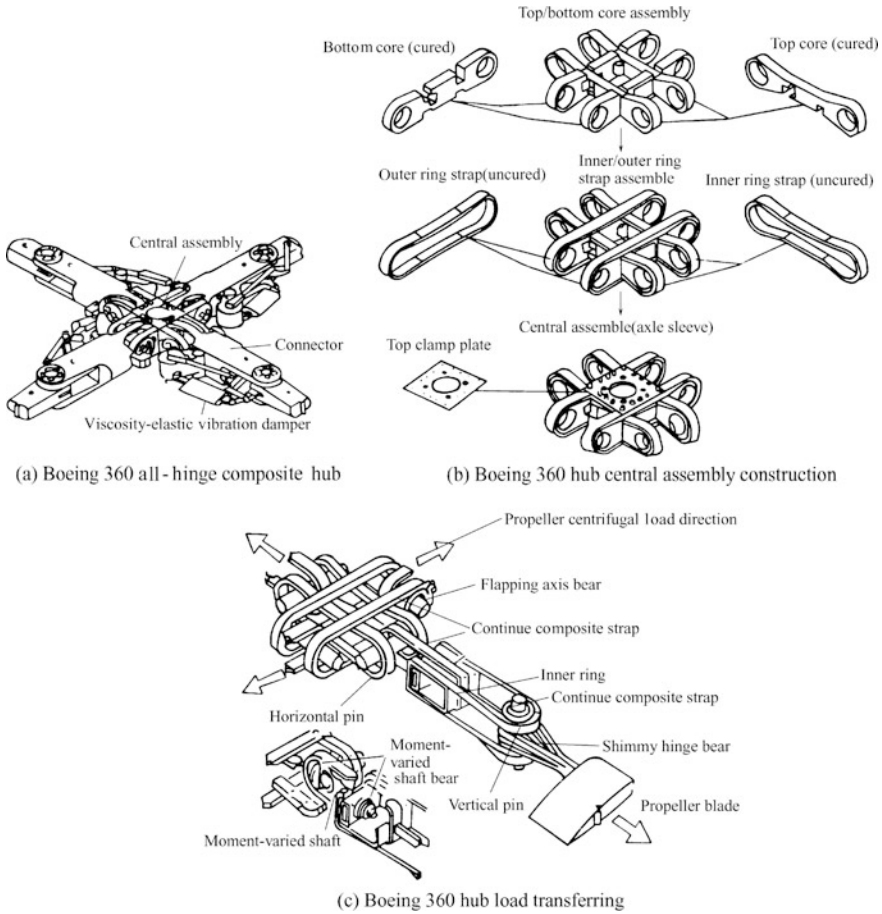
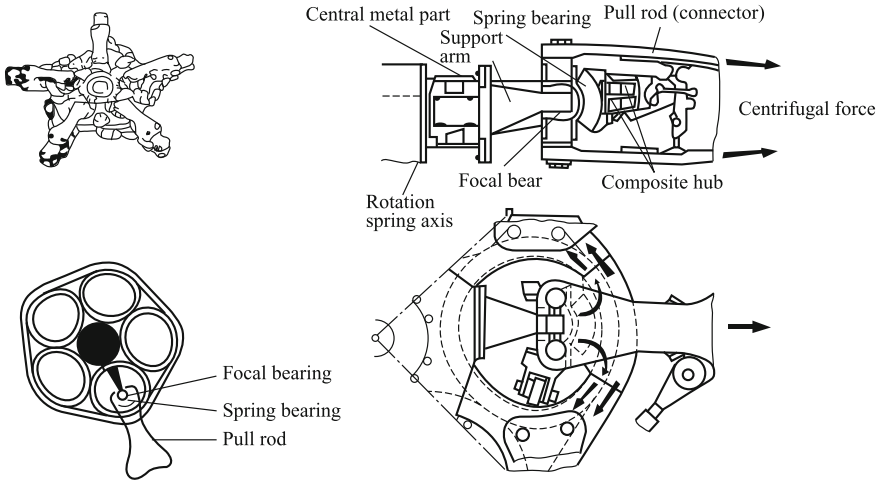


Fig. 1.72 Boeing 360 composite hub construction and processing chart

support arm. Both of these are joined to satisfy the propeller blade’s load-bearing and aerodynamic performance needs.

The asterisk flexible structure was designed based on the failure safety criterion, in which the first failure in a composite will be interlaminar delamination (interlaminar shear delamination) rather than glass fiber breakage (positive stress tensile fracture). The delaminated cracks can be restricted to slow their growth. This can guarantee the reliability of the asterisk flexible structure using “dependent maintenance” to ensure flight safety.

The asterisk flexible structure is a laminated and press-molded component that is processed by half-dry prepreg press molding. The main procedures include prepreg cutting, mold packing, press molding, and curing and inspection. The processing features are given below:



(a) EH101 propeller hub construction and multi-load transferring

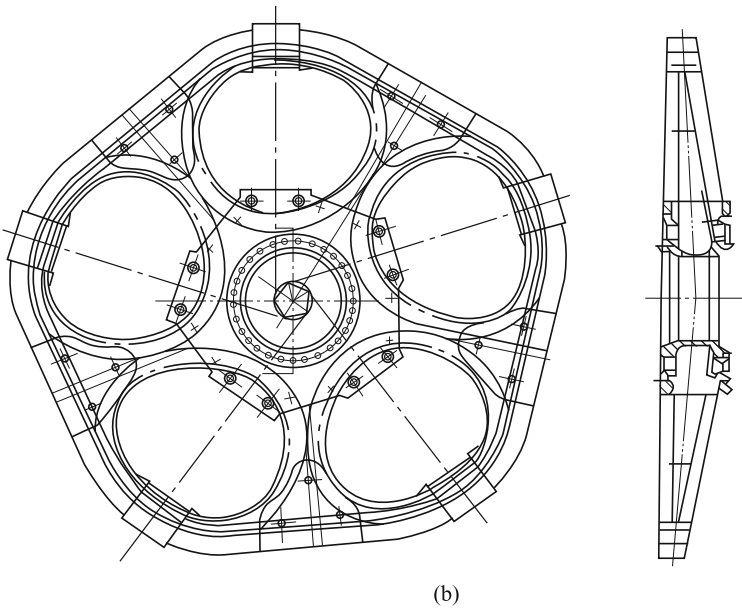
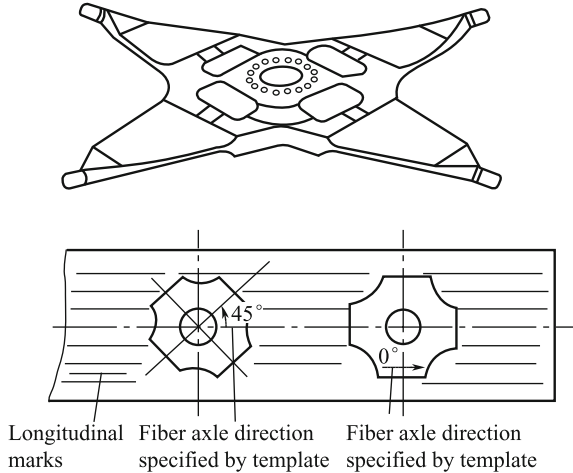


Fig. 1.73 EH101 composite propeller hub structure and its processing

- ① The prepreps should comply with related quality standards. When cutting prepreps, the fiber longitudinal direction should be absolutely guaranteed, and marks showing the fiber's longitudinal direction must be made during the cutting procedure to guarantee precise fiber stacking orientations, as shown in Fig. 1.74.

Fig. 1.74 Dolphin hub central asterisk flexible structure and prepreg cutting

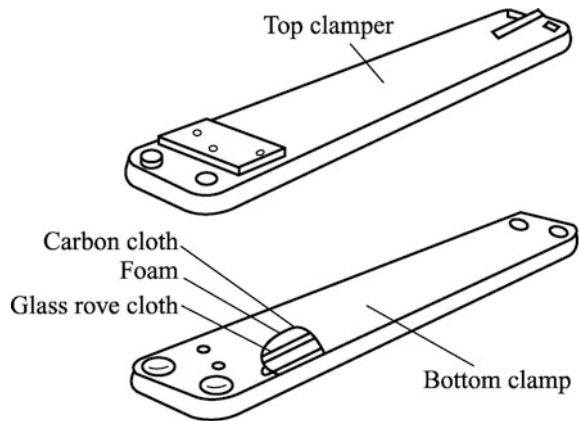


- ② To guarantee the exchangeability of asterisk flexible structures, very high dimensional precision is required. The selected mold material should meet the requirements of high-temperature curing and easy room temperature release as well as have lower expansion at high temperature. Usually, invar alloys (low expanding alloys) are the mold materials of choice in asterisk flexible structure processing. They deliver high part dimensional accuracy and surface finishing as well as other design requirements.
- ③ Ply stacking should exactly follow the designed ply sequence, layer numbers, and fiber orientations. In prepreg laminate packing into molds, to guarantee each prepreg layer perfectly fits the mold shape surface without wrinkles or waves, the molds should be preheated and controlled to about 35 °C.
- ④ Press molding and curing control are the important steps in guaranteeing the asterisk's flexible structure processing quality. For this reason, a specialized hot press with computer-controlled oil mold heating, mold closure, and pressure application and cooling should be used to guarantee part processing quality.
- ⑤ X-rays should be used to inspect part inner mold quality. Dimensional precision should then be acceptable.
- ⑥ The static bending stiffness of the support arms that ensure the stiffness and exchangeability of support arms in accordance with design requirements should be strictly controlled.

Example 3: Propeller system clamps

The helicopter hub and blades are joined by clamps. The top and bottom clamps have the same construction, as shown in Fig. 1.75. Centrifugal loads are transferred from the wound glass rove ring straps in the sleeves between the clamp ends to the central asterisk structure. The gaps between the fiber rove straps are filled with a plastic foam core. The foam core is wrapped with carbon cloth to increase the

Fig. 1.75 Helicopter hub clamp construction



compression and bending strength and the stiffness. The clamp's outer surface is wrapped in $\pm 45^\circ$ carbon ply layers to form an integrated clamp construction and to increase the clamp's torsion strength and stiffness. The material system designed and used for clamps is the 120 °C curing epoxy resin system, high-strength glass rove strips, and high-strength carbon plane woven cloth.

Both the top and bottom clamps are manufactured by half-dry prepreg press molding. The main procedures include prepreg cutting, circular winding, mold packing, press molding, and curing and inspection. The circular winding of impregnated glass rove straps is the key factor in part quality assurance. To ensure the clamps can bear centrifugal loads, quality defects like dislocations between wound fiber layers, fiber distortion, and wrinkles should be eliminated during the winding process. The impregnated fiber roves have to be inspected and accepted before use. Special attention should be given to the following steps for circular winding and packing into molds:

- ① The impregnated fiber roves should be shelved for a specific time after removal from the freezer. This is to ensure that the material's temperature is consistent with the environmental temperature, and when the flexibility condition is met, winding may begin.
- ② In the circular winding process, the fiber tension should be precisely controlled by a specialized tension controlling device.
- ③ Additionally, the prepreg temperature should be exactly controlled (30–35 °C) during the winding process because a temperature change will directly affect the resin viscosity in the prepregs, possibly resulting in inconsistent fiber tension or skew and flat fiber dislocations or wrinkles resulting in the parts. Again, the environment temperature in the workshop should be also controlled during fiber winding; otherwise, fibers will peel apart and filament ruptures can occur.
- ④ In mold packing, the wound ring straps should be kept flat and straight with a certain tension to exclude dislocations and wrinkles.

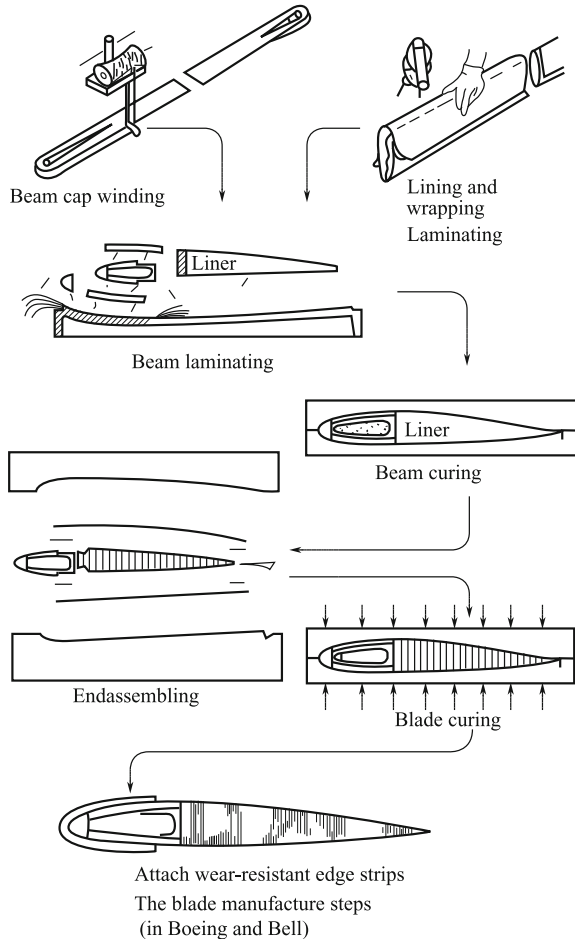
In the mold packing process, the mold's preheat temperature and packing sequence should be controlled. The curing temperature of the clamp assembly should be equal to the measured mold temperature. During part curing, the curing temperature, pressure, and time should be applied by exactly following the designed curing curves. The cured part should be subjected to X-ray inspection. The pinholes at the clamp ends should be subject to a boring process to guarantee interchangeability.

The composite hub of the Dolphin helicopter propeller has a weight of 82 kg, and this is about 25% the weight of identical metal hubs.

Example 4: The fabrication of propeller blades by secondary adhering co-curing in closed molding processes

The processing steps of the D-beam propeller blade fabrication by the secondary adhering curing technique are shown in Fig. 1.76 with the advantages presented below:

Fig. 1.76 Processing steps in propeller blade fabrication by the secondary adhering curing technique



- ① Some critical elements in a blade can be procured and fabricated by high-temperature curing (180 °C) resin systems or by filament winding processes and other mechanical techniques with a large selection range.
- ② The mold residence time can be considerably reduced.
- ③ Suitable for the manufacture of complex D-beam blades, multipipe beam blades, and large metal-beam blades.

For these reasons, this kind of processing technique is widely used to make helicopter propeller blades in some countries, for example, the CH-46 and Boeing 360 principal propeller blades.

1.3 Advanced Resin Matrix Composite Performance

In this section, the performance of advanced resin matrix composites that are very critical in structural designs, manufacturing, and applications will be extensively discussed. These include correlated mechanical properties, physical properties, and processing performance.

Reinforcing fibers in composites play a very important role in part load bearing, and they dominate the direction-dependent performance characteristics in a single laminar composite. The performance of some composites is dominated by fiber properties, content, and ply stacking angles, while other performances depend on the resin matrix (interface involved). The resin matrix is a principal constituent material in composites. The transverse properties, interlaminar performance, thermal resistance, moisture absorption, wet/hot performance, medium resistance, and processing performance are basically dominated by resin matrix performance. The development of resin matrixes is a critical milestone that exemplifies the achievements in advanced composite research and applications. For this reason, advanced resin matrix composite performance will be presented on the basis of composites that are classified as epoxy resin matrix, bismaleimide (BMI) resin matrix, and polyimide resin matrix composites in this chapter. The highlights will focus on empirically used resin matrixes and their corresponding performance. These matrixes are recommended for composite applications as they have good combined performance and comprehensive data are available. The data listed were compiled from several documents and can serve as a reference.

Composite performance parameter symbols are listed in Table 1.31.

1.3.1 Epoxy Resin Matrix Composite Performance

Epoxy resin systems have a series of advantages such as good processing performance, superior mechanical properties, low curing shrinkage, large modification margins, and low prices. They have become the most widely used resin systems in

Table 1.31 Composite performance parameter symbols

Property	Symbol	Unit
Laminar longitudinal tensile strength	X_t	MPa
Laminar longitudinal tensile modulus	E_{1t}	GPa
Laminar longitudinal compression strength	X_C	MPa
Laminar longitudinal compression modulus	E_{1C}	GPa
Laminar principal Poisson's ratio	ν_{12}	
Laminar transverse tensile strength	Y_t	MPa
Laminar transverse tensile modulus	E_{2t}	GPa
Laminar transverse compression strength	Y_C	MPa
Laminar transverse compression modulus	E_{2C}	GPa
Laminar longitudinal/transverse shear strength	S	MPa
Laminar longitudinal/transverse shear modulus	G_{12}	GPa
Laminar bending strength	σ_b^f	MPa
Laminar bending modulus	E^f	GPa
Laminar interlaminar shear (SBS) strength	τ_b^i	MPa
Laminate longitudinal tensile strength	σ_{xt}	MPa
Laminate longitudinal tensile modulus	E_{xt}	GPa
Laminate transverse tensile strength	σ_{yt}	MPa
Laminate transverse tensile modulus	E_{yt}	GPa
Laminate principal Poisson's ratio	ν_{xy}	
Laminate shear strength	S_x	MPa
Laminate shear modulus	G_{xy}	GPa
Laminate longitudinal compression strength	σ_{xc}	MPa
Laminate longitudinal compression modulus	E_{xc}	GPa
Laminar transverse compression strength	σ_{yc}	MPa
Laminar transverse compression modulus	E_{yc}	GPa
Laminate longitudinal bending strength	σ_x^f	MPa
Laminar model-I fracture toughness	G_{IC}	J/m ²
Laminar model-III fracture toughness	G_{IIIC}	J/m ²
Laminate open-hole tensile strength	σ_t^{OP}	MPa
Laminate open-hole compression strength	σ_C^{OP}	MPa
Laminate compression strength after impact	CAI	MPa
Density	ρ	g/cm ³
Void content	V_v	%
Fiber volume content	V_f	%
Longitudinal thermal expansion coefficient	α_1	K ⁻¹
Transverse thermal expansion coefficient	α_2	K ⁻¹
Longitudinal moisture expansion coefficient	β_1	
Transverse moisture expansion coefficient	β_2	
Thermal conductivity	λ	W/(m · K)
Specific thermal capacity	c	J/(kg · K)
Thermal diffusion coefficient	D_t	m ² /s
Laminar thickness	t	mm
Glass transition temperature, T _g	T_g	°C

different applications. In terms of curing temperature, the epoxy resins used for aerospace applications can be generally divided into three classes: low-temperature (cure temperature $-80\text{ }^{\circ}\text{C}$), medium-temperature (cure temperature $-120\text{ }^{\circ}\text{C}$), and high-temperature (cure temperature $150\text{--}180\text{ }^{\circ}\text{C}$) curing epoxy resins with a service temperature below $130\text{ }^{\circ}\text{C}$ under wet conditions and below $150\text{ }^{\circ}\text{C}$ under dry conditions. Modifications of epoxy resin composites are basically done by modifications to the epoxy resin matrixes to increase toughness and to maintain other high-performance properties.

1.3.1.1 Performance of High-Temperature Curing Epoxy Composites

The first generation of composite structures for use in airplane applications was carbon fiber-reinforced epoxy 648 in China, and it has been more than ten years since its introduction. Comprehensive design and application data have been accumulated for this composite system. Epoxy 648 is the first generation of high-temperature curing epoxy resins with advantages like a long shelf life, good drape ability, and a simple curing process. Its drawbacks are brittleness and low hot/wet resistance. The second generation of high-temperature curing epoxy resins developed in China is the 5222 resin system containing TGDDM/DDS as the main chemical component. It is equivalent to the 3506 and 5208 resins in the USA and the BG-2526 resin in Russia. Design data are widely available for this resin system, and good processing performance can be provided, but low hot/wet resistance and toughness still pose obstacles to its application. In the late 1980s to the 1990s, a new generation of epoxy resins was developed with the aim of further improving hot/wet resistance and toughness. The main products include 5224, 5228, and 5288. Among these, the hot/wet resistance and toughness of epoxy 5224 have been improved and good processing performance has been maintained, while epoxy 5228 and epoxy 5288 have excellent toughness, but their drape ability is lower because of the higher amount of thermoplastic toughening agents added.

(1) A review of high-temperature curing epoxy composites in China

The high-temperature curing epoxy composites available in China are given in Table 1.32.

(2) Physical properties of the high-temperature curing epoxy composites available in China

The physical properties of the high-temperature curing epoxy composites in China are shown in Table 1.33, and their thermal physical properties are listed in Table 1.34.

(3) Mechanical properties of high-temperature curing epoxy composites in China

The mechanical properties of high-temperature curing epoxy composites in China are given in Table 1.35, the hot/wet resistance mechanical properties are

Table 1.32 High-temperature curing epoxy composites available in China

Designation	Composition	Company	Application	Features
HT3/5222	Multifunctional group epoxy, amine curing agent, HT3 high-strength CF	Beijing Institute of Aeronautical Materials	Some aircraft structures	Suitable for autoclave, hot-press molding and thermal expansion processes. Parts are high temperature resistant and can serve wet/80 °C, dry/120 °C
HT3/HD03	HD03 epoxy resins, HT3 high-strength CF	Xi'an Aircraft Industry Company	Vertical tail stabilizer, rudder, fin and space parts	Suitable for autoclave, hot-press molding and thermal expansion processes. Good processing ability, parts are high temperature resistant and can serve at 120 °C
HT3/NY9200G	NY9200G epoxy resins, HT3 high-strength CF	Nanchang Aircraft Industry Company	Vertical stabilizer and rudder in training and other airplanes	Suitable for autoclave, hot-press molding processes. Parts have good mech. performance and medium resistance, cure temp. 175 °C and can serve at 120 °C
HT3 and G803, G827/5224	5224 epoxy resins, HT3 high-strength CF, Carbon cloth 803,827	Beijing Institute of Aeronautical Materials	Helicopter body parts	Suitable for autoclave, hot-press molding processes. Parts have good mech. performance, good medium resistance, and fatigue resistance and can serve at 120 °C over a long period
HT3 and HT8/5228	5228 epoxy resins, HT3 and HT8 high-strength CF	Beijing Institute of Aeronautical Materials	XX antenna Candidate materials for wing skins in integrity of wing/fuselage	Suitable for autoclave, hot-press molding processes to make plane primary structures. Parts have good toughness and comprehensive performance, can serve at -55-130 °C over a long period
HT3 and HT8./5288	5288 epoxy resins, HT7 and HT8 high-strength CF	Beijing Institute of Aeronautical Materials	Candidate materials for wing skins in integrity of wing/fuselage	Suitable for autoclave, hot-press molding processes to make plane primary structures. Parts have good toughness and comprehensive performance and can serve at -55-130 °C over a long period

Table 1.33 Physical properties of high-temperature curing epoxy composites in China

Performance	HT3/5222	HT3/5224	HT3/5228	HT8/5228	HT7/5288	HT8/5288	HT3/HD03	HT3/NY9200G
$\rho/\text{g} \cdot \text{cm}^{-3}$	1.55–1.60	1.57	1.57	1.59	1.58	1.59	1.50–1.61	1.5–1.61
$V_v/\%$	<2	<1.0	<1.0	<1.0	<1.0	<1.0	<2	<1.5
$V_f/\%$	62–68	60–65	63 ± 3	63 ± 3	60 ± 3	60 ± 3	62–68	65 ± 5
$T_g/^\circ\text{C}$	258	230	220	220	220	220	182	150
Service temp./ $^\circ\text{C}$	120	130	130	130	130	130	125	120

Table 1.34 Thermal physical properties of high-temperature curing epoxy composites in China

Performance	$\alpha_1/10^{-6} \text{ K}^{-1}$	$\alpha_2/10^{-6} \text{ K}^{-1}$	$\lambda/W \cdot (\text{m} \cdot \text{K})^{-1}$ (thick direction)	$D_t/10^{-6} \text{ m}^2 \cdot \text{s}^{-1}$ (thick direction)	$c/J \cdot (\text{kg} \cdot \text{K})^{-1}$
HT3/52222	0.1–0.12	25–31	0.76–0.99	0.44–0.53	1000

given in Table 1.36, and the interlaminar toughness and damage-dependent properties are given in Table 1.37.

(4) Epoxy 648 composite performance

Epoxy 648 is a phenolic-type epoxy resin and was developed in the 1960s. It is referred to as epoxy 4211. The data presented here were obtained experimentally and can be used as a reference. All the data are of the classical allowable base except those indicated as B-allowable values.

In Table 1.38, for the basic mechanical properties of HT3/4211 epoxy composites, the data with an * are the average value of 30 specimens prepared using unidirectional laminates with a fiber volume content of $60 \pm 3\%$ and a void content of less than 2%.

The mechanical property data for the HT3/4211 epoxy composite tested at 25 °C and 100 °C are given in Table 1.39. The specimens were prepared using unidirectional laminates with a fiber volume content of $60 \pm 3\%$ and a void content less than 2%. The data marked with an * are experimental results from tests at 110 °C.

In Table 1.40, the mechanical properties of the HT3/4211 laminate composite are listed.

The physical properties of HT3/4211 laminates are given in Tables 1.41, 1.42, 1.43, 1.44, and 1.45.

Table 1.46 lists the thermal cycling effects on the mechanical properties of HT3/4211 composites.

1.3.1.2 Performance of Medium-Temperature Curing Epoxy Composites

Medium-temperature curing epoxy composites have advantages such as good performance, short processing cycles, lower costs compared with high-temperature curing resins, a maximum service temperature usually below 100 °C. Carbon fiber-reinforced epoxy 3234 composites give good combined performances. Resin systems have good performance stability and a long shelf life at room temperature (2 months). They are suitable for a wide range of applications. G814NT/3233 is a type of composite with a flame-retardant property and superior impact resistance as well as fatigue resistance. HT3/NY9200Z is mostly used for composite repair. HT3/HD58 has very limited applications.

Table 1.35 Basic mechanical properties of high-temperature curing epoxy composites in China

Performance	HT3/ 5222	HT3/ 5224 ^a	HT3/ 5228	HT8/ 5228	HT7/ 5288	HT8/ 5288	G803/ 5224	G827/ 5224	HT3/ HD03	HT3/ NY9200G ^a
X_c /MPa	1490	1400	1744	2405	2880	2630	573	1300	1854.8	1430
E_{1l} /Gpa	135	140	137	155	146	172	71.6	136	141.0	143
ν_{12}	0.28	0.35			0.334	0.35	0.06	0.316	0.348	0.31
X_c /Mpa	1210	1100	1230	1800	1470	1480	693	1180	1257.9	1174
E_{1c} /Gpa	134	120	110	150	128	169	66.2	111	143.7	143
Y_c /Mpa	40.7	50	81	65	66	62			65.1	48
E_{2l} /Gpa	9.4	8.6	8.8	9.4	9.69	7.0			9.1	9.3
Y_c /Mpa	197.0	180	212	205	210	213			200.2	209
E_{2c} /Gpa	10.8	9.0	9.3	9.4	11.0	8.1			9.6	9.3
S /Mpa	92.3	99	124	104		109	94.1	104	82.7	77
G_{12} /Gpa	5.0	50	4.4	5.4		3.9	4.06	4.9	5.1	4.9
σ_b^i /MPa	1860	1600	1780	1600	1770	1830	845	1630		
E^i /Gpa	121	108	130	154	120	151	59	110		
τ_b^i /Mpa	100	97	106	105		107	78	105		

^aHT3/5224 and HT3/NY9200G are B-allowable; others are classically allowable

Table 1.36 Hot/wet resistant mechanical properties of high-temperature curing carbon/epoxy composites in China

Performance	HT3/5222	HT3/5224 (48 h in boiling water)			HT8/5228				
	120 °C, 1% moisture absorption	Room temp.	70 ° C	120 ° C	Room temp. (dry)	130 ° C (dry)	150 ° C (dry)	170 ° C (dry)	130 ° C (wet) ^a
X_t /Mpa	1557								
E_{1t} /Gpa	112								
ν_{12}	0.30								
X_c /Mpa	1016								
E_{1c} /Gpa	125								
Y_t /Mpa	15.7								
E_{2t} /Gpa	5.9								
Y_c /Mpa	136.0								
E_{2c} /Gpa	8.1								
S /MPa	70.6								
G_{12} /GPa	2.7								
σ_b^t /MPa		1550	1400	1120	1830	1780	1258	1101	1112
E^t /GPa		106	108	110	151	134	139	143	137
τ_{12}^t /MPa		92	75	50	107	58	59	53	45

Note Courtesy of Beijing Institute of Aeronautical Materials

^aRefers to 48 h of immersion in soft water at 95–100 °C

- 1) Review of medium-temperature curing epoxy composites in China in Table 1.47 introduces the medium-temperature curing epoxy composites available in China.
- 2) Physical properties of medium-temperature curing epoxy composites available in China in Table 1.48 list the physical properties of medium-temperature curing epoxy composites in China.
- 3) The mechanical properties of medium-temperature curing epoxy composites in China in Table 1.49 list the basic mechanical properties of medium-temperature curing epoxy composites available in China. Their hot/wet performances are listed in Table 1.50.

1.3.1.3 Performance of Low-Temperature Curing Epoxy Composites

- (1) Review of low-temperature curing epoxy composites available in China

Low-temperature curing epoxy composites are expensive because of the very expensive molds and tools and high-energy-consuming equipment. If high-performance auxiliary material costs can be significantly reduced, the part costs would be relatively low. For low-temperature cured composite parts, low deformation, high dimensional precision, and stability can be expected. The HT3/

Table 1.37 Interlaminar toughness and damage-dependent properties of high-temperature curing carbon/epoxy composites in China

Performance	HT3/5222	HT3/5224	HT3/5228	HT8/5228	HT7/5288	HT8/5288	HT3/NY9200G
σ_t^{OP}/MPa			333	473		464	322
σ_c^{OP}/MPa			341	316		274	309
CAI/MPa	151.1	182	190	230 ^a	260	245	173
$G_{IC}/J \cdot m^{-2}$		208	227			470	175
$G_{IIC}/J \cdot m^{-2}$		375	1105			765	348

^aSACMA SRM2-88 impact testing standard, others of the NASA RP 1142 specification

Table 1.38 Basic mechanical properties of HT3/4211 epoxy composites

Performance	Average value	Mean square deviation	$C_V/\%$	B-allowable base
X_t/MPa	1415	161	11	1186
E_{1t}/GPa	126	4.5	4	
ν_{12}	0.33	0.02	5	
Y_t/MPa	35.0	9.27	26	21.0
E_{2t}/GPa	8.0	0.5	6.0	
X_C/MPa	1232	140	12	928
E_C/GPa	116	4.9	4.0	
Y_C/MPa	457	31.5	20	100.2
E_{2C}/GPa	8.34	0.85	10	
S/MPa	63.9*	11.3	18	46.5
G_{12}/GPa	3.7*	0.21	5.6	
σ_b^f/MPa	1590*	78	4.7	
E^f/GPa	120*	3.7	3.1	
τ_b^i/MPa	82.6*	0.2	7.5	

Table 1.39 High-temperature mechanical properties of the HT3/4211 unidirectional laminate

Performance	Test temperature/ $^{\circ}\text{C}$			
	25		100	
	Typical value	$C_V/\%$	Typical value	$C_V/\%$
X_t/MPa	1300	7.7	1179	
E_{1t}/GPa	146	2	140*	
Y_t/MPa	49.3	12	30.6	
E_{2t}/GPa	9.2	3	6.1	
X_C/MPa	1204	7	789	9.4
E_{1C}/GPa	150	4	123*	
Y_C/MPa	159.2	5.0	113.7	17.4
E_{2C}/GPa	9.0		5.8*	
S/MPa	71.5	4.3	55.9	3.7
G_{12}/GPa	4.7			
$\sigma_b^f Z/\text{MPa}$	1650	6.5	1166	5.6
E^f/GPa	122	8.9	113	3.6
$\tau_b^i Z/\text{MPa}$	87.6	5.9	56	4.4

LT01 composite system developed for autoclave low-temperature curing can be used at medium service temperatures. Their performance is equivalent to medium-temperature cured composite systems, and their maximum service temperatures are 80–100 $^{\circ}\text{C}$. Low-temperature curing and pressure bag mold HT7/LT-03 composites eliminate high energy consumption and dimension limitations.

Table 1.40 Mechanical properties of HT3/4211 laminate composites

Stack code	σ_x /MPa	σ_y /MPa	ϵ /%	E_x /GPa	E_y /GPa	ν_{xy}	σ_{xz} /MPa	σ_{yz} /MPa	E_{xz} /GPa	E_{yz} /GPa
1	134.9	134.9	1.80	15.55	15.55	0.760	160.3	160.3	14.30	14.30
2	531.1	150.5	1.01	49.91	22.58	0.749	448.9	192.4	45.76	25.07
3	896.4	141.0	0.97	84.87	19.96	0.710	641.8	227.8	74.54	21.61
4	1080.2	76.0	0.94	109.03	16.12	0.590	807.1	131.2	107.12	17.97
5	1427.0	45.6	0.93	135.46	8.76	0.318	1124.0	185.7	132.35	10.44
6	150.5	531.1	0.76	22.58	49.91	0.345	192.4	448.9	25.07	45.76
7	511.0	511.0	0.98	52.42	52.42	0.330	516.1	516.1	54.68	54.68
8	696.0	436.6	0.94	72.36	48.31	0.220	689.8	411.5	74.39	45.98
9	1024.4	356.2	0.85	109.77	42.78	0.075	918.9	462.6	89.56	45.76
10	141.0	896.4	0.77	19.96	84.87	0.197	227.8	641.8	21.61	74.54
11	436.6	696.0	0.84	48.31	72.36	0.126	411.5	689.8	45.98	74.39
12	801.2	801.2	0.97	76.26	76.26	0.038	738.0	738.0	66.28	66.28
13	76.0	1080.2	0.54	16.12	109.03	0.101	131.2	807.1	17.97	107.12
14	356.2	1024.4	0.79	42.78	109.77	0.022	462.6	918.9	45.76	89.56
15	45.6	1427.0	0.51	8.78	135.46	0.018	185.7	1124.0	10.44	132.35

Note The stack codes are listed below

- 1 [-45/+452/-452/+452/-45]_s
- 2 [+45/-45/02/-45/+452/-45]_s
- 3 [+45/-45/02/-45/+45/02]_s
- 4 [02/+45/-45/04]_s
- 5 [0]₁₆
- 6 [-45/+45/902/+45/-452/+45]_s
- 7 [+45/-45/0/90/-45/+45/0/90]_s
- 8 [02/45/-45/90/0/900]_s
- 9 [02/90/02/90/02]_s
- 10 [-45/+45/902/+45/-45/902]_s
- 11 [902/-45/+45/0/90/0/90]_s
- 12 [0/902/02/902/0]_s
- 13 [902/45/-45/904]_s
- 14 [902/0/902/0/902]_s
- 15 [90]₁₆

Table 1.41 Density of the HT3/4211 laminate composites

Laminar stacking	Density $\rho/g \cdot cm^{-3}$	Laminar stacking	Density $\rho/g \cdot cm^{-3}$
[0] ₁₆	1.57	[±45] ₄₅	1.558

Table 1.42 Linear expansion coefficient of HT3/4211 laminate composites

Laminate code	θ	Test direction	$\alpha (20-T)/10^{-6} K^{-1}$				
			70	90	110	130	150
[0] ₁₆	0°	0°	0.02	0.09	0.07	0.11	0.12
		15°	1.94	2.0	2.1	2.2	2.2
		30°	7.3	7.6	7.7	7.8	8.0
		45°	14.8	15.5	15.7	15.9	16.2
		60°	21	22	22	22	23
		75°	26	28	28	28	28
		90°	28	30	30	30	31
[± θ] ₄₅	0°	0°	-0.12	-0.03	0.01	0.07	0.13
		15°	-1.69	-1.71	-1.71	-1.79	-1.79
		30°	-4.5	-4.8	-4.9	-5.3	-5.8
		45°	4.0	4.0	4.1	4.1	4.1
		60°	21	22	23	24	26
		75°	32	33	35	36	37
		90°	34	36	37	38	40
[0 ₂ /± θ] _{2s}	0°	0°	-0.12	-0.03	0.01	0.07	0.13
		15°	-0.94	-1.02	-0.95	-0.92	-0.97
		30°	-1.45	-1.51	-1.46	-1.41	-1.46
		45°	-0.15	-0.15	-0.12	-0.07	-0.09
		60°	1.34	1.30	1.35	1.40	1.43
		75°	2.4	2.4	2.5	2.5	2.6
		90°	2.7	2.7	2.8	2.8	2.9
[90 ₂ /± θ] _{2s}	0°	0°	2.7	2.7	2.8	2.8	2.8
		15°	2.9	2.9	3.0	3.1	3.2
		30°	5.5	5.6	5.7	5.9	6.0
		45°	13.6	14.1	14.3	14.8	15.2
		60°	26	26	27	28	29
		75°	30	31	32	33	35
		90°	34	36	37	38	40
[45/0/-45/90/-45/0/45/90/0/90] _s		0°	2.1	2.1	2.2	2.3	2.4
		90°	2.6	2.7	2.6	2.6	2.6
[45/-45/90/0/90] _s		0°	2.8	2.8	2.8	2.9	2.9
		90°	1.19	1.15	1.16	1.17	1.17
[0 ₂ /±45/0 ₄] _s		0°	-0.06	-0.10	-0.06	-0.06	-0.08
		90°	16.6	17	18	18.6	18.7
[0 ₂ /±45/0 ₂ /±45] _s		0°	-0.08	-0.20	-0.19	-0.23	-0.26
		90°	11.1	11.8	12.1	12.2	12.4

Table 1.43 Thermal conductivity of HT3/4211 laminates

Laminates	Test direction	Thermal conductivity $\lambda/W \cdot (m \cdot K)^{-1}$			
		60 °C	75 °C	95 °C	115 °C
[0] ₁₆	Thick direction	0.72	0.76	0.78	0.82
[±45] ₄₅	Thick direction	0.76	0.78	0.80	0.86

Table 1.44 Specific thermal capacity of HT3/4211 laminates

Laminate	Average temperature/°C	Average specific thermal capacity $C/J \cdot (kg \cdot K)^{-1}$
[0] ₁₆	60	972
[±45] ₄₅	60	990

Table 1.45 Thermal diffusion coefficient of HT3/4211 laminates

Laminate	Test direction	Average temperature/°C	Thermal diffusion coefficient $D_T/10^{-6}m^2 \cdot s^{-1}$
[0] ₁₆	Thickness direction	60	
[± 45] ₄₅	Thickness direction	60	

Table 1.46 Thermal cycling effects on the mechanical properties of HT3/4211 composites

Performance	Thermal cycle number/times	[0] ₁₆		[(45/0-45) ₂ -45/0/45]	
		Longitudinal	Transverse	Longitudinal	Transverse
X_t 0 °tensile strength (20 °C)/MPa	0	1472		635	148
	200	1420		625	146
E_{11} 0 °tensile modulus (20 °C)/GPa	0	143		47	20
	200	118		50	21
X_t 0 °tensile strength (130 °C)/MPa	0			586	143
	200			604	140
E_{11} 0 °tensile modulus (130 °C)/MPa	0			39	15
	200			40	15
τ_b^i Z interlaminar shear strength/MPa	0			67	38
	200			66	36
σ^f /MPa	0			916	322
	200			889	312
E^f /GPa	0			54	23
	200			55	22
Compression strength σ_c /MPa	0			591	220
	200			611	222

(continued)

Table 1.46 (continued)

Performance	Thermal cycle number/times	[0] ₁₆		[(45/0-45) ₂ -45/0/45]	
		Longitudinal	Transverse	Longitudinal	Transverse
Compression modulus E_c /GPa	0			51	20
	200			54	20
Thermal expansion coefficient $\alpha/10^{-6} \text{ K}^{-1}$	0			0.68	9.9
	200			0.64	9.0

Table 1.47 Medium-temperature curing epoxy composites available in China

Designation	Composition	Company	Application	Features
HT3, G827, G803, G814NT, and 750/3234	Epoxy 3234 resins, HT3 high-strength CF, C cloth G827, G803, G814NT and G cloth 759	Beijing Institute of Aero Materials	In helicopter part applications	Suitable for autoclave, hot-press molding, soft mold molding, and vacuum bag molding processes. Parts have good hot/wet resistance, serve at -55-80 °C
HT3/HD58	Epoxy HD58 resins, HT3 high-strength CF	Xi'an Aircraft Industry Company	Vertical tail trial part in the Y7 airplane	Suitable for autoclave, hot-press molding, soft mold molding and vacuum bag molding processes. Parts serve at -55-80 °C
HT3/NY9200Z	Epoxy NY9200G resins, HT3 high-strength CF	Nanchang Aircraft Industry Company	Repair of composite parts	Curing temp. 90 °C, parts serve below 80 °C

Table 1.48 Physical properties of medium-temperature curing epoxy composites

Performance	G814NT/3233	G827/3234	G803/3234	G814NT/3234	G803/3236	G8031/3242	HT3/NY9200Z
$\rho/\text{g} \cdot \text{cm}^{-3}$	1.52	1.52	1.53	1.55		1.45	
$V_v/\%$	<1.0	<1.0	<1.0	<1.0	<1.0	<1.0	<2
$V_f/\%$	55	56	57	60	50 ± 3	54-60	65 ± 5
$T_g/^\circ\text{C}$	120-140	162	162	162	130	≥ 100	115

Table 1.49 Basic mechanical properties of medium-temperature curing epoxy composites

Performance	G814NT/3233		G827/3234		G803/3234		G814NT/3234	
	R.T.	80 °C	R.T.	80 °C	R.T.	80 °C	R.T.	80 °C
X_f /MPa	670	610	1656	1153	756	748	673	630
E_f /GPa	57	49	131	110	69	65	70	62
ν_{12}	0.07	0.084	0.332	0.317	0.064	0.063	0.062	0.063
X_C /MPa	410	320	903	500	557	437	423	430
E_{1c} /GPa	57	47	110	95	64	60	63	
Y_f /MPa								
E_{2f} /GPa								
Y_C /MPa								
E_{2c} /GPa								
S /MPa	110	85	114	104	118	99	118	98
G_{12} /GPa	2.8	2.3	3.6	3.4	4.2	4.0	4.1	3.7
σ_b^z /MPa	780	530	1647	1430	924	772	847	725
E^z /GPa	52	52	111	110	59	62	59	61
τ_b^z /MPa	59	39	89	66	68	56	66	53
Performance	G803/3236		G803/3242		G803/3242		HT3/NY9200Z	
R.T.	HT3/3234		R.T.		60 °C			
X_f /MPa	567		507	700	692	1747	1632	
E_{1f} /GPa	53.6		52.7	56	54	137	137.3	
ν_{12}	0.061		0.074			0.312	0.33	
X_C /MPa	453		361			1357	1179	
E_{1c} /GPa	57		56.2			136	121	
Y_f /MPa				700	660	67	63.9	
E_{2f} /GPa				56	52	9.3	7.82	
Y_C /MPa						170	192	
E_{2c} /GPa						9.4	9.0	
S /MPa	112		78.4			124	123	

(continued)

Table 1.49 (continued)

Performance	G814NT/3233		G827/3234		G803/3234		G814NT/3234	
	R.T.	80 °C	R.T.	80 °C	R.T.	80 °C	R.T.	80 °C
$G_{1/2}$ /GPa	3.49		2.83				5.3	4.1
σ_b^f /Z/MPa	809		628		870	650	1615	
E^f /GPa	51.7		53.6		63	60	132	
τ_b^f /Z/MPa	64.6		43.5		60	50	93	

Table 1.50 Hot/wet resistance in medium-temperature curing epoxy composites

Performance		G814NT/3233	G827/3234	G803/3234	G814NT/3234
σ_b^f /MPa	Boiling water A	560	1120	696	654
	Boiling water B	780	1580	890	666
E^f /GPa	Boiling water A	69	100	58	57
	Boiling water B	52	106	60	63
τ_b^i /MPa	Boiling water A	37	59	52	46
	Boiling water B	55	75	62	67

Note 1. In boiling water A, specimen immersed in a vapor water container and put in an oven for 48 h at 100–105 °C

2. In boiling water B, specimen after water A treatment and immediately dried for 24 h at 100–105 °C

3. Test performed at R.T.

This method takes advantage of low-temperature composite curing and is far more suitable for large composite structure manufacturing and low-cost composite production. The long-term service temperature of the parts is -55–80 °C.

Low-temperature curing epoxy composites are supplied by the Beijing Institute of Aeronautical Material (BIAM) and are basically used in unmanned aircraft.

(2) Physical properties of low-temperature curing epoxy composites available in China

Table 1.51 lists the physical properties of low-temperature curing epoxy composites in China.

(3) Mechanical properties of low-temperature curing epoxy composites available in China

The mechanical properties of low-temperature curing epoxy composites available in China are listed in Table 1.52. Their hot/wet resistance is listed in Table 1.53. Their interlaminar toughness and damage-dependent performances are listed in Table 1.54.

Table 1.51 Physical properties of low-temperature curing epoxy composites

Performance	HT3/LT-01A	G803/LT-01A	HT3/LT-01	HT7/LT-03
ρ /g · cm ⁻³	1.5–1.55	1.5–1.55	1.54–1.60	1.50–1.58
V_v /%	<1	<1.5	<1	<2
V_f /%	55–60	55 ± 3	63 ± 3	60 ± 3
T_g /°C	153	153	210	210

Table 1.52 Basic mechanical properties of low-temperature curing epoxy composites

Performance	HT3/LT-01A	G803/LT-01A	HT3/LT-01	HT7/LT-03	HT3/LT-03
X_t /MPa	1537	620	1560	2377	1545
E_{1t} /GPa	121	59.5	136	120	119
ν_{12}	0.31		0.31	0.316	0.329
X_C /MPa	1064	403	1380	1074	1023
E_{1c} /GPa	116		136	128	119
Y_t /MPa	57.8	614	43.7	42.8	171
E_{2t} /GPa	6.44	57.6	8.1	7.3	7.0
Y_C /MPa	142	403	215	128	85.6
E_{2c} /GPa	6.4		8.1	7.2	4.38
S /MPa	104		83.7	104	
G_{12} /GPa	3.8		4.9	4.7	
σ_b^f /MPa	1329	670	1627	1497	1385
E_b^f /GPa	111	55.1	135	120	113
τ_b^i /MPa	78.6	51	94.6	75	66

Table 1.53 Hot/wet resistance of low-temperature curing epoxy composites

Performance	HT3/LT-01A		G803/LT-01A		HT3/LT-01		HT7/LT-03	
	80 °C (dry)	80 °C (wet)	80 °C (dry)	80 °C (wet)	130 °C (dry)	130 °C (wet)	80 °C (dry)	70 °C (wet)
X_t /MPa	1509	1450	601	595	1550		2310	
E_{1t} /GPa	120	118.5	58.5	57.7	130		120	
ν_{12}								
X_C /MPa	811	709.4	342	233	1224	964	926	
E_{1c} /GPa					130		7	
Y_t /MPa			598	555			34.6	
E_{2t} /GPa			57.6	52.8			6.78	
Y_C /MPa				232			96	
E_{2c} /GPa							6.8	
S /MPa	91.5	45.1			67.9		83.8	
G_{12} /GPa	3.4				4.11		4.1	
σ_b^f /MPa	1054	943	597	447	1321	1045	1198	994
E_b^f /GPa	107	107	54.9	48	133	121	113	112
τ_b^i /MPa	64.4	45.1	45.9	27.6	65.5	43.6	62	43.4

Note Wet specimen immersed in water for 48 h at 95–100 °C

Table 1.54 Interlaminar toughness and damage-dependent performance of low-temperature curing epoxy composites

Performance	HT3/LT-01A	HT3/LT-01	HT7/LT-03
σ_t^{OP} /MPa	273	257	482
σ_C^{OP} /MPa	258	207	277
CAI/MPa	187	156	195
G_{IC} /J · m ⁻²		122	309
G_{IIC} /J · m ⁻²		326	761

1.3.1.4 Processing Performance of Epoxy Resin Matrix Composites

As shown in Table 1.55, compared with bismaleimide resin, polyimide resin and various thermoplastic composites, and epoxy resin matrix composites have several good processing properties. These include good tack and drape ability, low curing temperature and pressure (usually below 0.7 MPa) as well as suitability for autoclave processing and RTM. Hot-press molding processes can be used to manufacture a variety of composites in different shapes.

Most of the current epoxy resins are suitable for autoclave and hot-press molding processes. LT-03 resin systems are specialized materials for low-temperature vacuum bag processing. Furthermore, in thermal compression molding techniques (mainly autoclave and hot-press molding), prepregs are prepared first. Hot melting prepreg preparations have advantages compared with wet wound preparations, for example, higher production rates, better product quality, less pollution, and good processing performance. Most epoxy resin systems available in China can be used in hot melting preparations of continuous fiber or fabric prepregs.

Table 1.55 Processing performance of epoxy composites

Material designation	Processing ability	Processing technique	Cure temperature/°C	Cure cycle
G803/3234	Proper tack, easy drape	Autoclave, press molding	125	Simple
G827/3234			125	
G814NT/3234			125	
G803/3242			125	
G814NT/3233			125	
HT3/NY9200Z			125	Need temperature maintenance
HT3/NY9200G			175	
HT3/4211			175	
HT3/5222			180	
HT3/HD02			175	
HT3/5222	180	Simple		
G803/5222	180			
G827/5224	Autoclave, press molding vacuum bag		180	
HT3/5228	Poor tack, heated	Autoclave, press molding	180	Need free state post-treatment
HT8/5288	Drape		180	
HT3/LT-01A	Proper tack, easy drape	Vacuum bag	70	
G803/LT-01A			70	
HT3/LT-01			75	
HT7/LT-03			75	

1.3.1.5 Evaluation of the Performance of Epoxy Resin Matrix Composites in China

A comprehensive evaluation and comparison of the performance of epoxy resin matrix composites available in China are listed in Table 1.56.

1.3.2 Bismaleimide Resin Matrix Composite Performances

1.3.2.1 Review of Bismaleimide Resin Matrix Composites Available in China

The bismaleimide resin matrix composites available in China are summarized in Table 1.57.

1.3.2.2 Mechanical Properties of BMI Composites

The mechanical properties of BMI composites available in China are listed in Tables 1.58 and 1.59. Their hot/wet resistance is listed in Tables 1.60, 1.61, 1.62, and 1.63. Their interlaminar toughness and damage-dependent performances are listed in Table 1.64.

1.3.2.3 Processing Performance of BMI Resin Matrix Composites

The processing performance data for BMI resin matrix composites are listed in Table 1.65.

1.3.2.4 Evaluation of BMI Resin Matrix Composite Performance in China

A comprehensive evaluation and comparison of BMI resin matrix composite performances in China are listed in Table 1.66.

1.3.3 Polyimide Resin Matrix Composite Performance

1.3.3.1 Review of Polyimide Resin Matrix Composites in China

The polyimide resin matrix composite systems available in China are listed in Table 1.67.

Table 1.56 Evaluation of the performance of epoxy resin matrix composites

Designation	Basic mechanical performance	Hot/wet resistance	Toughness ^a	Processing ^a	Max. service temperature/°C	
					Dry	Wet
HT3/LT-01A	Moderate	Good	4	8	100	80
HT3/LT-01	Higher	Superior	4	8	150	130
HT7/LT-03	Moderate	Good	4	8	80	70
G 803/3234	Moderate	Good	4	8	100	70
G 827/3234	Higher	Good	4	8	100	70
G 14NT/3234	Moderate	Good	4	8	100	70
HT3/NY9200Z	Higher	Good	4	6	80	70
G814NT/3233	Moderate	Good	4	8	80	70
HT3/4211	Higher	Bad	1	6	150	100
HT3/NY9200G	Higher	Good	4	6	120	100
HT3/HD03	Higher	Bad	2	4	150	120
HT3/5222	Higher	Bad	2	4	150	120
G827/5224	Higher	Good	6	6	150	120
HT3/5228	Higher	Superior	6	4	150	130
HT8/5288	High	Superior	6	4	150	130

^aThe number indicates performance grades; the larger the number, the better the performances

Table 1.57 The bismaleimide resin matrix composites available in China

Material system	Designation	Composition	Company	Application	Features
Modified BMI composite systems	HT3/5405	Toughened BMI resins, HT3 high-strength CF	North Western Polytechnical University and Beijing Institute of Aero materials	Aircraft wings	Good toughness, suitable for wet preparation of prepregs, long-term service at 130 °C
	HT3/QY8911	Propylene modified BMI resins, HT3 high-strength CF	Beijing Institute of Aviation Technology	Front fuselage sector, vertical stabilizer skin	Good processing performance, parts high temp. resistant, good toughness, long-term service at 150 °C
Toughened BMI composite systems	HT3/QY8911-III	Toughened BMI resins, HT3 high-strength CF	Beijing Institute of Aviation Technology	Under development	Good performance and toughness, service below 150 °C
	HT3, HT8/QY9511	Thermal plastic modified BMI 9511, HT3 and HT8 high-strength CF	Beijing Institute of Aviation Technology	Under development	Simple processing, good toughness, serve in wet conditions/−55–177 °C
	HT7/5428	Thermal plastic modified BMI 5428, HT7 high-strength CF	Beijing Institute of Aeronautical Materials	Under development	Superior toughness (CAI up to 260 MPa), good hot/wet, processing, mechanical performance, long-term service at 170 °C, post-curing at 210 °C
	HT7/5429	Thermal plastic modified BMI 5429, HT7 high-strength CF	Beijing Institute of Aeronautical Materials	Under development	Superior toughness (CAI up to 260 MPa), good hot/wet processing, mechanical performance, long-term service at 150 °C, post-curing at 200 °C

(continued)

Table 1.57 (continued)

Material system	Designation	Composition	Company	Application	Features
High temp. BMI composite systems	HT3/QY8911-II	Polyether sulfone modified BMI resins, HT7 high-strength CF	Beijing Institute of Aviation Technology	Missile skin, cabin segment	Good processing, post-curing temp below 230 °C, time less than 6 h, service at 230 °C
RTM special BMI composite systems	HT3/QY8911-IV	RTM special low-viscosity BMI resins, HT3 high-strength CF	Beijing Institute of Aviation Technology	Under development	Suitable for RTM and long-term service at 150 °C
	HT3/6421	RTM special low-viscosity BMI resins, HT3 high-strength CF	Beijing Institute of Aviation Technology	Under development	Suitable for RTM, good hot/wet resistance and fatigue resistance, long-term service at 180 °C
RTM special BMI composite systems	HT3,HT8/QY9512	RTM special low-viscosity BMI resins, HT3 and HT8 high-strength CF	Beijing Institute of Aviation Technology	Under development	Suitable for RTM and long-term service at 150 °C

1.3.3.2 Mechanical Properties of the Polyimide Resin Matrix Composites Available in China

The basic polyimide resin matrix composite systems available in China are listed in Table 1.68, and their high-temperature mechanical performance is listed in Table 1.69. Their interlaminar toughness and damage-dependent performances are listed in Table 1.70.

1.3.4 Performance of Advanced Resin Matrix Composites from Global Sources

There are many global sources of advanced resin matrix structural composites, and these are of different types, grades, and performance to meet the different requirements of aerospace applications. Some of the most commonly used and generally accepted composites will be introduced.

Table 1.58 Basic mechanical properties of C fiber/BMI composites (1)

Performance	HT3/QY8911		HT3/5405		HT3/ QY8911-III	HT8/ QY8911-III	HT3/ QY9511	HT8/ QY9511
	Classical allowable	B-allowable	Solution prepregs	Melting prepregs				
X_t /MPa	1548	1239	1660	1841	1464	2319	1530	2741
E_{1t} /GPa	135		135	157	135.4	149.1	75	163
ν_{12}	0.33		0.34	0.36		0.289	126	
X_c /MPa	1426	1281	1033	1102		1491	10	1513
E_{1c} /GPa	126		136	144		149	177	163
Y_t /MPa	55.5	38.7	75	88.6	78	68		70
E_{2t} /GPa	8.8		8.1	9.2	9.8	9.6		9.1
Y_c /MPa	218	189.4	170	186				
E_{2c} /GPa	10.7		8.1	10.3				
S /MPa	89.9	81.2	140	126		99	98	91
G_{12} /GPa	4.47		4.1	4.59		5.0	4.7	4.8
σ_b^f /MPa	1915		1750	1810	1841	1631	1868	1830
E^f /GPa	134		120	122	124.4	147.5	128	178.8
τ_b^i /MPa	110.5		97	101	114	114	121	105

Table 1.59 Basic mechanical properties of C fiber/BMI composites (2)

Performance	HT7/5428	HT7/5429	HT3/QY8911-II	HT3/QY8911-IV	HT3/YQ9512	HT8/YQ9512	HT3/6421
X_t /MPa	2150	2010	1537	1425	1464	2413.0	1670
E_{1t} /GPa	125	129	129.7	137.4	135.4	149.1	143
ν_{12}	0.32	0.31	0.324	0.303	0.289	0.289	
X_c /MPa	1210	1430	1305	1288		1493	
E_{1c} /GPa	107	116	129.7	137.4		149.1	
Y_t /MPa	65		60.7	58	77.6	67.6	
E_{2t} /GPa	7.8		9.0	9.5	9.84	9.65	
Y_c /MPa	220		209.3	209	209		
E_{2c} /GPa	10		10.4	9.5	9.5		
S /MPa	111		80.6	73		99.5	
G_{12} /GPa	5.6		5.2	5.6		5.04	
σ_b^f /MPa	1640	1530	1758	1830	1628		1730
E_b^f /GPa	120	100	120.5	124	113.8		138
τ_b^i /MPa	97	103	107.4	98	102		192

Table 1.60 Hot/wet resistance of C fiber/BMI composites (1)

Performance	HT3/QY8911				HT3/5405							
	130 °C (dry)	150 °C (dry)	150 °C (wet)	200 °C (dry)	R. T. (wet)	80 °C (dry)	80 °C (wet)	130 °C (dry)	130 °C (wet)	150 °C (dry)	150 °C (wet)	
X_C /MPa	1579	1448	1250		1835	1739	1787	1744	1653	1742	1558	
E_{11} /GPa	128	128			138	139	136	141	138	141	135	
ν_{12}						0.279		0.282		0.300		
X_C /MPa	1344	1221			977	1150	934	1200	741	1130	683	
E_{1C} /GPa	119	114				106		117		101		
Y_f /MPa	51.1	44.6	25.8		67	52	49	47	25	34	17	
E_{21} /GPa	9.2	8.2			8.0	7.1	7.4	6.1	4.8	4.8	2.7	
Y_C /MPa	172	154			136	182	126	143	87.8	150	75	
E_{2C} /GPa	8.2	7.9				10.6		11.7	11.1	10.1		
S /MPa	80.8	73.5	56.5		133	123 ^b	107	107	79	88	64	
G_{12} /GPa	4.0	3.5			3.86	3.42 ^b	3.2	3.14	1.85		0.65	
σ_b^f /MPa	1655	1725	986	1261	1556		1387	1276	927	1100		
E^f /GPa	131	136		131	118		115	119	113	116		
τ_b^f /MPa	82.8	77.0	54.0		86	69 ^b	68	61	49 ^c	57		

^aWet specimen immersed in soft water for 340 h at 71 °C^bTested at 90 °C^cIn boiling water for 48 h

Table 1.61 Hot/wet resistances of C fiber/BMI composites (2)

Performance	HT3/QY8911-III					HT8/QY8911-III						
	20 °C (dry)	130 °C (dry)	150 °C (dry)	20 °C ^a (wet)	130 °C ^a (wet)	150 °C ^a (wet)	20 °C (dry)	130 °C (dry)	150 °C (dry)	20 °C ^b (wet)	130 °C ^b (wet)	150 °C ^b (wet)
σ_b^f /MPa	1841	1550	1293	-	-	-	1597	1284	1021	-	-	-
E^i /GPa	124.4	127.6	124.7	-	-	-	145.1	146.9	143.3	-	-	-
τ_b^i /MPa	108	81	63	114	56	46	95	78	54	103	52	44

^aMoisture content 1%

^bIn boiling water for 48 h

Table 1.62 Hot/wet resistances of C fiber/BMI composites (3)

Performance	HT3/QY9511			HT8/QY9511						
	20 °C (dry)	150 °C (dry)	20 °C (wet)	150 °C (wet)	20 °C (dry)	150 °C (dry)	177 °C (dry)	20 °C (wet)	150 °C (wet)	177 °C (wet)
σ_b^f /MPa	1868	1685	–	1089	1830	1357	1386	–	1067	991
E^f /GPa	129	119	–	122	178.8	174	121	–	121	116
τ_b^i /MPa	121	83	110	–	105	71	62	111	53	–

Table 1.63 Hot/wet resistances of C fiber/BMI composites (4)

Performance	HT3/QY8911-IV			HT3/6421			HT3/5428			HT3/5429			
	20 °C (dry)	150 °C (wet)	20 °C (wet)	150 °C (wet)	20 °C (dry)	150 °C (dry)	180 °C (wet)	150 °C (wet)	180 °C (wet)	170 °C (dry)	170 °C (wet)	150 °C (dry)	150 °C (wet)
σ_b^f /MPa	1830	1420	1905	1123	1730	1420	1330	1380	1010	1240	950	1130	900
E_b^f /GPa	124	129	131.5	126.2	138	117	–	–	–	120	116	105	100
τ_b^i /MPa	98	64	97	54	92	70.6	56.4	58.8	50.4	64	48	55	42

Table 1.64 Interlaminar toughness and damage-depended performances of C fiber/BMI composites (relative to NASA RP 1142 impact testing standards)

Performance	HT3/QY8911	HT3/5405	HT3/QY8911-III	HT8/QY8911-III	HT3/QY9511	HT8/QY9511	HT3/QY9511	HT8/QY9511	HT3/QY8911-II	HT7/5428	HT7/5429	HT3/QY8911-IV	HT3/QY9512	HT8/QY9512
σ_t^{OP}/MPa	390.6	286	345	418	374	439	290	454	290	454	587	306	345.3	582.5
σ_c^{OP}/MPa	257.6	293	331	331	282	300	314	280	314	280	291	321	286	292
CAI/MPa	171	170	211	219	277	286	169 ^a	260	169 ^a	260	296	175 ^a	211	193.1
$G_c/\text{J}\cdot\text{m}^{-2}$	267	236	-	-	-	-	129	301	129	301	281	-	-	-
$G_{IC}/\text{J}\cdot\text{m}^{-2}$	252	130	-	-	-	-	502	780	502	780	764	-	-	-
$G_{IIC}/\text{J}\cdot\text{m}^{-2}$	665	-	-	-	-	-	635	-	635	-	-	-	-	-

^aRelative to SACMA SRM2-88 impact testing standards and others relative to NASA RP 1142 impact testing standards

Table 1.65 Processing performance data for BMI resin matrix composites

Material designation	Processing ability	Processing techniques	Curing temperature/time	Post-curing temperature/time	Curing cycle	Others
HT3/QY8911	Tacky at R.T.	Autoclave, hot-press mold	185 °C/2 h	195 °C/3 h, pressure	10 h	-
HT3/QY89110-II	Tack-free, heated draping	Autoclave, hot-press mold		200 °C/2 h + 210 °C/2 h + 230 °C/4 h pressure	18 h	-
HT3/QY89110-III		Autoclave, RFI		200 °C/4 h, pressure	12 h	-
QY8911-IV	Lowest melt state low viscosity	Autoclave, RFI	190 °C/6 h	210 °C/8 h, pressure	22 h	-
HT3/QY9511		Autoclave, RFI	185 °C/2 h	200 °C/4 h, pressure	12 h	Zero-resin sucking
HT3/QY9512	Easy film making	RFI	185 °C/2 h	200 °C/4 h, pressure	12 h	-
HT3/5405	Tacky at R.T.	Autoclave, hot-press mold	180 °C/2 h	195 °C/3 h, pressure	10 h	Zero-resin sucking
HT7/5428	Tack-free, heated draping	Autoclave, hot-press mold	180 °C/2 h	205 °C/4 h, pressure	11 h	
HT7/5429			180 °C/3 h	200 °C/4 h, pressure	10 h	
6421	Lowest melt state low viscosity	RTM	130 °C/1 h + 190 °C/3 h	200 °C/8 h	16 h	-

Table 1.66 Evaluation of the performance of epoxy resin matrix composites

Designation	Basic mechanical performance	Hot resistance	Hot/wet resistance	Toughness	Processing	Price
HT3/QY8911	5	5	5	3	6	5
HT3/QY8911-II	5	9	5	4	2	6
HT3/QY8911-III	5	5	5	6	6	5
HT3/QY8911-IV	5	5	5	5	4	5
HT3/QY9511	5	5	6	8	5	9
HT3/QY9512	5	5	6	6	6	5
HT3/5405	5	5	5	5	7	5
HT7/5405	7	5	5	6	7	3
HT3/5428	7	8	7	8	5	4
HT7/5429	7	6	7	9	6	4
HT3/6421	5	8	6	4	5	5

Note The number indicates performance grades from 1–9 with a higher number indicating better performance

Table 1.67 Polyimide resin matrix composite systems available in China

Designation	Composition	Company	Application	Features
HT3/KH-304	KH-305 polyimide resin, HT3 high-strength CF	Institute of Chemistry, Chinese Academy of Sciences and Beijing Institute of Aviation Technology	Engine out culvert	Good processing in prepregs, suitable for autoclave, hot-press molding processes. service at 316 °C, short term at 400 °C
HT3/BMP316	BMO polyimide resin, HT3 high-strength CF	Beijing Institute of Aviation Technology	Engine out culvert	Good processing in prepregs, suitable for autoclave, hot-press molding processes. service at 316 °C, short term at 400 °C
AS4/Lp-15 GB27/Lp-15	LP-15 polyimide resin HT3 high-strength CF and GB carbon cloth	Beijing Institute of Aeronautical Materials	Engine flow dividing ring	Good processing in prepregs, superior thermal oxidation, good hot/cool resistance, MDA-free service above 300 °C

Table 1.68 Basic mechanical properties of C fiber/polyimide composites

Performance	HT3/KH304		HT3/BMP316		G803/BMP316		AS4/LP-15
	Classical allowable	B-allowable	Classical allowable	B-allowable	Classical allowable	B-allowable	
X_c /MPa	1320	1126	1300	1061	612.9	1850	
E_{1t} /GPa	134.7		129		68	140	
ν_{12}	0.329		0.328		0.035	0.32	
X_c /GPa	971	767.1	1068	839.1	608	980	
E_{1c} /GPa	125.4		125		60.4	138	
Y_t /MPa	48.3	39.4	64.0	49.1	470.8	45	
E_{2t} /GPa	8.6		8.94		52	9.8	
Y_c /MPa	193.8	160.5	185	136.6	507.5		
E_{2c} /GPa	9.4	66.2	8.23		48.6		
S /MPa	92.5		79.4	71.9	4.4	180	
G_{12} /GPa	4.1		5.66		4.4	6.5	
σ_b^f /MPa	1705		1780			1950	
E_b^f /GPa	126.3		140			134	
τ_b^i /MPa	108		105			87	

Table 1.69 High-temperature mechanical performance of C fiber/polyimide composites

Performance	HT3/KH304			HT3/BMP316			AS4/LP-15	
	150 ° C	230 ° C	280 ° C	150 ° C	230 ° C	280 ° C	260 ° C	280 ° C
X_U /MPa	1204.0	1244.6	908.7	726.3	988.2	945.3	1790	1650
E_{1U} /GPa	142.4	146.7	153.6	160.0	168.8	166.0	138	136
ν_{12}								
X_C /MPa	541.9	386.7	450	552.8	438.2	394.0		
E_{1C} /GPa								
Y_U /MPa	38.0	33.6	22.0	21.0	19.2	19.8		
E_{2U} /GPa								
Y_C /MPa	128.5	102.4	65.3	106.3	103.9	92.8		
E_{2C} /GPa								
S /MPa			41.5				1650	1050
G_{12} /GPa								
σ_b^f /MPa			1020					
E^f /GPa								
τ_b^i /MPa			55					

Table 1.70 Interlaminar toughness and damage-dependent performance of C fiber/polyimide composites

Performance	HT3/KH304	HT3/BMP316	AS4/LP-15
σ_t^{OP} /MPa	276	308.2	
σ_C^{OP} /MPa	276	324.0	
CAI /MPa	196.5	181.6	
$GIC/J \cdot m^{-2}$			214

The high-temperature curing composites T300/5208 and AS4/3501 are earlier applied materials, and a comprehensive database is available and thus can be used as a baseline.

T300/913 and 1300/914C are empirical and old brand resin matrix composites that were developed more than 30 years ago. They are still widely used in the aerospace industry.

IM7/381 and 8552 resin matrix composites are used far more in helicopter structural applications.

The 977 series composites are currently used for military purposes and in commercial airplanes.

BMI composites are mostly used in military aircraft (fighters), while polyimide composites are primarily used in engine structures.

Table 1.71 lists a number of carbon fiber composites that are supplied by global sources. Their performances are presented as a reference.

Table 1.71 Performances of carbon fiber composites (supplied by global sources)

Perfor.	Medium temp. epoxy composites		High temp. epoxy composites										BMI composites					Polyimide
	IM7/	T300/	T300/	AS4/	T300/	IM7/	IM7/	IM7/	AS4/	IM7/	IM7/	IM7/	IM7/	G30 600	IM7/	IM7/	IM7/	
	381	913 ^a	5208 ^a	3501 ^a	914C ^a	977-2	977-3	8552	8552	8552	5250-4	5260	5260	5260	5260	2691	2932	2458
X_b /MPa	2468	1540	1496	1165	1673	2863	2510	2200	2200	2721	2314	2314	2314	2314	2314	162	168	144
E_{10} /GPa	166	141	180	128	134	175	162	141	164	164	139	139	139	139	165	162	168	144
ν_{12}	–	–	0.28	0.3	–	–	–	–	–	–	–	–	–	–	–	–	–	–
X_{Cj} /MPa	1482	–	1496	1060	1018	1638	1680	1529	1688	1688	1551	1551	1551	1551	1310	1746	1794	1384
E_{1C} /GPa	148	–	158	128	101	159.6	154	128	149	149	137	137	137	137	159	152	152	143
Y_b /MPa	38	61	40.1	41	60.8	76.3	64.1	81	111	111	57	57	57	66	72	74	74	29
E_{20} /GPa	8.83	8.6	10.3	11.0	9.6	7.7	8.34	9.6	11.7	11.7	7.9	7.9	7.9	9.7	9.7	9.0	9.0	8.6
Y_{Cj} /MPa	–	222	249	207	–	–	–	–	304	304	223	223	223	223	–	–	–	–
E_{2C} /GPa	–	8.9	11.3	11.0	–	–	–	–	12.5	12.5	14.9	14.9	14.9	14.9	–	–	–	–
S /MPa	128	–	67.2	69	99	110.6	–	127	120	120	115	115	115	81.4	110	108	108	–
G_{12} /GPa	4.3	–	7.2	5.9	5.8	5.6	4.96	–	–	–	5.0	5.0	5.0	6.34	5.1	–	–	–
σ_b^t /MPa	1455	1550	–	–	–	–	1765	1888	1860	1860	–	–	–	1550	1842	1863	1863	1508
E_b^t /GPa	–	131	–	–	–	–	150	127	151	151	–	–	–	–	148	152	152	121
τ_b^t /MPa	92	98	–	–	94	–	127	–	137	137	107	107	107	–	159	166	166	104
σ_{1c}^{OP} /MPa	–	–	–	–	–	504	–	–	428	428	434	434	434	–	490	518	518	–
σ_{2c}^{OP} /MPa	–	–	–	–	–	336	322	–	–	–	328	328	328	–	352	373	373	–
C_{AI} /MPa	234	–	–	–	–	280	193	220	213	213	–	–	–	213	352	406	406	–
G_{1C} /Jm ⁻²	303	–	–	–	–	–	315	–	–	–	–	–	–	–	352	–	–	–
G_{1IC} /Jm ⁻²	–	–	–	–	–	–	577	–	–	–	–	–	–	–	845	–	–	–

^aT300/913, T300/5208, AS4/3501, and T300/914C are resins that were developed earlier with incomplete data available

1.4 Latest Advances and Developing Trends for Advanced Composites

1.4.1 General Trends—Reduction of Processing Costs

The historical development and application of advanced composites has been characterized by superior performance and high costs. High costs are required to achieve superior performance in advanced composites. Therefore, cost reduction and the optimum balance between performance and cost have been critical trends in the development of advanced composites since the mid-1980s. The focus is now on the development of low-cost processing techniques for high-performance composite manufacturing. These include specialized resin systems, equipment, and facilities. As computer technology is widely used for control and numerical simulations of processing procedures, the processing techniques in advanced composites have become more effective and benefits have resulted. Experimental work has declined significantly, and production costs have apparently decreased.

The advances in composite low-cost technologies can be summarized as follows:

- 1) Preform/liquid molding processes are in development and are being applied in preform preparation, specialized resin systems, and digital simulations of injection processes.
- 2) The development of low-temperature and low-pressure processing techniques. Highlights are researched into specialized resin systems and their related prepreg preparations for low-temperature and low-pressure processing technologies.
- 3) Automated tape or fiber bundle placement to achieve fiber layer automated stacking and complex contours, high precision, and quality fiber placement to satisfy the multifunctional needs in aerodynamics, stealth and structures, as well as the necessary software for fiber placement.
- 4) Software development for the integration of composite part design and manufacture.

In modern composite design and manufacture, digital techniques as well as related software are widely applied for integration in part design and manufacturing. For example, the software “Fiber SIM” developed by “Composite Design Inc. US” can be incorporated into the computer-aided systems “Catia” “ProEngineer”, or “Unigraphic” to constitute a complete software system for the integration of composite part design and manufacture. In this software system, feasibility, evaluation, and design work can be automated and used to generate necessary production documents and graphics. The use of this software in composite production has led to cost reductions, processing cycle reductions, and raw material savings. This system has been used for aerospace structural design for parts such as the cowl in the RAH-66 helicopter, the F-35s air-intake channel, the X-32s wing skin, the EF-2000s fuselage cabin panels, and the Delta’s rocket cowl. More than 30% of the total costs have been saved.

FiberSIM operating platform:

CATIA edition: version 4.1 or above

IBMAIX edition: version 3.2.5 or above

SGRIRIX edition: version 6.3 or above

Unigraphic: version 13 or above

- 5) Control and simulation processing procedures (virtual manufacturing): The control and simulation of composite processing procedures are recent trends in composite technologies and have been used over the last decade. They will be separately introduced in the next section.

Co-curing techniques for the integrated processing of large and complex parts or foam sandwich constructions will not be discussed further.

1.4.2 Manufacturing Process Control of Advanced Composites

The manufacturing processes for advanced composites are those processes in which constituent materials are subjected to fiber orientation and placement, resin matrix polymerization, and curing under desired operation conditions. They are finally processed into products with desired shapes, dimensions, and performance. Different processing techniques require different processing equipment to meet production requirements. For some processing techniques, specialized equipment, facilities, and resins are required. Essentially, manufacturing process control refers to the control of composite curing processes.

The completion of final composite part production simultaneously with material processing requires the in situ dynamic monitoring of equipment and material changes. For processing equipment, the geometric size, operating temperature and pressure, heating rates, and other technical characteristics are specific and do not change until the equipment is modified or replaced. Composite performance will continuously change as the resin matrix curing progresses until the fully cured composite parts are produced.

The essential requirements for the in situ monitoring of composite processing should be the ability to observe changes in processing parameters and to implement necessary changes. Therefore, in composite processing control, it is important to control and adjust the processing equipment to a state that satisfies processing requirements and guarantees part quality.

Figures 1.77, 1.78, 1.79, and 1.80 show current models for composite processing control.

Fig. 1.77 Model applicable to autoclave processes

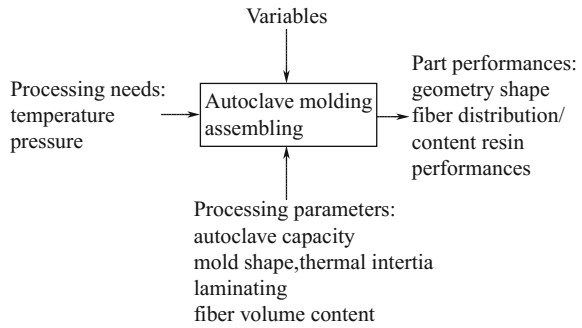


Fig. 1.78 Model applicable to hot-press molding

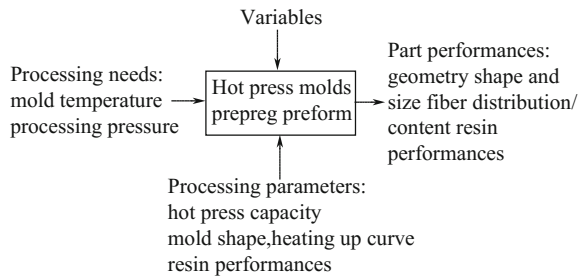


Fig. 1.79 Model applicable to filament winding

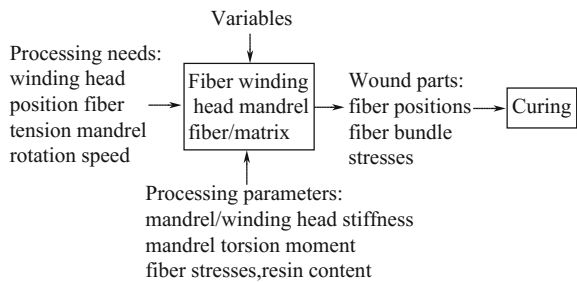
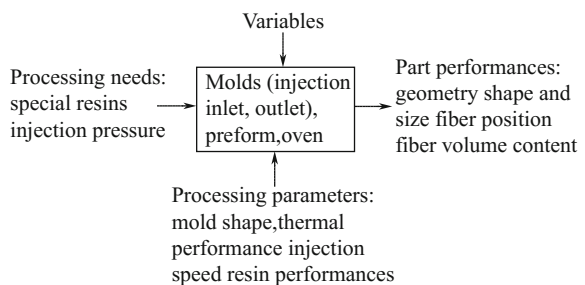


Fig. 1.80 Model applicable to RTM



1.4.3 Simulation and Optimization of Composite Processing (Virtual Manufacturing)

The simulation of composite processing is a computerized numerical modeling technique for the prediction of composite physical and chemical property changes during resin matrix curing reactions. Numerical models are mathematic equations that can calculate and produce numerical results for systemic engineering analyses on processing or product quality. Simulations of composite processing can be used for processing scheme design to provide guidelines for mold design, material optimization, production cycle determination, and part performance. Additionally, processing in situ optimization using different parameter inputs can be used by personnel to operate models for the selection and optimization of critical in situ parameters.

The simulation flow for polymer base composite processing is shown in Fig. 1.81.

Process design (off-line parameter optimization) and process optimization (in situ parameter adjustment) are the two main aspects of computer simulations. The primary model consists of reaction kinetics, thermal transfer, resin flow (viscosity), and void submodels. For processing and part descriptions, boundary conditions are provided to solve reaction heat, energy, and dynamics equations. The primary model is combined with processing and partial boundary conditions, and the processing simulation system is generated (“processing simulation and optimization” in Fig. 1.81). This can be used for processing simulations and optimization.

Parameter optimization in processing (in situ parameter optimization) is a feedback problem in processing design. Parameter simulations and optimization systems are changed to parameter adjusting systems. The data or information

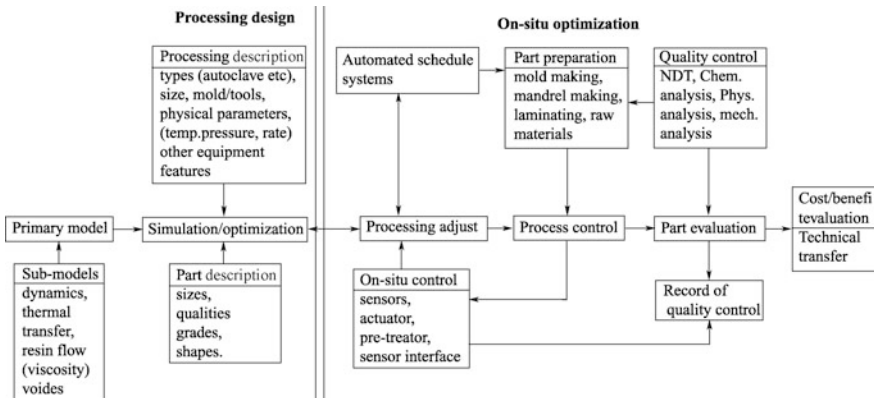


Fig. 1.81 Simulation scheme for polymer-based composite processing (in case of product rejection, messages are fed to the primary model and processing design resumes)

generated during process in situ monitoring is input into the parameter adjustment systems, and the treated information is then fed into automated adjustment systems to incorporate parameter modifications and thus improve processing conditions.

The COBRA program developed by Lockheed can be used for autoclave processing optimization and has been used for F-22 and F-35 fighter parts manufacturing.

It is necessary to point out that very complicated chemical reaction variables such as viscosity, voids, resin flow in fibers, heat conduction, and energy balance are involved in composite processing simulations. It is very difficult to establish and express mass transfer equations; nevertheless, simulation techniques have limited use in applications despite related research being carried out over more than 20 years.

1.5 Applications of Advanced Composites

Advanced composites are light, and high-performance materials but composite costs—that is, the life cycle expenses that consist of expensive raw materials, manufacturing, inspection, maintenance, and repair—are very high. Therefore, advanced composites are primarily used in aerospace applications, high-speed trains, racing cars, and sports boats where high-input and high-performance products are required.

In this section, the advanced composites used in aerospace applications are mainly introduced.

1.5.1 Applications in Aircraft Structures

Pioneering research and development of advanced composites originated because of the high structural efficiency and improved performance requirements of aircraft parts. Their application in aircraft structures is of great benefit, and development continues as composite technologies become more mature. For the military fighter planes developed in the 1990s, the use of composites has reached 24–30% of the total structure's weight, as shown in Table 1.72 and Figs. 1.82, 1.83, 1.84, 1.85, 1.86, 1.87, 1.88, and 1.89. This means that the unique advantages of aerodynamic elastic tailoring are significantly exploited by composites. This is impossible for fighter swept-back wing aerodynamic configurations using conventional isotropic engineering materials. For example, the X-29 experimental plane in the USA (first flight in Dec. 1984) and the Su-47 in Russia (gold eagle in Sept. 1997) are shown in Fig. 1.87. For the huge B-2 bomber, composites are used for 37% of the total structure weight, while 60% of its wing structural weight comes from composites as shown in Fig. 1.88. In helicopters, for example, the RAH-66, Tiger, NH-90, and EH-101, the propeller blades are mostly composites, with composite parts making up at least 50% of the total structure.

Table 1.72 Composites in aircraft applications

Aircraft	Composite	Applications	Weight saving/%
F-4	Graphite/epoxy	Check port	
F-111	Glass/epoxy, boron/epoxy	Cabin panel, fair cowl	
F-14	Boron/epoxy	Horizon tail skin, horizon stabilizer torsion box	0.8
F-15	Boron/epoxy	Horizon/vertical tail skin, reducer plate	1.6
Mirage F1	Boron/epoxy	Horizon tail skin	
F-16	Graphite/epoxy	Horizon/vertical tail skin, flight control surface	
F-18	Graphite/epoxy (IM7/977-3,	Wing skin, extended front	12.1
	F-18/E/F)	Back flap,	
	Graphite/epoxy	Horizon/vertical tail skin, flight control surface	
		Hatch cap, reducer plate	
	Graphite/epoxy, (graphite/BM, I F-18/E/F)	Fuselage panel, door	
AV8B	Graphite/epoxy	Wing skin/torsion box beam, rib, horizon tail skin	26.3
		Front fuselage, control surface, cowl, flap, aileron, landing gear support rod	
	Graphite/epoxy	wing after edge	
B-1	Graphite/epoxy	Horizon tail structure, flap skin, check port	
	Boron/epoxy	Flap sliding track,	
	Graphite/epoxy(AS-1/3501-5A)	missile module door,	
	Graphite/epoxy T330/5208	flight control surface	
	Graphite/epoxy T330/934	Missile launch unit	
F-22	Carbon/BMI	Skin, inlet, frame, spacer frames	
EF2000	Carbon/BMI	Wing, middle fuselage	
	Carbon/BMI	Vertical tail, duck wing, front fuselage, landing gear	
A-6	IM6/3501-6	Cabin door, air-intake, wing (modified)	
AS300	Graphite/epoxy	Wing, rudder	
–	Graphite/epoxy	Tail skin	
XF-2	Carbon/epoxy	Tail, wing, landing gear cabin door	18

(continued)

Table 1.72 (continued)

Aircraft	Composite	Applications	Weight saving/%
Mirage2000	Graphite/epoxy	Flap, vertical tail torsion box skin	17
		Rudder, flipper, by-wing, electronic cabin elevator	
–	Graphite/epoxy	Wing, fuselage (50%)	24
		Control surface, landing gear cabin door, wing	
JA539	Graphite/epoxy	Wing, vertical tail, front fuselage, landing gear cabin door	30
J- XX	Carbon/BMI	Vertical stabilizer, rudder, hatch	6
J-XIII	Carbon/BMI	Front fuselage, vertical tail,	2
Q-5	Carbon/BMI	vertical stabilizer, front fuselage,	>2
J-X	Carbon/BMI	rudder, reducer plate	≤ 1
CH53D	Kevlar49/epoxy	Fuselage skin	15-20
	Glass/epoxy	Fuselage frame	
	Glass/epoxy/Al interlaminar mix.	After fuselage	14
	Graphite/glass/epoxy	Main propeller	24
	Glass/epoxy	Hub	
S-76	Glass/Nomex honeycomb	Main propeller	
	Graphite/epoxy	Tail propeller	
	Kevlar, glass/epoxy	Fuselage skin	
	Kevlar/epoxy	Horizon tail skin	
	Glass/epoxy/Nomex honeycomb	Horizon tail	
AH-64	Carbon/epoxy	Extended cabin, driving cap, vertical tail back edge	15
AH-I	S-glass/epoxy	Propeller skin, main beam	
UH-6A	Kevlar49/epoxy	Fuselage skin	
WG-13	Graphite/epoxy	Shaft	
Bo105	Graphite/epoxy	Propeller blade	
SA330	Graphite, glass/epoxy, Nomex	Propeller blade	
RAH-66	S-2/IM7/PR500	Propeller	
EC120		Propeller, body, vertical tail/beam, horizon stabilizer	

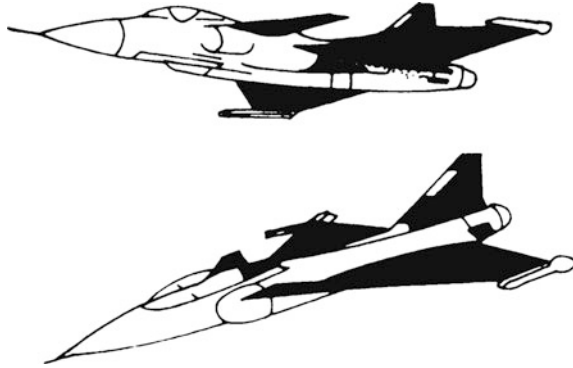


Fig. 1.82 Composites in the JAS39 (dark area)

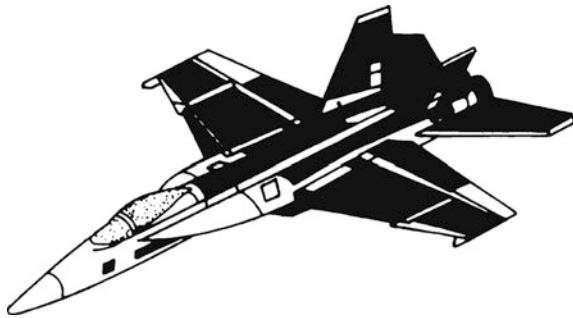
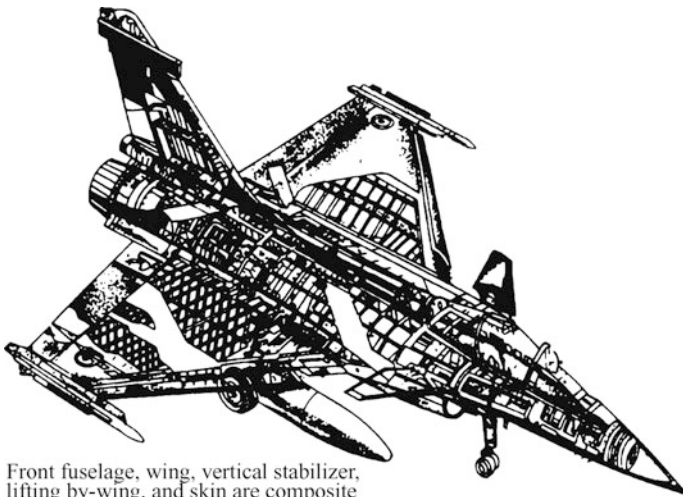


Fig. 1.83 Composites in the F/A18E (dark area)



Front fuselage, wing, vertical stabilizer, lifting by-wing, and skin are composite structures

Fig. 1.84 Rafale C's structural configuration

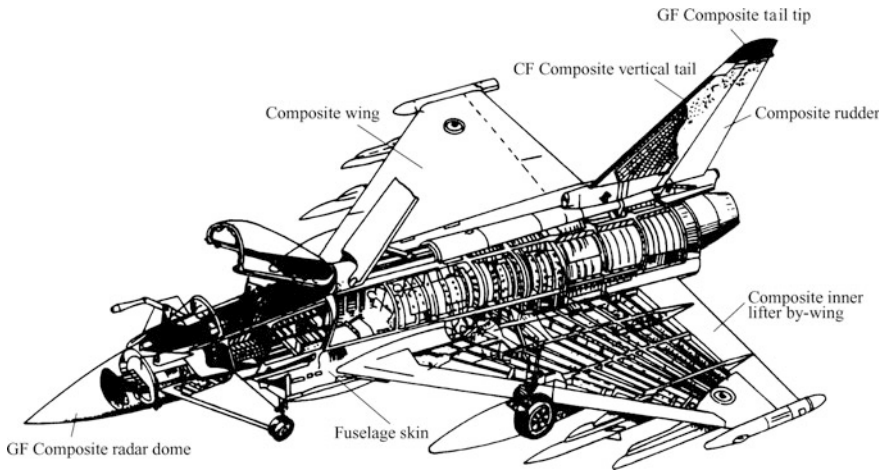


Fig. 1.85 EF2000's structural configuration

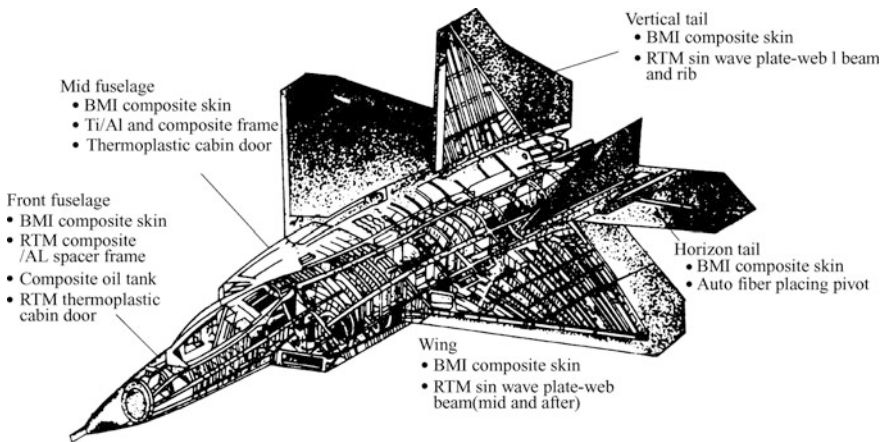


Fig. 1.86 Composites in the F-22 jet

In unmanned aircraft, 70–80% of the structure is composed of composites.

Composite structure applications in the large commercial airplane industry have been expanded for weight saving, pollution-proofing, fatigue resistance, and possible cost reduction purposes, as shown in Table 1.72 and Fig. 1.89. Composite technologies for use in commercial airplanes have been developed and are now mature. In large passenger planes such as the Boeing 787 and the Airbus A-380, composite use has increased to 50% and 25% of the total structure weights, respectively. The percentage of composite use is 37% for the A-350, showing the benefits of weight reduction and a performance increase. In terms of small business

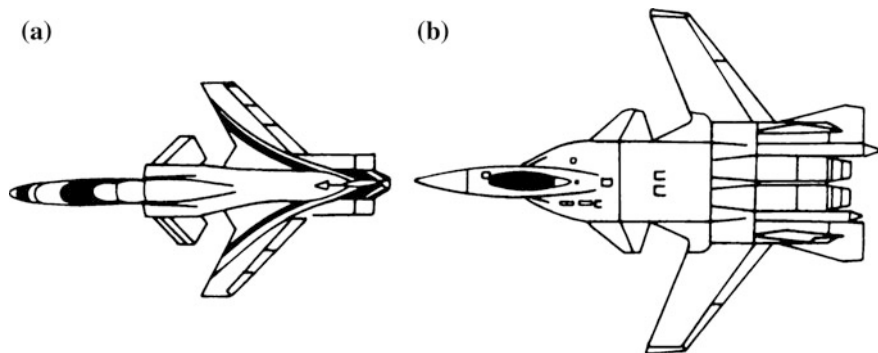


Fig. 1.87 Experimental jet with composites in the swept-forward wings

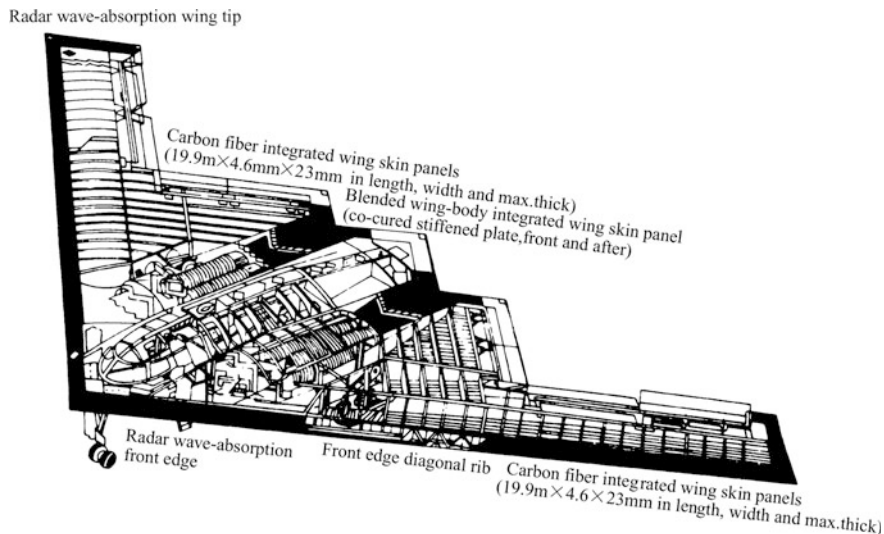


Fig. 1.88 Composites in the stealth B-2 bomber

and sport aircraft, almost all the main structure is composed of composites as the ratio is as high as 70% or above. These are referred to as all-composite airplanes with good examples being the “Star ship” and “Voyager”.

It is necessary to point out that currently the composites used in plane structures are mostly carbon/epoxy composites, even in fighter applications, rather than carbon/BMI composites. For example, IMM/977-3(carbon/epoxy) is used in the F/A-18E/F composite structures; IM7/977-3 and other carbon/epoxy composites make up 50% of the total composite structure in the F-22 with the others being BMI composites (IM7/5250-4). In Space Ship One, most of the structure consists of carbon/epoxy and ceramic composites.

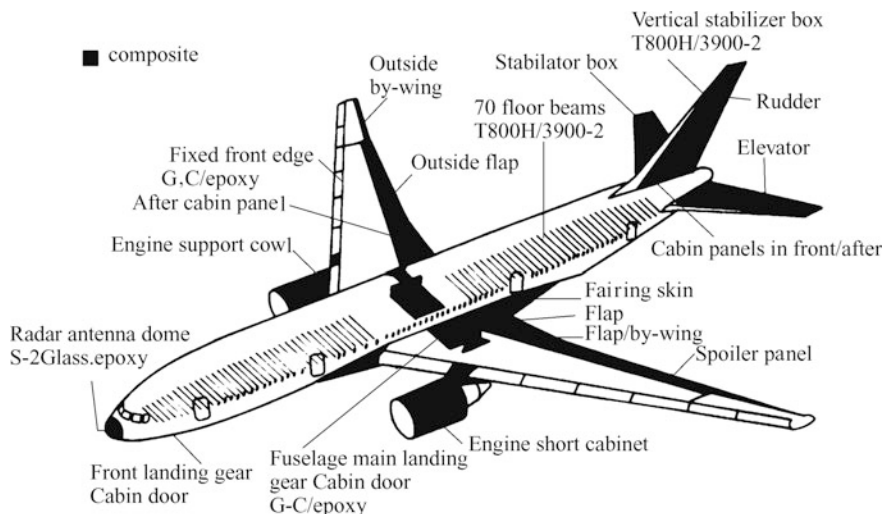


Fig. 1.89 Composites in the Boeing 777

Pioneering work on composite development and application in China began in the 1980s as a key technology. Composites in aeronautical applications have progressed from secondary structures to primary structures; for example, composite vertical stabilizers, horizon tails, rudder, and front fuselages are used in jet planes and can be supplied in small volume. Critical primary composite structures like wings with an integrated oil tank and blended middle wing-body structures have been also developed indicating new milestones of composite technologies in China.

1.5.2 Applications in Aeronautical Engines

The application of advanced composites in aeronautical engines started in the 1970s and the main manufacturers involved were Rolls-Royce in the UK, Pratt & Whitney, and GE in the US. Composite aeronautical engine parts from Pratt & Whitney will be discussed.

In 1970, nose cones made using glass/epoxy were approved for use in JT9D turbine engines; in 1981, aramid/epoxy nose cones were used in the JT9D-TR4 for further weight saving. After that, composites were largely applied to the PW engine series such as the fan cases in PW2037 and PW4000 (2388_2540 mm); the RTM carbon/epoxy parts in fan spacers in PW4084/90/98; the inner and outer rings of exhaust stator blades in the fan outlet in PW4056/4168/4084. In PW4168 composite engine nacelles were used (basically honeycomb structures), including BMI composite cowls and carbon/epoxy reverse thrust devices. Approximately 400 composite parts have been used in the PW engine series.

GE used the fan bypass made from polyimide composites in F404 engines in the 1980s, and composites were used for up to 15% of the total engine structure’s weight. Recently, by adapting the experiences of the R-R company, the fan blades with a large aspect ratio made using advanced resin matrix composites have been successfully developed and used in the GE 90 engine series. This is regarded as a new milestone for composites in engine applications, which fulfills the transfer from static structures to load-bearing rotation structures.

In China, polyimide composite fan bypass (outer bypass) for aeronautical engines has been developed indicating a major technical breakthrough in advanced composite applications.

The thrust–weight ratio is a critical parameter in military plane engines, and a thrust–weight ratio increase can benefit jets in terms of cruise speed, mobility, and combat radius. Research indicates that the increase in the thrust–weight ratio in aeronautical engines will be 50–70% depending on new materials and corresponding structures. Composites are becoming more favorable for use in a new generation of aeronautical engines because of their superior performance. Currently, resin matrix composites (PMCs) are widely applied in the cool-end parts of new engines. Table 1.73 shows the PMC parts used in aeronautical engines in recent years. The service temperatures of engines increase from the air-intake fan to the out bypass condenser burning chamber. Currently, the PMC parts are mostly used for the air-intake fan and the bypass sections in aeronautical engines with a lower service temperature.

Table 1.73 The PMC parts used in aeronautical engines

Manufacturer	Engine parts	Materials	Features	Remark
GE	F404	CFR/PMR15	Replace cladding melted Ti parts with special F rubber coating, weight-saving 15–20% and cost saving 30–35%	
RR	Tay bypass	CFR/PMC	Weight-saving 25%, noise reduced	
Do-pone		Avimid N	Good thermal stability and used in engines as intermediate cases, compression case, static blades, rings, pipes, to be used in F119 engines	
PW	F119 varied-shape exhaust blade, pipes and exhaust blades in F100-PW-229			

(continued)

Table 1.73 (continued)

Manufacturer	Engine parts	Materials	Features	Remark
GE	GE90 fan blades	CFR/epoxy	Use Hercules 8551-7/IM7 toughened epoxy/CF composite with a layer of cladding on Ti alloy skin on front edge, to prevent falloff, after edge was knitted with Kevlar wires. The composite blades have a weight of 14.5 kg and a weight saving of 30%-40% compared with hollow Ti blades	the linear speed on the blade tip is limited to less than 355–365 m/min
GE	GE90 fan containing ring	Kevlar/epoxy	Prevent plane damage caused by broken blades	
Rolls	Core faring dome in CF6 nacelles	CFR/PMR-15	Weight saving of 25% compared with Al or Ti parts; service temp. reaches 232–288 °C, used in modified CF6.	
RR,GE,PW	Fan containing a ring in large civil engines	Kevlar/epoxy tape wound on Al cases	Service temp. below 130 °C	
Textron Lycoming	T800 accessories gear box cover	Press-molded chopped fiber/PMR15	Passes 15-min flame test without linkage (1093 °C)	PEEK molded parts replace ball holding frames, Al oil-hole plates and eccentric rings
	ALF502 ice-proof pipes	Press-molded CFR/PEEK		
	ALF502 faring	CFR/winding		
Snecma	M88 out bypass	CFR/PMR 15		
Lycoming	T55 ACE inlet case	Composites		
PW	SCFN small thrust vector/reverse jet-pipe	PMR15 and AFR700 are used on two sided wall surfaces	Used in F119 jet-pipes and in navy advanced attack airplanes	

1.5.3 Applications in Solid Rocket Motors

1.5.3.1 Applications in Solid Rocket Motor Bottles

Composite applications in solid rocket engine shells can basically be divided into three generations:

Table 1.74 Typical composite use in rocket motors from the US

Engines		Bottle materials	Diameter/m	Length/m	Developed year
Polestar A2 s rocket		E-glass/epoxy	1.37	2.14	1958–1960
Polestar A3	First	S-944 glass/epoxy	1.37	4.60	1960–1964
	Second	S-944 glass/epoxy	1.37	2.26	
Militia II	Third	S-944 glass/epoxy	0.95	2.29	1962–1965
Militia III	Third	S-944 glass/epoxy	1.32	2.35	1966–1970
Sea-god C3	First	S-901 glass/epoxy	1.88	4.77	1966–1971
	Second	S-901 glass/epoxy	1.88	2.48	
Trident I (C4)	First	Kevlar 49/epoxy	1.88	4.72	1971–1979
	Second	Kevlar 49/epoxy	1.88	2.50	
	Third	Kevlar 49/epoxy	0.77	3.10	
MX	First	Kevlar 49/epoxy	2.34	8.34	1979–1986
	Second	Kevlar 49/epoxy	2.34	5.598	
	Third	Kevlar 49/epoxy	2.34	2.33	
Trident II (D5)	First	IM7 CF/epoxy	2.11	7.11	1980–1989
	Second	IM7 CF/epoxy	2.11	2.87	
	Third	Kevlar 49/epoxy	0.813	3277	
Manikin	First	IM7 CF/epoxy	1.168	5.08	1984–1995
	Second	IM7 CF/epoxy	1.168	2.74	
	Third	IM7 CF/epoxy	1.168	1.83	

In the 1960s, glass/epoxy was mainly used; in the 1970s, aramid fibers/epoxy was used; and in the 1980s, carbon/epoxy composites were mainly used. Typical use in engines from the USA is listed in Table 1.74.

In the former Soviet Union, the APMOC aramid fibers have a strength of 4900 MPa and a modulus of 145 GPa, which is 35% and 21%, respectively, higher than Kevlar 49. Its density is only 1.45 g/cm³, and its specific strength is 12% higher than that of IM-7 CF (strength 5300 MPa, density 1.77 g/cm³). Therefore, in the former Soviet Union, the motor bottles in the SS-24 and SS-25 missiles were all made from APMOC aramid/epoxy and these reached third shell composite levels.

1.5.3.2 Applications in Solid Rocket Motor Jet-Pipes

The early jet-pipes in solid rocket motors were made using alloy steels, and usually a thermal-isolated layer of zirconium oxide was applied to the inner surface.

As propellant efficiency increased, the gas temperature increased and the working time became extended. The working environment became harsher especially for the throats, which have to bear high temperatures, pressures, speeds and mechanical washing, chemical attack, and thermal vibrations caused by the condensed particles. Therefore, the throat liners, contraction sections (inlets), and extended sections (outlets) were gradually made from graphite or other composites. In shell and joining parts, filament winding and ceramic composites are used to replace metals.

The throat liner materials have undergone a revolution because of oxidation ceramics, high strength and density graphite, thermal degradation graphite, infusible metals and porous tungsten penetrating silver (copper) and modern FW composites and ceramic composites.

For contraction, extended sections, and back wall thermal isolation parts, thermal isolation and ablating materials are used such as high silicon–oxygen/phenolic press-molded parts or cloth tape winding parts. Carbon–phenolics are commonly used in large motors. The material densities used in contracting sections are 1.45 g/cm^3 , while 1.0 g/cm^3 is used in extended sections.

For example, in Sea-god C3 missiles, graphite/phenolic composites are used as throat liner materials in the jet-pipes and carbon/phenolic composites are used in the extended sections as thermal isolation layers; in Trident I (C4) missiles, thermal degradation graphite is used as the throat liner of jet-pipes, carbon/epoxy is used as the outer structure layers, and carbon/phenolics are used as the inner thermal isolation layers in the extended sections; in Trident II (D5) missiles, the jet-pipe throat liner is made from 3D carbon/carbon composites, the extended section is made from carbon/phenolics in the section raket, and the exit cone of the jet-pipe in the engine is made from carbon/phenolic composites; in MX missiles, the throat liner in the engine jet-pipes is made from 3D carbon/carbon composites and the extracting section and throat liner in the second jet-pipe are an integrated 3D carbon/carbon braided part, which is supported by a steel structure with carbon/phenolic cladding as a thermal isolation layer. The inner layer of the extended section is a wound tape of carbon/phenolics, and the third jet-pipe shell is aluminum alloy. Both the extraction and extended sections are pre-impregnated graphite/phenolic tape as thermal isolation layers, and the extended cone in the jet-pipe is also made from 3D carbon/carbon composites.

The solid rocket motor bottle with a diameter of 3.2 m is manufactured by an IM-7 carbon fiber/epoxy winding process, and its jet-pipe throat diameter is nearly 1 m. The corresponding multiple-D braided throat liner has an outer diameter of 1.5 m and a height of 1.2 m. The Russian extended cone of engine jet-pipes in submarine-to-land missiles is a thin-walled carbon/carbon part with a diameter of 2.5 m, indicating a high level of composite material and processing in rocket engine applications.

1.5.3.3 All-Composite Solid Rocket Engines

With progress in missiles and composites, the ratio of composites in rocket engine mass has increased. For example, in the US Pegasus rocket the composites used in the three-rocket engines compose 94% of the total structure mass.

Multiple-D braided high-strength and density C/C composites have advantages of high-temperature resistance and anti-ablating. They can be used for integrated thermal resistance in structural materials. The all-C/C jet-pipe can be used to replace traditional building-block jet-pipes that consist of many segments, layers, and materials and to simplify the structures, increase reliability, and save 30–60% of the weight.

C/C jet-pipes are the only materials capable of withstanding high-temperature working conditions. Connectors made using metal and carbon/phenolics between jet-pipes and composite bottles cannot be used at such high temperatures. Therefore, thermal linking composites (referred to as TLC) have been developed. TLC consists of inner and outer rings with the outer ring being the connector to the bottle base. The inner ring is a part of the jet-pipe; both the outer and inner rings are joined by bolts, and they connect the bottles and jet-pipes. The outer ring is made of 6D braided aluminum oxidation fiber/carbon composites, and this is used as a rocket bottle connector; the inner ring is also made from a carbon-based composite, and it is a kind of gradient functional composite, which uses T300 CF as the internal layer in the braided structure, and the external layer is 6D braided aluminum oxidation fiber. TLC embodying allows for an all-composite solid rocket engine.

Solid rocket engines that largely use advanced composites are being used more in missile and space industries.

1.5.4 *Satellite and Space Station Applications*

1.5.4.1 Satellite Applications

Earth satellites have to survive launch, orbit, and atmospheric reentry if recovery is required. During their launch, satellites are subjected to great acceleration overload and extreme vibration; therefore, the materials used for satellites must have sufficient strength. To avoid resonance between satellites and launching devices, the satellite should have enough stiffness, and during orbit motions, satellites are subjected to alternating high- and low-temperature conditions. Some parts such as the parabolic antenna require very high dimensional accuracy and a minimized linear expansion coefficient. For open-type structures (such as solar cell array base panels), sufficient stiffness is also required to avoid non-preferable attitude control during orbit. Satellite materials are also required to be stable enough to resist high vacuum, particles, and ultraviolet (UV) radiation. Recoverable satellites have thermal resistance because an air dynamic thermal environment exists during

reentry. Weight saving is more important in satellites than in airplanes or other space vehicles. In summary, the overall requirements of satellite materials are high specific strength and modulus, small linear expansion coefficient, good dimensional stability, and performance stability in varied space environmental conditions.

Based on the above discussion, advanced composite materials (ACMs) have features that can suit the requirements of satellite structural materials. ACM is widely used in satellite structures, but its application is not limited to structures as thermal-resistant layers of phenolic-based composites are also used in recoverable satellites. Further discussions will focus on the application of ACM to different satellite sections, structure patterns, and property requirements.

Satellite Main Body Structures

Carbon/epoxy has high specific modulus and is suitable for satellite main body structures. For example, in Japan, the EIS-1 satellite shell contains internal composite parts such as the thrust cylinder made from M40 composite and is 0.5 m in diameter, the equipment frame, the 8 support rods, and the split ring. The thrust cylinder is a primary structure that supports the equipment frame and any attached devices and solar cell array. The split ring is the interface between the satellite and the fixture devices in the rocket.

The central thrust cylinder in the international communication satellite V was divided into the cylinder shell and the cone shell. The cylinder body is a sandwich structure containing aluminum honeycomb cores and graphite/epoxy skins. The skins are made of T300 carbon cloth and unidirectional tape composites. The other parts were mostly made of graphite/epoxy.

The design principle in satellite structures is that permanent deformation or over deformation should be avoided under critical load, and the deformation should not influence part functions. Under limit loads, there should not be fractures or other failures. As satellite sizes and effective loads have continuously increased, the structure mass ratio of the total satellite mass has decreased from 13–20% to 10% or even less; therefore, large quantities of ACM have been used in satellite structures.

Antenna Structures

The earliest application of ACM in antenna structures was in the Applications Technology Satellite (ATS), and in ATS-F, the antenna subtruss was constructed using high modulus graphite/epoxy. The surface layer was an S-glass/epoxy circular composite, and it was used for lateral strength and impact resistance. It also meets the thermal expansion requirements. The graphite/epoxy truss can save up to 50% of the weight compared with aluminum alloys. In addition, ACM is widely used in space vehicle parts and in satellite antenna reflectors, as shown in Table 1.75. As satellite technology has advanced, the antenna size has become larger and much higher dimensional accuracy is required. To guarantee structural

Table 1.75 ACM in space vehicle antennae

Space vehicle (satellites)	Part designation	Materials
“The Pirate”, Mars orbit voyage antenna	High gain antenna reflector (Φ 3.7 m)	GY-70 graphite-934epoxy; Al honeycomb cores
US Defense Meteorological Satellite	Precise antenna reflector	GY-70 graphite-934epoxy
EIS-1 Satellite	Large extendable antenna	Graphite/epoxy
RCA Communication Satellite	Integrated or single shell reflector	Graphite-Kevlar/epoxy skin, Kevlar/epoxy honeycores
International Communication Satellite V	Antenna, feed source, waveguide antenna truss multichannel modulator, solar cell array (more than 4000 CM parts with different sizes)	GY-70-Kevlar/epoxy skin, T300/epoxy, Kevlar/epoxy honeycores
US Technical Satellite F and G Model	Reflector truss pipes	GY-70graphiter/epoxy
India INSAT Communication System	Antenna reflector	Graphite/epoxy
Space vehicles	Focal extendable parabolic antenna	Graphite–Al alloy composites

dimension stability, materials with a small linear expansion coefficient (LEC) must be adopted. Carbon fibers have negative LEC in the longitudinal direction and positive LEC in the transverse direction. By proper ply orientation design, ACM with zero LEC can be produced. This can also be realized by a hybrid of graphite and Kevlar 49 fibers. The antenna is the satellite’s information collector, and to increase signal emission or receiving efficiency and to reduce signal loss, the dimensional stability of the antenna supporting truss is very important and carbon/epoxy pipes have been most commonly used. To reduce heat leakage and to provide electromagnetic wave penetration, Kevlar/epoxy can be also used. The ACM supporting truss weighs 60% less than comparative metals.

Solar Cell Array Structures

Solar cell arrays are essential energy resources for a satellite’s long-term operation. With the development of satellites, the power needed by satellite instruments and devices has increased. Large extendable space solar cell arrays are currently used in satellites, and the corresponding materials required high specific modulus and low thermal deformation. Carbon/epoxy is suitable for this purpose. For example, the French MBB company has developed two solar cell array structures. One is a

stiffened solar cell array consisting of carbon/epoxy surface panels, square thin beams, and an Al honeycomb. The array is hinged by sandwich panels, folded during satellite launch, and extended when in space. This array has been used in the orbit testing of satellites and has an area of 11.4 m². The international communication satellite V has a solar cell array area of 18.12 m². The other type of array is a half-stiffened solar cell array in which the thin square pipe frame is made from carbon/epoxy. A pretensed flexible film is attached onto the frame to support the solar cells, and this structure has a lower area density.

In China, second-generation meteorological satellites are self-spinning stable synchronous satellites in which solar cell shells are both the satellite's main body and carriers for solar cell silicon pellets. The solar cell shell is a large, light honeycomb sandwich structure with a diameter of 2.1 m and a height of 0.72 m. The surface panels are made of epoxy-phenolic-base glass composites, while the inner panels are LF2Y Al alloys. The core materials are durable Al honeycombs. In the late 1960s, in China ACM sandwich space structures were developed including instrument cabin caps, solar cell shells, solar screens, instrument attachment panels, parabolic antennae and their trusses, satellite interface support stands, beam/girder beams, and multifold carbon fiber stiffened solar electric wings.

In satellite structural materials, glass composites have a lower specific modulus and are not suitable for primary structure, while boron fiber composites have a high specific modulus but are complex to process and are expensive. Kevlar composites have high specific strength and low thermal expansion and can be used in satellites to a certain extent. However, their low specific modulus and compression strength have limited their use. SiC metals are suitable for high-temperature structures but are still being investigated. In general, future principal structural satellite materials will consist of high modulus graphite polymer matrix composites.

1.5.4.2 Space Station Applications

Space stations (also referred to as space platforms) usually orbit the earth at an altitude of 240–450 km and are subjected to microgravity, high vacuum, and alternative high- and low-temperature conditions. They are also subjected to solar rays, atomic oxygen radiation, as well as micrometeor or space fragment impacts. Permanently manned space stations are large, complex structures and should have a long work life (15–30 years). They should be subjected to far longer space environmental testing than other space vehicles. Space stations should have the ability to support accessory systems such as solar panels, heat sinks, a variety of modules, and a large stiff platform. Structural complexity and a long work life will be the main features that differentiate it from other space vehicles. The structural stiffness, dimensional stability, building-block type quick assembly and recovery as well as its suitability and durability in a space environment are important requirements. To satisfy these structural requirements, apart from high specific strength and modulus and low thermal expansion, the materials used for some parts should have good thermal conductivity, be flameproof, have low vacuum gas emission, have atomic

Table 1.76 T_g in epoxy resins after radiation

Total radiation/ 10^{-2} Gy	Glass transition temperature, $T_g/^\circ\text{C}$			
	Room temperature/ open to atmosphere	Room temperature/ vacuum	100 $^\circ\text{C}$ /open to atmosphere	100 $^\circ\text{C}$ / vacuum
0	260	230		
4.4×10^7	231	230	236	235
8.8×10^7	230	235	239	230
1.4×10^8	234		240	238
3.2×10^8	225		238	237

oxygen resistance and anti-fragment penetration as well as resistance to high-energy electric-magnetic waves and particle radiation. Polymer composites do not satisfy all these requirements and can only be used for some station parts. For example, the visible and infrared radiation from solar radiation can affect the station's surface temperature, but generally will not damage the materials. Ultraviolet (UV) quanta have enough energy to damage the chemical bonds in resins and cause material degradation. However, UV has a low penetrating ability and can only affect film polymers. When γ -rays and X-rays are at 10^4 Gy or above, the T_g of epoxy resins will decrease, as shown in Table 1.76. Therefore, working modules (pressure modules or living modules) must be made of Al alloys because of their sealing requirements. However, as experimental stations become large and permanently manned space stations, the station parts will be delivered from the ground to near earth orbit and will be assembled in space. As the size of parts increase, metal materials will be less desirable for use in space stations and ACM including graphite/epoxy will gradually be applied more.

The "Peace" space station's large truss-frame earth antenna reflector (EAR) was made of carbon fiber composites and hinged using light alloys. Its fold-over dimensions are $0.6 \times 0.6 \times 1.0$ m and 3.8×3.6 m in extended form.

In the USA, the structures of the "Freedom" permanently manned space station will be delivered to orbit by a space shuttle in 15 trips,

In the USA, the robot in the space station is composed of high-strength CF composites or Ti alloys. In the Japanese space laboratory, the robot arm was made of high modulus graphite/epoxy and Nomex honeycomb structures with Kevlar/epoxy wound on the outer layers.

(Translated by Jianmao Tang.)

References

1. Chen XB (2004) Polymer matrix comp handbook. Chemical Industrial Press, Beijing (in Chinese)
2. China Aero mater Handbook: vol.6 (2002) Composite Adhesives, 2nd edn. China Standard Press, Beijing (in Chinese)

3. Jiang ZY, Zhang HS (1990) Fiber-resin matrix composite technology and application. China Standard Press, Beijing (in Chinese)
4. Michael C et al (1992) Composite airframe structures. Conmilit Press LTD, Hong Kong
5. Shen Z et al (2001) Composite structure design handbook. Aero Industrial Press, Beijing (in Chinese)
6. Timothy GG (1997) Advanced composites manufacture. Wiley, New York
7. Wo DZ et al (2000) Encyclopedia of composites. Chemical Industrial Press, Beijing (in Chinese)
8. Yang NB, Zhang YN (2002) Composite airplane structure design. Aero Industrial Press, Beijing (in Chinese)
9. Zhang YL et al (2003) Advanced composite manufacture tech handbook. Mechanical Industrial Press, Beijing (in Chinese)
10. Zhao QS (2003) Advanced composite handbook. Mechanical Industrial Press, Beijing (in Chinese)

Chapter 2

Industrial Polymer Matrix Composites and Fiber-Glass-Reinforced Plastics

Qixian Liu, Zhongmin Xue, Zaiyang Liu, Hongmei Gao, Rongqi Zhang, Weizhong Li, Zhihua Du and Dexu Yang

Today, the most commonly used composites, with the largest market share, are resin matrix composites. Glass-fiber-reinforced plastics (GFRPs) have excellent performance/price ratios and weathering properties and can be easily molded into complex shapes. They also perform better in many applications and have lower densities, than metals.

The appropriate design, manufacture, and choice of GFRP depend on an understanding of this type of composite. Firstly, coordination between the resin and reinforcing fiber is needed. For example, the elongation at rupture of glass fibers is about 5.3% and the resin should have at least the same elongation to give the composite the optimum properties. The resin and fiber also must be adhered firmly. Resistance to environmental factors, water, and other corrosive media, and the ability to withstand a constant stress cycle are essential properties of resin systems. For a given resin–fiber system, the higher the fiber volume fraction is, the better the mechanical properties of the composite are. However, the fiber volume fraction is limited by the manufacturing technique. In the shipbuilding industry, the fiber volume fraction of a composite produced by hand lay-up is generally about 30–40%. In the aerospace industry, the fiber volume fractions of composites produced using complicated and precision processes can be up to 70%. The orientation of the fibers in a composite depends on the composite loading method. This anisotropy can be an important advantage of a composite or may be a shortcoming if dealt with poorly.

Secondly, the personnel who fabricate the final structures can do almost nothing to change the inherent properties of metals. However, composite materials and structures are made simultaneously with the composites. An appropriate and

Q. Liu (✉) · Z. Liu
Harbin FRP Institute, Harbin, Heilongjiang 150036, China
e-mail: lqx888@mail.hl.cn

Z. Xue · H. Gao · R. Zhang · W. Li · Z. Du · D. Yang
Beijing FRP Institute, Beijing 102101, China

reasonable choice of manufacturing process is therefore the most important step in determining the composite structures and properties. It is difficult to draw up a national composite material standard, and only a composite products standard has been compiled. Because of the anisotropy of composites and the close relationship between the composite properties and manufacturing process, methods for testing composites are complicated. Methods for property testing and composite characterization are important aspects of resin matrix composites.

2.1 Core Materials

According to engineering theory, the bending stiffness of a panel is directly proportional to the cube of the thickness, so increasing the panel thickness is an effective way of enhancing its bending stiffness. This concept is widely used in the design of engineering structures. A low-density core material is used as a core board for addition to a composite laminate to increase the thickness and stiffness of the laminate.

Figure 2.1 shows a sandwich core laminated with a core board under a bending load. The sandwich-core laminate can be regarded as an I-beam. The laminate skin acts as the flange of the I-beam, and the sandwich core acts as a web and is subjected to shear. In this loading model, the top skin is under compression, the bottom skin is under tension, and the core is under shear. The most important property of the core material is therefore the shear strength or shear stiffness. In addition, when lightweight and thin laminate skins are used, the sandwich board can be subjected to a compressive load to avoid damaging the thin skins, stabilizing the structure surfaces to protect the sandwich structure from premature failure.

Sandwich structures are widely used in various environments, from the seabed to outer space, and many processing methods are available. Designers therefore have to select core materials with appropriate properties based on the service requirements and process. The properties required for sandwich structures and core materials are listed in Table 2.1. One or more core material properties must meet every property requirement of the sandwich structure. The properties of a sandwich structure should therefore be guaranteed, and appropriate related core materials must be selected.

Fig. 2.1 Sandwich laminate under bending load

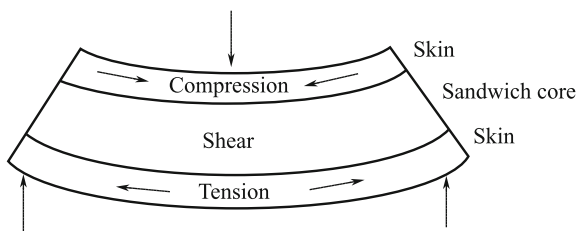


Table 2.1 Relationship between structural properties of sandwich core and core materials

Required structure properties	Properties that core materials should own
Weight optimization	Wide density range
Lateral load capacity	High shear strength
Low plane deformation	High shear modulus
Protect sandwich board buckling	High shear modulus
Protect partial skin buckling	High tensile and compression modulus
Fatigue property	High shear strength, shear strain, and fracture toughness
Impact property	High compression, shear strength, and energy absorption
Allowable stress concentration	High shear strain
Damage allowance	High fracture toughness and high shear strain reduce the faults whenever possible
Creep property	High compression strength, elastic modulus, and heat resistance
Insulation property	Low thermal conductivity, water absorption, and vapor tight
Moisture regain	Low water absorption and vapor tight
Heatproof property	High glass-transition temperature, T_g
Process ability	Good adhesion can be machined and formed, heat and solution resistance, good dimensional stability

2.1.1 Types of Core Material

2.1.1.1 Foam Core

Foams are the most popular core materials. They can be fabricated from various synthetic polymers such as poly(vinyl chloride) (PVC), polystyrene (PS), polyurethane (PU), poly(methyl methacrylate) (PMMA), polyetherimide (PEI), and styrene-acrylonitrile. All these can be supplied with densities over a wide range, from 30 to 300 kg/m³. For composite structures, the most popular density range is 40–200 kg/m³. Various thicknesses can be chosen, and the typical thickness is 5–50 mm [1].

(1) PVC foam

Closed-pore PVC foam is a core material that is used in a wide range of high-performance sandwich structures. Strictly speaking, this type of foam is a blend of PVC and PU, but is usually simply referred to as PVC foam. The PVC foam properties depend on the static, dynamic, and water absorption properties of the foam. In general, foams can be processed at a wide range of operating temperatures, i.e., –240 to 80 °C, and have good resistance to many chemicals. Although PVC foams are usually flammable, flame-resistant products are also available and are generally used in applications with higher fire-resistant requirements, such as train parts. When foam is used as the core material in a GFRP skin sandwich structure, it must be resistant to styrene, to enable its safe use with

polyester resins. PVC foam is therefore used in many industries and is usually supplied in the form of ordinary or grid sheets to facilitate shape formation.

There are two main types of PVC foam: cross-linked and non-cross-linked. The former, which is often called “linear” (e.g., Airex R63.80), is softer and easier to heat-set. However, some of the mechanical properties of such foams, e.g., density, and heat and styrene resistances, are poorer than those of cross-linked PVC foams. Cross-linked PVC foam is hard and brittle, and a panel made of such foam is much stiffer, hard to soften, and has low creep under heating. Typical cross-linked PVC products are Herex C series foam, Divinycell H and HT-class, Polimex Klegecell, and Termanto.

A new generation of toughened PVC foams is available. For these foams, some of the mechanical properties of cross-linked PVC are sacrificed to improve the stiffness of the linear foam. Typical products are Divinycell HD-class ones.

Because of the chemical structures of PVC/PU, such foams must be coated and sealed with resin to enable curing of the cross-linked PVC foam with prepreg tape at low temperatures. The foam can be treated specifically for thermostability, but the treatment merely improves the foam dimensional properties and reduces the amount of gas during high-temperature processing.

(2) PS foam

PS foam is lightweight (40 kg/m^3), cheap, and easily ground; it is therefore widely used in the manufacture of sailing boats and surfboards. It is not suitable for high-performance components because of its poor mechanical properties. This foam cannot be used in combination with polyester resin because styrene can dissolve in polyester resin.

(3) PU foam

PU foam has medium mechanical properties. The foam surface at the resin/core material interface tends to deteriorate with time, resulting in delamination between the skin and core materials. Usually, PU foams are only used in the manufacture of models and skeletons, and the sideboards of strengthened components in various structures. However, PU foam can also be used in sandwich panels that are subjected to small loads. These panels are widely used as insulating boards. PU foams have good high-temperature properties, good sound-absorbing properties and can be easily cut to required contours.

(4) Polyacrylamide foam (acrylic foam)

Acrylic foam has the highest strength and stiffness for a given density, and excellent dimensional stability. In addition, it is easy to use with commonly used high-temperature-cured prepreg tape. However, it is expensive and its use is limited to the manufacture of aeronautic composite parts such as the rotor wings of helicopters and aircraft covers.

(5) SAN foam

The properties of SAN foam are similar to those of toughened cross-linked PVC foam, but SAN foam has a higher elongation and toughness. Its impact-absorbing ability is therefore superior to that of toughened PVC foam. The difference between the stiffness of SAN foam and that of toughened PVC foam is that the SAN stiffness is inherent, whereas a toughener is added to the PVC. The stiffness of SAN foam therefore does not change significantly over time.

Because SAN foam has the same toughness and elongation as linear PVC foam, and it has better heat-resistant and static properties, it is now replacing linear PVC foam in many applications. In addition, SAN foam can be hot-formed to produce curved parts. Thermally stable SAN foam does not interfere with the inherent chemical structure of PVC and can therefore be used with PVC in low-temperature-cured prepregs. Typical SAN foam products are ATC Core-cell series.

(6) Other thermoplastic foams

New techniques for preparing thermoplastic foams are constantly being developed; therefore, the number of types of available foam cores is increasing. Typical products are PEI foam and polyetherimide (PEI), which combine excellent fire-resistant properties and high service temperatures. Although they are relatively costly, they are used in heat- and fire-resistant structures with service temperature in the range -194 to 180 °C. They are particularly suitable for the inner decoration of aircrafts and trains to meet the most stringent fire-resistant specifications.

2.1.1.2 Honeycomb Core

Various materials can be used to make honeycomb cores for sandwich structures. The core can be made of paper or cardboard for applications that need lower strength, stiffness, and smaller loads, such as interior doors.

Aluminum honeycomb can be used to make high-strength, high-stiffness, and lightweight parts of aircraft structures. Planar and curved surface composite structures can be fabricated based on honeycombs. The honeycomb can be made to conform to a complex camber without using excessive mechanical force and heating.

Thermoplastic honeycombs are usually produced by extrusion molding, and then worked to a required thickness. Other honeycombs such as paper and aluminum honeycombs are produced using a multistep process. In this process, many adhesive strips are first attached to many large and thin material sheets, and then the stacked materials are loaded on a hot press to cure the adhesive strips. For an aluminum honeycomb, the stacked materials are cut to the size of the core sheets based on the required thickness of the core material. The core sheet is then slowly stretched, resulting in a continuous honeycomb sheet with a hexagonal grid.

For a paper honeycomb, the core sheet is stretched slowly and enlarged to give a large honeycomb stack of thickness several Chi (1 Chi = 1/3 m) in thickness. This brittle honeycomb core is then immersed in a resin pan, while maintaining the stretched hexagonal structure. The excess resin is drained away, and the honeycomb is cured in an oven. Once the impregnated resin has been cured, the honeycomb core stack is sufficiently strong and can be cut to a honeycomb core sheet of a required thickness.

For both paper and aluminum honeycombs, the honeycomb grid contours can be regulated by changing the stretching level, to give regular hexagonal grid or over-stretched structures. The mechanical properties and processing conformations can be varied by changing the grid contours. Because the honeycomb is a bonding structure, it has different mechanical properties in directions 0° and 90° to the core sheet.

The skin of the sandwich structure is usually made of a fiber-reinforced plastic (FRP) material. Any sheet material with appropriate properties can be used, including wood, plastics (such as melamine), and metals (aluminum or steel). The grid holes in honeycomb structures can also be filled with hard foam. This increases the binding area of the skins and the stability of the grid walls, and the mechanical, insulating, and sound-proofing properties of the core sheet are improved accordingly.

The properties of honeycomb materials depend on the grid size, and the thickness and strength of the web materials. Generally, the thickness of honeycomb core board is 3–50 mm, and the board dimensions are 1200 mm \times 2400 mm, but honeycomb core sheets of size up to 3 m \times 3 m can be manufactured.

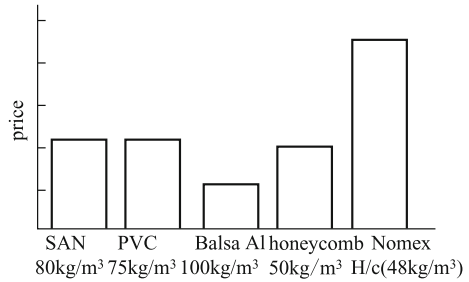
Honeycomb core sheets can be used to produce high-performance and light-weight laminates. However, because of the small binding surfaces of the skin and core sheets, high-performance resin systems such as epoxy resins have to be used to ensure binding between the laminate skin and core materials as required.

(1) Aluminum honeycomb

Aluminum honeycomb can be used to produce structural materials with optimum strength/weight ratios. Aluminum foil adhesion can be achieved in various ways; therefore, honeycombs with different grid contour patterns can be obtained by changing the thickness of the aluminum foil and the grid size. Honeycomb materials are normally supplied as unstretched stacks, which are stretched out into sheets on site.

Although aluminum honeycombs have good mechanical properties and are fairly cheap, they should be used carefully in some applications such as large marine structures. There are potential corrosion problems in briny environments. It is therefore necessary to ensure that the aluminum honeycomb is not in contact with carbon composite skins because the conductivity of the skin will aggravate electrochemical corrosion. Another problem with aluminum honeycombs is that they do

Fig. 2.2 Comparison of various core prices



not show a mechanical memory effect. If the sandwich structure is subjected to an impact, the honeycomb is deformed irreversibly, but the FRP skin recovers because of its flexibility. As a result, the skin debonds and the mechanical properties deteriorate.

(2) Nomex foam

A Nomex honeycomb is made from Nomex paper, which consists of Kevlar fibers. Generally, this raw paper honeycomb is impregnated with phenolic resin to make Bakelite and honeycomb cores with high strength and heat resistance. This foam is combined with a phenolic resin skin to make light wallboards inside aircraft. To meet the flame-resistant requirements for applications such as the inner wallboards of public transport vehicles, and to produce special-grade honeycomb cores, the core cells are filled with phenolic foam to increase the binding area and enhance the insulating properties. Because of its good mechanical properties, low density, and good long-term stability, Nomex combs are being increasingly widely used in high-performance non-aerospace parts. However, it is more expensive than other core materials, as shown in Fig. 2.2.

(3) Thermoplastic honeycomb

Honeycombs made of other thermoplastics are lightweight, useful for enhancing some properties, and recyclable. The main drawbacks are difficulties in achieving a firmly bonded interface, and low stiffness. Such honeycombs are generally used in structures bearing heavy loads and in ordinary inner wallboards.

The following polymers are used for general purposes.

1. ABS resin: This is used in structures that require high stiffness, toughness, impact strength, surface hardness, and dimensional stability.
2. Polycarbonate: This is used in structures that require good UV stability, transparency, heat resistance, and self-extinction.
3. Polypropylene: This is used in structures that require good chemical resistance.
4. Polyethylene: This is used in general structures that must be cheap.

2.1.1.3 Wood

Wood can be considered as a natural honeycomb. The microscopic structure of wood is similar to the hexagonal porous structures of man-made honeycombs. When sandwich structures are produced with wood in such a way that the direction of the grain is perpendicular to the skin plane, the performances of manufactured components are similar to those of man-made honeycomb components. Although various chemical treatments can be used to give moisture resistance, all wood core materials are sensitive to moisture. If the wood is not well packed with laminate board or resin, it will be easily corrupted.

(1) Light wood

The most common wood core material is end-grained light wood. Light wood cores were first used in 1940 as airship shells. Aluminum skin–light wood sandwiches are used to withstand repeated shocks when landing on water. End-grained light wood core materials are used in FRP structures in the marine industry because of their shock-resistant properties. In addition to having high compressive strength, light wood is a good insulating material and its absorption properties are good. The material does not deform when heated, and in a flame it is involved in the insulation and ablation layers. When the core material is slowly burned, the skin that is not exposed can still maintain its structural integrity. In addition, it can float and can be processed using simple tools and equipment.

Light wood cores can be produced in accordance with a specific contour size, of thickness 3–50 mm, and coated with fabric. The thickness of a hard end-grained core material can be up to 100 mm. This core material can be easily coated with resin and can be processed using vacuum bag or prepreg methods or manufactured under pressure, e.g., by resin transfer molding (RTM).

A disadvantage of light wood is its high density; the minimum density is usually 100 kg/m³. This results in deterioration caused by absorption of excess resin during lamination, although this can be reduced by using presealed foam. However, it is often used in structures where weight is not a serious consideration, or in local high-stress areas.

(2) China fir

China fir is also commonly used as a core material. In the marine industry, it often serves as the core of lath structures, with composite skins on both sides. The grain direction of China fir is parallel to the laminate surface. The fiber orientation of China fir is arranged along the ship length to achieved vertical stiffness. The FRP skin is laminated at $\pm 5^\circ$ to obtain stiffness and protect the wood.

2.1.1.4 Other Core Materials

Although other materials are not usually used as the cores of sandwich structures, there are many thin and low-density fabric materials that can be used to reduce the density of solid laminated structures. These materials such as COREMAT and SPHERETEX consist of a hollow ball filled with a nonwoven mat fabric; this reduces the density. Their thickness is usually 1–3 mm. They are laid on the middle of the laminate board, like another layer of reinforcing material, and leached with laminating resin during laying. However, although the middle layer consisting of a hollow ball instead of resin is heavier than a foam or honeycomb core, its density is lower than that of glass-fiber laminated board of similar thickness. This type of sandwich material is very thin and easy to lay up on a double-curvature surface. Methods for its use are convenient and fast.

2.1.2 Comparison of Mechanical Properties of Core Materials

Figures 2.3 and 2.4 show the changes in shear strength and compressive strength with density of some of the core materials discussed above [2].

The figures show that the properties of the core materials improve with increasing density. However, checking the weight of the core materials in the sandwich shows that other factors in addition to the density are involved. For example, a low-density foam core accounts for a small portion of the weight of a sandwich structure, but it absorbs a large amount of resin at the binding interfaces between the skin and the core because of its porous surface, and this increases the weight of the structure. The larger the pores are, the lower the foam density is, and the more serious the effect is. In contrast, for a honeycomb, this problem can be solved by painting an adhesive around the grid walls of the honeycomb to form a small adhesion gap, as shown in Fig. 2.5.

Fig. 2.3 Relationship between compressive strengths and densities of core materials

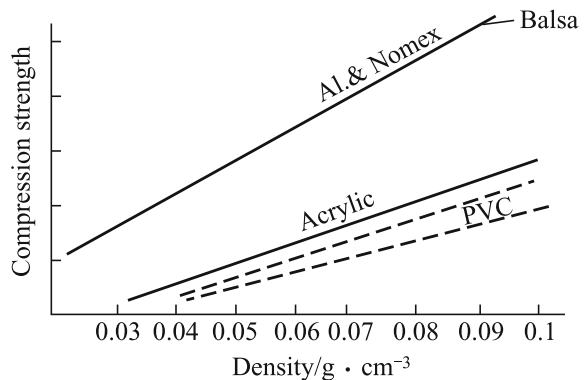


Fig. 2.4 Relationship between shear strengths and densities of core materials

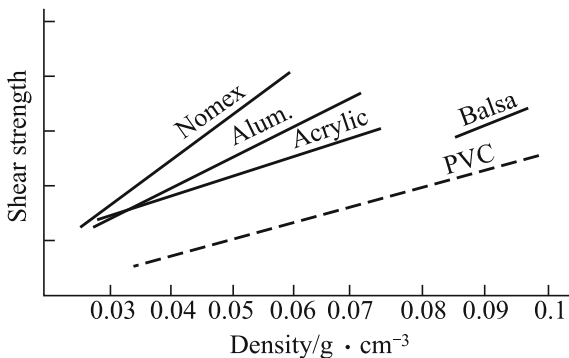
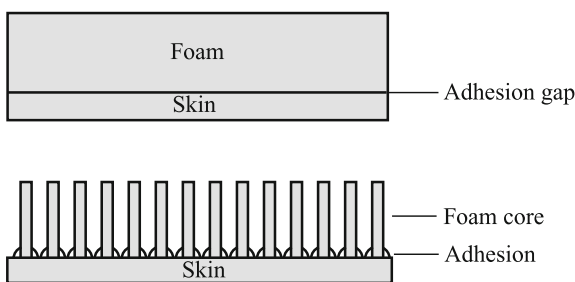


Fig. 2.5 Two types of binding between skin and core



Finally, the shape of the core material must be considered, and it must completely match the component shape. Any mismatches and large gaps must be filled with adhesive, resulting in a considerable increase in weight, which can be prevented by using an appropriate core material. For example, small square pieces of core material can be placed on a light and loose fabric. A foam or balsa core with a loose fabric can be easily matched with curved surfaces. Slots can be cut in the back of core materials to form contours that match the components, achieving the same results as above. These core sheets need large quantities of adhesive to fill the gaps between square foam pieces to enhance the structural properties.

When the weight required for components is critical, thermo-formed core materials have to be considered. For example, linear PVC and SAN foams can be heated to above their softening points and prebent to match a mold. For a honeycomb core, a common method used to match the core material with curved surfaces is to stretch the honeycomb core by expansion. Different expanded forms can be made to meet the needs of various configurations.

2.2 Forming Processes

2.2.1 Hand Lay-up Processes

Hand lay-up processes are low-pressure contacting and forming processes. They are performed mainly by hand, and equipment and tools are only needed to complete auxiliary work. Hand lay-up is simple, easy to learn, and easy to grasp. The equipment used is simple, needs low investment, and is quickly started. The product size and shape are not limited. However, hand lay-up processes have the drawbacks of low efficiency, poor working conditions, and high labor intensity. The product quality relies greatly on the worker's operational skill and is difficult to control. The product structure is inferior to those of products obtained using other techniques. Nevertheless, the hand lay-up process is still irreplaceable, especially for small quantities, and large or complex-shaped GFRP products. A large proportion of GFRP products are produced using hand lay-up processes. Most medium and small GFRP mills focus on production using hand lay-up processes. For large-lot producers, it is difficult to replace this process.

Because of the strong relationship between product quality and the worker's operational skill, much effort is expended on operator training and operating procedures and methods. All the details of the impact on product quality must be understood to produce reliable and stable products.

2.2.1.1 Materials

(1) Reinforcing materials

The main reinforcing materials used in hand lay-up processes are glass-fiber plaid, cloth, chopped strand mats, and chopped fibers. Other types of fiber fabric can also be used, depending on demand.

These reinforcing materials must be suitable for use in molds and set in surfaces without folds.

Tables 2.2 and 2.3 list the performance requirements of reinforcing materials used in hand lay-up processes.

Plaid is the main reinforcement used in hand lay-up processes. The advantages of this material are good shape variability, easy resin infiltration, thickening efficiency, and high stiffness and strength. Chopped fiber-glass mat is mainly used for anti-cracking on both sides of GFRP structures or anti-corrosion layers of anti-corrosive structures. The product structure can also be enhanced using chopped fiber glass if high strength is not required. Chopped fiber-glass mat has good soaking properties, air bubbles are easily removed, it is conformal, construction is convenient, and it contains 60–80% rubber.

Table 2.2 Specifications and purposes of some reinforcing materials

Name	Trademark	Specification/mm	Purpose
Plaid	EWR200-90	180 ± 18	Enhance the structure layer
	EWR400-90	365 ± 37	Enhance the structure layer
	EWR500-100	485 ± 49	Enhance the structure layer
Chopped strand mat	MC300-104 (208)	300	Enhance the impermeable layer and the transition layer
	MC360-104 (208)	360	Enhance the impermeable layer and the transition layer
	MC450-104 (208)	450	Enhance the impermeable layer and the transition layer
	MC600-104 (208)	600	Enhance the impermeable layer and the transition layer
	MC900-104 (208)	900	Enhance the impermeable layer and the transition layer
Unidirectional cloth	WF600	600	One-way reinforced
	WF800	800	One-way reinforced
Unidirectional woven material	WF1000	600/400 cloth/carpet	Enhance the structure layer
	WF1200	800/400 cloth/carpet	Enhance the structure layer
Surface mat	FW-30 M	30	Enhance the resin-rich surface layer
	FW-40 M	40	Enhance the resin-rich surface layer
	FW-50M	50	Enhance the resin-rich surface layer

Table 2.3 Properties of several reinforcing materials for glass-fiber-reinforced polyester

Type	Specification	Tensile strength/MPa	Tensile modulus/GPa	Shear strength/MPa	Rubber content/%
Plaid	400 g/m ²	223	14.9		50
Unidirectional cloth	Roving	563.7	32	52.5	40
Chopped strand mat	450 g/m ²	49.3	7.9		75

Surface mat is used on the outer layer of GFRP products. It has good soaking properties and good conformality and contains 90% rubber. It is also used to decorate the surface and improve the surface corrosion resistance of anti-aging materials.

Unidirectional cloth and GFRP cloth are used for local reinforcement.

Fiber roving or chopped fibers are sometimes used to fill local corners. Other types of fiber and fabric products can also be used to meet the structural performance requirements of products.

(2) Resin systems

Several types of resin are used in resin systems, such as polyester resins, vinyl ester resins, phenolic resins, and furan resins. Polyester resins, vinyl ester resins, and epoxy resins are most commonly used. Phenolic resins are not generally used because of the need for pressure curing. In China, phenolic resins that can be cured under normal pressure are currently used in winding and hand laying. However, they are rarely used because of their instability. Because their manufacture produces toxins and pollutants, furan resins are not often used except for specific temperature- or corrosion-resistant applications.

The resin systems used in hand lay-up processes must have low viscosity, good immersion properties, be curable at room temperature and normal pressure, have low flow during curing, and the curing process must be non- or low-toxic. Polyester and vinyl ester resins are suitable, and Table 2.4 lists the properties of several polyester and vinyl ester resins. Gel-coating resins are also used as hand lay-up resins. Gel-coating resins are applied to product surfaces to decorate the surface and make it hard, corrosion resistant, and anti-aging.

Table 2.4 Properties of various resins

Project		Epoxy resin	Polyester resin			Vinyl ester
		Bisphenol A	o-type	m-type	Bisphenol A	Bisphenol A
Viscosity		200–600	300–400	500	450–550	400–700
Density/g cm ⁻³		2.5–6	1.23	1.21	1.123	1.13
Physical properties of cast	Pap hardness	50	29	32	25	35
	Shrinkage %	1–2	8.5	9.6	8.5	8.0
	Heat distortion temperature/°C	110–150	70–90	90–110	90–120	100–150
	Tensile strength/MPa	65.6	30	52	33	80
	Flexural strength/MPa		10.4	95	10.5	150
	Compressive strength/MPa		179	150–180	1.35	150–260
	Impact toughness/J cm ⁻²		3.0	2.1	2.3	7.5
	Flexural modulus/GPa		3.4	3.5	3.5	2.7
Elongation/%		1.5	1.8	1.2–3	1.5–3.2	6

(3) Supplementary material

The supplementary materials used in hand lay-up processes are reactive materials that form curing systems with resins, and fillers that constitute functional systems with resins. For epoxy resins, the components of the curing system are curing agents (amine curing system) and catalysts (acid anhydride curing system). For polyester resins and vinyl ester resins, the curing system contains components such as initiators and promoters.

The supplementary materials that constitute functional systems with GFRPs include tougheners, thinners, defoamers, air cutoff agents, coloring agents, release agents, and fillers.

With the development of composite molding techniques and the composite materials industry, supplementary materials such as flexibilizers, thinners, defoamers, and air cutoff agents are being considered by resin manufacturers for use in resin production. Supplementary materials that can be used independently by composite manufacturers include fillers, colorants, flame retardants, and release agents.

Calcium carbonate, barium sulfate, silica, talc, diatomite, mica, asbestos, aluminum hydroxide, glass-fiber powder, and graphite are used as fillers. The properties of composites, such as reduced shrinkage rates, reduced stress during resin curing, improved mechanical properties, improved surface states, thixotropy, flame retardancy, heat resistance, electrical conductivity, and anti-aging, can be changed by using different fillers; the cost can also be reduced. Table 2.5 lists some filler types and functions.

2.2.1.2 Mold and Release

Molds are the main tools used in hand lay-up processes. An appropriate choice of mold material and mold structure design ensure product quality, reduce costs, and increase efficiency. They are important components in the hand lay-up process.

(1) Mold material

Many types of mold material are used in hand lay-up processes. Different materials are used, depending on the situation. When choosing a mold, factors such as technology, economy, and feasibility should be considered. Mold manufacture should be simple, mold production and source materials should be cheap, and the quality of the mold must meet the product requirements. There are many mold materials, e.g., timber, paraffin, cement, metal, GFRPs, and clay. Table 2.6 compares the properties of various materials.

1. Timber: The general requirements of timber for mold materials are uniform texture, non-section, and good stiffness. Wood molds are only used for large-scale, single products or small numbers of products. For large-volume products, wood molds can be used as mother molds.

Table 2.5 Filler types and functions

Filler	Approximate density/g cm ⁻³	Bulk density/g cm ⁻³	Filler ratio in every ten resins	Interoperability ^a	Effect ^b
Chalk powder	2.7	1–2	50–300	a, c, h	1, 7, 15
Clay	2.6	0.25–0.45	25–200	a, d, h	2, 7
Talc	2.7	0.5–0.6	25–200	a, e, h	1, 4, 5, 7, 11
Slate powder	2.5	0.45–0.70	25–150	c	2, 5, 7, 14
Quartz powder	2.65	1.0–1.1	100–400	a, c, e	3, 5, 7, 8, 12, 14
Ceramic powder	2.4	1.0	100–400	a, c, e	3, 5, 7, 8, 12, 14
Quartz sand	2.65	1.3–1.6	300–700	c, e	3, 5, 7, 8, 12, 14
Mica powder	2.6–3.2	0.45–0.55	25–100	b, d	1, 4, 5, 13, 14
Cork powder	0.2–0.3	0.05–0.10	5–10	b, d, f, h	1, 10, 11, 13, 15
Graphite	2.3–2.6	0.25–0.45	30–80	c, g	1, 4, 5, 7, 12, 15
Metal powder	–	–	–	c, e, g	1, 4, 6, 7, 8, 9, 12
Silica uncompressed	2.1	0.0048	3–15	a, b, f	2, 14
Glass flake	2.5	–	20–35	a, b, c, f	3, 5, 7, 8, 13, 14

^aInteroperability: a-added easily; b-adding a small amount of filler, lead to increased viscosity; c-easily mixed; d-difficult mixed; e-rapid precipitation; f-keeping suspension; g-promoting curing; h-hygroscopicity

^bEffect: 1-good mechanical properties; 2-general mechanical properties; 3-poor mechanical properties; 4-good sliding properties; 5-good abrasion resistance; 6-reducing heat; 7-low shrinkage properties; 8-low coefficient of linear expansion; 9-high density; 10-low density; 11-high impact strength; 12-high thermal conductivity; 13-good thermal insulator; 14-good electrical insulator; 15-poor electrical properties

Table 2.6 Comparison of various materials

Type	Production cycle	Production process	Weight	Frequency of use	Cost	Range of using
Timber	Short	Simple	Light	General	General	Small- and medium-sized products with complex structure and small number
Gypsum	Short	Simple		1–5	Low	Large products or one-off products with complex structure
Paraffin	Short	Simple	Light	1	Low	Products with small number, difficult to paint, melting demoulding
Cement	General	Simple	heavy	General	Low	Simple product
GFRP	General	Relatively simple	General	frequently	High	Small- and medium-sized products with complex structure and larger number, high surface requirements
Foam	Short	Simple	Light	1	High	The inner core without releasing
Metal	Long	Complex	Heavy	100	Expensive	Surface

2. Paraffin: Paraffin molds are suitable for small dies, which are not demolded or difficult to demold.
3. Cement: The characteristics of cement are high strength, low cost, and ease of manufacture. Generally, it is used in the manufacture of simple shapes and products with simple surface requirements. It can also be used as a mother mold material.
4. Metal: Metal molds are made of steel. Large-scale and small products can be made using metal molds. Metal molds are suitable for manufacturing large quantities of products with high dimensional accuracy, and small products with rough surfaces. However, metal molds have the drawbacks of the high processing costs of steel, high weight, and long manufacturing cycles.
5. Gypsum: Gypsum plaster can be used to manufacture products with small volumes and complex shapes. Low-intensity gypsum is used with cement to improve its strength.

6. GFRPs: GFRP molds are suitable for small- and medium-volume production. They are made with the mother dies.

(2) Release agents

Release agents for molds should be easy to use, non-corrosive to the mold, and have low adhesion with the resin. They should also be uniformly smooth, non-toxic to humans, cheap, easily manufactured, and safe and easy to use.

There are many types of release agent. Common types are thin, mixed, solution based, and oil-wax. Release agents for use with products with high-quality surface requirements can be bought from GFRP manufacturers.

Useful release agents include the following.

1. Thin film: Films such as polyester, PVC, polyethylene, poly(vinyl alcohol) (PVA), and cellulose acetate films are used as release agents. The mold can be used after treating the surface with Vaseline or butter. Wrinkling or blanks must be prevented when using thin films.
2. PVA. Formula (wt%): PVA 5–8, ethanol 35–60, water 65–35
Low-molecular weight and water-soluble PVA should be selected. A release agent containing a small amount of ethanol is easy to dry, but the solubility is poor and it is difficult to prepare a film of the agent. Ethanol is sometimes omitted. A uniform film can be obtained by adding 2wt% of a surfactant, e.g., a soft-soap powder, to the release agent. A smooth film can be obtained by adding 1% of succinic acid salt aerosol to the release agent. The addition of 0.1% silicon defoamer to the solution reduces air bubble formation during brushing. The addition of 4–5% glycerol promotes film formation and improves the film flexibility. Rusting of a metal surface can be prevented by adding 0.75% sodium benzoate. The addition of blue ink or Berlin blue prevents leakage. PVA used with wax gives a better effect.
3. Release agents such as ointment and paraffin. Silicon ester (methyltriethoxysilane or its 50% toluene solution), HK-50 heat ointment, transformer oil, yellow oil, and Vaseline oil are used. Car polish wax, paraffin oil (5:95) solution, paraffin, asphalt and fuel, and other solutions are also used. These types of release agent are cheap, easily obtainable, and non-toxic.

(3) Mold design and manufacture

A mold is the main piece of equipment in a hand lay-up process. The mold design and manufacture directly affect the product quality and cost. In mold design, the following requirements must be considered.

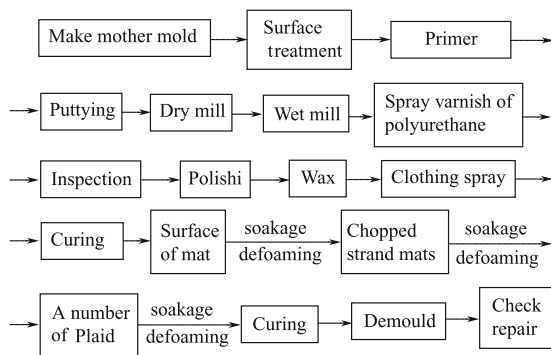
1. Products must meet performance requirements for factors such as dimensional accuracy, surface roughness, and flatness.
2. The mold must have sufficient strength and stiffness to withstand the load generated.
3. Demolding must be easy, labor saving, and must not damage the product.

4. Resin curing is exothermic; therefore, the mold must be heat resistant to prevent heat deformation.
5. The materials must be lightweight, cheap, and easily obtainable.

Molds can be negative mode, positive mode, matched mode, or combination mode. The mold type is chosen based on surface requirements. When dimensional accuracy and surface roughness are required, the negative mode is chosen. The positive mode is used when dimensional accuracy and inner surface roughness are required. Matched mode is used when dimensional accuracy and roughness of both surfaces are required. Combination mode is used when the product has complex dimensions and demolding is difficult.

An FRP mold is the most commonly used tool in hand lay-up processes. It has advantages such as ease of design, ease of manufacture, high surface roughness, and high intensity and stiffness; it can be reused and is suitable for mass production.

The following diagram shows the process for manufacturing a GFRP mold.



The mother mold is usually manufactured from wood, plaster, or cement. The mother mold is directly used if possible. The dimensional accuracy and surface roughness of the mother mold are the most important points. When a GFRP mold is being made from the mother mold, it is necessary to control spraying of the coating and to ensure that there are no bubbles in chopped strand mats and surface mats and that impregnation is complete. The quality of the forming mold not only affects the dimensional accuracy and surface roughness but also determines the service life of the mold.

2.2.1.3 Processes

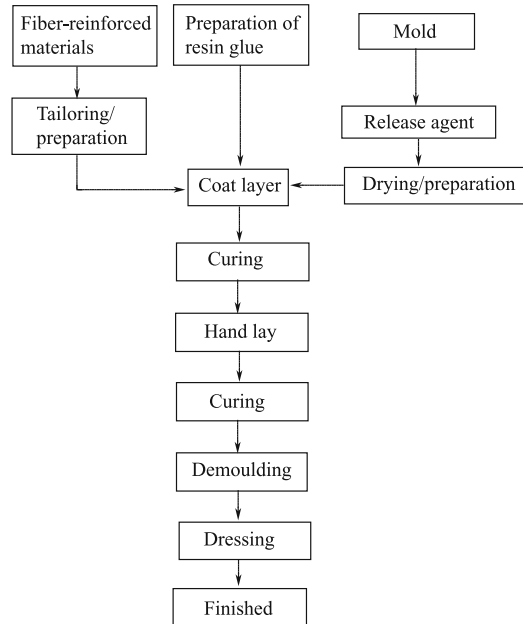
(1) Production process

The following diagram shows the hand lay-up process.

(2) Tools for hand lay-up

The tools used in hand lay-up are important for increasing productivity and ensuring product quality.

1. Spray gun: A spray gun is used for spraying a gel coating on the surface layer. Specific spray guns are commercially available. A spray gun with spray nozzles of various dimensions enables use of liquids of different viscosities.
2. Wool roller: A wool roller is used to impregnate and coat resin during the hand lay-up process; 4-inch, 6-inch, and 8-inch wool rollers are available.
3. Bristle roller: A bristle roller is used to drive out air bubbles. Rollers with bristles of the following sizes are available: ϕ 20 mm and 50 mm; length 50–150 mm.



4. Spiral roller: Spiral rollers are made of aluminum, steel, or hard plastic. They have a spiral groove on the surface circumference. A spiral roller is used to drive out bubbles and form a uniform resin by rolling the surface layer.
5. Scraper: Scrapers are generally made of polyethylene or glass plate of thickness 3 mm. They are used to drive out bubbles and form a uniform resin with high efficiency.

A number of other power tools such as angle grinders, electric drills, polishing and cutting machines are used for cutting cloth conference.

(3) Quality control

A hand lay-up operation is completed by hand, even if power tools are available. The key factors in quality control during hand lay-up processes are standardization of operations, the quantity of material, the complexity of the composition decomposition during operations, and operational simplicity.

1. Selection and preparation of materials: Raw materials of a certain size and quality must be obtained from manufacturers. The raw materials should not be changed frequently because there are differences among materials supplied by different manufacturers. Differences among resins are obvious. Replacement of a specific grade of resin may lead to changes in curing.

Environmentally friendly raw materials should be used. Humidity affects the moisture content of fibers for reinforcing materials. A large moisture content affects the quality of impregnation. Reinforcing materials should be stored under dry conditions and dried before use. Resins should be stored at constant temperature. This controls the stability of the resin system during application.

2. Dealing with mold. The internal properties of the mold, such as size and surface roughness, should be considered and controlled during production processes. Dealing with the release agent on the product surface is important in terms of product quality and die life. The release agent coating affects the product surface and mold release. Uneven coating or leakage of the release agent coating affects the surface quality of the product. An increase in the release force can potentially damage the product or mold surface. A mold release force that is too high shortens the service life of the mold.
3. Layer structure: A symmetric layer prevents deformation. Generally, the distribution of hand-lay products from the inside out is SM + GM + n (RC + GM) + GM + SM, or SM + GM + n RC + GM + SM (SM: surface mat; GM: chopped strand mat; RC: plaid). Unless the middle enhanced layer (RC) is sufficient, we cannot simplify the outer surface layer of GM and SM.
4. Control of resin volume: The amount of resin between layers must be controlled as follows: surface of mat 90%; chopped strand mat 70%; plaid 50%. Two layers of glue can be used according to the following equation:

$$w_{\text{total}} = w_{\text{layer}} + w_{\text{roller}} + w_{\text{other}}$$

w_{total} is the volume of the total plastic layer;
 w_{layer} is the actual volume of resin in the layer;

$$w_{\text{layer}} = w_r w_g / (1 - w_r);$$

w_r is the amount of resin with standard requirements;
 w_g is the total weight of enhanced material;
 w_{roller} is the volume of resin on the roller;
 w_{other} is the amount of resin lost for other reasons.

5. Specification: The operations performed by workers should be standardized and must not vary from person to person. Glue containers, stirring tools, mixing methods, and the number of steps in resin stirring and impregnation should all be standardized.

6. Environmental control: The environmental humidity and temperature greatly affect the product quality because they affect factors such as the amount of resin, impregnation quality, and bubble content. The humidity and temperature must be controlled in a stable range.
7. Demolding: Demolding should be taken into account in mold design. The quality of demolding affects the product quality.
8. Curing: The curing quality affects the structure performance and demolding of the product. Generally, hand-lay processes use room-temperature resin curing. Cured products are not completely produced in a natural environment because temperature changes in the natural environment affect the curing properties. A stable curing environment must be created.

2.2.2 Injection Molding Techniques

In injection molding, resin and fibers are simultaneously sprayed into a mold, using a spray gun, to make an FRP. A spray gun is the main equipment used in injection molding. The specific characteristic of this method is that a cutter is installed on the spray gun. The cutter is used in combination with resin spraying to cut continuous fibers into the required short fibers. The gun then injects the fibers into dies together with the resin. Injection molding is a development of hand lay-up and is a semi-mechanized hand-lay method. Its advantages are as follows.

1. It can reduce the cost of materials by using roving cloth instead of glass cloth.
2. The method has a high degree of mechanization and production efficiency (two to four times that of hand-lay processes) and is suitable for large-scale GFRP products.
3. There are no ride joints, and products are better overall.
4. Flash, cut, and loss of glue are reduced.

The disadvantages of injection molding include high resin contents, on-site dust, and the need for isolated operations. Injection molding can also be used in combination with other processes, bringing their respective advantages into play. For example, injection molding is combined with a hand-lay process to make tapetum structures, followed by spreading glass cloth by hand and foam removal, completely eliminating the coating operation. In the production of pipeline and storage tanks, a winding process is combined with a lining molding injection method to increase the degree of mechanization, to improve the production efficiency, quality, and stability. The injection molding has an almost irreplaceable role in manufacturing large molded products such as ships.

2.2.2.1 Materials

The only raw materials used in injection molding are continuous-fiber roving and the injecting resin, as determined by the technological features.

(1) Continuous-fiber roving

Continuous winding fiber roving in injection molding is different from fiber roving in winding and pultrusion processes. The characteristics of continuous-fiber injection are as follows.

1. A good cutting performance, and less generation of static electricity during cutting. To achieve a good cutting performance, coupling agents such as silane and organic chromium compounds are often used.
2. After roving has been cut off, the decentralization efficiency should be high; usually greater than 90% is required.
3. The original wire should give an excellent lodging performance after being cut off and should cover every corner of the mold without tilting.
4. Dipping is fast, and an easily used drive roller expels bubbles.

(2) Injection resin

The injection process characteristics are fast curing of the sprayed resin system, fast dipping, few air bubbles, ease of bubble expulsion, and easy lodging when mixed with chopped fibers. The main resins used for injection molding are polyester and vinyl ester resins. During injection, mixing occurs in the spray gun or spray nozzle. There is no mixing time, unlike in other techniques, and gelatinizing and lying, which are needed in hand lay-up, are unnecessary, which also saves time. The ratio of curing larger, the product can be solidified faster. Hyrizon resin, developed in the USA, consists of a polyester resin and isocyanate resin. It is used for injection molding and gives a good lodging performance, with almost no need for additional operations for foam removal, which greatly increases the production efficiency. The performance of GFRPs obtained after curing is better than that of polyester resin. Before use, the resin is a mixture of two components, A and B. A is a mixture of isocyanate and styrene, and B is a polyester resin mixed with an esterification catalyst. During injection, the two components are mixed in the spray gun; cross-linking occurs between the polyester resin and a benzene–ethylene mixture, and isocyanate is esterified by mixing with the esterification catalyst. The two reaction products mix with each other to form entangled polymer composite materials. The cured product has the strength of a polyester resin and the stiffness, toughness, and water resistance of polyisocyanate urethane.

2.2.2.2 Injection Molding Equipment

The injection molding process is almost completely performed using equipment, unlike hand lay-up processes. The process parameters are determined by the equipment, e.g., the group distribution ratio, mixture quality, length of short fibers, and uniformity of amount of resin. These factors improve the stability and efficiency of production and decrease the influence of operational factors.

Figure 2.6 shows a schematic diagram of spraying equipment. To increase productivity and reduce wear and tear, the structure of the mobile trolley, and

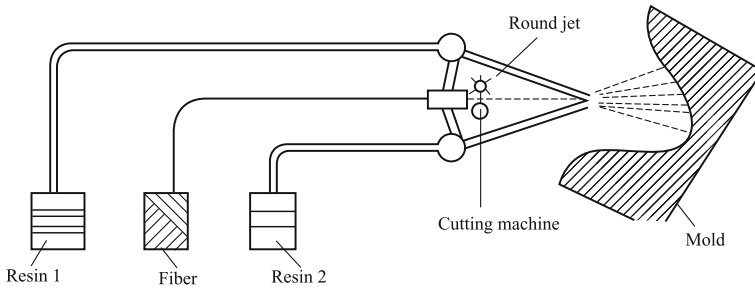


Fig. 2.6 Schematic diagram of spray forming

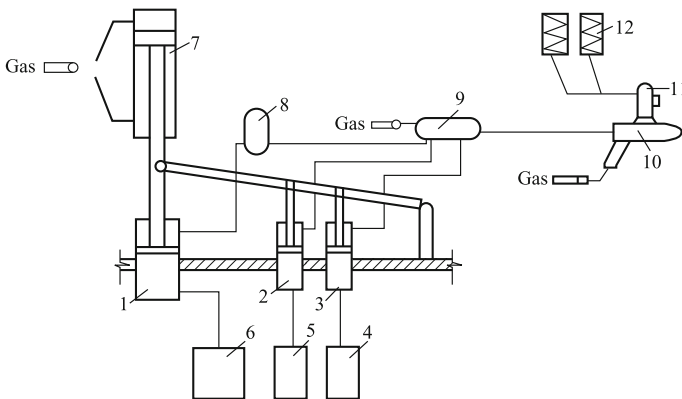


Fig. 2.7 Schematic diagram of pump jet 1—resin pump; 2, 3—auxiliary pump; 4, 5—auxiliary tank; 6—resin tank; 7—cylinder; 8—buffer; 9—mixed gas; 10—spray gun; 11—fiber cutters; 12—yarn emission

height, ventilation, temperature control, and energy-saving factors should also be considered in equipment design.

(1) Types of equipment

Sub-jet methods use compressed air jets and non-compressed air jets. Delivery points are pressure tank and pump-type conveyors.

1. Pump jet (Fig. 2.7): The resin, initiator, and promoter are each transferred to a static mixer pump and then emitted by the gun after being fully mixed. This method is called mixing within the gun. The gun components are a pneumatic control system, resin pump, auxiliary pump, mixer, spray gun, and jet fiber cutter. The resin pump and auxiliary pump are connected by a rigid arm with regulation of the arm's position. The proportions of ingredients are accurate. Resins and additives, which are evenly mixed in the mixer under compressed air, are formed into droplets by the spray gun, and then the mixture with the treated fibers is sprayed on the mold surface.

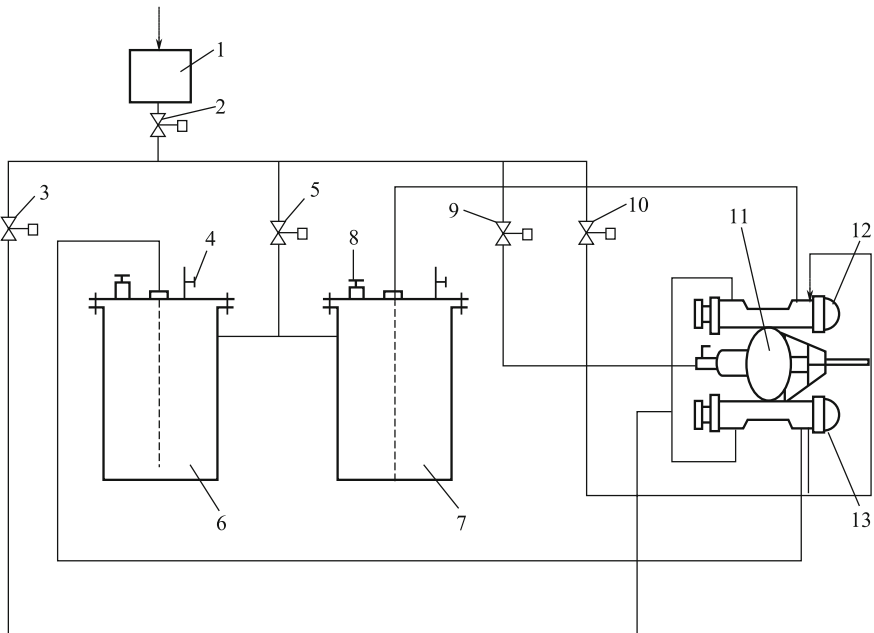


Fig. 2.8 Schematic diagram of tank pressure jet 1—gas-water separator; 2—gas valve; 3—adjusting switch; 4—release valve; 5—adjusting valve; 6, 7—pressure tank; 8—safety valve; 9, 10—adjusting switch; 11—fiber cutter; 12, 13—resin injector

This type of jet with only one glue gun has the advantages of a simple structure, low weight, and less initiator waste. Because the raw materials are mixed in the gun, it has to be cleaned immediately to prevent injection plugging.

2. Tank pressure jet (Fig. 2.8): Resin glues are individually stored in a pressure tank and then sprayed by the gas pressure through the spray gun. The system consists of two tanks, piping, valves, a spray gun, and a fiber-cutting jet. Resin and glass fibers are continuously emitted by the spray gun and then go through a vertical aerosol, fiber dispersion, and even mixing and then fall to the die. Resin mixing outside the spray gun reduces spray nozzle plugging.

(2) Auxiliary equipment

Auxiliary equipment is needed in injection molding to ensure product quality, personal safety, and environmental protection. Figure 2.9 shows the injection molding equipment and layout.

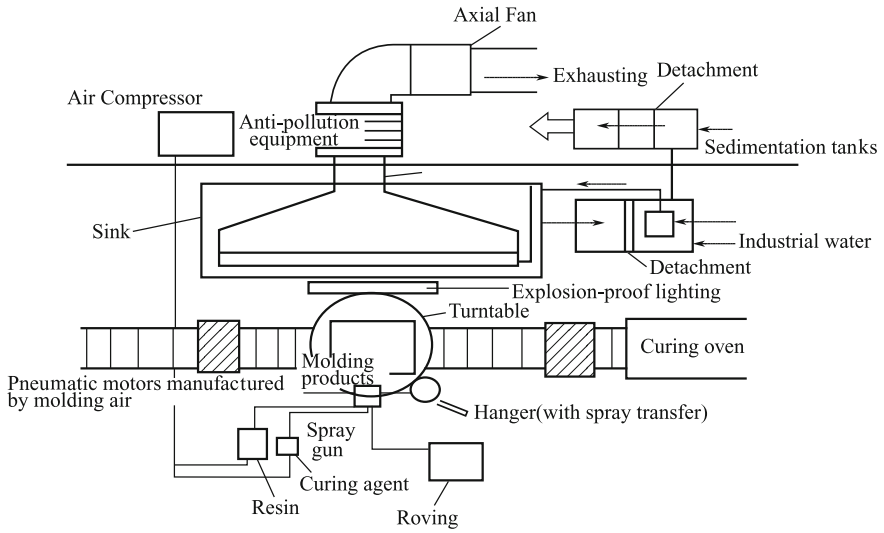
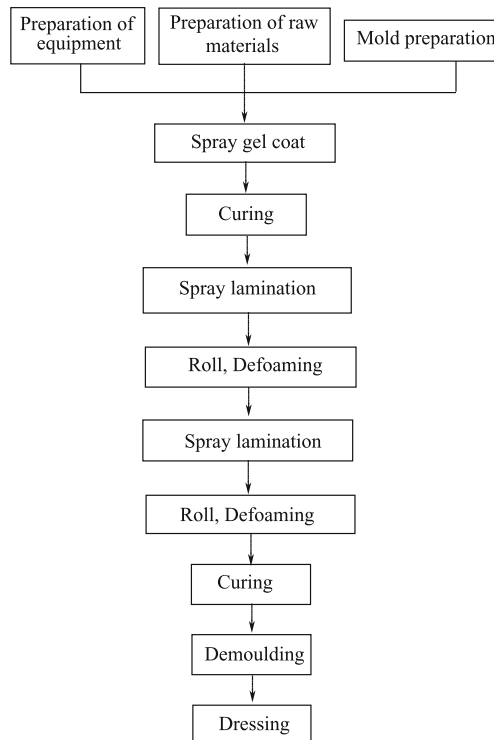


Fig. 2.9 Spray-forming equipment layout

2.2.2.3 Spray Process

(1) Process



(2) Control of process parameters

1. Environmental temperature: The environmental temperature for injection molding is 15–35 °C, and the recommended temperature range is (25 ± 5) °C. Fast resin curing at excessively high temperatures can lead to system blocking or curing stress inequality. Low temperatures lead to low viscosity, slow curing, and resin facade flow.
2. Resin content requirements: The resin content for injection molding should be about 60%. At a low volume of resin, fiber dipping is incomplete and the bending strength of the resin as an adhesive is not strong enough.
3. Spray pressure and tank pressure: These two parameters affect the mixture uniformity and resin content. The resin content in injection molding is about 60%, the spray pressure is 0.3–0.35 MPa, and the resin tank pressure is about 0.05 MPa.
4. Spray angle: The mixing degree of two resins with different components mixed outside the point of the spray depends on the angle of the spray gun. Generally, the spray gun angle is 20°. The distance between the nozzle and the mold surface is 350–400 mm.
5. Plot-level number: If the thickness is high, the product structure should be formed at various times. Generally, the single-layer thickness is less than 1–3 mm. If the laminated layer is thick, compaction will be not easy, with the exclusion of bubbles, and this may result in resin flow. If it is too thin, the production efficiency is low.
6. Flatness control: Injection molding is performed with a handheld spray gun, while the mold is moving. The thickness of the sprayed layer depends on the moving speed. The degree of overlap determines the lamination uniformity. The initial distance between the two jet trajectories can be determined as $d = (\text{width} + \text{thickness})/2$.

To sum up, injection molding process parameters can summarized as follows:

pressure of resin tank 0.05 MPa;

resin spray pressure 0.3–0.35 MPa;

jet diameter 3.5 mm;

angle between nozzle of resin spray gun 20°; length of cut glass fibers 40 mm;

glass-fiber content 30–40%;

distance between spray nozzle and forming surface 300–400 mm.

2.2.3 Compression Molding Techniques

In compression molding, a material (powder, particles, or fibers) is placed in a metal die and then cured at a certain temperature and pressure to give a desired product. During compression molding, a certain temperature and pressure are needed to make the material plastic or molten, so that it can fill the metal die. Curing occurs

under certain conditions. During flow of the compressed material, both the resin and reinforcing material are flowing, therefore a higher molding pressure is applied. Hydraulic pressure machines that can accurately control the pressure and metal dies of high-strength/high-precision/high-temperature resistance are needed [3].

(1) Characteristics of compression molding

Compression molding was first used industrially in 1909. The technique developed rapidly with the invention of new molding compounds such as sheet-molding compounds (SMCs) and bulk-molding compounds (BMCs). The merits of compression molding include good repetition, easy operation, a good operating environment, easy flow of mold products/wide temperature and pressure ranges, molding of sheet products, good surface quality, and high production efficiency. The drawbacks of compression molding are complicated manufacture of metal dies, higher investment, and the restrictions of hydraulic pressure machines [4].

Developments in metal-machining techniques, hydraulic pressure machine technology, and methods for resin synthesis, increases in press tonnage and table size, and decreased molding temperatures and pressures have led to the large-scale use of compression molding. Compression molding is now used to mold large products such as auto parts, tubs, and toilets.

(2) Categories of compression molding techniques

Compression molding techniques can be divided into various categories based on the types of reinforcing and molding materials.

1. Fiber-reinforced material molding: In this method, a material prepreg is placed in metal dies at a certain temperature and pressure and molded into composite products.
2. Scrap material molding: In this method, textile prepreps are cut into scrap and placed in metal dies at a certain temperature and pressure, and the scrap is molded into composite products.
3. Textile material molding: In this method, textile prepreps [two-dimensional (2D) or three-dimensional (3D)] are placed in metal dies at a certain temperature and pressure and molded into composite products.
4. Laminated molding: In this method, textile prepreps are cut into desired shapes and placed in metal dies at a certain temperature and pressure and molded into composite products.
5. Winding molding: This method uses a special winding machine to provide a tensile force and temperature. A prepreg fiber/belt is wound into a core mold and then placed in metal dies and molded into products.
6. BMC/dough-molding compound (DMC): In this method, a thickener, initiator, filler, internal release agent, and pigment are mixed into a paste and milled with short fibers. The mixture is placed in metal dies and molded into products at a certain temperature and pressure.

7. SMC: In this method, the SMC is placed in metal dies and molded into products at a certain temperature and pressure.
 8. Preform molding: In this method, glass fibers are formed into products and placed in metal dies. Resin is then injected, and the mixture is molded into products.
 9. Directional lay molding: In this method, directional prepregs are placed along the direction of major stress and molded into products.
- (3) Development of compression molding techniques

Compression molding techniques were first used in the twentieth century, and the products were mainly based on phenolic resin filled with wood flour and quartz powder. Two other resins, namely melamine–formaldehyde and urea–formaldehyde, were then used. However, these resins have various shortcomings, e.g., they are difficult to machine and mold, and give poor performances, which influenced the development of this type of molding compound. Molding compounds based on unsaturated polyester resins appeared in the 1950s. This type of molding compound avoids the problems encountered with phenolic and urea–formaldehyde resins. In the UK, they were referred to as DMCs. DMCs are easily molded, low cost, easily pigmented, and give good electrical performances. However, as production techniques and applications for DMCs were developed, the disadvantages of DMCs such as feed problems and poor mechanical properties became apparent. It took 20 years to overcome the disadvantages of DMCs. In the 1970s, modified DMCs, known as BMCs, were introduced. The SPI definition of a BMC is a DMC that shows low shrinkage and chemical thickening. SMCs, which can solve problems such as low production efficiency and poor mechanical properties, appeared in the 1960 in the Federal Republic of Germany. SMCs are more suitable than DMCs and BMCs for use with large molds and provide complex products with good mechanical properties.

2.2.4 Other Forming Processes

2.2.4.1 Filament Winding

In filament winding, which is a resin matrix composite fabrication technique, continuous fibers are wound onto a mandrel according to an established form after impregnation with a colloid and then solidified into specific shapes at a certain temperature. The continuous fibers can be impregnated beforehand and stored until winding onto the mandrel, or wound onto the mandrel and made into products directly after impregnation, or impregnated and continuously wound onto the mandrel after a liquid glue has been formed by primary cross-linking by passing through baking equipment. The first process is dry forming, the second is wet forming, and the third is semi-dry forming. Each of these methods has its own characteristics. Wet forming is most widely used [5].

Products made by filament winding make full use of the features of composites and give the optimum required structures. For example, the axial/ring direction internal force ratio of a cylindrical pressure vessel is 1:2. If the vessel is made from a metal, the structural strength is the same in all directions, but in terms of the required ring direction strength, half of the axial strength is redundant. By varying the winding angle (the angle between the filaments and the generatrix), the filament-winding process can be used to make the ring strength of the vessel double the axial one, therefore the product has the optimum properties, and redundant material consumption is avoided. Furthermore, the fibers are continuous and strained, therefore the fiber strength is better than that of fabric fibers (lamination technique and hand lay-up technique), and short cut fibers (products made of short cut fibers by injection). The fiber content can be up to 80%, whereas for other composite fabrication techniques, such as mold pressing, hand lay-up, and injection, a maximum of 60% is achieved. The composite strength comes mainly from the fibers, so the higher the fiber content is, the higher the product structural strength is.

Filament winding was inspired by the reinforcement of the tensile strengths of some structures through binding. It was first used as a fabrication technique in the 1950s, after the emergence of techniques for fiber enhancement of composites. It is a high-level mechanized technique for composite fabrication and has been widely used and rapidly developed since it first appeared. In the 1960s, it was used in almost every possible field. In the aerospace industry, because of their high specific strength, modulus, insulation, and ablation resistance, filament-wound composites are the best structural materials for applications such as rocket engine cases, nozzles, energy storage vessels, and antenna frames. They are also used to build large chemical storage tanks and pipelines for transporting liquids. In military applications, they are used as structural materials for rocket engine cases. In electrical equipment, they are used as high-voltage insulation products. In aviation, they are used to make radomes on high-speed aircraft.

For more than half a century, filament winding has been developed, improved, and matured. Raw material production has become industrialized and winding equipment, including devices making members with diameters of several millimeters, spot winding machines for making chemical storage tanks of diameter more than 20 m, and two-axes winding machines to multifunctional winding machines with dozens of axes have been developed. This is an advanced technique and its products are widely used in aviation, aerospace, national defense, and civil industries.

2.2.4.2 Pultrusion

Pultrusion is a technique for molding composite profiles. Continuous glass fibers and glass-fiber products such as continuous strand mats are pulled by a traction device through oriented devices, a paste groove, premold, and heated mold to form

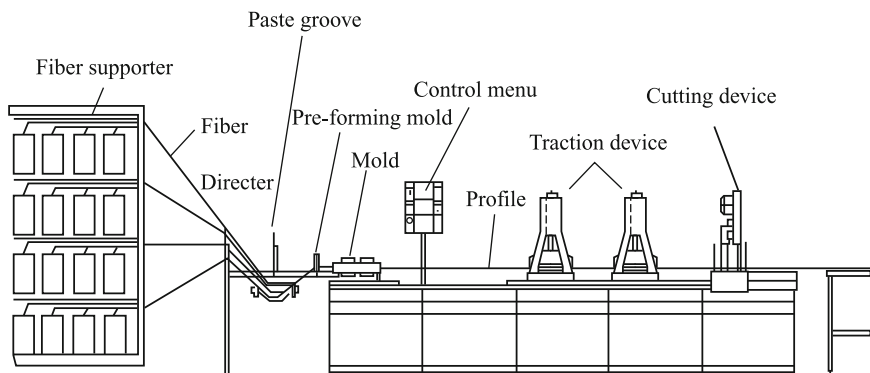


Fig. 2.10 Diagram of typical pultrusion process

a continuous profile. The length depends on the product needs. The product is completed by a cutting device [6].

In pultrusion, a composite material is formed using the highest level of mechanization. Figure 2.10 shows a diagram of a typical pultrusion process.

Compared with steel manufacturing, pultrusion has greater flexibility and requires a smaller investment in equipment, and is used for the production of a larger number of products.

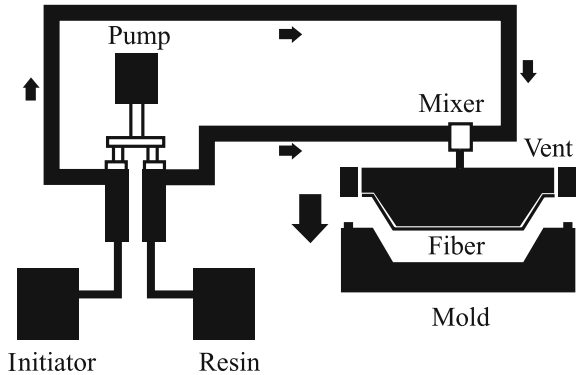
The pultrusion profile density is lower than that of aluminum. The profile has the advantages of high specific strength, a high modulus and corrosion resistance, no need for surface finishing, good insulating properties, stability during long-term use in the natural environment, high efficiency, a high degree of mechanization, and low production costs.

2.2.4.3 Resin Transfer Molding

In RTM, matched die molding is used to produce polymer composites. A thermosetting resin in a reactive liquid state and dry fibers are injected into a cavity under low pressure to discharge air from the cavity and wet the fibers [7]. When the resin appears at the air vent, this means that the mold cavity is full of resin and the curing stage begins. Products can be taken out until the resin reaches a specific strength. The entire process is shown in Fig. 2.11. Compared with other FRP-forming processes, RTM has the following advantages.

1. Mold manufacture and material selection are flexible, and RTM has economic benefits if the product output is around 1000–20,000 pieces.
2. Complex components with good surface quality and high dimensional accuracy can be made, and there are advantages in the manufacture of large-scale components.

Fig. 2.11 Schematic diagram of RTM



3. A partially enhanced sandwich structure can be easily obtained from molding components. Reinforced materials and layer structures can be designed.
4. The fiber content is up to 60%.
5. It is a closed-mold process, with clean working conditions and low-styrene emissions from the forming process; this is beneficial to the environment.
6. It has a high degree of freedom in terms of mold design, and low tooling costs. FRP molds can be made using a low injection pressure, including epoxy molds, FRP molds with electroformed nickel surfaces, and aluminum molds.

2.2.4.4 Vacuum Bag Pressure Forming

Vacuum bag pressure forming is a depression shaping technique. The process is as follows. Depending on the design requirements, and mainly by hand, reinforced materials and resins (including preimmersed materials) are placed on a mold one by one until the specified thickness is achieved. The process is completed by pressurizing or evacuating, heating, solidifying, demolding, and truing. The difference between the four types of process and shaping by hand is solidification. They are simply an improvement of shaping by hand to improve the compactness and splicing intensity of products.

The advantages of bag pressure molding are that (1) both sides are smooth; (2) it can be used with polyester, epoxy, and phenolic resins; and (3) the product quality is higher than that of products shaped by hand.

(1) Technique

There are two types of bag pressure molding, i.e., the pressure bag method and the vacuum bag method.

1. Pressure bag method

- (a) Non-solidified products laid by hand are placed in a dracone, and then a cover is fixed on the dracone.
- (b) Air or steam is compressed (0.25–0.5 MPa) in the dracone to enable product solidification under hot-pressing conditions.

2. Vacuum bag method

- (a) A vacuum bag is placed on the non-solidified product, laid by hand, to sandwich the product between the vacuum bag and mold.
- (b) The edges are sealed, and the system is evacuated (0.05–0.07 MPa) to remove blisters and volatile matter in the product. Because of the low vacuum pressure, this method can be used to shape polyester composites and epoxy composites.

Scrimping is a technique that combines a vacuum bag method and RTM. First, a reinforced layer is laid on a single mold. Secondly, the layer and mold are sealed in a vacuum bag. Thirdly, the layer is evacuated. Finally, the resin is injected into the layer. The advantages are good dipping, high speed, and compensation for undipped parts. The products have good consistency, smooth surfaces, and high fiber contents. The disadvantages are that the ancillary materials are expensive and not readily available.

(2) Notes

1. The molds used in the pressure bag method must be strong enough to withstand hot pressing and shaping, and external forces.
2. The molds and rubber bag or vacuum bag should be examined carefully before use to prevent air leakage. The rubber bag and vacuum bag should not be corroded by the resin.
3. In a vacuum bag method at low vacuum pressures, a drawing stick can be used to assist pressurizing to eliminate blisters.

(3) Applications and development

High-performance composite products based on high-strength glass, carbon, boron, and aramid fibers, and ethoxy resins produced using pressure bag methods have been used in airplanes, missiles, satellites and space shuttles, e.g., in airplane ports, false ogives, radomes, base frames, wings, empennage, clapboard, wainscot, and stealth planes.

2.2.4.5 Winding Shaping

Winding shaping is a composite-shaping method. A prepregged fabric is placed on a hot-rolling machine. The hot roller in a pipe-coiling machine softens the fabric and then the resin on the fabric melts. Under a certain tension, the roller rolls the

fabric up to the core barrel by the frictional force between the roller and the core mold until the required thickness is reached. Then, the fabric is cooled and shaped by a cool roller. Finally, the fabric is removed from the pipe-coiling machine and loaded in a curing oven to solidify. After solidification, the mandrel is removed.

2.2.4.6 Techniques for Preparing Sandwich Structures

A sandwich structure is a three-layered composite. The materials used in the first and third layers must have high tension and a high modulus [8]. These layers are called the panel and thin-gauge skin. A lighter material is used for the middle layer, which is called the core. The distance between the two thin-gauge skins enlarges the inertial moment of the section. This increases the bending rigidity and makes full use of the strengths of the materials. A composite sandwich structure consists of a composite and another lighter material. This structure increases the effective rate of utilization and decreases the weight.

Composites with GFRP honeycomb sandwich structures and GFRP foamed sandwich structures, which have good thermal stabilities and electrical properties, have been developed.

Composite sandwich structures include foam plastic sandwich structures, honeycomb sandwich structures, echelon form, orthogonal structure, and round sandwich structures.

2.3 Composite Properties and Testing

Composites are anisotropic materials, and their design and testing differ from those used for metals. The determination of material properties is important and basic information in material research, development, design, and applications [8–13]. Designers can obtain the property parameters of conventional materials from handbooks or the material specifications provided by manufacturers based on the material properties (or trademark) when selecting materials. Composites are considered to be structures rather than materials. The composite properties are relevant to many factors such as type of matrix reinforcement, material state manufacturing processes, interfacial conditions, and storage time and environment. Before design, the composite properties and their relationship to all factors must be known. However, property data for certain processing conditions are only the basis for raw material selection rather than all the necessary design data. At present, micromechanical results are only qualitative estimates because of their limitations. The property data needed for composite part design must be obtained by basic property testing; this is critically important in design.

Much research has been performed, and large amounts of test data have been accumulated. A series of specifications have been built, which lay the foundations for correctly evaluating material properties and determining the relationships

between material properties and test conditions and the relevant factors that affect them.

Composite property testing is the crucial basis for selecting the material composition, and evaluating the reinforcements, matrix, interfacial properties and their compatibility, processing conditions, manufacturing techniques, and product design.

2.3.1 Mechanical and Physical Properties and Testing

Methods for determining the mechanical and physical properties of composites, and the data obtained, are widely used in practical engineering. Test methods are available for oriented fiber-reinforced composites and fabric-reinforced composites, according to the composite reinforcement and forming process. Material property data obtained from these tests form the basis for evaluating material systems, processing levels, and structural design. In addition, laminate properties can be determined theoretically from these basic data [8, 9].

2.3.1.1 Tests for Mechanical and Physical Properties

(1) Property tests for unidirectional composites

According to the national standard GB 4550-84, *Preparation of unidirectional orientated fiber reinforced plastic plates for test purposes*, unidirectional FRP plates for testing are prepared by filament-winding and vacuum bag-autoclave processes. The elastic properties of unidirectional composites are determined based on the tensile, compressive properties at 0° , 90° , and 45° . The resin-fiber interfacial properties are determined by flexural and in-plane shear testing. Fiber composite plates for evaluating material properties must be machined to the required dimensions and amounts specified in GB 3354-82, GB3355-82, GB3356-82, GB3357-82, and GB3856-82.

1. Specimen machining: Surface dust or impurities should be removed before the preparation of unidirectional fiber plates. The cutting direction and machining areas of specimens for tensile, compressive, and flexural tests at 0° , 90° , and 45° are marked on the plates using a special pencil. In addition, the amount of specimen and cut width should be taken into account, according to the national standard requirements. The specimen shape and dimensions are shown in Fig. 2.12 and Table 2.7. The flexural and interfacial shear specimen dimensions must meet the span:depth ratio requirements.
2. Tab bonding: End tabs are made of cross-ply glass-fiber/resin laminates of thickness 2–3 mm or 1–3 mm aluminum laminates. If aluminum laminates are

Fig. 2.12 Unidirectional laminate specimen dimensions **a** tensile specimen: L —overall specimen length, mm; h —specimen thickness, mm; D —tab length, mm; b —specimen width, mm; l —gauge length, mm; θ —chamfered angle of tabs, mm. **b** compressive specimen: 1—specimen; 2—tabs

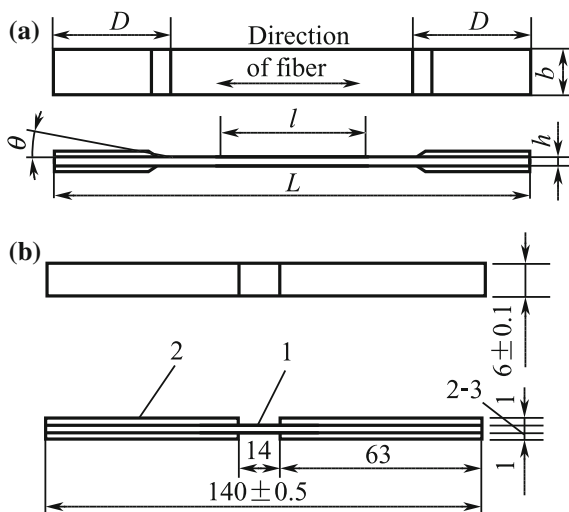


Table 2.7 Tensile specimen dimensions

Specimen type	Size/mm					
	L	b	h	l	D	θ
0°	230	12.5 ± 0.5	1–3	100	50	≥ 15°
90°	170	25 ± 0.5	2–4	50	50	≥ 15°
45°	250	25 ± 0.5	2–4	100	50	≥ 15°

used for tabs, the tab surfaces are smoothed and roughened with sandpapers to eliminate oxidized layers, and heated at 65 °C in acid solution for 15 min. The tabs are cleaned with freshwater and then baked for 2 h to evaporate the water. The treated tab surfaces must not be touched by hands. The solution mass composition is sulfuric acid:distilled water:potassium dichromate = 10:30:1.

Before bonding the tabs, the specimen surfaces are smoothed with 100# abrasive paper. Dust is removed from the surfaces, and the mold release and grease are removed using ethyl acetate. The specimens are cleaned with acetone and dried. Tab slippage easily occurs during tensile tests because of the high tensile strength along the fiber direction of a unidirectional composite; therefore, a good adhesive is used. The mass ratios of the components are 618 epoxy:200# polyamide:diglycidyl ether:iminazole = 100:80:15:2. The adhesive is painted on the specimens and tabs, cured under contact pressure in the curing system at 60 °C for 2 h and then 120 °C for 8 h, and cooled. Tensile specimens for tests at 45° and 90° to the fiber direction use an adhesive cured at normal room temperature because of their low strength.

After the tabs have been cured, the exposed fibers on the test section surfaces are roughened. Grease is removed using acetone and ethyl acetate. Gauge marks are drawn. The strain gauge is bonded with 502 adhesive. It must be ensured

that the bonding direction of the strain gauge is the same as that of the tested material. Specimen preparation is finished by adhesive curing.

3. Tensile property testing. Specimens are tested along the fiber orientation (0°), perpendicular to the fiber orientation (90°), and at a 45° orientation; the tensile modulus of elasticity E_{Lt} , E_{Tt} , Poisson's ratio V_{LT} , V_{TL} , tensile strength F_{Lt} , F_{Tt} , and the shear strength F_{Lt} and modulus G_{LT} are separately tested.

- (a) Tensile property testing along fiber orientation. The tensile properties at 0° depend on the fiber type, volume content, fiber straightness, and saturated resins. Two tabs are bonded perpendicularly in the middle of the effective length at 0° and 90° to the fiber direction after preparing the specimens. The width and thickness of the test specimen are measured at three points, and the average value is calculated. The measurement accuracy is verified in accordance with GB1446, and a specimen number is subsequently assigned. The strain gauge leads must be isolated from the measurement wires during welding. Carbon fibers are conductive; therefore, not only the leads themselves but also carbon composites should be separated and insulated. When placing the specimen in the grips of the testing machine, the long axis of the specimen and the grips must be aligned with an imaginary line, and then the measurement wire is joined to the strain indicator. To avoid the effects of temperature variations in practical tests, the strain gauge that is bonded to the specimen is made of the same material as the tested specimen and aligned with the strain indicator to form a semi-bridge. For determining the tensile modulus of elasticity, Poisson's rate, elongation at break, and stress-strain curve, specimens of various grades are loaded, with break load differentials of 5–10% (at least five grades are used when determining the tensile modulus of elasticity and Poisson rate). The loads at different grades, the strain, the load at break, and the strain at break, are recorded. The tensile strength is calculated using Eq. (2.1):

$$F_{Lt} = \frac{P_b}{bh} \quad (2.1)$$

where

- F_{Lt} = tensile strength at 0° , MPa;
- b = specimen width, mm;
- P_b = maximum load value at break, N;
- h = specimen thickness, mm.

The tensile modulus of elasticity is calculated using Eq. (2.2):

$$E_{Lt} = \frac{\Delta P}{bh\Delta\varepsilon} \quad (2.2)$$

where

- E_{Lt} = tensile modulus of elasticity, MPa;
 ΔP = increment in load of primary straight line in load–strain curve, N;
 $\Delta \varepsilon$ = strain increment corresponding to ΔP .

The Poisson rate is calculated using Eq. (2.3):

$$V_{Lt} = \frac{\varepsilon_T}{\varepsilon_L} \quad (2.3)$$

where

- V_{Lt} = Poisson rate;
 ε_L = strain at 0° corresponding to ΔP ;
 ε_T = strain at 90° corresponding to ΔP .

- (b) Tensile property testing at 90° : The tensile properties in the 90° direction mainly depend on fiber infiltration and the fiber–resin interfacial properties. The specimen thickness must be carefully measured because of the low tensile strength in the 90° direction. The wires are welded, and the specimen is placed in the grips. The tensile strength in the 90° direction is determined using Eq. (2.4):

$$F_{Tt} = \frac{P_b}{bh} \quad (2.4)$$

where

- F_{Tt} = tensile strength at 90° , MPa;
 P_b = maximum load at break, N.

The tensile modulus at 90° is calculated using Eq. (2.5):

$$E_{Tt} = \frac{\Delta P}{bh\Delta \varepsilon} \quad (2.5)$$

where E_{Tt} = tensile modulus at 90° , MPa.

- (c) Tensile property testing at 45° . The tensile properties at 45° depend mainly on the fiber–resin interfacial state, fiber infiltration, and resin properties. At a high stress, most composites show nonlinear behavior. Tensile property testing is commonly used to evaluate the fiber–resin interfacial properties. The fiber direction greatly affects the test results. In sampling, the specimen axis should be 45° to the fiber direction. The cross-shear strength is calculated using Eq. (2.6):

$$F_{Lt} = \frac{P_b}{2bh} \quad (2.6)$$

where

F_{Lt} = cross-shear strength, MPa.

The cross-shear modulus is calculated using Eq. (2.7):

$$G_{Lt} = \frac{\Delta P}{2bh(\Delta\varepsilon_X - \Delta\varepsilon_Y)} \quad (2.7)$$

where

G_{Lt} = cross-shear modulus, MPa;

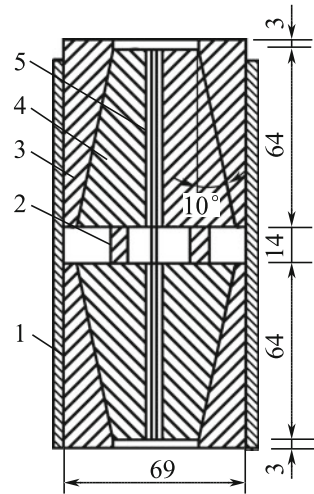
ΔP = selected load increment of straight line in load–strain curve, N;

$\Delta\varepsilon_X$ = strain increment on specimen axis corresponding to ΔP ;

$\Delta\varepsilon_Y$ = strain increment perpendicular to specimen axis corresponding to ΔP .

4. Compressive property testing. Composite tensile properties differ greatly from their compressive properties, unlike the case for metal materials. Generally, the compressive properties are much poorer than the tensile properties. The aim of compression testing is to determine the compressive strength, compressive modulus of elasticity, and Poisson's ratio in the 0° and 90° directions for unidirectional composites.
 - (a) Compressive property testing along the fiber orientation. Compressive property testing of unidirectional composites is difficult because of the requirements for factors such as specimen thickness, gauge length, and tab width. To induce compression rupture rather than buckling breakage, special testing jigs are used and the requirements for the gauge length are high (Fig. 2.13). To prevent slippage between the specimens and metal jigs, the tabs must be long enough to resist the test load when the test specimen is being placed in the jig; the specimen is first placed in the wedges, the outer clamps are put in place, and then the sleeves are fitted. Preloaded washers in the sleeve windows are used to prevent wedge slippage and provide easy connection to the strain wires. After clamping, the specimen is placed in the testing machine and focused on the center. Preloading ensures that the jigs can completely clamp the specimen and enable the sleeve to move freely. The preloaded washers are unloaded and removed. The compressive modulus and Poisson's ratio are determined using specimens of more than five grades, with breakage load differentials of 5–10%. A uniform load is applied during the test until the specimen breaks. The stress–strain and breakage

Fig. 2.13 Test jigs for compressive properties
 1—sleeve; 2—preloaded washer; 3—clamp;
 4—wedge; 5—specimen



load for different grades are recorded. The compressive strength is determined using Eq. (2.8):

$$F_{LC} = \frac{P_b}{bh} \tag{2.8}$$

where

F_{LC} = compressive strength in 0° direction, MPa.

The compressive modulus of elasticity is determined using Eq. (2.9):

$$E_{LC} = \frac{\Delta P}{bh\Delta\varepsilon} \tag{2.9}$$

where

E_{LC} = compressive modulus of elasticity, MPa;

ΔP = load increment, N;

$\Delta\varepsilon$ = strain increment corresponding to ΔP .

If there is no onset straight line on the stress–strain curve, the onset tangent modulus or secant modulus is taken as the elastic modulus.

Poisson’s ratio is calculated using Eq. (2.10):

$$U_{LC} = \frac{\varepsilon_T}{\varepsilon_L} \tag{2.10}$$

where

U_{LC} = Poisson's ratio in the compression test.

- (b) Compressive property testing in 90° direction. When preparing specimens with an orientation perpendicular to the fiber orientation for testing compressive properties, welding and jiggling should be performed carefully to prevent breakage during installment because of the very low strength of such specimens. A uniform load should be applied. The compressive strength in the 90° direction is calculated using Eq. (2.11):

$$F_{TC} = \frac{P_b}{bh} \quad (2.11)$$

where

F_{TC} = compressive strength perpendicular to fiber direction, MPa.

The compressive modulus of elasticity in the 90° direction is calculated using Eq. (2.12):

$$E_{TC} = \frac{\Delta P}{bh\Delta\epsilon} \quad (2.12)$$

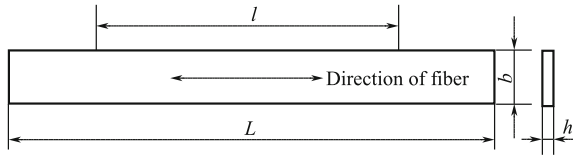
where

ETC = compressive modulus of elasticity perpendicular to the fiber direction, MPa.

If there is no onset straight line, the onset tangent modulus or secant modulus is taken as the elastic modulus.

5. Flexural property testing. Flexural property test methods using three-point and four-point loadings on a simple supported beam are used to determine the flexural strength, flexural modulus of elasticity, and load–deflection curve of unidirectional FRP plates to assist material choice and for quality control. China national standard GB3356-82 uses a three-point bending system with a simple supported beam. The tensile modulus of composite elasticity usually differs from the compressive modulus, which results in the non-duplication of a neutral axis and geometric center and double modulus laminar beam, so this must be taken into account.
- (a) Three-point bending method on simple supported beam. A bar specimen with the shape and dimensions shown in Fig. 2.14 is used to ensure that tensile or compressive break occurs at the outer fiber layer under the flexural load. The recommended span:depth ratio is $l/h = 16, 32, \text{ and } 40$; $l/h = 16 \pm 1$ is suitable for GFRPs; $l/h = 32 \pm 1$ is suitable for carbon-fiber-reinforced plastics because of the high flexural modulus; and $l/h = 32 \pm 1$

Fig. 2.14 Shape and dimensions of specimen for three-point bending L —specimen length; l —specimen span; h —specimen thickness; b —specimen width



or 40 ± 1 is used for aramid-fiber-reinforced composites to ensure flexural break, rather than interlaminar shear break, because of the low interfacial shear strength and the flexural modulus, which is higher than those of glass-fiber composites. The loading noses and fillet radius of the supports should conform to the national standard. In the tests, loads of various grades are used, with a break load differential of 5–10%, to determine the flexural modulus of elasticity or load–deflection curve. The loadings at different levels and relative deflections are recorded separately. The flexural strength is determined by applying successive loads until the specimen breaks. If interlaminar shear break occurs or the break area exceeds one-third of the support span, the specimen is not accepted. At least five effective specimens should be tested. The flexural strength is calculated using Eq. (2.13):

$$\sigma_f = \frac{3P_b l}{2bh^2} \quad (2.13)$$

where

σ_f = flexural strength, MPa;

l = flexural span, mm.

The flexural modulus of elasticity is calculated using Eq. (2.14):

$$E_f = \frac{\Delta P l^3}{4bh^3 \Delta f} \quad (2.14)$$

where

E_f = flexural modulus of elasticity, MPa;

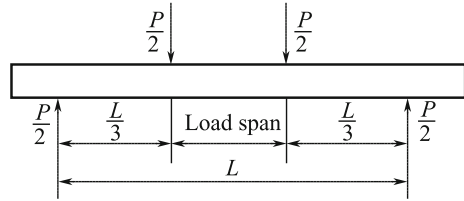
ΔP = load increment on straight line on the load–deflection curve, N;

Δf = midspan deflection corresponding to ΔP , mm.

(b) Simple supported beam four-point bending test.

The four-point bending test method is shown in Fig. 2.15. Unlike the three-point bending test using a simple supported beam, the working length in the four-point bending test is determined by the real bending load, and the maximum bending load is applied to an area of the span rather than a point; this ensures that the specimen breaks in the maximum stress area. The

Fig. 2.15 Four-point bending test using simple supported beam



loading changes from one point in the three-point bending test to two points, which reduces local bearing stress and avoids bearing break. A specimen with high bending strength must have large dimensions for use in the four-point bending test. In addition, the jigs are more complex than those for the three-point bending test. The flexural strength in the four-point bending test is calculated using Eq. (2.15):

$$\sigma_f = \frac{3P_b L}{4bh^2} \quad (2.15)$$

where

- σ_f = flexural strength, MPa;
- L = support span of four-point bending, mm;
- P_b = break load at the loading point, N;
- b = specimen width, mm;
- h = specimen thickness, mm.

The flexural modulus of elasticity is calculated using Eq. (2.16):

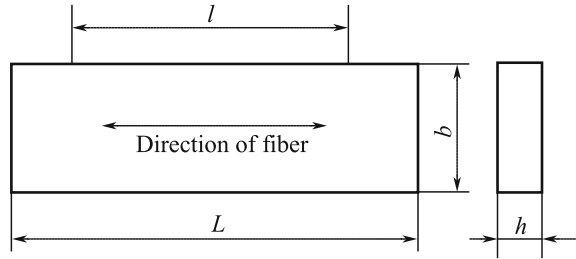
$$E_f = \frac{0.17 \Delta P L^3}{\Delta f b h^3} \quad (2.16)$$

where

- E_f = flexural modulus of elasticity, MPa;
- ΔP = load increment, N;
- Δf = deflection increment corresponding to ΔP ;
- L = support span in four-point bending.

6. Interlaminar shear property testing: Interfacial shear strength tests are used to evaluate the interfacial properties of fibers and resins to assist material choice and for product quality control. The national standard GB 3357-82, *Test methods of the interfacial shear strength for unidirectional fiber reinforced plastics*, specifies use of the short-beam method to test the interfacial shear strengths of unidirectional FRP plates.

Fig. 2.16 Specimen shape and dimensions for interfacial shear strength tests L —specimen length; l —support span; h —specimen thickness; b —specimen width



A bar specimen is used in the test. The specimen shape and dimension are shown in Fig. 2.16; specimen thickness $h = 2\text{--}5$ mm, specified support span $l = 5h$. Because of the small support span, more care must be taken when choosing the span:depth ratio. The loading nose radius and support fillet radius must conform to the national standard to prevent bearing break of the specimen during the test. For effective specimens, the ratio is not less than 10. The interfacial shear strength is calculated using Eq. (2.17):

$$\tau_s = \frac{3P_b}{4bh} \quad (2.17)$$

where

- τ_s = interfacial shear strength, MPa;
- P_b = maximum load at shear break, N.

7. Property testing using NOL ring: Composite property testing using an NOL ring is closely related to fiber-winding techniques. A ring specimen was first used at the US Naval Ordnance Laboratory and is therefore called an NOL ring. Netting theory is used to design filament-wound high-pressure tanks and solid motor cases. Netting theory neglects the matrix rigidity, and the fiber bears all the loads; this is the basis of the NOL ring testing method.

An NOL ring specimen is usually filament wound using a specific small winding machine. There are two methods for NOL ring fabrication. In one method, a single ring is wound using a specific tool assembly; in the other, a shell is wound first and then cut into rings. The outer surface can be machined or non-machined. A machined ring has high strength and a low discrete factor. A non-machined ring with a rough surface has a high resin content and relatively high dimensional tolerance. The strength of a ring cut from a shell is lower than that of a single ring because some continuous fibers are broken when the ring is cut from the shell, and this reduces the bearing load of the ring. A single ring is therefore usually used in practical tests. The ring properties are affected by factors such as the winding tension, curing system, water content of the fibers, surface state of the fibers, and the resin system.

- (a) Tensile property testing using NOL rings. Tensile property testing using NOL rings, which is easier than unidirectional plate tests, is performed

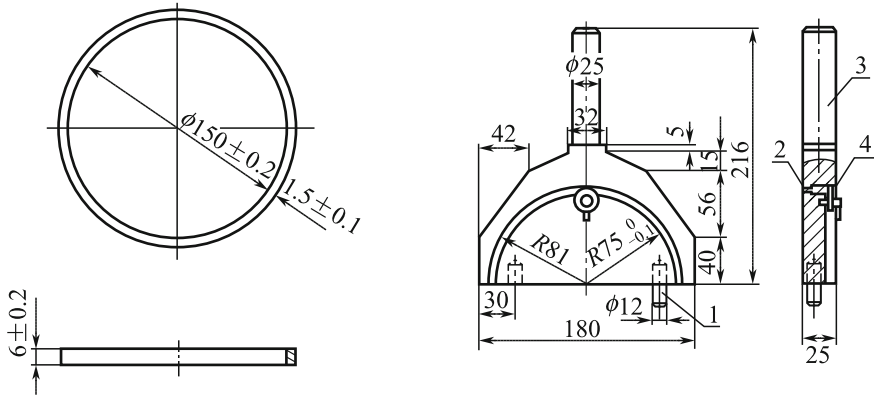


Fig. 2.17 Jigs for NOL ring tensile test 1—positioning pin; 2—access hole; 3—disk; 4—closure cam

using specific jigs; the jig types are shown in Fig. 2.17. Two half disks are assembled, and the NOL ring is placed in the circle groove. The test method can be used to determine the tensile strength and tensile modulus of the ring specimen along the fiber orientation, enabling calculation of the fiber tensile strength. The tensile strength of an NOL ring is calculated using Eq. (2.18):

$$F_{Lt} = \frac{P_b}{2bh} \quad (2.18)$$

where

- F_{Lt} = tensile strength of NOL ring, MPa;
- P_b = tensile load at break of NOL ring, N;
- b = specimen width, mm;
- h = specimen thickness, mm.

The fiber strength is calculated using Eq. (2.19):

$$F_f = \frac{P_b}{2bhV_f} \quad (2.19)$$

where

- F_f = average tensile strength of fibers in ring, MPa;
- V_f = volume content of fibers, %.

A strain gauge is bonded along the fiber direction on the ring for determining the tensile modulus. The tensile modulus is calculated using Eq. (2.20):

$$E_{Lt} = \frac{\Delta P}{2bh\Delta\varepsilon} \quad (2.20)$$

where the symbols definitions are the same as those in Eq. (2.2).

Although fabrication of NOL ring specimens is easy, they are only used for testing properties along the fiber direction, and extra bending during the test cannot be excluded.

- (b) Interlaminar shear strength testing using NOL rings. Small-arc specimens cut from a ring specimen are used in the three-point bending test to determine the interfacial shear strength. The specimen shape and dimensions, and jigs are shown in Fig. 2.18 and 2.19, respectively. The support span should be such that the specimen can extend freely but the supporting position does not change. The loading nose radius is 3 mm. The interfacial shear strength is calculated using Eq. (2.17).

(2) Test methods for glass-fiber fabric or short glass-fiber composites

The properties and preparation methods for glass-fiber-fabric-reinforced composite plates and those for short-glass-fiber composites are different. Directional fiber composite plates have orthotropic properties, so they have high strength along the fiber direction and very low strength perpendicular to the fiber; therefore, a specimen shape that keeps the fiber consistency is needed. Filament-winding or vacuum bag–autoclave techniques are usually used to prepare oriented FRPs. It is difficult to machine thick specimens because of the high break load and hard grip. Hand lay-up, RTM, and pressure molding are usually used to prepare fabric-reinforced plates and short-glass-fiber-reinforced plates. Machining thick specimens is not difficult. The specimen shape, dimensions, and test methods are different from those for directional fiber-reinforced composite plates because the fibers are uniform in two directions, so differences are smaller.

Fig. 2.18 Specimen shape and dimensions for shear test

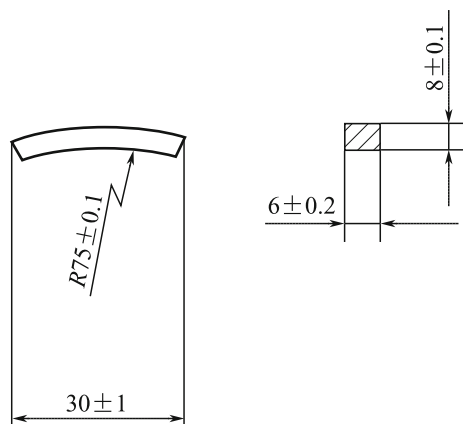
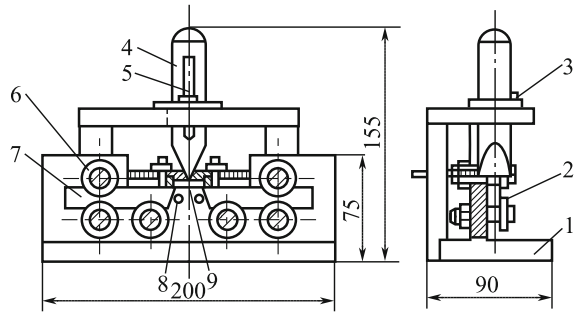
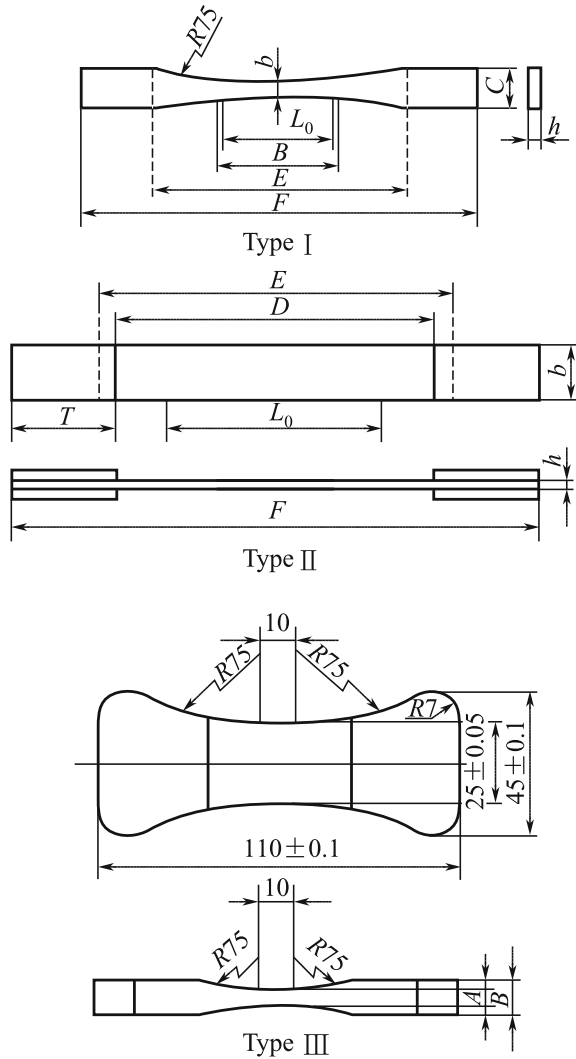


Fig. 2.19 Jigs for shear test
 1—base; 2—nut for fastening bearing; 3—key; 4—loading bar; 5—sliding groove to ensure loading direction; 6—sliding bearing of support; 7—sliding support; 8—positioning pin for support span; 9—specimen



1. Methods for testing tensile properties of glass-fiber-fabric-reinforced plates and short-glass-fiber-reinforced plates: National standard GB1447-82 stipulates that three specimen types can be used to test glass-fiber-fabric-reinforced plates and short-glass-fiber-reinforced plates. Specimen dimensions are shown in Fig. 2.20, Tables 2.8, and 2.9. Specimens of type I are used for glass-fiber-fabric-reinforced thermoplastics and reset composite plates; type II specimens are used for glass-fiber-fabric-reinforced thermosetting composites; type III specimens are used to test the tensile strength of molded short-glass-fiber-reinforced composite plates. Type I or type II specimens are used in other tensile tests. In the machining of type I specimens, there must be a smooth transition between the gauge length and grip areas to prevent specimen breakage in these areas. Specific jigs are used for type III specimens. At least five specimens are tested for each sample, regardless of the specimen type. The tensile strength, tensile modulus, and Poisson's ratio are calculated using Eqs. (2.1)–(2.3).
2. Methods for testing compressive properties of glass-fiber-reinforced composite plates and short-glass-fiber-reinforced composite plates: National standard GB1448-83 stipulates two types of specimen for testing the compressive properties of glass-fiber-fabric-reinforced composite plates and short-glass-fiber-reinforced composite plates. The plates are shown in Fig. 2.21, and the dimensions are shown in Table 2.10. Type I specimens are prepared by mechanical machining, and type II specimen is molded. Unlike the case for fiber-reinforced composite compression specimens, buckling does not usually occur because of the large thickness of the compression specimens of fabric-and short-glass-fiber-reinforced composites, therefore specific jigs are not needed for these tests. Care should be taken to ensure that the upper and lower surfaces are parallel during the test to prevent fracture of the specimen. The draw ratio for measuring the compressive strength is 10, but if buckling occurs, a draw ratio of 6 is used. The compressive modulus of elasticity is determined using a draw ratio of 15. The compressive strength and compressive modulus of elasticity are calculated using Eqs. (2.8) and (2.9).
3. Methods for flexural testing of glass-fabric composites: Bar specimens are used for flexural property testing of glass-fiber composites plates and glass-fabric composite plates; the shapes, dimensions, and arbitral specimen dimensions are

Fig. 2.20 Specimen shapes and dimensions



shown in Fig. 2.22, Tables 2.11, and 2.12, respectively. If either surface of the specimen is machined, the machined surface is subjected to an upward load. The test span greatly affects the flexural properties, and the national standard stipulates that the span L is equal to $(16 + 1)h$. When choosing materials or comparing solutions, the span:depth ratio should be changed appropriately for specimens that are too thick or too thin (L/h can be 10, 32, or 40), but it is best to use the arbitrary dimensions when recording material flexural property data.

4. Methods for testing interfacial shear strength of glass-fabric-reinforced composites: Two methods are used for testing the interlaminar shear strength of glass-fiber-fabric-reinforced composites. For thin specimens, the short-beam

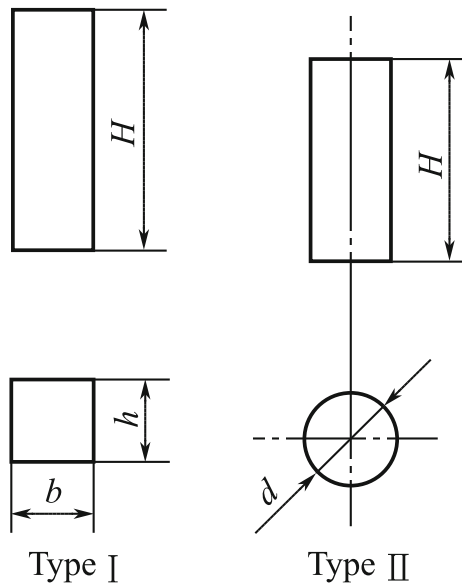
Table 2.8 Type I and II specimen dimensions (mm)

Dimension	Type I	Type II
Total length (min) F	180	250
End width C	20 ± 0.5	
Thickness h	2–10	2–10
Middle parallel length B	55 ± 0.5	
Middle parallel width b	10 ± 0.2	25 ± 0.5
Gauge length L	50 ± 0.5	100 ± 0.5
Distance between jigs E	115 ± 5	170 ± 0.5
Distance between tabs D	15	0 ± 5
Minimum length between tabs T		50

Table 2.9 Type I and II specimen dimensions (mm)

Specimen thickness	A	B
6	6 ± 0.05	10
3	3 ± 0.05	6

Fig. 2.21 Shapes and dimensions of specimens for compression testing of fabric-reinforced and short-glass-fiber-reinforced composite plates



three-point test for unidirectional fiber-reinforced composites can be used. The span is chosen to ensure interfacial shear breakage. The other method, i.e., GB 1450.1-83, is used for special specimens and assemblies, shown in Figs. 2.23 and 2.24. The specimen is machined to ensure that A, B, and C are parallel to each other and perpendicular to the layers. D has a smooth surface, and D, E, and F must be parallel to the layers. Smooth loading of A and C is required. Test jigs can be used to adjust C. The clamping tightness should allow the specimen

Table 2.10 Specimen dimensions for compression testing of fabric- and short-glass-fiber-reinforced composite plates (mm)

Dimension	Type I		Dimension	Type II	
	Common specimen	Arbitral specimen		Common specimen	Arbitral specimen
Width b	10–14	10 ± 0.2	Diameter d	4–16	10 ± 0.2
Thickness h	4–14	10 ± 0.2	Height H	^a /4d	25 ± 0.5
Height H	^a /3.46 h	30 ± 0.5			

^aλ is the draw ratio that is the ratio of height of cylinder with uniform section to the minimum inertia radius

Fig. 2.22 Specimen shape for testing flexural properties of fabric- and short-glass-fiber-reinforced composites

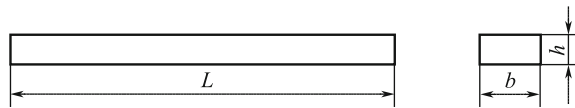


Table 2.11 Specimen dimensions for testing flexural properties of fabric- and glass-fiber-reinforced composites (mm)

Nominal dimension h	Width b	Length L	Nominal dimension h	Width b	Length L
1 < h ≤ 10	15 ± 0.5	20 h	20 < h ≤ 35	50 ± 0.5	20 h
10 < h ≤ 20	30 ± 0.5		35 < h ≤ 50	80 ± 0.5	

Table 2.12 Arbitral specimen dimensions (mm)

Material type	Thickness h	Width b	Length L
Glass-fabric-reinforced composites	4 ± 0.2	15 ± 0.5	≥ 80
Short glass-reinforced composites	6 ± 0.2	15 ± 0.5	≥ 120

to move freely up and down, with low friction. The platen surface must be smooth, and its height should be greater than the size of the next step. The specimen should be in a sheared state during the test. The specimen should be clamped in the interfacial shear jigs so that A faces upwards. It is better to allow the specimen to move freely up and down. The jigs are then placed in the testing machine, and the center of loading of face A is aligned to that of the platen on the testing machine. The load is uniformly and continuously applied until breakage occurs.

5. Methods for testing the impact toughness of GFRPs using a simple supported beam: Specimens for impact-resistant tests using a simple supported beam have a rectangular (or square) cross section machined with a V notch. The specimen

Fig. 2.23 Specimen dimensions and shape for testing interfacial shear strength of glass-fabric-reinforced composites

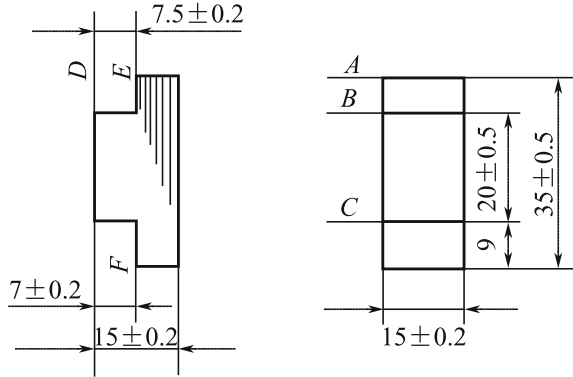
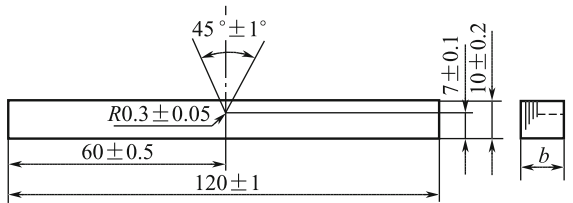
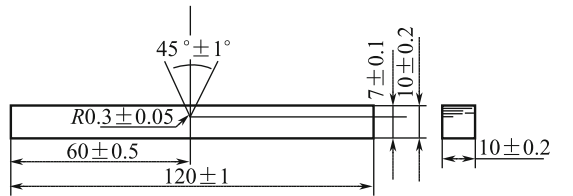


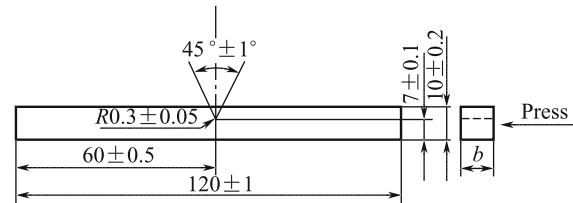
Fig. 2.24 Specimen dimensions for impact test



(a) Direction of the notch perpendicular to laminates



(b) Direction of the notch parallel to laminates



(c) Specimen of short fibre reinforced plastics

dimensions depend on the V notch machined on the specimen surface, the layer direction, and reinforcement (Fig. 2.25). The test equipment is a nonmetal pendulum testing machine with a simple supported beam, and the main dimensions of the pendulum and supporter are shown in Fig. 2.26. The impact speed is 3.8 m/s. The span is 70 mm. An appropriate pendulum is chosen to

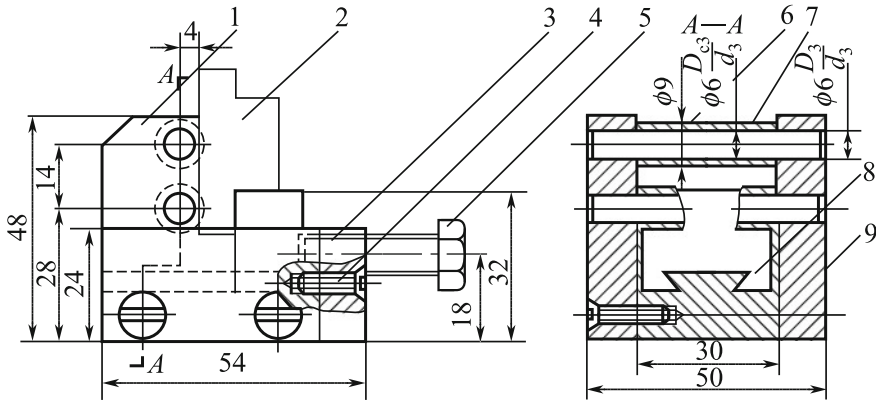
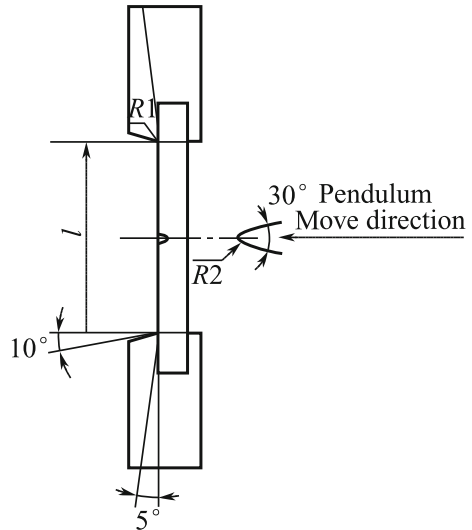


Fig. 2.25 Jigs for testing interfacial shear strength 1—front cover; 2—specimen; 3—side cover; 4—screw M4 × 14; 5—bolt M8 × 30; 6—axis sleeve; 7—axis; 8—block; 9—base

Fig. 2.26 Dimensions of pendulum and base



keep the energy for full specimen breakage in the range from 10% to 85% of the full energy. The notched specimen surface is placed opposite the pendulum, and the specimen is fixed with positioning plates so that the notch center is focused on the impact position. A specimen that is deficient or for which break does not occur at the notch is not accepted. If there are fewer than five effective specimens in a sample, the test is repeated. The impact toughness is calculated using Eq. (2.21):

$$\alpha_k = \frac{A}{bh} \quad (2.21)$$

where

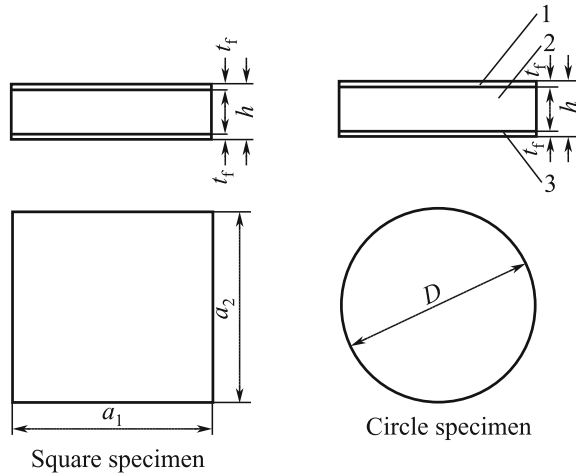
- α_k = impact resistance, J/cm²;
- A = power consumed to break specimen, J;
- b = width of the specimen notch, cm;
- h = thickness of the specimen notch, cm.

(3) Methods for testing composite sandwiches

Composite sandwiches are usually used to significantly reduce the weight and improve the bending rigidity, and acoustic and thermal insulation. Composite sandwiches consist of upper and lower panels and light cores. Foamed plastics, light wood, and corrugated and honeycomb materials are usually used as light cores. Composite panels can provide the necessary strength and bending rigidity to withstand compressive and shear loading. Engineering designers consider the bending strength and rigidity of the core of a composite sandwich structure, adhesion between the composite panels and light core, and compressive properties to be important. The purpose of composite sandwich structure testing is to provide data for these properties, to evaluate the effects of various sandwich structures on these properties, and to determine interfacial adhesive properties for reference in material choice and structural design.

1. Methods for testing flat tension strength of composite sandwich structures: The flat tension strength is mainly determined to evaluate the interfacial bonding properties between composite panels and cores, which are related to the adhesive type and technique. Rectangular or circular specimens of thickness equal to that of the sandwich product are used. Specimens of length or diameter 60 mm are used for continuous cores of materials such as foamed plastics and light wood. For honeycomb, corrugated, or cellular cores, the specimen length or diameter is 60 mm or at least four cells. If the thickness of the sandwich product is uncertain, a core thickness of 15 mm and panel thickness of 0.3–1.0 mm are used. The upper panel must be parallel to the lower panel, and the shape and dimensions of the loading block are the same as those of the specimen. After roughening with sandpapers and cleaning with the solution, two loading blocks are bonded separately with the upper and lower panels. The bonding curing temperature is room temperature or 30 °C lower than that of the sandwich adhesive. The bonded specimens are placed in the jigs for tensile testing. The 0 point scale of the testing machine is adjusted to the specific speed needed to apply a uniform loading until the specimen breaks. Specimens that debond from the loading blocks are invalid. The flat tension strength is calculated using Eq. (2.22):

Fig. 2.27 Specimen shapes for flat compression tests 1,3 —panels; 2—core; a_1, a_2 —edge lengths; D —specimen diameter; t_f —panel thickness; h —specimen thickness



$$\sigma_t = \frac{P}{F} \tag{2.22}$$

where

σ_t = flat tension strength, MPa;

P = load at break, N;

F = cross-sectional area of specimen, $F = a_1, a_2$ (for rectangular specimens)

or

$$F = \frac{\pi D^2}{4} \quad (\text{for circular specimens});$$

a_1, a_2 = specimen length, mm;

D = specimen diameter, mm.

- Method for testing flat compressive properties of composite sandwich structures: Rectangular or circular specimens, shown in Fig. 2.27, are used for testing the flat compressive properties of composite sandwich structures. The specimens used for testing the flat compressive strength are the same size as those used for flat tension strength tests. A specimen thickness of 15–80 mm is recommended for testing the core elastic modulus. The ball support is adjusted to make the upper block parallel to the indenter surface of the testing machine. The meter readings are checked, and the two side meter reading are made the same. The load is applied at levels 5–6% that of the break load until the specimen breaks. The flat compressive strength is calculated using Eq. (2.23).

$$\sigma = \frac{P}{F} \quad (2.23)$$

where

- σ = flat compressive strength, MPa;
- P = load at break, N;
- F = cross-sectional area, see Eq. (2.22).

The flat compressive modulus of elasticity of the core is calculated using Eq. (2.24):

$$E_C = \frac{\Delta P(h - 2t_f)}{\Delta h F} \quad (2.24)$$

where

- E_C = flat compressive modulus of elasticity, MPa;
- ΔP = load increment on straight line on the load–deflection curve, N;
- h = specimen thickness, mm;
- t_f = panel thickness, mm;
- Δh = compressive deflection increment corresponding to ΔP , mm.

For a core of known dimensions, E_C is calculated using Eq. (2.25):

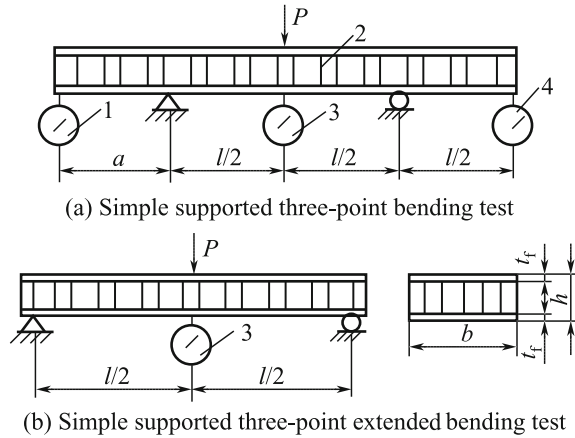
$$E_C = \frac{\Delta P h_C}{\Delta h_C F} \quad (2.25)$$

where

- E_C , ΔP , and F are as defined for Eq. (2.24);
- h_C = core specimen thickness, mm;
- Δh_C = compressive deflection increment corresponding to ΔP , mm.

3. Flexural tests for FRP sandwich structures. Flexural tests for FRP sandwich structures are used to determine the panel strength when the sandwich structure bears a flexural load, the core shear strength, and the flexural shear rigidity of the sandwich. Two types of specimen, i.e., transverse and longitudinal, are used, and the specimen thickness is equal to the product thickness. National standard GB 1456-78 stipulates the panel thickness, sandwich thickness, lee lattice edge length, specimen width and length, and test span. A simple supported three-point bending test is used to test the flexural strength and shear strength, and a simple supported three-point extended bending test is used to test the flexural rigidity, as shown in Fig. 2.28. Flexural strength testing requires blocks at the loading points and supporting points. The block width in the loading noses is $h \leq B \leq 1.5h$. The block width to enable the supporting points to

Fig. 2.28 Flexural tests for sandwiches



move freely is $h/2 \leq B \leq h$. The load is applied at a regulated speed at a level 5% of the breakage loading and 30–50% for deflection measurements. If complete load deflection data are needed, the test is continued until the specimen breaks. The core shear strength is calculated using Eq. (2.26):

$$\tau_c = \frac{PK}{2b(h - t_f)} \tag{2.26}$$

where

- τ_c = core shear stress, MPa;
- P = break load, N;
- b = specimen width, mm;
- h = specimen height, mm;
- t_f = panel thickness, mm;

$$K = 1 - e^{-AA} = \frac{1}{4t_f} \sqrt{\frac{6 G_C (h - t_f)}{E_f t_f}}$$

where

- E_f = elastic modulus of panels, MPa;
- G_C = shear modulus of core, MPa.

The panel flexural strength is calculated using Eq. (2.27):

$$\sigma_f = \frac{P_b l}{4bt_f(h - t_f)} \tag{2.27}$$

where

σ_f = panel flexural strength, MPa;
 l = span of three-point bending, mm.

The flexural rigidity of a sandwich structure is calculated using Eq. (2.28):

$$D = \frac{\Delta P l^2 a}{16 f_{\text{out}}} \quad (2.28)$$

where

D = flexural rigidity of sandwich structure, N mm²;
 ΔP = load increment corresponding to straight line on the load-displacement curve, N;
 f_{out} = displacement increment corresponding to extending point ΔP , mm;
 a = extending length, mm.

The shear rigidity of a sandwich structure is calculated using Eq. (2.29):

$$N = \frac{\Delta P l}{4 \left(f_{\text{mid}} - \frac{f_{\text{out}}}{3a} \right)} \quad (2.29)$$

where

N = shear rigidity of sandwich structure, MPa;
 ΔP = load increment corresponding to straight line on load-deflection curve, N;
 f_{mid} = midspan deflection of specimen, mm.

The definitions of other symbols are the same as those for the equations above. The shear modulus of elasticity is calculated using Eq. (2.30):

$$G_C = \frac{N}{b(h - t_f)} \quad (2.30)$$

where

G_C = shear modulus of elasticity, MPa;

Other symbols have the same meanings as in the equations above.

(4) Methods for testing composite physical properties

The mechanical properties of composites are closely related to their physical properties. A knowledge of their mechanical properties and test methods enables determination of the physical properties of composites (including insoluble content

of composite resin and composite resin content), and these data and test methods can be widely used in practical engineering projects.

1. Methods for determining insoluble content of fiber-reinforced composite resin: The insoluble content of a fiber-reinforced composite resin is a major index for evaluating the composite properties and reflects the degree of cross-linking of thermosetting resins to some extent. The insoluble content is closely related to the mechanical and heat-resistant properties, and when the mechanical property data of composites are given, resin-insoluble content data also need to be supplied.

Acetone extraction is used to determine the resin-insoluble content. Sampling is performed 20–30 mm from the plate edges to avoid defects such as blisters, delamination, resin pocket wrinkles, and chips. The specimen mass is (1 ± 0.2) g. At least, three test specimens should be used. During specimen machining, water should be used for cooling; oil cooling is forbidden. After machining, the specimens are dried under appropriate conditions for an appropriate time. File cullers or other tools are used to grind specimens to powders, avoiding resin heating, and then screened with a 40# sieve. The residues are grounded again and stirred uniformly. Specimens that are sticky because of a degree of resin curing are not sieved. The specimen is dried for 2 h at (80 ± 2) °C after sampling and placed in a desiccator until it cools to room temperature or for 24 h. The specimen $[(1 \pm 0.2)$ g] is weighed on a filter paper. The weighing accuracy should be 0.0001 g. The specimen is packed in an extracting machine and extracted at a constant temperature of (80 ± 2) °C in a water bath for 3 h with a backflow velocity greater than 80 ± 2 times per hour. Several specimens can be extracted simultaneously, but the extraction time will be prolonged: 4 h for two specimens and 6 h for three specimens. When extraction is complete, the dried specimen is placed in a weighed bottle and heated for 2 h in a drying box at (105 ± 5) °C, cooled to room temperature in a desiccator, and weighed. The weighing accuracy is maintained during the test. The extraction time must be sufficient for complete extraction of the non-cured resin. The resin-insoluble content of the composite is calculated using Eq. (2.31):

$$C_r = \left(1 - \frac{G_1 - G_2}{G_1 \times W_r} \right) \times 100 \dots \quad (2.31)$$

where

- C_r = resin-insoluble content, %;
- G_1 = specimen quantity before extraction, g;
- G_2 = specimen quantity after extraction, g;
- W_r = resin content, %.

2. Method for determining resin contents of FRPs: The method for determining the resin contents of glass-reinforced plastics is different from that for carbon-fiber-reinforced plastics. An ignition method is used to determine the

resin contents of glass-reinforced plastics, whereas sulfuric acid digestion is used for carbon-fiber-reinforced plastics.

- (a) Method for determining resin contents of glass-reinforced plastics. The sampling position and method for determining the glass-fiber-reinforced composite resin content are the same as those for determining the resin-insoluble content. The specimen weight is 2–5 g; at least, three specimens are tested for each sample. The specimen thickness is less than 5 mm. After sampling, the specimens are cleaned with a solvent and then placed in a desiccator at room temperature for 24 h, or dried at 80 °C for 2 h, and then cooled to room temperature in a desiccator. The specimen is heated in a crucible in a muffle furnace at (600 ± 20) °C for 10–20 min, cooled to room temperature, and weighed to the nearest 0.1 mg. The test is repeated until the crucible weight is constant. The crucible is placed in the muffle furnace at (600 ± 20) °C until all the carbonaceous material disappears; this takes approximately 30 min for epoxy and polyester FRPs, and about 90–120 min for phenolic FRPs. The crucible and residue are removed from the muffle furnace, cooled to room temperature in a desiccator, weighed, and burned again, at a constant temperature. This process is repeated until the difference between two successive results does not exceed 1.0 mg. Weighing is performed to the nearest 0.1 mg. The resin content is calculated using Eq. (2.32):

$$W = \frac{G_2 - G_3}{G_2 - G_1} \times 100\% \quad (2.32)$$

where

W = resin content, %;

G_1 = crucible mass, g;

G_2 = total weight of crucible and specimen, g;

G_3 = total weight of crucible and residue after ignition, g.

Equation (2.32) includes the impregnated reinforcer and a small amount of small molecular materials formed by combustion. Blank tests can be used as a check if necessary.

- (b) Method for determining resin contents of carbon-fiber composites. Sulfuric acid digestion is used to determine the resin contents of carbon composites. Heating with sulfuric acid assimilates the resin matrix rather than corroding the carbon fibers. Each sample contains three specimens. The specimen quantity is 0.5 g. The specimen thickness is less than 3 mm. If the thickness is more than 3 mm, the specimen is cut into pieces of thickness less than 3 mm. The specimen can be any shape that fits the container. The specimen (0.5 g) is placed in a flask, and 95–98% sulfuric acid (30 mL) is injected into the flask. A thermometer is inserted, and the temperature is adjusted to the digestion temperature. The digestion temperature is the temperature at

which dropwise addition of hydrogen peroxide (30%) makes the digestion solution clear and fibers float above the liquid level. The digestion temperature for an epoxy or polyester matrix is (220 ± 10) °C, a non-constant temperature; and for a phenolic resin matrix is (285 ± 5) °C, constant temperature for 1 h. The container of sulfuric acid and the specimen is heated in a ventilator. The time taken to increase the solution temperature from room temperature to the digestion temperature is not less than 15 min. Then, 30% hydrogen peroxide is dripped slowly along the bottle wall until the digestion solution becomes clear and fibers float above the solution level. The clear solution is then heated at the digestion temperature for 10 min. If the solution is turbid, hydrogen peroxide is added dropwise and the solution is stirred well until it becomes clear. A constant-weight filter apparatus is cleaned and weighed. The cooling digestion solution is diluted with distilled water under a vacuum of 17 kPa or better and filtered. The residue is washed with distilled water and acetone. The filtered fibers and filter apparatus are placed in an oven at (150 ± 5) °C and dried for 2 h. The filter or crucible is cooled to room temperature. Representative specimens are weighed, and blank tests are performed under the above conditions. The weight of the fibers equals the amount digested, and the length approximates to the fiber length. The percentage weight loss is calculated. The measurement accuracy is 0.1 mg. The resin content of the carbon-fiber-reinforced plastic is calculated using Eq. (2.33):

$$W = \left[1 - \frac{G_2}{G_1(1 - W_1)} \right] \times 100 \% \quad (2.33)$$

where

W = resin mass percentage in the carbon-fiber-reinforced plastic, %;

G_1 = mass of the specimen before digestion, g;

G_2 = final mass of carbon fibers after digestion, g;

W_1 = the percentage weight loss of fibers in the blank test.

The resin content of the carbon-fiber composite calculated using the above equation excludes the fiber coating and impregnant. If an impregnant was included in the resin content, the fibers used in the blank test should be extracted and then digested.

2.3.1.2 Composite Mechanical and Physical Properties

Composite mechanical property data provide an important basis for material choice and structural design in projects. Different composites have significantly different mechanical properties. It is commonly thought that the reinforcing fibers are load bearing and the resin matrix acts as an adhesive and transfers loads. The tensile and

compressive properties of a material mainly depend on the types and forms of reinforcements (continuous, fabric, short fibers). The interfacial properties and thermal resistance are determined by the resin matrix. The mechanical properties obtained using a given type of reinforcement differ depending on the fiber content and the fiber reinforcement form. Information on material properties and the factors that affect them is needed for material choice and structural design.

(1) Mechanical and physical properties of composites for hand lay-up

Hand lay-up is one of the most common methods used in composite processing. It has advantages such as low investment, simple processing equipment, and easy molding processes. Composite mechanical and physical properties vary depending on the type of reinforcement and resin matrix. The properties of composites for hand lay-up under specific conditions are shown in Table 2.13.

(2) Mechanical and physical properties of composites for SMC and BMC molding

SMC and BMC molding processes are widely used in engineering projects. The SMC or BMC is placed in a preformed mold and cured by pressing at a specific pressure, temperature, and time. The process has high mechanical efficiency. This process is suitable for applications such as production of large batches of water tank panels, vehicle parts, and electric switches. The composite properties are shown in Table 2.14.

(3) Mechanical and physical properties of composites for laminates

Laminates, which are widely used in electrical insulation, are made by curing and hot pressing a resin matrix impregnated with glass-fiber cloth. The composite properties are shown in Table 2.15.

(4) Mechanical and physical properties of composites for RTM, vacuum-assisted RTM (VARTM), and spray-up

RTM and VARTM are closed-mold processes. They cause less environmental pollution than hand lay-up and spray-up, but need special processing equipment. The composite properties are given in Table 2.16.

(5) Mechanical and physical properties of composites for prepregnation

Prepregnation can be categorized into hot-melt prepregnation and solvent prepregnation, based on the prepregning forms of the resins and fibers, and their fabrics. In hot-melt prepregnation, hot, molten resin films are painted uniformly on the surfaces of fibers and fabrics and then rolled using isolating films into intermediate products. In solvent prepregnation, fibers and fabrics prepregated with resin solution are cured and rolled into intermediate products. The intermediate products are cut according to design requirements, placed in molds, and pressed using a vacuum bag into composite products. This process gives precise control of the resin content and flexible material design, and products with good mechanical

Table 2.13 Mechanical and physical properties of composites for hand lay-up

Composition	1:1 fabric (glass/epoxy)	4:1 fabric (glass/epoxy)	1:1 fabric (glass/epoxy-polyester)	1:1 fabric (glass/306 polyester)	Chopped fiber mat/polyester
Longitudinal tensile strength/MPa	294.2	365.8	284.4	215.8	60-140
Longitudinal tensile modulus/GPa	17.7	25.5	16.7	13.7	5.5-12
Longitudinal compressive strength/MPa	245.2	304.0	245.2	176.5	110-180
Longitudinal compressive modulus/GPa	16.2	23.0	15.0	12.5	5.0-10.8
Transverse tensile strength/MPa	294.2	139.7	284.4	215.8	60-140
Transverse tensile modulus/GPa	17.7	11.8	16.7	13.7	5.5-12
Transverse compressive strength/MPa	245.2	225.6	245.2	176.5	110-180
Transverse compressive modulus/GPa	16.2	11.0	15.0	12.5	5.0-10.8
Shear strength/MPa	68.6	65.7	55.3	50.0	50.0
Shear modulus/GPa	3.53	2.84	3.34	3.20	1.40
Poisson's ratio	0.14	0.20	0.14	0.14	0.23
Flexural strength/MPa	298.0	340.0	273.4	193.3	108-280
Flexural modulus/GPa	16.7	23.4	16.7	14.2	6.9-13
Impact strength/kJ m ⁻²	230	294	265	240	98-180
Fiber content by volume V _f (or resin content W _R)/%	W _R = 45	W _R = 45	W _R = 47	W _R = 52	W _R = 40-55

Table 2.14 Mechanical and physical properties of composites for SMC and BMC

Composition	Food SMC	Common SMC	Electric SMC	BMC polyester	BMC phenol	BMC epoxy
Tensile strength/MPa	100	60–130	140.0	30–70	29–49	20–59
Compressive strength/MPa	150	60–100	130	20–40	98–147	98–147
Flexural strength/MPa	150	130–210	150	70–140	10–13	12–14
Shear strength/MPa	90	80	93			
Flexural modulus/GPa	9.5	9.6–13	11.5	9.6–13	13.5	15.0
Impact strength/kJ m ⁻²	63.7	43–85	60	16–32	20	20
Poisson's ratio	0.3	0.3	0.3	0.3	0.3–0.5	0.3–0.5
Density/g cm ⁻³	1.78	1.7–2.1	1.75–1.95	1.8–2.1	1.9	1.85
Barcol hardness	≥ 45	40–60	50–60	50	60	60

Table 2.15 Mechanical and physical properties of composites for laminates

Composition	Phenolic laminates	High-strength phenolic laminates	Epoxy/phenolic laminates	Epoxy laminates	BMI laminates
Density/g cm ⁻³	1.30–1.42	1.30–1.50	1.70–1.90	1.70–1.90	1.70
Martin thermal resistance/°C	125	125	200	130	280
Tensile strength/MPa	64	69	314	330	320
Flexural strength/MPa	103	118	313	340	343
Impact strength/kJ m ⁻²	25	29	200	37	147

properties. The mechanical and physical properties of fabrics and unidirectional fibers for prepregation are shown Tables 2.17 and 2.18.

(6) Mechanical and physical properties of composites for pultrusion

In pultrusion, a reinforcing material such as fibers, mat, or fabric and a prepregating resin are cured in heated molds under a pulling force to give continuous products with required cross-sectional shapes. This process has high mechanical requirements and is suitable for manufacturing a range of products such as cable supports for insulating rods and protective covers for rails. The composite properties are given in Table 2.19.

Table 2.16 Mechanical and physical properties of composites for RTM, VARTM, and spray-up

Composition	Glass mat, fabric/polyester	Glass mat, fabric/vinylester	E-glass cloth/epoxy	E-glass/poly-ester 0/90 nonweave (vacuum assistant)	E-glass/polyester 0/90 nonweave (vacuum bag)	T300/epoxy polyester 0/90 nonweave (vacuum assistant)	T300/epoxy polyester 0/90 nonweave (hotpress)		Short glass/polyester (spray-up)	
							30°	60°		
Tensile strength/MPa	80-140	148.3	350	506	590	730	813	682	700.3	60-130
Tensile modulus/GPa	8.30-13	9.5-14	18.5	32	34	60	62	52.3	48.1	5.5-12.5
Compressive strength/MPa	72-126	133.5	390							110-180
Compressive modulus/GPa	7.5-11.7	12.0	14.5							
Flexural strength/MPa	150-260	215.4	480	624	790	878	977	786.6	555.4	110-200
Flexural modulus/GPa	8.39-13	13.5	19.5			60	63	44.1	31.5	6.9-8.2
Shear strength/MPa	36	40	38			51	64	36.8	48.1	
Impact strength/kJ m ⁻²	50-110	80-140	170							40-80
Density/g cm ⁻³	1.4-1.6	1.55	1.75			1.50	1.55			1.4-1.6

Table 2.17 Mechanical and physical properties of fabric composites for prepregnation

Composition	Glass cloth/polyester	Glass cloth/polyester (auto-extinguish)		Glass cloth/polyester (dielectric)		E-glass cloth/epoxy		Thornel 300 Fiber cloth/epoxy Vacuum bag	Kevlar49 cloth/epoxy	
		Vacuum bag	Molding pressing	Vacuum bag	Molding pressing	Vacuum bag	Molding pressing		Weave285	Weave120
Tensile strength/MPa	284.1	441.3	358.5	377	361.3	471.0	483	598.0	538	463
Tensile modulus/GPa	18.6	22.6	23.4	19.0	23.6	26.9	27.53	64.0	31	30
Compressive strength/MPa	395.1	283.4	362.7	317.7	360.6	481.0	477	401	179	174
Compressive modulus/GPa	16.7	20.3	21.0	17.1	21.2	29.19	30.50	65	26	30
Shear strength/MPa	23.0	25.0	26.3	25.3	27.1	28.77	29.33	74	23.2	
Flexural strength/MPa	405.4	450.9	556.4	451.5	547.5	647.0	740	752	443	
Flexural modulus/GPa	18.6	22.6	23.4	19.0	23.6	27.90	29.12	53	30	
Fiber content by volume V_f (or resin content W_R)/%	$W_R = 38$	$W_R = 36.7$	$W_R = 35.3$	$W_R = 36.0$	$W_R = 33.6$	$W_R = 32$	$W_R = 32$	$W_R = 39$	47	48

Table 2.18 Mechanical and physical properties of fiber composites for prepregation

Composition Properties	Angle/ (°)	E-glass/epoxy (autoclave)	S-glass/epoxy (autoclave)	Carbon/epoxy (T300/5208) (autoclave)	Carbon/epoxy (AS-12 k) (autoclave)	Kevlar 7100/epoxy (autoclave)	Kevlar 49/epoxy (autoclave)
Tensile strength/MPa	0	965.0	1790	1500	2044.0	1064	1400
Tensile modulus/GPa	90	20	43	40	56	23.1	12
Compressive strength/MPa	0	39.3	48.3	143.0	140.0	68.6	76.0
	90	9.7	14.5	10.0	9.3	6.02	5.5
Compressive modulus/GPa	0	880.0	1000	1500	1435	253.4	235.0
	90	195	200	246	263.0	124.6	53.0
In-plane shear strength/MPa	0	35.3	46.9	128.7	128.8	68.6	
	90	8.7	12.4	9.0	8.3	5.6	
In-plane shear modulus/GPa	±45	145.0	97	68.0	144.9	60.2	34.0
	±45	10.3	5.5	7.17	5.60	1.89	2.30
Poisson's ratio		0.31	0.30	0.28	0.28	0.39	0.34
Flexural strength/MPa	0	1150	1520.0	1453.0	1855.0	728.0	
	90	75					
Flexural modulus/GPa	0	38.6	48.3	132.0	125.3	60.9	
	90	11.1					
Interfacial shear strength/MPa		75.8	83.0	80.0	119.0	40	36
Fiber content by volume V_f (or resin content W_R)/%		$W_R = 36.5$	$W_R = 29$	$V_f = 60$	$V_f = 60$	$V_f = 57$	$V_f = 60$

Table 2.19 Mechanical and physical properties of fabric composites for pultrusion

Composition Properties	Direction	Mat/glass/polyester	E-glass/polyester	E-glass/vinyl ester	Glass/mat/polyester (polyglas TM)	Polyglas-epoxy rod	E-glass/epoxy rod	Glass/polyester rod
Tensile strength/MPa	0°	205.0	550–1270	850	210.0	1232.0	1000.0	490.0
	90°	48.0	23.0	30.0	105.0	32.0	34.0	28
Tensile modulus/GPa	0°	17.0	27–41	27.5	14.0	48.6	45.0	34
	90°	5.5	7.5	9.10	5.6	11.2	12.0	8.0
Flexural strength/MPa	0°	205.0	690–1270	805.0	210.0	1183.0	1000.0	490.0
	90°				105.0			
Flexural modulus/GPa	0°	13.7	22–41	24	14.0	47.3	45.6	21.0
	90°			9.0	5.6			
Compressive strength/MPa	0°	205.0	210–480	765.0	210.0	1108.8	900.0	280.0
	90°	103.0	21.0	27.0	105.0	28.8	30.6	140.0
Poisson's ratio		0.33	0.30	0.30	0.33	0.30	0.3	0.3
Impact strength/kJ m ⁻²		120–160	220.0	230.0	228.0	350.0	400.0	228.0
Interfacial shear strength/MPa		38.0	36.0	37.0	38.5	80.5	50.0	40.0
Density/g cm ⁻³		1.7–1.9	1.6–2.2	1.9	1.7	2.0	2.0	1.95

(7) Mechanical and physical properties of composites for filament winding

In filament winding, continuous fibers prepregged with resin are wound uniformly on the surface of a mandrel. Continuous fibers of high specific strength and rigidity can be obtained. Flexible design allows the winding angle for each layer to be changed, and materials can be chosen based on the product property requirements. This process is suitable for manufacturing all types of pressure vessels and rotating structures. The material properties are given in Table 2.20.

(8) Envelope curves of composite laminates

Many factors affect the mechanical properties of composite laminates, including the components and their proportions, the laying angle, stacking sequence, and loading conditions. The mechanical properties of laminates are determined based on theoretical calculations and testing.

A symmetric laminate of $[0^\circ/\pm 45^\circ/90^\circ]_s$ is a common lay-up product, and the unidirectional laminates mechanical properties base on the envelope curve of laminates.

The $[0^\circ/\pm 45^\circ/90^\circ]_s$ laminate envelope curve assumes that laminates bear only an interfacial tensile, compressive load in a linear elastic state rather than suffering breakage from cracks, delamination of free edges, and other factors. A $[0^\circ/\pm 45^\circ/90^\circ]_s$ laminate in the linear elastic state is produced by lay-up in the 0° , $+45^\circ$, -45° , and 90° directions, and full lay-up is not less than 10%. The stress-strain curves of an AS1/3501 carbon-fiber/epoxy composite unidirectional laminate are shown in Figs. 2.29, 2.30, 2.31, and 2.32. The envelope curves of the AS1/3501 carbon-fiber/epoxy $[0^\circ/\pm 45^\circ/90^\circ]_s$ laminate are given for reference in Figs. 2.33, 2.34, 2.35.

2.3.2 Thermal Properties and Testing

Composites have not only good structural properties but also many other properties such as corrosion resistance, ablation and heat resistance, non-conductivity, and weatherability. Composites can be designed because they differ in terms of composition, processing, layer parameters, and thermal properties. Composites are anisotropic; therefore, their thermal properties have a certain direction, so methods for their testing differ from those used for non-composite materials. This is taken into account in composite design.

2.3.2.1 Thermal Property Testing

Composite thermal property testing is important for predicting and evaluating material properties. A wide range of methods are used, including *Test method for coefficient of linear thermal expansion of FRPs* (GB2572-81), *Test method for*

Table 2.20 Mechanical and physical properties of composites for filament winding

Composition Properties	Direction	E-glass/polyester 199	E-glass/polyester 189	S ₂ fiber (240 Tex)/epoxy	S ₂ fiber (280 Tex)/epoxy	Carbon T300/epoxy	Carbon T700/epoxy	Carbon M40/epoxy
Tensile strength/MPa	0°	936.0	757.0	1250.0	1344.0	1200.0	1400.0	1050.0
	90°	25.7	22.9	33.1	31.78	18	18.0	16.0
Tensile modulus/GPa	0°	37.3	36.4	44.6	58.20	120.0	120.0	190.0
	90°	10.6	12.0	10.7	28.61	8.9	8.3	8.2
Flexural strength/MPa	0°	924.0	763.0	1230.4	1350	1320.0	1380.0	1020.0
	90°							
Flexural modulus/GPa	0°	36.4	36.7	43.7	54.3	123.0	125.0	180.0
	90°							
Compressive strength/MPa	0°	484.0	464.8	715.0	688.0	800	850.0	925.0
	90°	143.0	141.5	130.0	135.0	95.0	96.0	90.0
Compressive modulus/GPa	0°	37.9	33.6	44.0	50.0	90.0	100.0	175.0
	90°	11.5	10.3	9.88	19.2	8.5	8.4	9.0
Shear strength/MPa	±45°	16.1	12.3	21.1	3.09	16.0	15.0	12.0
Shear modulus/GPa	±45°	4.5	3.7	3.34	6.78	4.8	4.8	4.2
Interfacial shear strength/MPa		62.6	62.5	70.5	59.35	60.0	60.0	46.0
Poisson's ratio		0.29	0.31	0.30	0.29	0.3	0.3	0.3
Fiber content by volume V _f (or resin content W _R)/%		W _R = 30	W _R = 30	W _R = 26.46	W _R = 18	V _f = 57	V _f = 57	V _f = 54

Fig. 2.29 Longitudinal tension stress–strain curve of AS1/3501

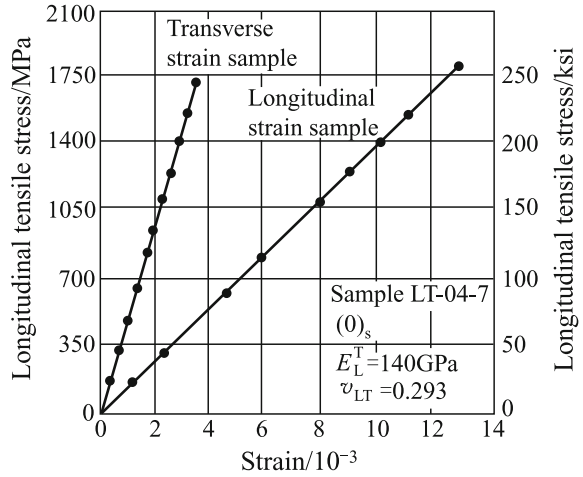


Fig. 2.30 Compressive stress–strain curve of AS1/3501

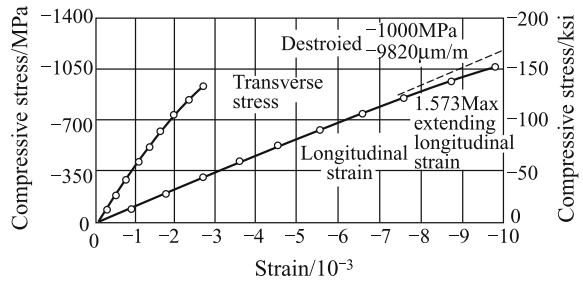


Fig. 2.31 Compressive stress–strain curve of AS1/3501[±45]_{ns}

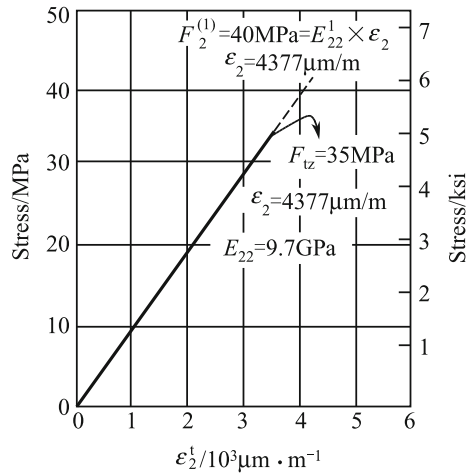


Fig. 2.32 Tension stress–strain curve of AS1/3501 90°

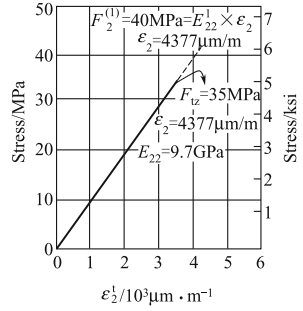


Fig. 2.33 Tensile and shear moduli of AS1/3501 laminate

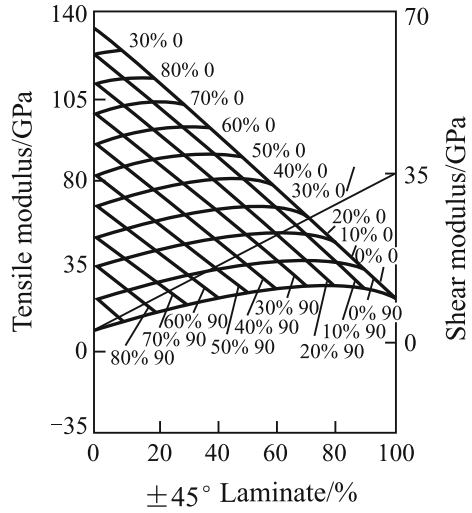


Fig. 2.34 Tensile and shear moduli of AS1/3501 laminate

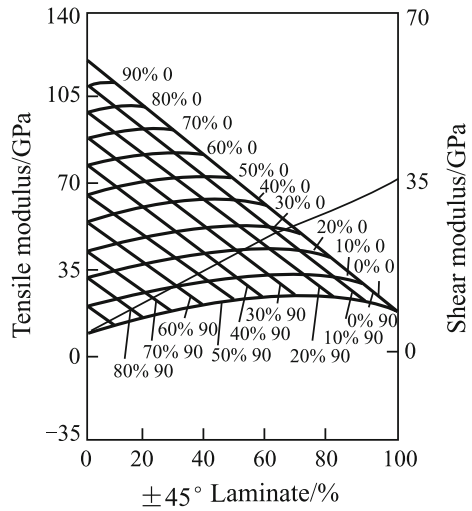
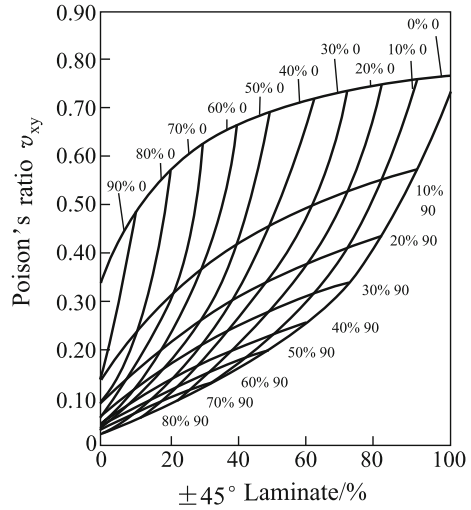


Fig. 2.35 Poisson's ratio for AS1/3501 laminate



thermal conductivity factors of FRPs (GB3139-82), Test method for average specific heat capacity of fiber-reinforced plastics (GB/T 3140—1995), Test method for Martin heat resistance of plastics (GB1035-70), and Test method for deflection temperature (GB1634-76).

(1) Methods for determining average coefficient of linear thermal expansion

The coefficient of linear thermal expansion of a composite is affected by many factors. The coefficient of thermal expansion continuously changes with increasing test temperature. The coefficient of thermal expansion of a certain type of material can only be obtained for a given relative temperature range, material composition, and composition content. Test methods for determining the coefficient of average linear thermal expansion are applicable to FRPs and referenced to carbon- or aramid-reinforced composites.

The test method stipulates that the cross section of the test specimen should be round or square. For round specimens, the diameter is 6–10 mm, and the circumference is 50 or 100 mm. Square specimens have a side length of 7 mm. At least, three specimens are used in each sample. The ends of the specimen are cut flat, with less than 0.04 mm of roughness. Any dilatometer can be used that is able to heat uniformly, to control the rate of temperature increase of the specimens, the test specimen temperature, and its relative extension. The accuracy of the device for measuring changes in length should be 0.001 mm. The accuracy of the device for temperature measurements should be 0.5 °C, and the rate of temperature increase should be $(1 \pm 0.2) \text{ }^\circ\text{C}/\text{min}$. Based on the expansion–temperature curve, the coefficient of linear thermal expansion over the temperature range $a_{T_1 \sim T_2}$ is given by

$$\alpha_{T_1 \sim T_2} = \frac{\Delta L}{KL_0 \Delta T} + \alpha_{\text{quartz}} \quad (2.34)$$

where

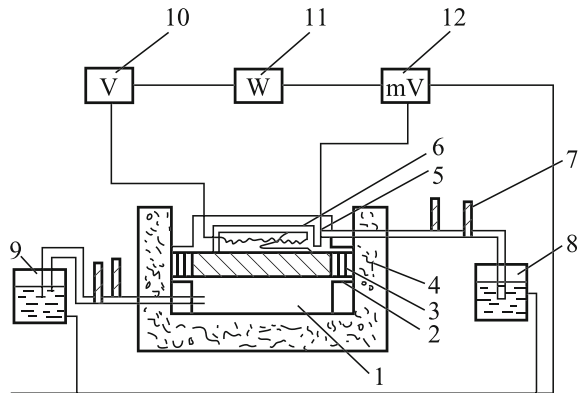
- L_0 = specimen length at room temperature, mm;
 K = multiples of extension length measured by device;
 ΔT = temperature difference, °C, $\Delta T = T_2 - T_1$;
 ΔL = extended length of specimen relative to ΔT , mm;
 α_{quartz} = average coefficient of linear thermal expansion of quartz at test temperature ($T_1 - T_2$), the value is usually $0.51 \times 10^{-6} \text{ K}^{-1}$.

(2) Methods for determining thermal conductivity of FRP

The thermal conductivity of a composite can be used to predict the thermal properties of materials. Factors that affect the thermal conductivity include the types of resins and fibers, and the fiber orientation. Generally, the thermal conductivity of a continuous-fiber-reinforced composite is better than that of a non-continuous-fiber composite. The thermal conductivity is improved by increasing the content of carbon fibers in a composite. The thermal conductivities of Kevlar-fiber composites are lower than those of carbon-fiber composites.

The test method for determining the thermal conductivity stipulates that the specimen side length or diameter should be the same as that of the heater plate. The specimen thickness should be at least 5 mm, and less than 1/10 of the side length or diameter. The specimen surface should be flat and of roughness less than 0.5 mm/mm. At least, three specimens should be used in each sample. The testing device is shown in Fig. 2.36.

Fig. 2.36 Device for measuring thermal conductivity 1—cooling plate; 2—specimen; 3—microcalliper; 4—heat protector; 5—heat-protecting plate; 6—heating plate; 7—thermometer; 8—constant-temperature water bath for heat-protecting plate; 9—constant-temperature water bath for cooling plate; 10—voltmeter; 11—watt-hour meter; 12—millivoltmeter



Specimens are pretreated before the test, below the temperature that would cause changes in quality and deformation (the maximum temperature should be less than 105 °C). The specimens are heated to constant weight or treated according to the product requirements. At constant weight, the specimen weight changes by less than 0.2% every 2 h at the treatment temperature. The side length or diameter of the heating plate is usually 100 mm. The width of the heat-protecting plate is one-quarter that of the side length or diameter of the heating plate to maintain the heat. The temperature differences between points on the main heating plate should be less than 2% of the temperature difference between both surfaces in a stable state and at most 0.5 °C. The temperature differences between points on the heat-protecting plate should be less than 5% of the temperature difference between specimen surfaces and at most 1 °C. The roughness of the heating plate surface should be less than 0.25 mm/m. The accuracy of the temperature measurements should be 1% of the temperature difference between the specimen surfaces in a stable state and at most 0.5 °C. The thermal conductivity λ [W/(cm K)] is calculated using Eq. (2.35):

$$\lambda = \frac{0.239Wd}{S\Delta t} \quad (2.35)$$

where

W = power of main heating plate in a stable state, W;

d = specimen thickness, cm;

S = calculated area of main heating plate, cm²;

Δt = temperature difference between specimen surfaces, °C.

(3) Method for determining average specific heat capacity of FRP

The average specific heat capacity of a composite is determined by uniformly heating a specimen to the test temperature, and then placing it with a copper thermometer of known heat capacity at a lower temperature, and measuring the increase in the thermometer temperature when they both have the same temperature. The heat absorbed by the thermometer is equal to that released by the composite. At least, three specimens should be used in each sample. The specimen is shown in Fig. 2.37. The measuring device is shown in Fig. 2.38. The thermometer is shown in Fig. 2.39. The thermometer material should be copper (heat capacity approximately 800 J/°C), and the heat capacity should be scaled to the electrical energy.

The water-bath temperature should not fluctuate by more than ± 0.1 °C during the test. The maximum temperature difference in a uniform area should not be more than 1 °C. The thermometer precision should not be lower than 0.01 °C. The precision of the thermocouple for measuring the specimen temperature should not be lower than 0.2 °C.

Fig. 2.37 Specimen dimensions

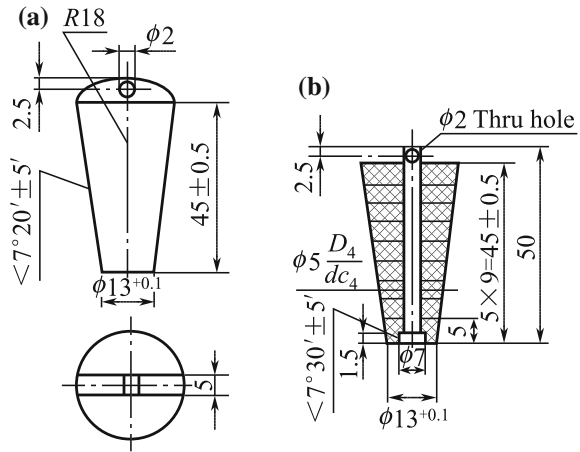
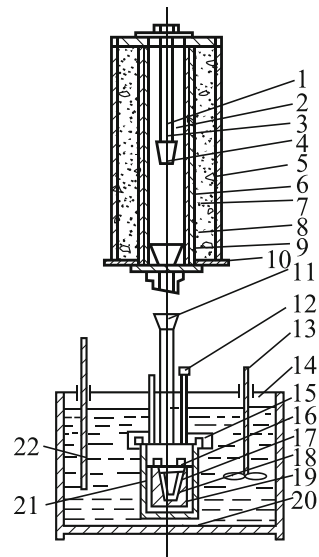


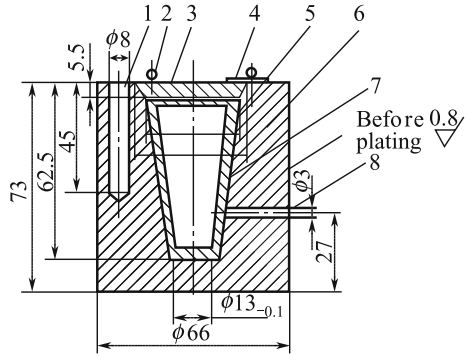
Fig. 2.38 Measuring device

- 1—specimen holder;
- 2—thermocouple thermometer;
- 3—metal wire;
- 4—specimen;
- 5—heating furnace;
- 6—copper pipe;
- 7—heating wire;
- 8—insulating material;
- 9—thermal insulation material;
- 10—furnace door;
- 11—rubber plug;
- 12—guy of movable cover;
- 13—agitator;
- 14—water bath at constant temperature;
- 15—outside cover of thermometer;
- 16—movable cover of thermometer;
- 17—thermometer;
- 18—scaled heating wire;
- 19—thermometer liner;
- 20—thermally insulated supporter;
- 21—platinum;
- 22—temperature gauge



The specimen is hung in the middle of a furnace of uniform area and heated to 100 °C. The thermometer is placed in a water bath, and the onset temperature of the thermometer and the bath temperature are kept at about 20 °C. The temperature of the water bath is adjusted to 1 – 1.5 °C higher than the onset temperature of the thermometer until a constant temperature is reached. After the temperature has stabilized, it is maintained for over 20 min and the temperature errors should not be more than ±0.2 °C. The temperature t is recorded when the specimen is lowered.

Fig. 2.39 Thermometers (chrome plated at thickness of 0.02 mm) 1—jack for thermometer; 2—guy of movable cover; 3—movable cover; 4—hinge; 5—thermometer liner; 6—copper thermometer; 7—scaled heating wire; 8—leading hole of heating wire



The thermometer temperature changes are measured in three stages and read every other minute. (1) The temperature t_0 is recorded at the 10th minute. (2) The temperature t_1 is recorded at the 11th minute. The maximum temperature t_n is recorded. (3) When the temperature starts to drop, the temperature is recorded for 10 min. After testing, the specimen is weighed to the nearest 0.01 g. The average specific heat capacity is given by Eq. (2.36):

$$C_p = \frac{C(t_n + t_s - t_0)}{m(t - t_n - t_\delta)} \tag{2.36}$$

where

- C_p = average specific heat capacity, J/(kg K);
- C = heat capacity of the thermometer, °C;
- t_n = highest temperature of the thermometer, °C;
- t_s = the recommended thermometer temperature, °C;
- t_0 = the thermometer temperature, °C;
- m = specimen quantity after testing, kg;
- t = specimen temperature, °C.

The recommended thermometer temperature is given by Eq. (2.27) or Eq. (2.38):

$$t_\delta = \frac{V_3 - V_1}{\bar{t}_3 - \bar{t}_1} \left(\frac{t_0 + t_n}{2} + \sum_{j=1}^{n-1} t_j - n\bar{t}_1 \right) + nV_1 \tag{2.37}$$

$$t_\delta = \frac{V_3 - V_1}{\bar{t}_3 - \bar{t}_1} \left(\frac{t_0 + t_n}{2} + \sum_{j=1}^{n-1} t_j - n\bar{t}_3 \right) + nV_3 \tag{2.38}$$

where

- V_1 and V_3 = rates of temperature change in first and second stages, respectively, °C/min;
 t_1 and t_2 = average temperatures in first and second stages, respectively, °C;
 n = number of recording times in the second stage;
 t_j = the temperature recorded in the second stage, °C.

(4) Method for determining thermal resistance of plastics

The thermal resistance of a composite is largely determined by the resin properties. The thermal resistance is an important index in choosing composites and their working conditions for a project. The Martin thermal resistance test method and deflection temperature test are usually used to evaluate the thermal properties of plastics and composites.

1. Martin thermal property test: The specimen is subjected to a flexural stress of (5 ± 0.02) MPa at (10 ± 2) °C/12 min below the static bending point. The temperature at which the flexural deflection is 6 mm is the Martin heat-resistant temperature. This test method is not applicable to plastics or FRPs with a thermal resistance below 60 °C. The Martin test specimen dimensions are (120 ± 1) mm \times (15 ± 0.2) mm \times (10 ± 0.2) mm. The surfaces of specimens of thickness more than 10 mm can be machined to 10 mm. Each sample consists of three specimens. The testing device and weight position adjustment are shown in Fig. 2.40. The weight position is first adjusted to apply a bending stress of 5 MPa to the specimen.

The weight position is calculated using Eq. (2.39):

$$L = \frac{\frac{bd^2}{\sigma_f} - P_1L_1 - P_2L_2}{P} \quad (2.39)$$

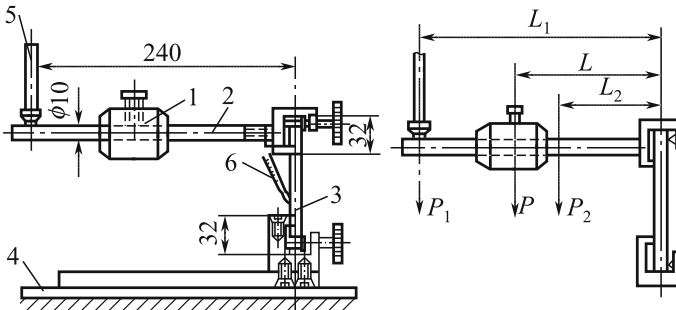


Fig. 2.40 Martin test apparatus and weight position 1—weight; 2—bar; 3—specimen; 4—support; 5—deflection indicator; 6—thermometer (divisions less than 2 °C)

where

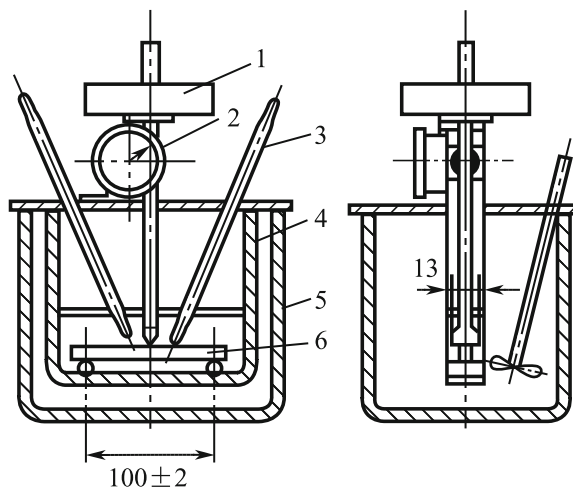
- P = weight mass (including screws), kg;
- P_1 = indicator mass, kg;
- L_1 = distance from deflection indicator to specimen center, cm;
- P_2 = bar mass (including nuts), kg;
- L_2 = distance from bar center to specimen center, cm;
- b = width of specimen, cm;
- d = thickness of specimen, cm;
- σ_f = bending stress, = 5 MPa.

The incubator in the testing apparatus is equipped with a blast device. The temperature difference at any position of the incubator can be up to 2 °C, and the initial temperature is (30 ± 1) °C. The specimen is installed vertically, and the bar is horizontal. The working length for specimen bending is (56 ± 1) mm. The temperature is increased after installation of the specimen. When the reading on the deflection indicator decreases to 6 mm, the temperatures of the two thermometers are recorded. The average temperature value is the Martin temperature.

2. Thermal deflection temperature: The specimen is immersed in silicone oil at a uniform elevated temperature, and the temperature at which specimen deflection under a simple supported beam flexural loading occurs is the thermal deflection temperature. The test device is shown in Fig. 2.41.

The specimen supports are made of metal, and the load is applied vertically midway between the supports. The distance between the two supports is 100 mm. The contact edges between the loading rod and specimen are rounded to a radius of (3 ± 0.2) mm. A bath of a suitable liquid heat-transfer medium such as silicone oil, which will not affect the specimen, is used to increase the

Fig. 2.41 Device for determining deflection temperature 1—load; 2—dial gauge; 3—thermometer; 4—specimen supports; 5—bath; 6—specimen



temperature at a uniform rate of $(12 \pm 1) \text{ }^\circ\text{C}/6 \text{ min}$. A set of weights of suitable sizes should be available so that the specimen can be loaded to a fiber stress of 1.82 or 0.455 MPa. The mass of the added weights is calculated using Eq. (2.40):

$$M_1 = \frac{2\sigma b h^2}{29.4l} - R \frac{T}{9.8} \quad (2.40)$$

where

- M_1 = weight mass, kg;
- σ = fiber stress, MPa;
- b = width of specimen, mm;
- h = thickness of specimen mm;
- l = midpoint of two supports, mm;
- R = mass of loading rod and indenter, kg;
- T = extra force of deflection device, N.

The divisions of the thermometer or thermal detector in the test apparatus should be $1 \text{ }^\circ\text{C}$. The divisions of the dial gauge or differential transformer for measuring the deflection should be 0.01 mm. The specimens should have smooth flat surfaces free from blisters. The specimen dimensions should be 120 mm \times 10 mm \times 15 mm; the flexural deflection point should be 0.21 mm. If the specimen thickness exceeds 15 mm, the specimen should be machined to 15 mm. If the thickness is less than 15 mm, the specified flexural deflection should be more than 0.21 mm. During the test, the specimen dimensions should be measured so that the weight mass can be calculated. The test specimen is aligned edgewise on the supports. The thermometer is positioned midway between the test specimen supports, within 3 mm but without touching it. The specimen frame is then placed in the liquid bath; the top of the specimen should be at least 35 mm below the liquid level of the bath. Weights are added to obtain the desired stress of 0.455 or 1.82 MPa. After stirring sufficiently for 5 min, the deflection measurement device is adjusted to zero and the liquid heat-transfer medium is heated. The deflection temperature is recorded, i.e., the temperature of the liquid heat-transfer medium at which the specimen has been deflected by the specified 0.21 mm.

2.3.2.2 Thermal Properties

Composites have anisotropic thermal properties. The thermal properties of composites differ significantly depending on the types of reinforcement and resin.

(1) Thermal properties of fabric- and fiber-reinforced plastics

Resins are often reinforced with fabric and chopped fibers. Hand lay-up, RTM, and pressure molding are usually used. Thermal properties are important in material

choice and performance evaluation. Thermal property data for composites produced using various manufacturing processes are given in Table 2.21.

(2) Thermal properties of unidirectional FRPs

The thermal properties of unidirectional FRPs are the basis of product design. The thermal properties vary depending on the material composition. The thermal properties of the finished products can be controlled to some extent based on composite design. The composite thermal properties are greatly affected by the manufacturing process. The thermal properties of several types of unidirectional composites and resin systems are given in Table 2.22.

2.3.3 Electrical Properties and Testing

Composites have a wide range of applications because they have good non-conductive properties as well as high specific strengths and rigidity. Knowledge, control, and testing of composite electrical properties are therefore important in material choice and property evaluation.

2.3.3.1 Electrical Property Tests

Methods for electrical property testing include methods for determining the electric strength of a solid insulating material at different power frequencies, methods for determination of the permittivity and dielectric dissipation factor of a solid electrical-insulating material at various power, audio, and radio frequencies, including meter wavelengths, and methods for testing volume and surface resistivity of a solid insulating material. National standards equivalent to the relevant IEC standards must be followed.

(1) Methods for testing electric strength of solid insulating materials at various power frequencies

These methods are used to determine the short-term electric strength of a solid insulating material at 50 or 60 Hz. The results obtained using this method do not represent the long-term electrical properties but are the basis of regular quality control testing.

The national standard GB 1408-90 stipulates that copper, stainless steels, and other metals can be used for electrode materials. The electrodes must be kept smooth, clean, and free from defects at all times. If the upper and lower electrodes are not of equal size, the larger one should be connected to the ground side of the transformer and arranged coaxially.

1. Specimens and electrodes for tests perpendicular to the surface of laminated materials

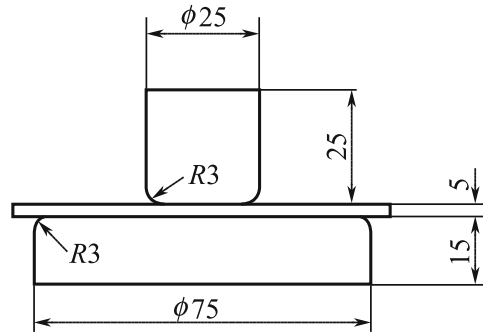
Table 2.21 Thermal properties of fabric- or fiber-reinforced plastics

Parameter	Glass reinforcement	Resin type	Glass content/%	Coefficient of linear thermal expansion/ 10^{-6} K^{-1}	Thermal conductivity rate/W (m K) $^{-1}$	Specific heat capacity/kJ (kg K) $^{-1}$	Thermal deflection temperature/ $^{\circ}\text{C}$	Martin thermal resistance/ $^{\circ}\text{C}$
Process								
SMC product	Short fibers	Polyester	15–30	14–22	0.186–0.244	1.3–1.5	150–180	110–150
BMC product	Short fibers	Polyester	15–35	14–22	0.186–0.244	1.3–1.5	150–180	110–150
Hand lay-up product	Short fiber mats	Polyester	30–40	18–36	0.186–0.267	1.3–1.4	130–160	100–130
Hand lay-up product	Cloth	Polyester	45–55	7–11	0.267–0.333	1.1–1.2	150–180	110–150
Molding product	Short fiber mats CSM performs	Polyester	25–35	18–32	0.186–0.2566	1.3–1.4	180–200	150–180
RTM product	CSM performs	Polyester	20–30	18–32	0.186–0.256	1.3–1.4	130–160	100–130
Spray-up product	Short fibers	Polyester	30–35	22–36	0.175–0.222	1.3–1.4	130–160	100–130
Laminating product	Cloth	Epoxy	50–65	7–11	0.278–0.333	1.1–1.2	200	180
Laminating product	Cloth	Epoxy phenolic	50–65	7–11	0.278–0.333	1.1–1.2	250	200

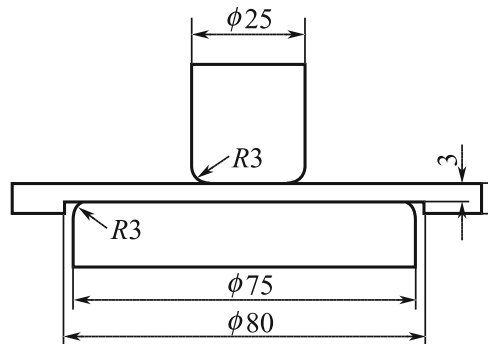
Table 2.22 Thermal properties of unidirectional FRPs

Materials	Coefficient of linear thermal expansion/ 10^{-6} K^{-1}	Thermal conductivity rate/W (m K) $^{-1}$	Specific heat capacity/kJ (kg K) $^{-1}$	Thermal deflection temperature/ $^{\circ}\text{C}$	Martin thermal resistance/ $^{\circ}\text{C}$	Fiber content by volume $V_f/\%$
Vinyl ester resin				117	90	0
Epoxy resin	66.5	0.27		130	95	0
E-glass fiber/epoxy	0 $^{\circ}$ 90 $^{\circ}$	0.85 0.30	0.96	180-200	180	55
T300 epoxy	0 $^{\circ}$ 90 $^{\circ}$	34 0.8	1.12	220	200	57
Kevlar49/epoxy	0 $^{\circ}$ 90 $^{\circ}$	-1.02 59	1.60	200	200	61
		0.14				61

Fig. 2.42 Specimens and electrodes for board and sheet tests



(a) Electrode arrangement of non-machined materials ($s \leq 3\text{mm}$)



(b) Electrode arrangement of materials ($s \leq 3\text{mm}$) machined to the effective thickness 3mm

- (a) Board and sheet specimens. The electrodes consist of two metal cylinders with the edges rounded to give a radius of 3 mm. One electrode is of diameter 25 mm and height 25 mm. The other electrode is of diameter 75 mm and height 15 mm. The electrode of diameter 75 mm is placed on boards or sheets; if the thickness is greater than 3 mm, it is reduced by machining on one side to (3 ± 0.2) mm (Fig. 2.42).
- (b) Tube specimens (of internal diameter up to 100 mm). The outer electrode consists of a band of metal foil of width 75 mm. The inner electrode is a metal-foil sphere of diameter 35 mm. The metal foil must be soft enough to give good contact with the specimen (Fig. 2.43).

2. Specimens and electrodes for tests parallel to laminated materials

- (a) Board and sheet specimens: The test specimen is a rectangle, with a length of 100 mm and a width of (25 ± 0.2) mm; its thickness is the same as that of the tested material. The long edges are cut as parallel planes at right angles to the

Fig. 2.43 Electrode arrangement for tubes and cylinders

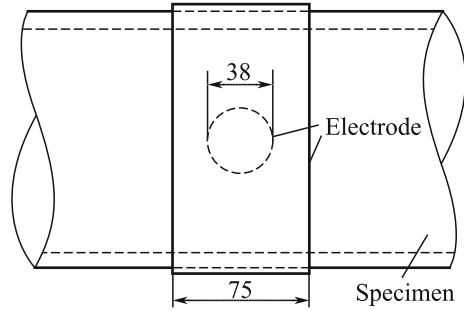
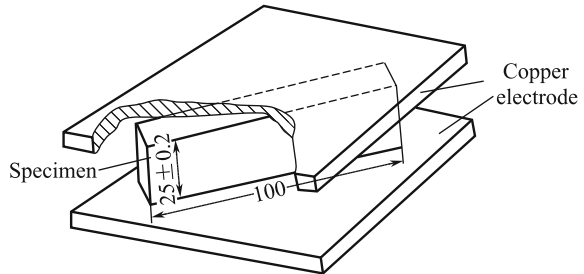


Fig. 2.44 Electrode arrangement for tests parallel to surface



surface of the material. The test specimen is placed between parallel metal electrodes, and a voltage is applied (Fig. 2.44). For thin specimens, two suitably placed test specimens are used to support the upper electrode. The electrode is of sufficient size to overlap the edges of the test specimens by 15 mm.

- (b) Tubes and cylinders: Both edges of the specimen are finished as parallel planes at right angles to the axis of the tube or cylinder. The test specimen is a complete ring or a 100-mm circumferential portion of a ring of axial length (25 ± 0.2) mm. The electrodes should be of sufficient size to overlap the edges of the specimens by 15 mm.

The voltage is raised from zero at a uniform rate until breakdown occurs, between 10 and 20 s. If the test specimen withstands the voltage for 20 s without failure, the voltage is increased in incremental steps until failure occurs. The electric strength is based on the highest voltage that is withstood for 20 s without breakdown. The electric strength is calculated using Eq. (2.41):

$$E_b = \frac{V_b}{d} \tag{2.41}$$

where

- V_b = breakdown voltage, MV;
- d = specimen thickness, m;
- E_b = electric strength, MV/m.

Five tests are conducted, and the electric strength or breakdown voltage is determined from the median of the test results. If any test result deviates by more than 15% from the median, five additional tests are performed. The electric strength or breakdown voltage is then determined from the median of the 10 results.

- (2) Methods for determination of permittivity and dielectric dissipation factor of solid electrical-insulating material at power, audio, and radio frequencies, including meter wavelengths

The relative permittivity ϵ_r of an insulating material is the ratio of the capacitance C_x of a capacitor, in which the space between and around the electrodes is entirely and exclusively filled with the insulating material in question, to the capacitance C_0 of the same configuration of electrodes in a vacuum. The dielectric loss angle δ of an insulating material is the angle of the phase difference between the applied voltage and resulting current, when the dielectric of the capacitor consists exclusively of the dielectric material. The composite permittivity and dielectric loss angle are related not only to frequency, temperature, moisture, and field strength, but also to the material composition, specimen thickness, and fiber orientation. The test conditions, including temperature and moisture, should therefore be noted. Sheet specimens are preferable for determining the permittivity and dissipation factor of a material, but the material may only be available in tubular form. The accuracy of the specimen thickness must be within $\pm(0.2\% \pm 0.001 \text{ mm})$, and the measuring points should be spread uniformly over the entire surface. The electrodes can be contact electrodes, contactless electrodes, and fluid displacement fixation electrodes. To avoid errors in the permittivity caused by edge effects, the electrode system can include a guard electrode. The guard electrode width should be at least twice the thickness of the specimen, and the gap between it and the main electrode should be smaller than the thickness of the specimen. Various types of electrode can be used, including metal-foil electrodes, fired-on metal electrodes, electrodes produced by spraying metal electrodes by cathodic evaporation or evaporation under high vacuum, mercury and other liquid-metal electrodes, conducting paint, and conducting rubber. Methods can be divided into two groups: null methods and resonance methods. Null methods are used at frequencies up to about 50 MHz. The networks normally used are a Schering bridge, transformer bridge, and parallel-T. Resonance methods can be used in the range 10–300 MHz. The reactance-variation and Q code-variation methods are generally used. The relative permittivity is measured accurately with a tolerance of $\pm 1\%$, and the dielectric dissipation factor is measured with a tolerance of $\pm(5\% + 0.0005)$. The relative permittivity of a specimen with its own electrodes is calculated using Eq. (2.42):

$$\epsilon_r = \frac{C_x}{C_0} \quad (2.42)$$

The relative permittivity of a specimen without a guard electrode is calculated using Eq. (2.43):

$$\varepsilon_r = \frac{C_x - C_c}{C_o} \quad (2.43)$$

where

- ε_r = relative permittivity;
- C_x = capacitance of insulating material;
- C_o = capacitance of capacitor in vacuum;
- C_c = correction for edge capacitance.

The dielectric dissipation factor $\tan\delta$ is calculated from the measured values in accordance with the equations applicable to the specific measuring arrangement.

(3) Methods for determining volume resistivity and surface resistivity of solid insulating materials

Direct and comparison methods are commonly used for measuring volume resistivity and surface resistivity. The direct methods can be divided into the voltmeter–ammeter method and current-amplifier method (resistor method). Comparison methods can be divided into ammeter and bridge methods. The measuring device must be capable of determining the unknown resistance with an overall accuracy of at least $\pm 10\%$ for resistances below $10^{10} \Omega$, and $\pm 20\%$ for higher values. Specimens commonly in use are either flat or tubular; specimen

Fig. 2.45 Electrode arrangement on flat specimen
 1—electrode (1);
 2—electrode (2);
 3—specimen; 4—electrode (3)

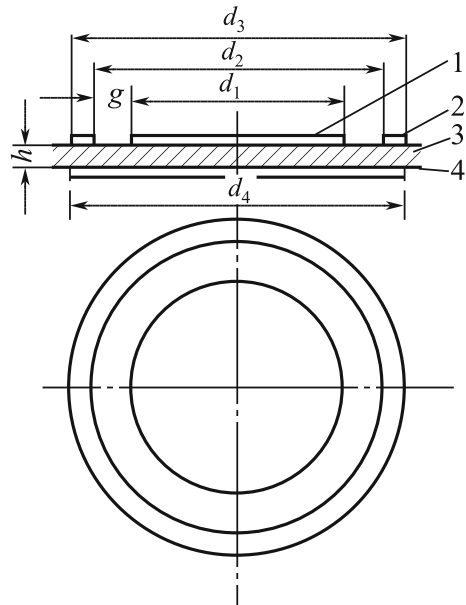
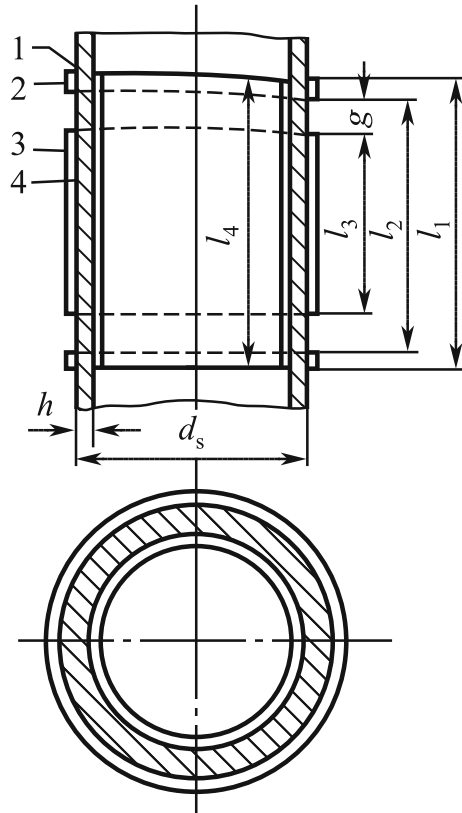


Fig. 2.46 Electrode arrangement on tubular specimen 1—electrode (3); 2—electrode (2); 3—electrode (1); 4—specimen



shapes and electrode arrangements are shown in Figs. 2.45 and 2.46. In measurement of the volume resistance, electrode (1) is a guarded electrode (measuring electrode), (2) is the guard electrode, and (3) is an unguarded electrode. The diameter d_1 or length L_1 of the guarded electrode should be at least 10 times the specimen thickness and for practical reasons usually at least 25 mm. The diameter d_4 (or length l_4) of the unguarded electrode and d_3 (or l_3) of the guard electrode should be equal to the inner diameter d_2 of the guard electrode (or length L_2) plus at least twice the specimen thickness. The values $d_1(l_1) = 50$ mm, $d_2(l_2) = 54$ mm, $d_3(l_3) = d_4(l_4) = 74$ mm are recommended.

In measurements of the surface resistivity, (1) is a guarded electrode, (3) is the guard electrode, and (2) is an unguarded electrode. In measurements of the surface resistivity between electrodes (1) and (2), the surface gap width g is at least twice the specimen thickness (1 mm is normally the smallest practicable width), so that the effect of the volume resistance is negligible. The diameter (or length) of the guarded electrode should be at least 10 times the specimen thickness, and for practical reasons at least 25 mm.

The recommended electrode arrangement is $d_1(l_1) = 50$ mm, $d_2(l_2) = 60$ mm, and $d_3(l_3) = d_4(l_4) = 80$ mm. The specimen should be 7 mm larger than the

maximum size of the electrodes at each side. At least, three samples should be tested. Electrode materials include evaporated metal, sprayed metal, and metal-foil conductive silver paint. A specified direct voltage is applied, and a timed device takes measurement after each of the following electrification times: 1, 2, 5, 10, 50, and 100 min. If the electrification time needed to reach steady state is long, the volume resistance is reported as a function of the electrification time. The electrification time is 1 min.

The volume resistivity is calculated using Eq. (2.44):

$$\rho_V = \frac{R_V A}{h} \quad (2.44)$$

where

ρ_V = the volume resistivity, Ω m

R_V = the volume resistivity of the specimen, Ω ;

A = the effective area of the electrodes, m^2 .

Circular electrodes	$A = \frac{\pi^4(d_1 + g)^2}{4}$;
Rectangular electrodes	$A = (a + g)(b + g)$;
Square electrodes	$A = (a + g)^2$;
Tubular electrodes	$A = \pi(d_0 - h)(l_1 + g)$;

where h = the average thickness, m.

The surface resistivity is calculated using Eq. (2.45):

$$\rho_S = \frac{R_S P}{g} \quad (2.45)$$

where

ρ_S = the surface resistivity, Ω ;

R_S = the surface resistance of the specimen, Ω ;

P = the effective perimeter of the electrode.

Circular electrodes	$P = \pi(d_1 + g)$;
Rectangular electrodes	$P = 2(a + b + 2g)$;
Square electrodes	$P = 4(a + g)$;
Tubular electrodes	$P = 2\pi d$.

where

g = the distance between the electrodes, m.

2.3.3.2 Electrical Properties

Generally, composites have good electrical properties. The electrical properties are anisotropic and greatly affected by the material composition, interfacial state, fiber orientation, and processing method.

(1) Electrical properties of insulating SMCs and BMCs

SMC and BMC products are widely used as insulating materials. SMCs and BMCs are used for complex products with high structural strength and good electrical insulation; examples are shown in Table 2.23.

(2) Electrical properties of laminated composites

Laminated composites are widely used for insulation in the electrical industry. A prepreg cloth made by impregnating glass cloth with resin is heated in a press and cured to give the laminated product.

This process involves a high molding pressure and gives low porosity; therefore, the products have good electrical properties (Table 2.24).

(3) Electrical properties of fabric composites

Fabric composites need to be non-conductive under some conditions as well as having good mechanical strength, e.g., for use in large FRP ground radomes. Information of their properties is therefore needed in designing such materials to assist choice of suitable materials and processing solutions. The electrical properties of various fabric composites are shown in Table 2.25.

(4) Electrical properties of unidirectional composites

Unidirectional composites have anisotropic mechanical properties, and their electrical properties vary depending on the fiber orientation because of the differences between the electrical properties of fibers and resins. Unidirectional composites are seldom used as structural materials, but they form the basic cells of laminates. The electrical properties of unidirectional composites are basic parameters of structural composites in the electrical insulation field and the basis of laminate design. Their properties are given in Table 2.26.

2.3.4 Corrosion Resistance and Testing

Composites have good corrosion resistance and are used widely in areas such as the chemical industry, oil exploration, papermaking, and the metallurgical industry. The main products include acid wash baths, chemical pipes, and tanks. The material compositions and processes used to fabricate composites vary depending on the stored material to meet the working requirements of products.

Table 2.23 Electrical properties of insulating SMCs and BMCs

Composition Properties	Universal polyester SMC	Electric polyester SMC	Phenolic SMC	Universal polyester BMC	Electric polyester BMC	Phenolic BMC
Density/g cm ⁻³	1.75–1.95	1.75–1.95	1.7–1.9	1.80–1.95	1.80–1.95	
Water absorbing capacity/mg	20	20	15	9–20	9–16	60
Volume resistivity/ Ω m	1.0×10^{12}	1.0×10^{13}	1.0×10^{14}	1.0×10^{13}	1.0×10^{15}	1.0×10^8 (Immersed in water for 24 h)
Electric strength/MV m ⁻¹	11.0	12.0	13.0	13.0	15.0	3.5(90 °C \pm 20 °C, in transformer oil)
Dielectric dissipation factor	0.015	0.015	0.05	0.015	0.007–0.015	0.1
Dielectric permittivity	4.8	4.8	8.0	6.5	4.3–4.8	
Surface resistivity/ Ω			1.0×10^{12}	1.0×10^{12}	1.0×10^{13}	
Arc resistance/s	180	180			185–190	

Table 2.24 Electrical properties of laminated composites

Properties	Epoxy phenolic glass laminate	Epoxy glass laminate	Organic silicon glass laminate	BMI laminate	Melamine glass laminate
Specific gravity/g cm ⁻³	1.7–1.9	1.7–1.9		1.7	
Water absorbing capacity/mg	15	16	28–85		107
Vertical interfacial electric strength/MV m ⁻³	22	16.9		22	9.1(90 °C ± 2 °C, in transformer oil)
Parallel interfacial breakdown voltage/kV	30	35	25	30	15(90 °C ± 2 °C, in transformer oil)
Surface resistivity/Ω	1 × 10 ¹³	1 × 10 ¹³		1 × 10 ¹²	
Volume resistivity/Ω m	1 × 10 ¹¹	1 × 10 ¹²		1 × 10 ¹¹	
Dielectric dissipation factor	0.03	0.04	0.07 (After immersed in water)	0.05	
Parallel interfacial insulation resistance/O	1 × 10 ¹⁰	1 × 10 ¹¹	1 × 10 ⁸ (After immersed in water)	1 × 10 ¹⁰	
Martin thermal resistance/°C	200	180	450	280	
Dielectric permittivity	5.8 (After immersed in water)	5.5 (After immersed in water)	6 (After immersed in water)		

2.3.4.1 Corrosion-Resistant Testing

The composite corrosion resistance is the mass or thickness of the corrosive parts in a specimen unit area per unit time when the composite is in a chemical medium (e.g., acid, alkali, organic salt, organic solvent). It indicates the resistance of composites to chemicals.

Resistance to chemicals is determined by regular static soaking of composite plates and checking changes in the appearances of the specimen and medium, Barcol hardness, and bending strength changing ratio, in addition to changes in the plate mass and flexural modulus of elasticity if required.

The test plate specimen is 130 mm in length, 130 mm in width, and 3.2 ± 0.2 mm in thickness, or 80 mm in length, 15 mm in width, and 3.2 ± 0.2 mm in thickness. The specimen surfaces must be smooth, uniformly

Table 2.25 Electrical properties of fabric composites

Properties	Glass cloth/thermoplastic resin	E-glass cloth/polyester resin	E-glass cloth, mat/epoxy resin	E-glass mat/epoxy resin	Kevlar49 cloth/epoxy resin
Specific gravity/g cm ⁻³	1.52	1.85	1.7	1.65	1.40
Water absorbing capacity/mg	12	25			
Surface resistivity/ Ω		1.2×10^{13}	6.0×10^{13}	1.0×10^{14}	5×10^{15}
Volume resistivity/ Ω m	1.0×10^{14}	3.9×10^{12}	1.7×10^{12}		7.0×10^{13}
Vertical interfacial electric strength/MV m ⁻¹	17.7	23.0	31.6	19.4	24.9
Dielectric permittivity	3.53		5.0	5.2	3.75
Dissipation factor		0.0145	0.0059	0.0049	0.0099
Fiber content by volume V_f (or resin content W_f)/%		0.40	0.38		0.40

Table 2.26 Electrical properties of unidirectional composites

Properties		E-glass fiber/ E-54 epoxy	E-glass fiber/E-51 epoxy	E-glass fiber insulated rod	Kevlar49	
					Polyester	Epoxy
Specific gravity/g cm ⁻³		1.90	1.92	1.95	1.34	1.34
Electric strength/MV m ⁻¹	Vertical	24.6	18.2	11.81 (in oil)		
	Parallel		12.0	1.96(in oil)		
Volume resistivity/Ω m		3.4 × 10 ¹⁵	1.1 × 10 ¹²		5 × 10 ¹³	7 × 10 ¹³
Dielectric permittivity		4.75	5.9	5.0	3.41	3.28
Dissipation factor		0.0184	0.0385	0.03	0.021	0.024
Fiber content by volume V _f /%		49.1	55.0	58.0	60	60

glossy, and free from visual blisters and exposed fibers. Four specimens are tested. The test chemicals are solution or industrial grade and diluted with distilled water or deionized water or chosen based on the technical requirements. The test temperature can be divided into room temperature (10–35 °C), 80 °C, or a temperature chosen based on the technical requirements. The periods for room temperature tests are 1, 15, 30, 90, 180, and 360 days. The periods for higher-temperature tests are 1, 3, 7, 14, 21, and 28 days. Specimens are prepared and tested separately based on the predicted specimen appearance, Barcol hardness, and bending strength. The specimen is immersed in the chemical, and the immersion time is recorded. The specimens are chosen according to test periods. The surface is cleaned, and the specimen appearance, Barcol hardness (or mass), and flexural strength are investigated. If delamination blisters form during the test, the test is terminated and the termination time is recorded. A table or curve based on the period and Barcol hardness during each period is compiled. The changes in flexural strength are calculated using Eq. (2.46). The percentage change is calculated when testing the flexural modulus of elasticity or mass.

$$\Delta\sigma_f = \frac{\sigma_{f2} - \sigma_{f1}}{\sigma_{f1}} \times 100\% \quad (2.46)$$

where

σ_{f1} = flexural strength before the test, MPa;

σ_{f2} = flexural strength after the test, MPa;

$\Delta\sigma_f$ = percentage change in flexural strength, %.

2.3.4.2 Corrosion-Resistant Properties

The corrosion resistance of a composite mainly depends on the resin matrix and the interface between the fibers and resins. Generally, composites have good acid resistance and poor alkali resistance. The choice of resin composite depends on factors such as the type of medium, temperature, and medium concentration. Corrosion accelerates with increasing temperature and concentration. Polyester, vinyl ester, epoxy, and phenolic composites are commonly used to manufacture anti-corrosive products. The processing conditions greatly affect the corrosion-resistant properties of products. The following data are provided for information purposes only.

(1) Corrosion resistance of unsaturated polyester composites

Unsaturated polyester composites are widely used in vessel liners, pipes, and because of their low cost, ease of processing and good corrosion resistance (Table 2.27).

Table 2.27 Corrosion resistance of polyester FRPs

Media	Concentration/ %	Temperature/ ^o C	Media	Concentration/ %	Temperature/ ^o C
H ₂ SO ₄	<50	104	HCN		100
	70	71	H ₂ SO ₃	<60	100
	75	25		70	50
HNO ₃	30	40	HNO ₂	<10	25
	40	25	HCIO	<20	50
HCl	<31	110	CH ₃ COOH	10–100	104–25
	37	71		COCH	<10
H ₃ PO ₄	<85	100	(COCH) ₂	>10	25
	≥ 85	93			100
HF	10	100	C ₆ H ₈ O ₇		100
	30	70	C ₆ H ₈ O ₇		100
HBr	<40	100	SC ₆ H ₆ O ₃		100
	50	70	H ₆ C ₇ O ₃		25
H ₂ CO ₃		104	NaOH	5–50	93–25
H ₂ CrO ₄	<5	100	KOH	10	60
	5–10	50		15	25
	10–20	25	NH ₄ OH	<29	100
H ₂ BO ₄		100		30–50	40
H ₂ AsO ₄		80	Ca(OH) ₂		100
HPO ₃		100	Mg(OH) ₂		100
Ba(OH) ₂		60	NaHCO ₃		80
Al(OH) ₃		60	Na ₂ CrO ₄ ·10H ₂ O		100
NaClO ₃		99	K ₂ SO ₄		100
NaClO	10	66	K ₃ PO ₄		100
NaCl		100			

Table 2.28 Corrosion resistance of vinyl ester FRPs

Media	Concentration/%	Temperature/°C	Media	Concentration/%	Temperature/°C
H ₂ CrO ₄	20	65	CuSO ₄		120
Citric acid		100	Cyclohexanone		65
Formic acid	10	80	Ethylene glycol		90
H ₂ SO ₄	≤ 50	99	Formaldehyde		65
	50–70	80	Gasoline	80	65
	75	49	NaOH	10	65
HCl	37	80		25	82
HNO ₃	5	80		50	90
H ₂ SiF ₆	10	20	NaClO	5–15	82
H ₃ PO ₄	50	40	Na ₂ SO ₄		100
		100	Toluene	100	49
HClO	10	82		20–37	82
	20	65	H ₂ O ₂	≤ 30	65
HF	10	65	CO ₂	20	85
	20	38	Wet Cl ₂		65
Seawater		100			

(2) Corrosion resistance of vinyl ester composites

Vinyl ester resins, which contain phenolic and epoxy groups, have good thermal and corrosive properties. They have the low curing temperatures of polyester resins, are easily processed, and are widely used in chemical-corrosion-resistant products. The corrosive properties of vinyl ester FRPs are shown in Table 2.28.

(3) Corrosion resistance of epoxy resin composites

Epoxy resins have good mechanical, thermal, and corrosive properties. Curing at room temperature or higher temperature is used, depending on the application requirements; resins cured below room temperature have poor thermal properties. The corrosive properties of epoxy resins are shown in Table 2.29.

(4) Corrosion resistance of phenolic resin composites

Phenolic resins have good thermal and acid-resistant properties, except to the thick sulfuric acid and nitric acid. Their alkali resistance is not better than those of epoxy resins. Phenolic resins have poor processing and corrosion properties (Table 2.30).

(5) Corrosion resistance of other resin composites

Furan resin composites are often used for resistance to chemical corrosion. They have good resistance to strong acids and alkalis and good thermal properties, but are difficult to process. Their properties are shown in Table 2.31. In terms of reinforcements, carbon fibers have good anti-corrosion properties. Because of the electronic conjugation of the benzene ring, aramid fibers are chemically stable and

Table 2.29 Corrosion resistance of epoxy FRPs

Media	Concentration/%	Temperature/°C	Media	Concentration/%	Temperature/°C
H ₂ SO ₄	<20 20–70 70–75	66 40 25	H ₃ AsO ₃		90
HNO ₃	<10	25			90
HCl	<20 20–37	90 66	HClO		90
H ₃ PO ₄	<85	90	HBF ₄		90
HF ^a		66	NaOH	10–30 30–50	90 40
HBr	<20 50	90 66	KOH	10–30 30–50	90 40
H ₂ BO ₄		90	NH ₄ OH	<10 20–30	100 66
H ₂ CrO ₄	<10 10–30	40 25	Ca(OH) ₂		100
HBrO ₃		66	Al(OH) ₃		90
H ₂ CO ₃		90	Ba(OH) ₂		90
Decanoic acid		66	KOH		90
HCN		66	Mg(OH) ₂		120
H ₂ SO ₃	<10 >10	90 40	NH ₄ F		25
			(NH ₄) ₂ SO ₄		90
H ₂ SiF ₆	10–30	40	NH ₄ NO ₃		120
Acetic acid	<50 >50	66 40	Na ₂ SO ₄		90
Formic acid		66	NaNO ₃		120
H ₄ SiO ₄		90	K ₃ PO ₄		90

^aIt is not applicable to the FRP applied Silicate filler

have good corrosion resistance except strong alkalis and acids. They would be affected little by organic solvents and oils. The properties of furan resins are given in Table 2.32.

2.3.5 Aging Properties and Testing

Composite aging properties are defined as variations in the composite performance with storage or exposure to weather conditions such as sunlight, rain moisture, and temperature. They are important indexes in predicting the long-term performances of composites.

Table 2.30 Corrosion resistance of phenolic FRPs

Media	Concentration/%		Temperature/°C		Media	Concentration/%	Temperature/°C	
			25	95			C	95
H ₂ SO ₄	50		√	√	Mixed acid	-	25	95
	70		√	×	(H ₂ SO ₄ /HNO ₃ = 57/28)		×	×
	93		√	×	NaOH	10	×	×
HNO ₃	5		√	×	NaOH	30	×	×
	-		√	√	NaOH	50	×	×
HCl	10		√	√	NaOH	-	×	×
Acetic acid	50		○	×	Al ₂ (SO ₄) ₃	-	√	√
Formic acid	90		√	√	NH ₄ Cl	-	√	√
					NH ₄ NO ₃ (NH ₄) ₂ SO ₄			
Acetone	-		√	√	CuCl ₂	-	√	√
					CuSO ₄			
					Cu(NO ₃) ₂			
Methanoe	-		×	×	FeCl ₃	-	√	√
			√	√	Fe(NO ₃) ₃ Fe ₂ (SO ₄) ₃			
Anilin	-				NiCl ₂	-	√	√
					NiSO ₄			
					Ni(NO ₂)			
Benzene	-		√	√	ZnCl ₂	-	√	√
			√	√	Zn(NO ₃) ₂			
CHCl ₃	-		√	√	ZnSO ₄		√	√

(continued)

Table 2.30 (continued)

Media	Concentration/%	Temperature/°		Media	Concentration/%	Temperature/°	
		C	95			C	95
Ethyl acetate	–	✓	✓	CaCl ₂	–	✓	✓
Vinyl chloride	–	✓	✓	Ca(NO ₃) ₂			
Formaldehyde	37	✓	✓	CuSO ₄			
Phenol	5	✓	✓	MgCl ₂	–	✓	✓
				Mg(NO ₃) ₂			
				MgSO ₄			
Trichloro ethylene	–	✓	✓				

Table 2.31 Corrosion resistance of furan FRPs

Media	Concentration/%	Temperature/°		Media	Concentration/%	Temperature/°	
		C	25			C	95
KCl	-	√	√	(H ₂ SO ₄ /HNO ₃ = 57/28)		25	95
KNO ₃							
K ₂ SO ₄							
NaCl	-	√	√	NaOH	10	√	√
NaNO ₃							
Na ₂ SO ₄							
Dry Cl ₂	-	√	○	NaOH	30	√	√
Wet Cl ₂	-	√	√	NaOH	50	√	√
SO ₂ (dry)	-	√	√	NH ₄ OH	-	√	√
SO ₂ (wet)	-	√	√	Al ₂ (SO ₄) ₃	-	√	√
Acetone	-	√	√	NH ₄ Cl	-	√	√
Methanol	-	×	×	NH ₄ NO ₃			
Anilin	-	√	√	(NH ₄) ₂ SO ₄			
Benzene	-	√	√	CuCl ₂	-	√	√
CCl ₄	-	√	√	Cu(NO ₃) ₂			
CHCl ₃	-	√	√	CuSO ₄			
Ethyl acetate	-	√	√	FeCl ₃	-	√	√
				Fe(NO ₃) ₂			
				Fe ₂ (SO ₄) ₃			
Vinyl chloride	-	√	√	NiCl ₂	-	√	√
				Ni(NO ₃) ₂			
				NiSO ₄			
Formaldehyde	37	√	√	ZnCl ₂	-	√	√
				Zn(NO ₃) ₂			

(continued)

Table 2.31 (continued)

Media	Concentration/%	Temperature/°		Media	Concentration/%	Temperature/°	
		C	25			C	95
		√	√	ZnSO ₄		√	√
Phenol	5	√	√	CaCl ₂ Ca(NO ₃) ₂ CaSO ₄	–	√	√
Trichlorethylene	–	√	√	MgCl ₂ Mg(NO ₃) ₂ MgSO ₄	–	√	√
Wet acid	–	×	×				

Table 2.32 Corrosion resistance of aramid fibers

Media	Concentration/%	Temperature/°C	Time/h	Reserve ratio of strength/%	
				Kevlar-29	Kevlar-49
Acetic acid	99.7	21	24	–	100
HCl	37	21	100	28	37
HCl	37	21	1000	12	19
HF	10	21	100	90	94
HNO ₃	10	21	100	21	23
H ₂ SO ₄	10	21	100	91	88
H ₂ SO ₄	10	21	1000	41	69
NaOH	10	21	1000	26	47
NH ₄ OH	28	21	1000	91	93
Acetone	100	21	1000	97	99
Ethanol	100	21	1000	99	100
Trichlorethylene	100	21	24	–	98.5
Methyl ethyl ketone	100	21	24	–	100
Transformer oil	100	60	500	95.4	100
Kerosene	100	60	500	90.1	100
Freshwater	100	100	100	100	98
Seawater	100	–	8760	98.5	98.5
Over heating water	100	138	40	90.7	–
Saturated stream	100	150	48	72	–
HCFC-22	100	60	500	100	96.4

2.3.5.1 Test Methods for Aging Properties

Methods for determining composite aging properties are divided into natural aging methods and accelerated aging methods. The properties determined using the natural aging method are unforced but limited by the test sites and long test times. The accelerated aging method can shorten the test time but needs more test data and mathematical simulation, and the data accuracy is worse than that achieved using the natural aging method. Both methods have limitations, which should be considered carefully.

(1) Method for determining effects of weather exposure on GFRPs.

The test method for investigating the effects of exposure of GFRPs to weather can be used to predict the effects of weathering on the appearance, and physical or mechanical properties of materials with no applied stress. Exposure test specimens can be direct specimens, specimen panels, or real products. At least, five samples should be tested. The properties of the test specimens before the test and the initial properties under standard conditions are recorded. The total amount of specimen needed is determined based on the exposure duration and the number of samples.

Exposure test specimens are fixed in racks 0.8 m above the roof. These racks are adjusted so that the exposed surfaces of the specimens are at an angle of $45^\circ \pm 1^\circ$ to the horizontal. Insulating materials are used to isolate the exposure test specimens and racks. The exposure duration is usually not less than 5 years. Pick up the specimens when they are exposed for 0.5, 1, 2, 3, 5, 7, and 10 years. The appearance of the exposed specimen is checked, and it is machined to the required specimen shape after the specified exposure duration has elapsed. The property retention rate is calculated using Eq. (2.47):

$$R_i = \frac{\overline{X}_i}{\overline{X}_0} \times 100 \% \quad (2.47)$$

where

R_i = the property retention rate, %;

X_0 = the arithmetic mean value of the initial property;

X_i = the arithmetic mean value of the specimen property for each sample after i periods.

(2) Method for testing resistance of GFRPs to damp heat

This method is used to predict the effects on the use and storage of glass-fiber-reinforced composites of constant or fluctuating damp heat. At least, five specimens are tested and the specimen dimensions conform to specific requirements. The temperature of the constant-damp heat box should range from $(25 \pm 2)^\circ\text{C}$ to $(60 \pm 2)^\circ\text{C}$. The relative humidity should be $(93 \pm 3)\%$ at high temperatures, and 80–96% at low temperatures. The test periods are 1, 2, 6, 14, 21, or 28 days. The specimens are removed from the constant-damp heat box and cooled to room temperature in a closed container and then tested. The mechanical property retention rate is calculated using Eq. (2.48):

$$R_i = \frac{\overline{X}_i}{\overline{X}_0} \times 100 \% \quad (2.48)$$

where

R_i = the mechanical property retention rate after i periods, %;

X_0 = the arithmetic mean value of the initial mechanical property;

X_i = the arithmetic mean value of the mechanical property of each sample after i periods.

(3) Method for testing resistance of GFRPs to water

This test is used to predict the effects of water on the mechanical properties of GFRPs and their maximum flexural strength in moist conditions. At least, five specimens are tested. The specimens must meet the relevant requirements for mechanical testing. The medium used to soak the test specimen is distilled water at $(23 \pm 2) \text{ }^\circ\text{C}$. The test specimens are soaked in either constant-temperature water or the water used in practical applications. The test periods are 30 days for water resistance, and 14 days for measuring the maximum flexural strength. A sample of specimens should be tested in each period until the rate of flexural strength change with time is nearest zero. The immersion period for specimen plates is usually not less than 5 years. Pick up the specimens when they are exposed to 0.5, 1, 2, 3, 5, 7, 10 years, or longer. The mechanical property retention rate is calculated using Eq. (2.49):

$$R_i = \frac{\bar{X}_i}{\bar{X}_0} \times 100 \% \tag{2.49}$$

where

- R_i = the mechanical property retention rate after i periods, %;
- X_o = the arithmetic mean value of the initial mechanical property;
- X_i = the arithmetic mean value of the mechanical property for each sample after i periods.

The maximum flexural strength in the moist state is calculated using Eq. (2.50) after the test. When $t \leq t_{0.05}$,

$$t = \frac{\bar{X}_1 - \bar{X}_2}{\sqrt{\frac{(n_1-1)S_1^2 + (n_2-1)S_2^2}{N}} \sqrt{\frac{1}{n_1} + \frac{1}{n_2}}} \tag{2.50}$$

where

- t = the calculated value after the test;
- S_1 and S_2 are standard differences in specimen property between last test and next test, respectively;
- X_1 and X_2 are the mean values of specimen property after last test and next test, respectively;
- n_1 and n_2 are specimen numbers in last test and next test, respectively;

$$N = n_1 + n_2 - 2$$

(4) Method for determining accelerated resistance of GFRPs to water

This method is used to predict the behavior of GFRPs used in water to sieve raw materials. At least, five specimens are tested. The specimen dimensions should

conform to the mechanical property requirements. The resistivity of the distilled deionized water used for soaking the specimens should be not less than $500 \Omega \cdot \text{m}$. Specimens should be soaked in water at $(80 \pm 2) ^\circ\text{C}$. Materials with good thermal properties are soaked in water at $(95 \pm 2) ^\circ\text{C}$ or boiling water. Materials with poor thermal properties are soaked in water at $(60 \pm 2) ^\circ\text{C}$. The specimen is soaked for 24 h. The period of soaking for epoxy phenolic resin composites is 1, 2, and 6 days. The period of soaking for polyester resin composites is 1/3, 1/2, 1, 2, 3, and 6 days. The appearance is checked after the specified test period has elapsed. The mechanical property retention rate is calculated using Eq. (2.48).

2.3.5.2 Composite Aging Properties

Composite aging properties, which are of great concern to designers, are affected by many factors. The aging mechanism is very complex and is therefore difficult to describe quantitatively. With the development of composites, a large number of studies are being performed to determine the effects of sunlight and accelerated aging, and large amounts of test data are available. The data shown in Tables 2.33, 2.34, 2.35, 2.36, 2.37, and 2.38 are for information and reference only.

2.3.6 Other Properties and Testing

Composites have not only high specific strengths, good chemical resistance, low thermal conductivities, and good non-conductive properties but also good flame retardancy, optical properties, and frictional properties; therefore, they are widely used in building and sports equipment. Knowledge of the fire-retardant, optical, and frictional properties of composites is necessary for solving practical problems in a project.

2.3.6.1 Other Property Testing

The flame retardancy, optical properties, and frictional resistance are often important in practical applications of composites. Methods for testing the flame retardancy and optical properties of composites are performed according to national standards. Frictional resistance tests are usually used to determine the coefficients of friction of plastics.

(1) Test method for determining flammability properties of GFRPs.

This test method is used to predict the necessary minimum concentration of oxygen needed to support flaming combustion of GFRPs. A sample should consist of at least five specimens. The specimen dimensions are length 70–150 mm, width

Table 2.33 Reserve ratio of flexure strength under weathering exposure (%)

Composition	Period/a	Harbin	Lanzhou	Qinhuangdao	Chengdu	Shanghai	Guangzhou
634 epoxy/phthalic anhydride 0.2 alkali-free cloth hand lay-up heat curing	Onset value/MPa	330.3	355.0	337.3	333.4	308.5	317.1
	1	90	93	93	95	101	95
	2	106	87	91	97	100	93
	3	104	92	93	101	103	95
	8	94	—	86	—	—	—
	Onset value/MPa	294.5	330.5	297.1	328.9	284.9	291.5
	1	94	83	98	94	103	93
	2	106	91	96	94	98	89
004 polyester benzaldehyde peroxide 0.1 alkali-free cloth hand lay-up heat curing	Onset value/MPa	292.2	293.2	316.8	279.5	259.4	249.3
	1	88	105	64	71	61	54
	2	109	96	64	77	65	60
	3	107	108	65	97	91	73
	8	111	—	69	—	—	—
	Onset value/MPa	302.4	266.7	265.8	270.7	227.3	190.6
	1	87	123	85	100	90	102
	2	92	108	85	88	91	92
604 polyester methyl ethyl ketone peroxide 0.1 alkali-free cloth hand lay-up heat curing	3	98	112	103	87	86	89
	8	92	—	—	—	—	—
	—	—	—	—	—	—	—
	—	—	—	—	—	—	—

(continued)

Table 2.33 (continued)

Composition	Period/a	Harbin	Lanzhou	Qinhuangdao	Chengdu	Shanghai	Guangzhou
616 phnolic 0.2 alkali-free cloth hot press	Onset value/MPa	221.2	176.5	22.6	177.5	172.8	199.4
	1	101	116	81	102	113	94
	2	97	105	86	99	113	93
	3	98	108	86	120	109	85
	8	96	—	92	—	—	—
003 polyester benzaldehyde peroxide 0.1 alkali-free cloth hand lay-up head curing	0.5	130	115			92	113
	1	132	108			98	70
	1.5	108	119			80	61
	2	100	95			53	55
	2.5	95	116			67	54

Table 2.34 Variations in mechanical properties of FRPs immersed in water

Resin type	Load type	Period/a						
		0	0.5	1	1.5	2.0	2.5	3
		Reserve ratio of properties/%						
Epoxy 634 hand lay-up	Tension	100	89	80	92	83	80	84
	Compression	100	93	49	47	43	42	37
	Bending	100	75	60	57	60	59	55
	Impact	100	108	118	164	158	182	144
004 polyester hand lay-up	Tension	100	80	70	93	88	98	68
	Compression	100	87	39	66	71	63	74
	Bending	100	74	30	40	46	53	47
	Impact	100	100	201	186	129	173	143
616 phenolic hot press	Tension	100	68	73	101	95	61	94
	Compression	100	124	121	123	140	120	149
	Bending	100	104	100	87	102	91	106
	Impact	100	114	106	102	106	127	109

(6.5 ± 0.5) mm, and thickness (3 ± 0.5) mm. The difference between the maximum and minimum resin contents can be up to 4%, and the curing degree should be more than 80%. A test device for determining the oxygen index is shown in Fig. 2.47.

The test specimen is mounted vertically in the specimen holder; the distance between the upper end of the specimen and the top of the combustion tube should be not less than 100 mm. The igniter flame length should be 15–25 mm. The flow valves should be adjusted to give the required concentration of oxygen in a flowing mixture of oxygen and nitrogen and to ensure that the gas flow rate in the combustion tube is (4 ± 1) cm/s. The tube is purged by the gas flow for at least 30 s, and the igniter is used to initiate burning only on the top surface of the upper end of the specimen. The igniter is removed once the specimen has been ignited. The burning period and burning behavior are recorded; the minimum concentration of oxygen needed to support combustion for 3 min is determined. The oxygen index is calculated using Eq. (2.51):

$$OI = \frac{[O_2]}{[O_2] + [N_2]} \times 100 \% \quad (2.51)$$

where

OI = oxygen index, %;

[O₂] = oxygen flow, L/min;

[N₂] = nitrogen flow, L/min.

Table 2.35 Storage aging of high-strength glass-fiber/epoxy composites

Properties	Original value	Harbin									Guangzhou								
		1	3	5	7	9	1	3	5	7	9	1	3	5	7	9			
0° tension	Strength	1398.8	1233.2	1202.9	1144.5	1109	1176.5	1184.9	1175.2	912.4	916.8	10072.3							
	Retained ratio/%		88	86	82	79	84	85	84	65	66	72							
	Modulus	49.2	47.6	47.1	44.6	46.4	45.2	48.9	39.2	44.9	44.4	42.3							
90° tension	Retained ratio/%		97	96	91	94	92	99	80	91	90	86							
	Strength	20.2	25.0	26.7	20.5	20.8	20.4	13.3	23.9	15.9	9.9	16.8							
	Retained ratio/%		124	132	101	102	100	66	118	79	49	83							
90° tension	Modulus	13.6	15.2	13.5	11.0	11.9	12.4	11.7	11.3	10.3	10.0	10.8							
	Retained ratio/%		112	99	81	87	92	86	83	76	73	80							
	Strength	19.5	20.0	24.6	21.5	28.3	26.7	10.4	26.7	15.8	13.0	15.3							
45° tension	Retained ratio/%		102	126	110	145	137	53	137	81	67	79							
	Modulus	5.1	5.7	6.0	3.9	4.0	4.3	5.1	6.1	4.3	3.8	3.6							
	Retained ratio/%		112	118	76	78	84	100	120	84	74	70							
Flexure	Strength	1410	1130.9	1231.0	1279.3	1264.2	1210.6	1082.5	1418.3	1181.7	1054.6	1084.5							
	Retained ratio/%		80	87	91	90	86	77	100	84	75	77							
	Modulus	44.5	42.4	42.6	38.5	37.8	36.5	42.5	44.9	35.7	30.6	31.2							
Shear	Retained ratio/%		95	96	86	85	82	95	101	80	69	70							
	Strength	67.4	59.2	74.4	63.1	63.8	63.5	53.0	69.4	59.0	52.6	53.6							
	Retained ratio/%		88	110	93	94	94	78	103	87	78	80							

Table 2.36 Storage aging of carbon-fiber/epoxy composites

Properties	Original value	Harbin						Guangzhou					
		1	3	5	7	9	1	3	5	7	9		
0° tension	Strength/MPa	898.5	993.0	915.3	769.9	905.4	860.7	902.9	933.8	933.2	916.8		
	Retained ratio/%	79	88	81	68	80	76	97	83	82	81		
0° tension	Modulus/GPa	100.4	92.8	97.8	86.2	85.3	94.3	95.3	90.5	92.4	91.3		
	Reserve ratio/%	97	89	95	83	82	91	92	87	90	88		
90° tension	Strength/MPa	12.9	13.5	14.6	15.2	14.5	13.9	13.0	10.8	10.3	10.6		
	Reserve ratio/%	94	98	107	110	106	101	95	79	75	77		
90° tension	Modulus/GPa	7.2	7.8		7.8	7.6	7.3	8.0	7.7	6.7	6.5		
	Reserve ratio/%	94	101		101	99	95	104	100	87	84		
45° tension	Strength/MPa	10.9	12.6	9.5	13.7	11.6	10.5	13.8	7.8	7.3	8.2		
	Reserve ratio/%	88	102	77	110	94	85	110	63	59	66		
45° tension	Modulus/GPa	4.2	4.2	3.5	5.1	4.6	4.1	4.8	3.8	3.0	3.9		
	Reserve ratio/%	93	93	78	113	100	91	107	84	67	87		
Flexure	Strength/MPa	1280.2	1436.9	1404.7	1398.5	1388.9	1183.1	1333.4	1315.5	1304.8	1320.0		
	Reserve ratio/%	87	97	95	94	94	80	90	89	88	89		
Flexure	Modulus/GPa	88.5	92.4	98.0	94.2	93.6	74.0	82.2	95.9	93.7	94.2		
	Reserve ratio/%	91	94	100	96	96	76	84	98	96	96		
Shear	Strength/MPa	54.3	58.2	51.5	50.2	51.8	49.5	50.3	48.5	50.9	49.6		
	Reserve ratio/%	85	91	81	78	81	76	79	76	80	78		

Table 2.37 Damp-heat aging of high-strength glass-fiber/epoxy composites

Periods	0° Tension		Flexure		Shear	
	Strength/MPa	Reserve ratio/%	Strength/MPa	Reserve ratio/%	Strength/MPa	Reserve ratio/%
Onset	1373.4		1325.5		71.2	
1 day	1304.7	95	1183.5	89	65.9	92
2 days	1309.5	95				
6 days	1344.6	98	1052.4	79	57.0	83
14 days	1227.4	89	1023.4	77	43.9	61
21 days	1231.4	90	1087.2	82	43.4	61
28 days	1081.2	79	1074.7	81	39.4	55
38 days			1069.0	80	383.3	54

Table 2.38 Damp-heat aging of carbon-fiber/epoxy composites

Periods	0° Tension		Flexure		Shear	
	Strength/MPa	Reserve ratio/%	Strength/MPa	Reserve ratio/%	Strength/MPa	Reserve ratio/%
Onset	1100.2		1223.7		61.4	
1 day	1053.3	96	1113.4	91	53.6	87
2 days	1103.6	100	1133.5	93	50.9	83
6 days	1209.1	110	1107.0	90	52.7	86
14 days	1071.9	97	1058.2	86	54.3	88
21 days	1133.3	103	1005.8	82	53.0	86
28 days	1041.4	95	1096.8	90	52.5	86

Note 1. Testing condition: $T = 60\text{ }^{\circ}\text{C} \pm 2\text{ }^{\circ}\text{C}$ $RH = 95\% \pm 2\%$

2. Resin content 43.5%, curing degree 93.5%

Fig. 2.47 Apparatus for determining oxygen index

1—combustion tube; 2—clamp; 3—igniter; 4—wire mesh; 5—tube containing glass ball; 6—base; 7—tee joint; 8—gas mixture; 9—gas gauge; 10—voltage valve; 11—rotameter; 12—regulating valve; 13—specimen

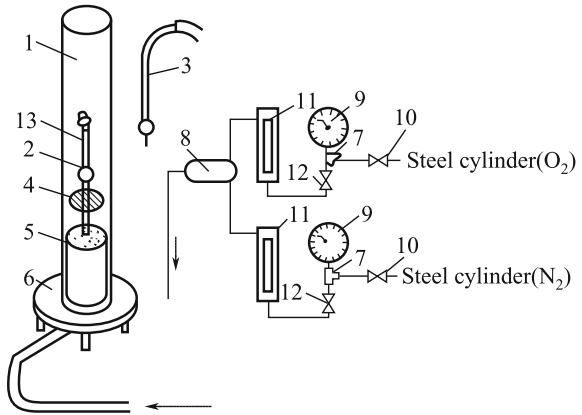
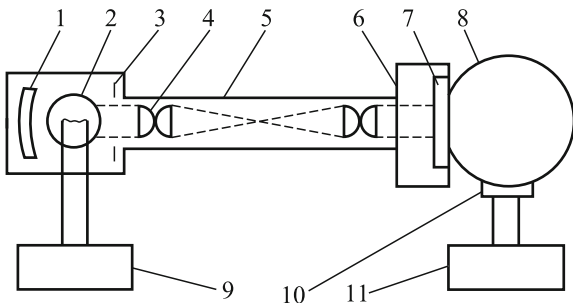


Fig. 2.48 Schematic diagram of integral ball apparatus for determining light transmittance

1—viewfinder; 2—light source; 3—raster; 4—lens; 5—collimator; 6—sample room; 7—sample; 8—integral ball; 9—display; 10—light receiver (with V_λ spectral filter); 11—voltage-stabilized source



(2) Test method for determining transmissivity of GFRPs

The transmissivity of a GFRP is the ratio of the flux of light passing through the specimen to that passing vertically through the specimen. The specimen size is 40 mm by 40 mm or ϕ 40 mm plates. There are not less than three specimens in a sample. The test principle is shown in Fig. 2.48. The light source is standard A. The light receiver has a V_λ spectral filter. The accuracy of the transmissivity should be not more than $\pm 2\%$. The specimen is fixed on the test frame, and the light is positioned. The specimen should be closely attached to the wall with a light input hole on the integral ball. The indicated value is the transmissivity.

(3) Test method for determining plastic coefficient of friction

The coefficient of friction of a plastic is measured based on the coefficient of kinetic friction of a plastic sheet. The speed and positive pressure of the friction-testing machine can be adjusted in the speed range 0.10–3.00 m/s (shown in Fig. 2.49). Specimen types are shown in Fig. 2.50. The dimensions of a rigid fixed specimen should be diameter (20.0 ± 0.1) mm and thickness

Fig. 2.49 Friction-testing machine 1—movable specimen; 2—fixed specimen; 3—hinge arm; 4—pendulum; 5—notch for pressure correction (with standard weights); 6—finder; 7—ruler; 8—button for pressure correction; 9—nut for choosing fast operation; 10—base; 11—drive belt

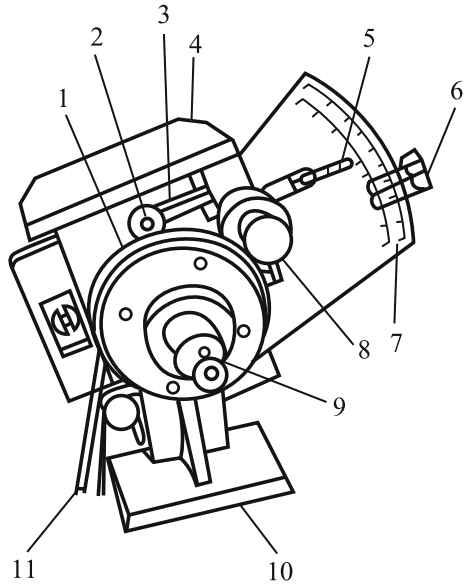
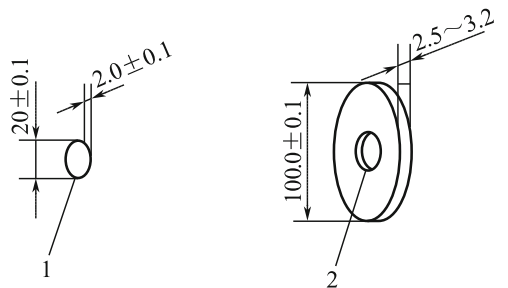


Fig. 2.50 Specimens 1—tightener combined with mounting screw; 2—tightener combined and concentric with mounting shaft



(a) Rigid fixed specimen (b) Rigid movable specimen

(2.0 ± 0.1) mm; the mass should be (5.0 ± 0.01) g. If the specimen mass is less than (5.0 ± 0.01) g, fine washers should be used to compensate. For a rigid movable specimen, the dimensions should be (100.0 ± 0.1) mm, and the minimum thickness should be such that 2.0 mm of the specimen length remains attached. The thickness is usually 2.54–3.18 mm. A fixed specimen can be used to determine the kinetic coefficient of friction at different speeds. A movable specimen is used to determine the kinetic coefficient of friction at different times. During the tests, the test machine is adjusted to be horizontal, according to the operational requirements, and then the fixed or movable specimen is positioned. A positive pressure is applied to the fixed or movable specimen. The positive pressure is adjusted to 0.5 N. The oscillation range is chosen based on the test material and positive pressure. The coefficient of friction as a function of time is investigated based on readings at 0.25,

0.50, 1.0, 2.0, 3.0, 1.0, 0.5, and 0.25 m/s; to reduce wear, the test time is limited to 1.5 min. The coefficient of friction as a function of time is investigated by taking readings at a fixed speed every 30 s until the reading becomes constant. A standard speed of 1.0 m/s is usually used to compare materials. The coefficient of friction is calculated using Eq. (2.52). The wear extent, which is also of concern, is determined as follows. The test material is moved on a grit surface under a certain pressure, and the volume of material lost is measured to predict the frictional properties.

$$\mu = M \sin \theta / 0.05 N \tag{2.52}$$

where

- μ = coefficient of friction;
- M = maximum oscillation distance, N m
- N = positive pressure, N;
- θ = displacement angle of oscillation, °.

2.3.6.2 Composite Flame-Proofing, Transparency, and Coefficient of Friction

Composites differ in terms of flame-proofing, transparency, and coefficient of friction. Specific resins, matched fibers, and assistants are chosen to obtain specific properties, and meet application requirements. Data on composite flame-proofing, optical, and frictional properties are generally obtained by performing tests under specific conditions. The data in Tables 2.39, 2.40, 2.41, and 2.42 are for information and reference purposes only.

Table 2.39 Flame retardancies of composites

Properties	Retardant polyester SMC	Retardant polyester BMC	Hand lay-up common polyester FRP	Hand lay-up retardant polyester FRP	Transparent retardant FRP	Polyester corrugated plate
Oxygen index/%	35	35	22	35	33	30
Flame retardance	FV-0	FV-0		FV-1		
Properties	Pultruded FRP doors & windows	Hand lay-up phenolic FRP	Phenolic FRP	Common polyester SMC	Common epoxy FRP	Retardant epoxy FRP
Oxygen index/%	34	80	60	23	24	32.7
Flame retardance						

Table 2.40 Relationship between transparency of FRP polyester corrugated plate and thickness

Thickness/%	0.5	0.7	0.8	0.9	1.0	1.2	1.5	1.6	2.0	2.5
Transparency/%	82	82	80	80	80	77	75	75	64	60

Table 2.41 Transparencies of composites

Properties	Transparent FRP	Transparent retardant FRP	Glass-fiber reinforced polyacrylate	Machined transparent retardant FRP laminates	Transparent FRP covered by anti-aging films
Transparency/%	85	82	90	88	86.5
Thickness/%	0.7	0.7	0.7	1	0.7

2.4 Latest Developments and Trends in Polymer Composite Industries

2.4.1 Development Status of Polymer Composites

Polymer composites are the main type of composite, and industrial techniques in this area have been improving for over 50 years. Composite products are widely used in fields such as transportation, construction, chemical resistance, ships, and electronics.

In 2002, the global output of polymer composites was about 4.5–4.6 million tons; North America, Europe, and Asia were the three largest manufacturers and customers. The major markets are for construction, transportation, electronics, and consumer goods.

In the 1990s (1991–1998), global polymer composite production increased by an average of 5.6% per year, and the output value was nearly twice as much as the GDP of developed countries.

Polymer composites reinforced with glass fibers (GFRPs) have dominated the polymer composite market. The amount of glass fiber used in 2002 was 2.2 million tons globally, with North America, Europe, Asia, South America, and other areas accounting for 33%, 32%, 30%, and 2%, respectively [14].

Recently, the use of high-performance fibers such as carbon fibers and Kevlar fibers to reinforce polymers have increased rapidly and become an important part and growing aspect of polymer composites [15, 16].

The development of polymer composites in different parts of the world is related not only to the local economy but also to the maturity of composite applications. North America, especially the USA, is the largest producer and sales market; its output of 1.9 billion tons in 2002 accounted for approximately half of the global demand. The CFA's statistics show that there are more than 13,000 composite production lines and 236,000 employees in the USA. Over 90% of composites

Table 2.42 Frictional resistances of composites

Properties	Temperature/ C	Glass fiber / phenolic	E-glass fiber / phenolic	High-strength glass fiber/epoxy	Carbon cloth/epoxy	Nylon-6 epoxy/glass	Nylon-6 epoxy/carbon
Friction coefficient	100	0.50	0.47	0.18-0.19	0.1-0.12	0.23	0.13
	150	0.51	0.51				
	200	0.48	0.51				
	250	0.44	0.46				
Wear rate	100	0.01	0.08	50	25		
	150	0.09	0.06				
	200	0.13	0.14				
	250	0.17	0.18				

Table 2.43 Polymer composite output in recent years in USA

Application	1997	1998	1999	2001
	Output/10 ⁴ t	Output/10 ⁴ t	Output/10 ⁴ t	Output/10 ⁴ t
Land transportation	49.3	51.3	54.8	48.9
Building/construction	31.5	33.8	34.5	30.4
Corrosion resistance	17.8	19.1	19.1	18.3
Marine	16.0	16.4	18.2	15.0
Electronics	19.7	16.2	17.0	14.9
Leisure/consumption	9.5	10.1	11.0	9.9
Apparatus/equipment	8.3	8.9	9.3	8.5
Aerospace/aviation	1.1	1.0	1.0	1.0
Others	5.0	5.3	5.5	4.8
Total	153.6	162.0	170.6	151.7

products are reinforced with glass fibers, and nearly 75% of products are based on unsaturated polyester resin (UP) or other thermosetting polymers, and the remaining 25% use thermoplastics as the matrix. The largest composite market in the USA covers transportation, building, and corrosion-resistant applications. Marine, electronic, and leisure good applications are also significant. Polymer composite outputs in the past few years are shown in Table 2.43 [17, 18].

Europe is another major area for the production and consumption of polymer composites. The annual average growth rate during the period 1991–1998 was 4.7%. The market slumped in 1993 and 1996, but the European polymer market growth has been relatively stable since 1997. For example, in 1998, the polymer market shares of various European countries were 33% in Germany and Austria; 19% in Italy; 14% in France; 13% in Belgium, the Netherlands, and Luxembourg; 9% in the UK; 8% in Spain and Portugal; and 4% in Sweden, Norway, Denmark, and Finland.

The Asia–Pacific region is the biggest potential market for polymer composites. Market analysis suggests that the demand for polymer composites will continue to increase for a long time. The annual growth rate is predicted to rise to 7%.

Japan is a major producer of polymer composites in the Asia–Pacific region. The outputs in 1998 and 1999 were lower than that in 1997 because of the Japanese economic slump, but the total output was higher than 600,000 t. The per capita quantity was about 5.29 kg (compared with 0.22 kg in China), higher than that of any other country in this region. The growth in polymer production in Japan in recent years is shown in Table 2.44.

The proportions of forming processes used in polymer composite production lines in Japan are given in Table 2.45.

China is also a large producer of polymer composites in the Asia–Pacific region. Production of FRPs slowed down during the three decades from 1958 when China was engaged in R&D of FRPs. In the early 1990s, FRP output reached nearly 100,000 t. Output increased significantly in the late 1990s. The output of glass-reinforced thermosetting composites reached 560,000 t, and that of glass

Table 2.44 Polymer composite output in recent years in Japan

Application	1997	1998	1999	2000	2001	2002
	Output/t	Output/t	Output/t	Output/t	Output/t	Output/t
Building/construction	48,200	45,400	47,900	53,500	50,900	49,800
Bath	123,100	100,200	101,670	102,200	98,900	96,200
Drain disposal	94,800	74,600	76,160	65,300	61,300	55,100
Marine	23,000	18,900	16,690	15,400	12,300	11,300
Land transportation	23,500	23,200	23,960	23,100	22,400	21,200
Tank/Container	41,400	35,800	33,190	32,300	30,600	28,400
Industrial equipment	51,500	49,700	48,260	46,800	40,100	40,100
Leisure/consumption	44,300	38,200	36,150	34,900	32,900	31,400
Others	11,200	8700	6780	8000	9800	12,600
Total	461,000	394,700	390,760	381,500	359,200	344,500
Polyester FRP	461,000	394,700	390,760	381,500	359,200	344,500
GFRTF	268,000	253,800				
Total	72,900	648,500				

Table 2.45 Proportions of polymer composite processes used in Japan

Processes	2000/%	2001/%	Processes	2000/%	2001/%
Hand lay-up	20.0	19.1	Filament winding	6.6	4.9
Spray-up	18.7	18.7	Continuous molding	4.8	5.6
Molding	43.0	45.4	Others	5.3	4.6
Other pressure molding	1.6	1.7			

Table 2.46 FRP/composites output (10 000 tons) in recent decades in China (excluding Taiwan)

Year	GF	UP	FRP	Year	GF	UP	FRP
1990	8.68	4.5	9.5	1997	17.5	20	22
1991	9.69	6	11	1998	18	25	25
1992	12.08	8	13.3	1999	20	32	30
1993	13.4	11	14.5	2000	21.5	45	48
1994	15	13	15	2001	28.3	50	50
1995	16	15	15	2002	36.9	58	56
1996	17	16	17				

thermoplastics was about 180,000 t, so the total output ranked second in the world. Table 2.46 shows the annual output of polymer composites in 1990–2002 in China.

Thermosetting FRP market shares in China are shown in Table 2.47.

At present, the FRP production facilities in mainland China are as follows: 300 production lines for filament-wound specific-length pipes, mortar pipes, and horizontal tanks; two production lines for continuous filament-wound pipes; three production lines for centrifugally cast pipes; 200 presses for SMCs and BMCs; 200

Table 2.47 Thermosetting FRP market shares in China (excluding Taiwan)

Applications	Proportion/%	Applications	Proportion/%
Construction	40	Marine	4
Pipes, tanks, chemical resistance	24	Industrial equipment	12
Land vehicles and auxiliaries	6	Other	14

Table 2.48 Proportions of various processes used in China

Processes	Proportion/%	Processes	Proportion/%
Hand lay-up (including spray-up)	65	Pultrusion	2
Filament winding	22	Others (Continuous profile, RTM)	1
SMC & BMC	10		

pultrusion production lines; 550 sets of spray-up machines; 10 continuous profile production lines; and 50 winding machines for vertical tanks. The proportions of various processes are shown in Table 2.48.

2.4.2 Latest Progress in Polymer Composite Technology

During the last 10 years of the twentieth century, much research on raw materials and processing techniques focused on issues such as lowering costs, enhancing polymer composite properties and functions, and environmental protection, and significant progress was made in these areas.

2.4.2.1 New Progress in Reinforcements

(1) Glass fibers

1. New glass-fiber compositions: High-performance glass fibers based on E-glass have been gradually introduced and are intended to replace E-glass. Owens Corning Fiber glass (OCF), USA, have done an excellent job in this respect. OCF recently introduced a chemical-resistant boron-free ECR containing ultrahigh-strength glass fibers, under the trademark Zen Tron. The tensile strength of this fiber is 50% higher than that of typical E-glass and 15% higher than that of S-2 high-strength fibers. The impact strength of products reinforced with this fiber is 50% higher than those of carbon-fiber-reinforced products, and the fatigue resistance is also enhanced. Advantex intends replacing E-glass with a composition that has the combined high strength, and electrical and chemical

properties of E-glass and ECR fibers. OCF has also produced dual-composition glass fibers for industrial production and applications [19].

MIRAFLEX, OCF's new and special type of flexible glass fiber, is produced using a combination of two techniques to melt two types of glass with different chemical compositions. These fibers are more flexible and elastic than typical glass fibers because they have disordered twisting and easily fill irregular cavities. Their heat resistance is higher than those of other synthetic and man-made fibers, and they produce less odor when they are heated. They have good fire resistance and are chemically stable. They also have valuable properties such as good processability and easy carding. They can be blended with synthetic and natural fibers and made into nonwoven materials as CCL cores by carding, providing a substitute for electric cloth.

2. New glass-fiber products and fabrics

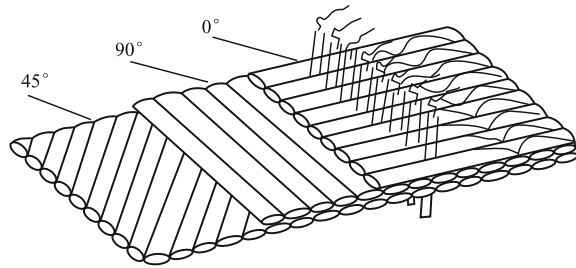
- (a) Air deformation roving. Air deformation roving is achieved by applying a high-pressure and high-speed air flow to the looped pile of a common roving in a special device. This device has many loops, with the result that many fibers are at right angles to the roving length direction. The use of this type of roving can improve the transverse strength of unidirectional composites.
- (b) TWINTEX is the trademark of raw materials made of glass-fiber-reinforced thermoplastics produced by VETRO TEX in the USA (part of the Saint-Gobain Group). During glass-fiber pulling, a thermoplastic (e.g., PP, PET, nylon) is applied to the glass; there are four types of product, i.e., roving, woven roving, panels, and granules.
- (c) OCF have successfully developed a type of roving for reinforcing thermoplastics. When the roving passes a cover head, fiber strands can be separated into single fibers and completely impregnated with thermoplastic. Mechanical damage can therefore be avoided, and fibers are evenly distributed in products made using injection processes. In addition, the mechanical strength of the end product is improved because the fibers are longer. Different sizes can be used for this glass roving, and it is suitable for resin systems such as nylon, polycarbonate, acetal, and thermoplastic polyesters.

3. Multiaxial woven preform full-thickness stitching is a type of reinforcement achieved using lay-up and stitching techniques and can significantly improve the impact properties (see Fig. 2.51).

(2) Carbon fibers

1. Development of large-tow carbon fibers. Most of the carbon fibers produced are 3 K and 6 K; 12 K is generally the largest one produced globally. The trend in carbon-fiber development is to produce larger-tow fibers. At present, many companies are working on large-tow carbon fibers, for example, 24 K fibers are being produced by the Toray Company of Japan, and carbon fibers larger than

Fig. 2.51 Reinforced preform production using lay-up and stitching techniques



48 K such as PANEX33-0160 (160 K) and PANEX33-0320 (320 K) are being produced by Zoltek in the USA. Zoltek considers that the use of large-tow carbon fibers decreases costs without affecting applications. Five additional carbon-fiber production lines have been installed and produce 48 K or more carbon fibers, with an annual output of 450 t.

2. Use of acrylonitrile textile strands: The carbon precursor is a key factor in carbon-fiber production. Toray and Toho in Japan and American Hercules in the USA all produce carbon fibers using special acrylonitrile strands. The techniques used for strand production are secret. The techniques have not been transferred, nor are the strands sold.

Zoltek recently made an important breakthrough in research on the use of acrylonitrile textile as a carbon-fiber precursor and produced PANEX33 carbon fibers equivalent to T300. In December 1995, Zoltek purchased the Magyar Viscosa Company, an acrylonitrile textile precursor producer, and researched the use of acrylonitrile textile as a precursor in carbon-fiber production.

The price of the acrylonitrile textile precursor is only one-quarter that of special precursors, which reduces the price of carbon fibers by a large margin.

The properties of the carbon fibers produced by Zoltek using the textile precursor were equal to those of T300, but its price was only half that of T300 fibers.

This was pioneering research in the carbon-fiber industry and represents a milestone in the development of new techniques for carbon-fiber production.

(3) New reinforcements

1. Super-high-performance PBO (polybutadiene) [20]: PBO is a high-polymer fiber that was commercialized in 1991 (trade name ZYLON). PBO is a heterocyclic aromatic polyimide and has high potential for use in a range of applications. PBO is superior to both organic and inorganic fibers in terms of thermal stability, specific tensile modulus, and specific tensile strength. The physical and mechanical properties of PBO are shown in Tables 2.49 and 2.50. The data in Tables 2.49 and 2.50 show that PBO has four superior properties, i.e., high strength, high modulus, and good heat and fire resistances. As shown in Table 2.49, the heat resistance of PBO is so high that its pyrolysis temperature is 650 °C, based on thermogravimetry in air, and its weight is unchanged

Table 2.49 PBO thermal properties

Thermal degradation temperature/°C	Pyrolytic residues		Thermal stability		Moisture regain/%
	660 °C	670 °C	316 °C for 100 h	370 °C for 100 h	
650	CO ₂ & CO	HCl	100% quality retained	80% quality retained	1

within 100 h at 316 °C. PBO does not melt, even at high temperatures, and its operating temperature is up to 330 °C. The physical properties of PBO are approximately twice as good as those of Kevlar 49. PBO plain fabrics do not shrink in vertical burning tests, and there is no residual fire. The flexibility is basically unchanged when the fire is removed. The properties of PBO are similar to those of inorganic fibers, but they are less brittle and have better bending resistance. PBO is therefore widely used in short or chopped fibers, textile yarns, mats, and fabrics.

Currently, research is being performed globally on the processing, structures, and performances of composites reinforced with PBO, including research on fiber-finishing methods and its effects, interfacial behavior between fibers and different matrices, composite fracture mechanisms, and applications. The properties of PBO fibers are considered to be superior to those of other polymer fibers.

- Basalt continuous fibers: Basalt fibers are made by milling natural basalt ores in a tank furnace at high temperatures, i.e., 1450–1500 °C, and pulling through bushing wells. Compared with glass fibers, basalt fibers have high mechanical strength, low electrical conductivity, good heat resistance (their properties are unchanged at –260 to 700 °C), good acid and alkali resistance, good sound-proofing, heat insulation, and dielectric properties and are lightweight. Their properties are compared with those of E-glass fibers in Table 2.51.

Basalt-fiber production does not produce waste gases, wastewater, and waste residues; therefore, basalt fibers are a cheap, high-performance, and clean material. Basalt-fiber-reinforced composites compare favorably with S-glass- or aramid-fiber-reinforced composites in many ways.

China is rich in basalt ores. Because of the outstanding properties of basalt fibers and their composites, plentiful resources, and wide applications, the prospects for their increased use as twenty-first century materials are good.

2.4.2.2 Radiation Curing Techniques

In recent years, many curing processes have been introduced, e.g., X-ray, laser, electron-beam (EB), microwave, and UV-curing methods. These methods all have

Table 2.50 Comparison of PBO performance with those of other high-performance fibers

Product	Fracture strength/N tex ⁻¹	Modulus/GPa	Fracture elongation/%	Density/g cm ⁻³	Moisture regain/%	LOI	Pyrolystic temperature/°C
Zylon HM	3.7	280	2.5	1.56	0.6	68	650
Zylon AS	3.7	180	3.5	1.54	2	68	650
Kevlar 49	1.95	109	2.4	1.45	4.5	29	550
HPPE Dyneema SK-75	3.5	105	3.8	0.97	0	–	T _m = 144–152
Steel fiber	0.35	200	1.4	7.80	0	–	–
Carbon fiber	2.05	230	1.5	1.76	–	–	–
High-modulus polyester	3.57	110	3.5	0.97	0	16.5	150
PBI	0.28	5.6	30	1.40	1.5	41	550

Table 2.51 Comparison of properties of basalt fibers and E-glass fibers

Fiber type	Thermal property		Physical properties			
	Operating temperature/°C	Sintering temperature/°C	Conductivity/W (m K) ⁻¹	Monofilament diameter/μm	Tex/g km ⁻¹	Density/g cm ⁻³
Basalt-fiber tows	-260-650	1050	0.031-0.038	7-17	88-420	2.6-2.8
E-glass fiber	-60-450	600	0.034-0.04	6-17	22-480	2.54-2.6
Fiber type	Physical property	Residual tension strength after heat-treatment/ %	Electric property			
	Elastic modulus/GPa	20 °C	400 °C	500 °C	Resistivity/Ω m	Dielectric loss angle tangent (1 MHz)
Basalt-fiber tow	89.2-107.8	100	95	82	1 × 10 ¹²	0.005
E-glass fiber	70.6	100	92	52	1 × 10 ¹¹	0.0047
Fiber type	Electric property	Acoustic property ^a	Chemical resistance stability (weight loss of roving, boiled for 3 h in aqueous solution)			
	Capacitivity (1 MHz)/F m ⁻¹	Acoustic absorptivity	In water	In 2 mol/L NaOH	In 2 mol/L HCl	
Basalt-fiber tows	2.2	0.9 - 0.99	1.6	2.75	2.2	
E-glass fiber	2.3	0.8 - 0.93	6.2	6.00	38.9	

^aThe materials are made of the super-fine fibers, and basalt filament is 13 μm in diameter. Above data are quoted from Russian Sudogda Glass fiber co.

their own advantages and disadvantages. Low-energy EB and UV-curing methods are the most attractive.

(1) EB curing

EB curing uses high-energy electrons or uses X-rays to generate electrons, to initiate polymerization and cross-linking reactions. This composite-curing technique was developed in the 1980s and 1990s. Its use has grown rapidly, and it has good potential.

EB curing has the following advantages.

1. Low cost: Its cost is 25–60% lower than that of thermosetting.
2. Fast curing: It is 10–1000 times faster than thermosetting.
3. Precise dimensions: No heating is needed for EB curing; therefore, it is free from thermal stress and avoids the drawbacks of tooling deformation.
4. Low porosity, shrinkage, and water absorption: The porosity ratio is less than 1%, the shrinkage ratio is about 2–3.5%, and water absorption is less than 1% after boiling for 48 h for most epoxy composites cured using an EB.
5. Low energy consumption: EB curing is energy saving, and the energy consumption is only 1/10–1/20 that of curing using an autoclave.
6. Good properties at low temperature and during thermal cycling: The composite properties are stable when they are subjected to low temperatures and during thermal cycling.
7. Long shelf life at room temperature if not exposed to sunlight and UV radiation.
8. Low toxicity: Because EB curing is performed at room temperature, no toxic hardeners are added to accelerate curing and save time. EB therefore reduces the use of materials that are toxic and harmful to human health and the environment.
9. Low-cost molds: The molds are 60% smaller than conventional molds and are easily made.

EB curing is suitable for free-radical and positive-ion resin curing.

Free-radical-cured resins are high polymers with terminal double bonds, e.g., epoxy acrylic acids and epoxy acrylic esters. When an acrylic ester system is cured using an EB, the EB not only causes polymerization of the double bonds of the acrylic ester but also causes free-radical cross-linking and reactions with acrylic acid groups. The disadvantages of this resin system are a low glass-transition temperature, low modulus, high moisture capacity, and high curing shrinkage (8–25%).

In positive-ion-cured resin systems, positive-ion initiators such as organic salts, aromatic sulfonium compounds, and iodine matte are added to an epoxy resin. This resin system is compatible with thermosetting composite processes (e.g., hand lay-up, RTM, VARTM, and fiber winding). EB-cured products have low porosity (no more than 1%), moisture content (no more than 1%), shrinkage (2.2–3.4%), and a high glass-transition temperature and are compatible with polyimides; they retain their good performance at low temperatures and during thermal cycling.

The EBs used for resin curing can be classified into three types based on the accelerator power and energy:

1. induced type, i.e., low energy (1–3 meV), high power (7–100 kW);
2. linear type, i.e., medium energy (4–5 meV), high power (50–150 kW)
3. radio frequency type, i.e., energy 4–10 meV, low power (0.2–5 kW)

A comparison of the performances of epoxy resins cured using an EB and heat is shown in Table 2.52.

(2) UV-curing techniques

UV curing is only suitable for composites consisting of transparent reinforcements and resins, e.g., glass-fiber composites. Use of a combination of UV curing and processes such as hand lay-up, spray-up, filament winding, and pultrusion can

Table 2.52 Comparison of EB- and heat-cured epoxy resins

Features	EB curable epoxy resins	Heat-cured epoxy resins
Mechanical properties	High	High
Manufacturing costs	Moderate(lower than heat cured by 25%–60%)	High
Prepreg storage	Extended life at 20 °C	Limited time below 0 °C
Environmental and health concerns	Low	Moderate to high (hardeners)
Material shrinkage on curing	2%–3%	4%–6%
Volatile emissions	<0.1%	<0.1%
Glass-transition temperature	Up to 400 °C	Up to 300 °C
Residual stresses	Very low	Moderate to high (thermal mismatch)
Water absorption	<2%	<6%
Production throughput	Fast	Slow
Maximum part thickness limit for a single cycle	50 mm (EB) 200 mm (X-ray) 1 mm (UV)	20 mm (thicker parts delamination caused by exotherm)
Materials of tooling	Metal, wood, ceramics, plastic, vax, and foam	Metal, ceramics, and graphite
Tooling costs	Low to moderate	Moderate to high
Cure time (10 mm-thick part)	Seconds to minutes	Hours
Energy requirements	Low to moderate	Moderate to high
Equipment cost	High	High to very high
Source material availability	Resins and initiators	Resins and hardeners
Resin system cost	4.4–11\$/kg (commercial) 17.6–44.1\$/kg (high performance)	4.4–8.8\$/kg (commercial) 17.6–44.1\$/kg (high performance)

improve the product performance, lower costs, and reduce environmental contamination (by reducing styrene emissions).

2.4.2.3 Latest Progress in Open-Mold Processes

In polymer-based composite techniques, hand lay-up, spray-up, and filament winding are considered to be open-mold processes. Such processes result in volatiles passing continually into the air from the resin, leading to environmental pollution and serious health hazards. In recent years, much research has focused on solving these problems and has achieved good results [21, 22].

(1) New type of low-volatile resin and gel coating

The Neste research technology group developed and patented a low-volatile process based on a unique unsaturated polyester. The polymer has an end group that is chemically compatible with styrene. Gel coatings formulated using this polymer cut monomer use by 30%. Tests showed that released volatiles were reduced by 50% during spray-up, but the properties of the final products were unchanged or improved slightly.

The PEAR thermosetting resin produced by Ashland has excellent processing properties, without volatile emissions and gas release, and the curing shrinkage is only 0.8%. Scott Bader, a polyester supplier in the UK, developed a new gel-coating resin with 66% less styrene volatiles than a typical coating, which is 80% less than for hand lay-up laminates and 50% less than for spray-up.

At present, many resin manufacturers are providing various low-styrene polyester and vinyl ester resins, e.g., the Hydrex LS series, D10 N VPC 7100, CoREZYN VEX 201-307, and H839-ECA.

(2) Spray-up equipment with low-styrene emissions

To meet the requirements of EP regulations, spray-up equipment manufacturers have developed many new techniques such as fluid impact techniques, air aid cover techniques, and low-pressure and non-atomizing techniques, aimed at reducing atomization caused by the spray gun during processing. The resin and catalyst are efficiently mixed by optimizing the design of the gun and nozzle so that air covers and shields the spray flow to prevent resin and catalyst particle dispersion into the air. Spraying at lower pressure than atomizing and improving the spray pattern between the gun and the mold results in the nozzle spraying a fluid fan, with lower levels of fumes, emissions, and overflows. The use of non-atomizing techniques is a growing trend in spray-up processes.

(3) UV curing

Commercial UV-cured resins are available in domestic and overseas markets. Their features include fast curing on exposure to sunlight or UV radiation (a couple

of minutes), a short profile time, lower cost, and less environmental pollution. UV curing is already used in hand lay-up and filament winding.

2.4.2.4 Latest Progress in Closed-Mold Process

During the past few decades, especially in recent years, much progress has been made in the use of closed-mold processes. RTM and related techniques are considered to be important.

Much research has been performed to increase the use of RTM and overcome its limitations, resulting in increased use of RTM and development of a mature complete system of materials, processes, and theories. The latest progress is described below.

(1) Multiaxial fabric preform technique

The main preforms are 2D and 3D fabrics, and 2D and 3D woven fabrics, especially multiaxial woven, full-thickness stitched (lay-up plus stitching, the preforms are laid down in desired ways and then stitched together), and OC-molded woven mats (including a woven core, two layers of chopped strand mat, and continuous reinforcement). Preform manufacture by filament winding can significantly improve the composite impact resistance.

(2) Use of various blenders to broaden resin applications

Various types of blenders and heating highly viscous resins to the temperature needed for RTM and air bubble release enable the wide use of RTM to produce high-performance composites.

(3) Obtaining high glass content with compacted reinforcement and vacuum assistance

1. Thermal expansion RTM (TERTM): The mold is assembled inside the preform, and then the mold and preform are heated, with simultaneous resin injection. The mold expands to compact the parts accordingly.
2. VARTM: In this method, the resin is absorbed into the RTM mold using a vacuum. It gives low porosity and a high glass content.

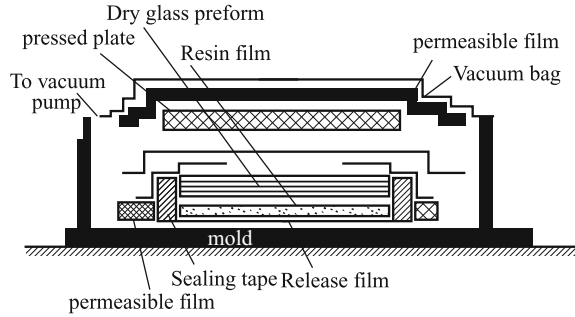
(4) Monitoring resin injection and curing using computer simulation

New computer-assisted engineering software has been developed and used to predict and control resin flow in the mold cavity. Computer analysis is used to display material loading in the cavity. This prediction and control system is used to monitor and control processing parameters.

(5) Vacuum bag and soft-film techniques

Resin film infusion (RFI) and Seaman's composite resin infusion molding process (SCRIMP) are the most notable developments.

Fig. 2.52 Resin film infusion



1. RFI: A precatalyzed resin sheet is loaded into the mold, and then the dry reinforcement is laid over it. The mold cavity is sealed with a vacuum bag. The mold is heated and evacuated at the same time. The melted resin impregnates the reinforcement (generally from the bottom to the top) and cures it (Fig. 2.52). For thicker laminates, several dry fabric and resin film plies can be used (semi-cured resins are also acceptable). This process is suitable not only for vacuum bags, but also for matched dies, pressure bags, and autoclaves.

The film infusion method has many advantages over RTM: (a) a short infusion path, even resin distribution, suitability for resins of high molecular weight, and a short production cycle; (b) low porosity; (c) large and thick laminates can be molded quickly and economically; (d) low reject rate and consistent quality; (e) low cost; and (f) high-performance products.

Hexcel Composites and SP Systems are now bringing RFI processes to market under the brand names HexFIT™ and SPRINT™, respectively. Figure 2.53 shows a cross section of the SPRINT CBS.

The British company TVR, a racing car manufacturer, used SPRINT for its Tuscan racing car (200 mph). RFI is attractive for making large and high-performance composite parts.

2. SCRIMP: This is a patented technique; its most prominent feature is provision of a system for controlling resin flow (a reusable resin diversion slot or pipe), and a distribution system based on dry glass impregnation. The process basically involves loading the dry reinforcement into a mold, making the preform parts, sealing with a vacuum bag, evacuating the mold to reduce the material volume, and delivering the resin from drums into the mold through an inlet and resin feed channel to wet the reinforcement quickly. A typical SCRIMP setup is shown in Fig. 2.54.

Fig. 2.53 Cross section of one ply of SPRINT CBS with alternative surface veil

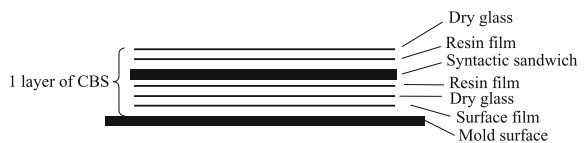
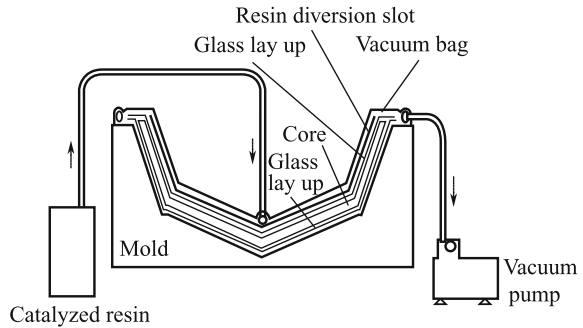


Fig. 2.54 Typical SCRIMP setup



The merits of SCRIMP are (a) a high fiber content (60–70%); (b) low-volatile emissions (less than 10×10^{-6}); (c) it is almost void free; (d) high specific strength; and (e) good process reproducibility.

SCRIMP has been used in yachts, and parts of buses and trailers. The weight of a bus body of length 9.1 m produced using SCRIMP is 30% less than that of a steel structure of the same size.

A catalyzed resin is drawn from drums through the inlet along the resin diversion slot into the bag and completely impregnates the lay-up (courtesy of TPI Technology Inc.)

The vacuum infusion process (VIP) is a further development of this process. A grooved surface on a PVC foam core is used to distribute the resin through dry glass reinforcements under vacuum. Yacht hulls of length 37.5 m have been molded using this process.

2.4.2.5 Fiber Placement

Fiber placement is a complex and unique process based on filament winding and tape placement, combining the merits of these two processes.

In the fiber placement process, a single fiber is gathered up to a band and the band is made into a prepreg on the unit. Tows are pulled off spools and fed through a fiber delivery system into the fiber placement head. The prepreg is laid down on a mandrel or mold surface.

A fiber placement unit (Fig. 2.55) is similar to a fiber-winding machine; it has five to seven axes and one placement head, which consists of parts such as a cutting band, clamp mechanism, and reset compaction roller. Its motion mechanism is similar to that of a filament machine.

Fiber placement differs from filament winding and tape placement and does not lay-up the band along the geodesic on the mold. The width can be controlled precisely. Each single band can be placed individually. The placing thickness can also be adjusted. In addition, fiber placement usually avoids delamination because filament winding compacts the band on the mold by way of the head.

Fig. 2.55 Fiber placement head

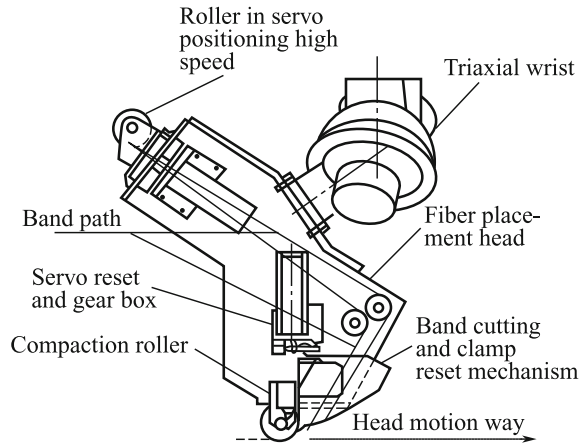


Table 2.53 Comparison of fiber placement, filament winding, and tape placement parameters

Item	Filament winding (wet)	Tape placement (prepreg tape)	Fiber placement (prepreg yarn)
Porosity	4–8%	<1%	<1%
Thickness	0.24–0.6	0.01–0.03	0.01–0.04
Winding angle/(°)	>15	0–90	0–90
Yarn cut	Not allowed	Allowed	Programming control
Over lap/cm	0.32	0.08	≤ 0.08
Geometry	The best is roundabout body	All are acceptable	Complex shape, concave
Reject rate	20%–40%	50%–200%	5%–20%

The advantages of fiber placement are (1) precise control of layer thickness; (2) in-process consolidation; (3) low porosity; (4) placement at any angle; and (5) low in-process scrap.

A comparison of fiber placement, filament winding, and tape placement is shown in Table 2.53.

2.4.3 Development Trends in Polymer Composite Use in Industry

Polymer composites face many new opportunities and challenges in the twenty-first century. There is a huge potential market for polymers in the repair, reinforcement, and renewal of infrastructures, exploration and applications of energy resources,

and marine offshore oil production and transportation. However, their high cost makes them less competitive than conventional materials. Low reliability, unstable qualities and properties, inconsistent and incomplete data, and incomplete data sets make designers and end users apprehensive about their applications. Polymers are difficult to recycle, and they need to conform to higher environmental standards since Japan and Europe have legislated to limit VOC emissions and waste disposal. Reducing pollution is now an urgent issue.

Based on the diversity of material demands and the merging of materials and functions, energy-saving strategies, population growth, and the need to protect the environment and achieve sustainable development, future polymer-based composites must be cheap, high-performance, multifunctional, intelligent, and compatible with environmental standards.

2.4.3.1 Development of Low-Cost Manufacturing Techniques

High cost is still an obstacle to the further development and wider application of polymer composites, although they are used widely in various industries. Extensive and comprehensive development studies have been conducted. The progress made is summarized below.

(1) Low-cost raw materials [23]

The reinforcement account for more than 60% of a polymer composite, so reducing the reinforcement cost is a key point. This can be achieved by actions such as glass-fiber manufacturers developing larger furnaces and larger tows, and carbon-fiber manufacturers taking measures to enhance production volume. Large-tow production, especially using acrylonitrile textile strands, can reduce costs by a large margin.

(2) Mechanized and automated processes

Hand lay-up, including spray-up, still represents a large percentage of all processes used, especially in developing countries. Hand lay-up suffers from low productivity, severe pollution, and inconsistent quality. Mechanized processes such as filament winding, pultrusion, SMC, and RTM have advantages such as high efficiency and consistent quality.

In recent years, optimized RTM and fiber placement techniques have been used to obtain high-precision products and high glass contents. Appropriate placement, low porosity (even zero porosity), and simpler processes, resulting in lower production costs, are significant. The development of RTM, pultrusion, and fiber placement are considered to be important in the twenty-first century.

(3) EB and low-temperature curing techniques

EB curing and low-temperature curing have advantages such as short curing times, low cost, low energy consumption, and low mold requirements, and therefore they increase productivity and reduce production costs.

(4) Integration of design and manufacturing techniques

Integrated computer-aided design (CAD) software can be used to design, analyze, and manufacture products using a simulated prototype. The integration of design and manufacturing techniques enables further mechanization and automation of polymer composite production. It has been reported that filament-wound products designed using CAD and FEA and produced using advanced winding machines require 20–30% less raw materials and have a 70% shorter production cycle. The integration of design and manufacturing techniques can improve the product quality, reduce raw material consumption, and shorten the production cycle, by enabling precise design and production. The target of lower costs can therefore be achieved.

Integrated design and manufacturing techniques were a milestone in the development of the advanced composite industry during the last 10 years of the twentieth century, and the core of new polymer composite technology.

2.4.3.2 Compatibility with Environment

Most polymer composite matrices and FRPs are thermosetting polymers, more than 70% of which are unsaturated polyester resins. Toxic volatile emissions during production and the difficulty of waste recycling are therefore problems. In the early twenty-first century, work began on green composites. Currently, developing models of FRP/composite industry pollution, more environmentally friendly closed-molding processes, materials that are environmentally benign, awareness of the requirements of international environmental laws, developing methods for the recovery, reuse, and recycling of composites, and drawing up plans for industry applications are hot topics and are high on the research agenda. Future research trends include:

1. low-volatile techniques, innovative low-volatile resins, non-atomizing fogless spray-up systems, and UV-curing techniques;
2. closed processes, including RTM, RFI, VARTM, and SCRIMP;
3. thermoplastic matrix materials;
4. natural fibers and degradable composites.

2.4.3.3 Trends in Development of High-Performance, Multifunctional, and Smart Materials and Products

The development of materials that are high performance, multifunctional, and smart relies on progress in industrial production techniques, materials, and material development from the low level to the high level, based on complex materials. This can be achieved using combinations of polymer composite processes to form super-combinations or super-hybrids; for example, the reinforcement of high-pressure FRP pipes by adding steel strips improves not only the pressure that they can withstand but the wall thickness; FRP tanks based on nanocomposite technology have good corrosion resistance and no scale deposits. New applications usually require the integration of high-performance and multifunctional materials or products. Applications of super-hybrid products consisting of plastics, and metals are becoming more widespread (e.g., for compressed natural gas cylinders). Super-complexation is an important method for obtaining high-performance, multifunctional, and smart polymer composites, and this method will broaden the application scope of polymer composites.

Much good, basic work has been done in the study of smart materials. For example, optical fibers are used in composite windmill blades in offshore wind-energy projects, and optical fiber sensors can monitor the real-time performances of the blades during operation so that costly overhaul and maintenance is minimized.

2.4.3.4 Development Trends in FRP Industry

Since they were first reported more than 50 years ago, FRPs have evolved from new materials into conventional ones and the performance of the FRP industry is strengthening in the intense competition with traditional materials such as metals, stone, wood, and concrete. Large-scale products and integration are the development trends in the FRP industry, e.g., large cooling towers (37.3 m wide, 11.3 m long, and 9.1 m high), chimneys (5 m in diameter, 187 m in height), wind turbine rotor blades (55 m long), and large-diameter GFRP mortar (3.2 m in diameter). Large and integrated FRP products are in demand for technological processes in all sectors and are also effective in enhancing productivity and quality, and reducing costs.

Other trends are precise manufacturing techniques and stable-quality products. Along with the fierce competition in industrial sectors, other customers are demanding better quality, appearance, makeup, and decoration of FRP products, and only products that are precision processed and of stable quality are competitive in the market.

Higher production efficiency, large-scale production, and lower costs are necessary for the continuing existence and development of the FRP industry. The achievement of high-speed, large-scale, and low-cost production will enable FRPs to compete effectively with traditional materials and broaden and strengthen their applications.

2.4.4 Development Potential of Polymer Composites

2.4.4.1 Development Potential for Infrastructures

Infrastructures such as bridges, tunnels, highways, railways, dams, water-work plants, power stations, and ports are necessary and basic installations for national economic growth. At present, many infrastructures such as bridges are faced with structural problems caused by overloading, varied functions, and decreases in strength caused by corrosion.

In recent years, polymer composites reinforced with carbon, aramid, and glass fibers have played major roles in the building, reconstruction, consolidation, and repair of infrastructures.

Extensive research has been performed worldwide, and much success and progress have been achieved. Research and prototype projects have shown that composites have the following advantages:

1. high strength and rigidity, low weight, and less additional weight resulting from repairs;
2. easy construction on site and efficiency four to eight times higher than that of steel;
3. a wide range of applications, and no changes in the shape and appearance of the original structures;
4. good chemical corrosion resistance and good weathering ability;
5. low cost, e.g., a cost reduction of about 20% of total costs compared with previous methods.

Table 2.54 shows a comparison of some repair methods made by Japanese researchers.

Composites have been used for the following:

1. reinforcement and repair of concrete, steel, and cast-iron structures;
2. whole composite structures (bridges);
3. concrete-reinforced bars;

Table 2.54 Comparison of some repair methods

Items	Carbon-fiber-reinforced	Concrete-reinforced	Steel panel-reinforced
Construction project	Bonding carbon fibers/resin composites over the damaged concrete	Adding steel bar to the damaged concrete	Wrapping steel panel the over damaged concrete
Construction days	15–20	20–30	20–30
Direct cost	40,000–80,000 yuan/m ²	50,000–120,000 yuan/m ²	80,000 yuan/m ²

4. outside skins for steel or concrete structures;
5. composite structures with bonded steel.

The successful use of composites, especially optimized super-complex structures made using steel, concrete, and composites, will bring revolutionary changes in architectural design, function, cost, service life, and repair. Composites are considered to be an important building material in the twenty-first century.

The American SPI Association estimated that 75,923 bridges, 8794 high dams in danger, and 10,131 water-disposal plants need to be consolidated, repaired, and rebuilt in the USA.

In Europe, more than one-third of 100-thousand rivet steel railway bridges are in need of consolidation to enable them to bear heavy trucks and express trains.

China has made extensive use of concrete engineering. In recent years, the Chinese government has invested considerable money in projects such as express trains, and many railway bridges need repair and consolidation.

New infrastructure building and maintenance worldwide will lead to the need for robust composites and important applications.

2.4.4.2 Development Potential in Transportation

The demand for resin matrix composites in transportation is high. The resin composites used in cars, express trains, light-rail vehicles, and other means of transport account for more than 30% of the total output of composites. Developed countries have established regulations to limit vehicle gas consumption rates, exhaust pollution, noise, and vibrations, and to increase safety and comfort. This has prompted vehicle manufacturers to use new designs and materials. Composites are used in automobiles to reduce weight and energy consumption, improve productivity, lower costs, and enable easy model modification. In the USA in 1998, thermosetting composites were used in more than 10 million vehicles and 510 types of parts. Composite parts include cover shells and bodies, driving shafts, bumpers, leaf spring hoods, CNCs, seat frames, heavy truck chassis, and brake disks. The amount of composites used in the automobile industry is rapidly increasing annually; the use of thermoset SMC and thermoplastic GMT is growing fastest.

The trend in the automobile industry is to use lightweight structural materials to replace steel. Use of a composite car body and chassis instead of steel can reduce the weight by 68% and reduce gas consumption by 40%. The advantages of carbon-fiber composites in the automobile industry are (1) low weight; (2) design and profile flexibility; (3) good chemical resistance; (4) modified damping; and (5) low investment. The use of carbon composites in the automobile industry is expected to grow. Design results show that 113 kg more carbon fibers could be used in a typical car. To meet the demand for this in North America alone, the need for carbon fibers will be up to 100 times the present total global capacity. At present, carbon prices limit carbon-fiber use in large amounts in the automobile industry.

Experts predict that growth in the use of polymer composites in automobiles will accelerate, and they have good prospects for the future.

The use of polymer composites in metroliners, subways, light rail, and other transport applications is also growing rapidly. Traffic networks consisting of subways, elevated light railways, and urban railways have become an important part of solving the problems associated with the increases in metropolitan traffic caused by rapid growth in the economy and urban populations, the expansion of cities.

In Japan, window frames, side window sills, decoration, and ceiling air conditioners in all carriages on the Shinkansen line are made of SMCs because they are lightweight, esthetically pleasing, heat resistant, and dew proof.

In Europe, polymer composites and SMCs are also widely used in railways. Switzerland, Germany, Italy, and the UK have developed carbon-fiber train carriages and locomotives. The main uses of polymer products in railway facilities and indoor decoration include cable conduits, third rail covers and brackets, side-walk grids, fence grids, anti-noise panels, carriages, doors, wall panels, ceilings, and floors.

In 1998, there were over 100 thousand passenger trains, and more than 6300 new carriages were produced per year; 80% were used in freight and suburban lines. There is a demand by European railways for metroliners and luxury trains such as the French TGV_S, Swedish bullet trains, and Austrian and German “Restaurant Trains.”

In Europe, tramcar and light-rail traffic networks have been built in over 100 cities, half of them located in Germany. The demand for railway carriages is therefore increasing. In addition, new robot subways are under construction or new subways are being built in many countries.

Recently, China has accelerated train construction, built faster trains, and reconstructed and built new high-speed railways. In 10–20 years, subways and light railways will be built in many cities. The polymer composites used in the communications and transport industries are finding new market opportunities in transportation.

2.4.4.3 Development Potential in Offshore Oil Extraction Industry

Along with advances in the petroleum industry, especially the requirements for unattended platforms and minimum facilities, the use of polymer composites in offshore oil exploration has significantly accelerated in recent years.

In oil and natural gas exploration, the weight, cost, and performance of a platform system are the primary factors in deciding its economic viability, safety, and reliability. Another key point is whether composite pipes can be used instead of steel ones. For platforms, the component parts used and installation costs depend on the platform weight. In terms of weight, composites are preferable to metals because of their low density. The use of composites in water-disposal systems on platforms or the raisers under the platform reduces the system deadweight by 50–60%, and sometimes by up to 80% in some special cases.

The main contributors to the cost of component parts for platforms are materials and installation. A comparison of the costs of typical materials used in offshore operation showed that the cost of a GRP pipe is equivalent to that of 316 stainless steel pipes and nearly six times that of carbon steel. If the installation costs and material weight are considered, the cost of a GRP pipe is close to that of carbon steel. Assuming that the cost of carbon steel is 1, then that of the GRP pipe will be 1.1; those of stainless steel, Cu/Ni 90/10 alloys, and high Mo alloys will be 1.55, 1.80, and 3.7, respectively.

Because seawater is highly corrosive, an FRP replacing carbon steel must have good chemical resistance. Test results showed that resin matrix composites retained 80–90% of their strength and rigidity after immersion in seawater for 5–10 years. In particular, the hoop stress value in a short-time bursting test of an epoxy resin FRP pipe used for crude oil and natural gas containing seawater was unchanged after 20 years, whereas the service life of a carbon-steel pipe was only 1–5 years.

At present, resin matrix composites are used in most platform structures. For example, in the Mars tension leg platform (TLP) in Mexico, resin matrix composites were used in 1.6×10^4 m² FRP lattice panels, a riser tensioner, lifeboats, a high-pressure vessel, torque shafts, component parts, sealant units, and fire and blast walls. FRP pipes installed in the Mars TLP as fire piping and a sewer system enabled reduction of the maximum weight by 72.6 t. In Ram-powell, which is the same type of TLP as Mars, an advanced composite material energy vessel was used as a tensioner in the production riser. The vessel consisted of carbon/glass epoxy resin composites, a 316 L stainless-steel shell, and a high-density polyethylene liner. The composite vessel dimensions were outer diameter 44 cm and length 209 cm, and it weighed 165 kg, which is one-third that of the steel vessel.

The offshore use of polymers reinforced with carbon fibers, aramid fibers, and glass fibers, or hybrid-reinforced polymers is growing rapidly.

It is estimated that there are 6100 platforms around the world and more platforms are being designed. The use of polymer composites at a water depth of 609–1220 m is considered to be economical, and their use below 1220 m is technologically feasible. It is estimated that in 10 years the offshore applications of polymer composites will enter a new stage, and the potential market is large.

2.4.4.4 Potential Use in Electrical Energy Applications

(1) Wind power

Wind is a sustainable energy source; it is renewable, does not cause pollution, and has large and widely dispersed sources. In the past 10 years, the average global growth rate in total wind-generated energy was close to 40%. In 2002, the total wind-generated energy was 31,128 MW, accounting for only 0.4% of global power supplies [24, 25].

Table 2.55 Lengths and masses of FRP blades for different powers

Rated power/MW	Blade length/m	Rotator mass/t	Rated power/MW	Blade length/m	Rotator mass/t
0.055	7.5	1.08	1.0	29.1	14.70
0.10	9.0	2.00	1.2	29.1	14.70
0.15	11.0	2.10	1.5	34.0	16.80
0.20	12.0	2.50	2.0	36.8	27.30
0.25	13.4	2.50	2.5	38.8	25.90
0.5	17.2	4.86	3.0	43.8	28.50
0.6	19.1	5.88	5.0	55.0	45.00
0.8	23.3	8.97			

Note Rotator mass is meant three blades, exclusive of the hub

The blades are the most important components of windmills. Because of the special needs of wind power, the blades have to be high strength, corrosion resistant, lightweight, and long-lived. Blades made of polymer composites reinforced with glass fibers and carbon fibers are generally used worldwide.

At present, FRP blades are mainly produced using hand lay-up, VIP, VARIM, SPRINT, and filament winding. Carbon composite blades of length up to 56 m have been produced, and carbon composite blades of length 61.5 m are being developed. The lengths and masses of FRP blades for different powers are shown in Table 2.55.

The mass of a 31-m FRP blade is 5 t and that of a 50–60-m FRP blade is 20 t. Thousands of blades are needed for only one wind farm; therefore, composites are in great demand.

Energy demands and the need for environmental protection are the motivation behind the rapid growth in wind energy. In Europe, the German government plans to increase the percentage of total energy produced using wind power from 3.5% to 25% by 2025. Denmark plans to use wind power to generate 50% of its energy by 2030. France planned to increase its use of wind power three- to sixfold in 5 years the total wind power generated would be 10,000 MW. The US Energy Sources Department estimated that annual wind power generation is 6000 billion and accounts for 20% of general power. Wind power sources in China represent approximately 1.6 billion kW, and exploitable wind power generation is nearly 250 million MW. Wind power will approach 20% of global power. Wind power has great promise.

(2) Potential applications in power infrastructures

Composite poles have been used for electrical utilities for over 10 years. The poles are generally used for transmission lines, telephone lines, and lighting circuits in mountainous and hilly areas, and corrosive environments such as industrial parks and coastal regions. In the past, poles were made by pultrusion, filament winding, and centrifugal casting and classified as grade 3, 4, or 5; the length was generally 20 m. Recently, the Strongwell Corporation in the USA produced a tapered pole of

length 20–24.4 m and classified as grade 1 or 2, with pultruded panels assembled using a proprietary method. Recently, FRP poles manufactured using an innovative process have been used as ideal alternatives to wooden, steel, and concrete pole. In the USA, there are about 21 million miles of power transmission lines and 595 million poles (28.5 poles/mile on average) and the wooden poles used in the aged distribution system need to be replaced yearly.

Composites are used in electrical applications because they have the following advantages.

1. Low weight: The weight of a composite pole is only one-third that of a wooden one. They can be installed manually or using small pieces of equipment, which reduces installation costs.
2. Non-conductive: Compared with reinforced concrete poles, composite poles have better insulating and anti-thunderbolt properties.
3. Non-toxic: Unlike wooden poles, composite poles do not need anti-corrosion treatment with toxic chemicals; this avoids environmental pollution and decreases costs.
4. As the amount of forest decreases, lumber prices will increase. In contrast, composite prices will remain relatively stable and will decrease with improved techniques and processes.

Several factors are increasing growth in the global power market. One factor is that existing aged infrastructures are approaching the ends of their service lives and need to be replaced. Another is the migration of populations to cities and the accompanying increased power demand. Global industrialization is also increasing power demands. A combination of these factors means that countries worldwide will have to increase power output as a priority, resulting in growth in the use of composites in poles, insulator cores, cross-arms, brackets, and other elements of power infrastructure.

(Sections 2.1, 2.2.4.1, 2.3, and 2.4 were translated by Baifeng Yu; 2.2.1–2.2.3 and 2.2.4.2–2.2.4.6 were translated by Linwen Zhang, Liang Yang, and Yong Shi.)

References

1. Qian ZP (ed) (1998) Foam plastics. Petroleum Industry Press, Beijing (in Chinese)
2. Chen XB et al (1999) High performance resin matrix. Chemical Industry Press, Beijing (in Chinese)
3. Liang GZ, Gu YJ (2000) Compression molding technology. Chemical Industry Press, Beijing (in Chinese)
4. Chen F (2003) BMC molding plastics and its forming technology. Chemical Industry Press, Beijing (in Chinese)
5. Ha B (ed) (2002) Filament winding technology. Science Press, Beijing (in Chinese)
6. Yue HJ (1995) FRP pultrusion process and products. Science Press, Beijing (in Chinese)
7. Micheal FF (1992) The flexible resin transfer molding (FRTM) process. *Sample J* 28 (6):15–57

8. Wang ST, Yang XZ et al (1997) Resin-based composite materials. China Building Materials Industry Press, Beijing
9. Ouyang GE, Ou GR (eds) (1993) Composite material testing technology. Wuhan University of Technology Press, Wuhan
10. Zeng JC et al (1998) Physical and chemical properties of composite materials. National Defense University Press, Changsha
11. Hollaway L (1994) Handbook of polymer composites for engineers. Woodhead Publishing Limited, Cambridge
12. Charles AH (1996) Handbooks of plastics elastomers and composites, 3rd edn. McGraw-Hill, New York
13. Hogg PJ, Woolstencroft DH (1992) Composites Tooling II Proceedings. Elsevier, Mayfield House
14. Asia-the future for the composites market (2003) Reinforced plastics, July and August, pp 28–30
15. Global opportunities reviewed at RP Asia (2002) Reinforced plastics, October, pp 20–21
16. Globalisation on the agenda at JEC (2003) Reinforced plastics, May, pp 38–46
17. How credible are the predictions? (2003) Reinforced plastics, May, pp 23–27
18. North America: what's up the world's largest composites market? (2000) Reinforced plastics, September, pp 26–32
19. Boron-free glass fibres-the trend for the future (2003) Reinforced plastics, June, pp 36–40
20. Reduced styrene content offers answer for Lse (2001) Reinforced plastics, December, pp 24–30
21. Reducing emissions by resin formulation (2001) Reinforced plastics, December, pp 32–35
22. Low cost carbon fibres open up new applications (2000) Reinforced plastics, Buyers' Guide, pp 10–14
23. Developments in composite materials for the railway industry (2003) Composites International, (52): 26–30
24. Wind energy-the fuel of the future? (2001) Reinforced plastics, Buyers' Guide, pp 10–13
25. Ana S (2002) Wind power for global electricity generating present and future opportunities. 47th International SAMPE Symposium, May, 12–16. pp 779–793

Chapter 3

Metal Matrix Composites

Lin Geng and Kun Wu

Metal matrix composites (MMCs) are a class of artificial materials compounded by the introduction of certain content reinforcements, such as fibers, whiskers, or particles, into the metal or alloy matrix materials. MMCs exhibit not only high specific modulus, high specific strength, good thermal conductivity, good electrical conductivity, controllable thermal expansion coefficient, and excellent high-temperature performance, but also designability and machinability. Therefore, they are an important class of advanced materials.

The appearance of metal matrix composites can be traced back to ancient civilizations. In 7000 BC, a copper awl, which was found in Turkey, exhibited metal matrix composite characteristics. To improve the service performance of metals, enhance their specific strength and specific stiffness, and satisfy the requirements of space technology development, investigations of metal matrix composites began in the 1960s and this research focused mainly on aluminum and copper matrix composites reinforced with tungsten, boron, and other fibers. In the 1970s, metal matrix composite development was restricted because of the difficult-to-solve matrix–reinforcement interface problem, fewer available reinforcement categories, complex fabrication processes, and high costs. However, after the 1980s, the research and applications of metal matrix composites were promoted further. In particular, aluminum, magnesium, copper, and titanium matrix composites entered the practical development stage. The reason for this is that at that time, science and technology developments, and especially the high-tech developments that included aerospace and nuclear energy use, urgently required such materials, with their high specific strength, high specific stiffness, wear resistance, corrosion resistance, and high-temperature resistance, along with their ability to maintain high chemical and

L. Geng (✉) · K. Wu
Harbin Institute of Technology, Harbin, Heilongjiang 150001, China
e-mail: genglin@hit.edu.cn

dimensional stability under abrupt temperature variations. In addition, intermetallic matrix composites with high-temperature resistance were also developed rapidly.

Metal matrix composites consist of the metal matrix, the reinforcement, and the interface between metal matrix and reinforcement. As an important component of such composites, the metal matrix plays the role of the reinforcement carrier. The matrix materials are selected according to their alloy characteristics and the intended composite uses. For example, both the shells and internal structures of airplanes, satellites, rockets, and other aerospace components require materials with lightweight, high specific strength, and high specific modulus, so magnesium, aluminum, and other light alloys can be used as the matrix materials. High-performance reinforcements are important components of such composites, and they determine the metal matrix composite performance to a certain degree. The reinforcement selection process mostly considers the reinforcement strength, the modulus, the processing costs, compatibility between reinforcement and matrix, and the high-temperature performance, but thermal conductivity and electrical conductivity are also considered for specific uses.

The metal matrix composite interface is the combination region between the matrix and the reinforcement. During composite manufacture and use processes, the matrix materials may react with the reinforcements to produce certain compounds, or diffusion between the matrix and the reinforcement may form certain diffusion layers. The great influence of the interface on the composite mechanical properties means that it is necessary to control the interface reaction to obtain the appropriate composite interface. Metal matrix composite interfaces can be classified into three types.

The first class includes interfaces where the reinforcement and the metal matrix are mutually non-reactive and insoluble, such as Cu/W, Cu/Al₂O₃, Al/SiC, Ag/Al₂O₃, and other interfaces. These interfaces exhibit relatively smooth planes and only have a molecular layer thickness. There are no materials other than the composite components in such interfaces.

The second class includes interfaces where the reinforcement and the metal matrix are non-reactive but are mutually soluble, such as Nb/W, Ni/C, Ni/W, and other interfaces. Such interfaces display staggered saw tooth structures, and they are formed through the dissolution and diffusion of the material components. The alloy elements of the metal matrix and the impurities may be enriched or depleted in such interfaces.

The third class of interfaces is a reactive product layer induced by chemical reactions between the reinforcement and the metal matrix, such as Ti/Al₂O₃, Ti/B, Ti/SiC, and other interfaces. Such interfaces have sub-micron-scale layers.

Metal matrix composites can be classified into two categories according to the reinforcement types: continuous fiber-reinforced composites and discontinuous fiber-reinforced composites (using short fibers, whiskers, and particles). Because continuous fibers play a primary role in supporting the load, a continuously reinforced composite has high specific strength, a high specific modulus, and strong

anisotropy because of the fiber reinforcement in one direction. However, their practical applications are hindered by the high costs incurred by both the expensive fiber materials and the complex preparation technology. For discontinuous fiber-reinforced composites, the metal matrix still plays the dominant role, and its strength is close to that of the raw metal. The addition of the reinforcements mainly remedies the matrix inadequacies, such as its stiffness, wear resistance, and high-temperature performance. The preparation technology of these composites is relatively simple, and commercial processing can be achieved using existing metallurgical processing equipment, so the lower fabrication cost is promising for the large-scale application of such composites. The metal matrix materials used include lightweight metals and their alloys (such as Al, Mg, Ti, and Zn), superalloys, and intermetallic compounds. Continuous reinforcements mainly use materials such as carbon fibers, graphite fibers, silicon carbide fibers, precursor pyrolysis fibers, boron fibers (with tungsten core), alumina fibers, stainless steel wires, and tungsten wires. For discontinuous reinforcements, the most commonly used short fibers are short alumina fibers containing mullite and silicate; the particles used include silicon carbide, alumina, zirconia, titanium diboride, titanium carbide, and boron carbide; the whiskers used include silicon carbide, aluminum oxide, boric acid, and potassium titanate.

The metal matrix composite fabrication methods depend on the choice of raw materials and can be divided into three categories: solid-state methods, liquid-state methods, and other preparation methods. Solid-state methods are a class of technologies for metal matrix composite fabrication under a solid matrix state. In some processing methods (such as the hot pressing method), a small amount of the liquid matrix can exist during fabrication to obtain better compounded materials. Therefore, the matrix alloy temperature is controlled in the temperature range between the solid-phase line and the liquid-phase line. The interface reaction between the metal matrix and the reinforcement is not serious because both matrix and reinforcement exist at a relatively low temperature during the entire fabrication process. Solid-state methods include powder metallurgy (PM), hot pressing, hot isostatic pressing (HIP), rolling, extrusion and pulling methods, and the explosive welding (EW) method. Liquid-state methods are a class of fabrication methods that combine a liquid-state metal matrix with solid-state reinforcements. To improve the wettability between the liquid-state matrix and the solid-state reinforcement and control the matrix–reinforcement interface reaction at high temperatures, pressure infiltration, surface treatment of the reinforcement, the addition of alloy elements into matrix, and other methods can be used during fabrication. Liquid-state methods include vacuum-pressure infiltration, squeeze casting, stirring casting, liquid metal infiltration, the co-deposition method, and thermal spray technology. Other manufacturing methods include *in situ* synthesis, physical vapor deposition (PVD), chemical vapor deposition (CVD), chemical plating, electric plating, and composite plating [1, 2].

3.1 Types of Metal Matrix Composite

This section describes metal matrix composites according to the type of metal matrix used, including aluminum, copper, titanium, magnesium, and other metal matrix composites [3, 4].

3.1.1 Aluminum Matrix Composites

Both pure aluminum and aluminum alloys can be selected as composite matrix materials, of which the most commonly used matrix materials are aluminum alloys. Aluminum alloys have been researched and developed for many years, resulting in a more mature alloy system. Al–Si, Al–Mg, and Al–Cu alloys, which are commonly applied in industry, have been used for fabrication of aluminum matrix composites. At present, aluminum matrix composite research is concentrated on two aspects: (1) continuous fiber-reinforced aluminum composites with excellent properties and with their general applications focused on very specific areas, such as the aerospace field; and (2) discontinuously reinforced aluminum matrix composites with excellent properties, with an applications' range that is rather wide. Also, the industrialization and volume production of such composites may be achieved because of the simple preparation technology used and the low reinforcement costs [5–7].

3.1.1.1 Continuous Fiber-Reinforced Aluminum Matrix Composites

The most commonly used long fibers are carbon fibers and boron fibers. Comparatively, boron fiber-reinforced aluminum composites offer better all-round performance, near-perfect compound processing because of the rich fabrication experience and more mature engineering applications.

Cascading methods are usually used to prepare carbon fiber-reinforced aluminum matrix composites. During the fabrication process, it is necessary to overcome the interface reaction between the Al matrix and the C fiber, because the Al matrix reacts with the C fiber to form an Al_4C_3 brittle phase which can diminish the composite performance. The preparation processing of boron fiber-reinforced aluminum matrix composites can be divided into two steps. First, the boron fibers are prepared in a prefabricated band, which usually includes four band types: the boron fiber resin band, the plasma spraying band, the preconsolidated boron aluminum single-layer band, and the fiber weave band. Second, liquid- or solid-phase synthesis technologies are used to fabricate the B/Al composites. The solid-phase synthesis technology involves hot pressing, diffusion bonding, and hot isostatic pressing. The B/Al composites exhibit not only lower density relative to aluminum, but also strength equal to that of a high-strength structural steel, and higher stiffness.

For example, B/Al composites with a fiber volume fraction of about 50% showed tensile strengths from 1350 to 1550 MPa, elastic moduli from 200 to 230 GPa, and a density of only 2.6 g/cm³.

Continuous fiber-reinforced aluminum matrix composites with high specific strength, high specific modulus, relatively high strength at high temperatures, good dimensional stability, and other advantages are mainly used as structural materials in aerospace fields, such as space shuttles, artificial satellites, and space stations. Load-carrying tube components produced using B/Al composites are widely applied in aerospace and aircraft. Such tube components have not only been made into the fan blades of turbofan engines but also into the fan blades and guide blades of high-performance aeroengines.

Although continuous fiber-reinforced aluminum composites have high specific stiffness and high specific strength, there are some questions that must be urgently addressed for their preparation and applications, such as the complex forming process, difficulties in secondary machining, and the high material costs. Therefore, applications of such composites are limited to only a few advanced fields, such as aerospace and nuclear weapons, where product performance is more important than the price factor. In contrast, aluminum matrix composites that are discontinuously reinforced with short fibers, whiskers, or ceramic particles not only offer a wide range of reinforcements, low costs, good formability, and isotropic material properties, but can also use traditional metal molding processes for secondary processing.

3.1.1.2 Discontinuously Reinforced Aluminum Matrix Composites

For discontinuously reinforced aluminum matrix composites, the reinforcements can be divided into short fibers, whiskers, and particles. Short fibers used include C, SiC, Si₃N₄, Al₂O₃, aluminum silicate, and mullite. Short fiber-reinforced aluminum matrix composites with high strength, high stiffness, and excellent abrasion resistance are usually prepared by the liquid infiltration method and have produced good results in practical applications. C fiber-reinforced aluminum matrix composites show high specific strength, high specific stiffness, a low thermal expansion coefficient, no moisture absorption, anti-radiation properties, high electrical conductivity, high thermal conductivity, and good dimensional stability. In addition, they do not release gas during use. As structural and functional materials, these composites have quite wide application prospects in the aerospace and civilian fields. SiC fiber-reinforced aluminum matrix composites with their lightweight, high heat resistance, high strength, and anti-fatigue properties can be used as components in airplanes, automobiles and machinery, as well as in sports equipment. Aluminum silicate fiber-reinforced composites exhibit excellent anti-wear properties.

In general, whisker-reinforced aluminum matrix composites are prepared by squeeze casting. First, the whiskers are prefabricated into whisker blocks with certain volume fractions; then, under pressure, liquid aluminum alloy infiltrates into

the whisker preform block to compound the composites. At present, the most commonly used whiskers are SiC, Si₃N₄, and Al₁₈B₄O₃₃. SiC whiskers are particularly widely applied because of their excellent all-round performance. The Mitsubishi and Toyota car companies in Japan have used SiC whisker-reinforced composites to produce important car parts, such as cylinders and pistons. However, the high cost of SiC whiskers restricts their extensive application in engineering. Recently developed low-cost aluminum borate whiskers have more optimistic application prospects. Whisker-reinforced aluminum matrix composites with their excellent performances can not only retain advantages of the aluminum alloy matrix, such as lightweight and corrosion resistance, but can also significantly improve the wear resistance and thermal fatigue properties. Also, they have a lower linear expansion coefficient. In general, their high-temperature tensile strength is significantly higher than that of the matrix materials alone. Some aluminum matrix composite strengths at 250 °C correspond to the matrix alloy strength at room temperature, suggesting that these composites can increase the service temperature limit of aluminum alloys to 250 °C. Aluminum matrix composites have been found to be optimal materials for engine pistons because of their low thermal expansion coefficient, and their wear resistance and heat resistance performances.

Particle-reinforced aluminum matrix composites have solved the high-cost problem of reinforcement preparation for fiber-reinforced aluminum matrix composites. Meanwhile, these composites with their isotropic properties have also overcome many preparation process shortcomings, such as fiber damage, microstructure asymmetry, mutual contact of fibers, and the very large reaction bands. These disadvantages affect composite properties directly. Therefore, particle-reinforced aluminum matrix composites have become one of the most attractive focal points in the metal matrix composite research field and are developing increasingly toward industrial-scale production and applications. Commonly used particle reinforcements include carbides (SiC, B₄C, and TiC), borides (TiB₂), nitrides (Si₃N₄), and oxides (Al₂O₃), as well as C, Si, and graphite crystal particles. Among these particles, SiC is the most commonly used reinforcement. The preparation technologies of particle-reinforced aluminum matrix composites have also been improved continuously to obtain particle-reinforced composites with perfect microstructures, and excellent mechanical, and other properties. At present, the most commonly used methods include liquid metal infiltration, stirring casting, powder metallurgy, in situ synthesis, and spray deposition. Both rational preparation processes and post-treatment processes can be used to obtain aluminum matrix composites with excellent mechanical properties. After addition of the reinforcement particles, both the tensile strength and the yield strength increase, but elongation decreases. This trend becomes more obvious with increasing particle content. Another important advantage of particle-reinforced aluminum matrix composites is their good corrosion resistance. Usually, the corrosion resistance of composites is lower than that of the corresponding metal matrix, and their main corrosion mechanism is pitting corrosion. However, the corrosion resistances of some aluminum matrix composites hardly decrease relative to the alloy matrix. This suggests that the addition of certain reinforcements will not reduce the corrosion resistance

as a result of improving the mechanical properties of aluminum alloys. For $\text{SiC}_p/6061\text{Al}$, $\text{SiC}_p/2014\text{Al}$, $\text{SiC}_p/2124\text{Al}$, $\text{SiC}_p/\text{A356Al}$, and other particle-reinforced aluminum matrix composites in media containing Cl ions, the material pitting potentials are close to that of the matrix metal. An increase in the average size and volume fraction of these particles hardly changes the pitting potential value. Particle-reinforced aluminum matrix composites can be used to manufacture not only satellite and aerospace structural materials, aircraft parts, metal mirror optical systems, and automotive components, but also microwave circuit plug-ins, precision components for inertial navigation systems, turbocharger components, electronic packaging, and many other devices.

3.1.2 Copper Matrix Composites

Copper matrix composites not only have high strength, electrical conductivity, and thermal conductivity similar to pure copper, but also have good arc erosion and abrasion resistance. These composites are a new kind of material with wide application prospects in high-tech electrical conduction energy-saving fields, such as aerospace, electronic, and electrical equipment and micro-motor applications. With the continuing development in the machinery and electronic industries, there are increasingly urgent demands for these copper matrix composites with their high strength and high electrical conductivity. Copper matrix composites can be classified into continuous fiber-reinforced copper composites and discontinuous fiber-reinforced copper composites [8, 9].

3.1.2.1 Continuous Fiber-Reinforced Copper Matrix Composites

Nonmetal or metal fiber-reinforced copper or copper alloy matrix composites not only retain the high electrical conductivity and high thermal conductivity of copper, but also exhibit high strength and high-temperature resistance. For example, carbon fiber-reinforced copper matrix composites combine the advantages of carbon fibers, such as self-lubrication, wear resistance, and a low thermal expansion coefficient, with the advantages of copper, such as good conductivity and thermal conductivity; consequently greatly extend the material service life; and enhance its reliability. Carbon fiber-reinforced copper matrix composites are not only used in sliding electrical contact materials, brushes, power semiconductor support electrodes and integrated circuit radiators, but also have a number of potential applications in the load bearings of the automobile engine, and the powder metallurgy bearings of printing machinery, papermaking machinery, textile machinery, and light industrial machinery.

In general, long carbon fiber-reinforced copper matrix composites are prepared by the hot pressing diffusion method. First, a composite preform is manufactured through winding, and then, hot press molding is performed in the pressing furnace

with a full- H_2 protective atmosphere. In addition, other fabrication methods include liquid metal infiltration, vacuum-pressure infiltration, the rolling diffusion method, and foil metallurgical methods.

3.1.2.2 Discontinuously Reinforced Copper Matrix Composites

Discontinuously reinforced copper matrix composites include short carbon fiber-reinforced copper matrix composites, particle-reinforced copper matrix composites, in situ copper matrix composites, and other copper matrix composites.

(1) Short carbon fiber-reinforced copper matrix composites

In short fiber-reinforced metal matrix composite fabrication, the important points are avoiding mechanical damage to the fibers when adding them to the matrix, completely dispersing the fibers into the matrix, and obtaining perfect bonding between fiber and matrix. Powder metallurgy methods are often used to manufacture discontinuous carbon fiber-reinforced copper matrix composites. This is mainly because the powder metallurgy method with its single forming process can avoid subsequent machining and save raw materials, and it is also superior to the liquid-state method and the diffusion bonding method. Consequently, this method has been widely used to manufacture short fiber-reinforced metal matrix composites. In addition, the hot pressing sintering method is also used to prepare short carbon fiber-reinforced copper matrix composites and is divided into two steps: sintering and forming. The hot pressing sintering method has been used to prepare uniform and dense C/Cu composites under lower pressure and relatively short time conditions.

The fibers used to reinforce copper alloys include carbon fibers, tungsten wires, graphite fibers, alumina fibers, carbon nanotubes, silicon carbide fibers, and steel fibers. Among these fibers, tungsten wires and carbon fibers are the most commonly used reinforcements.

Also, the addition of carbon nanotubes and buckytubes into copper alloys is conducive to the resulting composites having high strength, low thermal expansion coefficients, and thermal conductivity, and particularly improves their wear resistance.

(2) Particle-reinforced copper matrix composites

The preparation methods for particle-reinforced copper matrix composites are similar to those of other particle-reinforced metal matrix composites and include conventional casting, conventional powder metallurgy, the co-deposition method, and the internal oxidation method. Tungsten, molybdenum, tungsten carbide, and alumina are usually used as reinforcements because of their high-temperature hardness, high melting points, and anti-adhesion properties. Using the powder metallurgy method, the reinforcements and Cu powders are mixed and are then sintered together to form copper matrix composites.

In addition, there are nanoparticle-reinforced copper matrix composites and particle-reinforced copper amorphous alloy matrix composites. For example, the nano- Al_2O_3 -reinforced Cu-0.3%Al composite prepared by the internal oxidation method shows good performance and has micro-hardness of more than 1000 MPa. Zirconium carbide particle-reinforced copper amorphous alloy matrix composites exhibit tensile strengths of up to 2200 MPa.

(3) In situ reinforced copper matrix composites

In situ reinforced copper matrix composites are fabricated by the following method. By forging, drawing, or rolling a series of Cu-X alloys, the X metals form filamentous or zonal distributions along the deformation direction, and consequently form Cu-X microstructure composites. During the drawing and rolling process, the X elements are elongated under the axial force into filamentous or zonal distributions with thicknesses of less than 10 nm. The contribution of the filamentous body to the overall strength of the microstructural composites is not large, because thinning of the filamentous body can increase the phase interface and hamper dislocation movement.

Cu-X microstructure composites exhibit not only ultrahigh strength (maximum tensile strength of more than 2000 MPa) and very high electric conductivity, but also good heat resistance, excellent composite microstructures, and high-preferred grain orientations. These composites can be used to produce thrusters and heat exchangers beside point welding electrodes. Compared with traditional copper alloys, the alloy elements of such composites have greater content and fewer types. The X materials include the refractory metals (W, Mo, Nb, and Ta), and other elements (e.g., Cr, Fe, V). Cu-X composites can be divided according to the X elements into two categories.

- 1) The X elements are refractory metals with high melting points and good heat resistance (e.g., W, Mo, Nb, Ta). As strengthening elements, the refractory metals have a good strengthening effect on the X-Cu composites.
- 2) Although the refractory metals exhibit good strengthening effects when acting as the strengthening phase, their cost is relatively high. In situ reinforced Cu-Fe, Cu-Cr, Cu-V, and other copper matrix composites have high strength with low cost. Their strengths are also above 1000 MPa, although this strength is lower than that of the Cu-Nb category. In such microstructured composites, the Cr, Fe, and V elements with band or filamentous shapes are also distributed along the axial direction.

3.1.3 Titanium Matrix Composites

Titanium matrix composites (TMCs), with their high specific strength, high specific stiffness, and good high-temperature resistance, are widely used in the aerospace

industry. TMC material research began in the 1970s. In the mid-1980s, the implementation of the National Aerospace Plane (NASP) and Integrated High-Performance Turbine Engine Technology (IHPTET) programs in the USA along with similar development projects in Europe and Japan played a major role in promoting the development of TMCs.

TMCs can be divided according to their reinforcement types into two categories: continuous fiber-reinforced titanium matrix composites and discontinuous particle- or whisker-reinforced titanium matrix composites [10–12].

3.1.3.1 Continuous Fiber-Reinforced Titanium Matrix Composites

The continuous fiber reinforcements used are mainly ceramic fibers such as alumina, boron carbide, and silicon carbide, and they exhibit high melting points, good thermal stability, high specific strengths, and high specific stiffnesses. Among these ceramic fibers, both alumina and boron fibers have thermal expansion coefficients that are very close to that of the titanium matrix, but boron fibers cannot resist high temperatures and alumina fibers react very strongly with the titanium matrix, so their applications are significantly restricted. At present, carbon-coated SiC fibers are commonly used in industry. Continuous SiC fiber-reinforced TMCs offer high specific strength, high specific stiffness, high service temperatures, and good fatigue and creep properties. For example, SCS-6 SiC/IMI834 composites developed in Germany have tensile strengths up to 2200 MPa and elastic moduli up to 220 GPa. These composites also exhibit extremely high thermal stability, and their mechanical properties are not reduced after heat exposure at 700 °C for 2000 h. Replacing compressor disks with TMC leaf joints can reduce component weight by 70%. Using the Pratt & Whitney's XTC-65 IHPTET demonstrator machine, TMC leaf joints fabricated in the USA have been successfully shown to satisfy performance requirements. Britain, France, and Germany have also developed TMC leaf joints and have successfully conducted bench tests.

The preparation of continuous fiber-reinforced titanium matrix composites is difficult and generally includes only two steps: synthesis through a solid-phase method and compaction forming through HIP or vacuum hot pressing (VHP).

3.1.3.2 Discontinuous Particle-Reinforced Titanium Matrix Composites

Reinforcements for particle-reinforced titanium matrix composites (PTMCs) include carbides such as TiC, B₄C, and SiC; borides such as TiB and TiB₂; metal oxides such as Al₂O₃, Zr₂O₃, and R₂O₃ (where R is a rare earth element); and intermetallic compounds such as Ti₃Al, TiAl, and Ti₅Si₃. Among these particles, the most commonly used reinforcements are TiB, TiB₂, and TiC.

Various preparation methods can be used to fabricate particle-reinforced titanium matrix composites, and they include melt casting, powder metallurgy (PM),

mechanical alloying (MA), self-propagating high-temperature synthesis (SHS), and the XD™ process (exothermic dispersion).

Melt casting for preparation of discontinuous reinforced titanium matrix composites has excellent qualities such as a simple process, good feasibility, and low costs and offers easy preparation of complex components. However, it also has weaknesses such as the strong reactivity of both titanium and the reinforcement in the liquid phase, poor wettability between the matrix and the reinforcement and uneven reinforcement distribution. To overcome these disadvantages, in situ synthesis melt casting has been investigated. In this method, carbon, boron, and other elements are added to the molten titanium metals, or other reactive gases are input into the molten titanium metals, and they then react with the liquid titanium alloys to form in situ products such as TiC and TiB particle reinforcements. The in situ synthesis of reinforcements can overcome the poor wettability between the reinforcement and the matrix to produce a uniform reinforcement distribution and consequently enhance the titanium matrix composite performances.

Using PM to fabricate titanium matrix composites can not only eliminate the melt casting defects, but can also adjust the particle size and volume fraction over a wider range. By using near-net-shape technologies, including PM densification technology (cold isostatic pressing and hot isostatic pressing) and powder injection molding processes, high-density particle-reinforced titanium matrix composites can be prepared in temperature ranges that are far lower than the melting point, consequently avoiding the high reactivity of liquid titanium and greatly reducing the machining required.

MA technology is used to fabricate nanoalloy powders with non-equilibrium states. Through cyclical processes of deformation, cold welding, breaking, then bonding again, and then breaking again, the powders can be refined to the nanometer scale, consequently forming a high activity surface. Because of the introduction of multiple distortion defects, the interdiffusion is enhanced and the activation energy is reduced, which consequently induces both the thermodynamics and the kinetics of the mechanical alloying process to differ from those of the common solid-state process. Therefore, the mechanical alloying method may be used to prepare many new alloys that are difficult to synthesize under conventional conditions, such as TiB/Ti, TiC/TiAl, and other discontinuous reinforced titanium matrix composites.

Self-propagating high-temperature synthesis (SHS) is an in situ synthesis technology. The process is as follows: Through an exothermic reaction, the raw material mixtures can react spontaneously and continuously, consequently producing the metal ceramics or compounds. This method is also known as combustion synthesis. The SHS method has advantages including simple processing, rapid reaction times, and reduced power consumption. This technology can be used to synthesize carbides, borides, silicides, and nitrides. However, it is necessary to perform densification because of the difficulty in controlling the reaction process and the high porosity of the products.

The XD™ Process is also an in situ synthesis technology, developed on the basis of SHS. First, the various raw powders used to synthesize the products are mixed

and compacted and are then heated to the temperature for automatic combustion synthesis. Finally, through an exothermic reaction between the raw powders, the required products are synthesized. This technology can be used to prepare borides, carbides and nitride reinforced Ti, TiAl, or Ti₃Al, and other titanium matrix composites.

The in situ synthesis method can also be used to fabricate titanium matrix composites. This method is conducive to preparation of high-performance composites because it can avoid the contamination caused by adding particles and resolve the problems of wettability between the ceramic particle and the matrix alloy. The melt casting, PM, and MA methods can be used to synthesize in situ particle-reinforced titanium matrix composites. TiB, TiB₂, and TiC particle-reinforced titanium matrix composites fabricated by in situ synthesis methods have good mechanical properties.

3.1.4 Magnesium Matrix Composites

Magnesium, which has extremely rich reserves on earth, is the lightest metallic material among the structural materials in nature, in which the density of pure magnesium is 1.74 g/cm³. Magnesium has high specific strength, high specific stiffness, good damping properties, and excellent processing performance. Therefore, magnesium and its alloys promise to become one of the most widely used metal materials in high-tech industries in the twenty-first century. However, magnesium alloy applications are restricted by their low hardness, low strength, low modulus, poor wear resistance, and high thermal expansion coefficient. Magnesium matrix composites can overcome or reduce these inadequacies of magnesium alloys; consequently, these composites also become the lightweight metal matrix composites with the most competitive advantages after aluminum matrix composites. Magnesium matrix composites exhibit high specific stiffness and high thermal conductivity, and some of their performance levels exceed those of aluminum matrix composites, giving them broad application prospects in the aerospace and automobile industries [13, 14].

Magnesium matrix composites can be divided according to their reinforcement types into three categories: continuously reinforced magnesium matrix composites, discontinuously reinforced magnesium matrix composites, and in situ reactive self-reinforced magnesium matrix composites.

3.1.4.1 Continuous Fiber-Reinforced Magnesium Matrix Composites

The main continuous reinforcements for magnesium matrix composites can be divided into two categories: Al₂O₃ fibers and carbon (graphite) fibers. Carbon (graphite) fiber-reinforced magnesium matrix composites are the most widely investigated type. The main methods used for their preparation are pressureless

infiltration or low-pressure infiltration. Graphite fiber-reinforced magnesium matrix composites have a low density of less than 2.1 g/cm^3 , a controllable thermal expansion coefficient from both negative and positive values, good dimensional stability, high specific strength, high specific stiffness and high damping properties. Carbon (graphite) fiber-reinforced magnesium matrix composites have been prepared in Japan, and their strength and elastic modulus values have reached 1200 MPa and 570 GPa, respectively. Continuous fiber-reinforced magnesium matrix composites have very broad application prospects in the aerospace and automotive fields. NASA has used graphite (Gr)/Mg composites to fabricate components including space power recovery system components, space station struts, and space mirror holders. However, their development is limited by the high cost of the long fibers and the difficulties of composite preparation.

3.1.4.2 Discontinuously Reinforced Magnesium Matrix Composites

Discontinuously reinforced magnesium matrix composites exhibit not only high strength, high modulus, high hardness, excellent wear resistance, and good damping properties, but also excellent machinability, good dimensional stability, and isotropic properties, which are advantageous for structure design.

Commonly used discontinuous reinforcements include short fibers (Al_2O_3), whiskers (SiC and $\text{Al}_{18}\text{B}_4\text{O}_{33}$), and particles (SiC and B_4C). The choice of reinforcement is based on the factors such as the intended composite applications, the fabrication methods, and the reinforcement cost. Magnesium alloy matrix materials can be divided into two categories: cast magnesium alloys and wrought magnesium alloys. The material is selected according to the factors such as the matrix alloy performance, wettability between the matrix and the reinforcement, and the interfacial reactions.

The preparation methods for discontinuously reinforced magnesium matrix composites can be divided into the following types: liquid metal infiltration (including squeeze casting, vacuum-pressure infiltration, and spontaneous infiltration), stirring casting, rheological casting, PM methods, and spray co-deposition.

The squeeze casting method is a most extensive and successful technology for preparation of short fiber- and whisker-reinforced magnesium matrix composites. It has been successfully used to fabricate Al_2O_3 short fiber-reinforced AZ91 and Mg–Zn composites, Al_2O_3 short fiber, and carbon silicon particle hybrid reinforced MSR alloy, SiC whisker-reinforced AZ91, AZ31, and Mg–Li composites, and $\text{Al}_{18}\text{B}_4\text{O}_{33}$ whisker-reinforced AZ91 and Mg–Zn magnesium matrix composites. Among these composites, SiC whisker-reinforced magnesium matrix composites have the best mechanical properties, and their properties vary with the reinforcement volume fraction, giving them strengths between 330 MPa and 370 MPa and elastic moduli between 80 GPa and 110 GPa. These composites also exhibit good heat resistance and interface stability. However, the preparation methods used to limit the reinforcement volume fraction range, which is generally in the range of 15–30%.

Several preparation methods can be used to fabricate particle-reinforced magnesium matrix composites. The typical fabrication technology, stirring casting, has many advantages such as a simple process, low cost, and good reinforcement volume fraction controllability, and it can be used to prepare larger size composites with low reinforcement volume fractions. The Dow Chemical Company (USA) developed a patent on the stirring casting method to fabricate magnesium matrix composites and manufactured SiC particle- and Al₂O₃ particle-reinforced AZ91, AZ31, and AZ61 magnesium matrix composites. The total weight of the fabricated composites reached 70 kg. In addition, PM, spray deposition, and squeeze casting are commonly used to prepare particle-reinforced magnesium matrix composites. For both the PM and spray deposition methods, the processing is more complex, the fabrication costs are higher, and the size of the prepared composite is limited. For particle-reinforced composites prepared by the squeeze casting method, the reinforcement volume fraction is generally above 45%, which consequently reduces the material machinability and limits the finished product size.

Discontinuously reinforced magnesium matrix composites exhibit low density, high wear resistance, high specific stiffness, excellent dimensional stability, and high-temperature performance. Therefore, they can be used to produce not only aerospace components such as satellite antennas and helicopters, but also car parts, including discoid impellers, piston ring grooves, gears, transmission bearings, differential bearings, forks, connecting rods, and rockers.

The Dow Chemical Company used Al₂O_{3p}/Mg composites to manufacture wear-resistant parts such as belt pulleys, sprockets, and pump covers; one car pump cover has traveled a total of 160,000 km. Simultaneously, this company has produced pumps consisting entirely of Al₂O_{3p}- and SiC_p-reinforced magnesium matrix composites for fabrication of car bearings, pistons, cylinder liners, and other car parts. The Textron Company and the Dow Chemical Corporation used SiC_p/Mg composites to produce airscrews, missile rudders, and internal cylinders. The US Office of Naval Research and Stanford University used B₄C_p/Mg–Li and B_p/Mg–Li composites to prepare aircraft antennas. The Fujitsu Company (Japan) used B_p/Mg–9 wt%Al composites to manufacture computer peripheral devices such as disk drives. Magnesium Elektron Ltd. (MEL, UK) has developed a series of specially designed discontinuous fiber-reinforced magnesium matrix composites with low costs, and recoverable and reusable values, as well as meeting their application requirements Electron. This company developed SiC_p/Mg–Zn–Cu–Mn tubular products and used them to manufacture a three-wheel bike.

3.1.4.3 In Situ Reactive Self-Reinforced Magnesium Matrix Composites

The preparation methods for in situ reactive self-reinforced magnesium matrix composites can overcome the shortcomings of other preparation methods, such as the process complexity, the thermodynamic instability of the matrix–reinforcement

interface, degraded performance caused by poor wettability between matrix and reinforcement, and the non-uniform reinforcement distribution. This is because the relatively uniformly distributed reinforcements can be synthesized into the matrix through an exothermic reaction. However, both the reinforcement and the matrix are approximately in an equilibrium state, and their low-energy interface induces the in situ composites to essentially be in a stable state. Meanwhile, the morphology and size of the in situ synthesis reinforcements can be controlled.

The preparation methods used for in situ reaction-reinforced magnesium matrix composites include stirring casting, MA, and the molten salt auxiliary synthesis method. The main material systems involved are Mg_2Si/Mg , MgO/Mg , TiC/Mg , TiB_2/Mg , and quasicrystalline Mg_3YZn_6/Mg .

3.1.5 Other Metal Matrix Composites

Along with the aluminum, magnesium, titanium, and copper matrix composites described above, there are also other metal matrix composites, such as zinc, iron, steel, nickel, silver, and refractory metal (tungsten, tantalum, niobium, molybdenum) matrix composites [15–17].

3.1.5.1 Zinc Matrix Composites

Zinc matrix composites with good wear resistance can be used for delivery vehicles and mechanical equipment components such as transmission gears, wheels, and other special wear-resistant components. Zinc matrix composites overcome the disadvantages of zinc alloys, such as their great loss of strength and hardness at high temperatures and their larger thermal expansion coefficients. Their high-temperature properties and other properties, such as their tribological properties, are also improved. When compared with zinc alloys, zinc matrix composites have the following advantages: higher strength at high temperatures, better wear resistance, higher hardness and elastic modulus, evidently increased fatigue life and high-temperature creep resistance, and lower thermal expansion coefficient. The reinforcements used for zinc matrix composites include graphite and carbon fibers, silicon carbide particles and whiskers, alumina particles and whiskers, and modified silicon and steel wires. The addition of both graphite and carbon fibers into zinc alloys can form a carbon-rich layer on the zinc surface, which consequently improves the tribological properties of the zinc alloys. Such materials are referred to as anti-friction zinc matrix composites. When the addition of other reinforcements enhances the zinc alloy strength, the resulting composites are called reinforced zinc matrix composites. With increasing reinforcement content, the tensile strength of

zinc matrix composites reaches a peak value, and the wear resistance increases. The fabrication methods used for zinc matrix composites include stirring casting, liquid infiltration, squeeze casting, and the spray deposition method.

3.1.5.2 Iron Matrix Composites

Iron matrix composites have been developed to satisfy the requirements for structural parts working under high-temperature, high-speed and high wear resistance conditions, such as the roll collar and guide wheel of a high-speed wire rod mill. Iron matrix composites can be divided into in situ composites, iron/metal-laminated composites, iron/ceramic-laminated composites, fiber-reinforced composites, and particle-reinforced composites. Fiber (tungsten, molybdenum, and titanium diboride)-reinforced Fe metal matrix composites have been successfully prepared. Many particles are used to reinforce iron, such as SiC, TiC, TiN, WC, VC, ZrO₂, WO₃, CeO₂, ThO₂, CaS, and Cr₃C₂. The preparation methods used for iron-based composites include PM, stirring casting, and in situ reaction techniques. The fabrication methods used for iron matrix surface-layer composites include the casting infiltration and casting sintering methods.

3.1.5.3 Steel Matrix Composites

Steel matrix composites are compounded by adding hard phases with good stability and anti-corrosion and antioxidation interfaces into the steel matrix with its high strength and high-temperature oxidation resistance, so the tribological properties of the material at high temperatures can be enhanced very greatly. Particles are the main reinforcement type used for steel matrix composites. TiB₂ particle-reinforced steel matrix composites with different volume fractions were prepared in the UK using PM, and their strengths can reach 1100 MPa. TiC, WC, SiC, VC, and other particles can also be used as reinforcements for steel matrix composites. The preparation methods used also include cast sintering and cast infiltration.

3.1.5.4 Nickel Matrix Composites

As the matrixes of high-temperature self-lubricating wear-resistant composites, nickel alloys have excellent high-temperature mechanical properties, good oxidation resistance and corrosion resistance and thus are the most commonly used matrix materials among the high-temperature self-lubricating alloys. Nickel matrix composites are mainly used for the full-flow cycle engine in liquid rocket engines, and also as highly wear-resistant coating layers. MoS₂-reinforced nickel matrix composites produced by PM have good self-lubricating anti-friction properties at high temperatures. Carbon nanotube-reinforced In1600 nickel alloy composites

prepared by rapid solidification exhibit perfect bonding between matrix and reinforcement and show a good strengthening effect.

3.1.5.5 Refractory Metal Matrix Composites

The research into refractory metal matrix composites began in the 1950s and 1960s. As a new kind of engineering material, refractory metal matrix composites have excellent physical and mechanical properties, including high strength, low density, good corrosion resistance, and heat resistance, and consequently attract widespread attention.

Ceramic particle-reinforced tungsten matrix composites with high melting points, such as ZrC or TiC particle-reinforced tungsten matrix composites produced by PM, can overcome these problems. The USA has developed special tungsten matrix composites to replace the lead content in light weapons ammunition.

Having solved their corrosion problems, tantalum matrix composites, such as the Ta-Ta₂C composites developed in the USA, can be used in certain harsh environments, including chlorine, molten salts, and molten metals. The preparation process for these materials is as follows. First, the carbides are coated on the parts; then, the carbide coating layer is melted into the matrix material; finally, the required microstructure is obtained by aging treatment of the materials.

Compared with other refractory metals, molybdenum and niobium series alloys are more compatible for using as high-temperature metal structural materials because of their high melting points, high elastic moduli, and low densities. However, pure molybdenum and niobium solid solutions have lower high-temperature strengths and lower antioxidant capacities. Therefore, molybdenum and niobium matrix composites have been developed to overcome these shortcomings. For example, in situ Nb₅Si₃- or Nb₃Si-reinforced niobium-silicon matrix composites have high melting points, high stiffnesses, low densities, and improved high-temperature strengths. Tungsten alloy wire-reinforced niobium matrix composites were developed in the USA, and their working temperatures can reach 980–1650 °C. Niobium matrix composites can be divided according to their reinforcement types into four categories: continuous fiber-, short fiber (such as Al₂O₃ fibers)-, layered Nb–ZrO₂-, and lamellar Nb–ZrO₂-reinforced niobium matrix composites. Niobium matrix composites are mainly used in aerospace propulsion systems and space nuclear power reactor components.

In addition to the metal matrix composites described above, there also are silver-based, lead-based, cobalt-based, and other metal-based composites. Silver-based composites with their good electrical conductivity and thermal conductivity can be used as contact materials for high-voltage and low-voltage apparatuses (such as brushes). Lead-based composites not only inherit the good anti-friction properties of the matrix, but also overcome the poor wear resistance of the matrix.

3.2 Properties of Metal Matrix Composites

The development of modern science and technology requires increasingly high standards for material properties. In particular, the development of advanced science and technology in the aerospace and military fields means that no single material can meet all the requirements of an actual project, and this has promoted the rapid development of metal matrix composites. Compared with traditional metal materials, metal matrix composites have relatively high specific strength, specific stiffness, and abrasion resistance. Compared with resin-based composite materials, metal matrix composites have excellent electrical and thermal conductivity, and better high-temperature properties and welding ability. When compared with ceramic materials, metal matrix composites have advantages such as high toughness, high impact resistance, and low linear thermal expansion coefficients.

Acceptable metal matrix composites should have low density and mechanical properties that can be compared with that of the applied engineering materials. Successful metal matrix composites should show low density, obvious temperature advantages, and certain mechanical properties. For these reasons, when compared with currently used materials such as advanced Al alloys, Ti alloys, and high-temperature alloys, most research results for metal matrix composites are expressed in terms of the density normalization property (σ/ρ).

3.2.1 *Physical Properties of Matrix Materials and Reinforcements*

3.2.1.1 Reinforcements of Metal Matrix Composites

The reinforcement is an important constituent part of metal matrix composite materials. The introduction of reinforcements can obviously improve the strength, modulus, heat resistance, and wear resistance properties of the metal matrices. Therefore, the properties of metal matrix composites are closely related to the selected reinforcements. The reinforcements of metal matrix composites should have the following basic features [17, 18].

- 1) The reinforcements should have excellent chemical stability. During the high-temperature preparation process and the application process, the structures and properties of the reinforcements will not show any obvious changes or degeneration. The reinforcements must have good chemical compatibility with the matrix materials, so no serious interface reactions that would damage the combination of the interfaces will occur.
- 2) The reinforcements and the matrix materials should have good wetting properties. Alternatively, after surface treatment, the reinforcements will have a good wetting state with the matrix materials to ensure a good compounding

effect between the reinforcements and the matrix during the preparation process.

- 3) The reinforcements should obviously have properties that can meet the requirements of the metal matrix. This will enable the metal matrix composites to meet the design requirements. The metal matrix composites will have excellent overall properties, such as high specific strength, high specific stiffness, high wear resistance, and a low thermal expansion coefficient.

In recent years, along with the improvements in reinforcement materials manufacturing technology, many more types of reinforcements have been developed. To design and prepare high-quality metal matrix composites, reasonable reinforcements should be selected. Here, the reinforcements that can be used for metal matrix composites will be classified simply. The reinforcements are divided into non-continuous and continuous strengthening reinforcements. The non-continuous strengthening reinforcements mainly include short fibers, whiskers, and particles, and the continuous strengthening reinforcements are long fibers.

- 1) Particles: SiC, Al₂O₃, B₄C, et al.
- 2) Whiskers: SiC, Al₂O₃, TiN, et al.
- 3) Short fibers: Al₂O₃, B₂O₃, Al₂(SiO₃)₃, TiN, et al.
- 4) Continuous strengthening reinforcements: C (graphite) fiber, SiC fiber (single or multi-filament), B fiber, Al₂O₃ fiber, Mullite fiber, et al.
- 5) Metal wires: W wire, stainless steel wire, iron wire, et al.

(1) Non-Continuous Strengthening Reinforcements

In general, particle reinforcements are nonmetal particles such as ceramics and graphite, which have high strength, high modulus, heat resistance, wear resistance, and high-temperature-resistance abilities. Particle reinforcements are very fine powders (<50 μm, and generally less than 10 μm), and they play a role in improving the wear resistance, heat resistance, and modulus of the metal matrix materials. Metal matrix composites are basically produced by the PM method, the liquid metal paddling process, the mutual spray method, and the pressure impregnation method. The cost of the particle reinforcements is very low, and the metal matrix composites produced by the introduction of the particle reinforcements are isotropic. Thus, particle reinforcements developed rapidly in the composite field, and especially quickly in the automobile industry.

Table 3.1 illustrates the properties of the particle reinforcements that are widely used in metal matrix composites.

Whiskers are fine single crystals which are grown under artificial conditions. With their fine dimensions, whiskers have few structural defects and have high strength and modulus. Generally, the diameters of whiskers are 0.2–1 μm and their lengths reach several tens of micrometers. The most commonly used whiskers in metal matrix composites are ceramic whiskers, such as SiC and Al₂O₃. Because whiskers are very fine, they have to be produced in preforms and then the composites are manufactured via the squeeze casting method. The properties of

Table 3.1 Properties of particle reinforcements used in metal matrix composites

Particle	Density (g cm^{-3})	Melting point ($^{\circ}\text{C}$)	Linear expansion coefficient (10^{-6}K^{-1})	Heat conductivity (KJ (cm K)^{-1})	Hardness (GPa)	Bending strength (MPa)	Elastic modulus (GPa)
SiC	3.21	2700	4.0	0.7524	27	400–500	–
B ₄ C	2.52	2450	5.73	–	30	300–500	360–460
TiC	4.92	3200	7.4	–	26	500	–
Al ₂ O ₃	–	2050	9	–	–	–	–
Si ₃ N ₄	3.2–3.35	2100	2.5–3.2	0.1254–0.2926	HAR89– 93	900	330
Al ₂ O ₃ ·SiO ₂	3.17	1850	4.2	–	–	–	–
TiB ₂	4.5	2980	–	–	–	–	–

whisker-reinforced metal matrix composites are basically isotropic. However, because these composites have a secondary processing feature, after extrusion or rolling deformation, the properties of the whisker-reinforced metal matrix composites are basically anisotropic. The properties of the whiskers that are used in metal matrix composites are shown in Table 3.2.

The main reasons for the high costs of composite materials are the production procedures used and, in particular, the high prices of the reinforcement materials. Because the whiskers have fine dimensions and no defects, they have very high elastic modulus and strength properties, and they are widely known for their excellent micro-reinforcement and filling capabilities. To date, more than 100 types of whiskers have been developed in laboratories, and they include carbides, nitrides, oxides, sulfides, salts, intermetallic compounds, metals, and graphite. Among these whiskers, only a few types can actually be used in composites. Development of low-cost and high-performance whiskers is an important research target for the future development of metal matrix composites.

The lengths of the short fibers are generally dozens of millimeters. The properties of the short fibers are lower than those of the longer fibers. Before use, short fibers should be produced as a preform, felt, or cloth. Then, the metal matrix composites are produced by squeeze casting and pressure impregnation methods. The short fibers that can be selected are aluminum silicate fibers (fireproof cotton), Al_2O_3 fibers, C fibers (directly produced or cut from long C fibers), and boron nitride fibers. The properties of the short fibers used in metal matrix composites are shown in Table 3.3.

(2) Continuous reinforcements

The lengths of all the continuous reinforcements (long fibers) are more than several hundred meters. In general, the long fibers have very high strength and elastic modulus properties. The continuous fibers are divided into single fibers and bonded fibers. C (graphite) fibers, Al_2O_3 fibers, SiC fibers (by a sintering process), and Si_3N_4 fibers are used as a batch of fibers composed of 500–12000 single fibers

Table 3.2 Properties of whiskers used in metal matrix composites

Whisker	Density (g cm^{-3})	Melting point ($^{\circ}\text{C}$)	Tensile strength (MPa)	Elastic modulus (GPa)
Al_2O_3	3.9	2082	13800–27600	482.3–1033
AlN	3.3	2199	13800–20700	344
BeO	1.8	2549	13800–19300	689
B_4C	2.5	2449	6900	448
C (graphite)	2.25	3593	20000	980
SiC (α)	3.15	2316	6900–34000	482
SiC (β)	3.15	2316	6900–34000	550–820
Si_3N_4	3.2	1899	3400–10000	379

Table 3.3 Properties of short fibers used in metal matrix composites

Short fiber	Diameter (μm)	Density (g cm^{-3})	Tensile strength (GPa)	Elastic modulus (GPa)
SiC fiber	10–20	2.32	1.8–2.0	180–190
Al_2O_3 fiber	5–7	3.2	0.8–1.0	130–190
Aluminum silicate	2–5	2.5–3.0	0.6–0.8	70–80
Boron nitride	5–7	1–9	1	70

with diameters of 5.6–14 μm . In contrast, B fibers and SiC fibers (by chemical vapor deposition processes) are used as single fiber forms with diameters of 95–140 μm . The properties of the continuous fibers used in metal matrix composites are shown in Table 3.4.

3.2.1.2 Matrix Materials of Metal Matrix Composites

Many types of alloys could be used as matrix materials in metal matrix composites, including Al and Al alloys, Mg alloys, Ti alloys, Ni alloys, Cu and Cu alloys, Zn alloys, Pb, and AlTi and AlNi intermetallic compounds. There are also many available kinds of reinforcements. The fibers used are C fibers, graphite fibers, B fibers, and oxide fibers. The whiskers used are mainly SiC whiskers, Al_2O_3 whiskers, and C whiskers. It is very important to properly select the types and chemical composition of matrix materials to fully use the specific characteristics of the matrix materials and the reinforcements, and meet the application requirements. When selecting the matrix materials, the following aspects should be considered.

(1) The application requirements of the metal matrix composites

The functional characteristics requirements of metal matrix composite parts are the main reference points for selection of the matrix materials and the reinforcements. Across the fields of space flight, aviation, advanced weapons, automobiles, engines, gas turbines, and electronics, the requirements for composite parts have significant differences. Therefore, we need to select different matrix materials and reinforcements according to the application requirements.

- 1) In the space flight and aviation fields, the most important requirements are high specific strength, high specific stiffness, and excellent dimensional stability. Therefore, low-density alloys such as Mg alloys and Al alloys can be selected as matrix materials, and the high-strength, high-modulus graphite fibers and B fibers can be used to produce continuous fiber composites for spacecraft and satellite components. For example, the elastic modulus of graphite fiber-reinforced magnesium matrix composites is higher than 345 GPa and the density is less than 2.1 g/cm^3 . This composite is therefore

Table 3.4 Properties of continuous fibers used in metal matrix composites

Continuous fibers	Fiber brand	Diameter (μm)	Density (g cm^{-3})	Tensile modulus (GPa)	Tensile strength (MPa)	Failure elongation (%)	Longitudinal direction linear expansion coefficient (10^{-6}K^{-1})
B	B	32–140	2.4–2.6	365–400	2300–2800	1.9	4.5
	B/W	100	2.57	410	3570	0.9	–
	B/C	100	2.58	360	3280	–	–
	B ₄ C–B/	145	2.57	370	4000	–	–
	Borsic	100	2.58	400	3000	–	–
SiC	SCS-2	140	3.05	407	3450	0.8	–
	SCS-6	142	3.44	420	3400	–	–
	Tyranno	1	2.4	120	2500	2.2	–
	Dow Corning	10–15	2.6–1.7	175–210	1050–1400	–	–
	Nicalon NL-201	15	2.55	206	2940	1.4	3.1
	Nicalon NL-221	12	2.55	206	3234	1.6	3.1
	Nicalon NL-401	15	2.30	176	2744	1.6	3.1
	Nicalon NL-501	15	2.50	206	2940	1.4	3.1
C	Amoco T-300	7	1.76	231	3650	1.4	–0.6
	Torayca-T1000	5.3	1.82	294	7060	–	–
	Torayca-M46 J	–	–	451	4210	–	–
	Torayca-M60 J	5	1.94	590	3800	–	–
	Thornel p120	10	2.18	827	2370	0.29	–1.45
	Thornel p100	10	2.15	724	2370	0.32	–1.45
Al ₂ O ₃	Nericl 312 (3 M)	11	2.7	154	1700	1.85	–
	FP	20	3.95	379	1380–2100	0.4	6.8
	Sumitomo	9	3.20	250	2600	–	–
	Saffil	3	3.30	300	2000	1.5	–
	Sumika	17	3.2	210	1775	0.8	8.8
	Nextel	13	2.5	152	1720	1.95	–
	Dupont	20	4.2	385	2100–2450	–	–
Si ₃ N ₄	Tonen	10	2.5	250	2500	–	–
BN	–	7	0.90	91	1400	–	–
ZrO ₂	–	–	4.84	350	2100	–	–
B4C	–	–	2.36	490	2300	–	–
TiB ₂	–	–	4.48	520	1100	–	–
W	–	13	1.94	413	4060	–	–
Steel	–	13	7.74	203	4200	–	–
Be	–	100–250	1.8	250	1300	–	–

suitable for use in space dynamic recovery system components, such as the stay bar in a space station, or a space mission mirror holder.

- 2) High-performance engines require the composite material to have not only high specific strength and a high specific modulus, but also excellent high-temperature-resistance ability. The composite material should have long-term normal operating ability in high-temperature oxidation atmospheres. Al and Mg alloys are thus unsuitable for this kind of composite. Ti alloys, Ni alloys, and intermetallic compounds can be selected as the matrix materials, and high-performance SiC fibers, or TiC and TiB₂ particles should be selected as the reinforcements. For example, SiC fiber-reinforced Ti alloy matrix composites and W fiber-reinforced Ni superalloy matrix composites can be used for important components such as jet blades and transmission shafts.
 - 3) The components in automotive engines require heat resistance, wear resistance, and low linear expansion coefficients and appropriate strength at certain temperatures. At the same time, they should also be low cost and suitable for mass production. Al alloys and ceramic particles or short fibers are usually selected to produce the composites. For example, SiC/Al, C/Al, and Al₂O₃/Al composites can be used as pistons, cylinder liners, and pitmans in engines.
 - 4) Electronic integrated circuits need metals and composites with high melting points, high heat conductivity, and low heat expansion coefficients to act as heat-loss components and base plates. Silver, copper, and aluminum, which have excellent electrical and heat conductivity properties, are usually selected as the matrix materials, and graphite fibers, which have low heat expansion coefficient and high-modulus properties, are selected as reinforcements.
- (2) The metal matrix materials of structural composites

Generally, the composites used in the fields of space flight, aviation, and advanced weapons require high specific strength, high stiffness, and high structural efficiency. Usually, Al, Al alloys, Mg, and Mg alloys are selected as matrix materials for these kinds of composites. However, the Al matrix composites and Mg matrix composites can be only applied at temperatures of less than 450 °C. In engines, and especially in gas turbines, heat-resistant composites are required. These composites can continuously and safely work at high temperatures in the 650–1200 °C range, and the composites should have excellent oxide resistance, creep resistance, fatigue resistance, and good high-temperature mechanical properties. Ti matrix composites can be used at 650 °C, and Ni and Co matrix composites can be used at temperatures up to 1200 °C. The developing intermetallic compound matrix composites can be used at even higher temperatures.

The matrixes of structural composites can basically be divided into two groups: light metal matrixes and heat-resistant alloys.

- 1) Light alloys for use at less than 450 °C. At present, the metal matrixes used at less than 450 °C are Al, Mg, and their alloys. Al matrix and Mg matrix composites are usually used in space flight, satellites, space stations, automotive engine components and brake wheels, and these composites are

already in commercial-scale production. For different types of composites, appropriate Al or Mg alloys should be selected as the matrixes. For continuous fiber-reinforced metal matrix composites, pure Al or single-phase Al alloys with alloying elements should be selected. However, for particle- or whisker-reinforced metal matrix composites, high-strength Al alloys are selected. The compositions and properties of the commonly used Al and Mg alloys are shown in Table 3.5.

- 2) The metal matrixes used in the 450–700 °C range. Considered from the viewpoint of density and mechanical properties, the structural metals that can be used in the 450–700 °C range are Ti and its alloys. After reinforcement with high-performance SiC fibers, or with TiC or TiB₂ particles, the high-temperature properties of Ti and its alloys showed obvious improvement. SCS-6 SiC fiber-reinforced Ti composites have already been developed, and this material is used for the blade wheels and hollow blades of turbine engines, blade wheels and blades of gas compressors, drive shafts of engines and rocket engine cases.

The compositions and properties of the Ti alloys that are used in Ti matrix composites are shown in Table 3.6.

- 3) The metal matrixes of high-temperature composites used at over 1000 °C. The main metal matrix materials used at over 1000 °C are Ni, Fe matrix heat-resistant alloys and intermetallic compounds. Ni and Fe matrix alloys are commonly used. The intermetallic compounds and Nb matrix composites intended for use at even higher temperatures are still at the research stage. The high-temperature endurance properties and high-temperature creep properties of Fe and Ni matrixes can generally improve by 100 h, and the endurance strength can improve from one to three times. These materials are mainly used to produce important components such as high-performance aviation engine blades and turbine blades. The compositions and properties of the matrixes of high-temperature metal matrix composites are given in Table 3.7.

(3) Matrixes of functional metal matrix composites

Along with the development of electronic, information, energy, and automotive technology, increased emphasis is being placed on the development of functional metal matrix composites. These materials have extensive long-term potential. The development of the high-tech field requires excellent integrative physical properties for the materials and devices. At the same time, the materials should have high mechanical properties, high heat resistance, low heat expansion coefficients, high electrical conductivity, high arc erosion resistance, high friction coefficients, and high wear resistance. By depending only on metals and alloys, it is difficult to have excellent integrative physical properties. Therefore, we should depend on optimized design and advanced manufacturing techniques to produce metal matrix composites that meet our requirements. For example, in electronic integrated circuits, the degree of electronic device integration is increasingly high and the component

Table 3.5 Compositions and properties of Al and Mg alloys

Alloy trademark	Main component							Density (g cm ⁻³)	Linear expansion coefficient (10 ⁻⁶ K ⁻¹)	Heat conductivity (W (m K) ⁻¹)	Tensile strength (MPa)	Elastic modulus (GPa)
	Al	Mg	Si	Zn	Cu	Mn						
Commercial pure Al3	99.5	-	0.8	-	0.016	-	-	2.6	22-25.6	218-226	60-108	70
LF6	Balance	5.8-6.8	-	-	-	0.5-0.8	-	9.64	22.8	117	330-360	66
LY12	Balance	1.2-1.8	-	-	3.8-4.9	0.3-0.9	-	2.8	22.7	121-193	172-54	71
LC4	Balance	1.8-2.8	-	5-7	1.4-2.0	0.2-0.6	-	2.85	28.1	155	209-618	68
LD2	Balance	0.45-0.9	0.5-1.2	-	0.2-0.6	-	-	2.7	23.5	155-176	347-679	70
LD10	Balance	0.4-0.8	0.6-1.2	-	3.9-4.8	0.4-1.0	-	2.3	22.5	159	411-504	71
ZL101	Balance	0.2-0.4	6.5-7.5	0.3	0.2	0.5	-	2.66	23.0	155	165-275	69
ZL104	Balance	0.2-0.3	8.0-9.5	-	-	-	-	2.65	21.7	147	255-275	69
MB2	0.4-0.6	Balance	-	0.2-0.8	-	0.15-0.5	-	1.78	26	96	245-264	40
MB15	-	Balance	-	5.0-6.0	-	-	-	1.83	20.9	121	326-340	44
ZM5	7.5-7.9	Balance	-	0.2-0.8	-	0.15-0.5	-	1.81	26.8	78.5	157-254	41
ZM8	-	Balance	-	5.5-6.0	-	-	-	1.89	26.5	109	310	42

Table 3.6 Compositions and properties of Ti alloys

Alloy trademark	Main composition							Density (g cm ⁻³)	Linear expansion coefficient (10 ⁻⁶ K ⁻¹)	Heat conductivity (W (m K) ⁻¹)	Tensile strength (MPa)	Elastic modulus (GPa)
	Mo	Al	V	Cr	Zr	Ti						
Commercial pure Ti TAl	-	-	-	-	-	Balance	4.51	8.0	16.3	345-685	100	
TC1	-	1.0-2.5	-	-	-	Balance	4.55	8.0	9.2	411-753	118	
TC3	-	4.5-6.0	3.5-4.5	-	-	Balance	4.45	8.4	8.4	991	118	
TC11	2.8-3.8	5.8-7.0	-	-	0.3-2.0	Balance	4.48	9.3	6.3	1030-1225	123	
TB2	4.8-5.8	2.5-3.5	4.8-5.8	7.5-8.5	-	Balance	4.83	8.5	8.9	912-961	110	
ZTC4	-	5.5-6.8	3.5-4.5	-	-	Balance	4.40	8.9	8.6	940	114	

Table 3.7 Compositions and properties of matrix materials in high-temperature metal matrix composites

Alloys and compositions	Density (g cm^{-3})	Endurance strength 1100 °C, 100 h) (MPa)	High-temperature specific strength (1100 °C, 100 h) (10^3 m)
Zh36Ni-12.5-7 W-4.8Mo-5Al-2.5Ti	12.5	1.38	112.5
EPD-16Ni-22 W-6Al-6Cr-2Mo-1.5Nb	8.3	51	63.5
Nimocast 713C Ni-12.5Cr-2.5Fe-2Nb-4Mo-6Al-1Ti	8.0	48	61.3
Mar-M322E Co-21.5Cr-25 W-10Ni-3.5Ta-0.8Ti	-	48	-
Ni-35 W-15Cr-2Al-Ti	9.15	23	25.4

density per unit area is increasing; the power is also increasing and the problem of heat production is very serious. Materials with low linear heat expansion coefficients and high thermal conductivity can be used to produce base plate and package parts, which can remove heat rapidly, reduce thermal stress, and improve device reliability.

The materials systems and matrix alloys selected are different under different conditions. The available functional metal matrix composites (not including bimetal composites) are mainly used for electronic packaging in microelectronics techniques, high heat conductivity and arc erosion-resistant integrated circuit materials and electronic head materials, high-temperature- and wear-resistant materials, and corrosion-resistant battery plate electrode materials. The main selected metal matrixes are pure Al, Al alloys, pure Cu, Cu alloys, Ag, Pb, and Zn.

- 1) The metal matrix composites used in electronic packaging are high-SiC particle volume-reinforced Al matrix and Cu matrix composites, high-modulus graphite fiber-reinforced Al and Cu matrix composites, diamond particle or multi-crystal diamond fiber-reinforced Al and Cu composites, and B/Al composites. The matrixes of these composites are mainly pure Al or pure Cu.
- 2) The metal matrix composites that are used as wear-resistant parts are SiC, Al_2O_3 , and graphite particle-, whisker-, or fiber-reinforced Al, Mg, Cu, Zn, and Pb metal matrix composites. The most commonly used matrixes are Al, Mg, Zn, Cu, and Pb, and their alloys.
- 3) The metal matrix composites used for integrated circuit materials and electronic head materials are C (graphite) fiber-, metal wire-, and ceramic-reinforced Al, Cu, Ag, and their alloys.

The matrixes used in functional metal matrix composites basically have good thermal and electrical conductivity and good mechanical properties, but they have disadvantages such as high linear heat expansion coefficients and weak arc erosion resistance. Through the addition of proper reinforcements to these matrixes,

excellent integrative physical properties can be obtained and the materials can then meet any special requirements. For example, when graphite fibers or SiC particles with good heat conductivity, high modulus, and low thermal expansion coefficients are added to pure Al, the resulting composites will have high heat conductivity and will then meet the heat emission requirements for integrated circuit packaging.

3.2.2 Particle-Reinforced Metal Matrix Composites

3.2.2.1 Particle-Reinforced Al Matrix Composites

After the particles are introduced into Al alloys, the microstructures of the matrix alloys are changed and thus induce the changes in their properties [18–23]. The mechanical properties of Al matrix composites vary with the production procedure, the types, dimensions and volume fractions of reinforcements used, and the heat treatment procedure. The mechanical properties of some particle-reinforced Al matrix composites are shown in Table 3.8. It is clearly shown that the addition of

Table 3.8 Mechanical properties of particle-reinforced Al matrix composites

Composites	$\sigma_{0.2}$ (MPa)	σ_b (MPa)	δ (%)	E (GPa)	Manufacturer
Al ₂ O ₃ /6061Al 10% (T6)	296	338	7.5	81	Duralcan, Alcan
15% (T6)	319	359	5.4	87	Duralcan, Alcan
20% (T6)	359	379	2.1	98	Duralcan, Alcan
SiC _p /6061Al 15% (T6)	405	460	7.0	98	DWA
20% (T4)	420	500	5.0	105	DWA
25% (T4)	430	515	4.0	115	DWA
Al ₂ O ₃ /4024Al 10% (T6)	483	517	3.3	84	Duralcan, Alcan
15% (T6)	476	503	2.3	92	Duralcan, Alcan
20% (T6)	483	503	1.0	101	Duralcan, Alcan
SiC _p /2024Al 7.8% (T4)	400	610	5–7	100 105	British Petroleum
20% (T4)	490	630	2–4		British Petroleum
25% (T4)	405	560	3		DWA
SiC _p /7075Al 15% (T651)	556	601	2	95	Cospray, Alcan
SiC _p /7049Al 15% (T6)	598	643	2	90	Cospray, Alcan
SiC _p /7090Al 20% (T6)	665	735	–	105	DWA

the particles obviously improves the elastic modulus, yield strength, and tensile strength properties of the composites, but decreases their elongation.

(1) Elastic Modulus

The addition of the reinforcements obviously improves the elastic modulus (E) of each composite. The main factors that influence the elastic modulus of a composite are the type, content, length-diameter ratio, and oriented configuration degree of the reinforcement used, the type of matrix alloy, and the heat treatment conditions. As shown in Table 3.8, the elastic modulus basically increased linearly with the addition of the reinforcements and the increase in their volume fraction. Compared with the use of Al_2O_3 particles, the addition of high-modulus SiC particles can produce high-modulus composites. In Table 3.8, the shapes and dimensions of the particles are not listed, but as a matter of fact, the shapes and dimensions of the particles have a major influence on the elastic moduli of the composites. Table 3.8 also shows that the composite produced using the 2024 Al matrix has a higher elastic modulus than that using the 6061Al matrix. However, some other researchers indicated that the elastic moduli of composites have no relationship to the matrix alloys used, and for different Al matrix composites, their specific moduli have certain differences. The specific modulus of the $\text{SiC}_p/\text{Al-Li}$ composite is 1.4 times higher than that of the Al-Li alloy.

Interface binding conditions are also an important factor influencing the elastic moduli of composites. Research results for aluminum borate whisker-reinforced Al matrix composites show that a certain interface reaction can increase the interface binding force and then increase the elastic moduli of the composites. Research results for SiC_p/Al composite also show that the degree of interface load transfer will affect the elastic modulus of the composite severely.

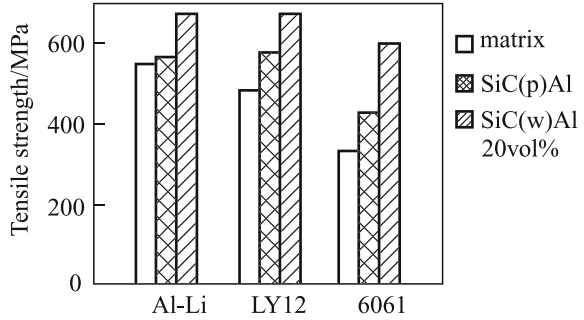
(2) Strength

Table 3.8 shows that the strengths of composites are different according to different types and contents of the reinforcements, the matrix alloys, and the heat treatment conditions.

The most important factors influencing the strengths of the composites are the yield strengths of the matrix alloys and the heat treatment conditions. The tensile properties of SiC whisker-reinforced solution-strengthened Al-Mg alloy (5456) matrix composites and age-strengthened Al-Cu-Mg alloy (2124) matrix composites show that the lower the matrix alloy's strength is, then the greater the improvement in the composite's strength will become. However, the 2124 matrix alloy can obtain age strengthening by heat treatment (T4, T6, or T8). Therefore, using the same reinforcement volume fraction, the SiC/2124 composite has higher strength than the SiC/5456 composite.

Figure 3.1 shows that the strengthening effects of SiC particles and whiskers used to reinforce different types of Al matrix composites have intimate relationships with the strengths of the matrix alloys. Particles and whiskers have strong strengthening effects for low-strength matrix alloys. Research results for SiCw/Al

Fig. 3.1 Room-temperature tensile strengths of some Al matrix composites

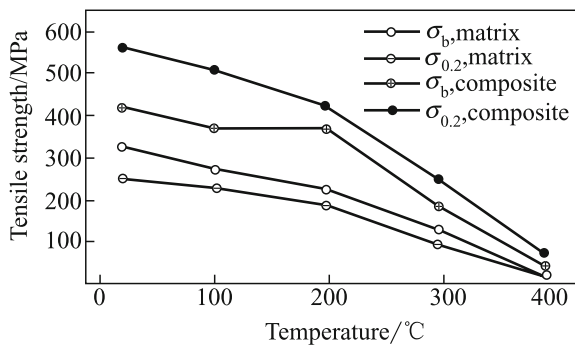


composites show that the lower the matrix strength is, then the more obvious the strengthening effects of the whiskers will be. However, for a super low-strength matrix alloy, the trend went against the strengthening effects of the whiskers. When the strength of the Al alloy is high enough, the addition of particles will inversely decrease the yield strength. The reason for this is that the strength of the matrix alloy is high enough, and the reinforcements sustain high loads when the composite experiences deformation. The SiC particles lacerated during the production procedure are easy to fracture and then induce the decrease in the yield strength and cause low-stress fractures.

Compared with matrix alloys, another important characteristic of composites is their high heat resistance capability. Figures 3.2 and 3.3 show the high-temperature tensile properties of 40% (volume fraction) $AlN_p/6061Al$ composites and some other composites. As shown in Fig. 3.2, the properties of the 40% (volume fraction) $AlN_p/6061Al$ composite have the same rules as that of its matrix alloy, but have higher high-temperature strength. From Fig. 3.3, we can see that the applicable temperature range of each composite is related to the type of matrix alloy used.

From the micromechanical viewpoint, the strengths of particle-reinforced composites mainly come from Orowan strengthening, grain and substructure strengthening, forest dislocation strengthening, heat treatment strengthening, work

Fig. 3.2 High-temperature strength of $AlN_p/6061Al$ composite and its matrix alloy



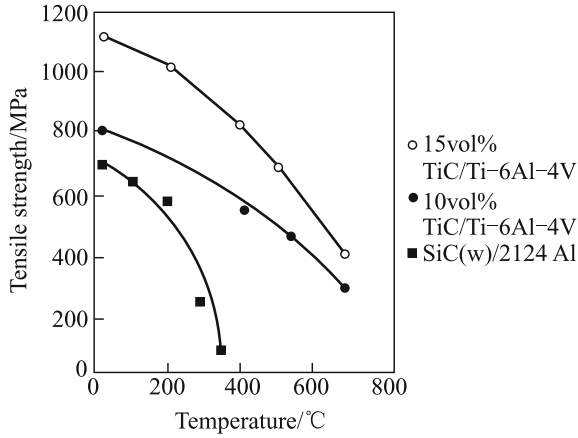


Fig. 3.3 Relationship curves between tensile strength and temperature for composites

hardening, and particle strengthening. The high strengths of the composites are not simply an overlay of the above strengthening effects and are the result of the combined actions of those effects.

(3) Heat Conductivity

For reasons of high electrical resistance, high thermal resistance, or high density, traditional Invar and Kovar alloys, Mo alloys, and W alloys cannot meet the requirements of modern aerospace electronic packaging integration materials. At present, Al₂O₃, SiC, and AlN ceramics are mainly used for these electronic packaging materials. The first two materials have low heat conductivity, but high density. The third material is difficult to mold. Table 3.9 illustrates the heat conductivity and thermal expansion properties of some traditional materials and the electronic packaging materials. The traditional electronic packaging materials have many disadvantages, and we therefore need to develop a series of new composites with low thermal expansion and high thermal conductivity. Figure 3.4 shows the relationships between the SiC volume fraction and the heat conductivity and the linear expansion coefficient of the SiC_p/Al composite. We can see that, under the appropriate conditions, different thermal conductivities and linear expansion coefficients can be obtained to enable the requirements for different electronic devices to

Table 3.9 Thermal conductivities and thermal expansion coefficients of selected materials

Materials	AlN	BeO	Al ₂ O ₃	W	SiC	Invar	Si	Mo	Kovar
Linear expansion coefficient (10 ⁻⁶ K ⁻¹)	4.7	6.7	8.3	4.5	3.8	0.4	4.1	5.0	5.9
Thermal conductivity (W (m K) ⁻¹)	250	250	20	174	70	11	13.5	140	17

Table 3.10 Physical properties of SiCp/Al composites and some conventional materials

Properties	A	B	420 stainless steel	Electroplated Ni
Linear expansion coefficient (10^{-6} K^{-1})	9.7	12.4	9.3	12.1
Thermal conductivity ($\text{W} (\text{m} \cdot \text{K})^{-1}$)	127	123	24.9	8.0
Elastic modulus (GPa)	145	117	200	2.0
Density ($\text{g} \cdot \text{cm}^{-3}$)	2.91	2.91	7.8	7.75

Notes: A is the composite used in the precision instrument and is 6061-T6 with 40 vol.% SiC_p. B is the composite used in the optical instrument and is 2124-T6 with 30 vol.% SiC_p

be satisfied. AlN has good thermal conductivity and a low linear expansion coefficient, no harmful effects, and an acceptable price; therefore, AlN_p/Al composites are highly promising materials for electronic device packaging.

(4) Thermal Expansion

Table 3.10 lists the physical properties of SiC_p/Al composites and conventional materials. The thermal expansion and thermal conductivity properties of the composites have obvious advantages. This gives the composites a good competitive advantage for the production of devices and parts with high-dimensional stability. In Fig. 3.4, the relationship between the linear expansion of the SiC_p/2024Al composite and SiC particle volume fraction indicates that the expansion coefficients of the composites can be arranged in a certain range. Therefore, SiC_p/Al composites have good application prospects in the optical instrumentation and aviation electronic component fields.

(5) High-Temperature Mechanical Properties

Table 3.11 gives the high-temperature properties of SiC_p/A356 composites. From this table, we can see that the high-temperature properties of the composite

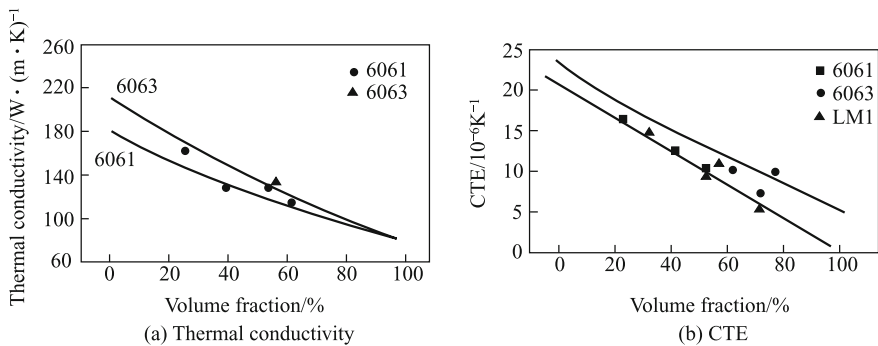


Fig. 3.4 Relationships between the properties of SiC_p/Al composites and the SiC volume fraction

Table 3.11 High-temperature properties of the SiCP/A356 composite

Temperature (°C)	Tensile strength (MPa)			
	0% ^a SiC	10% ^a SiC	15% ^a SiC	20% ^a SiC
22	262	303	331	352
149	165	255	283	296
204	103	221	248	248
260	76	131	145	152
316	28	69	76	76

^avolume fraction

increased with increasing SiC particle volume fraction. When the volume fraction is 20%, the strength of the composite at 200 °C is similar to the strength of the Al matrix alloy at room temperature.

(6) Influence of Hot Extrusion on the Properties of Composites

After hot extrusion, the distribution of particles in composites is more even, and the properties of the composites are improved. Large deformation is good for even distribution of the particles in composites. The results of superplasticity properties research for Al matrix composites show that superplastic pretreatment techniques, such as hot extrusion or rolling, obviously refine the grains of the composites.

Research results for hot extrusion particle-reinforced Al matrix composites show that, after hot extrusion, the composite densities have obviously increased, and most of the casting defects have been eliminated. At the same time, extrusion induces large compressive stresses in the composites, and all these factors will improve the mechanical properties of the composites. Hot extrusion usually leads to two effects. First, the extrusion will induce a large number of dislocations and then improve the yield strengths of the composites. Second is the continuous high temperature after the extrusion process will act as an annealing treatment. The diffusion coefficients of atoms at high temperature are relatively high, and the diffusion energy will decrease. The atoms will have high diffusion ability, meaning that the dislocations will be recovered and the dislocation density will decrease. The thermal vibration of the atoms will increase and a portion of the atoms will recover from non-equilibrium positions to equilibrium positions, and thus reduce the inner stress of the composites. This part of the procedure does not improve the mechanical properties of the composites. These two procedures in hot extrusion have contradictory effects. For a small extrusion ratio of 2.25:1, the latter procedure plays the main role; and for a larger extrusion ratio of 10:1, the former procedure plays the main role. Under these conditions, the mechanical properties of the composites will be obviously higher than those of cast composites.

Table 3.12 Mechanical properties of SiC_p/Mg composites at different temperatures

Materials	Temperature (°C)	$\sigma_{0.2}$ (MPa)	σ_b (MPa)	δ (%)	E (GPa)
15.1% SiC _p /AZ91	21	207.9	235.9	1.1	53.9
19.6% SiC _p /AZ91	21	212.1	231.0	0.7	57.4
25.4% SiC _p /AZ91	21	231.7	245.0	0.7	65.1
25.4% SiC _p /AZ91	177	159.6	176.4	1.5	56.0
25.4% SiC _p /AZ91	260	53.2	68.6	3.6	–
20% SiC _p /AZ91	25 + rolling	251.0	336.0	5.7	79.0

3.2.2.2 Properties of SiC_p/Mg Composites

The properties of SiC_p/Mg composites are given in Table 3.12. From this table, we can see that, at the same temperature, the yield strengths, tensile strengths, and elastic moduli increase, while the elongations decrease, with the addition of reinforcement particles and increasing particle volume fraction. However, for composites that have the same volume fraction of reinforcement particles, the yield strengths, tensile strengths, and elastic moduli are reduced, while the elongations are increased with increasing temperature. This indicates that the temperature has a great influence on the properties of the composites. In contrast, rolling can greatly improve the mechanical properties of the composites. The reason for this effect is that rolling can distribute the ceramic reinforcements more evenly in the composites and can also remove defects such as gas holes and shrinkage porosities.

The failure mechanism of SiC_p/AZ91 composites is mainly brittle rupture, and the main reason for failure is the aggregation of the particles. SiC_p/Mg composites have excellent wear resistance and corrosion resistance. The research results for wear behavior in SiC_p/AZ91 composites show that the wear resistance of the composite increased with increasing SiC particle volume fraction. In the salt mist corrosion test, when the SiC particle content is lower than a certain value, the corrosion rates of the composites do not change [23–25].

3.2.2.3 Properties of SiC_p/Zn Composites

The properties of SiC_p/Zn composites are shown in Table 3.13. From this table, we can see that the elastic modulus and hardness of SiC_p/ZA27 composites increase with increasing SiC particle volume fraction, but the tensile strength is reduced. This can be caused by the poor plasticity of the ZA27 matrix alloy. There is a peak value in the tensile strengths of the SiC_p/ZA22 composite, and this may be a result of the increase in dislocation density [15, 26].

Research results for the effects of the content and granularity of SiC particles on the high-temperature frictional wear properties of SiC_p/ZA27 composites indicate that the abrasion loss and friction factor decrease linearly with increasing particle content, and the best particle granularity is 20 μm . With increasing temperature, the

Table 3.13 Properties of SiC_p/Zn composites

Materials	σ_b (MPa)	δ (%)	E (GPa)	Hardness (HBS)
10% SiC _p /ZA27	396	0	92	121.0
20% SiC _p /ZA27	330	0	110	159.0
5% SiC _p /ZA22	485	3.6	96	101.0
10% SiC _p /ZA22	518	2.8	105	116.5
20% SiC _p /ZA22	480	0	131	121.6

wear mechanisms change from micro-cutting wear to stripping wear, and finally to severely adhesive wear.

3.2.2.4 Other SiC Particle-Reinforced Metal Matrix Composites

Pressing SiC particles into the internal surface of a cylinder by the press-embed method can improve the service life of a cylinder from 2000 h to 8000 h. In SiC particle-reinforced steel composites, the SiC particles are tightly combined with the steel matrix, and there are no interface chemical reactions. When the Si content in the steel matrix is 11.2%, the wear resistance ability of the composite is 20 times higher than that of high Cr cast iron. Under dry wear conditions, the wear resistance of the SiC particle-reinforced steel composite has been improved to be 2.5 times that of the matrix steel, and the wear mechanism is adhesive wear; under oil lubrication conditions, the wear resistance of the composite has been improved to be 18 times higher, and the wear mechanism is based on slight peeling and massive flaking. SiC particle-reinforced wear-resistant composites were produced by the electrolytic deposition method. The hardness of these composites can be improved by 70%, and the wear resistance could be improved to be three times higher. 5–10% SiC particle-reinforced Fe composites were produced by the powder metallurgy method. The tensile strength of the composite is approximately 230 MPa, the impact ductility is about 75 kJ/m², the hardness is about 130 HBS, and the wear resistance can be improved to be at least 10–20 times higher. The SiC_p/Cu composite was produced by the hot isostatic pressing method. The SiC particle content is the main factor affecting the linear expansion coefficient and the thermal conductivity of the composites. The linear expansion coefficient decreases while the thermal conductivity increases with increasing SiC particle content [8].

The mechanical properties of the TiB₂-Cu matrix composite and TiB₂ ceramic materials are shown in Table 3.14. The results show that the tightness, bending strength, and fracture toughness of the TiB₂-Cu matrix composite are greatly improved by the introduction of Cu. The melting point of the adhesive agent, Cu, is only 1083 °C, and during the combustion synthesis procedure, the melting Cu is in liquid flow conditions and can effectively fill the free spaces between the in situ formed TiB₂ particles in the pressing procedure. Simultaneously, the Cu metal will

Table 3.14 Mechanical properties of TiB₂-Cu matrix composite

Materials	Density (g cm ⁻³)	Tightness (%)	Hardness (HRA)	Bending strength (MPa)	Fracture toughness (MPa m ^{1/2})
TiB ₂ -Cu	5.417	96.1	76.5	583	8.32
TiB ₂	4.13	91.4	82	424.8	4.71

offer lubrication for rearrangement of the TiB₂ particles, and thus, the addition of Cu can improve the tightness of these materials.

With the improved tightness of the TiB₂-Cu matrix composite, the bending strength of the composite is also improved. However, the addition of Cu refined the TiB₂ particles. According to dislocation pileup theory, the number of pileup dislocations will increase with decreasing grain size. The large numbers of dislocations mean that the material requires a large external shear stress to initiate the dislocation sources between the adjacent grains, and then, the strength of the composite is improved.

For excellent electrical conductivity and heat transfer properties, pure Cu and alloys with high Cu content are widely applied in the industrial and military fields. However, the strengths of these materials are not high, and their ability to resist deformation at high temperatures is poor. Although we can improve the strength of the materials by alloying or cold working, the electrical conductivity and heat resistance ability will be affected and then cannot meet the requirements of modern industrial and military equipment. Therefore, the high strength, high electrical conductivity, and heat resistance of Cu materials are an important research area. The most important technical point in the study of high-strength, highly electrically conductive, and heat-resistant Cu materials is how to solve for the contradictions among the strength, electrical conductivity, and heat resistance of the Cu materials. In recent years, research results have shown that oxide dispersion strengthening of Cu matrix composites can effectively solve this problem.

Table 3.15 Mechanical and electrical properties of Al₂O₃/Cu composites

Fabrication method	Mass fraction (%)	Test temperature (°C)	σ_b (MPa)	$\sigma_{0.2}$ (MPa)	δ (%)	HRB	Relative conductivity (IACS) (%)
Mechanical alloying	0.9	25	405	400	6.5	60	84
		427	182	156	6	—	—
Internal oxidation	0.89	25	565	545	12	85	78.83
		427	525	470	8	—	—

Fig. 3.5 Relationships between working and rates and strengths of the composites

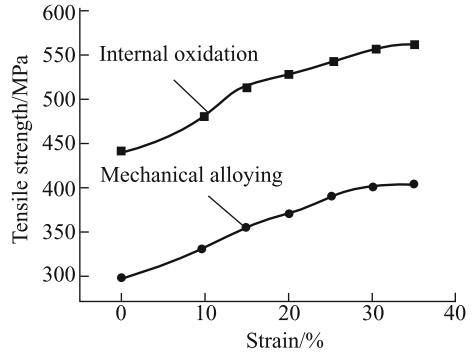
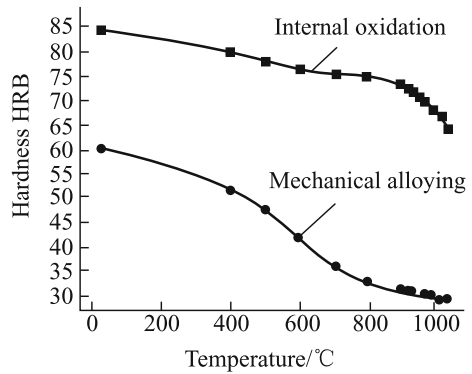


Fig. 3.6 Relationships between hardness annealing temperature of the composites



The Cu matrix composite was produced by the internal oxidation method. The mass fraction of the Al_2O_3 reinforcement is 0.89%, and this fraction is similar to that of the same composite produced by the mechanical alloying method. The properties of these two composites after sintering, extrusion, and cold drawing are listed in Table 3.15. The relationship between the working rates and the strengths of the composites is shown in Fig. 3.5, and the relationship between hardness and the annealing temperature is shown in Fig. 3.6. We can see that the mechanical properties and the heat resistance of the Cu matrix composite that was produced by the internal oxidation method are better than those of the composite produced by the mechanical alloying method. The cold working procedure has equivalent effects on the mechanical properties of the two composites and has almost no influence on the electrical conductivities of the composites. However, the electrical conductivity of the composite that was produced by the mechanical alloying method is obviously better than that of the composite produced by the internal oxidation method.

3.2.3 Whisker-Reinforced Metal Matrix Composites

3.2.3.1 Whisker-Reinforced Al Matrix Composites

(1) Elastic Modulus of SiC_w/Al Composites [23, 26–30]

The introduction of whiskers can obviously improve the elastic modulus and strength of composite materials. Table 3.16 shows the room-temperature tensile properties of SiC_w/Al composites produced by the powder metallurgy method.

From this table, we can see that heat treatment has little effect on the elastic modulus of SiC_w/Al composites. A higher elastic modulus can be obtained by increasing the volume fraction of the SiC whiskers. In terms of improving the elastic modulus of the composites, the contribution of the whiskers is better than that of particles. When the volume fraction V_f of the whiskers is low and the yield strength of the matrix is high, the improvement in the elastic modulus of the composite is more obvious; when V_f is high and the yield strength of the matrix is low, then the increment ratio of the elastic modulus is more obvious. When the whisker volume fraction is 8–20%, the elastic modulus of SiC_w/Al is 88–130 GPa. Compared with the matrix alloy, the elastic modulus is improved by 30–70%. After extrusion, the longitudinal elastic modulus of the SiC_w/Al composite will have

Table 3.16 Tensile properties of SiC_w/Al composites

Material	Heat treatment	E (GPa)	$\sigma_{0.2}$ (MPa)	σ_b (MPa)	δ (%)
PM5456	Quenching	71	259	433	23
8 vol.% SiC _w /5456	Quenching	88	275	503	7
20 vol.% SiC _w /5456	Quenching	119	380	635	2
8 vol.% SiC _p /5456	Quenching	81	253	459	15
20 vol.% SiC _p /5456	Quenching	106	324	552	7
PM2124	T4	73	414	587	18
PM2124	T6	69	400	566	17
PM2124	T8	72	428	587	23
PM2124	Annealing	75	110	214	19
8 vol.% SiC _w /2124	T4	97	407	669	9
8 vol.% SiC _w /2124	T6	95	393	642	8
8 vol.% SiC _w /2124	T8	94	511	662	9
8 vol.% SiC _w /2124	Annealing	90	145	324	10
20 vol.% SiC _w /2124	T4	130	497	890	3
20 vol.% SiC _w /2124	T6	128	497	880	2
20 vol.% SiC _w /2124	T8	128	718	897	3
20 vol.% SiC _w /2124	Annealing	128	221	504	2
8 vol.% SiC _p /2124	T4	91	368	–	–
8 vol.% SiC _p /2124	T8	87	475	–	–
20 vol.% SiC _p /2124	T4	110	435	–	–
20 vol.% SiC _p /2124	T8	110	573	–	–

improved further, but the transverse modulus will be reduced. The tensile elastic modulus and the compressive elastic modulus of the SiC_w/Al composite are the same.

In addition, with regard to the test and experimental aspects, the proportional limit of SiC_w/Al is similar to that of Al alloys, which is relatively low. The relaxed dislocations, residual stresses, and centering abilities of the specimens have a strong effect on the initial stages of the strain–stress curve, and these aspects will affect the measurement accuracy. The reported elastic modulus values are 101.3, 107.6, 119.7, and 121.7. One possible test method is to carry out periodic unloading during normal tensile testing, and measure the E_c of the composite according to the unloading curve. We found that the repetitive nature of the results obtained from the unloading curve was very good, and the value of the unloading stress has little influence on the results. In the unloading curve, the linear section can be artificially prolonged, and therefore, the measurement accuracy of E_c can be improved.

(2) Strengths of SiC_w/Al Composites

The strengths of SiC_w/Al composites are correlated with the volume fraction of the whiskers, the arrangement and distribution of the whiskers, the interface conditions, the type of matrix alloy used, and the heat treatment conditions. While the proportional limits of SiC_w/Al composites are similar to those of Al alloys, or even lower than those of Al alloys, the yield strengths and tensile strengths are much higher than those of Al alloys.

The yield strength and the heat treatment conditions are the main factors influencing the strengths of SiC_w/Al composites. In terms of the tensile properties of the solution-strengthened Al–Mg alloy (5466) and age strengthening Al–Cu–Mg alloy (2124) matrix SiC_w/Al composites, the lower the matrix alloy strength is, then the greater the improvement in the composite strength will be. However, the 2124 matrix alloy can be age-strengthened by heat treatments (T4, T6, or T8). Therefore, for the same V_f , the $\text{SiC}_w/2124$ composite has higher strength than the $\text{SiC}_w/5456$ composite. The heat treatment conditions are also an important factor in the strengths of the composites. For four $\text{SiC}_w/2124$ composite samples, after annealing treatment, T4 treatment (room-temperature aging), T8 treatment (145 °C aging for 10 h), and T6 treatment (160 °C aging for 10 h or 190 °C aging for 16 h), the T8-treated composite has the highest yield strength, followed by the T4-, T6-, and annealing-treated composites. For the 20 vol.% $\text{SiC}_w/2124$ composite, the yield strength of the T8-treated composite is almost 500 MPa higher than that of the annealing-treated composite (as shown in Table 3.16). In addition, underaging treatments can obviously improve the composite yield strength more than peak-aging treatments, but the resulting fracture toughness values are similar. On the one hand, this indicates that the heat treatment conditions of the composite have a prominent influence on the strength (i.e., proportional limit, yield strength) in the low-strain region. On the other hand, this indicates that, apart from precipitation strengthening, there are other strengthening factors (including relaxed dislocation-induced strengthening and dislocation forest hardening).

Research results show that when the strengths of matrix alloys are high enough, the addition of SiC reinforcements will inversely decrease the yield strengths of the resulting composites. The reason for this is that the high strength of the matrix alloy means that the reinforcements will sustain very high external loading during the deformation of the composite. Thus, defective SiC particles caused by the fabrication procedure are easily broken, which then lowers the yield strength of the composite and induces low-strain ruptures.

The volume fraction of whiskers is another important factor affecting the strengths of composites. On the one hand, with increasing volume fraction of SiC whiskers, the proportional limit of the composites increases slightly; on the other hand, the distance between the whiskers is decreasing, and thus, the source-shortening stress is increasing. The composite has a higher work hardening rate and then greatly improves the yield strength and rupture strength of the composite. Research results show that as long as the composite materials have sufficient plasticity, they can attain their maximum strength values. The strengths of SiC_w/Al composites increase with increasing volume fractions of the SiC whiskers. When the volume fraction is 30–40%, the matrix alloys do not have sufficient plasticity to transfer the high local internal stress; therefore, rupture can occur before the composite reaches its stable plastic flow and normal rupture strength. Thus, the actual improvement in strength can conversely decrease.

The orientation of the whiskers is another factor influencing the strengths of the composites. Through extrusion, the longitudinal direction fracture strength of SiC_w/Al composites will be enhanced, while the transverse direction fracture strength will decrease. The longitudinal direction fracture strength is 20% higher than the transverse direction fracture strength. However, the orientation of the SiC whiskers has no obvious influence on the yield strength of SiC_w/Al composites.

The SiC_w-Al interface conditions also directly affect the strength of SiC_w/Al composites. Research results on the effects of interface precipitation on the tensile properties of SiC_w/2124 composites show that overaging treatment (where the hardness of the matrix alloy is equal to that after underaging treatment) will reduce the fracture strength and strain. Interface precipitations make the whiskers sustain higher loads, and then, the whiskers are easily ruptured. This will induce reductions in the fracture strength and strain.

There are many theoretical approaches to calculating the strengths of SiC_w/Al composite materials and the simplest one is the mixture law. However, the theoretical value given by the mixture law is quite different to the actual strength value. The main reason for this is that the mixture law does not consider structural factors, such as the shape and spatial distribution of the reinforcements. In addition, for SiC_w/Al composites, the constant strain hypothesis predicts failure, and the predicted flow stress and elastic modulus according to this model are normally at the upper limits of the correct values.

(3) Fracture Toughness

The research into the fracture behavior of SiC whisker- and particle-reinforced Al matrix composites mainly includes tensile fracture, compression fracture,

bending fracture, fatigue fracture, creep, and stress corrosion fracture. Among these fracture types, research on tensile fracture and fatigue fracture occupies the majority of the studies, and the latter places the research emphasis on the composite fatigue field. Therefore, in this section, we will mainly discuss the tensile fracture behavior of SiC_w/Al composites.

- 1) The fracture characteristics of SiC_w/Al composites. The main fracture characteristics of SiC_w/Al composites are small fracture strain and low fracture toughness. These are also the main problems that restrict the application of this type of material.

From the macroscopic viewpoint, the fracture of the SiC_w/Al composite appears as a brittle fracture feather; while in the microscopic view, it behaves as a dimple-type plastic fracture feather. From the viewpoint of the materials themselves, the fracture problems can be related to the production method, the heat treatment of the SiC_w/Al composites, the characteristics of the matrix alloys, the geometrical features of the whiskers (e.g., the length-diameter ratio and the spatial feature distribution and orientation), the SiC_w-Al interface conditions, and other problems. These problems are correlated with the initiation and spreading of cracks in the composites. From the viewpoint of the external conditions, the composite fractures are closely related to the test temperature and the loading method. Research into the fracture processes of SiC_w/Al composites can be carried out by observation of the fracture surface or of the acoustic emission signals that are transferred during the deformation and fracture of the materials. More direct methods include in situ deformation and fracture observation by scanning electron microscopy and transmission electron microscopy.

The research results show that the normal fracture surfaces of SiC_w/Al composites have typical macroscopic fracture features. There are a small number of drawn-out whiskers that are covered with Al alloy, and at higher magnifications, many Al dimples can be observed on the fracture surfaces. This indicates that there are significant local plastic deformations near the fracture surface. Sometimes, small numbers of sharp-cornered polygonal or rectangular intermetallic compounds and cracked impurities (particularly for PM SiC_w/Al composites) can be found on the fracture surface. On a high-speed tensile fracture surface, almost no drawn-out whiskers can be found, but longitudinal cracks are observed. These longitudinal cracks are a result of the high-speed running crack "bifurcation" or "kinking" and indicate that a large range of yield and tearing processes may be occurring in the adjacent matrix alloy. The research results for the low-temperature tensile fracture surfaces (-100 °C, -190 °C) of SiC_w/2124Al and SiC_w/2024Al composites show that their low-temperature fracture surface features are similar to those of the normal temperature features. The SiC whiskers have an obvious inhibiting effect on low-temperature fracture along the grains of the Al alloys.

For the analysis of the crack spreading route of the tensile fracture surface, the results of in situ dynamic observation of the tensile fracture procedure of the SiC_w/Al composite in particular indicate that the tensile fracture behavior of composite materials is controlled by the crack initiation procedure.

- 2) The fracture strain and fracture toughness of SiC_w/Al composites. Normally, SiC_w/Al composites have relatively low plasticity. Table 3.17 lists the tensile fracture strains of different Al matrix composite materials. We can see that, for SiC_w/Al composites with 15–30% volume fraction V_f whiskers, the maximum fracture strain (ε_b) values are only about 3%, and the changes of the matrix alloys and the reinforcement content (within the above V_f range) have no strong effect on ε_b . Generally speaking, matrix alloys with good plasticity and heat treatments that are beneficial for improved matrix plasticity can slightly improve the ε_b of the resulting composite materials. In addition, the longitudinal plasticity of extruded SiC_w/Al composites will also be improved. Although SiC_w/Al composites have low fracture strains at room temperature, under certain specific conditions, large plastic deformations can occur in these materials. Experimental results show that this kind of material has excellent

Table 3.17 Tensile fracture strain of SiC_w/Al composites at room temperature

Materials	Whisker volume fraction (%)	Production method	Status	Fracture strain (%)
$\text{SiC}_w/1100\text{Al}$	20	SQ	–	4
	28	PM	–	4
	28	SQ	–	3.7
$\text{SiC}_w/6061\text{Al}$	15	PM	T6	3.6
	17	SQ	T6	3.5
	18	PM	T6	2.8
	20	PM	T6	2.3
	20	PM	T6	2.2
	20	SQ + EXTR	T6	3.5
	22	SQ	T6	2.85
	25	PM	T6	1.9
	30	PM	T6	1.5–1.8
$\text{SiC}_w/2024\text{Al}$	20	PM	T6	2.0–2.5
	20	PM	T6	2.4
$\text{SiC}_w/2124\text{Al}$	20	PM	T4	3
	20	PM	T6	2
	20	PM	T8	3
	15	PM	T6	3.7
	20	PM	T6	3.0
	13.2	PM	T6	4.0
	30	PM	T6	1.4–1.8
$\text{SiC}_w/7075\text{Al}$	17.5	PM	T6	2.8
	20	PM	T6	3.4
	30	PM	T6	1.2–1.5
$\text{SiC}_w/5456\text{Al}$	20	PM	Quenched	2

technical plasticity. If the material is at a high temperature and the deformation speed is slow enough, then hot extrusion deformation with a large ratio, cross rolling, and even superplastic deformation can be carried out.

Research results show that the fracture toughness of any SiC_w/Al composite is obviously lower than the relevant matrix alloy. In general, the fracture toughness of Al alloys is in the range of 25 to 75 $\text{MPa m}^{1/2}$, and that of SiC_w/Al composites is only in the range of 7 to 25 $\text{MPa m}^{1/2}$. The basic reason for the low fracture toughness of this kind of composite is generally considered to be that the deformation of the materials is not even because of the addition of fragile reinforcements; micro-cracks and holes are thus initiated early through different modes and then spread rapidly, and therefore the early-stage fracture is induced.

The low fracture toughness of SiC_w/Al composite is caused by early cracking of the matrix alloy near the ends of the whiskers. The stress concentrations at the ends of the whiskers and strong local plastic deformation induce the formation and spreading of holes at relatively low levels of macroscopic stress. We consider the whiskers as rigid bodies and the matrix alloys as elastic plasticoviscous bodies; therefore, the mechanical conditions for the initiation of interface holes at the ends of the whiskers during tensile stress can be given by finite element analysis. This analysis also indicates that the sizes, shapes, and locations of these holes are closely related to the interface strength, the properties of the matrix alloys, and the geometrical properties of the whiskers. The high strength of the interface bonding can restrict the initiation of holes at the middle parts of the whiskers. The main reason for the low tensile toughness of the SiC_w/Al composites is therefore the uneven distribution of the SiC whiskers. The uneven distribution of these whiskers causes fractures in some whiskers and then initiates early-stage cracking. Some research results indicate that the low fracture toughness of the $\text{SiC}_w/2124\text{Al}$ composite is caused by massive impurity phase breaking

To date, the test for the fracture toughness of SiC_w/Al composites has not yet been standardized. The main reason for this is that it is difficult to produce prefabricated cracks, and the fatigue crack threshold value, K_{th} , is relatively high. After the crack initiation, the cracks spread rapidly and are difficult to control. Many research works refer to the standards for metal materials, such as the plane fracture toughness test methods in ASTM399 and the integration test methods in ASTM813J. During testing, compact tensile samples are mostly used, and the prefabricated crack problems are solved by the computer-controlled curvature radius at the bottom of the notched specimen. Based on the properties of SiC_w/Al composites, many research works focus on the test for the crack initiation fracture toughness of the composites. Others research the fracture toughness of the composites during the crack growth procedure, but these researchers mainly consider particle-reinforced composites.

The fracture toughness of SiC_w/Al composites is influenced by factors that include the volume fraction and degree of dispersion of the whiskers and the type and microstructure of the matrix alloy, the $\text{SiC}_w\text{-Al}$ interface features, and the aging treatment method. The research results show that an increase in the whisker volume

Table 3.18 Effects of heat treatments on the fracture toughness of SiC_w/6061Al composites

Materials	Status	Fracture toughness K _{IC} (MPa m ^{1/2})	Remarks
SiC _w / 6061Al	Commercial	19.5	No heat treatment before test
	T6	23.4	Solution treated for 1 h at 527 °C, then water quenched, and aged for 8 h at 177 °C
	Vacuum degassing	18.9	Vacuum temperature preservation for 48 h at 500 °C
	Vacuum degassing + T6	22.4	Vacuum degassing and then T6 treatment
6061Al	T6	36.8	Solution treated for 1 h at 527 °C, then water quenched, and aged for 8 h at 177 °C

fraction, uneven distribution of the whiskers, an increase in the SiC particle size, and generation of precipitated phases at the interface, or high bonding strength and the poor toughness of the matrix alloy can reduce the fracture toughness of composite materials. Table 3.18 shows the effects of heat treatments on the fracture toughness of 20% SiC/6061Al composites. Under these heat treatment conditions, we can see that the fracture toughness of the composite is only half that of its matrix alloy. The research results for the SiC_p/Al composite show that the fracture toughness in the overaged condition is lower than that in the underaged condition. We also found that from -136 to 190 °C, the fracture toughness of the SiC_p/Al composite remains constant.

Overall, we should increase the fracture toughness of SiC_w/Al composites by controlling the distribution of the SiC whiskers, improving the toughness of the matrix alloy, purifying the matrix alloy, and carrying out heat treatments.

3.2.3.2 Properties of Whisker-Reinforced Mg Matrix Composites

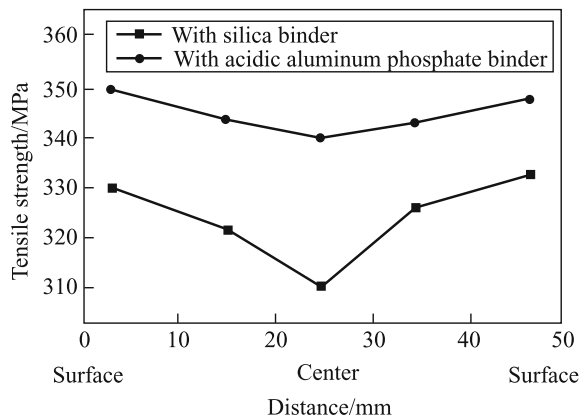
Table 3.19 shows the tensile properties of squeeze cast SiC_w/AZ91 Mg matrix composites that use different kinds of bonding agent. Compared with the AZ91 matrix alloy, the yield strengths, tensile strengths, and elastic moduli of the SiC_w/AZ91 composites are largely improved, but the elongation is reduced. The bonding agents have obvious effects on the properties of the composites. Of the SiC_w/AZ91 composites that use different bonding agents, the composite that uses acidic aluminum phosphate bonding agent has the highest yield strength, tensile strength, and elongation, while the properties of the composite that uses silica gel bonding agent are poor. The properties of SiC_w/AZ91 composites with no bonding agents are also poor [23, 31–33].

Figure 3.7 shows the tensile strengths of different parts of the composite ingot along the squeeze casting direction of SiC_w/AZ91 composites that use silica gel and

Table 3.19 Tensile properties of SiC_w/AZ91 composites that use different bonding agents

Materials	V _f (%)	σ _{0.2} (MPa)	σ _b (MPa)	E (GPa)	Elongation (%)
AZ91	0	102	205	6.00	46
SiC _w /AZ91 (acidic aluminum phosphate bonding agents)	21	240	370	1.12	86
SiC _w /AZ91 (silica gel bonding agents)	21	236	332	0.82	80
SiC _w /AZ91	22	223	325	1.08	81

Fig. 3.7 Tensile strengths of different parts of SiC_w/AZ91 composite ingot which use different bonding agents



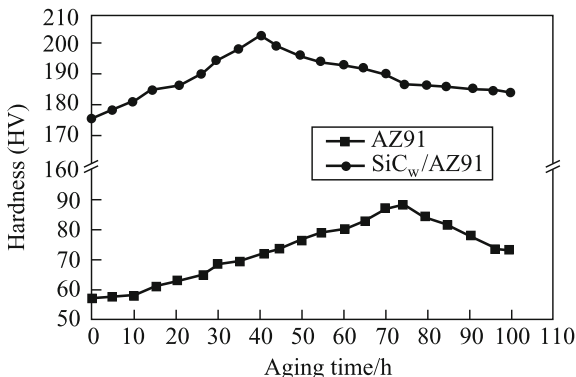
acidic aluminum phosphate bonding agents. In the composites that use silica gel bonding agents, the tensile strengths are low and the dispersibility of the strength is obvious. The strength near the surface is higher than that in the middle part. In the composites that use acidic aluminum phosphate bonding agents, the strength distributions are even and the strength near the surface is slightly higher.

Table 3.20 shows a comparison between the properties of the SiC_w/AZ91 composite that uses the acidic aluminum phosphate bonding agent and the SiC_w/6061Al composite. Using the hydrostatic force method, the density of the

Table 3.20 Tensile properties of SiC_w/AZ91 and SiC_w/6061Al composites

Materials	V _f (%)	ρ (g cm ⁻³)	E (GPa)	σ _{0.2} (MPa)	σ _b (MPa)	E/ρ (10 ³ m)	σ/ρ (10 ³ m)	Elongation (%)
SiC _w /AZ91 (using acidic aluminum phosphate bonding agents)	20	2.08	86	240	370	4.19	17.8	1.1
SiC _w /6061Al	20	2.80	110	300	500	3.83	17.9	2.5

Fig. 3.8 Age-hardening plots at 175 °C of AZ91 alloy and SiC_w/AZ91 composite



SiC_w/AZ91 composite is measured as 2.08 g/cm³, which is only 74% of that of the SiC_w/6061Al composite. Although the strength and elastic modulus of the SiC_w/AZ91 composite are lower than that of the SiC_w/6061Al composite, its specific elastic modulus is higher than that of the SiC_w/6061Al composite, and the specific strength is similar to that of the SiC_w/6061Al composite.

Numerous studies indicate that the best artificial aging temperature for AZ91 magnesium alloys is 175 °C. Aging treatments were carried out at 175 °C for Mg alloys and SiC_w/AZ91 composites, and Fig. 3.8 shows the age-hardening plots of the AZ91 Mg alloy and the SiC_w/AZ91 Mg matrix composite that uses the acidic aluminum phosphate bonding agent. From Fig. 3.8, we can see that, under the same aging conditions, the introduction of SiC whiskers causes the hardness of the composite to be much higher than that of the matrix alloy. Both the matrix alloy and the composite have aging peaks, and, after the aging peak, overage softening occurs. From Fig. 3.8, we can also see that the peak aging of the composite takes place earlier than that of the matrix alloy. The peak aging of the matrix alloy occurs after aging for 75 h at 175 °C, while that of the composite is after 40 h at 175 °C. The reason for this is that the linear heat expansion coefficients of the whiskers and the Mg alloys are different, and residual thermal stresses and large numbers of dislocations are introduced into the matrix alloy during the quenching procedure after solution treatment.

Table 3.21 gives the tensile properties of the SiC_w/AZ91 Mg matrix composite under different heat treatment conditions. Solution treatment obviously improves the fracture strain of composite materials. Peak-aging treatment (T6) obviously improves the strength of the SiC_w/AZ91 composite, but strongly reduces its fracture strain, and this is related to the age precipitation of the composite. At the peak-aging

Table 3.21 Tensile properties of SiC_w/AZ91 composites under different heat treatment conditions

Conditions	HV	σ _{0.2} (MPa)	σ _b (MPa)	E (GPa)	Elongation (%)
As cast	178	240	370	86	1.12
As quenched	175	220	355	85	1.40
T6 (175 °C, 40 h)	202	–	398	92	0.62

condition, two aging-precipitated phases exist in $\text{SiC}_w/\text{AZ91}$ composites. They are the laminae-precipitated phase in the crystal and cystiform-precipitated phase at the $\text{SiC}_w\text{-AZ91}$ interface. The two phases are Mg_{17} and Al_{12} .

3.2.4 Short Fiber-Reinforced Metal Matrix Composites

In the early 1980s, the Toyota Company and the Art Metal Company produced Al_2O_3 short fiber partially reinforced AC8A Al pistons via the squeeze casting technique and obviously improved the wear resistance of the piston ring groove. After reinforcement with 5–7% volume fraction (V_f) of Al_2O_3 short fibers, the wear resistance of the AC8A alloy is 70% higher than that of high-nickel austenitic iron [15, 34, 35].

(1) Room-Temperature Tensile Strength

Table 3.22 shows the tensile strengths of Zn alloys and Zn matrix composites. We can see that the room-temperature tensile strength of the composite is slightly lower than that of the matrix alloy. One reason for this is that the fibers have variable degrees of defects and respectable levels of impurities, which will reduce the load transfer ability of the fibers and then reduce the strength of the composite. The other reason for this is that the room-temperature strength of the fiber-matrix alloy interface is lower than that of the matrix alloy. It is difficult to distribute the external load evenly to each fiber through these interfaces, and the reinforcement functions of the fibers cannot be used. At the same time, the cracks are initiated at these fragile interfaces. The large numbers of defects will also reduce the strength of the composite.

(2) Compression Strength

The compression strengths of the Zn alloy and the Zn matrix composites can be seen in Table 3.23. From this table, we see that the introduction of short fibers into the matrix alloy can greatly improve the compression strength. The reason for this is

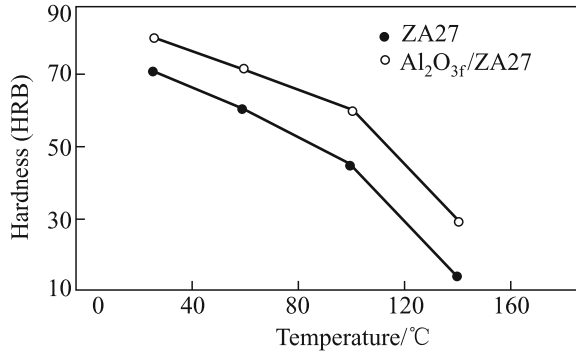
Table 3.22 Tensile strengths of Zn alloys and Zn matrix composites

Specimens	ZA27	ZA4-3	$\text{Al}_2\text{O}_3/\text{ZA27}$	$\text{Al}_2\text{O}_3/\text{ZA4-3}$
Tensile strength (MPa)	319	272.6	281.14	290.8

Table 3.23 Compression strengths of Zn alloys and Zn matrix composites

Specimens	ZA27	ZA4-3	$\text{Al}_2\text{O}_3/\text{ZA27}$	$\text{Al}_2\text{O}_3/\text{ZA4-3}$
Compression strength (MPa)	453.6	443.6	639.2	604.6

Fig. 3.9 Comparison of hardness between ZA alloy and $Al_2O_3_f/ZA27$ composite



that the high hardness, high stiffness, and high modulus of the Al_2O_3 fibers can greatly improve the deformation resistance of the material.

(3) Hardness

The hardness of the Zn alloy and one Zn matrix composite is shown in Fig. 3.9. We see that the hardness of both the composite and the matrix alloy increases with increasing temperature. At high temperatures, the internal structures of the metal change, and creep and relaxation occur, and then, a reduction in the high-temperature hardness of these materials is induced. At the same temperature, the hardness of the composite is clearly higher than that of the matrix alloy because of the introduction of the high hardness, high modulus, and high strength Al_2O_3 fibers in the softened ZA alloy. The fibers increase the deformation and rupture resistance abilities of the composite.

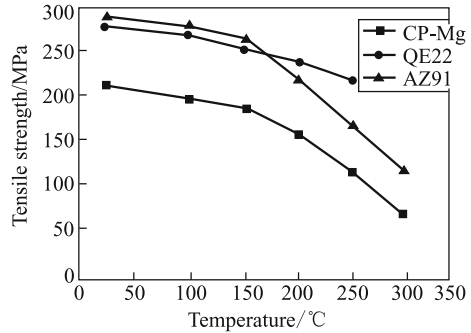
(4) Linear Heat Expansion Coefficient

The linear heat expansion coefficients of the Zn alloy and a Zn matrix composite are listed in Table 3.24. We can see that the introduction of low heat expansion coefficient short fibers can reduce the linear expansion coefficient of the material. Although the interface bonding of the composite is relatively weak, it still has a strong restricting action in the matrix alloy and obviously reduces the micro-stress. Therefore, the ZA matrix composite material can be used as a mold. The effects of

Table 3.24 Linear heat expansion coefficients of ZA27 and $Al_2O_3/ZA27$

Specimens	$T_0-150\text{ }^\circ\text{C}$		$T_0-250\text{ }^\circ\text{C}$		$T_0-350\text{ }^\circ\text{C}$	
	$\frac{\Delta L}{L}/10^{-3}$	$\alpha/10^{-6}K^{-1}$	$\frac{\Delta L}{L}/10^{-3}$	$\alpha/10^{-6}K^{-1}$	$\frac{\Delta L}{L}/10^{-3}$	$\alpha/10^{-6}K^{-1}$
ZA27	4800	48	7400	49.34	11000	44
$Al_2O_3/ZA27$	2200	20	4800	22.86	7800	25.16

Fig. 3.10 Relationships between tensile strength and temperature of Al₂O₃-reinforced Mg composites



temperature on the mold are very small, and this ensures the dimensional precision and stability of the components.

(5) High-Temperature Properties of Mg Matrix Composites

The properties of unreinforced Mg alloys are obviously reduced at temperatures higher than 100–150 °C. The addition of reinforcements can greatly improve the high-temperature properties of these matrix alloys.

The high-temperature properties of the composites are correlated with the type of matrix alloy used. As shown in Fig. 3.10, for squeeze cast 20% Saffil Al₂O₃ short fiber-reinforced CP-Mg, AZ91, and QE22 Mg matrix composites, the matrix alloys have an obvious influence on the high-temperature properties of the resulting Mg matrix composites. At temperatures higher than 150 °C, the strength of the CP-Mg matrix composite is obviously reduced and is similar to that of the unreinforced matrix alloy. The Al₂O₃ short fiber-reinforced AZ91 composite still has high strength at 150 °C, but when the temperature increases above 150 °C, the strength rapidly decreases. When the temperature reaches approximately 300 °C, the strength of the composite is almost equal to that of the matrix alloy. The high-temperature-resistant temperatures of the AZ91 and QE22 matrix composites are about 50 °C higher than that of their respective matrix alloys. At 200 °C, the QE22 matrix composite still has relatively high strength. Under 200 °C, the fibers have a small influence on the tensile properties of the composites. The fracture strains of the matrix alloys increase rapidly with increasing temperature. At 200 °C, the fracture strain is 12%. For the composite materials, however, the fracture strain is still very low at 300 °C. At 200 °C, the fracture strain is only 3%.

3.2.5 Long Fiber-Reinforced Metal Matrix Composites

Continuous fiber-reinforced Cu matrix composites not only have high specific strength and high specific stiffness, but also have excellent thermal and electrical conductivities and wear resistance [36–38]. This kind of composite is a candidate

material for use in high-performance structural components in the modern aerospace and weaponry fields. Fiber-reinforced metal matrix composites have the following features: (1) high specific strength and high specific stiffness; (2) good high-temperature properties; (3) good thermal and electrical conductivities, and electromagnetic induction shielding properties; (4) a low linear expansion coefficient along the fiber direction; (5) good fatigue resistance; (6) no moisture absorption or degassing; and (7) low shear strength and low tensile strength between the layers.

3.2.5.1 C Fiber-Reinforced Al Matrix Composites

Among the available metal matrix composites, there has been considerable scientific research into C fiber-reinforced Al matrix composites, and they are among the most widely applied types of composite material. C fiber-reinforced Al matrix composites have low density, high specific strength, high specific modulus, good electrical and thermal conductivities, good high-temperature strength, and good dimensional stability at high temperatures. Therefore, these materials are widely applied in many fields, and particularly in the aerospace field. For example, C fiber-reinforced Al matrix composites can be used to produce electrical cables, pistons, propeller blades, and all kinds of components for rockets, satellites, and airplanes.

Table 3.25 shows the mechanical properties of C fiber-reinforced Al matrix composites. This kind of composite has high strength and a high modulus. The densities of these composites are lower than those of the Al alloys, but their moduli are 2–4 times higher than those of the Al alloys. Therefore, the components made using this kind of composite have lightweight and good stiffness. Structurally stable components can be made with thin-walled materials to improve the charge capacities of the equipment. They can be used in aerospace vehicles, artificial satellites, and high-performance aircraft.

Table 3.25 Mechanical properties of C fiber-reinforced Al matrix composites

Fiber	Matrix	Fiber volume fraction V_f (%)	Density (g cm^{-3})	Tensile strength (MPa)	Modulus (GPa)
C fiber T50	201 Al alloy	30	2.38	633	169
C fiber T300	201 Al alloy	40	2.32	1050	148
Asphalt C fiber	6061Al alloy	41	2.44	633	320
C fiber HT	5056 Al alloy	35	2.34	800	120
C fiber HM	5056 Al alloy	35	2.38	600	170

Fig. 3.11 High-temperature properties of Al alloys and Al matrix composites

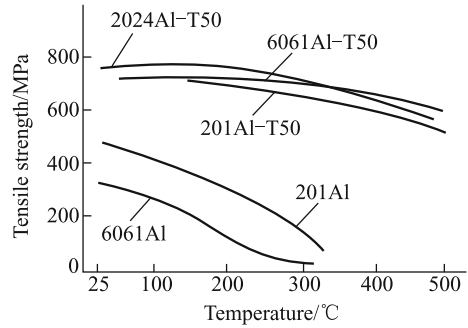


Figure 3.11 shows the high-temperature properties of the composites and the Al alloys. In the composites, the fibers are the main supporting bodies. The fibers maintain their high strength and high modulus at high temperatures, and therefore, the fiber-reinforced metal matrix composites can also maintain their high strength and high modulus at relatively high temperatures. This is highly beneficial for aerospace components and engine parts.

3.2.5.2 C Fiber-Reinforced Ag Matrix Composites

Electrical contact materials require good electrical conductivity, fusion welding resistance, and wear resistance (to both electrical wear and mechanical wear) properties. Ag matrix composites are basically this kind of material. Normally, these composites are prepared and sintered using highly electrically conductive and chemically stable Ag and high melting point, wear-resistant reinforcements via the powder metallurgy method. For example, Ag-graphite, Ag-W, and Ag-ZnO are all commonly used contact materials.

C fibers have not only high strength and high modulus, but also have certain electrical and thermal conductivities. With the appropriate complex techniques, C fiber contact material reinforcements can improve the electrical properties and mechanical properties and prolong the service life of the contact materials.

Table 3.26 Physical properties of Ag contact materials

Name	Brand	Density (g cm^{-3})	Hardness (HV)	Electric resistivity ($\mu\Omega \text{ cm}$)	Remarks
Ag-C fiber 3	CAgCF ₃	8.98	80–84	2.51	–
Ag-C fiber 5	CAgCF ₅	8.24	72–80	2.83	–
Ag-C fiber 7	CAgCF ₇	7.82	65–75	3.28	–
Ag-graphite 5P	CAgC ₅	8.6	25–40	3.2	Normal type
Ag-graphite 5Q	CAgC ₅ Q	8.6	30–35	2.4	Extrusion type
Ag-ZnO	Ag-ZnO	9.6	83–100	3.8	–

Table 3.27 Electrical wear properties of Ag head materials

Head materials	On-off tests (number of times)	Wear capacity (g)	Remarks
Moving contact Ag-ZnO	2700	–	–
Static contact Ag-graphite 5P		Static contact polished	Normal type
Moving contact Ag-ZnO	12000	–	–
Static contact Ag-graphite 5Q		0.09	Extrusion type
Moving contact Ag-ZnO	12000	–	–
Static contact Ag-C fiber 3		0.011	–

Table 3.26 lists the physical properties of Ag contact materials. The Ag content of Ag-C fiber 3 is equal to that of Ag-graphite 5. However, while their electric resistances are similar, the hardness of Ag-C fiber 3 is considerably higher. When compared with Ag-ZnO, the hardness values of the composites are basically the same, but the electrical resistance of Ag-C fiber 3 is relatively low. Table 3.27 shows the electric service life test results for Ag-C fiber 3 and Ag-graphite 5, where the matching moving contact materials used are all Ag-ZnO. From this table, we can see that the electric wear capacity of Ag-C fiber 3 is much smaller than that of the Ag-graphite 5 material.

3.2.5.3 C Fiber-Reinforced Cu Matrix Composites

C fiber-reinforced Cu matrix composites have the combined advantages of the good electrical and thermal conductivities of Cu alloys and the self-lubrication, wear resistance and low linear expansion coefficients of C fibers. Thus, this type of composite can be used for sliding electric contact materials, electric brushes, semiconductor supported electrodes, and integrated circuit cooling plates. For

Fig. 3.12 Coefficients of thermal expansion (CTE) of C/Cu composites

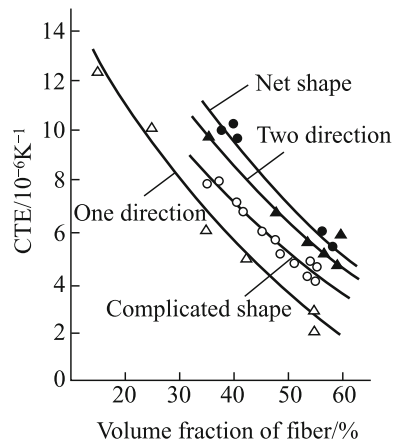


Table 3.28 Tensile strengths of fiber-reinforced Cu matrix composites

Composite materials	ρ (%)	V_f (%)	σ_b (MPa)
Cu _f /Cu	95	30	432
C _f /Cu	97	45	455
C _f /Cu	98.5	60	581
C _f /Cu	>95	32 (55)	410 (490)
C _f /Cu	>95	55	630–680

example, a cooling plate is fixed to the insulation board (Al_2O_3) inside the integrated circuit device. Normally, the cooling plate is produced using highly conductive materials (e.g., Ag, Cu), but the differences between the linear expansion coefficients of the insulation boards are large and they are easily bent and ruptured. We can control the C fiber content and distribution to adjust the linear expansion coefficient of the C fiber-reinforced Cu matrix composite to be close to that of Al_2O_3 . Then, the cooling plate is not easily ruptured. Figure 3.12 shows the change in the linear expansion coefficient of C fiber-reinforced Cu matrix composites with changes in the content and distribution of the C fibers. We can see that the linear expansion coefficients of the composites can be controlled within a wide range.

Table 3.28 shows the tensile strengths of fiber-reinforced Cu matrix composites, which were deposited over 8 h under experimental conditions, along with other reported data. For Cu_f/Cu composites, there are more Cu fiber bridge connections and drawn-out phenomena with further addition of Cu fibers, and then, the material strength is improved. For C_f/Cu composites, the tightness is relatively high, and the glass fibers and layers match well with the matrix. Therefore, they have relatively high strengths. If we further optimize the deposition conditions to improve the tightness of the materials, then the material strengths can be further improved. Related research results show that the tensile strengths of chemically deposited C_f/Cu composites increase to 600–680 MPa under certain temperature (600–700 °C) conditions. Hot pressure treatment under high-temperature conditions can further increase the composite densification and remove defects such as holes and micro-cracks.

Another application example of C fiber-reinforced Cu matrix composites is sliding blocks. The sliding blocks on trolley pantographs are the most worn parts of trolleys and are electromotive. In the early stages, metal sliding blocks were used, and now, graphite blocks have been adopted. However, they both have disadvantages. C fiber-reinforced Cu matrix composites can reduce the contact electrical resistance and avoid overheating. At the same time, they can improve the strength and overload electric current, and they have excellent lubrication and wear resistance abilities.

3.2.5.4 C Fiber-Reinforced Pb Matrix Composites

Pb metal has features such as high density, irradiation resistance, and strong acid corrosion resistance. Pb has a wide range of applications, such as its use in lead-acid storage batteries. However, the poor mechanical properties of Pb restrict its application. Sometimes, we have to enlarge the dimensions, add weight, and waste large amounts of materials. The appearance of fiber-reinforced composites has aroused the attention of researchers. The strength of a C fiber is 100 times that of pure Pb, and the density of a C fiber is only 1/7 of that of Pb. The introduction of C fibers can fully exert the strength of these fibers. For example, the tensile strength of a storage battery plate grid that is made with C fiber-reinforced Pb composite is 1.5 times higher than that of a normal plate grid, and the weight is reduced by 35%, while the capacity is enhanced by 15%. The composite can thus improve the properties of the storage battery.

3.2.5.5 Ti Matrix Composites

Recently, some European researchers studied continuous SiC fiber Ti alloy matrix coatings and developed the plasma spraying equipment that is used to produce SiC fiber-matrix alloy coatings. In their experiments, the Ti-6Al-4 V alloy was selected. A magnetic spray system is currently under development, which will be used to produce SiC fiber IMI834 matrix alloy coatings. They found that, at 700 °C, the interface reaction zone has very small growth, and there was no change in the thickness of the original C coating of the SiC fibers. This composite is shown in Fig. 3.13. The strength of this composite can remain unchanged after treatment for over 900 h at 700 °C.

Over the past few years, research emphasis was placed on the Ti-24Al-23Nb/SCS-6SiC composite system. This composite is under development because of its high mechanical strength, optimized microstructure, acceptable fracture toughness, increasing thermal fatigue response and an oxidation resistance that is better than the α -alloy. Dudek is now researching Ti-24Al-23Nb/SCS-6SiC via a magnetic spraying system.

Fig. 3.13 Blade fracture surface of SiC fiber composite sprayed with IMI-834 alloy

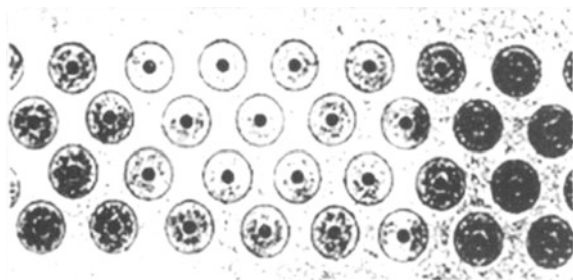
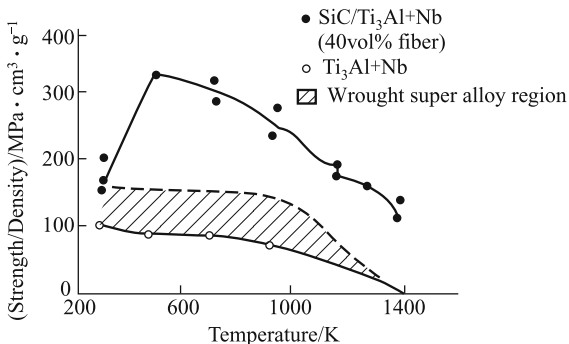


Fig. 3.14 Strength–temperature plots for $Ti_3Al + Nb$ and $SiC/Ti_3Al + Nb$ and the calculated values according to the mixture law



3.2.5.6 Intermetallic Compounds

The powder technique for fiber-reinforced intermetallic compound matrix composites is relatively mature. Here, we analyze the mechanical properties of $Ti-Al$ intermetallic compound matrix composites that are produced by this technique.

Figure 3.14 shows the strengths of the SiC fibers, the Ti_3Al-Nb matrix alloy, the SiC/Ti_3Al-Nb composite and the calculated strength of SiC/Ti_3Al-Nb according to the mixture law at different temperatures. Within the temperature range discussed, the strength of the SiC/Ti_3Al-Nb composite is higher than that of Ti_3Al-Nb . At the same time, the measured strength value of the composite is lower than the calculated value according to the mixture law.

Figure 3.15 shows the relationships between the tensile strengths and temperatures of $SiC/Ti-24Al-11Nb$ composites produced by the powder technique, the foil fold technique, and the plasma spray technique. From this figure, we see that the ultimate tensile strengths σ_u of the $SiC/Ti-24Al-11Nb$ composites decrease linearly with increasing temperature. σ_u is strongly dependent on the strength of the fibers.

Fig. 3.15 Longitudinal tensile strengths of $SiC/Ti-24Al-11Nb$ composites produced by various methods

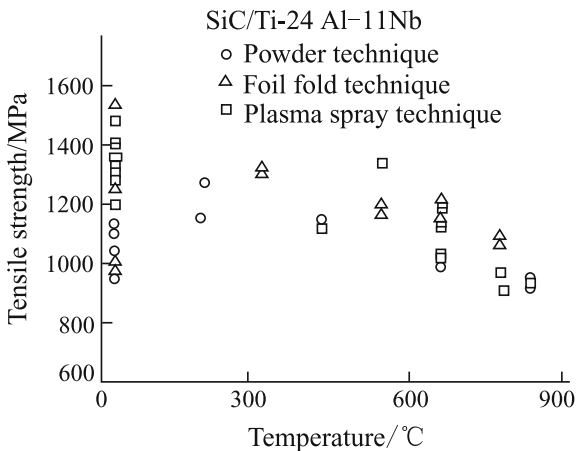
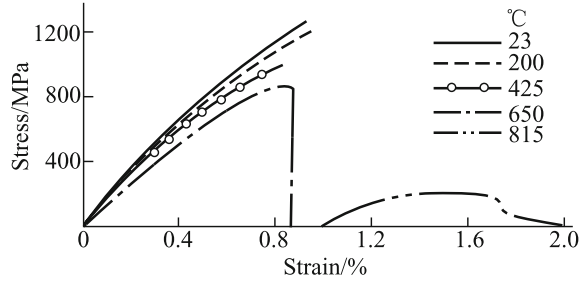


Fig. 3.16 Typical stress–strain plots of SiC/Ti–24Al–11Nb composites



The actual measured σ_u value is 77% of the value calculated according to the mixture law. The reason why the measured σ_u is lower than the calculated value is not because of a reduction in the strength of the fibers during the composite production procedure. The difference may be because, during the composite production procedure, the strength of the erosive fibers is only 96% of that of the original fibers. Until now, we have not been able to explain why the actual strength of SiC/Ti–24Al–11Nb is lower than the calculated value according to the mixture law.

Figure 3.16 shows typical stress–strain plots of SiC/Ti–24Al–11Nb composites at different temperatures. The volume fraction of fibers in the samples is 27.8–33.8%, and its mean value is 31%. When the test temperatures are 23, 200, and 425 °C, before the samples fracture, there are two separate linearity sectors. Between these two linearity sectors, there is a transition zone with a total length of 0.02%. At stage I, elastic deformation occurs in both the matrix and the fibers; and at stage II, elastic deformation occurs in the fibers, but plastic deformation is present in the matrix alloy. At 23 °C, for some samples, there is also a short and soft stage III before fracture occurs.

At temperatures of 650 and 815 °C, unlike the low-temperature states, there is a definite stage III with a relatively large curvature in the stress–strain plot before the fracture. This phenomenon is particularly obvious at 815 °C. Before fracture, the SiC fibers are always in an elastic deformation condition. Therefore, at 815 and 650 °C, the stage III behavior has nothing to do with the plastic deformation of these fibers. Apart from its relationship to the plastic deformation and creep of the matrix, stage III is also related to local fracture of the fibers, separation of the fiber/matrix interface, and the drawing out of the fibers.

In the typical stress–strain plots at 23 and 815 °C shown in Fig. 3.17, the moduli of the composite at stage I and stage II are E_1 and E_2 , respectively. The elasticity limit of the composite is σ_{c1} . The modulus of stage III is E_f .

Figure 3.18 shows that the modulus E_1 of SiC/Ti–24Al–11Nb decreases linearly with increasing temperature. The figure also shows the E_1 values calculated according to the mixture law (based on a V_f of 31% and a fiber modulus of 400 GPa). We can see that, at all temperatures, the calculated E_1 values and the actual measured E_1 values are similar.

Fig. 3.17 Performance parameters illustration using the stress–strain plots of SiC/Ti–24Al–11Nb

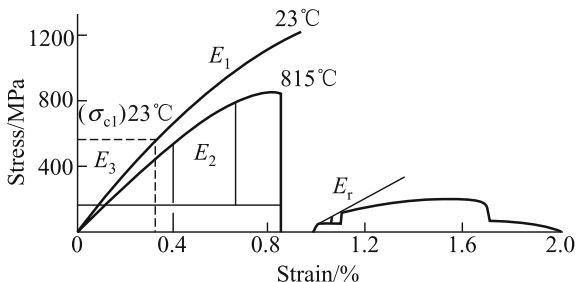


Fig. 3.18 Relationship between temperature, the measured elastic modulus E_1 , and the ROM-calculated value of SiC/Ti–24Al–11Nb composites

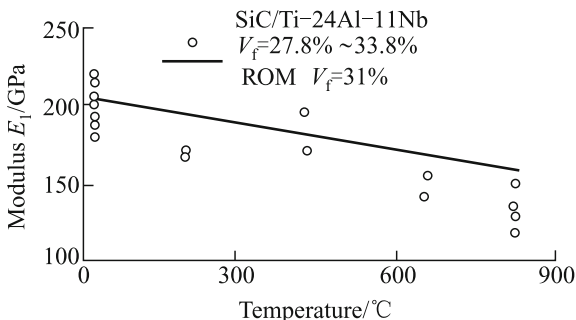


Fig. 3.19 Elastic modulus values of SiC/Ti–24Al–11Nb composite and matrix alloy at different temperatures

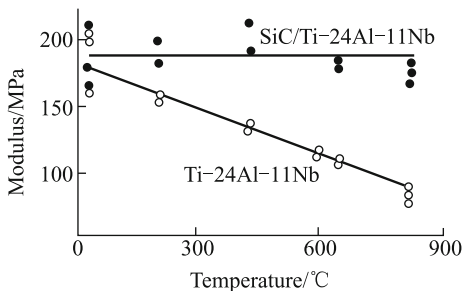


Figure 3.19 shows the limits of the elasticity σ_{e1} of the Ti–24Al–11Nb matrix and the SiC/Ti–24Al–11Nb composite. The σ_{e1} of the composite is a constant value of 567 MPa, and it does not change under these temperature conditions. However, with increasing temperature, the σ_{e1} of Ti–24Al–11Nb is decreased linearly.

In contrast, the longitudinal properties of SiC/Ti–24Al–11Nb composites are controlled by the fibers, and their transverse properties are obviously lower than those of the matrix alloy. The creep property and the endurance strength in the longitude direction are both one order of magnitude higher than those in the direction perpendicular to the fibers. The fatigue crack initiation behavior is determined by the strain features and the service life of the matrix. When there are gaps in the sample, the longitudinal service life is decreased, but the transverse

properties will not be greatly affected. This indicates that, under transverse loading, the fibers act as the weighted gaps. Under periodic loading, the crack spreading speed along the fiber direction is five times that in the direction perpendicular to the fibers. The transverse strain strength factor is $14\text{--}19 \text{ MPa}\cdot\text{m}^{1/2}$, which is equal to that of the matrix material. However, in the longitudinal direction, obvious toughening occurred. For the bridge connection of the cracks, under room-temperature conditions, the fracture strength can reach $110\text{--}150 \text{ MPa}$.

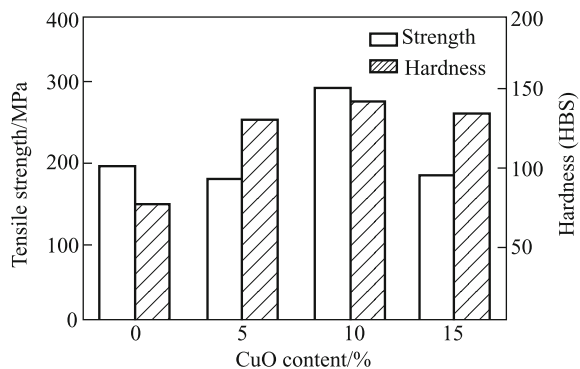
3.2.6 Self-Generated Reinforced Metal Matrix Composites

3.2.6.1 Self-Generated Reinforced Al Matrix Composites

The liquid stirring method was used to produce the CuO/Al system. The research results show that, at $1000 \text{ }^\circ\text{C}$, the system produced a good reaction. An Al–Mg alloy was used as the matrix alloy and, through control of the alloy composition, a particle-reinforced 2017 matrix composite was produced. However, $1000 \text{ }^\circ\text{C}$ is relatively high, and it restricts practical production. The XD™ technique was used to produce the composites, and it was found that the reactions can take place when the system temperature reached $800 \text{ }^\circ\text{C}$. However, because of the poor wetting properties between Al and CuO and because the diffusion conditions required for formation of the reaction products (mainly Cu) are difficult to satisfy, continuous processing of the reaction is restricted. At the same time, the liquid stirring method can accelerate the diffusion and improve the occurrence of the reactions. A CuO/Al self-generated Al_2O_3 -reinforced metal matrix composite was produced by the liquid stirring method at low temperature ($800 \text{ }^\circ\text{C}$), and the matrix alloy used was ZL303. The mechanical properties and fracture surfaces of this composite were then studied [39, 40].

Composites with different CuO contents were machined into tensile specimens ($\text{Ø}8 \text{ mm} \times 90 \text{ mm}$), and the room-temperature tensile test was carried out using

Fig. 3.20 Tensile strength and Brinell hardness values of composites with different CuO contents



the DG10TA universal tensile testing machine. The hardness test was carried out using the BHTH 3000 Brinell hardness tester. From Fig. 3.20, we can see that the tensile strength of the 10% CuO composite is relatively high and that the mean value can reach 297 MPa, which is 53% higher than that of the matrix alloy. However, in the other two conditions, the tensile strengths are lower than that of the matrix alloy. This phenomenon coincides with the structures of the materials, i.e., the strength of the composite increases with increasing Al_2O_3 content. The decrease in the other two alloys may be caused by low-added CuO content, and low reaction-produced Al_2O_3 content. Also, during the continuous stirring procedure, Mg and some other elements will be oxidized and burned, and the content of these elements will be decreased. The matrix alloy properties are reduced, and the low-produced Al_2O_3 content cannot compensate for the decrease in strength and hardness caused by stirring. With increasing addition of CuO, the Al_2O_3 content produced also increases. Therefore, the composite properties are also improved. However, the amount of CuO added to the alloy by self-generation has limitations. When the added amount is high, it is conversely not good for the material. When 15% CuO is added to the alloy, because the added amount is high, the stirring time is relatively long and the alloying elements are burned heavily. There is a large amount of slag on the liquid surface, which makes it difficult to continue to add CuO to the alloy. However, the unreacted CuO in the liquid can easily contact and adhere to the slag. The effective CuO content is then relatively low and the reaction-produced Al_2O_3 is reduced, which then reduces the strength and hardness of the composite.

From Fig. 3.20, we can see that the hardness of the three composites is high, and the addition of the high melting point hard Al_2O_3 phase is the direct cause of this result. The hardness of the 10% CuO composite is the highest, and the value can reach 136 HBS, which is higher than the matrix alloy. However, the elongations of these three composites are reduced by varying degrees, and they are all lower than 1%.

3.2.6.2 Properties of $\text{TiB}_2/\text{Ti-Al}$ Composites

The XD technique was used to produce $\text{TiB}_2/\text{Ti-Al}$ composites. The research results show that dispersal-distributed TiB_2 particles introduced into Ti-Al matrix by the XD technique improve the tensile strengths of the composites and will not reduce other properties. Table 3.29 lists the tensile properties of the composites under two temperature conditions.

Table 3.30 gives the creep rupture lives at 800 and 900 °C of Ti-47Al matrix alloys and 6% volume fraction $\text{TiB}_2/\text{Ti-47Al}$ composites produced by the XD technique. From this table, we can see that, under normal forging conditions, the endurance life Q of the Ti-47Al matrix alloy is slightly higher than that of its composite. When the 6% volume fraction $\text{TiB}_2/\text{Ti-47Al}$ composite was heat treated for 50 h at 1200 °C, its creep rupture life was obviously increased and was much higher than that of the Ti-47Al matrix alloy.

Table 3.29 Tensile properties of TiB₂/Ti–45Al composites

Status	20 °C			800 °C		
	$\sigma_{0.2}$ (MPa)	σ_b (MPa)	Elongation (%)	$\sigma_{0.2}$ (MPa)	σ_b (MPa)	Elongation (%)
Extrusion	–	793	0	448	710	11
Heat treated	793	862	0.5	427	600	20

Table 3.30 Creep rupture life of Ti–Al matrix alloy and its composites

Materials/processing status	Temperature (°C)	Stress (MPa)	Creep rupture life (h)
Ti–47Al (forging)	900	69	75.4
6 vol.% TiB ₂ /Ti–47Al (forging)	900	69	35.3
6 vol.% TiB ₂ /Ti–47Al (forging + heat treatment at 1200 °C for 50 h)	900	69	276.4
Ti–Al47 (forging)	800	138	171.1
6 vol.% TiB ₂ /Ti–Al47 (forging)	900	138	82.7
6 vol.% TiB ₂ /Ti–Al47 (forging + heat treatment at 1200 °C for 50 h)	800	138	588.2

The reason for the results above is mainly because of the changes in the microstructures of the materials. Under forging conditions, the microstructure of the matrix alloy is a mixture of layered and equiaxed $\alpha_2 + \gamma$. The forging structure of the TiB₂ composite contains rather fine α_2 -grains, and these grains are distributed on a gross and continuous γ -matrix. During forging and heat treatment, dynamic recrystallization occurs easily in the particle-reinforced composites, and the layered structure will gradually change into equiaxed grains. After heat treatment for 50 h at 1200 °C, the layered structure changes completely into equiaxed grains. The grains of α_2 and γ have a growth trend, but TiB₂ restricts their growth. The composite has high creep resistance caused by the fine equiaxed grains, and the heat treatment then improves the endurance life of the composite.

3.2.6.3 TiC_p/Ni₃Al Composites

The density of the TiC_p/Ni₃Al composite, which is produced under high temperature and high pressure, is 6.24 g/cm³, which is higher than 98% of the theoretical value. At 1473 K, a change in the resultant pressure did not obviously change the density of the sample, and this indicated that, within the pressure range of 1.5–6.5 GPa, compact TiC_p/Ni₃Al composites can be produced.

Using the typical framework of homogeneous crystallization theory, the influence of pressure on the nucleation and generation behavior was studied. The results indicate that nucleation is promoted and its growth is inhibited by the high-pressure conditions. With a constant cooling rate, grains are refined by the high pressure, which agrees with experimental results for nano-TiC reinforcement particles formed in the composites. The effects of pressure on grain size at certain temperatures are studied, and the results indicate that the relative degree of supercooling is enhanced by the pressure and that there is a critical pressure P_c . When the pressure is lower than P_c , the mean grain size d decreases with increasing pressure; when the pressure is higher than P_c , d increases with increasing pressure. Figure 3.21 shows the change in the mean grain size of TiC in the composite when fabricated at 1473 K under different pressures, and the results agree with the discussion above.

The mechanical properties of composites fabricated by the high-temperature and high-pressure method are measured by means of micro-hardness measurement.

Fig. 3.21 Relationship between mean grain size of TiC and resultant pressure of composites

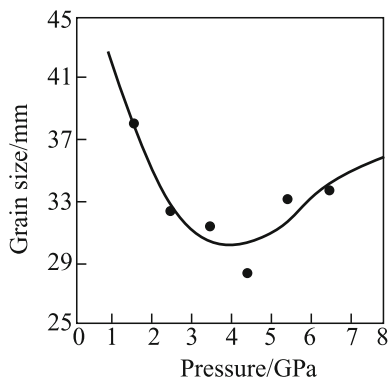


Fig. 3.22 Relationship between micro-hardness and the mean TiC grain size of the composites

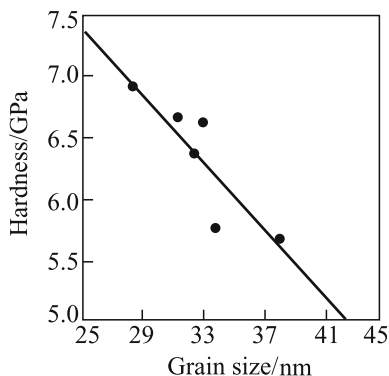


Figure 3.22 shows the relationship between the micro-hardness of the composite and the mean grain size of TiC. The micro-hardness of the composite increased with a reduction in the mean grain size of the TiC particles. Therefore, the micro-hardness of the composites can be adjusted by changing the fabrication conditions.

3.2.7 Other Reinforcements for Reinforced Metal Matrix Composites

Mixture-reinforced composites appeared in the early 1970s at the earliest, and they were mainly mixture-reinforced resin matrix composites. The purpose of this kind of composite is to retain the advantages of each constituent element and also obtain excellent combined properties. This can not only reduce the material costs, but can also improve the practicability of these materials. In recent years, researchers have moved their attention to mixture-reinforced metal matrix composites to satisfy the requirements of design and structure forms. Al matrix composites are one of the metal matrix composites that have been widely studied. The addition of ceramic reinforcements can obviously improve the strength and modulus of Al and Al alloys. In particular, for non-continuous reinforced Al matrix composites, the costs of the reinforcements are much lower than those of long fibers. Currently available metal working methods and equipment can also be used to greatly reduce the cost of this kind of composite [41, 42].

3.2.7.1 Room-Temperature Mechanical Properties

From the research on the strengthening behavior of $\text{SiC}_w/\text{Al}_2\text{O}_3$ composites, we found that when the total volume fraction of reinforcements remains constant, the tensile strength of the mixture-reinforced composite reached 507 MPa by adjusting the ratio of SiC whiskers to Al_2O_3 particles. The tensile strength of the composite

Table 3.31 Tensile properties of $\text{SiC}_w\text{-SiC}_p/2024\text{Al}$ composites

Composites	Tensile strength (MPa)	Elastic modulus (GPa)	Maximum elongation (%)
20% SiC_w/Al	452.1	112.10	0.83
(20% $\text{SiC}_w + 2\%$ $\text{SiC}_p)/\text{Al}$	464.0	128.80	0.72
(20% $\text{SiC}_w + 5\%$ $\text{SiC}_p)/\text{Al}$	470.2	124.10	0.85
(20% $\text{SiC}_w + 7\%$ $\text{SiC}_p)/\text{Al}$	612.8	126.60	0.80

Table 3.32 Elastic modulus values of some composites

Materials	Elastic modulus (GPa)	Yield strength (MPa)
(1Euc + 3ABO)/4032Al	101	177
(3Euc + 1ABO)/4032Al	85	184
(2Euc + 2ABO)/4032Al	90	170
(2Euc + 2ABO)/p-Al	91	162
(2Euc + 2ABO)/2024Al	89	–
(2Euc + 2ABO)/6061Al	99	–

improved obviously. The addition of particles improved the dispersivity of whiskers and reduced the fractures of these whiskers, and therefore improved the tensile strength of the composite. Table 3.31 shows the effects of nanometer SiC particles on the room-temperature tensile properties of SiC_w·SiC_p/2024Al composites. The results show that the addition of SiC particles effectively improves the tensile strength and the elastic modulus of these composites.

Table 3.32 lists the elastic modulus and yield strength values of eucryptite and aluminum borate-reinforced composites. We can see that the elastic moduli of these composites are all higher than 90 GPa. For the first three composites in this table, the matrix alloy is the same while the ratios of eucryptite and aluminum borate are different. The higher that the relative particle contents are, then the higher the yield strengths of the composites will become.

3.2.7.2 Wear-Resistant Properties

There is a development trend for metal matrix composites to add third-phase particles to the basis of the original composites to improve their wear resistance, or to

Fig. 3.23 Relationship between the wearing loss capacity and the sliding distance of composites

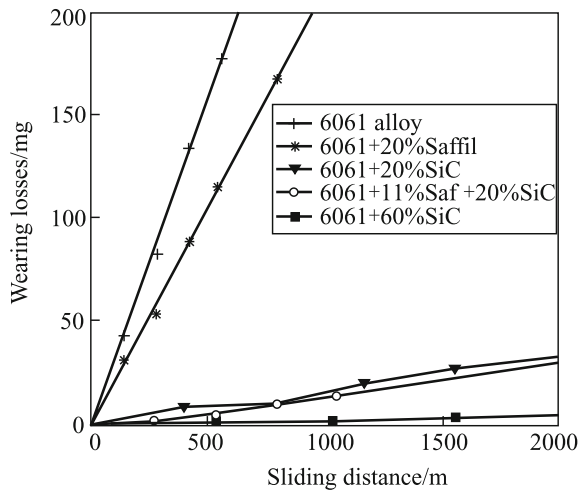
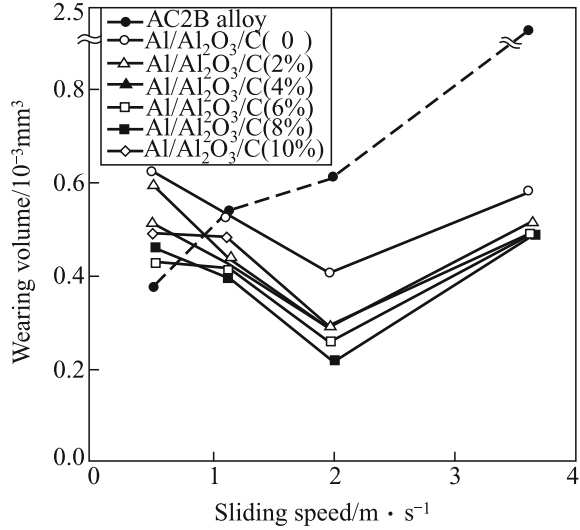


Fig. 3.24 Influence of sliding speed on the wear capacity of composites



mix wear-resistant reinforcements and anti-attrition reinforcements according to the “mixture effect.” There is a great deal of scientific research on the wear resistance of mixture-reinforced composites, and their abrasion mechanisms have also been discussed in depth.

Figure 3.23 indicates that the wear losses of the composites decreased with increasing reinforcement volume fraction. The wear resistance of the (11% Al₂O_{3f} + 20% SiC_p)/6061Al composite is higher than that of 20% SiC_p/6061Al and 20% Al₂O_{3f}/6061Al, and it is similar to that of 60% SiC_p/6061Al.

Figure 3.24 shows that, with the addition of C fibers, the wear resistance of mixture-reinforced composite is improved by 20–30% over that of Al₂O_{3f}/Al composites. Under medium-speed slide conditions (1.14–1.97 m/s), the wear resistance of the mixture-reinforced composite with 8% volume fraction of C fibers is the best. A solid lubrication layer is formed between the composite and the mated couple by the addition of the C fibers. The layer reduces the friction force between the composite and the mated couple and therefore improves the wear resistance of the composite.

The research results on the influence of fiber orientation on the frictional wear properties of Al₂O₃ fiber and C fiber mixture-reinforced AlSi₁₂ CuMgNi composites show that, compared with composites in which the fibers are perpendicular to the wear direction, when the fibers are parallel to the wear direction, the wear rate of the mixture-reinforced composite is relatively high, and its wear factor is relatively low.

Table 3.33 Physical properties of materials

Materials	Linear expansion coefficient (10^{-6} K^{-1})	Thermal conductivity ($\text{W m}^{-1} \text{ K}^{-1}$)	Elastic modulus (GPa)
6061Al	23.0	201	69
50% C _f /6061Al	5.68	102	112.10
(50% C _f + 1% SiC _p)/6061Al	5.55	152	128.80

3.2.7.3 Thermo-Physical Properties

Al matrix composites retain both the thermal conductivity of the matrix Al alloy and the low linear expansion coefficients of the reinforcements. Their thermo-physical properties can also be designed by selecting different reinforcements or by controlling the volume fraction of the reinforcements. Table 3.33 shows that the mixture-reinforced composite retained a relatively low linear expansion coefficient, and good thermal conductivity, which is higher than that of the singly reinforced composites.

3.2.7.4 High-Temperature Properties

Metal matrix composites have relatively good high-temperature properties, and they are more suitable for use at high temperatures. The research into the deformation rules of metal matrix composites at high temperatures can provide the basis of a reliable theory for the high-temperature mechanical properties, the expansion of the working temperature range, and the secondary working techniques of these composites.

Fig. 3.25 Stress–strain plot of mixture-reinforced composites (450 °C, strain rate of $7.97 \times 10^{-2} \text{ s}^{-1}$)

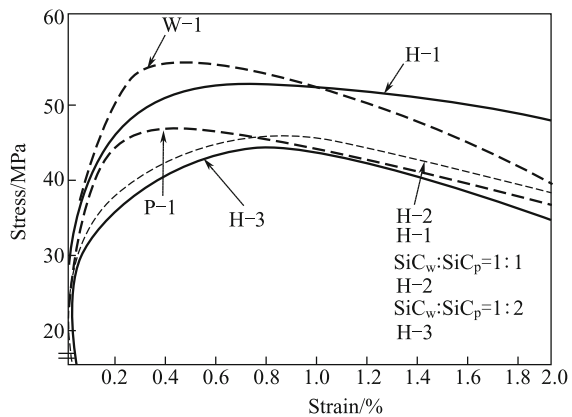


Fig. 3.26 Relationship plot of the wear capacity with temperature of composites

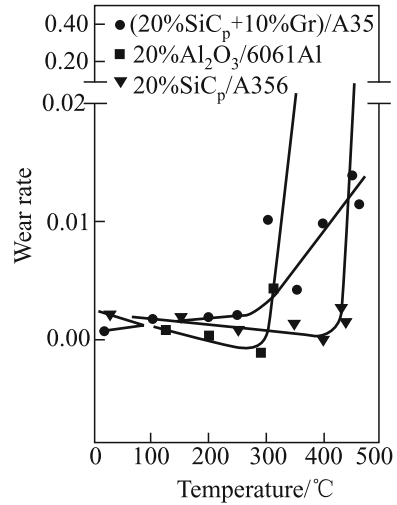


Figure 3.25 shows that, at 450 °C and with a strain rate of $7.97 \times 10^{-2} \text{ s}^{-1}$, the whisker-reinforced composite has the highest flow stress. The flow stress of mixture-reinforced composites increased with increasing SiC whisker content. The SiC whiskers can improve the strength and flow stress of the composites more effectively than SiC particles.

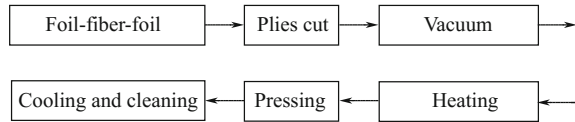
The transition temperature of these composites from light wear to heavy wear was also studied. Figure 3.26 shows that the addition of Al₂O₃ and SiC particles increases the transition temperatures of the 6061Al and A356 alloys to 310–350 °C and 440–450 °C, respectively. Also, at 460 °C, the SiC_p-Gr/A356 composite can still maintain light wear. For the single reinforced composites, the wear factor shoots upward at the transition temperature from light wear to heavy wear. In contrast, for mixture-reinforced composites, the wear factor shows strong stability at the transition temperature.

3.3 Fabrication of Metal Matrix Composites

3.3.1 Continuously Reinforced Metal Matrix Composites

The main shortcomings of metal matrix composites (MMCs) are high processing temperatures, complex manufacturing processes, fluctuating performance levels, and high costs. The research into fiber-reinforced metal matrix composites has focused on the development of manufacturing processes and reduction of production costs. Many techniques have been developed for fabrication of long fiber-reinforced metal matrix composites, such as squeeze casting, vacuum-pressure casting, powder metallurgy, extrusion, rolling, co-deposition, hot pressing, and the

Fig. 3.27 Flowchart of hot pressing process



liquid metal infiltration method. Among these methods, the hot pressing and liquid metal infiltration methods are widely used [43, 44].

3.3.1.1 Hot Pressing

Hot pressing, which is also called diffusion bonding, is a type of pressure welding method. Hot pressing is the principal method for manufacturing of the coarse boron fiber- and silicon carbide fiber-reinforced aluminum and titanium matrix composites. The products of this process have been used as the supporting framework of space shuttles, turbine blades, and rocket parts, among others. Hot pressing is also used to fabricate tungsten wire superalloys and tungsten wire-copper alloy composites. The hot pressing process solidifies foil–fiber–foil preform by hot pressing under vacuum or inert gas atmospheres. The flowchart of the process is shown in Fig. 3.27. The hot pressing process can be divided into powder cloth, foil–fiber–foil process, and hot spray stages.

During the hot pressing process, atoms in the contact area diffuse into each other under high-temperature and low deformation conditions. The process can be divided into 3 stages: (1) close surfaces come together, deform, move, and the oxide layer breaks under heat and pressure; (2) as time passes, interface, and volume diffusion occur, and the contact surfaces are welded; and (3) the thermal diffusivity interface ultimately disappears, and the bonding process is complete. Parameters including temperature, pressure, holding time, and atmosphere all influence the process. Among these factors, temperature is the most important factor.

The hot pressing process usually requires metal/fiber/metal preform to be made first, according to the required volume fraction of reinforcement. After this, the plies are cut, laid up, and consolidated through hot pressing. To ensure composite quality, the consolidation process can be carried out under vacuum or inert gas atmospheres.

Foil–fiber–foil plies (ribbons) can be made in four ways: plasma spraying to produce coarse fiber-metal plies; liquid metal infiltration to produce bunches of thin fiber-metal plies; and plasma spraying; and finally, sticking the fibers to the metal foils. Plies made by the first three methods have good interface bonding between the reinforcement and the metal matrix, while those made by the last method are not composited together. The plies fabricated by the last method are called “green plies.” The glue used in the last method should be vaporized completely in the early stages of heating and pressurization.

The temperatures used for hot pressing are higher than those of diffusion welding and usually slightly lower than the solidus line of the matrix metal to

prevent reaction between the reinforcement and the metal matrix. A small amount of liquid is sometimes beneficial for good interface bonding, especially when hot pressing “green plies.” Under this condition, the temperature is controlled between the solidus temperature and the liquidus line. The pressure can change over a wide range, but much higher pressures will damage the fibers. The pressure is usually maintained at less than 10 MPa and is dependent on the temperature, i.e., the pressure can be lower when the temperature is higher. One reason for consolidation in air is that the mold is sealed well and the volatile glue has a protective effect. Another reason is that the stiff fiber can break the oxide film of the metal, so that the exposed fresh surface can bond well with the fiber.

The main advantages of this process are as follows: (1) wide variety of available metal matrixes, and (2) the controllable orientation and volume fraction of the fiber. Shortcomings include the following: (1) several hours required for welding, (2) high process temperature and pressure, leading to higher costs, and (3) limitations of the part sizes.

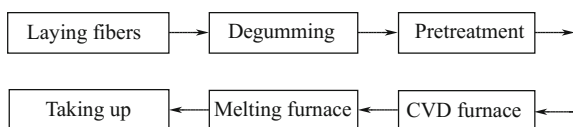
3.3.1.2 Liquid Metal Infiltration

Liquid metal infiltration, which is also known as the continuous casting method, uses long fibers dipped into liquid metal to produce composite materials. In this way, the long fibers can be easily dispersed in the liquid metal and fully composited. However, the wettability of the fibers is an important problem. To improve the fiber wettability, we can use surface coatings on the fibers, add alloy elements to the liquid metal, or use ultrasound. Another option that can be considered is overreaction between the fibers and the liquid metal under high-temperature conditions.

(1) Surface treatment of reinforcements

The most important point for production of carbon (graphite)/Al (or Mg) composites by liquid metal infiltration is the surface treatment of the carbon (graphite) fiber. After treatment, the liquid metal will infiltrate into gaps between the treated fibers. The process involves degumming, pretreatment, chemical vapor deposition (CVD) on the fibers, and metal infiltration. The process flowchart is shown in Fig. 3.28. Glue coated on the surfaces of the carbon fibers is removed by heating. When the temperature is lower than 450 °C, this process can be carried out in air. However, the process must be carried out in a protective atmosphere when the temperature is higher than 450 °C to avoid oxidation of the fibers. In a protected pretreatment furnace, residual glue and waste gases are cleared away at 700 °C with Ar protection.

Fig. 3.28 Process diagram of liquid metal impregnation



(2) Chemical vapor deposition

Chemical vapor deposition (CVD) is an important process for liquid metal infiltration. In this process, the fiber is treated with BCl_3 and TiCl_4 . A Ti–B coating will form on the fiber surface. BCl_3 is gaseous at room temperature. The vapor tension of TiCl_4 is 907 Pa below 25 °C, so that in cold seasons, heating is necessary to enhance the vapor tension and ensure sufficient gas concentration. Argon gas is used as the carrier gas for BCl_3 and TiCl_4 and is the protective gas for the whole system. A small amount of zinc and titanium sponge should be added to the furnace, and the temperature should be controlled at 700 °C.

In the melting furnace, the matrix metal is heated up to 50–100 °C higher than its melting point. The liquid metal is better protected by the inert gas to prevent oxidation. However, if the chemical vapor deposited carbon fiber enters the melting furnace beneath the liquid surface and does not contact the oxide on the surface, then the inert gas is unnecessary. Coated fibers are protected under nitrogen before entering the melting furnace. Once they contact the molten metal, they will be soaked by the molten metal spontaneously. The composite wire or band is then collected for secondary processing. If the surface-treated fiber is in contact with air, the surface coating will be disabled, and fiber then cannot form the composite with the matrix alloy.

(3) Infiltration technique

Before infiltration into the liquid metal, the surfaces of the fibers should be treated. For example, carbon fibers can be coated with TiB, liquid Na (or K), or other compounds. Another way to improve the wettability between the fibers and the matrix metal is to add alloying elements to the matrix alloy. For aluminum, many elements can be added as alloying elements, but the amounts must be strictly controlled to ensure that the carbide products cover the whole carbon fiber surface without significantly increasing the melting point of the matrix alloy. Good effects can be obtained by adding 0.5%Ti (Zr) or 1%Cr. The latter is the best option.

Ultrasound is also used to improve fiber wettability. The infiltration technique is used to fabricate not only continuous SiC fiber-reinforced Al composites, but also continuous B fiber-reinforced Al composites. However, the applications of this technique are greatly limited by the complicated process (particularly the requirement for fiber surface treatment), the product size limitations, the need for secondary processing to make parts or materials, and the high overall cost.

3.3.1.3 Typical Long Fiber-Reinforced Metal Matrix Composites

(1) Long fiber-reinforced titanium composites

- 1) Fibers The reinforcements should have excellent mechanical properties (elastic modulus, tensile strength), maintain these properties up to at least 1000 °C, and maintain stable thermal performance and mechanical properties (coefficient of thermal expansion mismatch) with titanium alloy. Table 3.34 lists the

Table 3.34 Characteristics of continuous reinforcements for titanium matrix composites

Type	Name	Producer	Diameter (μm)	UTS (GPa)	Elastic modulus (GPa)
SiC	SM1140+	DERA-Sigma	106	3.4	400
SiC	SCS-6	Textron	140	4	400
SiC	SCS-Ultra	Textron	140	6.2	420
SiC	Trimarc	ARC	125	3.5	410
Al_2O_3	Sapphire	Saphikon Inc.	120	3.4	410

properties of several commercial fibers, most of which are large-diameter monofilament fibers fabricated by CVD. At high temperatures, SiC fibers have high strength, thermal stability, and good antioxidation properties. There are two kinds of SiC fiber, distinguished by their core materials. One has a carbon core with a diameter of 33 μm , fabricated by Textron (SCS-6, SCS-Ultra). The other is fabricated by DERA-Sigma (SM1140 +) or ARC (Trimarc) with a 13- μm tungsten core. The SiC fiber with the carbon core has better thermal stability than that with the tungsten core. All SiC fibers have a protective layer to prevent chemical reaction with the Ti matrix during the service period. The coating is a 3–5- μm -thick carbon layer. Another possible reinforcement is the Al_2O_3 single crystal fiber fabricated by the Saphikon Corporation. Compared with SiC fibers, Al_2O_3 fibers have higher mechanical properties, better thermal stability, and little difference in coefficient of thermal expansion with the matrix. At present, the price of this expensive fiber has hampered its titanium matrix composite material applications.

- 2) Matrix alloys Several Ti alloys are listed in Table 3.35. The first application of titanium alloy is Ti–6–4. The γ -Ti–Al alloy has the highest high-temperature performance. The β -Ti alloy has better deformation than $\alpha + \beta$ -alloys and can be fabricated under lower temperatures, but β -Ti alloy has poor creep properties, which limit its application. Because the operating temperatures of new turbines are increasingly high, the matrix alloy used should have better high-temperature properties. This is the reason why near α -alloys are gaining increasing interest. Compared with Ti–1100 and IMI834, the Ti–6–2–4–2 alloy is better, although its anti-creep property is lower than the other two alloys.

Table 3.35 Main matrix alloys for Ti-MMCs

Type	Name	Chemical constituents
β	Ti-15-3	15 V–3Al–3Cr–3Sn
β	β -21S	15Mo–2.7Nb–3Al–0.2Si
$\alpha + \beta$	Ti-6-4	6Al–4 V
Near α	Ti-6-2-4-2	6Al–2Sn–4Zr–2Mo–0.1Si
Near α	Ti-1100	6Al–2.7Sn–4Zr–0.4Mo–0.45Si
Near α	IMI834	5.8Al–4Sn–3.5Zr–0.7Nb–0.5Mo–0.35Si
α_2	Ti–24Al–11Nb	14Al–21Nb
O	Ti–24Al–23Nb	11Al–40Nb
γ	Ti-48Al–2Cr–2Nb	33Al–2.6Cr–4.8Nb

- 3) Fabrication methods Fabrication of Ti matrix composite (TMC) parts is very difficult because Ti alloys have high melting points and high activity. As a result, TMCs can only be fabricated in the solid state and at less than 1000 °C. To effectively fabricate high-quality parts, many manufacturing methods have been developed, such as foil–fiber–foil, plasma spraying, and physical vapor deposition (PVD). Ti alloys with good deformation properties and reasonable manufacturing costs, such as β -, $\alpha + \beta$ -, and a number of near α -alloys, can be used as matrix alloys to fabricate TMCs by the foil–fiber–foil method. However, uneven distribution of the fibers, or fibers contacting each other, will affect the mechanical properties of the products. To reduce the damage, Ti powders can replace Ti foils as the matrix material. The plasma spray method uses vacuum plasma spraying to produce TMCs. During the process, 20–100- μm Ti powders are melted and ejected onto single-layer fibers by the plasma to fabricate composite plates. The composite plates are then cut and piled up into dice, followed by final hot pressing. The PVD method has been developed in recent years and has great potential.

The advantages and disadvantages of the foil–fiber–foil (FFF) method, the plasma spray coating method (MCM), and physical vapor deposition (PVD) are listed in Table 3.36. Physical vapor deposition (PVD) is divided into two categories: electron beam evaporation deposition (EBED) and sputtering (triode sputtering, or TS, and magnetron sputtering, or MS). These methods are used to spray metals onto the fiber uniformly before compression. These methods reduce manufacturing costs by using metal coatings instead of metal foils or powders. The main advantages of these technologies are evenly distributed fibers, no contact between the fibers, little fiber damage, controllable fiber volume fractions, and an ability for near-net-shape processing.

(2) Long fiber-reinforced aluminum composites

- 1) Fibers C fibers and Al_2O_3 fibers are commonly used as reinforcements for aluminum matrix composites. There are two types of C fibers, classed according to their mechanical properties: high-stress fiber (T800, M40 J) and high-modulus fiber (FT700, KC139). They perform differently within the matrix. Table 3.37 lists the characteristics of several fibers used as reinforcements for aluminum matrix composites.
- 2) Matrix alloy Several Al alloys are listed in Table 3.38. Pure Al and low alloys, such as Al–2Cu, Al–1Mg–0.6Si (6061), are used as matrixes for Al_2O_3 fiber (Nextel 610)-reinforced aluminum composites. High alloys, such as Al–4.5Cu, Al–10Mg, and Al–7Si–0.6Mg (A357), are used as matrixes for C fiber-reinforced aluminum composites. Compared with pure Al, high alloys have lower liquidus lines. The liquidus lines of Al–4.5Cu and Al–10Mg are 25 °C lower than that of pure Al, and that value will be 50 °C for Al–7Si–0.6 Mg (A357). The lower liquidus line will decrease the reactivity between Al and C and avoid reduction of the mechanical properties.

Table 3.36 Advantages and disadvantages of techniques for fabricating TMCs

Composite method	Technical process	Advantages	Disadvantage	Alloys
Foil-fiber-foil method	Foil-fiber-foil placed together, heating and compressing	Cheap	Uneven distribution of fibers, easy contact of fibers, easy formation of fatigue crack	β , $\alpha+\beta$, near α
Plasma spray coating method	Using vacuum plasma spray metal into high-speed rotating woven fibers, stacking compaction	Dense, little interface reaction	Uneven microstructure of matrix, fiber damage, uncontrollable composition of alloy	Near α , $\alpha+\beta$, α , β
Electron beam evaporation deposition	Electron beam gun evaporating titanium atoms sticking to the fiber in the form of condensate	Hard control of consist	Low using efficiency of materials	Ti-64, TiAlTi3Al+V
Triode sputtering	-	Controllable volume fraction, High utilization rate	Low deposition speed	Ti-64, 6242, IMI834
Magnetron sputtering	-	Even interval between fibers, controllable interface	-	Ti-64, MI834, Ti-22A1-23Nb

Table 3.37 Characteristics of fibers used as reinforcements for Al matrix composites

Kind	Name	Producer	Diameter (μm)	UTS (GPa)	Elastic modulus (GPa)
C	T800	Toray	5	5.5	290
C	M40 J	Toray	5	4.4	380
C	FT700	Tonen	10	3.3–3.8	700
C	DC139	Mitsubishi	9	3.8	750
Al ₂ O ₃	Nextel 610	3 M	10–12	2.8–3.5	400

3) Process The process flow diagram for fabrication of continuous fiber-reinforced aluminum matrix composites is shown in Fig. 3.29. Preforms (wire, tape, or sheet covered with metal) can be fabricated by liquid metal infiltration, plasma spraying, PVD, or electrodeposition. The preforms are then thermal diffusion-bonded with each other to form composites. A small amount

Table 3.38 Main aluminum alloys for continuous fiber-reinforced aluminum matrix composites

Serial number	Chemical constituent (wt.%)
1	Pure Al
2	Al-2Cu
3	Al-1 Mg-0.6Si(6061)
4	Al-4.5Cu
5	Al-10 Mg
6	Al-7Si-0.6 Mg(A357)

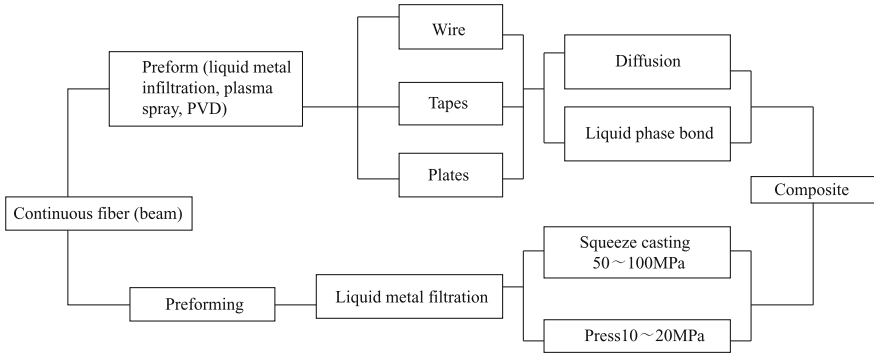


Fig. 3.29 Process diagram for fiber-reinforced aluminum matrix composites

of the liquid phase is beneficial for bonding. A higher pressure is also needed when fabricating composites in the solid phase, which will increase the possibility of fiber fracture.

3.3.2 Fabrication of Discontinuous Reinforced Metal Matrix Composites

3.3.2.1 Casting Process

The bottleneck restricting the practical use of metal matrix composites is their cost, and especially their manufacturing cost [45–47]. To produce composites with good performance at low cost, the following requirements should be considered for the manufacturing techniques:

- 1) The reinforcements should have the appropriate volume fraction and should be evenly distributed in the matrix.
- 2) The process should not undermine the original properties of the matrix and reinforcement materials and particularly should not damage the reinforcements.

- 3) The process should prevent unfavorable reactions between the reinforcements and the matrix material and obtain the proper interface structure and properties.
- 4) The process should be simple, nearly net-shaped and suitable for mass production.

Manufacturing methods for MMCs include solid-state methods, liquid-state methods, and solid–liquid-state methods. Table 3.39 summarizes the different fabrication methods. Liquid methods are widely adopted with simple equipment, easy operation, and ease of mass production. At present, the liquid methods are the most widely used, including gravity casting and pressure casting.

(1) Gravity casting of Al matrix composites

- 1) Characteristics During gravity casting of aluminum matrix composites, the reinforcement and the liquid metal are mixed uniformly and are then cooled under certain conditions. The method is particularly suitable for mass production. However, this method has some shortcomings. It is difficult to guarantee uniform distribution of the reinforcements, and the liquid metal will react with the reinforcements easily with long contact times between reinforcement

Table 3.39 Techniques for MMC fabrication

Category	Techniques	System		Composites
		Reinforcements	Matrix material	
Solid state	Powder metallurgy	Particles, whiskers, short fibers of SiC, Al ₂ O ₃ , B, and C	Al, Cu, Ti	Parts, sheets, ingots of SiC _p /Al, SiC _w /Al, Al ₂ O ₃ /Al, TiB ₂ /Ti
	Hot pressing	B, SiC, C (Gr), W	Al, Ti, Cu, heat-resistant alloy	Parts, pipes, sheets of B/Al, SiC/Al, SiC/TiC/Al, C/Mg
	Hot isostatic pressing	B, SiC, W	Al, Ti, superalloys	B/Al, SiC/Ti
	Extrusion, rolling	–	Al	Rods, pipes of C/Al, Al ₂ O ₃ /Al
Liquid state	Squeeze casting	Fibers, whiskers, Al ₂ O ₃ , SiO ₂ , C, Al ₂ O ₃ , SiC _p	Al, Zn, Mg, Cu	Parts, sheets, ingots of SiC _p /Al, SiC _w /Al, C/Al, C/Mg, Al ₂ O ₃ /Al, SiO ₂ /Al
	vacuum-pressure infiltration	Fibers, whiskers, particles	Al, Mg, Cu, Ni	Sheets, ingots of SiC _p /Al, C/Al, C/Mg, Cu/Al, SiC _p + SiC _w /Al
	Stirring	Particles, short fibers	Al, Zn, Mg	Ingots
	Co-deposition	Al ₂ O ₃ , SiC _p , B ₄ C, TiC _p	Al, Ni, Fe	Sheets, ingots of SiC _p /Al, Al ₂ O ₃ /Al
	Vacuum casting	Al ₂ O ₃ , C fiber	Mg, Al	Ingots
Other	Reaction synthesis	–	Al, Ti	Ingots
	Electroplating, chemical plating	SiC _p , B ₄ C, Al ₂ O _{3p} , C fiber	Ni, Cu	Coatings
	Thermal spraying	SiC _p , TiC	Ni, Fe	Pipes, rods

and matrix. Therefore, to improve the properties of composites, manufacturers should reduce the stirring temperature, reduce the contact time, solidify the liquid metal rapidly, or add alloying elements into the matrix alloy.

Another way to reduce the interface reactions is to form a dense layer on the reinforcement surface, which can prevent further reactions. For example, adding 7% of Mg into SiC/Al composite can form a dense oxide layer rapidly on the surfaces of the SiC particles. This layer can protect SiC particles from direct contact with the liquid aluminum alloy.

Coating reinforcements with a protective layer is also effective. However, changing the alloying elements and coating the reinforcements will both increase the procedure numbers and costs of the process. So, using fibers (particles) such as Al_2O_3 , which do not react with Al alloys, undoubtedly has many advantages.

During the solidification of evenly mixed reinforcements and liquid metal, the reinforcement tends to congregate in the matrix grain boundary area because of the influence of liquid–solid interface forces. This is a unique phenomenon of gravity casting. As a result, it is very important to investigate the reinforcement distribution and control methods during the solidification process. The impact factors of the reinforcement distribution in composite materials include both mixing and solidification. These factors are discussed in detail in the following.

The process of mixing reinforcements with matrix alloys is changing from solid–gas systems to solid–liquid systems. During the process, the interface energy plays an important role. Addition of the reinforcements is now usually performed when the matrix alloy is heated up to a semisolid state. The mixture is then heated to a liquid state and solidified immediately. The stirring method and the blade shape also influence the distribution of the reinforcements in the liquid metal.

The solidification rate is one of the most important factors that affects the reinforcement distribution in composites fabricated by gravity casting and has been investigated in depth both theoretically and experimentally. Theoretical analysis of the capture and exclusion of particles in $\text{Al}_2\text{O}_3/\text{2014Al}$ composites suggests that there is a critical cooling rate. When the cooling rate is higher than the critical rate, the reinforcement distributes homogeneously in the composite.

The volume fraction, particle size, and gravity conditions also influence the composite particle distribution. Studies of $\text{SiC}_p/\text{Al–Cu}$ composites suggest that uniform particle distributions are easily obtained when the volume fraction is higher. Investigations of $\text{SiC}_p/\text{AlSi}_7\text{Mg}$ composites found that the particle distribution depends on the particle size and the grain size. When the particle size is equal to or larger than the interdendritic distance of α (Al), the distribution is uniform. Control of the cooling rate can thus produce better microstructures. Density differences between particles and metals will also cause uneven particle distributions. For example, after remelting of TiB_2/Al composites under conditions of weightlessness, the TiB_2 distribution is more uniform. Increasing the solidification temperature gradient is also conducive to solving particle agglomeration problems.

Wetting conditions between the reinforcement and the metal will significantly affect the distribution. Al_2O_3 particles are repelled in untreated $\text{Al}_2\text{O}_3/\text{Al}$ and $\text{Al}_2\text{O}_3/\text{Al–Si}$ composites. After addition of Sr and Ca to the liquid Al alloy, Al_2O_3 particles

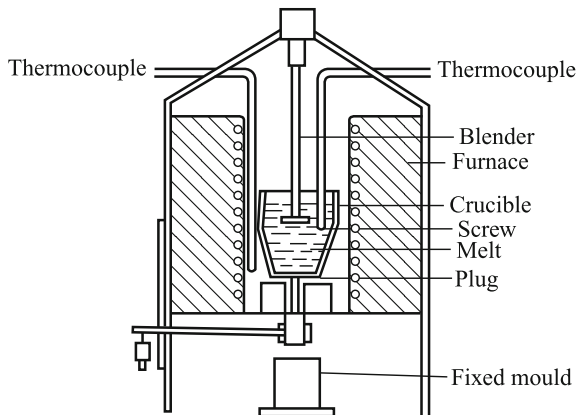
are easily captured by the matrix alloy. The reason for this is that the addition of Sr and Ca increases the wettability of the reinforcements to the liquid metal.

- 2) Technology Gravity casting must overcome two problems: The first is the wettability and distribution of the reinforcement; the other is oxidation and gas contamination of the liquid metal during the mixing process. To solve these problems, several methods are usually used and are listed as follows.
 - ① Adding elements to the metal alloy, melt can improve particle wettability. For example, adding Ca, Mg, and Li to the Al melt can significantly reduce the surface tension of the melt and improve the wettability of ceramic particles.
 - ② Surface treatment of the particles. Particles are usually heated to high temperatures to remove water, gas, and other contaminants on the particle surfaces. Some particles, like SiC, will be oxidized at high temperatures and form a SiO₂ layer. This layer can significantly improve the wettability of the particles.
 - ③ Gas control. A vacuum or an inert gas is generally used to protect the liquid metal from oxidation and gas contamination.
 - ④ Effective mechanical stirring. Effective mechanical stirring is one of the most important technologies for homogeneous mixing of the particles with the liquid metal. Intensive stirring can make the liquid metal form a strong shearing flow pass by the particles, which can effectively improve the wettability between particles and metal and promote uniform particle distribution in the liquid metal. To achieve higher stirring effects, we can use high-speed rotating mechanical stirring or ultrasonic stirring.

Accounting for all the above considerations, as well as the technology characteristics and the equipment, gravity casting can be divided into the vortex technique, Duralcon, and composite casting.

- a) **Vortex technique** The vortex technique uses high-speed rotating blades to stir liquid metal into a strong flow, into which the ceramic particles are added. The particles enter the metal melt owing to the vacuum suction of the vortex. After a period of strong stirring, the particles are evenly distributed in the metal. The technical mechanism of the vortex is shown in Fig. 3.30.

Fig. 3.30 Schematic diagram of stir casting

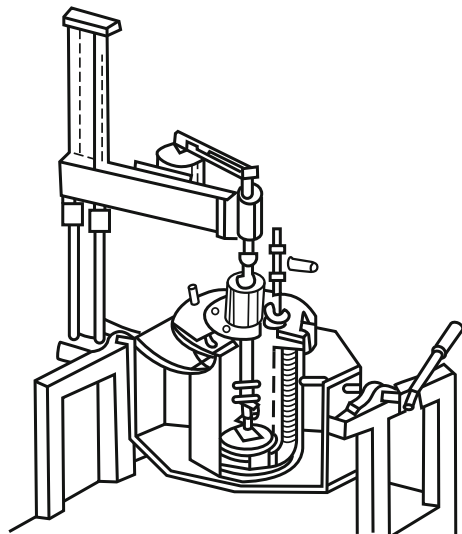


The processes of the vortex technique consist of melting the metal matrix, degassing, refining, particle pretreatment, stirring, and casting. Among these processes, stirring is most important. The important parameters of the vortex technique are the stirring rate, the melt temperature, and the particle addition speed. The technical parameters are as follows.

- i) Stirring speed: 500–1000 rad/min.
 - ii) Temperature: 100 °C above the liquid line of the matrix metal.
 - iii) Blender shape: screw.
 - iv) Diameter ratio of blender to crucible: 0.6–0.8.
 - v) Advantages and disadvantages: simple technique, low cost, suitable for production of larger particles (diameter of 50–100 μm), but not suitable for fabrication of high-performance structure particle-reinforced MMCs.
- b) **Duralcon** Duralcon was developed by the Alcan Corporation in the mid-1980s and is used to fabricate particle-reinforced Al, Mg, and Zn composites. This technique has become an industrial production method and can produce high-quality SiC_p/Al , $\text{Al}_2\text{O}_{3p}/\text{Al}$, and other composite materials. Factories for fabrication of particle-reinforced MMCs with outputs of 11000 tons have been established in Quebec, Canada. Figure 3.31 illustrates the equipment used for this technique.

During the Duralcon process, melted metal is placed into a stirring stove under vacuum or inert gas protection, and then the reinforcements are added to the melt. The blender is then stirred at high speed in a vacuum or an argon gas atmosphere. The blender is composed of major and assistant agitators. The major agitator has coaxial blades. The rotation speed of the major agitator is high, and it shears the melt and particles to make small particles that are distributed evenly and form the composite with the melt. The assistant agitator rotates slowly along the wall of the stove to eliminate vortex formation and pull particles that are adhering to the

Fig. 3.31 Equipment of Duralcon method



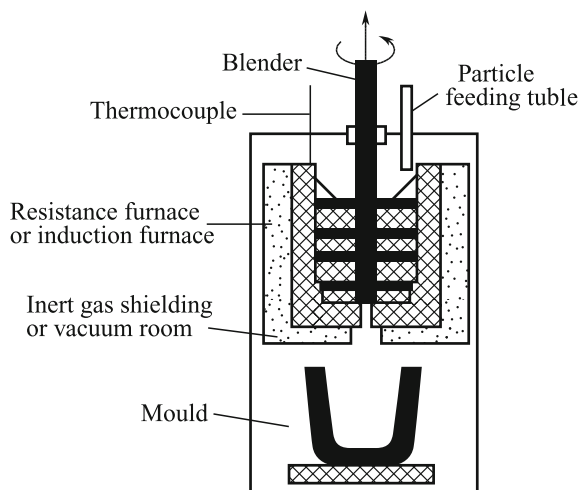
wall into the melt. The agitator shape, stirring speed, and temperature are the key parameters and are determined by the alloy components, the fraction and size of the particles, and other factors. The technical parameters are as follows.

- i) Speed of major agitator: 1000–2500 r/min.
- ii) Speed of assistant agitator: <100 r/min.
- iii) Temperature of the melt: 50 °C above the liquid line of the melt.
- iv) Stirring time: around 20 min.
- v) Merits and application scope: low gas content in the MMC melt, uniform distribution of particles, billet porosity of less than 1%, dense microstructure, good performance, and applicability to various particles and matrixes.

Duralcon is mainly used to fabricate Al MMCs, including deformation Al alloys, LD2, LD10, LY12, and LC4, and cast Al alloys, ZL101 and ZL104. The biggest ingot produced by this technique weighs 600 kg. Duralcon is currently the primary industrial technique for production of particle-reinforced Al matrix composites.

- c) **Composite casting** Composite casting also mixes particles with a metal melt by mechanical stirring. The difference is that the stirring is performed in a semisolid metal instead of liquid metal. The particles are taken into the melt by solid-phase metal granules. The solid-phase content of the melt is controlled in the range of 40–60% by controlling the temperature. The particles collide and grind with the metal granules and are evenly distributed into the semisolid melt by strong stirring. After stirring, the melt with the evenly distributed particles is then heated up to the casting temperature and cast into parts or billets. A schematic of the composite casting process is shown in Fig. 3.32. The most important aspect of the whole process is the speed and shape of the blender. The parameters, application, and the advantages and disadvantages of the technique are as follows.

Fig. 3.32 Schematic of composite casting process



- i) Materials system: the metal has 40–60% precipitation at a certain temperature.
- ii) Stirring temperature: at which a large amount of metal precipitation occurs.
- iii) Application: high-content fine particle-reinforced MMCs, whiskers, and short fiber-reinforced composites.
- iv) Shortcomings: restrictions of materials system.

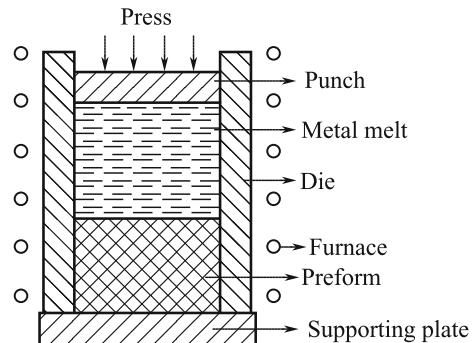
(2) Squeeze casting of Al MMCs [48]

- 1) Characteristics Squeeze casting is mainly used to fabricate ceramic short fiber-, whisker-, or particle-reinforced Al or Mg composites. Pistons made from ceramic fiber-reinforced Al composites have been widely used because of their low cost. Figure 3.33 is a schematic illustration of the equipment used to fabricate composites by squeeze casting.

Compared with other solid fabrication techniques, such as powder metallurgy, squeeze casting has several advantages:

- (1) Various cheap metal matrixes can be used;
- (2) There is little damage to the reinforcement during the fabrication process;
- (3) Fabrication is fast;
- (4) Simple equipment is used;
- (5) The process provides good size precision;
- (6) The process does not require wettability between reinforcement and matrix metal;
- (7) Low possibility of reaction between reinforcement and matrix metal;
- (8) The metal can infiltrate the preform even when the preform temperature is below the melting point of the metal;
- (9) The order of metal solidification is controllable with effective feeding;
- (10) The material has low porosity;

Fig. 3.33 Schematic illustration showing the equipment used to fabricate composites by squeeze casting



- (11) The pressure is beneficial for heat release, refining the grain of the metal matrix, and reducing interface reactions.

Shortcomings:

- (1) It is difficult to precisely control the volume fraction;
- (2) High pressure is applied, so the mold must be strong;
- (3) It is difficult to fabricate large or local composites.

The squeeze casting die is usually made of tool steel. The design of the squeeze casting die must take into account the following factors:

- i) Ability to withstand high temperature and high pressure during casting and have a long lifetime;
- ii) Ability to measure various parameters, especially temperature, during the squeeze casting process;
- iii) Exhaust channel requirement;
- iv) Process simplicity.

The pressure equipment of the squeeze casting process consists of punch-driven and gas-driven equipment. The process pressure is as high as 100 MPa. The die undergoes tensile stress, so high-intensity die material is required. Tool steel is often used to make the squeeze casting die. When using punch-driven equipment, the die temperature is lower than the melting point of the metal matrix, which extends the service life of the die, prevents the metal escaping from the die gap under high pressure, prevents liquid aluminum from sticking to the die, and speeds up the composite ingot's cooling and solidification. Gas-driven equipment is also widely used. Use of gas-driven equipment is accompanied by lower pressure (less than 10 MPa), slower infiltration, slower cooling, and greater porosity.

2) Squeeze casting process

- ① **Fabrication of reinforcement preform** The mold used to produce whisker preforms is shown in Fig. 3.34. The reinforcements are first washed and then dispersed in a liquid medium by ultrasonic processing. Glue is added to the liquid medium before it is mechanically mixed. The materials are then poured into the mold and pressed to obtain a preform with specific content. The preform is then dried and sintered. During the preform production process, the glue determines the preform quality. Two commonly used types of binders are: a) silica gel; and b) aluminum phosphate glue.

Silica gel is primarily used for preform preparation and is a high-temperature binder. The components of silica gel are shown in Table 3.40. The preparation method involves melting polyethylene alcohol in boiling water, followed by addition of silica sol and glycerin. The following processes will occur during heating: The mixture will become amorphous in the 200–500 °C range; cristobalite SiO₂ will form at 800 °C; and a mixture of cristobalite and SiO₂ will be formed at 1000 °C. The mixture is generally sintered at 800 °C for 1 h for transformation of

Fig. 3.34 Schematic drawing of the die used for preform manufacture

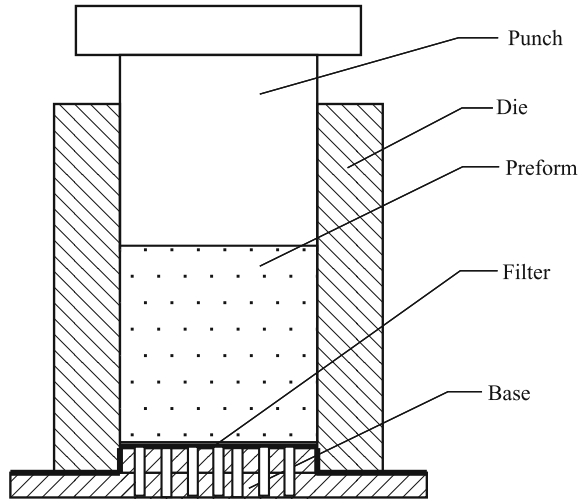


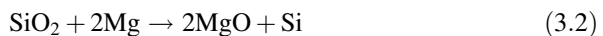
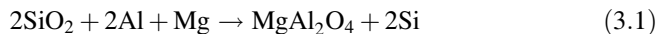
Table 3.40 Components of silica adhesive

Silica sol (mL)	Polyvinyl alcohol (g)	Glycerin (mL)	Water (mL)
1	1	1	15

the silica gel. The silica gel will not be crystallized or transformed. The bonding effect of the silica gel is good and it is widely used in the preparation of various types of reinforcement preform.

The compression strength of the preform generally increases with increasing gel content. Too little gel cannot effectively improve the strength of the preform, while too much gel will react with the metal and produce more impurities, which will then reduce the performance of the composite materials. Studies of SiC whisker preforms show that addition of 2 mL of silica gel is the optimum.

Silica gel is effective for most composite systems. The strength of the preform is increased, while the performance will not be diminished by using silica gel. Most matrix alloys will not obviously react with silica gel. However, when the matrix alloy contains more Mg or Li, it will react with SiO₂ as follows:



Aluminum phosphate glue is also a high-temperature binder; it does not contain SiO₂ and therefore will not react with certain elements in the matrix alloys, such as Li and Mg. Its components are shown in Table 3.41. The preparation method is as follows: First, a solution of Al(OH)₃ and H₃PO₄ (85%) is prepared with a P/Al atomic ratio of 1:23; then, 15-part water is added and mixed. The transformations

Table 3.41 Components of aluminum phosphate glue

Al(OH) ₃ and H ₃ PO ₄ (85%) with P/Al ratio of 1:23 (mL)	Water (mL)
1	15

during the heating process are: changing into amorphous state at 200 °C; crystallization into B-type sub-aluminum phosphate at 500 °C, formation of A-type sub-aluminum phosphate at 800 °C, while at the same time releasing P₂O₅ and H₃PO₄; and transformation into amorphous phosphite at 1000 °C. Aluminum phosphate glue that has been sintered at 800 °C for 1 h has better bonding effects.

Tests of silica gel and aluminum phosphate glue for production of SiC whiskers and carbon fiber preforms show that layered damage occurs when using silica gel, and shearing damage occurs when using aluminum phosphate glue. Aluminum phosphate glue has a strong bonding effect. When using silica gel, there is little gel within the preform, and a lot of gel on the top and side surfaces of the preform. When using aluminum phosphate glue, it is uniformly distributed in the preform. In addition, aluminum phosphate glue will not react with Mg, Li, or other elements as easily as the silica gel.

- ② **Choice of squeeze casting temperature** During the squeeze casting process, the preheating temperature of the preform and the melt temperature are determined by the matrix alloy. To infiltrate the preform completely, the appropriate temperature ranges must be used. Figure 3.35 shows the appropriate range of temperatures in the SiC_f/Al composite system. It shows that the range is narrow for squeeze casting of SiC_f/pure Al composites. The temperature ranges of other composites can also be calculated.
- ③ **Choice of best infiltration pressure** The critical infiltration pressure can be calculated according to the capillary model, which is shown in Fig. 3.36. Because the fiber has a disorderly distribution in the composite material, in a single plane, the section ratio of the fibers at different angles is same, as shown in Fig. 3.37.

Fig. 3.35 Range of preheating and melt temperatures

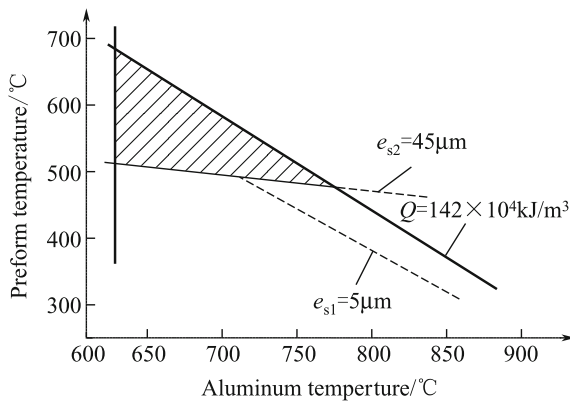


Fig. 3.36 Force analysis of the liquid metal at the infiltration front

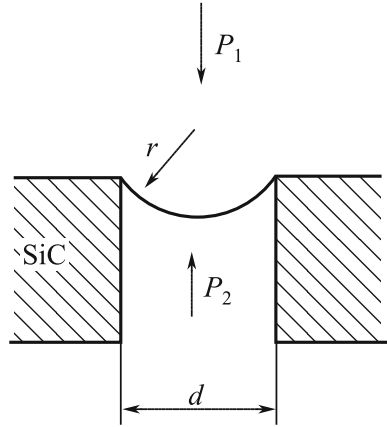
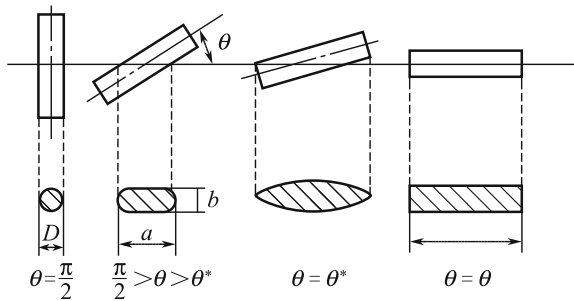


Fig. 3.37 Sections of the SiC whiskers at different angles



Suppose that the fibers are evenly distributed at different angles and that the interspaces between the fibers are round in shape; then, the diameter of an interspace is given by:

$$d = 2\sqrt{\frac{S(1 - V_f)}{\pi V_f}} \tag{3.3}$$

S is the elliptical projection area of fiber sections along the plane, which can be calculated using:

$$S = \frac{\theta^* [LD + \frac{\pi D^2}{4 \sin \theta^*}]}{\pi} + 0.25D^2 \ln\left(\frac{1 + \cos \theta^*}{1 - \cos \theta^*}\right), \tag{3.4}$$

where D is the fiber diameter, L is the fiber length, and θ^* is the angle of the fiber to the plane.

Using $P^* = 4\gamma/d$:

$$P^* = 4\pi\gamma\sqrt{\frac{V_f}{1 - V_f}} \frac{1}{\sqrt{[0.07999(DL + 39.28D^2) + 9.21\pi D^2]}} \tag{3.5}$$

For SiC_w preforms with a volume fraction of 20%, $D = 0.5 \mu\text{m}$, $L = 25 \mu\text{m}$, $\gamma = 0.8 \text{ N/m}$ (800 °C), and the critical infiltration pressure is 1.2 MPa.

The relationship between the critical infiltration pressure and the volume fraction can be obtained based on the above. Figure 3.38 shows the relationships for the three diameters based on Eq. (3.5). It shows that the smaller the fiber diameter is, then the higher the pressure becomes.

The calculated and experimental results for the critical pressure show that for a volume fraction of 11–16%, the liquid metal can infiltrate the preform at pressures higher than 2 MPa. The pressure determines the volume fraction of the reinforcement and the porosity. When the pressure is low, the preform deforms less and the porosity ratio is large. Increasing pressure is beneficial for reducing the porosity, but leads to deformation of the preform. Further research found that the reason for the increasing volume fraction is preform deformation under the pressure of liquid Al before infiltration. The reason for the decreasing porosity is that liquid Al solidified under high pressure after infiltration. If the two pressures can be controlled

Fig. 3.38 Relationship between critical infiltration pressure and volume fraction

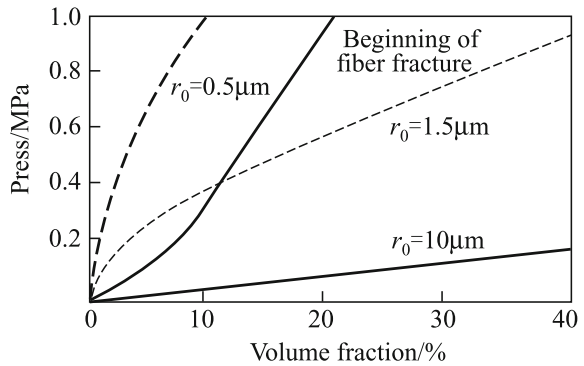
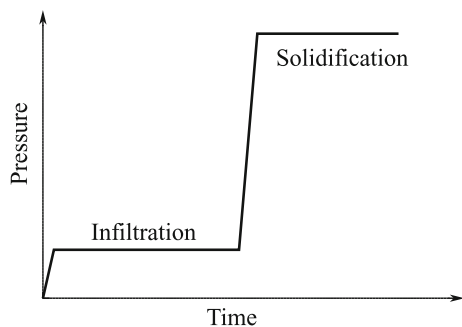


Fig. 3.39 Illustration of two-stage pressure process



separately, then the volume fraction and the porosity can be controlled. This is called a two-stage pressure process. The pressures in the two steps are the infiltration pressure and the solidification pressure. During the two-stage pressure process, it is essential to ensure that the infiltration pressure increases to the solidification pressure after all liquid Al has infiltrated into the preform and before the liquid Al has solidified. The two-stage pressure process is shown in Fig. 3.39. For SiC_w/Al composites, the infiltration pressure is about 5 MPa, and the solidification pressure is in the 50–100 MPa range.

3.3.2.2 In Situ Synthesis

The in situ synthesis technique fabricates composites by forming a fine and thermodynamically stable reinforcement phase within the matrix. The reinforcements can be eutectic precipitations, or be products of the reactions between raw materials. The former produces directional solidification eutectic composite materials, while the latter produces in situ composite materials. As a result, this provides thermodynamic compatibility at the matrix–reinforcement interface. The reinforcement surfaces are also likely to be free of contamination. Therefore, a stronger matrix–dispersion bond can be achieved, especially when the interface between the reinforcements and the matrix is a coherent lattice or semicoherent lattice [39, 40, 49, 50].

(1) Directional solidification

Directional solidification is a technique used to fabricate metal matrix composites by controlling the cooling direction of eutectic alloys. During this process, directionally aligned whisker- or platelike reinforcements grow in the matrix. The reinforcement sizes range from a few millimeters to several hundred microns, depending on the technical parameters. The volume fraction can be from a few percent up to 20%. Generally speaking, the shapes of the reinforcements depend largely on the reinforcement volume fraction and the interface energy. With regard to the properties of the composites, whisker-like reinforcements are better than platelike reinforcements and easily grow under large thermal gradients and low eutectic growth rates.

Directional solidification eutectic composite materials are primarily used for high-temperature materials like those of engine blades and turbine blades. These materials require both the eutectic and the matrix to have good high-temperature performance. To date, most research has focused on nickel- or cobalt-based alloys, in which the reinforcements are intermetallics with good high-temperature properties, like heat resistance and high strength. Research on intermetallic matrix composites has also been performed.

The main problems with directional solidification are that the growth rate of the eutectic must be very slow for control of the microstructure, and the choice of

materials systems is limited. These problems limit the further study and application of such materials.

(2) Reaction synthesis

Reaction synthesis is an effective route for fabrication of metal matrix composites. The technique was developed in the late 1980s and involves Lanxide, XD, and liquid reaction methods. The characteristic features of these techniques are that the reinforcements are formed in situ rather than being added.

- 1) Lanxide: The Lanxide Corporation has developed a series of methods, and one of these methods is directional oxidation. It is a type of liquid reaction method, which is used to fabricate composites by adding oxygen to an Al melt to form $\text{Al}_2\text{O}_3/\text{Al}$ composites. The most important point of this process is the even Al_2O_3 distribution.

Another Lanxide method is known as PRIMEX. In this process, liquid metal pressurelessly infiltrates into a ceramic preform, which involves placing metal ingots on a ceramic preform, setting them in a graphite die together, and then heating up to the melting point of the metal in a N_2 atmosphere. Finally, the molten metal spontaneously infiltrates into the preform. To enable molten metal to infiltrate smoothly into the porous preform, it is very important to eliminate any oxide films, improve the wetting ability, and degas the adsorption gas. All of these functions can be achieved by adding active alloying elements into the melt, e.g., by adding Mg and/or Ti into Al.

- 2) XD: XD is a trademark of the Martin Marietta Corporation. During the XD process, the powders that react with each other to form the reinforcement and the matrix are mixed together and then heated up to the ignition temperature. After the reaction begins, the heat released by the reaction will let it continue. Finally, a composite with fine particles ($< 1 \mu\text{m}$) evenly distributed in the matrix will be formed. This technique is also called self-propagating high-temperature synthesis (SHS).

The numbers of particles can be adjusted by controlling the quantities of the reactants. The technique has been used to fabricate carbide, boride, or nitride particle-reinforced Al, Ti, Ni, or intermetallic matrix composites, e.g., TiC–Al, TiB_2 –NiAl, and TiB_2/TiAl composites. It is also used to fabricate composites with high reinforcement volume fractions, which are then remelted with the matrix alloy to obtain composites with appropriate volume fractions.

- 3) Liquid reaction: During the liquid reaction process, an element or compound that will react with the matrix is added to the liquid metal. At a specific temperature, fine and dispersed particles are formed. For example, following addition of C or hydrocarbons into a molten Al–Ti alloy, C will react with Ti and form TiC particles, as follows: $\text{Ti} + \text{CH}_4 \rightarrow \text{TiC} + \text{H}_2$. The size and number of the particles are influenced by the process and the amounts of available reaction elements. This technique is suitable for production of Al, Mg, and Fe matrix composites.

3.3.2.3 Spray Co-Deposition

Spray co-deposition, which has become popular over the last 20 years, is widely used to fabricate composite materials because of its unique advantages. In this technology, an inert gas is used to atomize liquid metal into tiny droplets and eject them in a certain direction. Meanwhile, the reinforcement is ejected using inert gas from another direction. The two join together and are spray deposited on a water-cooled substrate platform and solidify into composite materials [23, 51].

Spray co-deposition is an effective way of fabricating particle-reinforced metal matrix composites. The matrix material can be Al, Cu, Ni, Fe, or intermetallics, among others. The process includes metal melting, liquid metal atomization, particle mixing with the atomized metal droplets, deposition, and finally consolidation. The main technical parameters are as follows: (1) the metal melting temperature; (2) the pressure, flux, and speed of the inert gas; (3) the additional speed of the particles; (4) the temperature of the substrate. These parameters sensitively affect the qualities of the resulting composite materials. Different metal matrix composites have their own best technical parameters, which must be strictly controlled.

Liquid metal atomization is the most important process of spray co-deposition. This process decides the size, size distribution, and cooling rate of the atomized metal droplets. The size of atomized metal droplets is in the range of 10–300 μm with an asymmetric statistical distribution. The size and size distribution of the droplets are decided by the properties of the liquid metal, the shape and size of the nozzle, the inert gas parameters, and other process factors. During the atomization of the metal liquid, the liquid metal droplets are cooled rapidly by the gas flow. The cooling rate depends on the size of the droplets; the smaller the droplet size is, then the faster the cooling rate can be. After atomization, the smallest droplets are cooled to a solid state, while most of the droplets are semisolid (solid on the surface, and liquid in the center). To obtain good composites, a certain size distribution for the metal liquid droplets is preferred, which is beneficial for maintaining the majority of the liquid metal droplets in semisolid or liquid states as the droplets arrive at the substrate surface. A thin layer of liquid metal will be formed on the surface of the sprayed layer and fills the gaps between particles to obtain uniform and dense composites.

Continuous and uniform addition of particles into the atomized metal droplets is very important for uniform distribution of the particles in the composites. It is therefore very important that the addition method, time, and direction, and the ejector structure are chosen properly. The numbers and the addition speed of the particles should be stable. Fluctuations in the particle numbers directly affect the volume fraction and distribution of particles in the composites and subsequently affect the microstructure and properties of the composites.

The mixing, deposition, and solidification of the atomized droplets and particles are highly important processes in composite fabrication. Deposition and solidification take place alternately. To ensure that these processes proceed smoothly, a liquid metal layer on the deposition surface is preferred during the entire process.

To maintain the balance between deposition and solidification, the right atomizing parameters must be chosen, and the substrate temperature should be stabilized.

The devices used for spray deposition consist of a melting room, an atomized deposition room, a particle addition device, a gas source, and a control board. The most important devices are the atomizing nozzle and the deposition substrate.

Spray co-deposition has attracted scientific and industrial attentions as a new technique for fabrication of particle-reinforced metal matrix composites. It has the following characteristics:

- 1) Wide applicability. The matrix can be Al, Cu, Ni, Co, Fe, or intermetallics. The reinforcements can be SiC, Al₂O₃, TiC, Cr₂O₃, graphite, and other particles. The products can be rods, round ingots, plates, belts, pipes, and many others.
- 2) The production process is simple and effective. Unlike PM, this technique does not require metal powder fabrication and mixing with particles, or pressing and sintering processes. Composite fabrication is completed in one step. The atomization speed is in the 25–200 kg/min range, and deposition and solidification are fast.
- 3) High cooling speed. The metal droplet cooling speed can be as high as 10^3 – 10^6 K/s. The microstructure of the metal matrix is similar to that of composites fabricated by rapid solidification, is fine, uniform, and has no macro-segregation.
- 4) Particles are distributed uniformly in the matrix by strict control of the process parameters.
- 5) Higher porosity. The porosity is in the range of 2–5%, but can be eliminated by extrusion.

The spray co-deposition process is complex and depends on the metal spray, the co-deposition conditions, and the entrance angle of the reinforcements. Faster solidification will undermine compositing between the reinforcements and the matrix material. Slower solidification will cause the reinforcements to be distributed unevenly in the matrix material. The advantages of this route are rapid processing, deposition rates in the 4–10 kg/min range, greater numbers of products, and continuous and automatic processing. Rapid solidification is beneficial for the solid solubility of the alloying elements, and for control of segregation and coarsening. The interface reaction is completely under control. No interface reaction layer or segregation layer is formed between the reinforcement and the matrix material. The interface bonding is by mechanical combination. The reinforcements are distributed evenly. The microstructures of the composites can be fine and non-equilibrium structures. The number of particles can be controlled and adjusted during the process. The composites suffer little oxidation because of the protection of the inert gas. However, this new method also has some problems. Raw materials can be taken away by the gas flow during processing. The material porosity is high, and the microstructure is loose. The reinforcement volume fraction is difficult to increase. The required equipment investment is high.

3.3.2.4 Powder Metallurgy

Powder metallurgy (PM) is a process for fabrication of metal matrix composites in the solid state. This method is mainly used to fabricate MMCs reinforced with short fibers, whiskers, and particles [5, 52]. Full-density composites can be fabricated by PM. The PM process usually involves the following: (1) powder screening; (2) mixing of the metal powder with the reinforcement; (3) pressing of the mixed powders to a relative density of 75%; (4) degassing; (5) solidification by extrusion, forging, rolling, or other hot deformation processes. Compared with the other methods, powder metallurgy has some unique advantages: (1) A lower temperature is used than in the casting methods, which reduces interface reactions between the reinforcements and the matrix alloys, and ensures good mechanical properties; (2) the reinforcement volume fraction is unrestricted; (3) some MMCs can only be fabricated by PM.

PM also has some disadvantages: (1) the high cost of producing the metal powders, coupled with the high possibility explosion of these powders during mixing with reinforcements; (2) high equipment costs; (3) restrictions on product size; (4) non-uniform product microstructures. Recently, to solve these problems, some new techniques, such as hot isostatic pressing (HIP) and mechanical alloying (MA), were developed.

PM is the first technique that has been used to fabricate metal matrix composites. PM can produce composite material parts directly or produce green billets for post-secondary processing, such as extrusion, rolling, forging, and spinning. Even mixing of the metal powder with the reinforcement particles (whiskers) and prevention of metal powder oxidation are the key elements to the whole process.

Powder treatment, which includes screening, electrostatic separation, gas separation, and chemical treatment, is important to guarantee the powder quality. Oxide layers formed during the fabrication and transportation of matrix powders will hinder solidification, which results in lower composite strength and plasticity. Meanwhile, gas contamination can form heat-induced pores during PM processing and heat treatment. These pores will lead to the formation of micro-cracks and seriously reduce the mechanical properties of the composites. Powder degassing, especially at high temperature, has thus become a hot topic in PM research.

PM is suitable for manufacturing SiC_p/Al , SiC_w/Al , $\text{Al}_2\text{O}_3/\text{Al}$, TiB_2/Ti , and other metal matrix composite parts, sheets, and ingots. Reinforcements used include ceramic particles, whiskers, and short fibers, such as SiC_p , Al_2O_3 , SiC_w , and B_4C_p . The matrix materials can be Al, Cu, Ti, intermetallics, and other metal alloys. In SiC_p/Al composites fabricated by PM, there are many types of interface between the matrix and the reinforcement. Apart from a few clean interfaces and step interfaces, the majority are tiny areas with nanoscale thickness. Each tiny area is composed of polycrystalline Al, a Mg congregation area, and MgAl_2O_4 oxide particles. In SiC_p/Fe composites, increasing the volume fraction of SiC particles will slightly reduce the density and hardness and reduce the strength and toughness more, but will greatly increase wear resistance. Nickel plating of SiC_p can also improve the wear resistance. When the volume fraction increases from 5 to 10%,

the wear resistance can be increased by 10–20 times. SiC_p/Zn composites fabricated using rapid solidification technology combined with powder metallurgy have excellent wear resistance. $\text{Al}_2\text{O}_3/\text{Fe}$ composites are made by PM of industrial reduced iron powder, Al_2O_3 particles, carbon powder, and a certain amount of binder material. During processing, some mesophases are formed at the interfaces and increase the bonding strength. The hardness and abrasion resistance of the composite are higher than those of steel materials.

Carbon nanotubes with copper and nickel chemical plating have been used to fabricate carbon nanotube-reinforced copper matrix composites by PM. Certain parameters are important to the performance of the composite, and among them, the carbon nanotube volume fraction is the most significant. When the volume fraction is around 12%, the density and hardness of the composite are at their highest. The optimum process is as follows: first, chemical plating of nickel; then, ball milling for 120 min; cold pressing at 450–500 MPa for 5 min; consolidation at 850 °C for 120 min in a vacuum stove, billet packaging with copper before rolling with 40–50% deformation; and finally, annealing at 600 °C for 120 min.

3.4 Heat Treatment and Processing of Metal Matrix Composites

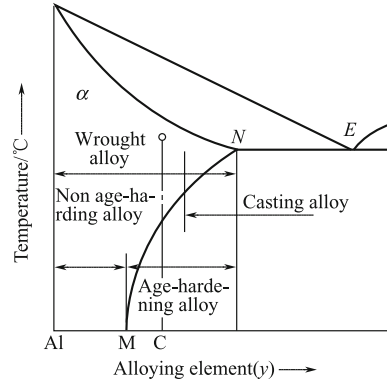
3.4.1 Strengthening Heat Treatment of Metal Matrix Composites

Metal matrix composites (MMCs) are advanced composites, in which metals and ceramics are fabricated together by certain techniques. MMCs have high specific strengths, high specific moduli, and improved creep and thermal resistance properties, and have been receiving a great deal of attention in the fields of materials science and engineering since their first appearance in the 1960s. Aluminum alloys, magnesium alloys, titanium alloys, and copper alloys are now widely used as matrix materials for metal matrix composites. One of the most important methods of improving the properties of MMCs is age hardening, which has become an engineering problem to be solved for the applications of MMCs. Therefore, it is necessary to understand both the technique and the theory of strengthening heat treatments for aluminum alloy matrix composites, magnesium alloy matrix composites, and titanium alloy matrix composites.

3.4.1.1 Strengthening Heat Treatment of Aluminum Alloy Matrix Composites

Aluminum alloys have a crystal structure with a face-centered cubic (FCC) lattice. They have many advantages such as high ductility and toughness, high

Fig. 3.40 Binary phase diagram of aluminum alloys and their classifications



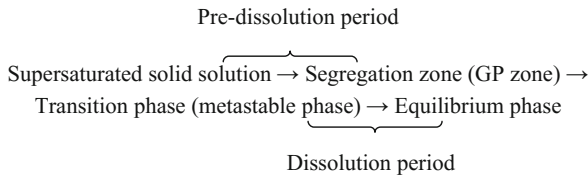
processability, high engineering reliability and low cost, and thus have been widely used as structural materials in the aviation, aerospace, and automobile industries, and are among the most attractive commercial structural materials in their various application fields [18, 19, 21, 23, 53–55].

The reinforcements used in aluminum matrix composites include continuous fibers, short fibers, whiskers, and particles. The properties of the matrix aluminum alloys greatly affect the properties of the aluminum alloy matrixes, so aluminum alloys that can be strengthened by age hardening are usually used as the matrix alloys of aluminum matrix composites. These alloys include wrought aluminum alloys (forged aluminum alloy (LD), Duralumin alloy (LY), super-Duralumin alloy (LC)), and cast aluminum alloy (ZL), with properties as shown in Fig. 3.40.

(1) Age-hardening treatment of aluminum alloys

To understand the age-hardening behavior of aluminum matrix composites, it is necessary to review the age-hardening theory of binary aluminum alloys. The strengthening heat treatment of aluminum alloys is realized through quench-aging. The aim of quench-aging is to improve the strength and hardness of an aluminum alloy through modification of its microstructure by curing, quenching, and aging. The aluminum alloy is heated to a specified temperature, and the alloying elements in the aluminum alloy are dissolved into the aluminum matrix at that temperature, and this is called solution treatment. Then, the aluminum alloy is cooled down at a high cooling rate so that the alloying elements cannot be precipitated from the matrix and no precipitates can be formed during the cooling process; this leads to the formation of a supersaturated aluminum-based solution. The condition required to form the supersaturated solution is that the solubility of the alloying elements in the aluminum matrix increases with increasing temperature (as in the case shown in Fig. 3.40). When the supersaturated aluminum-based solution is maintained at temperatures below its solubility curve, the second-phase (the precipitate) and the solute atom segregation zone (Guinier-Preston or GP zone) will be precipitated from the supersaturated solid solution, forming a dissolution and aging process. The precipitate is usually not an equilibrium phase in the diagram, but is a

non-equilibrium phase or a segregation zone of the solute atoms. XRD and electron microscopy results showed the following dissolution sequence:

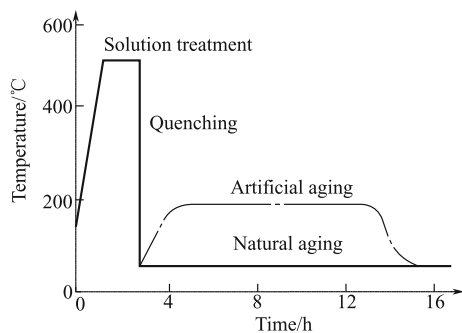


For an Al–Cu alloy, the dissolution sequence of the age precipitate phases is as follows: supersaturated solid solution \rightarrow GP zone \rightarrow θ'' \rightarrow θ' \rightarrow θ (CuAl_2). It should be noted that it is not true that all four aging periods will occur at any aging temperature, and the GP zone is not always the first period of the aging precipitation process. The new precipitate is usually formed more easily if the crystal defect density increases in the solid solution, and the dissolution rate increases. The formation of the GP zone relates to the vacancy density, and the formation of the transition phase depends on the dislocation density of the solid solution. The aging of aluminum alloys includes natural aging and artificial aging, and these processes are shown schematically in Fig. 3.41. The GP zone is the main product of natural aging, and the precipitate phase is the main result of artificial aging.

The first condition for formation of the age-hardening effect is that the alloying elements have high solubility in aluminum, and this solubility increases with increasing temperature, as shown in Fig. 3.41. The second condition is that the GP zone and the transition phases can be formed during the aging process and an obvious lattice distortion can be produced in the matrix. Only when both of these conditions are satisfied can an obvious age-hardening effect can be obtained in aluminum alloys. There are large age-hardening effects in the aluminum alloys of the Al–Cu, Al–Cu–Mg, Al–Mg–Si, Al–Zn–Mg–Cu, and Al–Li systems.

The age-hardening behavior of aluminum alloys is well understood. However, it will become more complicated if reinforcements are added to the aluminum alloy matrix. Therefore, it is important to introduce the aging mechanism and

Fig. 3.41 Schematic of the aging processes of aluminum alloys



characteristics and the factors that influence the aging behavior of aluminum alloy matrix composites. Typical heat treatment processes of some common aluminum matrix composites are also introduced.

(2) Age-hardening characteristics and mechanisms of aluminum alloy matrix composites

In aluminum alloy matrix composites, the addition of reinforcements cannot change the basic age-hardening process of the matrix aluminum alloys. In both aluminum alloy matrix composites and unreinforced matrix aluminum alloys, the morphological characteristics of the precipitates are the same. Both the age-hardening process and the age precipitation sequence of the aluminum matrix composite are the same as those of the unreinforced matrix aluminum alloy. Figure 3.42 shows the differential scanning calorimetry (DSC) curves of a $\text{SiC}_w/2124\text{Al}$ composite and a non-reinforced 2124Al alloy. Although the precipitation temperature of the $\text{SiC}_w/2124\text{Al}$ composite is a little lower than that of the unreinforced 2124Al alloy, the shapes of both DSC curves are very similar to each other and the numbers of the exothermic peaks in the two curves are the same. This indicates that there is no natural difference in the precipitate phase and the precipitation sequence between aluminum matrix composites and the corresponding unreinforced aluminum alloys. Like Al–Cu alloys, the age precipitation sequence of the $\text{SiC}_w/2124\text{Al}$ composite and that of the unreinforced 2124Al alloy is as follows: supersaturated solid solution \rightarrow GP zone \rightarrow metastable phase S' \rightarrow equilibrium phase S (Al_2CuMg).

Compared with the unreinforced aluminum alloys, the age-hardening process of aluminum alloy matrix composites is accelerated by the addition of the reinforcements, and the time required to reach peak hardness is shortened, as shown in Fig. 3.43. Also, the addition of the reinforcements may inhibit or delay the formation of the GP zone.

Fig. 3.42 DSC curves of $\text{SiC}_w/2124\text{Al}$ composite and unreinforced 2124Al alloy

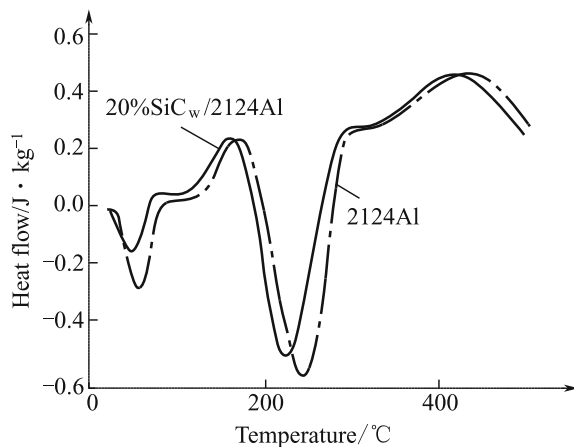
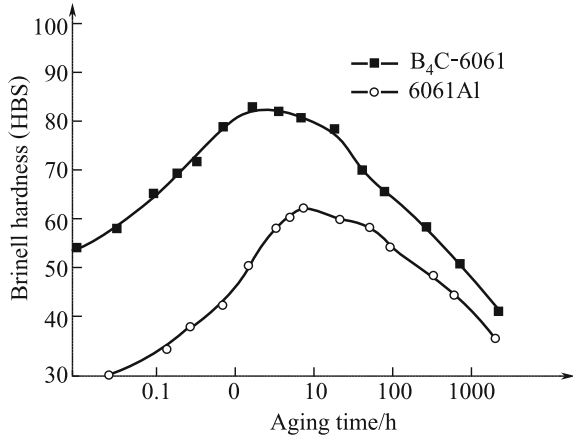


Fig. 3.43 Age-hardening curves of $B_4C/6061Al$ composite and 6061Al alloy



The acceleration of the age-hardening process in aluminum alloy matrix composites is considered to be related to the high density of dislocations in the matrix of the composites. The high dislocation density is increased in the aluminum alloy matrix composites because of the large difference in coefficients of thermal expansion between the reinforcement and the matrix. These high-density dislocations affect the aging processes of the composites in two respects. First, these dislocations provide heterogeneous nucleation positions for some precipitate phases, such as the transition S' -, θ' -, and β' -phases, where nucleation depends heavily on the dislocations and other crystal defects. Therefore, the activation energy required to form these precipitate phases is reduced and the precipitation process is improved. Second, short path diffusion caused by these dislocations increases the diffusion rate of the solute atoms, improves the nucleation and growth of the precipitate phase, and accelerates the composite aging process. In fact, these two phenomena usually occur simultaneously during the aging process of aluminum alloy matrix composites. In the microscale, the precipitation kinetics are improved in the composite, and in the macroscale, the age-hardening process of the composite is accelerated.

(3) Factors affecting the age hardening of aluminum alloy matrix composites

The factors that influence the age-hardening behavior of aluminum matrix composites include the following: the chemical composition of the matrix alloy; the aging temperature; the type, size, shape, and volume fraction of the reinforcements; and the composite fabrication method.

- 1) **Chemical composition of matrix alloy** In aluminum alloy matrix composites, the addition of the reinforcement cannot change the precipitation processes and the characteristics of the precipitates. The age-hardening abilities of aluminum alloy matrix composites depend not only on the quenching and aging technical parameters, but also on the properties and composition of the matrix alloy. Therefore, it is necessary to determine the precipitates and their

Table 3.42 Precipitate phases of some typical aluminum alloys

Alloy system	Precipitate	Characteristic*	Application
Al–Mg	Spherical G.P zone β' β ($Mg_5 Al_3$)	TP, S, hexagonal structure EP, N, FCC structure	Anti-rust aluminum alloy
Al–Cu	Disciform G.P zone Disciform θ'' Plate θ' θ (Al_2Cu)	TP, C, square structure TP, S, square structure EP, N, body-centered square	Casting aluminum alloy
Al–Cu–Mg	Rod-like G.P zone S' ($Al_2Cu Mg$) S ($Al_2Cu Mg$)	TP, S, orthogonal structure EP, N, orthogonal structure	Hard aluminum alloy
Al–Mg–Si	Needle-like G.P zone Rod-like β'' (Mg_2Si) Plate β (Mg_2Si)	TP, S, hexagonal structure EP, N, FCC structure	Forged aluminum and casting aluminum alloys
Al–Zn–Mg–Cu	Spherical GP zone η'' η ($Mg Zn_2$) T'' T	TP, S, hexagonal structure TP, S EP	Super-duralumin alloy

*TP—Transition phase, EP—Equilibrium phase, C—Coherent, S—Semi-coherent, N—Non-coherent

dissolution sequences during the aging treatment of aluminum matrix composites for the different matrix aluminum alloy compositions. Aluminum alloys with different chemical compositions have different precipitate phases and precipitation sequences. The precipitate phases and precipitation sequences of some typical aluminum alloys are shown in Tables 3.42 and 3.43.

- 2) **Aging temperature** The aging temperature is one of the most important parameters in the age-hardening processes of aluminum matrix composites. With increasing aging temperature, the activity of the atoms increases so that the dissolution rate also increases. However, if the aging temperature is too high, then the supersaturation degree of the alloy increases and the free energy difference for dissolution decreases, leading to a reduction in the dissolution rate. It is therefore very important to choose the optimum aging temperature for the aging treatment of aluminum matrix composites.

It was found that the natural aging process of an aluminum matrix composite is slower than that of the unreinforced aluminum alloy, while the artificial aging

Table 3.43 Precipitation sequences of some typical aluminum alloys

Alloy system	Precipitation sequence and equilibrium precipitate phase
Al–Cu	GP zone (disciform) $\rightarrow \theta'' \rightarrow \theta' \rightarrow \theta$ (Al_2Cu)
Al–Ag	GP zone (spherical) $\rightarrow \gamma' \rightarrow \gamma$ ($Al Ag_2$)
Al–Zn–Mg	GP zone (spherical) $\rightarrow \eta' \rightarrow \eta$ ($Mg Zn_2$) or GP zone (spherical) $\rightarrow T' \rightarrow T$ ($Al_2Mg_3 Zn_3$)
Al–Mg–Si	GP zone (needlelike) $\rightarrow \beta' \rightarrow \beta$ (Mg_2Si)
Al–Cu–Mg	GP zone (needlelike or spherical) $\rightarrow S' \rightarrow S$ ($Al_2Cu Mg$)

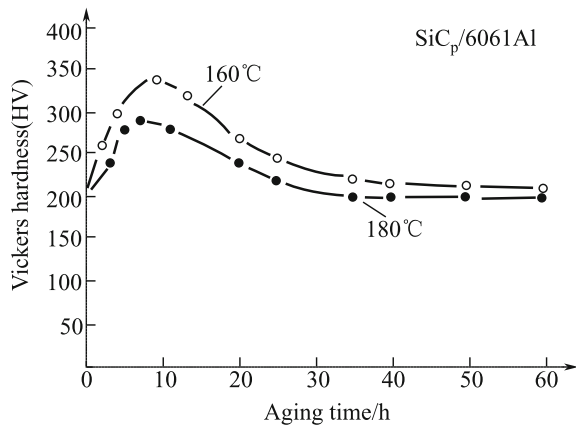
process of the composite is faster than that of the unreinforced aluminum alloy. This is because of the change in the type of precipitate phase with increasing aging temperature (from the GP zone to the transition phase).

With increasing aging temperature, the age-hardening behavior of aluminum matrix composites changes in the same way as that of the unreinforced matrix aluminum alloys. Depending on the type of matrix aluminum alloy, the hardening rate of the composite is faster than that of unreinforced matrix by different degrees. For example, at an aging temperature of 160 °C, the time required to form the hardness peak decreases from 14–16 h for the 15 vol.% SiC_w/6061Al composite to 4–5 h for the 6061Al alloy; at an aging temperature of 177 °C, the time required to form the hardness peak decreases from 12 h for the 13.2 vol.% SiC_w/2142Al composite to 4 h for the 2124Al alloy.

The age-hardening behavior of aluminum matrix composites is greatly affected by the aging temperature, as shown in Fig. 3.44. With increasing aging temperature, the dissolution rate of the strengthening phase increases and the age-hardening process of the composite is accelerated, leading to a reduction in the time required to reach peak hardness. In addition, with increasing aging temperature, the supersaturation degree of the solid solution decreases, and thus, the amount of precipitate decreases, which results in a fall in the value of the peak hardness.

- 3) Type, volume fraction, and size of reinforcement The age-hardening behavior of aluminum matrix composites is related to the type of reinforcement used. It is known that certain matrix aluminum alloys will react with certain reinforcements. Such interfacial reactions may change the compositions of the matrix aluminum alloys and in turn change the age-hardening properties of the aluminum alloy matrix composites. The age-hardening behavior of SiC_p/6061Al and Al₂O_{3p}/6061Al composites has been studied. The results indicate that the time needed to reach peak hardness is the same for both composites, but the age-hardening ability of the SiC_p/6061Al composite is greater than that of the Al₂O_{3p}/6061Al composite. The reason for this is that in the Al₂O_{3p}/

Fig. 3.44 Age-hardening curves of the SiC_p/6061Al composite at different aging temperatures



6061Al composite, the Mg element in the matrix 6061Al alloy can react with Al_2O_3 particles to form an interfacial reaction product (MgAl_2O_4 spinel), and this interfacial reaction will consume Mg elements in the matrix 6061Al alloy, so that the amount of the strengthening precipitate in the $\text{Al}_2\text{O}_3/\text{6061Al}$ composite decreases and the age-hardening ability of the composite also decreases.

The age-hardening behavior of aluminum alloy matrix composites is also affected by the volume fraction of the reinforcement. Figure 3.45 shows the effect of the SiC particle volume fraction on age-hardening behavior of the $\text{SiC}_p/7075\text{Al}$ composites. When the SiC particle volume fraction is less than 20%, the age-hardening curves of the $\text{SiC}_p/7075\text{Al}$ composites are similar to those of the unreinforced 7075Al alloy, and the difference is that the time needed to reach the peak hardness of the $\text{SiC}_p/7075\text{Al}$ composite is shorter than that for the unreinforced 7075Al alloy. The reason for this difference is that with increasing SiC particle volume fraction, the dislocation density in the $\text{SiC}_p/7075\text{Al}$ composite also increases, leading to accelerated growth speeds for the GP zone and the β' -phase, so that the aging process increases. The age-hardening curves of $\text{SiC}_p/7075\text{Al}$ composites with higher SiC particle volume fractions (i.e., higher than 20%) are different to that of the unreinforced 7075Al alloy, especially when the SiC particle volume fractions are 30% and 40%. There is almost no age hardening in the $\text{SiC}_p/7075\text{Al}$ composites, which may be because the formation of the GP zone and the precipitation are inhibited by the addition of a large number of SiC particles.

The age-hardening behavior of aluminum alloy matrix composites is also affected by the size of the reinforcement. The precipitation mechanism of aluminum alloy matrix composites reinforced with sub-micron-scale reinforcements is quite different to that of composites reinforced with common micron-scale reinforcements. The age-hardening speed of the aluminum alloy matrix composites reinforced with sub-micron-scale reinforcements is slower than that of the unreinforced matrix aluminum alloys, irrespective of the changes in aging temperature and the volume fraction of the reinforcement. This phenomenon is illustrated by the

Fig. 3.45 Age-hardening curves of $\text{SiC}_p/7075\text{Al}$ composites with different SiC particle volume fractions at 120 °C. ●—7075Al; ▽—5 vol.% SiC particle; ▼—10 vol.% SiC particle; □—20 vol.% SiC particle; ■—30 vol.% SiC particle; △—40 vol.% SiC particle

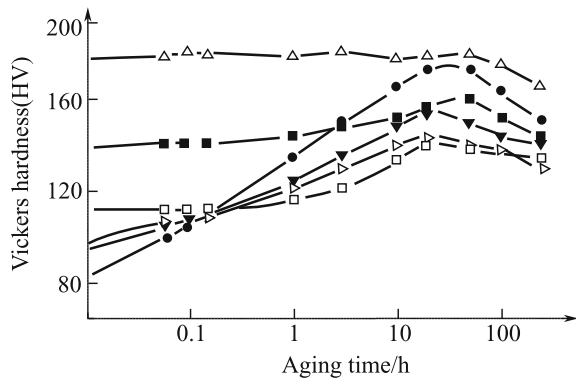
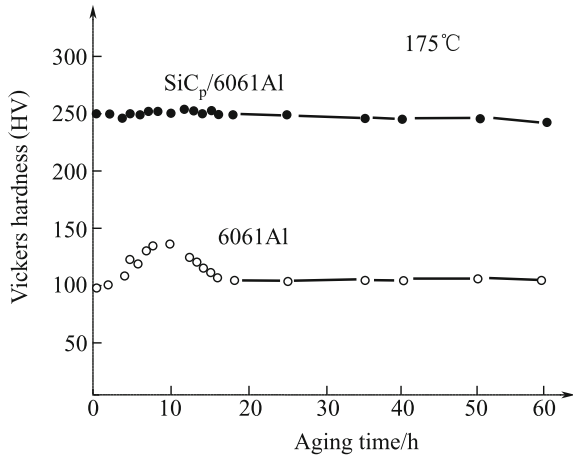


Fig. 3.46 Age-hardening curves of the 6061Al matrix composite reinforced with sub-micron-scale SiC particles and the unreinforced 6061Al alloy



experimental results for the age-hardening curves at 170 °C of the 6061Al matrix composite reinforced with 35 vol.% sub-micron-scale SiC particles and the unreinforced 6061Al alloy, as shown in Fig. 3.46.

The age-hardening behavior of aluminum alloy matrix composites is also affected by the fabrication of the composites. For example, if the SiC particle reinforcement is sintered at a high temperature before fabrication of the composites, a SiO₂ layer will be formed on the SiC surface; this layer will react with the Mg element in the aluminum alloy matrix, resulting in consumption of the Mg element in the aluminum alloy matrix and a change in the age-hardening behavior of the SiC_p/Al composites. If the aluminum alloy matrix composites are fabricated by the squeeze casting method, the SiO₂ added to the reinforcement preform as a binder will also react with the Mg element. The reaction between SiO₂ and Mg will release the Si in the aluminum alloy matrix, and if an Al–Mg binary alloy, which is a nonage-hardening alloy, is used as the matrix, then age hardening may occur because the Mg₂Si phase may be precipitated as a strengthening phase.

(4) Technical parameters of aging heat treatment of aluminum alloy matrix composites

The technical parameters of the aging heat treatment of the aluminum alloy matrix composites can be determined by considering those used for their unreinforced aluminum alloys, but they are not the same. For each specific aluminum alloy matrix composite, the optimum aging parameters are obtained experimentally and the effects of the fabrication method, the matrix chemical composition, the properties of the reinforcement, and the aging conditions on the age-hardening process must be taken into account. The technical parameters of aging heat treatment for some typical aluminum alloy matrix composites are shown in Table 3.44.

Table 3.44 Aging parameters of some typical aluminum alloy matrix composites

Composite	Fabrication method	Size of reinforcement (μm)	Reinforcement content	Solution		Aging	
				Temp ($^{\circ}\text{C}$)	Time (h)	Temp ($^{\circ}\text{C}$)	T_p^a (h)
SiC _p /2024Al	Powder metallurgy	20	(5–20) vol.%	490	1	170	5
SiC _p /2024Al	Squeeze casting	49	5 wt.%	500	2	170	15
SiC _p /2024Al	Squeeze casting	49	10 wt.%	500	2	170	13
SiC _p /2024Al	Squeeze casting	49	20 wt.%	500	2	170	9
SiC _w /2024Al	Squeeze casting	–	27 vol.%	520	1.5	170	14
SiC _w /2024Al	Squeeze casting	–	25 vol.%	490	2	190	–
SiC _w /2024Al	Squeeze casting	–	20 vol.%	495	–	190	2, 5, 20
SiC _w /2024Al	Squeeze casting	–	15 vol.%	495	2	120	6
SiC _w /2024Al	Squeeze casting	–	15 vol.%	495	2	150	6
SiC _w /2024Al	Squeeze casting	–	15 vol.%	495	2	170	4
SiC _w /2014Al	Squeeze casting	–	15 vol.%	495	2	200	2
(Al ₂ O ₃ + SiO ₂)/AA336	Squeeze casting	–	10 vol.%	520	9	205	4
(Al ₂ O ₃ + SiO ₂)/AA336	Squeeze casting	–	15 vol.%	520	9	205	3–4
(Al ₂ O ₃ + SiO ₂)/AA336	Squeeze casting	–	20 vol.%	520	9	205	3–4
SiC _p /6061Al	Squeeze casting	85	50 vol.%	557	2	160	5
SiC _p /6061Al	Squeeze casting	30	50 vol.%	557	2	160	5
SiC _p /6061Al	Squeeze casting	14	50 vol.%	557	2	160	3
SiC _p /6061Al	Squeeze casting	14	15 vol.%	520	1	160	8
SiC _p /6061Al	Squeeze casting	–	(17–32) vol.%	520	1	170	10
SiC _w /6061Al	Squeeze casting	–	20 vol.%	520	1	170	10
SiC _w /6061Al	Squeeze casting	–	20 vol.%	500	1	180	2, 5, 12
Al ₂ O _{3p} /6061Al	Powder metallurgy	0.3	10 vol.%	530	1	–	–

(continued)

Table 3.44 (continued)

Composite	Fabrication method	Size of reinforcement (μm)	Reinforcement content	Solution		Aging	
				Temp ($^{\circ}\text{C}$)	Time (h)	Temp ($^{\circ}\text{C}$)	T_p^a (h)
SiC _p /6013Al	Reaction infiltration	200, 45, 25	50 vol.%	495	4	170	10
SiC _p /6063Al	Powder metallurgy	20	(5–20) vol.%	525	1	150	5
SiC _p /7075Al	Spray deposition	14	15 wt.%	470	1	120	24
SiC _p /7075Al	Powder metallurgy	12.5	(5–40) vol.%	470	1	120	13–14
SiC _p /7020Al	Stir casting	40–100	5 vol.%	540 \pm 10	2	170	18
SiC _p /7020Al	Stir casting	40–100	10 vol.%	540 \pm 10	2	170	15
SiC _p /7034Al	Powder metallurgy	–	15 vol.%	490	4	120	24
SiC _w /Al–Li–Cu–Mg–Zr	Squeeze casting	–	22 vol.%	530	40 min	160	40
SiC _w /Al–Li–Cu–Mg–Zr	Squeeze casting	–	22 vol.%	530	40 min	190	12–15
SiC _w /Al–Li–Cu–Mg–Zr	Squeeze casting	–	22 vol.%	530	40 min	220	2.5–3
SiC _p /ZL102	Stir casting	10	10 vol.%	535	5	170	8–16
(Al ₂ O ₃ + SiO ₂)/ZL 107	Squeeze casting	–	8, 16 vol.%	550	7	140 205	25 5
SiC _p /ZL109	Liquid forging	10	(5–10) vol.%	510	6	150	8
SiC _p /ZL109	Stir casting	–	10 vol.%	535	5	170	12
(Al ₂ O ₃ + SiO ₂)/ZL109	Powder metallurgy	12.5	20 vol.%	515	1	190	0.5
(Al ₂ O ₃ + SiO ₂)/ZL109	Liquid infiltration	–	10, 20, 30 vol. %	500	1.5	200	8
(Al ₂ O _{3f} + C _f)/ZL109	Squeeze casting	–	20 vol.%	510	4	170	4–8
SiC _p /ZL201	Stir casting	10, 20, 40	5, 10, 15 wt.%	520–530	9	175	5

^a T_p —Time needed to reach peak hardness

(5) Properties of aluminum alloy matrix composites after age-hardening treatment

The strength, hardness, and ductility of the aluminum alloy matrix composites have been changed quite obviously by the age-hardening heat treatment. Table 3.45 shows the mechanical properties of some typical aluminum alloy matrix composites.

Table 3.45 Mechanical properties of some typical aluminum alloy matrix composites

Composite	Elastic modulus (GPa)	Yield strength (MPa)	Tensile strength (MPa)	Fracture elongation (%)
25% SiC _p /6013Al-T6	121	469	565	4.3
25% SiC _p /6061Al-T6	119	427	496	4.1
25% SiC _p /6091Al-T6	117	396	486	5.5
25% SiC _p /7475Al-T6	117	593	655	2.5
25% SiC _p /2124Al-T4	117	496	738	5
20% SiC _p /6061Al-T6	97	415	498	6
10% Al ₂ O ₃ /6061Al-T6	81	296	338	–
15% Al ₂ O ₃ /6061Al-T6	87	317	359	–
20% Al ₂ O ₃ /6061Al-T6	98	359	379	–
15% SiC _p /6061Al-T6	91	342	364	–
15% SiC _p /6061Al-T4	98	405	460	–
20% SiC _p /6061Al-T4	105	420	500	–
25% SiC _p /6061Al-T4	115	430	515	–
10% Al ₂ O ₃ /2014Al-T6	84	483	517	–
10% Al ₂ O ₃ /2014Al-T6	92	476	503	–

3.4.1.2 Strengthening Heat Treatment of Magnesium Alloy Matrix Composites

Magnesium alloys have many advantages, including low density, high specific strength, high specific modulus, high damping capacity, and good casting and processing ability [56–58]. However, their disadvantages of low hardness, strength, modulus, and wear resistance have limited the widespread application of magnesium alloys. These disadvantages are being overcome by the appearance of high-performance discontinuously reinforced magnesium alloy matrix composites, which are among the most promising metal matrix composites in current high-tech areas. To further widen the potential application fields of magnesium alloy matrix composites, the research into the strengthening heat treatment of these composites

Table 3.46 Precipitates and melting points in some typical magnesium alloys

Alloy system	Maximum solubility (%)	Precipitate	Melting point (°C)
Mg–Al	12.7	Mg ₁₇ Al ₁₂	437
Mg–Zn	8.4	MgZn	347
Mg–Ca	2.2	Mg ₂ Ca	714
Mg–Ce	0.74	Mg ₁₈ Ce	611
Mg–Nd	3.6	Mg ₁₈ Nd	580
Mg–Th	5.0	Mg ₃₃ Th	772
Mg–Y	12.0	Mg ₂₄ Y ₅	620
Mg–Bi	8.85	Mg ₃ Bi ₂	823
Mg–Si	~0	Mg ₂ Si	1087
Mg–Sb	~0	Mg ₃ Sb ₂	1245
Mg–Sn	14.85	Mg ₂ Sn	772
Mg–Sr	~0	Mg ₁₇ Sr ₂	606

is becoming increasingly important. Metal matrix composites are usually used in environments where high strength and a high modulus are required. The high performance of continuously reinforced metal matrix composites is mainly due to the contribution of the continuous fibers in the composites. However, for discontinuously reinforced metal matrix composites, the properties of the matrix alloy have a major effect on the properties of the composites, so any modification of the matrix alloy properties in discontinuously reinforced metal matrix composites is very important. Similar to the aluminum alloy matrix composites described above, age-hardening heat treatment is an effective method to improve the properties of the matrix alloys in magnesium alloy matrix composites. The age-hardening kinetics and degree are affected by the characteristics of the reinforcement, the composite fabrication method, the aging temperature, and the interface between matrix and reinforcement. Table 3.46 shows the precipitates and corresponding melting points of some typical magnesium alloys.

The mechanical properties of magnesium alloys can be improved by the following: (1) solution strengthening; (2) precipitation strengthening; and (3) dispersion strengthening. The alloying elements can be classified into three types according to their effects on the mechanical properties of the magnesium alloy: (1) the elements that increase the strength and ductility of the alloys simultaneously, which are Al, Zn, Ca, Ag, Ce, Ni, Cu, and Th; (2) the elements that increase the ductility of the alloys, which are Cd, Ti, and Li; and (3) the elements that increase the strength but reduce the ductility of the alloys, which are Sn, Pb, Bi, and Sb. The methods that increase the creep resistance of magnesium alloys include the following: (1) fine and dispersed precipitates at the grain boundaries of the magnesium alloy, which can inhibit grain boundary sliding; (2) large size grains, which can enlarge the diffusion distance and reduce the effects of grain boundary diffusion; (3) increasing the elastic modulus of the magnesium matrix by increasing solution strengthening. It has been found that rare earth (RE) elements (such as Ce, Nd, Y),

Th, Si, Ca, Sr, Ba, and Sb can increase the creep strength of magnesium alloys. The addition of these elements to magnesium alloys may enhance the alloy properties at elevated temperatures. The reasons for this are as follows: (1) The precipitates formed by these elements contain large fractions of Mg atoms, such as $Mg_{12}Ce$, $Mg_{12}Nd$, $Mg_{23}Th_6$, and $Mg_{24}Y_6$, so that larger fractions of precipitates can be formed for a specific added amount of these elements; (2) the precipitates have higher melting points and thermal stabilities; (3) the RE, Th and Y elements have higher melting points (798–1663 °C) and lower diffusion rates in the magnesium matrix.

The maximum age-hardening effect can be achieved by solution treatment and aging treatment. However, the strengthening precipitates will grow and may even be dissolved back into the solid solution, leading to a reduction in the hardness and strength of the magnesium alloys. If some fine particles, which have high melting points and are not dissolved into the magnesium solid solution, are added to the magnesium alloys, a kind of dispersed strengthening magnesium alloy is obtained, which can maintain the high mechanical properties at higher temperatures. The dispersed magnesium alloy has higher creep properties because of the pinning effect of the dispersed phases and the high density of the dislocations in the alloys.

(1) Strengthening heat treatment of cast magnesium alloy matrix composites

A 20 vol.% $SiC_w/AZ91$ composite has been fabricated using a squeeze casting method. A two-step heating technique was used for solution treatment of the composite to inhibit melting of the low-melting point compound at the grain boundaries. The $SiC_w/AZ91$ composite and the unreinforced AZ91 magnesium alloy were heated to 380 °C and kept at this temperature for 2 h; they were then heated to 415 °C and kept at this temperature for 24 h, followed by water quenching. Aging treatment was carried out at 175 °C for 0–200 h, and the hardness values of the $SiC_w/AZ91$ composite and the AZ91 alloy at different aging times are shown in Fig. 3.47.

Figure 3.47 shows that when the $SiC_w/AZ91$ composite and the AZ91 magnesium alloy are aged at 175 °C, the peak hardness of the $SiC_w/AZ91$ composite is

Fig. 3.47 Age-hardening curves at 175 °C for the $SiC_w/AZ91$ composite and the AZ91 magnesium alloy

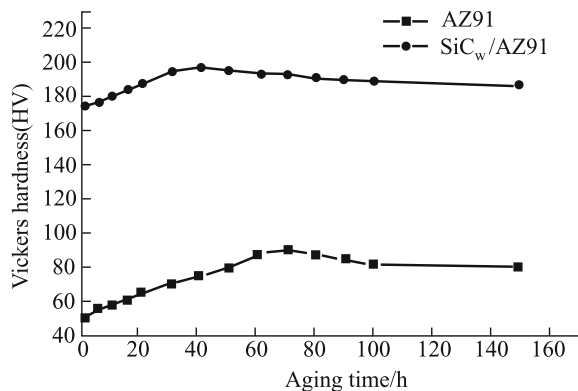
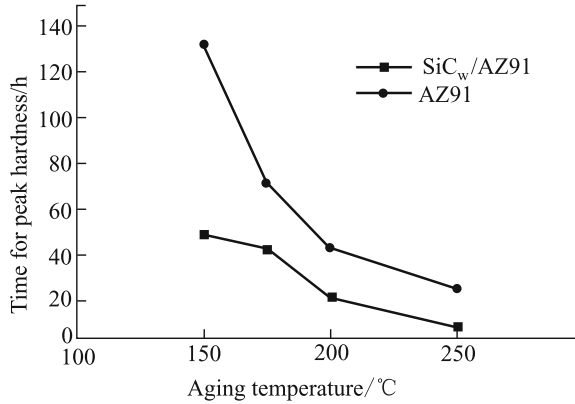


Fig. 3.48 Effect of aging temperature on the time needed to reach peak hardness of the SiC_w/AZ91 composite and AZ91 magnesium alloy



reached at an aging time of 40 h and that of the AZ91 magnesium alloy is reached at an aging time of 70 h. This result indicates that the aging process of the SiC_w/AZ91 composite is faster than that of the AZ91 magnesium alloy at the aging temperature of 175 °C.

Figure 3.48 shows the effect of the aging temperature on the time needed to reach the peak hardness of the SiC_w/AZ91 composite and the AZ91 magnesium alloy. For both materials, the time needed to reach peak hardness decreases with increasing aging temperature. The reason for this is that the age-hardening kinetics accelerates when the aging temperature increases. At all aging temperatures, the time needed to reach the peak hardness of the SiC_w/AZ91 composite is shorter than that required for the unreinforced AZ91 magnesium alloy.

Figure 3.49 shows the effect of the aging temperature on the peak hardness increment (the difference between peak hardness and hardness in the solution state) of the SiC_w/AZ91 composite and the AZ91 magnesium alloy. At all aging temperatures, the peak hardness increment of the SiC_w/AZ91 composite is lower by 20–30% when compared with that of the unreinforced AZ91 magnesium alloy. This

Fig. 3.49 Effect of aging temperature on the peak hardness increments of the SiC_w/AZ91 composite and AZ91 magnesium alloy

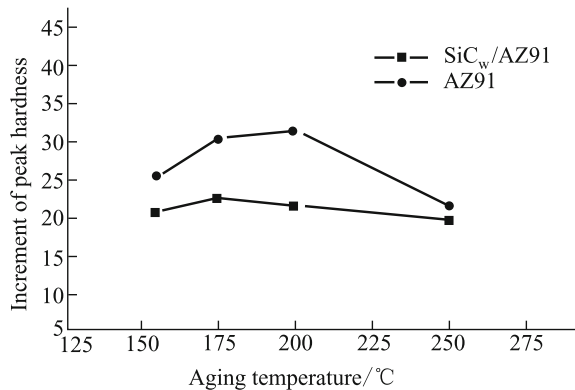


Table 3.47 Tensile properties of the SiC_w/AZ91 composite in different heat treatment states

Property State	Hardness (HV)	Yield strength (MPa)	Tensile strength (MPa)	Elastic modulus (MPa)	Elongation (%)
As cast	178	240	370	86	1.12
Solid solution	175	220	355	85	1.40
T6 (175 °C, 40 h)	202	–	398	92	0.62

result indicates that the age-hardening degree of the SiC_w/AZ91 composite is lower than that of the unreinforced AZ91 magnesium alloy.

The tensile properties of the SiC_w/AZ91 composite in different heat treatment states are shown in Table 3.47. It is shown that the ductility of the composite is increased by the solid solution treatment. Peak hardness aging treatment (T6) obviously improves the tensile strength of the SiC_w/AZ91 composite because of the dispersed precipitate phases, but the ductility of the composite decreases. In the peak hardness aging treatment (T6) state, the dispersed precipitate in the SiC_w/AZ91 composite is Mg₁₇Al₁₂, which is distributed in the grain of the matrix in sheet form and also at the SiC_w-AZ91 interface in cellular form.

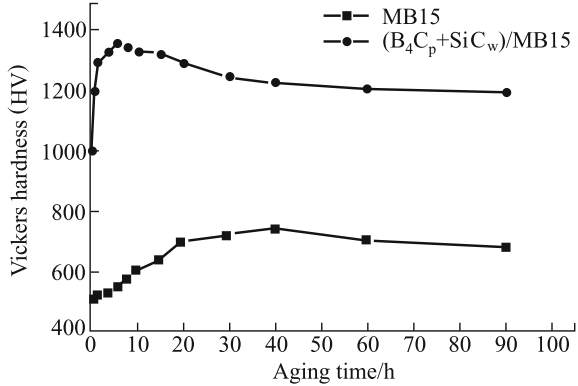
(2) Strengthening heat treatment of wrought magnesium alloy matrix composites

A (B₄C_p + SiC_w)/MB15 composite has been fabricated by the vacuum-pressure infiltration technique, and the volume fraction of both the B₄C particles and the SiC whiskers in the composite is 12%. Samples of the (B₄C_p + SiC_w)/MB15 composite and the unreinforced MB15 magnesium alloy are sealed in a vacuum glass tube and are solution treated at 360 °C for 4 h, followed by ice water quenching and are then aged in a vacuum at 170 °C for various times.

It is known from the DSC experimental results that the precipitation temperatures of the (B₄C_p + SiC_w)/MB15 composite and the unreinforced MB15 magnesium alloy are 218 and 233 °C, respectively, indicating that the aging process of the (B₄C_p + SiC_w)/MB15 composite is accelerated by the residual stress and the high-density dislocations in the composite, which are caused by the addition of the B₄C particles and SiC whiskers to the composite. The DSC results also show that the solution temperatures of the β'-phases (Laves MgZn₂) in the (B₄C_p + SiC_w)/MB15 composite and the unreinforced MB15 magnesium alloy are 292 °C and 288 °C, respectively, indicating that the stability of the precipitate in the (B₄C_p + SiC_w)/MB15 composite is higher than that in the unreinforced MB15 magnesium alloy. It is also found from the DSC results that the amount of precipitate in the (B₄C_p + SiC_w)/MB15 composite is larger than that in the unreinforced MB15 magnesium alloy under the same aging conditions.

The age-hardening curves of the (B₄C_p + SiC_w)/MB15 composite and the unreinforced MB15 magnesium alloy are shown in Fig. 3.50. They show that the hardness in the solution state of the (B₄C_p + SiC_w)/MB15 composite is 1000 MPa, which is much higher than that of the unreinforced MB15 magnesium alloy

Fig. 3.50 Age-hardening curves of $(B_4C_p + SiC_w)/MB15$ composite and MB15 magnesium alloy at 175 °C



(500 MPa). It is also shown that the time needed to reach the peak hardness of the $(B_4C_p + SiC_w)/MB15$ composite is only 6 h, but it takes 40 h for the unreinforced MB15 magnesium alloy, indicating that the aging process of the $(B_4C_p + SiC_w)/MB15$ composite is accelerated. The peak hardness increment for both materials is 200 MPa, indicating the same degree of age hardening for both the $(B_4C_p + SiC_w)/MB15$ composite and the unreinforced MB15 magnesium alloy.

3.4.1.3 Strengthening Heat Treatment of Titanium Alloy Matrix Composites

The microstructure of the matrix in metal matrix composites is changed by the addition of the reinforcement [10, 11, 59, 60]. High-density dislocations are formed in the matrix because of the thermal mismatch between reinforcement and matrix, which induces heterogeneous nucleation of precipitates in the matrix during the addition process. This causes a change in the precipitation kinetics of metal matrix composites compared with those of the unreinforced matrix metals. Although ceramic reinforcements such as SiC, B_4C , and Al_2O_3 are not affected by the aging treatment, they have an obvious influence on the precipitation behavior of metal matrix composites. Therefore, the strengthening heat treatment of titanium matrix composites will be greatly influenced by the existence of the ceramic reinforcement, and thus, the heat treatment parameters for titanium matrix composites are different to those for the unreinforced titanium alloys.

(1) Properties and heat treatment of titanium alloys

Titanium has two types of crystal structure: One is α -titanium with a close-packed hexagonal structure ($a = 0.29511$ nm, $c = 0.46843$ nm, $c/a = 1.5873$), which is stable below 885 °C; the other is β -titanium with a body-centered cubic structure ($a = 0.3282$ nm), which is stable above 885 °C. Titanium alloys are thus classified by their structural characteristics: α -titanium

Table 3.48 Classification of titanium alloys

No.	Grade	Nominal composition	Type	Service temperature (°C)	Strength (MPa)
1	TA0	Ti	Pure	300	≥ 280
2	TA1	Ti	Pure	300	≥ 370
3	TA2	Ti	Pure	300	≥ 440
4	TA3	Ti	Pure	300	≥ 540
5	ZTA	Ti	Pure	300	≥ 345
6	ZTA	Ti	Pure	300	≥ 440
7	ZTA	Ti	Pure	300	≥ 540
8	TA7	Ti-5Al-2.5Sn	α	500	≥ 785
9	ZTA	Ti-5Al-2.5Sn	α	500	≥ 760
10	TA1	Ti-2.5Cu	α	350	≥ 610
11	TC1	Ti-2Al-1.5Mn	Near	350	≥ 590
12	TC2	Ti-4Al-1.5Mn	Near	350	≥ 685
13	TA1	Ti-8Al-1Mo-1 V	Near	500	≥ 895
14	TA1	Ti-5.5Al-4Sn-2Zr-1Mo-0.25Si-1Nd	Near	550	≥ 980
15	TA1	Ti-6.5Al-2Zr-1Mo-1 V	Near	500	≥ 930
16	TA1	Ti-3Al-2.5 V	Near	320	≥ 620
17	TA1	Ti-6Al-2Sn-4Zr-2Mo	Near	500	≥ 930
18	TC4	Ti-6Al-4 V	$\alpha + \beta$	400	≥ 895
19	TC6	Ti-6Al-2.5Mo-1.5Mo-1.5Cr-0.5Fe-0.3Si	$\alpha + \beta$	450	≥ 980
20	TC1	Ti-6.5Al-1.5-Zr-3.5Mo-0.3Si	$\alpha + \beta$	500	≥ 1030
21	TC1	Ti-3Al-5Mo-4.5 V	$\alpha + \beta$	350	≥ 1030
22	TC1	Ti-5Al-2Sn-2Zr-4Mo-4Cr	$\alpha + \beta$	430	≥ 1120
23	ZTC	Ti-5Al-2Sn-5Mo-0.3Si-0.02Ce	$\alpha + \beta$	500	≥ 930
24	ZTC	Ti-6Al-4 V	$\alpha + \beta$	350	≥ 835
25	ZTC	Ti-5.5Al-1.5Sn-3.5Zr-3Mo-1.5 V-1Cu-0.8Fe	$\alpha + \beta$	500	≥ 930
26	TB2	Ti-5Mo-5 V-8Cr-3Al	β	300	≥ 1100
27	TB3	Ti-10Mn-8 V-1Fe-3.5Al	β	300	≥ 1100
28	TB5	Ti-15 V-3Cr-3Sn-3Al	β	290	≥ 1080
29	TB6	Ti-10 V-2Fe-3Al	Near	320	≥ 1105

alloys (TA), $\alpha + \beta$ -titanium alloys (TC), and β -titanium alloys (TB). The classification of titanium alloys in China is shown in Table 3.48.

Strengthening heat treatment is usually carried out for $\alpha + \beta$ -titanium and β -titanium alloys. Through solution treatments and aging treatments, the strengths of the titanium alloys can be increased and a good combination of strength and ductility can be achieved for these titanium alloys. The microstructural evolution of titanium alloys during these solution and aging treatments is very complicated. The α -phase remaining in the solution state will be maintained during the cooling

Table 3.49 Heat treatment parameters for some titanium alloys

Grade	Stress relief annealing ^a		Full annealing ^b		Solution treatment		Aging treatment			
	Temp. (°C)	Time (min)	Temp. (°C)	Time (min)	Temp. (°C)	Time (min)	Temp. (°C)	Time (h)	Cooling mode	
TA1	500–600	15–60	680–720	30–120	–	–	–	–	–	
TA2	500–600	15–60	680–720	30–120	–	–	–	–	–	
TA3	500–600	15–60	680–720	30–120	–	–	–	–	–	
TA4	550–650	15–60	700–750	30–120	–	–	–	–	–	
TA5	550–650	15–60	800–850	30–120	–	–	–	–	–	
TA6	550–650	15–120	750–800	30–120	–	–	–	–	–	
TA7	550–650	15–120	750–850	30–120	–	–	–	–	–	
TA8	550–650	15–120	750–800	60–120	–	–	–	–	–	
TB2	480–650	15–240	800	30	800	30	Air or water cooling	500	8	Air cooling
TC1	550–650	30–60	700–750	30–120	–	–	–	–	–	–
TC2	550–650	30–60	700–750	30–120	–	–	–	–	–	–
TC3	550–650	30–240	700–800	60–120	820–920	25–60	Water cooling	480–560	4–8	Water cooling
TC4	550–650	30–240	700–800	60–120	850–950	30–60	Water cooling	480–560	4–8	Water cooling
TC6	550–650	30–120	750–850	60–120	860–900	30–60	Water cooling	540–580	4–12	Water cooling
TC7	550–650	30–120	850–950	60–120	–	–	–	–	–	–
TC9	550–650	30–240	600	60	900–950	60–90	Water cooling	500–600	2–6	Water cooling
TC10	550–650	30–240	760	120	850–900	60–90	Water cooling	500–600	4–12	Water cooling

^aThe cooling mode for stress relief annealing for all alloys is air cooling^bAnnealing before use as product: 950 °C/1 h, air cooling or water cooling; final annealing: 870 °C/30 min + 650 °C/60 min, air cooling; final annealing of TC9 alloy: 930 °C/30 min, air cooling + 530 °C/360 min, air cooling

process of the solution treatment, but the β -phase may be changed into α' -, α'' -, ω -, or β' -metastable phases, depending on the compositions of the alloys. These metastable phases will change into the dispersed ($\alpha + \beta$)-phase during the aging process, resulting in an obvious strengthening effect. Table 3.49 shows the heat treatment parameters of some titanium alloys.

(2) Heat treatment of titanium matrix composites

1) Important items One of the most important functions of the heat treatment of titanium matrix composites is to reduce the residual stress that forms during the casting, deformation, welding, and mechanical processing, while at the same time obtaining the required properties, such as fracture toughness, fatigue properties, and thermal resistance. Considering the special physical properties of these titanium alloys, attention must be paid to the heat treatment of the titanium matrix composites.

- ① Titanium alloys are very active and have a high affinity to nitrogen, hydrogen, and oxygen, so to prevent gas pollution of the sample, heat treatment is usually carried out in a vacuum furnace or a furnace with a partial-pressure oxidization atmosphere.
- ② Because the microstructures of titanium alloys coarsen easily at higher temperatures, the times that the titanium matrix composites are at the solution temperature should be controlled to be as short as possible.
- ③ If overheating occurs during the heating process, the resulting striped structure in the titanium alloy cannot be removed by heat treatment, so the heating temperature must be controlled.
- ④ If the titanium matrix composites are heated to temperatures above the ($\alpha + \beta$)/ β -transformation temperature, the β -phase grows rapidly, resulting in high brittleness, so it is better for the heating temperature to be lower than the ($\alpha + \beta$)/ β -transformation temperature.

2) Effects of heat treatment on reinforcement of titanium matrix composites Many researchers have concluded that most ceramic reinforcements, such as SiC, B₄C, and Al₂O₃, are not affected by the aging treatment of the titanium alloy matrix composites. The evolution of the microstructure of Ti–Al–C alloys during heat treatment indicates that the morphology of the TiC phase can change during heat treatment processes.

The evolution of the morphology of primary TiC and eutectic TiC during heat treatment processes has been studied for TiC_p/Ti composites fabricated by the melt casting method. It is known that carbon solubility in β -titanium with a BCC crystal structure is very low. When the composite is kept at high temperature in the β -phase zone, TiC is first dissolved at the position with the larger curvature and then the dissolved carbon atoms diffuse to other positions with smaller curvatures and form TiC again. Therefore, the morphology change mechanism of TiC from dendrite to particle is a dissolution-precipitation mechanism. The driving force comes from the curvature effect and the surface energy.

When the composite is treated in the α -Ti + TiC high-temperature zone, TiC is dissolved into the matrix and is then precipitated during the cooling process, according to the dissolution-solution-precipitation mechanism. When the carbon content in the alloy is lower, all TiC phases are dissolved and a single-phase α' is obtained after quenching; when the carbon content is higher, the fine eutectic TiC dissolves first and the primary TiC dendrites cannot be completely dissolved, and some of them remain. If the aluminum content of the alloy is higher, the Ti_3Al phase will be precipitated.

When the composite is treated in the α -Ti + β -TiC + TiC temperature zone, the morphology change mechanism of the TiC phase is different in the different matrixes (α and β). In the α -phase matrix, the mechanism is a dissolution-solution-precipitation mechanism; in the β -phase matrix, both mechanisms exist for the morphology change of the TiC phase.

- 3) Effect of heat treatment on matrix of titanium matrix composites The SCS-6SiC fiber-reinforced Ti-22Al-23Nb composite is heat treated using the process parameters shown in Table 3.50. The results indicate that the composite sample solution is treated at temperatures above the β -transformation temperature of the matrix alloy and then aged. The transverse creep properties of the composite increase at 650–760 °C and the longitudinal tensile strength of the composite is not reduced. The increase in the creep properties is caused by the increasing volume fraction of the orthorhombic structure phase (O-phase) and the formation of a platelike (O + β) dual-phase zone.

During the heat treatment, the samples are covered with titanium foil to remove the oxygen. The solution temperature of the first type of sample is chosen based on the β -transformation temperature of 1100 °C for the Ti-22Al-23Nb alloy. The solution temperature of the second type of sample is chosen as 1125 °C, which is a little higher than the β -transformation temperature. Table 3.51 shows the longitudinal tensile test results of the samples at room temperature. The results indicate that the tensile properties of the composite are not obviously affected by the heat treatments.

Table 3.50 Heat treatment processes of the SiC_f/Ti-22Al-23Nb composite

Heat treatment method	Solution treatment, 2 h (°C)	Cooling rate (°C min ⁻¹)	Aging treatment (°C/h)
Heat treatment above T_β (Type I)	1125	28	815/8
Heat treatment below T_β (Type I)	1050	28	815/8
Heat treatment above T_β (Type II)	1160	2.8	815/8
Heat treatment below T_β (Type II)	1085	2.8	815/8

Note: T_β — β -phase transformation temperature

Table 3.51 Longitudinal tensile properties of SiC_f/Ti–22Al–23Nb composites in different states

Composite state	Tensile strength (MPa)	Elongation (%)	Elastic modulus (GPa)
HIP state	1600–1800	1.0–1.2	175–220
Heat treatment above T_{β} (Type I)	1605	1.0	192
Heat treatment below T_{β} (Type I)	1685	1.04	201
Heat treatment above T_{β} (Type II)	1680	1.09	190
Heat treatment below T_{β} (Type II)	1605	1.07	195

Based on the reaction $\text{TiB}_2 + \text{Ti} \rightarrow \text{TiB}$, TiB/Ti–6Al–4 V composites with volume fractions of 20% and 40% are fabricated by an in situ reaction sintering method using the TiB₂ powder and Ti–6Al–4 V powder as starting materials. The as-sintered unreinforced Ti–6Al–4 V alloy consists of a needlelike α -phase and an intergranular β -phase, and under the same conditions, the matrix of the TiB/Ti–6Al–4 V composite consists of an equiaxed α -phase and an intergranular β -phase. After heat treatments at 1100 and 1200 °C, the α -phase is equiaxed in the matrix, and after heat treatments at 1300 and 1400 °C, along with the equiaxed α -phase, β -grains also appear in the matrix.

When the TiB/Ti–6Al–4 V composites are heat treated at 1200 °C, some TiB₂ particles remain, and they are covered with fine TiB whiskers. When the composites are kept at 1200 °C for 5 h, all the TiB₂ particles are transformed into TiB whisker clusters. When the composites are kept at 1200 °C for 100 h, the TiB whisker clusters change into separated TiB whiskers, which are distributed uniformly in the composite.

When the TiB/Ti–6Al–4 V composites are heat treated at 1300 and 1400 °C, the microstructure changes are similar to that at 1200 °C. The microstructure of a composite treated at 1300 °C for 5 h is the same as that treated at 1400 °C for 1 h, which contains a large amount of separated TiB whiskers and a small number of TiB whisker clusters. The driving force for the transformation from TiB₂ particles to TiB whiskers increases with increasing heat treatment temperature. With sufficient heat treatment temperature and holding time, all the TiB₂ particles and TiB whisker clusters will be transformed into separate TiB whiskers, and these TiB whiskers will be distributed in the matrix uniformly. If the starting TiB₂ particles and Ti–6Al–4 V particles are smaller than 40 μm in diameter, then heat treatment at 1300 °C for 6 h will result in a fine matrix grain size and uniform distribution of the TiB whiskers, which is an optimum heat treatment parameter.

Research on Ti–Al alloy matrix composites fabricated by forging and investment casting methods indicates that the morphology of the matrix alloy can be controlled to be an equiaxed and laminar structure by heat treatment. The morphology of the boride reinforcement can also be controlled to be particles or fibers in shape by heat

Table 3.52 Effects of heat treatment on microstructures of boride-reinforced Ti–Al alloy composites

Composition	1200°C/16 h/900°C/5 h		1400°C × 5 h	
	Morphology	Size	Morphology	Size
7 vol.% TiB ₂ /Ti–47Al–2 V (forged)	Equiaxed matrix	20 μm	Laminar matrix	45 μm
	Particle reinforcement	–	Particle reinforcement	–
7 vol.% (Ti,Nb) B/Ti–47Al–2Nb (forged)	Equiaxed matrix	10 μm	Laminar matrix	27 μm
	Fiber reinforcement	–	Fiber reinforcement	–
8 vol.% TiB ₂ /Ti–47Al–2 V (investment cast)	Laminar matrix	95 μm	Equiaxed matrix	96 μm
	Particle reinforcement	–	Particle reinforcement	–
8 vol.% (Ti,Nb) B/Ti–47Al–2Nb (investment cast)	Laminar matrix	15 μm	Equiaxed matrix	90 μm

treatment. Table 3.52 shows the effects of the heat treatment process on the microstructures of boride-reinforced Ti–Al alloy matrix composites.

Commercial metals and alloys are usually used as the matrixes for metal matrix composites, particularly for particle-reinforced metal matrix composites. However, because of the addition of reinforcements, the heat treatment mechanism and processes are different for the metal matrix composites and the unreinforced matrix alloys, and sometimes, the difference is quite large. Therefore, it should be remembered that different results may be produced if the heat treatment processes used for commercial metals and alloys according to their standard parameters are used for the heat treatment of metal matrix composites using these same metals and alloys as the matrixes.

3.4.2 Dimensionally Stabilizing Heat Treatment of Metal Matrix Composites

Dimensional stabilization implies resistance to the permanent deformation of a material after heat treatment and processing without external loading or under a stress that is below the elastic limit of the material. It can be classified into three types.

- 1) Dimensional change in a constant environment, which is considered to be a result of structural transformation and relaxation of residual stress. Sometimes, material micro-creep is included in this type.

- 2) Dimensional change in a changing environment, which is considered to be a result of micro-yield deformation caused by external loading and size changes caused by temperature changes in the environment.
- 3) Dimensional change by an elasticity, which is a result of the recovery of elastic deformation.

Dimensional stabilization can be divided into two types, depending on whether or not a load is applied to the material. Dimensional stabilization under a load includes the micro-yield strength under a short-term load and the micro-creep resistance under a long-term load; dimensional stabilization without a load includes dimensional stabilization in a constant temperature environment and that in a variable temperature environment.

Many factors will cause dimensional changes in materials, including external stress, residual stress and the microstructures of the materials. External stress can result not only in elastic deformation of the material, but may also produce anelastic deformation, micro-plastic deformation and micro-creep deformation, leading to dimensional changes in the products. Residual stress includes macro-residual stress and micro-residual stress. It has been found that the relaxation of the macro-residual stress is the main reason for product dimensional change, although the micro-residual stress also has some effect on the dimensional changes. Microstructural changes in metals and alloys usually result in a change of their specific volume. Although the speed of microstructural change is very low at room temperature, after long-term accumulation, the degree of transformation will be large enough to produce a large-dimensional change that exceeds the limitations of the products.

Table 3.53 Characterization of dimensional stabilization of materials

Characterization method	Definition	Mechanism	Influencing factor
Micro-yield strength	Stress when a residual strain of $(1-2) \times 10^{-6}$ is formed after the sample is unloaded	1) Single-dislocation mechanism by Stein 2) Double-dislocation mechanism by Brown and Ekvall 3) Dislocation depletion mechanism by Marschall	1) Grain size 2) Alloying elements 3) Prestrain
Resistance to micro-creep	Time needed to get strain of 10^{-6} in the sample under constant temperature and constant load conditions	1) Dislocation climb mechanism 2) Dislocation sliding mechanism 3) Mechanism of anelastic sliding of grain boundary	1) Stress value 2) Temperature 3) Prestrain
Relaxation limit of residual stress	The maximum stress where the residual stress cannot occur under certain conditions. It is usually evaluated using the residual stress value σ after a certain time t under experimental conditions	It has the same mechanism as the micro-creep. Both involve the evolution of plastic strain with time under external stress. The difference between the mechanisms is the experimental conditions	1) Grain size 2) Temperature 3) Initial stress

Therefore, to obtain greater dimensional stability, a higher shear modulus, lower macro-residual stress, uniform micro-residual stress, stable dislocations or no dislocations, stable phases and structures (including precipitation, interfacial reaction, and grain refining) are required for the materials.

Dimensional stabilization is usually characterized by resistance to the micro-plastic deformation of the materials, including the micro-yield strength, the resistance to micro-creep, and the relaxation limit of the residual stress, as shown in Table 3.53.

Aluminum matrix composites have high specific strength and specific modulus values, and their thermal conduction and coefficient of thermal expansion values can be adjusted by material design, so they are promising for application not only as structural materials but also in the field of optical precision components and instruments. Aluminum matrix composites have been used as a base material for optical mirrors and in infrared detection-based guidance systems and super light astronomical telescopes. These applications have high-dimensional stability requirements for the materials, so dimensional stabilization treatment is very important for the applications of aluminum matrix composites. The dimensional stabilization treatments used include mechanical methods, heat treatment methods,

Table 3.54 Classifications and definitions of the dimensional stabilization treatment methods

Method	Classification	Definition
Mechanical method	Tensile or compressive method	For products with simple shapes, a permanent uniform plastic deformation is carried out over the whole section of a product after heat treatment. Plastic deformation is formed by the combination of external stress and residual stress, so that the residual stress can be reduced and released
Mechanical method	Vibratory stress relief method	This method can effectively decrease the macro-residual stress in machine tool casting and large-scale welded structural components
Heat treatment method	Isothermal aging method	The components are heated to a certain temperature and kept at that temperature for a certain time, followed by air cooling
	Anti-quenching method	The components are cooled to $-196\text{ }^{\circ}\text{C}$ and kept at that temperature for a certain time and are then placed in boiling water or sprayed with high-speed steam
	Thermal cycling method	The components are heated and cooled repeatedly many times. This is a widely used dimensional stabilization treatment method
	Thermo-mechanical method	Based on deformation strengthening and transformation strengthening, this method is a combination of press working and heat treatment and improves both component strength and toughness
Magnetic treatment method	Pulsed magnetic field treatment method	This is a technique used to release the residual stresses in metals and alloys without heating

and magnetic treatment methods, which all have different effects from each other. The classifications and definitions of the dimensional stabilization treatment methods are shown in Table 3.54.

3.4.2.1 Thermal Cycling Dimensional Stabilization Treatment of Aluminum Matrix Composites

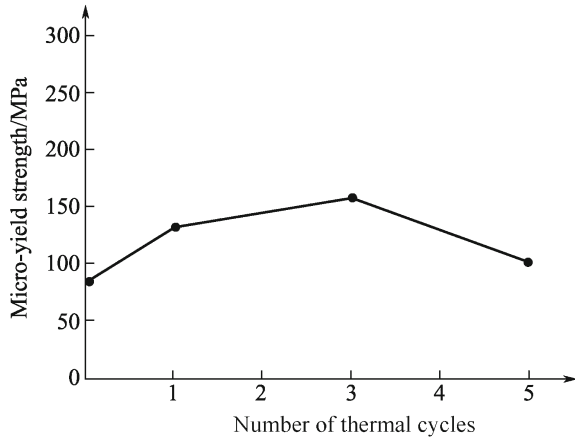
In ceramic-phase-reinforced aluminum alloy matrix composites, the difference in coefficient of thermal expansion between the reinforcement and the matrix is very large [61, 62]. A change of external temperature may cause high interfacial mismatch stress and even plastic deformation of the matrix near the interface. For whisker- and short fiber-reinforced aluminum alloy matrix composites, a large stress concentration will form at the sharp corners of the reinforcements, so it is difficult to release the thermal residual stress and improve the dimensional stabilities of the whisker- and short fiber-reinforced aluminum alloy matrix composites by thermal cycling treatment.

For particle-reinforced aluminum alloy matrix composites, the stress concentration in the composites is reduced, so thermal cycling treatment can be used as a thermal cycling stabilization treatment method. By controlling the size, shape, and volume fraction of the particles in the aluminum alloy matrix composites, the micro-yield strength of the composites is improved, but there are also internal residual stresses and high-density movable dislocations, which affect the dimensional stabilities of the composites. It is found that smaller particle sizes are beneficial when improving dimensional stability in these composites by thermal cycling treatment.

Thermal cycling treatment has been widely used for the dimensional stabilization treatment of aluminum alloy matrix composites. However, the thermal cycling treatment mechanism is not very clear. There is insufficient work to show the effects of the thermal cycling parameters (e.g., temperature, holding time, heating-cooling, transfer rate, and number of cycles) on the residual stress and the resistance to micro-plastic deformation. The effects of thermal cycling treatment are different for different material systems, so it is very important to find optimum thermal cycling treatment parameters for certain composites.

With increasing numbers of thermal cycles, the micro-yield strength of metal matrix composites first increases and then decreases, which is caused by aging strengthening, thermal cycling stresses, and the dislocation states. In the initial and middle stages of the thermal cycling processes, the micro-yield strengths of the composites increase because of age-hardening effects. With further increases in the number of thermal cycles, the age-hardening effect is reduced, and the thermal mismatch stresses and especially the induced movable dislocation densities in the composites increase, resulting in a decrease in the micro-yield strength of the composites. Figure 3.51 shows the dependence of the micro-yield strength of the 35% SiC_p/2024Al composite on the number of thermal cycles.

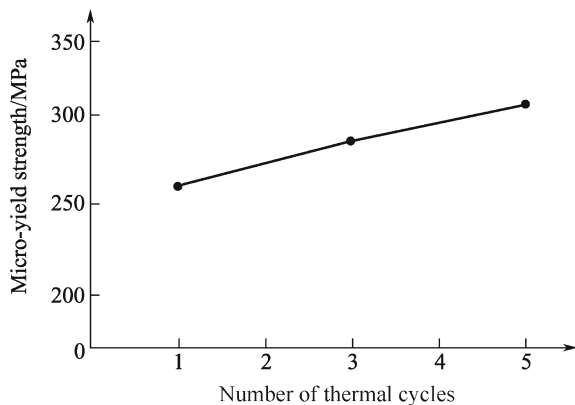
Fig. 3.51 Dependence of the micro-yield strength of 35% SiC_p/2024Al composite on the number of thermal cycles



When the size of the reinforcement in metal matrix composites is very fine, the micro-yield strengths of the composites increase with increasing numbers of thermal cycles. The range of deformations caused by thermal mismatch is very small for small-sized reinforcements, and such a small-range (e.g., 1–2 atom spacing) cannot induce dislocations, so the lower dislocation density leads to higher micro-yield strength in the composites. Figure 3.52 shows the effects of the number of thermal cycles on the micro-yield strength of the 33% Al₂O_{3p}/6061Al composite, in which the Al₂O₃ particle diameter is 0.4 μm. It is found that the micro-yield strength of the composite increases with increasing numbers of thermal cycles, and the micro-yield strength of the composite is 298.2 MPa when the number of thermal cycles is five.

Dislocation recovery is easy when the thermal cycling upper limit temperature is higher and the holding time is longer. Bigger particle sizes and interparticle spacings also make dislocation recovery easier. If the dislocations move to the grain boundaries and interfaces, or dislocations with opposite signs meet each other, the

Fig. 3.52 Effect of number of thermal cycles on the micro-yield strength of the 33% Al₂O_{3p}/6061Al composite, in which the diameter of the Al₂O₃ particle is 0.4 μm



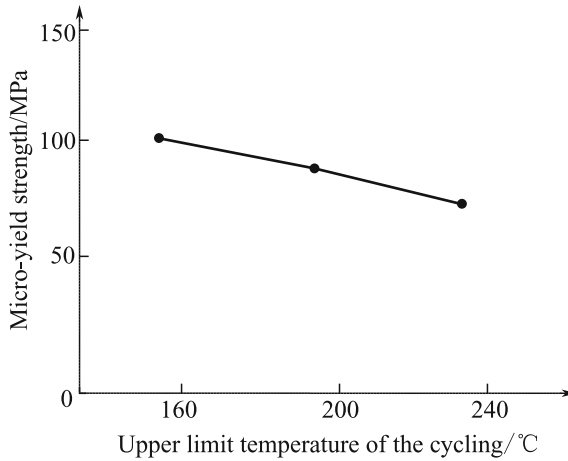


Fig. 3.53 Effect of the upper limit temperature of the thermal cycling treatment on the micro-yield strength of 33% SiC_p/LY12 composite

Table 3.55 Thermal cycling treatment processes and the resulting properties of some aluminum matrix composites

Composite	Thermal cycling treatment process	Micro-yield strength (MPa)	Accumulated plastic strain
22% SiC _w /6061Al	530 °C, 1 h + 160 °C, 15 h + (160 °C, 4 h ↔ -196 °C, 2 h, twice)	–	–
35% SiC _p /LY12	500 °C, 1 h + (150 °C, 2.5 h ↔ -196 °C, 1 h, once)	110	–
35% SiC _p /2024Al	500 °C, 1 h + (190 °C, 2.5 h ↔ -196 °C, 1 h, three times)	155	–
35% SiC _p /6061	530 °C, 1 h + 160 °C, 15 h + (160 °C, 4 h ↔ -196 °C, 2 h, three times)	227	–
35% SiC _p /6061	530 °C, 1 h + 160 °C, 15 h + (160 °C, 4 h ↔ -196 °C, 2 h, five times)	140	–
50% SiC _p /6061	500 °C, 1 h + (160 °C, 1 h ↔ -196 °C, 2 h, three times)	–	0.8×10^{-4}
22% Al ₂ O ₃ /6061Al	530 °C, 1 h + 160 °C, 15 h + (160 °C, 4 h ↔ -196 °C, 2 h, once)	241	–
33% Al ₂ O ₃ /6061Al	530 °C, 1 h + 160 °C, 15 h + (160 °C, 4 h ↔ -196 °C, 2 h, five times)	298	–
35% Al ₂ O _{3p} /6061	530 °C, 1 h + 160 °C, 15 h + (160 °C, 4 h ↔ -196 °C, 2 h, five times)	310	–
40% AlN _p /6061	530 °C, 1 h + 160 °C, 15 h + (160 °C, 4 h ↔ -196 °C, 2 h, three times)	257	–
50% SiC _p /pure Al	400 °C, 3 h + (160 °C, 1 h ↔ -196 °C, three times)	–	-0.4×10^{-4}

dislocation density will decrease and the micro-yield strength will be reduced. Figure 3.53 shows the effect of the upper limit temperature on the micro-yield strength of the 33% SiC_p/LY12 composite. The micro-yield strength of the composite is shown to decrease with increasing upper limit temperature.

Table 3.55 shows the thermal cycling treatment processes and the resulting micro-yield strengths of some aluminum matrix composites.

3.4.2.2 Deep Cooling Dimensional Stabilization Treatment of Aluminum Matrix Composites

Very little research has been conducted into deep cooling dimensional stabilization treatment for aluminum matrix composites. On the one hand, the deep cooling treatment leads to a reduction in the dimensional stability of the aluminum matrix composite, because a higher dislocation density is formed because of the thermal interfacial mismatch stress when the composite is cooled to a very low negative temperature, resulting in a reduction in micro-yield strength of the composite. On the other hand, the residual stress caused by the thermal mismatch stress at room temperature in the composite can be reduced by the deep cooling treatment, which will increase the dimensional stability of the aluminum matrix composite. The residual thermal mismatch stress in the aluminum matrix composites is mainly affected by the deep cooling temperature and is not related to the deep cooling times. In theory, the residual thermal mismatch stress at room temperature in the aluminum matrix composites can be adjusted to zero by choosing suitable deep cooling temperatures. Deep cooling treatment process parameters for some aluminum matrix composites are shown in Table 3.56.

A variety of methods have been used to evaluate the dimensional stability of metal matrix composites. Both macro-residual stress and micro-plastic deformation resistance have been measured to evaluate the dimensional stability, but no comprehensive evaluation has been carried out. In certain dimensional stabilization treatments, it is impossible to reduce the macro-residual stress and increase the microstructural stability simultaneously. The dimensional stability of the metal matrix composites is important in many application fields, such as aviation and aerospace. Therefore, the dimensional stability of metal matrix composites is an interesting topic for materials science and engineering.

Table 3.56 Deep cooling treatment process parameters for some aluminum matrix composites

Composite	Deep cooling treatment process
35% SiC _p /2024Al	500 °C, 1 h + 190 °C, 8 h + (-196 °C, 1 h)
50% SiC _p /pure Al	500 °C, 1 h + (-196 °C, 1 h)
SiC _w /LD2	510 °C, 1 h + 175 °C, 10 h + (-196 °C, 6 h)
SiC/6061	520 °C, 1.5 h + 205 °C, 50 h + (-196 °C, 10 min)

3.4.3 Plastic Forming Processes of Discontinuously Reinforced Metal Matrix Composites

Compared with common metal materials, metal matrix composites have very low ductility, and their elongation at room temperature is usually less than 10%. When using a common plastic forming technique, the ductility of metal matrix composites does not increase obviously, even at elevated temperatures. Therefore, the difficulty in performing plastic forming of metal matrix composites has become one of the most important factors inhibiting further application of these materials. Plastic forming is an important processing technique for aluminum matrix composites, by which the relative density and distribution of the reinforcements can be improved and the designed shapes of the composites can be obtained. With the increasing numbers of applications of aluminum matrix composites, increasing attention is being paid to the plastic forming of these composites, and investigation of the plastic forming of metal matrix composites has an important meaning in practice. The most important plastic forming processes of metal matrix composites include tension, compression, extrusion, and rolling processes.

3.4.3.1 Tensile Ductility of Aluminum Matrix Composites

The mechanical properties of particle-reinforced aluminum alloy composites at room temperature and at elevated temperatures are shown in Tables 3.57 and 3.58, respectively [18, 19].

Table 3.57 Mechanical properties of some particle-reinforced aluminum alloy composites

Composite	State	$\sigma_{0.2}$ (MPa)	σ_b (MPa)	δ (%)	E (MPa)	Manufacturer
Al ₂ O _{3p} /6061Al	10% (T6)	296	338	7.5	81	Duralcan, Alcan
	15% (T6)	319	359	5.4	87	Duralcan, Alcan
	20% (T6)	359	379	2.1	98	Duralcan, Alcan
SiC _p /6061Al	10% (T6)	405	460	7.0	98	DWA
	20% (T6)	420	500	5.0	105	DWA
	25% (T6)	430	515	4.0	115	DWA
Al ₂ O _{3p} /4024Al	10% (T6)	483	517	3.3	84	Duralcan, Alcan
	15% (T6)	476	503	2.3	92	Duralcan, Alcan
	20% (T6)	483	503	1.0	101	Duralcan, Alcan
SiC _p /2024Al	7.8% (T6)	400	610	5–7	100	British Petroleum
	20% (T6)	490	630	2–4	116	British Petroleum
	25% (T6)	405	560	3	105	DWA
SiC _p /7075Al	15% (T651)	556	601	2	95	Cospray, Alcan
SiC _p /7049Al	15% (T6)	598	643	2	90	Cospray, Alcan
SiC _p /7090Al	20% (T6)	665	735	–	105	DWA

Table 3.58 Mechanical properties of some particle-reinforced aluminum alloy composites at elevated temperatures

Composite	Particle size (μm)	Particle volume fraction (%)	200 °C			400 °C		
			σ_b (MPa)	$\sigma_{0.2}$ (MPa)	δ (%)	σ_b (MPa)	$\sigma_{0.2}$ (MPa)	δ (%)
AlN _p /6061Al ^a	0.8–4	40	422	372	5.0	75	51	5.9
6061Al	–	–	226	189	14.5	29	24	44.3
Al ₂ O _{3p} /6061Al ^b	0.15	20	329	235	24.9	101	43	7.6
Al ₂ O _{3p} /6061Al ^b	0.15	30	300	219	32.0	176	94	6.1
Al ₂ O _{3p} /6061Al ^a	0.4	20	366	312	2.8	89	66	4.4

^aAs-cast state, T6 treatment^bAs-extruded state, T4 treatment

3.4.3.2 High-Temperature Compressive Deformation of Metal Matrix Composites

Strain softening is a characteristic of high-temperature compressive deformation of metal matrix composites [63, 64]. There is a stress peak in the stress–strain curve of high-temperature compressive deformation of metal matrix composites, and with further increases in strain after the stress peak, strain softening appears. In whisker-reinforced aluminum alloy composites, the orientation of the whisker changes during compressive deformation; the whiskers are oriented perpendicular to the compression direction after compressive deformation. The strain softening in whisker-reinforced aluminum alloy matrix composites is related to the orientation of the whiskers. When the whiskers are oriented perpendicular to the compression direction, the loading ability of the whiskers in the composite is reduced and results in the strain softening behavior in the composite.

The compressive strength of a metal matrix composite is given by:

$$\sigma_c = \sigma_m \left(\frac{l}{d} \right) V_f \sum_{i=1}^n \frac{\cos \alpha_i}{n} + \sigma_m, \quad (3.6)$$

where (l/d) is the average aspect ratio of a whisker; α_i is the angle between the whisker axis and the compression direction; σ_m is the flow stress of the matrix alloy; and V_f is the whisker volume fraction. During compressive deformation of whisker-reinforced metal matrix composites, the orientation distribution function of the whisker axis is:

$$f(\theta) = A \exp(-B\theta) + C \sin \theta, \quad (3.7)$$

where A and B are linear functions of the strain ε . The flow stress of the high-temperature deformation of whisker-reinforced metal matrix composites then is obtained as:

$$\sigma_c = V_f(\bar{l}/d)\sigma_m \int_0^{2\pi} \int_0^{\pi/2} \sin 2\theta \cos \theta f(\theta) d\theta d\varphi + \sigma_m. \quad (3.8)$$

Whiskers will rotate and break during high-temperature compressive deformation of whisker-reinforced metal matrix composites. Although there has been a quantitative study of the whisker rotation, no basic understanding of the whisker rotation process has been reached. The whiskers will bear a moment during the tensile deformation of the whisker-reinforced metal matrix composite, and whisker rotation takes place under this moment. The whisker rotation is described by

$$\varepsilon = \sigma \sin(2\alpha)/4G \quad (\text{Elastic stage}), \quad (3.9)$$

$$\varepsilon = 0.75\delta \sin(2\alpha) \quad (\text{Plastic stage}), \quad (3.10)$$

where ε is the whisker rotation angle; σ is the tensile stress of the composite; α is the angle between the whisker axis and the tensile direction; and δ is the tensile strain of the composite.

The whisker rotation is caused by plastic deformation of the matrix alloy in the whisker-reinforced metal matrix composites, so plastic deformation mechanisms such as dislocation sliding and dislocation climbing will greatly affect the whisker rotation. The matrix alloys of whisker-reinforced metal matrix composites are usually polycrystalline, so studies of the relationship between the whisker rotation and dislocation sliding and dislocation climbing are very complicated.

The compressive deformation of as-extruded whisker-reinforced metal matrix composites in which the whiskers are oriented has been studied. The results indicate that whisker rotation is easier at higher deformation temperatures, and that the degree of whisker rotation is larger when the amount of compressive deformation is larger. The whisker breakage degree decreases with increasing deformation temperature and uses a deformation mode that is suitable for the plastic flow of matrix alloys. Easier whisker rotation produces a lower degree of whisker breakage. Whisker breakage during plastic deformation of whisker-reinforced metal matrix composites is caused by the stress concentration at the ends of the whiskers, which is caused by the lack of coordination between the whiskers and the matrix alloys.

High-temperature compressive deformation of metal matrix composites is also carried out at temperatures between the solidus and the liquidus of the matrix alloys. It is known that the stress-strain curves of metal matrix composites at temperatures below the solidus of the matrix alloys can be divided into three stages: the elastic

deformation stage, the strain softening stage, and the strain hardening stage. When the composites are compressed at high temperatures near or above the solidus of the matrix alloys, the whisker breakage is mainly because of interactions between the whiskers, but not by interactions between whisker and matrix. The strengthening effect of the whisker is reduced when the composites are deformed in this temperature range. When the composites are compressed at temperatures between the solidus and the liquidus of the matrix alloys, the flow stresses of the composites increase with increasing strain rate. When a liquid phase appears during plastic deformation, the plastic deformation mechanism of the composite involves coordination between the dislocation sliding and the movement of the grain boundaries and interfaces; meanwhile, there is also a liquid coordination effect.

3.4.3.3 Rolling Plasticity of Aluminum Matrix Composites

Rolling is a common technique used to form plate products of metals and metal matrix composites. The microstructures and properties of metal matrix composites change greatly during rolling processes. Depending on the rolling temperature, the process can be hot rolling or cold rolling [65].

The orientation of the reinforcement changes by rolling deformation, which will affect the plastic deformation behavior and anisotropy of the composites. Voids, reinforcement fractures, and micro-cracks are easily formed during rolling deformation of the composites, and the cooling rate of the rolling sample is very high because of the contact between the sample and the cold roller. Therefore, rolling processes are not used to increase the relative densities of composites directly. An extrusion process is usually carried out before the rolling process, so that both the relative density and the microstructural uniformity of the metal matrix composites can be improved.

(1) Effect of rolling temperature on relative density of aluminum matrix composites

Table 3.59 shows the relative density of the 25% SiC_p/Al composite after hot extrusion deformation with an extrusion ratio of 16:1 and rolling by three passes at different temperatures. After rolling at 350 °C, the composite has a lower relative density, which may be caused by particle fracture during rolling deformation, because the composite has lower ductility and higher deformation resistance at lower deformation temperatures.

(2) Effect of deformation amount on relative density of aluminum matrix composites

Table 3.60 shows the relative densities of the 25% SiC_p/Al composite after extrusion at an extrusion ratio of 16:1 and hot rolling at 350 and 450 °C by different deformation amounts. The relative density of the composite is not sensitive to the amount of deformation caused by rolling under these experimental conditions, and

Table 3.59 Relative densities of 25% SiC_p/Al composites rolled at different temperatures

Rolling temperature (°C)	350	400	450	500	550
Relative density (%)	98.8	99.0	99.2	99.4	99.3

Table 3.60 Relative density of 25% SiC_p/Al composite rolled by different deformation amounts

Deformation amount	50%	75%	85%
Relative density (350 °C)	99.0	98.9	98.9
Relative density (450 °C)	99.2	99.2	99.2

also the relative density of the composite when rolled at 350 °C is lower than that rolled at 450 °C, which is the same result as that shown in Table 3.60.

(3) Effect of rolling temperature on strength of aluminum matrix composites

The 15% SiC_p/Al composite is hot-extruded at an extrusion ratio of 25:1 and then hot-rolled with different preheating temperatures. The tensile strengths of the rolling composite with rolling temperatures of 350 and 500 °C are 230 MPa and 245 MPa, respectively. When the rolling temperature is lower, the rolling deformation resistance is higher, so the SiC particle cannot rotate to coordinate the deformation of the matrix at a higher rolling deformation rate; this leads to fracture of the SiC particle during rolling deformation. In the rolling composite with a rolling temperature of 350 °C, although the interfacial bonding between SiC and the matrix is good, the SiC particle breaks in the composite. This is the main cracking source in the composite during tensile fracture, leading to a lower tensile strength in the 15% SiC_p/Al composite with a rolling temperature of 350 °C.

(4) Effect of deformation amount on strength of aluminum matrix composites

Table 3.61 shows the tensile strength of the 25% SiC_p/Al composite after hot extrusion at an extrusion ratio of 25:1 and hot rolling at 450 °C with different deformation amounts. The tensile strength of the composite is not affected by the amount of deformation caused by rolling. This indicates that the densification of the SiC_p/Al composite has been finished during the hot extrusion process, and hot rolling deformation cannot increase the relative density of the composite any further.

Table 3.61 Tensile strength of 25% SiC_p/Al composite after rolling with different deformation amounts

Deformation amount	50%	75%	85%
Tensile strength (MPa)	245	247	244

3.4.3.4 Extrusion Plasticity of Aluminum Matrix Composites [66, 67]

In many plastic forming methods, such as extrusion, rolling, forging, and drawing, extrusion is a widely used and important technique for plastic forming of discontinuously reinforced metal matrix composites. The addition of certain volume fractions of the reinforcements, such as whiskers and particles, to the metal matrix can greatly reduce the ductility of the composite, leading to high plastic deformation resistance and more difficulty in plastic forming. In addition, the hard reinforcements will cause wear of the extrusion dies. Therefore, for the extrusion of metal matrix composites, the extrusion parameters for common metals should be modified, including the extrusion temperature, extrusion speed, and extrusion force. During the extrusion processes, many factors will affect the material flow in the extrusion die, such as the extrusion method, the shape and size of the extruded products, the type of extruding materials, the structure and size of the extrusion die, the extrusion parameters, and the lubrication conditions. Factors that influence the extrusion formability of metal matrix composites include the preheating temperature of the extrusion die and composite billet, the extrusion ratio, the extrusion speed, and the lubricant.

(1) Lubricant

The function of the lubricant is to reduce the friction force between the extrusion composite billet and the extrusion die. The incidental tensile stress caused by the uneven plastic flow of the composite billet surface decreases with decreasing friction force. At the initial stage of the hot extrusion process, there is sufficient lubricant and it is distributed uniformly. As the extrusion process continues, more and more lubricant, which is mainly composed of graphite, is removed by the flow of the composite, and in positions where the material flow rate is very high, the lubricant will be depleted in a short time.

(2) Extrusion temperature

To choose the optimum extrusion parameters, the following quantities should be considered: the extrusion billet ductility, the plastic deformation resistance of the billet, the properties of the extruded material, efficiency, and cost. For extrusion of a SiC_p/Al composite, the extrusion temperature must be chosen in a range where SiC_p/Al composites have better ductility. The extrusion force required to extrude the SiC/Al composite obviously decreases with increasing preheating temperatures of the composite billet and the extrusion die, as shown in Table 3.62. The table shows that the maximum extrusion stress decreases by 10–20 MPa with each 50 °C temperature increment

Table 3.62 Effect of extrusion temperature on the maximum extrusion stress of SiC_p/Al composite

Extrusion temperature (°C)	350	400	450	500
Maximum extrusion stress (MPa)	280	265	248	235

(3) Extrusion ratio

During hot extrusion processes, the extrusion force relates to the deformation degree of the extrusion. Different methods are used to show the deformation degree of the extrusion, and the shrinkage of the cross section ε is widely used to describe the deformation degree of the extrusion process:

$$\varepsilon = \frac{F_0 - F_1}{F_0} \times 100\%, \quad (3.11)$$

where ε is also called the extrusion ratio, F_0 is the area of the cross section of the billet before extrusion, and F_1 is the area of the cross section of the extruded rod.

From Eq. 9.4.6, it can be seen that the plastic deformation degree of the composites increases with increasing extrusion ratio. It is found that when the extrusion ratio is more than five, obvious shear deformation will occur in the center of the extruded products, so that the mechanical properties will tend to be uniform across the whole section of the composite products. To obtain composite extrusion products with uniform properties, the extrusion ratio should be higher than five. Experimental results indicate that when the extrusion ratio is 36:1, the surface of the extruded rod is perfect and no cracks are formed.

(4) Extrusion speed

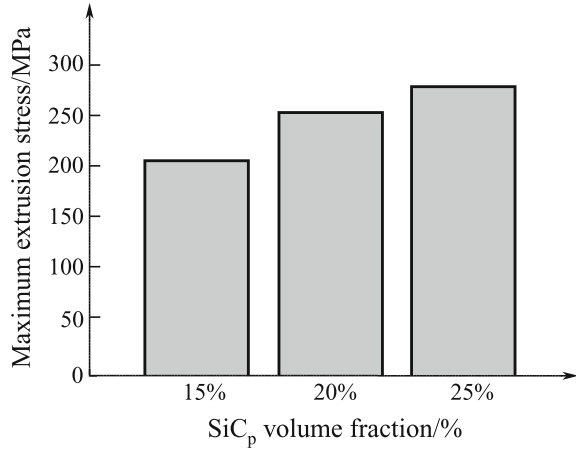
The plastic deformation resistance of SiC_p/Al composites is higher than that of the unreinforced matrix aluminum alloys because of the addition of the SiC particles to the matrix, so the first and second types of cracks are easily formed on the surfaces of the extrusion products. However, these cracks can be inhibited by reducing the extrusion speed, which can remove the excess heat by the heat transmission from the highly deformed area. However, a third type of crack will appear if the extrusion speed is too low. Experimental results indicate that when the SiC_p/Al composite is extruded at 450 °C at an extrusion speed of 5 mm/s, serious tear cracks appear on the surface of the extruded rod. The crack density decreases with increasing extrusion speed. All cracks are eliminated when the extrusion speed is 10 mm/s or much higher. The choice of extrusion speed is also limited by the extrusion temperature.

(5) Volume fraction of the reinforcement

Figure 3.54 shows the effect of the SiC particle volume fraction of SiC_p/Al composites on the maximum extrusion stress during extrusion of these composites with an extrusion ratio of 25:1. The figure shows that the maximum extrusion stress increases with increasing SiC volume fraction.

Clearly, many extrusion parameters can affect the extrusion forming ability of metal matrix composites, and these extrusion parameters are interactive and affect each other. For example, the extrusion stress decreases with increasing extrusion temperature, but in contrast, the ablation of the lubricant increases with increasing extrusion temperature, which results in increased extrusion stress. Because the

Fig. 3.54 Effect of SiC particle volume fraction on the maximum extrusion stress of SiC_p/Al composites

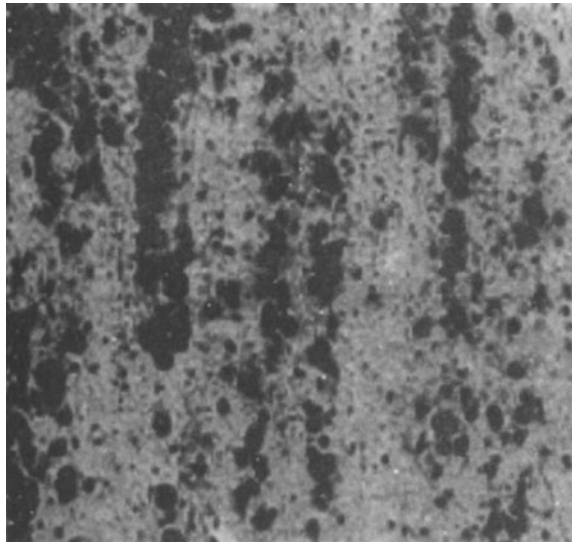


mechanical energy changes into heat, when the extrusion speed increases, then the preheating temperature of the extrusion die must be changed accordingly. When SiC_p/Al composites are extruded, extrusion temperatures below 500 °C are usually chosen, and the chosen extrusion speeds are usually less than 8 mm/s.

(6) Microstructures of extruded metal matrix composites

The reinforcements in metal matrix composites are easily broken during the extrusion process. Along with reinforcement breakage, another microstructural characteristic of extruded metal matrix composites is the formation of reinforcement-enriched bands, which are oriented parallel to the extrusion direction,

Fig. 3.55 Microstructure of an extruded SiC_p/Al composite showing the formation of the reinforcement-enriched bands



as shown in Fig. 3.55. Although the mechanism of this phenomenon is not completely clear to date, some experimental results have indicated that the extrusion conditions and the aspect ratio of the reinforcement are important factors that influence the formation of these reinforcement-enriched bands, and the uniformity of the original microstructure of the composites is not important.

3.4.3.5 Creep Properties of Metal Matrix Composites [68, 69]

Metal matrix composites have excellent properties at elevated temperatures, and their high-temperature creep behavior is one of the most important properties required for engineering applications of these composites in high-temperature environments. Compared with common metals and alloys, metal matrix composites usually have higher stress exponent, creep active energy, and creep resistance properties, which are explained by the threshold stresses of metal matrix composites. The threshold stress originally comes from the creep of dispersion-strengthened alloys. Therefore, the creep equation of metal matrix composites can be given as:

$$\dot{\epsilon} = A[(\sigma - \sigma_0)/E]^n \exp\left(-\frac{Q_c}{RT}\right), \quad (3.12)$$

where $\dot{\epsilon}$ is the creep rate, A is a constant, σ_0 is the threshold stress, E is the elastic modulus related to temperature, Q_c is the creep active energy, n is the true stress exponent, R is the gas constant, and T is the absolute temperature.

Table 3.63 Creep data of metal matrix composites

Composite	Temperature (°C)	Stress exponent n	Creep active energy (kJ/mol)
20% SiC _p /2124Al	300–450	9.5	400
20% SiC _w /2124Al(T4)	149–302	$n = 8.4$ (177 °C) $n = 21$ (288 °C)	277 (310 MPa) 431 (90 MPa)
20% SiC _w /6061Al	232–371	20.5	390 (60 MPa)
15% SiC _w /6061Al	300	18.7	–
30% SiC _p /6061Al	345–405	>7.4	270 (30 MPa) 494 (12 MPa)
10% SiC _p /1100Al	350	~7 (Compression) ~11.7 (Tension)	–
SiC _p (20 μm)/Al	573–673	21.3–19.9	253
SiC _p (10 μm)/Al	573–673	21.2–18.3	256
SiC _p (3.5 μm)/Al	573–673	26.1–24.4	261
1% Si ₃ N ₄ /Al	573–673	16.5–13.4	221
2% Si ₃ N ₄ /Al	573–673	16.0–15.5	259
10% TiC _p /Ti-6Al-4v	550–650	2.88	274
20% TiC _p /Ti-6Al-4v	550–650	2.96	282

Although some of the creep behavior of metal matrix composites can be explained by the threshold stress, there are also some disputes over the origin and evaluation of the threshold stress. Table 3.63 shows the creep data of some metal matrix composites.

3.4.4 Superplasticity of Discontinuously Reinforced Metal Matrix Composites

Metal matrix composites have excellent all-round properties but have poor mechanical machining properties that limit their wider application and further development. The “near-net-shape” plastic forming technique provides an effective method for producing metal matrix composite components with complicated shapes. Superplastic forming is the key aspect of the “near-net-shape” plastic forming technique. During superplastic deformation of metal matrix composites, the strain rate is usually described by:

$$\dot{\epsilon} = A \frac{DEb}{KT} \left(\frac{b}{d} \right)^p \left(\frac{\sigma - \sigma_0}{E} \right)^n, \quad (3.13)$$

where b is the Burgers vector, D is the diffusion coefficient, E is Young’s modulus, K is the Boltzmann constant, T is absolute temperature, d is the grain diameter, p is an index of the grain size, σ is the flow stress, σ_0 is the threshold stress, n is the stress exponent, and A is a geometrical constant.

According to the conditions of formation of superplasticity, there are three types of superplasticity: microstructural superplasticity, phase transformation superplasticity, and other superplasticity. Microstructural superplasticity is also called fine grain superplasticity and isothermal superplasticity. In microstructural superplasticity, the grains in the materials are refined, super-refined, equiaxed, and stable during superplastic deformation, and then superplasticity forms in a certain temperature range ($T > 0.5T_m$) and at a certain strain rate (10^{-4} – 10^{-1}). Phase transformation superplasticity is also called transformation superplasticity. Phase transformation superplasticity is obtained by repeated cycling phase transformation in a variable temperature environment. The other superplasticities include transient superplasticities, phase transformation-induced superplasticity, and internal stress superplasticities.

In metal matrix composites, the coordination between the reinforcement and the matrix during plastic deformation of the composite is an important factor that influences the superplasticity of the composites. However, in common metals and alloys, grain boundary movement is considered to be the superplasticity mechanism. The grain growth of the matrix is limited by the reinforcement in metal matrix composites. Large numbers of dislocations accumulate near the reinforcement, forming a stress concentration that enhances the formation and growth of voids at

the interfaces. Therefore, the most important factor influencing the superplasticity of metal matrix composites is not the grain size of the matrix, but the conditions for the nucleation and growth of voids in the composites caused by the existence of the reinforcements. Because of the limitation of the reinforcement to the matrix in metal matrix composites, the grains of the matrix are usually small in size and difficult to grow during tensile deformation of the composites, so complex heat treatments are not needed for the metal matrix composites to obtain a fine grain structure. The interfacial state is the other main factor that influences the superplasticity of metal matrix composites. Other influential factors include temperature, strain rate, strain hardening, grain shape, internals influential stress, microstructure, volume fraction, and the size and distribution of the reinforcements.

The characteristics of the structural evolution during superplastic deformation of metal matrix composites include the following.

- 1) The change in the shape and size of the grains of the matrix alloy. The grains are equiaxed during superplastic deformation and elongated after superplastic deformation.
- 2) Sliding, rotation, and transposition during superplastic deformation.
- 3) The striated band. The initial grain boundaries are widened after superplastic deformation. There are stripes in the wide grain boundary zone, and this is called the striated band. One viewpoint is that the striated band is evidence of the formation of diffusion creep. The other viewpoint is that diffusion creep is not the only reason for the formation of the striated band and that the striated band is caused by grain boundary sliding and new grain formation.
- 4) Dislocations. The density of the movable dislocations in metals during superplastic deformation is much higher than that before deformation, because the fine grains have large numbers of grain boundaries, so grain boundary sliding becomes very easy. Meanwhile, the stress concentration at the grain boundaries also increases, so more dislocations will be formed to relax the stress concentration. These processes occur rapidly so that grain boundary sliding goes on continuously. When a large amount of plastic deformation occurs, the dislocation density will be very high, especially at the grain boundaries and the triangular grain boundaries. However, no dislocation pileup has been found at the grain boundaries or the triangular grain boundaries, indicating that dislocation climbing occurs strongly at the grain boundaries.
- 5) Voids. Void formation is a common phenomenon in microstructure evolution during the superplastic deformation processes. At a certain stage of the superplastic deformation process, voids will nucleate in the deformed material. With increasing amounts of deformation, the voids will grow, accumulate, and bond with each other, which results in the fracture of the material.

Depending on the void shape, there are two kinds of void: One is a wedge void (or a V-type void), located at the triangular grain boundaries, which is caused by the stress concentration; the other is a spherical void (or an O-type void), which is

located at grain boundaries and interfaces in the metal matrix composites, and which is caused by the accumulation of supersaturated voids at the grain boundaries and interfaces.

There are two views about the nucleation of the voids in metal matrix composites. According to one viewpoint, the voids exist before the plastic deformation of the composites. According to the other viewpoint, the voids are formed at the interfaces by interface sliding during the superplastic deformation of the composite. Suppose that a crack is formed at the triangular grain boundary during grain boundary sliding under shear stress; the condition for void formation is given as follows:

$$\tau^2 > \frac{12\nu G}{\pi L}, \quad (3.14)$$

where τ is the shear stress, ν is the surface energy of the void, L is the length of the sliding interface, and G is the shear modulus.

In metal matrix composites, the physical properties, such as the elastic modulus, are different for the reinforcement and the matrix. During the superplastic deformation of metal matrix composites, the hard reinforcement will inhibit grain boundary sliding and cause stress concentration at the interface. When the reinforcement particle size is larger, it is more difficult to release the interfacial stress, and the interface between particle and matrix will become a position for void formation. The critical particle size is as follows:

$$\Delta = (\Omega\sigma\delta D_{\text{gb}}/KT\dot{\epsilon})^{1/3}, \quad (3.15)$$

where Ω is the volume of an atom, σ is the flow stress, δD_{gb} is the boundary diffusion coefficient, K is the Boltzmann constant, T is absolute temperature, and $\dot{\epsilon}$ is strain rate. When the particle size in a particle-reinforced metal matrix composite is smaller than a critical value, the formation of voids in the composites is limited; when the size is larger than the critical value, voids will obviously form.

In particle-reinforced metal matrix composites, bonding of the voids usually occurs at the interface between particle and matrix, and there is a specific angle between the bonding direction and the tensile direction. Therefore, the bonding of voids during superplastic deformation of particle-reinforced metal matrix composites may be related to the shear stress at the interface between particle and matrix in the composites. The stress concentration is an important factor for improvement of void nucleation of the metal matrix composites.

There are two void growth mechanisms during superplastic deformation: One is void growth caused by void diffusion along the grain boundaries; the other is void growth caused by plastic deformation around the void. In the void diffusion growth mechanism, the void growth rate can be described by the following:

$$\left(\frac{d_r}{d_\varepsilon}\right)_d = \frac{2\Omega\delta_{gb}D_{GB}}{kT} \cdot \frac{1}{r^2} \left(\frac{\sigma - 2\nu/r}{\dot{\varepsilon}}\right)\alpha, \quad (3.16)$$

where Ω is the volume of an atom, δ_{gb} is the width of the grain boundary; r is the void radius, ν is the surface energy of the void, D_{gb} is the diffusion coefficient of the grain boundary, σ is the flow stress, T is the absolute temperature, $\dot{\varepsilon}$ is the strain rate, K is the Boltzmann constant, and α is the diffusion coefficient of the grain boundary. Considering the size and interspacing of the voids, the diffusion coefficient of the grain boundary (α) is given by the following:

$$\alpha = \frac{1}{4 \ln(\lambda/2r) - [1 - (2r/\lambda)^2][3 - (2r/\lambda)^2]}, \quad (3.17)$$

where λ is the void interspacing.

The relationship between the volume fraction of the void and the strain is as follows:

$$C_v = C_{v0} \exp(\eta\varepsilon), \quad (3.18)$$

where C_v is the volume fraction of void at a strain ε , and C_{v0} is the volume fraction of the void when the strain is zero. The void growth rate is the slope of the $\ln C_v - \varepsilon$ curve.

Strain-rate sensitivity (the m value) is an important characteristic parameter of superplastic deformation of materials. It is affected by the strain rate, the deformation temperature, and the microstructure of the materials. The strain-rate sensitivity (m value) is always considered to be a constant under a specific superplastic deformation condition. Based on this viewpoint, a model of the void growth controlled by the plastic deformation of the matrix is given by the following:

$$df_v/d\varepsilon = \eta_v f_v, \quad (3.19)$$

where η_v is a material constant. The equation used to calculate η_v is as follows:

$$\eta_v = \frac{1+m}{m} \sinh \left\{ \frac{2(2-m)}{2+m} \times \frac{1}{3} K_s \right\} (K_s = 1 \sim 2). \quad (3.20)$$

Methods to reduce and inhibit void formation include the following: (1) changing the composition and microstructure of the materials; (2) preheating treatment to obtain a very fine grain structure; (3) annealing treatment after plastic deformation; and (4) hot isostatic pressing after plastic deformation.

Nucleation, growth, and bonding of the micro-voids will result not only in the formation of macro-cracks and the final fracture of the materials, but also in the

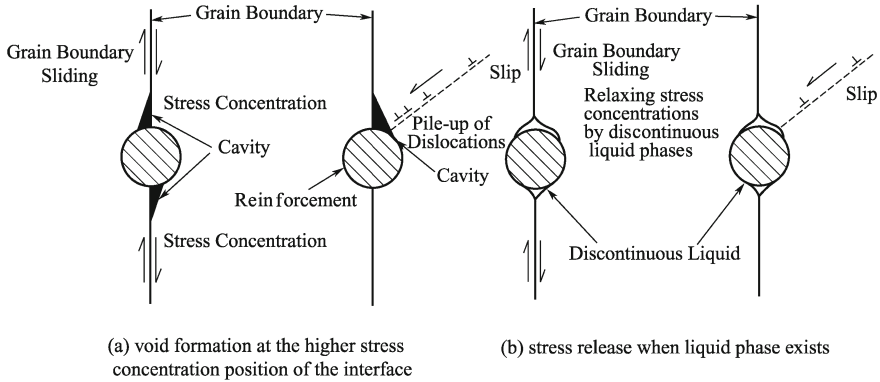


Fig. 3.56 Schematic drawings showing the formation of voids

reduction of the strength, modulus, and toughness of the deformed materials. The micro-void is considered to be a damage variable in damage mechanics. The damage evolution equation for superplastic deformation of a material is given by the following:

$$\begin{aligned}
 D &= \left[B' \int_0^p \exp\left(\frac{\sigma_m}{\sigma_e}\right) dp \right]^{B_1} \\
 &= (B')^{B_1} \left[\int_0^p \exp\left(\frac{\sigma_m}{\sigma_e}\right) dp \right]^{B_1} \\
 &= B_0 \left[\int_0^p \exp\left(\frac{\sigma_m}{\sigma_e}\right) dp \right]^{B_1},
 \end{aligned}
 \tag{3.21}$$

where $B_0 = (B')^{B_1}$, which are characteristic constants of the materials and can be determined by uniaxial tensile testing. If the characteristic constants of materials B_0 and B_1 are determined by a uniaxial tensile test, then the damage variable D can be determined. Figure 3.56 is a schematic showing the void formation process.

Materials with superplasticity are usually sensitive to voids. Void formation during plastic forming will greatly reduce the forming abilities and properties of the deformed products. Superplastic forming of materials is usually carried out at higher temperatures in a closed die with a very complex deformation mechanism, so the common analysis methods and measurements are difficult for these problems. Numerical simulation by the finite element method can solve these problems effectively and has become one of the most promising subjects in the materials processing field. Tables 3.64 and 3.65 show the superplastic deformation properties of metal matrix composites.

Table 3.64 Superplastic deformation properties of aluminum matrix composites

Composite	Temp. (K)	Grain size (m)	<i>m</i> value	Q_{app} (J mol ⁻¹)	Strain rate (s ⁻¹)	Elongation (%)
15% SiC _p /IN9052	823	–	0.5	–	5	610
15% SiC _p /PM-64	773–789	8	0.3	–	2×10^{-4}	450
20% Si ₃ N _{4p} /5052Al	818	1	0.5	–	1	700
20% Si ₃ N _{4p} /6061Al	818	3	0.5	–	1×10^{-1}	450
20% Si ₃ N _{4p} /6061Al	833	1	0.5	–	2	620
12% SiC _w /7475Al	773	6.4	0.5	–	1×10^{-3}	450
20% SiC _w /2124Al	798	–	0.5	218	3×10^{-1}	300
20% SiC _w /2124Al	748–823	1	0.3	218	1.3×10^{-1}	300
Si ₃ N _{4w} /2124Al	798	–	0.4	140	5×10^{-1}	150
β-Si ₃ N _{4w} /2124Al	798	–	0.5	–	1.7×10^{-1}	250
Si ₃ N _{4w} /7064Al	798	–	–	–	2×10^{-1}	250
β-Si ₃ N _{4w} /6061Al	798	–	–	–	2×10^{-1}	250
β-Si ₃ N _{4w} /2124Al	798	–	0.5	–	2×10^{-1}	250
20% β-Si ₃ N _{4w} /6061Al	798	–	0.5	–	1.6×10^{-1}	300
20% Si ₃ N _{4w} /6061Al	818	3	0.5	–	2×10^{-1}	600
20% β-Si ₃ N _{4w} /7064Al	818	3.5	0.4	–	2×10^{-1}	230
15% SiC _p /2014Al	753	–	0.4	–	2×10^{-4}	349
15% SiC _p /7475Al	788	–	0.4	–	2×10^{-4}	310
(10–15)% SiC _w /7475Al	793	–	0.5	–	2×10^{-4}	350
15% SiC _p /Al–Zn–Mg–Cu	773	–	0.3	–	2×10^{-4}	450
15% SiC _p /2618Al	833	–	–	–	3.3×10^{-3}	400
15% SiC _p /Al–Zn–Mg–Cu	783	–	–	–	8.33×10^{-3}	210
10% SiC _p /2024Al	788	–	0.4	–	5×10^{-4}	293–685
19% Al ₂ O ₃ /6061Al	803	–	0.6	–	7.2×10^{-3}	135

Table 3.65 Superplastic deformation properties of Mg, Zn, and Ti alloy matrix composites

Composite	Temperature (K)	Elongation (%)	<i>m</i> value	Strain rate (s ⁻¹)
20% TiC _p /Mg–5Zn	743	340	0.33	6.7×10^{-2}
17% SiC _p /Mg–5.5Zn–0.5Zr	723	360	0.33	1
19.7% SiC _w /MB15	613	200	0.35	1.67×10^{-2}
12% AlN _p /Mg–5%Zn	673	150	0.3	10^{-3}
(5–10)% SiC _p /AZ31	773	100	0.3	2×10^{-3}
(5–15)% SiC _p /Zn–4Al–3Cu	513	260	0.4	2×10^{-3}
10% TiC _p /Ti–4Cr	1013	200	0.3	4.17×10^{-3}
10% TiC/Ti–6Fe	963	820	0.3	4.17×10^{-3}

3.4.4.1 Superplasticity of Semisolid Metal Matrix Composites

The existence of the reinforcements in metal matrix composites will cause changes in the microstructure during superplastic deformation in three ways: (1) The grains are refined during thermal processing; (2) grain growth is inhibited during superplastic deformation; and (3) a large number of interfaces are formed. The addition of reinforcements results in segregation of the alloying elements, which helps with the formation of the liquid phase during hot plastic deformation. A small amount of the liquid phase can coordinate grain boundary sliding, release the stress concentration, and inhibit void growth. A greater elongation can be obtained by controlling the optimum amount of the liquid phase in metal matrix composites. The plastic deformation mechanism and void formation during high-strain-rate superplastic deformation are thus important subjects, particularly with respect to the problem of interaction between the liquid phase and voids. The optimum temperature for superplastic deformation of aluminum matrix composites is around the solidus temperature of the matrix, so some of the liquid phase may be formed during superplastic deformation of aluminum matrix composites. It is very important to study the effect of the liquid phase on the superplastic deformation of aluminum matrix composites. A small amount of the liquid phase may reduce the void growth rate because the liquid phase can change the stress state of the grain boundaries. The liquid phase can reduce the stress concentration, but if the amount of liquid phase formed is too large, then the interfacial bonding strength of the metal matrix composites will decrease; voids can then form easily, resulting in a large reduction in the elongation. This indicates that the plastic deformation and fracture of the metal matrix composites are affected by the size and distribution of the liquid phase. The formation of high-strain-rate superplasticity depends on the liquid phase at the interfaces, but the liquid phase is not a necessary condition for the formation of high-strain-rate superplasticity. High-strain-rate superplasticity can be found in all metal matrix composites fabricated by the mechanical alloying method.

When the deformation temperature is higher than the matrix solidus temperature, the high-strain-rate superplastic deformation behavior of a whisker-reinforced metal matrix composite can be explained by the shearing of the viscous layer between the whisker and the matrix. Suppose that the whisker is a rigid body; a speed gradient then exists in the viscous layer between the whisker and the matrix. The interfacial sliding is the movement of the non-Newtonian fluid of the viscous layer, and the shearing can be expressed as follows:

$$\tau = \eta \frac{dv}{dh} \quad (3.22)$$

where v is the relative deformation speed of the viscous layer and h is the thickness of the viscous layer.

The rheological model can explain the superplastic deformation of metal matrix composites when a large amount of the liquid phase appears during plastic deformation. However, for most of the superplastic deformation of metal matrix

composites, the amount of the liquid phase is not too large, because most of the superplastic deformation of metal matrix composites is carried out at a temperature near or slightly above the solidus temperature of the matrix. Therefore, a new model based on grain boundary sliding and interface sliding is given to explain the high-strain-rate superplasticity of metal matrix composites:

$$\dot{\epsilon}_t = \dot{\epsilon}_{\text{GBS}} + \dot{\epsilon}_{\text{IS}}, \quad (3.23)$$

$$\dot{\epsilon}_t = \frac{\pi(1-\nu)b^3}{18 \times 3^{1/2}GKTh^2} \left[\frac{2d_m - d_r}{d_m} D_{\text{gb}} + \frac{d_m - d_r}{d_m} D_{\text{I}} \right] (\sigma - \sigma_0)^2, \quad (3.24)$$

$$\dot{\epsilon}_t = \frac{1}{1 - f_{\text{li}}} \frac{\pi(1-\nu)b^3}{18 \times 3^{1/2}GKTh^2} \left[\frac{2d_m - d_r}{d_m} D_{\text{gb}} + \frac{d_m - d_r}{d_m} D_{\text{I}} \right] (\sigma - \sigma_0)^2, \quad (3.25)$$

where $\dot{\epsilon}_t$ is the total strain rate, h is the dislocation climbing distance, b is the Burgers vector, $\dot{\epsilon}_{\text{GBS}}$ is the grain boundary sliding rate, and D_{gb} is the grain boundary diffusion coefficient. σ is the external stress, $\dot{\epsilon}_{\text{IS}}$ is the interface sliding rate, d_m is the matrix grain size, G is the shear modulus, ν is the Poisson ratio, d_r is the reinforcement size, σ_0 is the threshold stress, T is the absolute temperature, D_{I} is the interface diffusion coefficient, and f_{li} is the liquid-phase fraction. Equation (3.24) is used when the deformation temperature is below the solidus of the matrix, and Eq. (3.25) is used when the deformation temperature is above the solidus of the matrix.

3.4.4.2 High-Strain-Rate Superplasticity of Metal Matrix Composites

The main factors that limit the wider application of superplastic forming of metal matrix composites are as follows [70, 71]: (1) The strain rate is lower, ranging from 10^{-5} s^{-1} to 10^{-4} s^{-1} ; (2) the deformation temperature is very high; and (3) large numbers of voids are formed in the material during the deformation processes. Therefore, for practical research, it is important to increase the strain rate and reduce the deformation temperature and the number of voids in the material. It is necessary to study and analyze the mechanical nature and microstructure evolution of these materials in detail during superplastic deformation. Depending on the matrix alloy, the reinforcement, and the composite fabrication technique used, different metal matrix composites attain superplasticity at different strain rates. Common superplasticity corresponds to a strain rate below $2 \times 10^{-2} \text{ s}^{-1}$, and high-strain-rate

superplasticity (HSRS) corresponds to a strain rate equal to or more than $2 \times 10^{-2} \text{ s}^{-1}$. High-strain-rate superplasticity promises to provide an effective route for formation of the “near-net-shape” of metal matrix composites.

For metals and alloys, about 90% of the deformation energy will be changed into heat. During high-strain-rate deformation, most of the heat will contribute to the temperature rise in the materials. High-strain-rate superplasticity is usually obtained at temperatures around the solidus temperature of the matrix, and because of temperature increases caused by the adiabatic phenomenon, the deformation temperature may be higher than the solidus temperature of the matrix. The temperature change during the deformation process can be expressed as follows:

$$\Delta T = \varepsilon \sigma t / c, \quad (3.26)$$

where t is the duration of the plastic deformation and c is the specific heat at a constant volume. From the plastic deformation viewpoint, it is found that

$$\Delta T = \frac{0.9}{\rho C_p} \int \sigma d\varepsilon, \quad (3.27)$$

where ρ is the material density.

The relationship between the deformation stress and the temperature, strain and strain rate is given by:

$$\sigma = (\sigma_0 + B\varepsilon^N)(1 + C \ln \varepsilon) \left[1 - \left(\frac{T}{T_m} \right) \right], \quad (3.28)$$

where σ_0 is the yield strength of the material, T_m is the melting point of the materials, and B , C , and N are constants.

By combining Eqs. (3.27) and (3.28), we obtain the following:

$$\int_{\frac{T_0}{T_m}}^{\frac{T_f}{T_m}} \frac{dT}{T} = \frac{0.9(1 + \ln \varepsilon^c)}{\rho c p} \int_0^{\varepsilon_f} (\sigma_0 + B\varepsilon^N) d\varepsilon, \quad (3.29)$$

where T_0 is the temperature when deformation begins, T_f is the temperature when the deformation is finished, and ε_f is the strain when the deformation is finished. The above equations reflect the relationships among the temperature change, the material characteristics, and the deformation conditions.

Metal matrix composites can attain superplasticity at higher strain rates, unlike common alloys. The most important problem for wider application of superplastic deformation is its lower strain rate, and thus, superplastic deformation is used only for materials that are difficult to machine. The high-strain-rate superplasticity in metal matrix composites provides an effective method for wider application of superplastic forming of metal matrix composites and other hard materials.

3.4.4.3 Mechanism of Superplastic Deformation of Metal Matrix Composites

The study of the mechanism of superplastic deformation of metal matrix composites is based on common superplasticity theory and the characteristics of metal matrix composites. The reinforcing effect of the reinforcement on the matrix during superplastic deformation depends on the flowability of the reinforcement and the crystal structure and chemical properties of the matrix. It is also affected by the chemical composition of the interface and the existence of the lower melting point zone and the liquid phase. No fully developed mechanism exists for the superplastic deformation of metal matrix composites. Grain boundary sliding is considered to be the main mechanism of microstructure superplasticity. Other mechanisms must also be considered to coordinate the grain boundary sliding to ensure that the deformation of the materials is continuous. Sliding between two grains cannot occur if their adjacent grain (i.e., a third grain) does not coordinate them. It is commonly considered that this coordination mechanism determines the kinetics of the superplastic flow of materials, which includes diffusion and dislocation slip. The differences between the various mechanisms of superplastic deformation relate to the way in which the stress concentrations caused by grain boundary sliding are adjusted [72, 73].

(1) Diffusion creep mechanism

The creep rate of aluminum matrix composites is considered to be controlled by lattice diffusion. In particle-reinforced aluminum alloy matrix composites, the sub-grains may be pinned by the particles. Because the strain rate is controlled by the lattice diffusion of the matrix, we have the following:

$$\frac{\dot{\epsilon}_m kT}{DGb} = A \left(\frac{\sigma - \sigma_0}{G} \right)^n, \quad (3.30)$$

where k is the Boltzmann constant, b is the Burgers vector, G is the shear modulus, D is the lattice diffusion coefficient of the matrix, A and n are constants, T is the absolute temperature, σ is the external stress, σ_0 is the ultimate stress, and $\dot{\epsilon}_m$ is the strain rate controlled by diffusion. The apparent active energy obtained by this mechanism is larger than the lattice diffusion active energy of the matrix, because of the complicated relationship between the temperature and the shear modulus, and especially that between the temperature and the ultimate stress. Suppose that $n = 5$; the ultimate stress of the composites then decreases with increasing temperature. This mechanism is suitable for a lower strain rate, so it is a creep mechanism at lower strain rates for metal matrix composites.

(2) Sliding deformation mechanism

Based on the grain boundary sliding, the following model is set up:

$$\frac{\dot{\epsilon}_m k T}{D G b} = A \left(\frac{\sigma - \sigma_0}{G} \right)^n \left(\frac{b}{d} \right)^p. \quad (3.31)$$

The active energy ($\dot{\epsilon}_m$) obtained by this mechanism is much larger than the lattice diffusion active energy of the matrix, so the superplastic deformation process of aluminum matrix composites is mainly the sliding of the grain boundary and the interface between the matrix and the reinforcement. As a coordination mechanism, diffusion also exists.

It is found that the strain-rate sensitivity (m value) changes greatly when the strain rate is higher, so it is considered that the deformation mechanism changes with the changing strain rate. When the strain rate is lower, the active energy is similar to the dislocation creep energy, so the deformation mechanism is a dislocation creep mechanism. When the strain rate is higher, the active energy is similar to the lattice diffusion active energy, and thus, the deformation mechanism is a grain boundary and interface sliding mechanism. It is widely accepted that grain boundary sliding is the main mechanism of microstructure superplasticity, and other mechanisms also exist as coordination mechanisms. The large elongation is contributed by grain boundary sliding, and in this process, other mechanisms will release the stress concentration at the interface and inhibit void growth. Most of the current mechanisms are set up by considering how to coordinate the sliding and rotation of the grains.

(3) Mechanism of high-strain-rate superplasticity

It is commonly considered that superfine grains and near-solidus temperatures are necessary conditions to realize high-strain-rate superplasticity. When the deformation temperature is higher than the solidus temperature, or the temperature is increased by the adiabatic phenomenon to the solidus temperature, liquid foils appear at the grain boundary and the interface, resulting in deformation in a solid-liquid dual-phase state. The grain boundary and interface sliding is caused by the shear of the liquid foil, which acts like a lubricant to make the sliding easier, so that the elongation is increased. The high-strain-rate superplasticity mechanism can be explained from the viewpoint of rheology, in which the deformation is considered as a non-Newtonian fluid, and thus, we have the following:

$$\eta = k \dot{\gamma}^{-p} \mu. \quad (3.32)$$

The sliding shear stress is described as follows:

$$\tau = k \dot{\gamma}^m, \quad (3.33)$$

Table 3.66 Results of high-strain-rate superplastic deformation of some metal matrix composites

Composite	Temperature (K)	Strain-rate sensitivity (m)	Strain rate (s ⁻¹)	Maximum elongation (%)
20% SiC _w /2124Al	798	0.3	0.3	300
20% Si ₃ N _{4p} (0.2 μm)/2124Al	773	0.3	0.3	280
20% Si ₃ N _{4p} (1.0 μm)/2124Al	788	0.4	0.04	840
20% β-Si ₃ N _{4w} /2124Al	798	0.5	0.2	250
20% Si ₃ N _{4p} (0.2 μm)/5052Al	818	0.4	1.0	700
20% SiC _w /6061Al	823	0.3	0.2	300
20% Si ₃ N _{4p} (0.2 μm)/6061Al	833	0.4	2.0	620
20% Si ₃ N _{4p} (0.5 μm)/6061Al	833	0.4	1.0	350
20% Si ₃ N _{4p} (1.0 μm)/6061Al	818	0.4	0.1	450
20% α-Si ₃ N _{4w} /6061Al	818	0.3	0.3	150
20% β-Si ₃ N _{4w} /6061Al	818	0.3–0.5	0.1–0.2	260–600
10% SiC _p (2.0 μm)/7075Al	793	0.5	5.0	300
20% α-Si ₃ N _{4w} /7075Al	773	0.35	0.18	260
15% AlN _p (0.7 μm)/6061Al	873	0.5	1.0	200
20% Si ₃ N _{4p} (0.2 μm)/7475Al	788	0.4	4.0	220
15% SiC _p /IN9021	823	0.5	5.0	600
20 vol.% SiC _w /2124Al	798	–	0.3	300
20 vol.% SiC _w /6061Al	873	–	0.17	440
20 vol.% SiC _w /2009Al	773	–	0.67	190
20 vol.% Si ₃ N _{4p} /6061Al	833	–	2	620
20 vol.% Si ₃ N _{4p} /2124Al	773	–	0.3	280
20 vol.% Si ₃ N _{4p} /5052Al	818	–	1	700
20 vol.% Si ₃ N _{4p} /Al–Cu–Mg	788	–	0.04	840
20 vol.% Si ₃ N _{4p} /Al–Zn–Mg	818	–	1	330
20 vol.% Si ₃ N _{4w} /6061Al	818	–	0.2	600
20 vol.% Si ₃ N _{4w} /Al–Mg–Si	833	–	0.1	480
12 vol.% SiC _w /7075Al	773	–	0.001	450
20 vol.% SiC _p /6061Al	853	–	0.13	200
17.5 vol.% SiC _p /8090Al	848	–	0.18	300
17.5 vol.% SiC _p /6061Al	853	–	0.1	375
15 vol.% SiC _p /2024Al	793	–	0.008	290
15 vol.% SiC _p /IN90	913	–	0.01	200

(continued)

Table 3.66 (continued)

Composite	Temperature (K)	Strain-rate sensitivity (m)	Strain rate (s ⁻¹)	Maximum elongation (%)
20 vol.% Si ₃ N _{4w} /Al–Zn–Mg	833	–	0.1	380
α–Si ₃ N _{4w} /2124Al	798	–	0.5	150
α–Si ₃ N _{4w} /7064Al	798	–	0.2	250
27 vol.% αSi ₃ N _{4w} /2024Al	773	–	0.17	175
27 vol.% αSi ₃ N _{4w} /7075Al	773	–	0.18	260
β–Si ₃ N _{4w} /2124Al	798	–	0.17	250
β–Si ₃ N _{4w} /6061Al	798	–	0.2	250
20 vol.% β–Si ₃ N _{4w} /6061Al	798	–	0.16	300
20 vol.% β–Si ₃ N _{4w} /2124Al	798	–	0.1	300
25 vol.% β–Si ₃ N _{4w} /6061Al	818	–	0.02	173
27 vol.% β–Si ₃ N _{4w} /Al	903	–	0.1	200
AlN _p /IN90	913	–	0.27	246
AlN _p /6061Al	873	–	0.8	500
10 vol.% TiC _p /Mg–Zn	743	–	0.07	200
15 vol.% AlN _p /Mg–Al	673	–	0.5	200
20% TiC _p (2–5 μm)/Mg–5Zn	743	0.3	0.07	340
15% AlN _p (0.7 μm)/Mg–5Zn	673	0.3	0.5	256
10% SiC _p (2.0 μm)/AZ31	798	0.4	0.5	228
5% SiC _p (14 μm)/Zn–4Al–3Cu	573	0.4	0.2	130
5% SiC _p (14 μm)/Zn–4Al–3Cu	533	0.4	0.02	254
(10–15)% SiC _p (14 μm)/Zn–4Al–3Cu	513	0.4	0.02	170

where η is the shear viscosity, $\dot{\gamma}$ is the shear strain rate, k and p are materials constants, and $m = 1-p$ is the strain-rate sensitivity. When the deformation temperature is higher than the matrix solidus and the strain rate is high, it is considered that the sliding of the grain boundary and the interface between the reinforcement and the matrix is the deformation mechanism, and the sliding is realized by the shear of the liquid viscous layer. The relationship between the liquid effect and the grain boundary sliding must still be investigated further. Table 3.66 shows the results of high-strain-rate superplastic deformation of some metal matrix composites.

3.4.5 Machining of SiC_w/Al Composites

3.4.5.1 Turning Machining of SiC_w/Al Composites

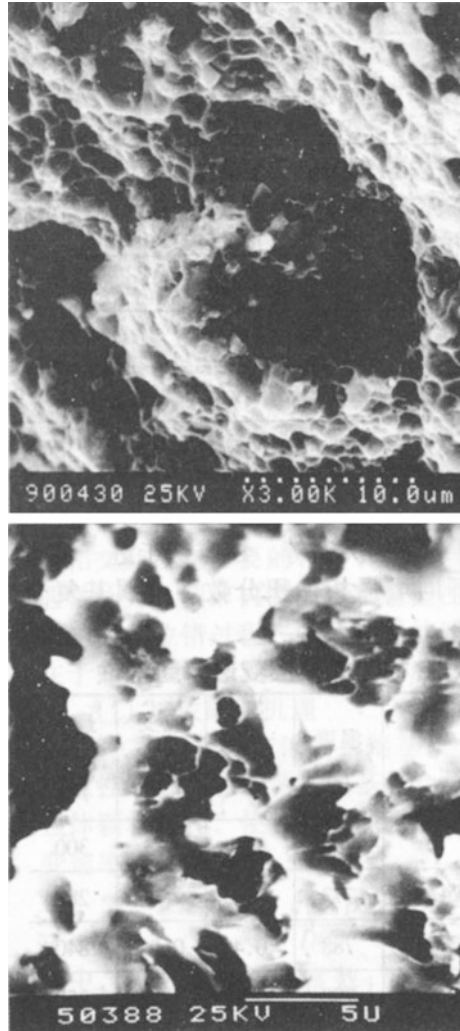
(1) Cutting mechanism of SiC_w/Al composites [74, 75]

- 1) Characteristics of plastic deformation of SiC_w/Al composites The SiC_w/Al composite is composed of an aluminum matrix alloy with high ductility and a SiC whisker, which is very brittle and has very high strength. All experimental results have indicated that the interfacial bonding strength between the SiC whisker and the aluminum matrix is very high, and the interface does not crack during the deformation and fracture of the composite. Therefore, the plastic deformation of SiC_w/Al composites combines the plastic deformation of the aluminum matrix and the rotation and breaking of the SiC whiskers in the matrix.

Plastic deformation of SiC_w/Al composites has the following three characteristics.

- ① The SiC_w/Al composite has lower yield strength but higher work hardening ability. When a force is exerted on a SiC_w/Al composite, stress concentrations will be formed in the matrix around the whiskers, resulting in local yielding at a lower external force, and therefore, the SiC_w/Al composite shows lower yield strength. With increasing external stress, more and more local yielding occurs; these local plastic deformations will be inhibited by other whiskers and the resistance to the plastic deformation increases. Therefore, the work hardening ability of the SiC_w/Al composite is high.
- ② The tensile fracture of SiC_w/Al composites shows as brittle fracture in the macroscopic view, because the fracture elongation is only about 2%; however, in a microscopic view, lots of plastic deformation occur before the fracture of the composite. The matrix aluminum alloy has high ductility and plastic deformation of the matrix is easy during the tensile process. This plastic deformation in the matrix is limited only to local areas because of the limitations of the whiskers, and as a result, the direction of plastic deformation in each local area is different. Therefore, although a great amount of plastic deformation has happened in many local matrix areas, the total elongation of the composite in the tensile direction is small. The tensile fracture surface of the SiC_w/Al composite is shown in Fig. 3.57. The fracture surface of the composite is shown as a typical dimple-type ductile fracture surface, although the tensile fracture elongation is only 2.5%, which indicates that large plastic deformation has happened in the matrix before fracture of the SiC_w/Al composite.
- ③ The plastic deformation ability of the SiC_w/Al composite is affected greatly by the stress state. In a tensile stress state, micro-cracks initiate in many areas because of the stress concentrations in the composite caused by the SiC

Fig. 3.57 Tensile fracture surface of SiC_w/Al composite



whiskers. These micro-cracks propagate easily under tensile stress, leading to a fracture of the composite. The tensile fracture elongation of the SiC_w/Al composite is thus very low. In a compressive stress state, on the one hand, rotation of the whisker is easy under the moment in the composite, which will coordinate the plastic deformation of the matrix in the composite, so initiation of macro-cracks is difficult; on the other hand, it is difficult for micro-cracks to propagate under compressive stress, so the SiC_w/Al composite exhibits a higher plastic deformation ability under compressive stress. The SiC_w/Al composite has much higher plastic deformation ability during hot extrusion because it is in a three-dimensionally compressive stress state in this case. The extrusion ratio for hot extrusion of SiC_w/Al composites can be 22:1.

- 2) Material removal mechanism of SiC_w/Al composites The material removal mechanism of SiC_w/Al composites is almost the same as that of common plastic metals. Scales will be formed at the cutting surfaces of these materials. However, some specific phenomena may exist during cutting of SiC_w/Al composites because of their special plastic deformation characteristics, as described above. Research into the cutting mechanism of SiC_w/Al composites has been carried out on an S1-225 ultraprecision lathe using a polycrystalline diamond turning tool.

The experimental results indicate that a build-up edge (BUE) is formed on the polycrystalline diamond turning tool during cutting of the SiC_w/Al composite. The BUE formation occurs because the SiC_w/Al composite has a certain ductility, and there is bonding between the matrix aluminum alloy and the polycrystalline diamond turning tool. The high work hardening ability of the SiC_w/Al composite is another reason for the BUE formation.

Associated with the BUE formation, scales are formed on the cutting surface of the SiC/Al composite, as shown in Fig. 3.58. The SiC_w/Al composite formation process is unlike that of other common metals because of the existence of the hard whiskers. The stress in different micro-zones of the plastic deformation area near the cutting edge is different during the cutting of the SiC_w/Al composite, because of the stress concentrations caused by the whiskers, so larger cracks will be formed in the areas with higher stress. Also, the chips staying at the crack face have a compressive effect on the cutting layer, which increases the compressive stress in the cutting layer near the cutting edge; this results in an increase in the plastic deformation ability of the SiC_w/Al composite and the formation of more serious scales on the cutting surface of the composite.

Fig. 3.58 SEM photographs showing scales on the cutting surface of the SiC_w/Al composite



There is also a tear fracture during cutting of the SiC_w/Al composite because of the micro-anisotropy of the composite. When cutting an isotropic material, the cracks in front of the cutting edge propagate only in the first deformation zone, along the direction of the main cutting force (the direction of the cutting speed). The cracks thus cannot propagate below the cutting plane, which is favorable for formation of a smooth cutting surface. When cutting the SiC_w/Al composite, which is anisotropic in the microscale view, the situation is different. The SiC whisker is a single crystal with an aspect ratio of about 20, so for each micro-zone around a SiC whisker in the SiC_w/Al composite, the tensile strength in different directions is different. The strength is lower in the direction perpendicular to the whisker axis, and thus, tensile fracture is easy in this direction. Also, when a crack propagates to meet a whisker, the resistance of the whisker to the propagation of the crack is different when the angle between the whisker axis and the crack propagation direction is different. The crack propagates easily in the direction along the whisker axis but with difficulty in the direction perpendicular to the whisker axis. Therefore, some cracks may propagate below the cutting surface because of the micro-anisotropy of the SiC_w/Al composite, which will affect the surface roughness of the cutting surface.

- 3) Residual stress formation mechanism in the cutting surface of the SiC_w/Al composite The residual stress formation mechanism in the cutting surface of the SiC_w/Al composite is complex. The residual stress is affected by many factors, in which the recovery of the elastic deformation of the internal material is the main factor. There is also a thermal residual stress in the cutting surface, because the coefficient of thermal expansion of the matrix aluminum alloy is five times higher than that of the SiC whisker.

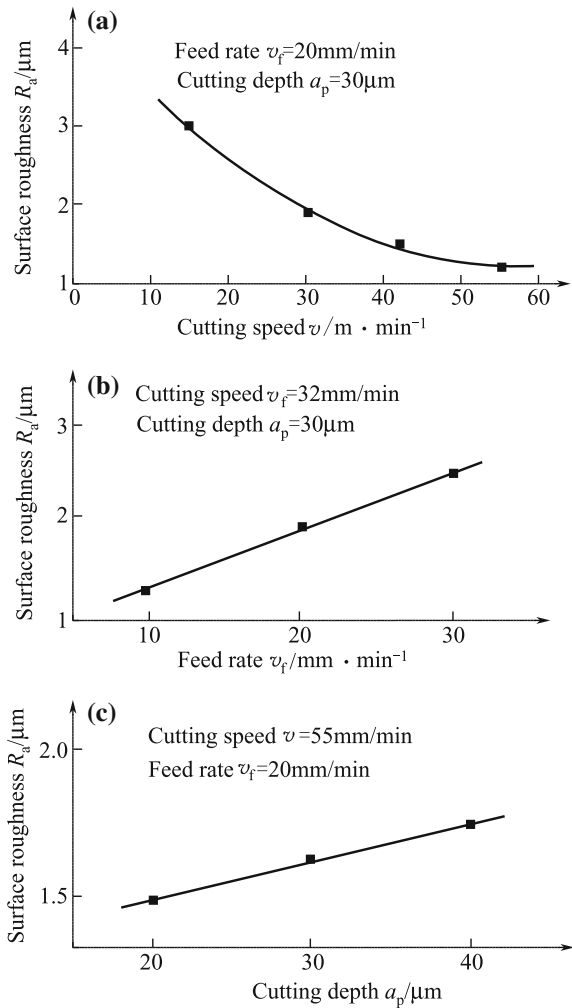
Both the analysis above and the results of electron microscope observation of the cutting surface indicate that a large amount of plastic deformation takes place in the cutting surface during the SiC_w/Al composite cutting process. During the plastic deformation of the cutting surface, elastic deformation occurs in the internal material of the cutting material. Recovery of the elastic deformation after the cutting process will result in a residual stress in the cutting surface. The experimental results indicate that the residual stress in the cutting surface of the SiC_w/Al composite is compressive residual stress, and thus, it is concluded that the elastic deformation of the internal material during the cutting process is a tensile elastic deformation.

The temperature of the cutting surface will be increased during the SiC_w/Al composite cutting process because of the formation of cutting heat. When the cutting process is finished, the temperature of the cutting surface will decrease, leading to shrinkage deformation of the SiC_w/Al composite. Because the coefficient of thermal expansion of the matrix aluminum alloy is much higher than that of the SiC whisker, the shrinkage of the matrix aluminum alloy will be limited, leading to the formation of tensile residual stress in the matrix aluminum alloy of the SiC_w/Al composite.

(2) Cutting properties of the SiC_w/Al composite

- 1) Effects of cutting parameters on surface roughness of the SiC_w/Al composite
The effects of cutting speed (V), feed rate (V_f), and cutting depth (a_p) on the surface roughness of the SiC_w/Al composite are shown in Fig. 3.59. Figure 3.59a shows that the surface roughness of the composite decreases with increasing cutting speed, and the decrement becomes smaller with increasing cutting speed, which is similar to the behavior of common metals. The effect of cutting speed on the surface roughness of the SiC_w/Al composite can be explained by the formation of scales and the tear fracture of the cutting surface. SEM observation results of the cutting surface show that the scale formation phenomenon reduces with increasing cutting speed, as shown in Fig. 3.60. The reason for this is that the cold sweat phenomenon is reduced

Fig. 3.59 Effects of cutting parameters on the surface roughness of the SiC_w/Al composite



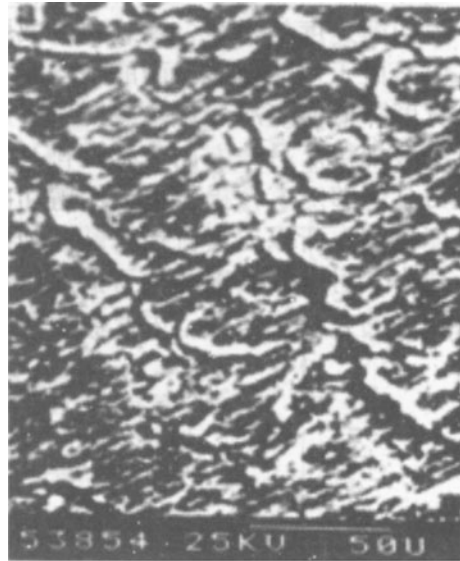
because of the reductions in the friction coefficient and the connecting width between the chip and the rake face. This phenomenon corresponds to the common cutting rules of ductile metals. With increased cutting speed, the cutting power and the input energy also increase, and thus, the possibility that the whiskers are cut directly increases. In this case, the tear fracture phenomenon is reduced and the frequency and size of cracks formed at the cutting surface are also reduced, resulting in a decrease in the surface roughness of the SiC_w/Al composite.

Fig. 3.60 Surface morphologies of the SiC_w/Al composite for different cutting speeds

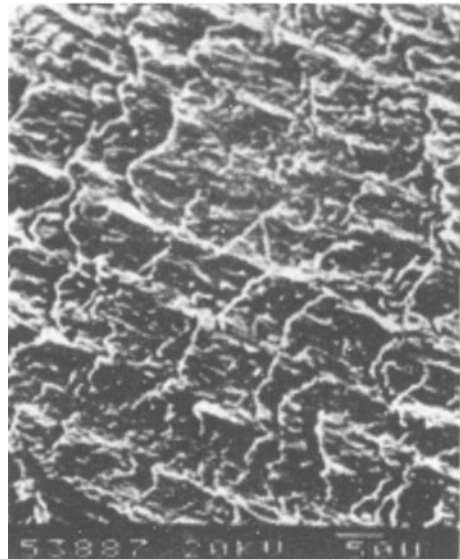


Figure 3.59b indicates that the surface roughness of the SiC_w/Al composite increases with increasing feed rate. An increase in the feed rate results in an increase in the amount and the height of the scales on the cutting surface of the composite, as shown in Fig. 3.61, and therefore, the surface roughness increases. Tear fractures take place on the surface during the cutting of the SiC_w/Al composite. When the feed rate is lower, some pits caused by the tear fractures are covered by the squeezing and rolling of the cutting tool to the cutting surface, resulting in a reduction in the surface roughness of the SiC_w/Al composite.

Fig. 3.61 Surface morphologies of the SiC_w/Al composite for different feed rates



(a) $v_f = 20 \text{ mm/min}$



(b) $v_f = 10 \text{ mm/min}$

Figure 3.59c shows that the cutting depth has no obvious effect on the cutting surface roughness of the SiC_w/Al composite. The surface roughness decreases slightly with increasing cutting depth. The reason for this is that the pits caused by the tear fractures on the cutting surface are covered by the rolling of the cutting tool to the cutting surface, which can slightly improve the surface quality of the SiC_w/Al composite.

- 2) Effects of whisker orientation on the surface roughness of the SiC_w/Al composite The specific characteristics of the SiC_w/Al composite cutting process are caused by the addition of the hard SiC whiskers to the matrix aluminum alloy, so the angle between the whisker axis and the cutting direction will have a major effect on the surface roughness of the composite. To study this effect, a SiC_w/Al composite in which the SiC whiskers are orientated in one direction has been made by hot extrusion. A cylindrical sample with its axis direction perpendicular to the whisker orientation direction is cut from the hot-extruded SiC_w/Al composite, and the whisker orientation in the composite can be seen on the cross section of the cutting sample, as shown in Fig. 3.62. By cutting the side surface of the cylindrical sample, various angles, from 0° to 100° , between the whisker axis and the cutting direction (which is referred to simply as the “whisker angle”) can be obtained at different cutting surface positions. In Fig. 3.62, the whisker angles are 0° , 45° , 90° , 135° , and 180° at positions A, B, C, D, and E, respectively.

The above experiments are carried out in a CM6125 lathe using a polycrystalline diamond turning tool, and the cutting results for two sets of cutting parameters are shown in Fig. 3.63. The results indicate that the lowest surface roughness is obtained when the whisker angle is 45° , and the highest is obtained when the whisker angle is 135° .

During the SiC_w/Al composite cutting process, when the cutting tool meets the SiC whiskers, there are three possible results of the interaction between the cutting tool and the whiskers: (1) The whiskers are pulled out from the matrix; (2) the whiskers are rotated in the matrix; and (3) the whiskers are cut directly by the tool. Pullout and rotation of the whiskers will result in major plastic deformation and

Fig. 3.62 Schematic of the whisker orientations and cutting directions

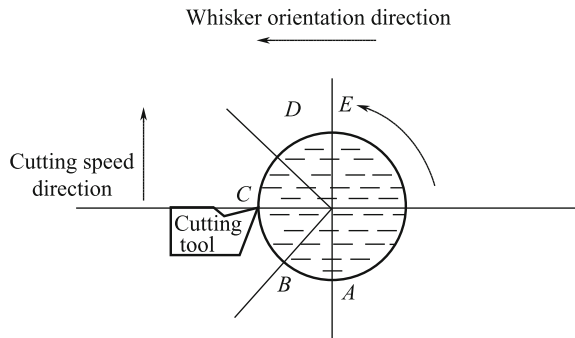
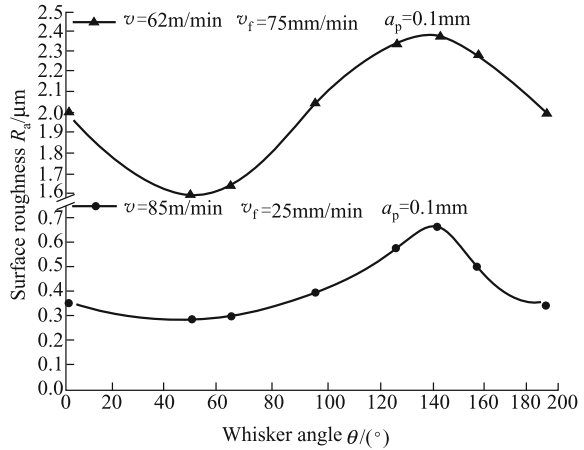


Fig. 3.63 Experimental results for the surface roughness dependence on the whisker angle for two sets of cutting parameters



even in the formation of cracks and voids in the internal material of the composite cutting surface, leading to an increase in the composite surface roughness. If the whiskers are cut directly by the cutting tool, then the fracture is limited within the cutting surface, and thus, a smooth cutting surface can be obtained.

At lower cutting speeds, it is almost impossible for the whisker to be cut directly by the cutting tool, and most of the whiskers will be pulled out or rotated during the cutting process. When the whisker angle is 0° , whisker pull-out is easy and whisker rotation is difficult. Because the whisker axis is parallel to the cutting direction, the pit left by whisker pull-out is shallow, so it does not greatly affect the surface roughness of the SiC_w/Al composite. With increasing whisker angle from 0° to 45° , whisker pull-out becomes increasingly difficult, so the surface roughness decreases. With increasing whisker angle from 45° to 135° , the surface roughness begins to increase. In this case, whisker pull-out is almost impossible, and whisker rotation becomes the main factor affecting the surface roughness of the SiC/Al composite cutting surface. With increasing whisker angle from 45° to 135° , the degree of whisker rotation also increases, so that the tear fractures of the cutting surface increase and the surface roughness also increases. When the whisker angle is 135° , the tear fractures caused by the whisker rotation are at their most serious, so the surface roughness reaches its maximum value. With further increases in the whisker angle, the degree of whisker rotation decreases and the surface roughness again begins to decrease. When the cutting speed is higher, the surface roughness of the SiC_w/Al composite is lower because the whiskers can be cut directly by the cutting tool, as shown by the lower line in Fig. 3.63. However, the effect of the whisker angle on the surface roughness of the composite is similar to that at lower cutting speeds.

Figure 3.64 shows SEM images of the morphologies of the cutting surfaces of the SiC_w/Al composite for different whisker angles. When the whisker angle is 0° , there are numerous strip-shaped pits parallel to the cutting speed direction, and the depths of these strip-shaped pits are low, indicating that the pits are formed by the

pull-out of whiskers, as shown in Fig. 3.64a. When the whisker angle is 45° , the numbers and sizes of the pits decrease, corresponding to lower surface roughness, as shown in Fig. 3.64b. When the whisker angle is 90° , whisker pull-out becomes very difficult, and the pits on the cutting surface are formed by tear fractures of the cutting surface caused by whisker rotation, as shown in Fig. 3.64c. When the whisker angle is 135° , numerous deep pits are formed on the cutting surface, indicating that a serious tear fracture has taken place, which results in high-surface roughness for the SiC_w/Al composite, as shown in Fig. 3.64d.

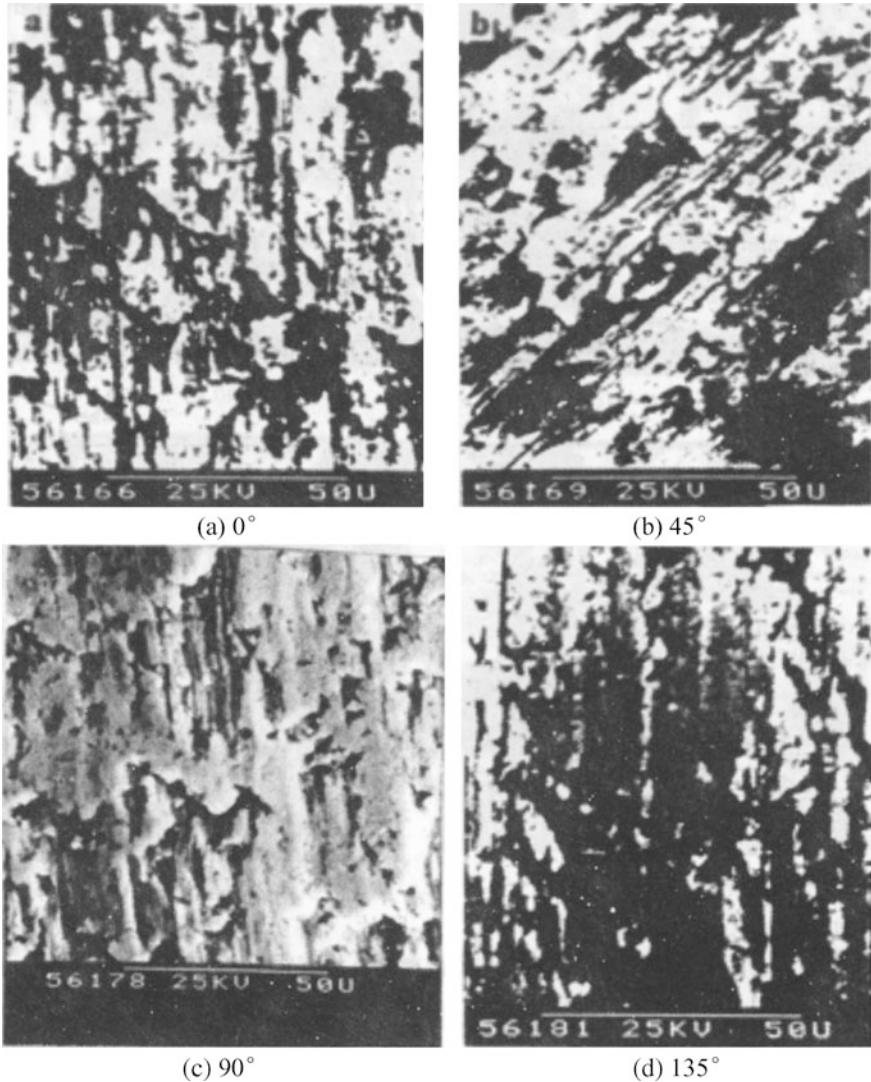


Fig. 3.64 SEM images of the morphologies of the cutting surfaces of the SiC_w/Al composite at different whisker angles ($v = 85$ m/min, $v_f = 25$ mm/min, $a_p = 0.1$ mm)

- 3) Effects of cutting parameters on the surface residual stress of the SiC_w/Al composite It is known from the above analysis that the residual stress formation mechanism in the cutting surface of the SiC_w/Al composite is complicated, and many factors can influence the residual stress. There is no suitable method for measurement of the residual stress in the cutting surface of the SiC_w/Al composite, so it is difficult to study the effects of the cutting parameters on the residual stress in the cutting surface of the composite. However, the surface residual stress is a negligible factor in the precision cutting of materials, so the residual stress in the cutting surface of the SiC_w/Al composite was measured for different cutting parameters using an X-ray stress analyzer. The measurement results were then analyzed and discussed.

The effects of the cutting speed, feed rate, and cutting depth on the surface residual stress of the SiC_w/Al composite are shown in Fig. 3.65. Figure 3.65a shows that the residual stress in the normal direction (perpendicular to the cutting speed direction) decreases with increasing cutting speed, for three reasons: First, the friction coefficient between the tool back slide and the sample surface decreases with increasing cutting speed, so the surface residual compressive stress that is formed by the recovery of elastic deformation decreases. Second, with increasing cutting speeds, increasing numbers of whiskers are cut directly by the tool, leading to a reduction of the plastic deformation in the cutting surface, and thus, the surface residual compressive stress formed by the recovery of elastic deformation again decreases. Finally, with increasing cutting speed, the temperature of the cutting surface also increases, which makes the surface residual tensile stress caused by the residual thermal stress of the cutting surface increase, so the residual compressive stress in the cutting surface of the SiC_w/Al composite then decreases.

Figure 3.65b shows that with increasing feed rate, the surface residual stress in the normal direction decreases, but the surface residual stress in the tangential direction increases. With increasing feed rate, the squeezing and rolling effects of the cutting tool on the material decrease, so that the plastic deformation in the cutting surface decreases, and the tear fractures of the cutting surface become serious. Meanwhile, the elastic deformation in the internal material of the composite increases, and thus, the surface residual stress in the tangential direction also increases.

Figure 3.65c shows that with increasing cutting depth, the surface residual stress decreases. The squeezing effect of the cutting tool on the material decreases with increasing cutting depth, so the surface residual compressive stress formed by the recovery of the elastic deformation decreases. In addition, with increasing cutting depth, the temperature of the cutting surface increases, which makes the surface residual tensile stress caused by the thermal residual stress of the cutting surface increase; this leads to reduced surface residual compressive stress in the SiC_w/Al composite.

It is found that the residual stress in the cutting surface of the SiC/Al composite is a type of compressive stress. With increasing cutting speed and cutting depth, the residual compressive stress in the cutting surface decreases, while, with increasing

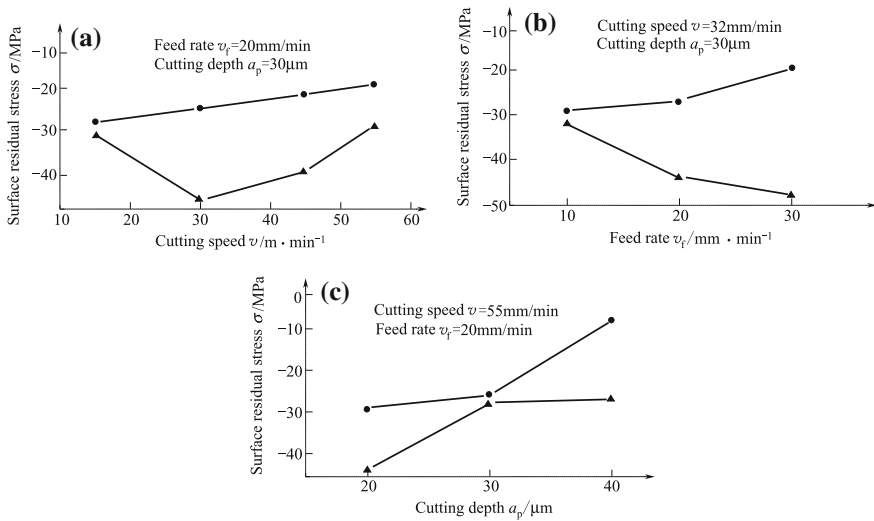


Fig. 3.65 Effects of cutting parameters on the surface residual stress of the SiC_w/Al composite.—●— Residual stress in normal direction; —▲— Residual stress in tangential direction

feed rate, the residual compressive stress in the normal direction decreases, but that in the tangential direction increases.

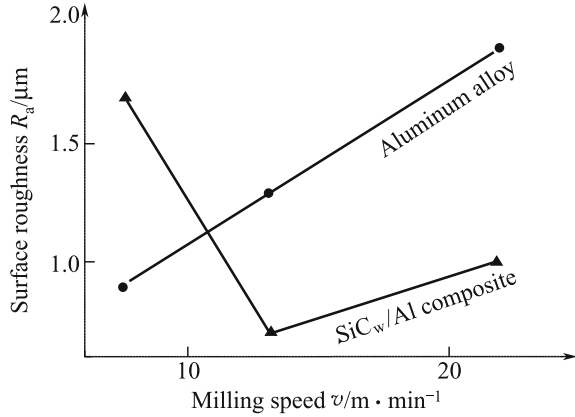
3.4.5.2 Milling Process of the SiC_w/Al Composite

(1) Surface roughness of the SiC_w/Al composite milling surface

Milling of the SiC_w/Al composite is carried out in a modified ZA4012 drilling machine using a cylinder end mill with a diameter of 5 mm. The feed rate is 2.2 cm/mm, and the turning speeds of the mill are 450 r/min, 800 r/min, and 1400 r/min, which correspond to milling speeds of 7.1 m/min, 12.6 m/min, and 22.0 m/min, respectively. Both the SiC_w/Al composite and the unreinforced aluminum alloy are machined by milling, and the surface roughnesses of the milled samples are measured using Taylor Hobson-6 equipment.

Figure 3.66 shows the surface roughness of the SiC_w/Al composite and that of the unreinforced aluminum alloy under different milling speeds. It is found that the surface roughness difference between the SiC_w/Al composite and the unreinforced aluminum alloy is not significant for the chosen milling parameters. The SiC_w/Al composite has its minimum surface roughness when the milling speed is 12.6 m/min. When the milling speed is lower or higher than this speed, the surface roughness will increase. In particular, when the milling speed is lower, the surface roughness is very high. The surface roughness of the unreinforced aluminum alloy increases with increasing milling speed.

Fig. 3.66 Surface roughnesses of SiC_w/Al composite and unreinforced aluminum alloy at different milling speeds



When milling an aluminum alloy, more heat is produced during the milling process with increasing milling speed, so that the sticking cutter problem is serious, leading to a reduction in the surface roughness of the aluminum alloy. The SiC_w/Al composite has the same milling characteristics as the aluminum alloy. However, with increasing milling speed, increasing numbers of SiC whiskers are cut directly by the milling cutter, leading to reduced surface roughness for the SiC_w/Al composite. Therefore, there is an optimum milling speed to obtain the minimum surface roughness for the SiC_w/Al composite, as shown in Fig. 3.66.

(2) Morphology of the milling surface of the SiC_w/Al composite

A typical milling surface morphology for the SiC_w/Al composite is shown in Fig. 3.67. Figure 3.67a is a SEM image with lower magnification, which shows that there are many scratches on the milling surface in the milling direction, and there are micro-cracks in the perpendicular direction that are similar to the scales on the turning surface of the SiC_w/Al composite. Figure 3.67b is a SEM image with higher magnification, which shows that there are exposed SiC whiskers on the milling surface of the SiC_w/Al composite, which is a different surface characteristic when compared with that produced by turning of the composite. It is also found that all exposed SiC whiskers are parallel to the milling direction, which may be caused by whisker rotation during surface plastic deformation of the SiC_w/Al composite in the milling process.

Figure 3.68 shows SEM images of the milling surfaces of the SiC_w/Al composite and the unreinforced aluminum alloy at different milling speeds. Figure 3.68a, c is the image of the milling surface of the SiC_w/Al composite. When the milling speed is lower (Fig. 3.68a), exposed SiC whiskers can be seen parallel to the milling direction on the milling surface of the composite. This indicates that the SiC whiskers in the milling surface layer are not cut by the milling cutter, but rotate to the milling direction. This will result in the existence of exposed SiC whiskers on the milled surface and increased surface roughness for the SiC_w/Al composite. With increasing milling speed, the number of exposed SiC whiskers

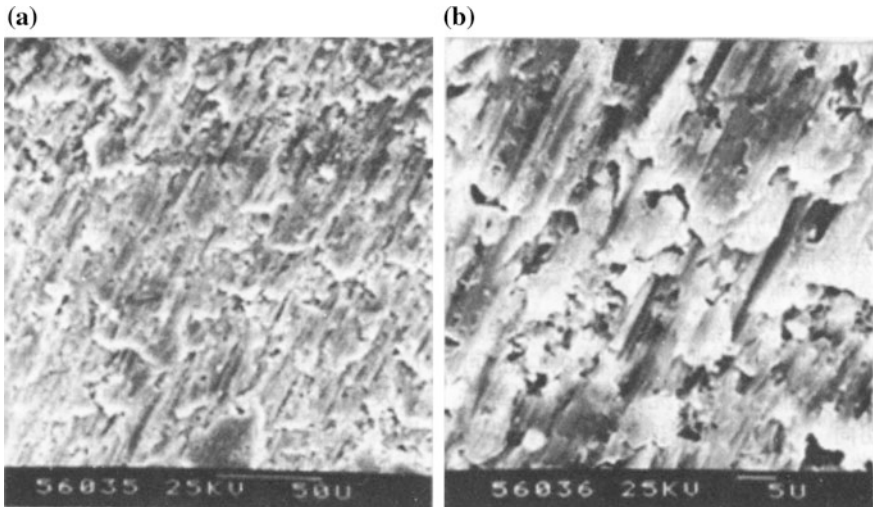


Fig. 3.67 Morphology of the milling surface of the SiC_w/Al composite

decreases, and the whisker cross section caused by the cutting of the milling cutter is found on the milled surface of the SiC_w/Al composite, as shown in Fig. 3.68c. Figure 3.68b, d are the images of the milled surface of the unreinforced aluminum alloy. The images show that with increasing milling speed, scratching, cracking, and tear fractures increase in number and size on the milling surface, leading to an increase in the surface roughness of the aluminum alloy. This phenomenon is also caused by serious cutter sticking as a result of the increasing temperature of the milling surface caused by increasing milling speeds.

(3) Milling force and wear of milling cutter during milling of the SiC_w/Al composite

During the milling experiments, the milling force on the SiC_w/Al composite and the unreinforced aluminum alloy was measured at different milling speeds. The results indicate that the milling force of the SiC_w/Al composite is five times that of the unreinforced aluminum alloy under the same milling conditions. The milling force of the SiC_w/Al composite increases obviously with increasing milling speed. Observation of milling cutter wear shows that when compared with the cutter used for the unreinforced aluminum alloy, the wear of the cutter used for milling of the SiC_w/Al composite is much more serious.

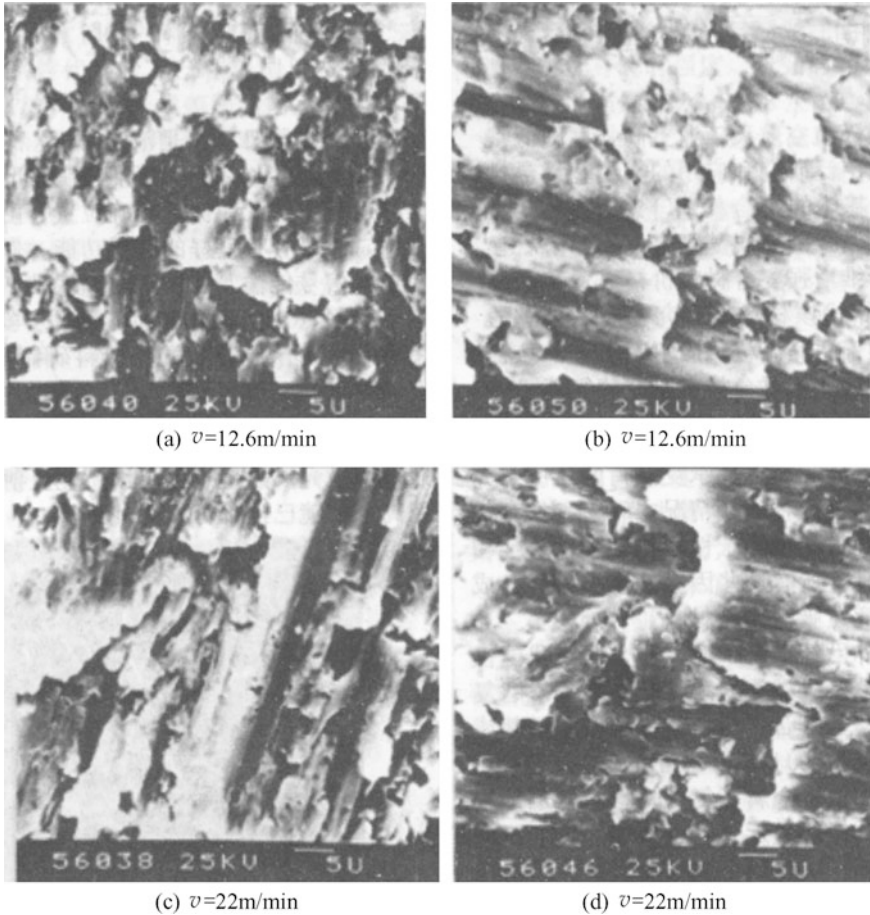


Fig. 3.68 SEM images of the milling surfaces of the SiC_w/Al composite and the unreinforced aluminum alloy at different milling speeds

3.5 Applications of Metal Matrix Composites

Metal matrix composites, especially those made using aluminum, magnesium, and other light metal matrixes, have been extensively researched and applied because the aerospace industry requires high-strength and low-density materials. In the 1960s, continuous carbon fiber- and boron fiber-reinforced metal matrix composites were rapidly developed. In the 1970s, research into continuously reinforced composite was restricted because of their high costs and complex manufacturing processes. When the high-temperature parts of turbine engines required high-temperature-resistant materials, investigations of metal matrix composites, and particularly of titanium matrix composites, were renewed.

In the 1980s, discontinuously reinforced composites were rapidly developed, and the research was mainly focused on aluminum matrix composites reinforced with silicon carbide and alumina particles, and with short fibers. These discontinuous reinforcements displayed strengthening performances between those of dispersed phases and those of continuous fibers. Discontinuously reinforced composites have demonstrated excellent lateral performance, low material consumption, and good machinability. Their performance levels offer significant improvement in comparison with those of the unreinforced alloys. These factors make such materials most commercially attractive for many application fields.

In countries overseas, the commercialization of metal matrix composites has already been achieved. In China, only small numbers of batch produced automotive and machinery parts have been fabricated from wear-resistant composites such as particle-reinforced aluminum and zinc matrix composites, and short fiber-reinforced aluminum and zinc–magnesium matrix composites. In addition, the annual output of these materials in China was only about 5000 tons, consequently exhibiting a large disparity with the production levels in foreign countries.

Similar to other advanced composites, metal matrix composites were originally developed in the aerospace and space technology fields. For nearly 40 years, the development of these materials has proved that metal matrix composites can be used not only in the aerospace and military fields but also in business fields such as transport facilities and electronic components. Typical examples of the engineering applications of metal matrix composites will be introduced in the following sections [6, 9, 12, 76–80].

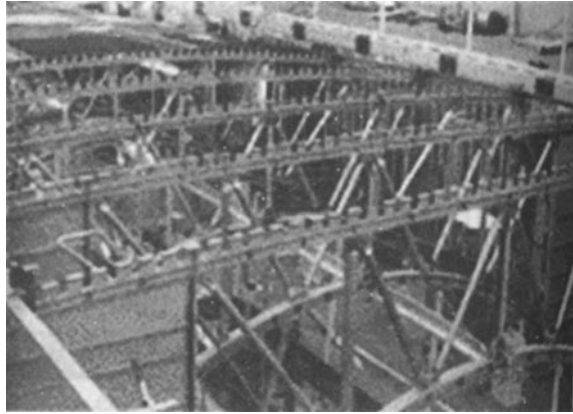
3.5.1 Applications of Metal Matrix Composites in Aerospace Fields

3.5.1.1 Applications of High-Performance Continuously Reinforced Metal Matrix Composites in Spacecraft

The most famous example of the successful application of metal matrix composites in spacecraft is that of boron fiber-reinforced aluminum composites (50% B_f/6061Al), which were used by NASA to fabricate the tube-shaped pillars of the fuselage framework in the midsection of the space shuttle orbiter (i.e., the cargo hold), as shown in Fig. 3.69. The entire fuselage framework consisted of a total of 300 B/Al composite tube-shaped supports with titanium rings and end joints. Compared with the original design plan (using aluminum alloys), the weight decreased by 145 kg, and the coefficient of weight reduction was 44%.

Another famous example application is that of 60% graphite fiber-reinforced 6061Al matrix composites, which have been successfully used to fabricate the high-gain antenna suspension (i.e., a waveguide) for the Hubble Space Telescope. This suspension, which is 3.6 m long (shown in Fig. 3.70), has sufficient axial

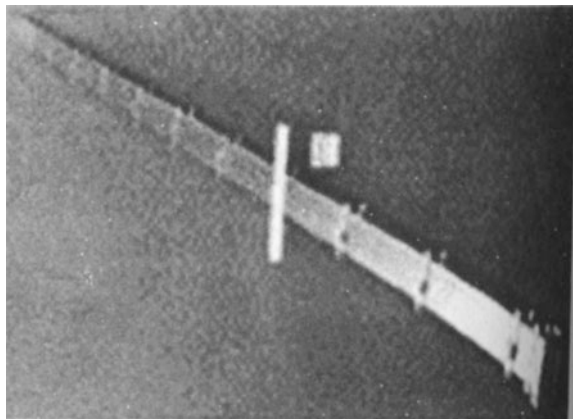
Fig. 3.69 B/Al fuselage framework in the space shuttle orbiter midsection



stiffness and an ultralow thermal expansion coefficient in the axial direction that keeps the antenna in the correct position in space during operation. In addition, the suspension has a good waveguide function because of the good electrical conductivity of the composites and can maintain signal transmission between the aircraft and the control system and can also resist both bending and vibration.

The ACMC Company, cooperating with the Optics Program of the University of Arizona (USA), used SiC particle-reinforced aluminum matrix composites to develop ultralightweight space telescope parts such as structural components and mirrors. This SiC/Al telescope has a primary mirror with a diameter of 0.3 m and weight of only 4.54 kg. Figure 3.71 shows the overall structure of the Hubble Space Telescope. The ACMC Company manufactured their SiC particle-reinforced aluminum matrix composites by powder metallurgy. In addition, these composites were used for mirrors, such as laser mirrors, satellite solar energy mirrors, and high-speed oscillating mirrors in space remote sensors, which have been partially put into practical service use.

Fig. 3.70 Gr/Al suspension of the Hubble Space Telescope



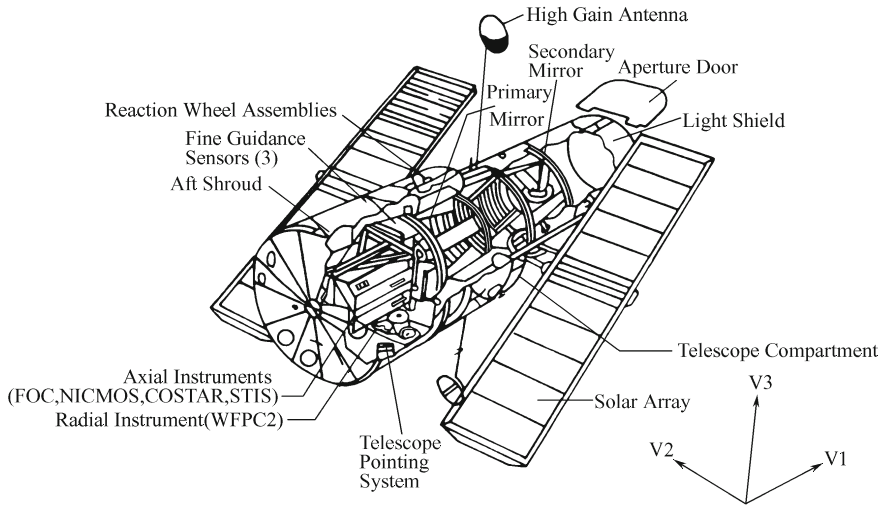


Fig. 3.71 Overall structure of the Hubble Space Telescope

3.5.1.2 Aluminum Matrix Composite Applications in Missiles

As third generation materials for aerospace inertial devices, instrument-grade high-volume SiC particle-reinforced aluminum matrix composites, replacing beryllium-based materials, have been applied by the USA in a type of ring laser gyro inertial guidance system, and they have become the subject of US Military Standards (MIL-M-46196). In addition, these materials have also been used successfully as inspection covers for both the inertial guidance ball and the inertial measurement unit (IMU) in the Trident missile, and their costs are two-thirds lower than those of the beryllium materials.

At present, missile manufacturers must compete in the international marketplace. To win their market share, they must satisfy the present and future requirements of the users, improve missile performance, and reduce both the initial life and life-cycle costs. Materials technology plays an important role in both improvement and development of missiles. For example, enhancing their strength and stiffness can reduce missile weight by using thinner missile walls. The missile weight reduction is beneficial for enhanced missile speed. An increase in the material stiffness not only enhances the stiffness of both the empennage and the wings, but also reduces warhead vibration and deflection, consequently improving missile guidance and precision. Therefore, it is necessary to develop and apply new materials to satisfy missile performance requirements including speed, guidance, and precision.

For many years, on the basis of the investment of the British Defense Ministry, the British Defense Evaluation and Research Agency and Matra BAE Dynamics have investigated aluminum matrix composite applications in missile parts, and

have achieved some successes. Al matrix composites are suitable for application to the missile body, empennage, wings, seeker components, optical components, propeller components, brake components, transmitting tubes, tripod, exhaust pipes, and other missile parts. Now, their first- and second-stage plans have been completed, a recent research plan is being implemented, and a future research plan has been established.

(1) The first-stage research plan

In the 1990s, the UK established a first-stage research plan for aluminum matrix composites. According to this plan, the UK researched and designed five Al matrix composite missile parts, including the anterior segment of the projectile body, the wings, the tail sleeve, the control empennage and axis and the control cylinders. The design and research content included the following aspects: The types of materials used to manufacture each part, the preparation methods used, the fabrication costs relative to those for traditional materials (the traditional manufacturing cost is 100%), and the degree of weight reduction. The results of the investigation are shown in Table 3.67.

According to the research plan, the UK also chose different types of metal matrix composites obtained from several companies and tried to manufacture them into various missile empennages by different preparation methods to verify the advantages of metal matrix composites and determine any possible difficulties in manufacturing of these composites into real missile empennages. The research results showed that particle-reinforced aluminum matrix composites made by powder metallurgy can be smoothly manufactured into the missile empennages. These empennages exhibit the increased stiffness, and it is also predicted that both weight and inertia can be reduced by 15%.

The UK also tried to use fiber-reinforced metal matrix composites to produce missile empennages, but failed due to the immature preparation technology that was

Table 3.67 Design and research results for the missile parts

Missile parts	Materials		
	Conventional materials	Advanced materials	
		Materials	Fabrication method
Anterior segment of projectile body	Steel	20% SiC _p /Al–Si–Mg	PM
Wing	Aluminum	20% SiC _p /Al–Cu–Mg	PM
Afterbody bushing	Aluminum	20% SiC _p /Al–Si	As cast
Combination of empennage and shaft	Aluminum/steel	SiC _f /Al	–
Control cylinder	Aluminum	C _f /Al	–

available at that time. These composites and their processing methods have been greatly improved since then, but their prices remain high.

(2) The second-stage research plan

In 1994, the UK established the second-stage research plan for aluminum matrix composites. This aim of this plan was to explore the feasibility of manufacturing the anterior segment of the projectile body of future high-speed short-range and medium-range air-to-air missiles from aluminum matrix composites. The main contents of the plan were to investigate the non-instantaneous high-temperature properties of particulate-reinforced aluminum matrix composites. It was expected that these materials would retain their instantaneous strengths in the temperature range between 350 and 400 °C. The materials investigated included 2124, 2618, Al-Fe-V-Si, and other aluminum matrix composites reinforced with silicon carbide particles with different weight percentages. The research conclusions were that for silicon carbide particle-reinforced 2000 series aluminum matrix composites, their strength values were higher below 200 °C, mainly because of the dominant influence of the aluminum matrix, but rapidly decreased above 200 °C, mainly because of silicon carbide particle precipitation. Therefore, apart from the anterior segment of the projectile body of the missiles, these materials are suitable for missile part applications. Al-Fe-V-Si is a specifically developed aluminum alloy for use at high temperatures, and this alloy, when reinforced with silicon carbide, has good prospects. All the investigated materials were evaluated for the missiles under simulated short-range and medium-range free flight conditions. The results showed that at 350 °C, both the tensile strength and the yield strength of silicon carbide particle-reinforced 2124 and 2618 aluminum matrix composites were lower than that of the 2618 reference aluminum cast alloy treated by the T6 process. For the 2618 reference aluminum alloy treated by T6, the ultimate tensile strength was about 180 MPa, and the yield strength was about 160 MPa. Among the investigated materials, 17% silicon carbide-reinforced Al-Fe-V-Si composites showed the highest performances, where their ultimate tensile strength was about 250 MPa, and their yield strength was about 210 MPa.

(3) Recent and future research plan

In recent research plans, the studies were mainly focused on SiC_p/Al-Fe-V-Si composites treated by the T1 process, while also contrasting these materials with 2618 aluminum alloy treated by T1, and silicon carbide particle-reinforced 2000 series aluminum composites. For 17% SiC_p/Al-Fe-V-Si composites treated by T1, the specific strength was lower than that of steel and titanium at 20 °C, but the strength was close to that of steel and below that of titanium at 350 °C. At 20 and 350 °C, the composite's specific stiffness was much higher than that of steel and titanium, and this stiffness was the highest value among the studied materials. Therefore, 17% SiC_p/Al-Fe-V-Si composite treated by T1 had the best all-round properties at 20 and 350 °C among the studied materials.

The research conclusion was that 17% SiC_p/Al–Fe–V–Si composite treated by the T1 process can be used to manufacture the anterior segment of the projectile body of missiles with thinner walls than that of the conventional Al–Cu–Mg alloy. Therefore, the missile weight decreased by 20%–35% and consequently helped to improve the missile performance by increasing its speed and improving guidance and precision. This thin-walled anterior segment of the projectile body can increase the payload capacity of the missiles.

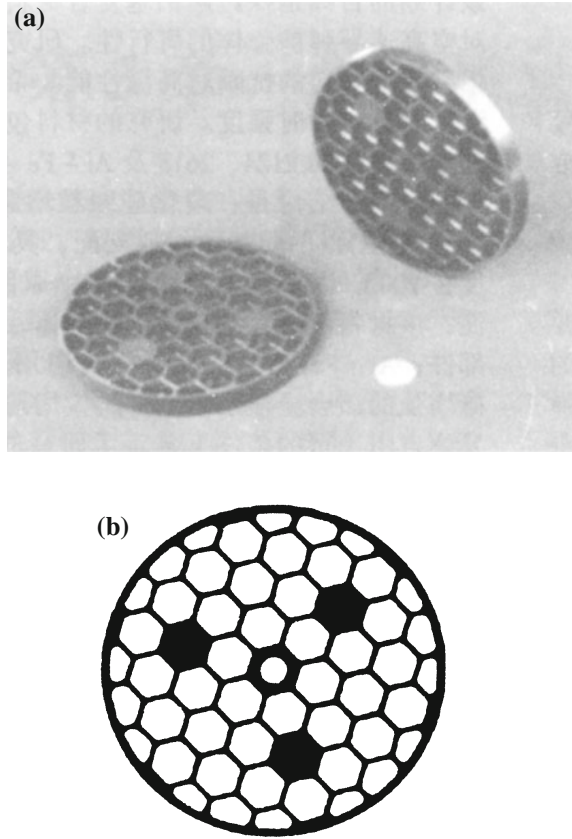
The deficiencies of SiC_p/Al–Fe–V–Si composites treated by T1 were as follows: (1) They need to improve their toughness and ductility; (2) their manufacturing process is more difficult because of the occurrence of higher strength during manufacturing; (3) they have a narrow processing range. In future studies, the researchers intend to use the funds obtained to manufacture silicon carbide particle-reinforced Al–Fe–V–Si composites into a small number of anterior segment projectile body samples to conduct machining tests and structural tests.

3.5.1.3 Applications of Aluminum Matrix Composites in Other Space Flight Fields

Recently, a material company in Florida, USA, has successfully developed a new class of discontinuously reinforced aluminum matrix composites with high strength and high heat resistance. As the matrix of these composites, the Al–Mg–Sc–Gd–Zr alloy has excellent strengthening ability at both low temperature and room temperature, at which its strength is 630 MPa. Its ductility (7%) at room temperature is at a moderate level and its high-temperature strength is also very good. The discontinuously reinforced aluminum matrix composites were manufactured through powder metallurgy from aluminum spherical powders with 325 orders (less than 45 μm) and hybrid silicon carbide and boron carbide powders with an average size of 5 μm and a volume fraction of 15%. The fabricated composite strength was more than 700 MPa. These composites, with their excellent stiffness, specific strength, abrasion resistance, and heat resistance, can be applied not only to aerospace vehicle materials, but also to rocket manufacturing.

In China, metal matrix composites were first formally applied to spacecraft around 2000. The Harbin Institute of Technology developed a SiC_w/Al pipe and applied it in a satellite antenna screw. The Beijing Aviation Materials Research Institute developed three SiC_p/Al castings (support round, mirror body, and box) and applied them in the calibration device of the satellite remote sensor and also successfully trial-produced the shrunken parts of a space optical reflector blank (Fig. 3.72).

Fig. 3.72 High-volume SiC/Al composite parts made by pressureless infiltration near-net-shape (a) and industrial CT images of the parts (b)

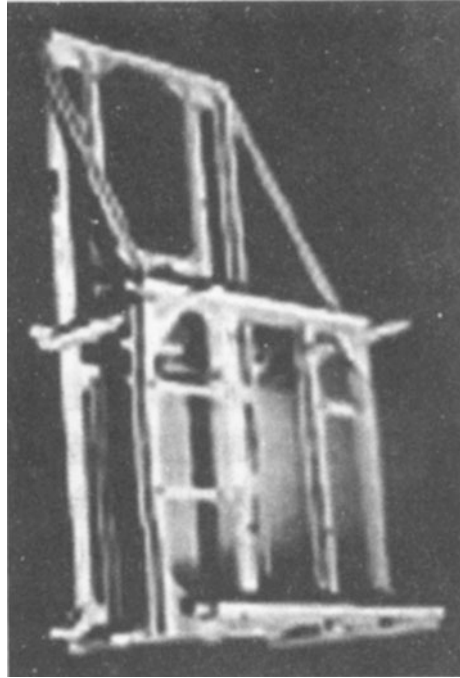


3.5.2 Applications of Metal Matrix Composites in the Aviation Field

The aviation industry, with its very high demand for both safety coefficients and use life, is always among the most challenging fields for metal matrix composite applications, and particularly for applications in commercial airplanes. Therefore, the aviation applications of metal matrix composites lag far behind the space flight industry applications. The earliest example of the aviation applications of composites was in the 1980s, when the Lockheed Martin Company used 25% SiC_p/6061Al composites (produced by the DWA Composite Company) to manufacture brackets for airplane electronic equipment. An equipment bracket with the very large size of about 2 m is shown in Fig. 3.73, and its stiffness was increased by about 65% relative to the 7075 aluminum alloy that it replaced; this alloy can be very greatly deformed under the loading caused by airplane reversing and rotation.

However, in recent years, particle-reinforced aluminum matrix composites as representative metal matrix composites have formally been used for manufacturing

Fig. 3.73 Aluminum matrix composite support frame for airplane electronic equipment



of the main support structure parts of advanced aircraft. A few of the most representative and symbolic engineering applications and the effects they induced will be introduced in the following.

On the basis of the “Title III” item support of the US Department of Defense, the DWA Composite Company, which cooperated with the Lockheed Martin Corporation and the US Air Force, used PM silicon carbide particle-reinforced aluminum (6092 Al) composites to produce the F-16 fighter ventral fin, as shown in

Fig. 3.74 Aluminum matrix composite ventral fin of F-16 fighter

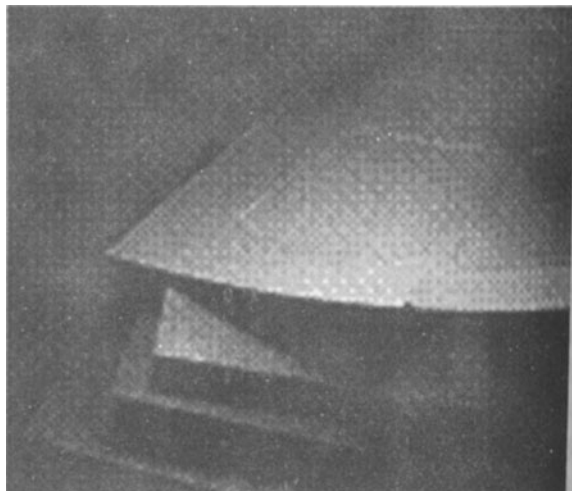
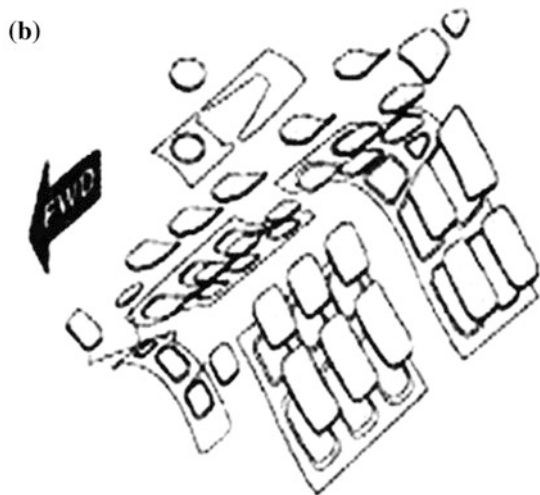


Fig. 3.74. Compared with the original 2214 aluminum alloy skin, its stiffness increased by 50%, and its service life increased from hundreds of hours to 8000 h, which was an increase of 17 times. At present, the US Air Force is using this aluminum matrix composite ventral fin as spare parts for active service F-16 fighters and is gradually replacing all of the older fins. The evaluation results of the Ogden Air Logistics Center showed that the application of aluminum matrix composites to ventral fins can significantly reduce the number of maintenance checks, save maintenance costs of 26 million US dollars, and improve airplane mobility. In addition, 26 fuel inspection covers in F-16 fighter upper bodies (Fig. 3.75) had lifetimes of only 2000 h and were checked two or three times annually. Use of

Fig. 3.75 a F-16 fighter and b its fuel inspection covers



composites meant that their stiffness increased by 40%, their carrying capacity increased by 28%, their prospective average overhaul life was more than 8000 h, and their crack examination period was extended for 2–3 years. Recently, there has also been a plan to use particle-reinforced aluminum matrix composites for fabrication of F-16 missile launcher tracks.

In F-18 “Hornet” fighters, the applications of silicon carbide particle-reinforced aluminum matrix composites in hydraulic brake cylinders not only reduced the weight and coefficient of thermal expansion of the cylinders, but also doubled the fatigue limit compared with the substituted aluminum and bronze materials. In Europe, the breakthrough evolution was initially achieved in the applications to helicopters. The British Aerospace Metal Matrix Composites Company (AMC) used high-energy ball milling powder metallurgy to prepare silicon carbide particle-reinforced aluminum (2009Al) composites with high stiffness and fatigue resistance. They manufactured these composites into the forgings of the helicopter rotor system connector pieces (hub plywood and oversleeve), which have been successfully used in the Eurocopter Company’s (EU straight) new N4 and EC-120 helicopters (Fig. 3.76). When compared with aluminum alloys, the stiffness of these parts increased by about 30%, and the useful service life increased by about 5%. When compared with titanium alloys, the weight decreased by about 25%.

It was noticeable that in the late 1990s, silicon carbide particle-reinforced aluminum composites had formal applications in large-scale passenger airplanes. From the early stages of PW4084 engines, Pratt & Whitney used the aluminum silicon carbide particle-reinforced wrought aluminum composites produced by the DWA Company to manufacture the guide vane of a fan outlet (Fig. 3.77), with applications in all PW4000 engines of the Boeing 777. Pratt & Whitney’s research and development work showed that when used as the diversion blade of fan export or compressor blades, the impact resistance capacity of aluminum matrix composites (e.g., to hail or bird impact) is better than that of resin-based composites (e.g.,

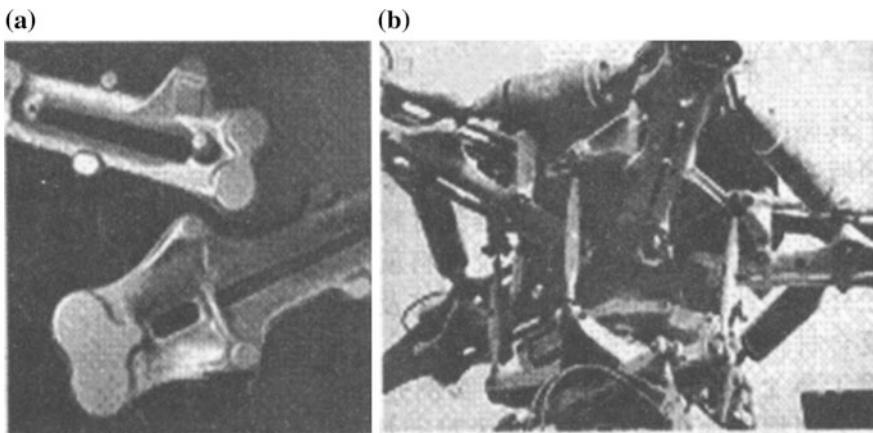


Fig. 3.76 **a** Helicopter rotor system and **b** its connecting pieces

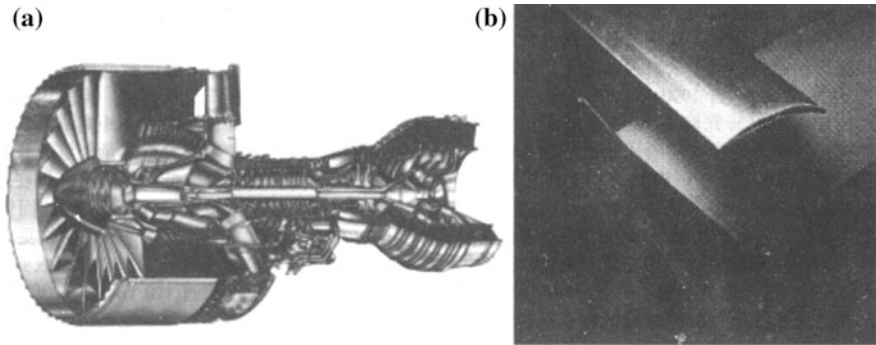


Fig. 3.77 a Pratt & Whitney's PW4000 aviation engine and b guide vane of the fan outlet

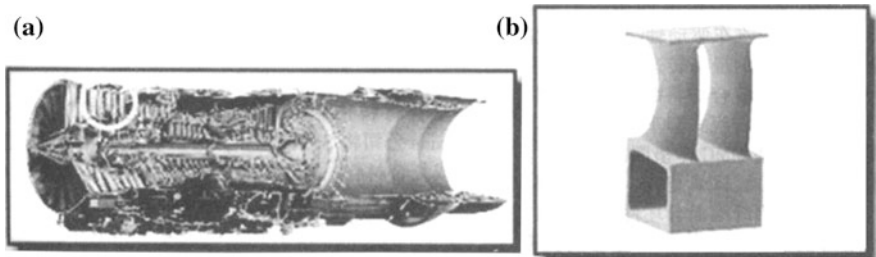


Fig. 3.78 a Aeroengine and b its static blade

graphite fiber/epoxy), and any damage is easy to find. In addition, their anti-erosion capacity (e.g., for sand, rain) is seven times that of the resin-based composites, and their costs are lower by one-third. Pratt & Whitney intended to use silicon carbide particle-reinforced aluminum matrix composites as standard materials in the PW4000 engine. America is developing particle-reinforced heat-resistant aluminum matrix composites. When these composites reach production, they will first be used in a single-stage compressor and as parts for a two-stage compressor, such as the static blades of the compressor (Fig. 3.78).

In 2003, America's Special Material Company produced silicon carbide fibers through chemical vapor deposition on carbon fibers and combined the silicon carbide fibers with titanium to fabricate titanium-based composites by plasma spraying. These metal matrix composites were used for the first time to produce landing chassis components, which were applied in the F-16 fighters of the Netherlands Royal Air Force. The replacement of the traditional high-strength steels with metal matrix composites can reduce their weight by 40% and gives them corrosion resistance that is better than that of aluminum or steel.

In the past decade, America, Canada, Sweden, and other countries have clandestinely investigated numerous metal matrix composites, particularly light-composite-armor materials that include aluminum and titanium matrix

composites. At present, the metal matrix composite armor is being used as protective armor for the US Air Force C-130 transport, but applications to ground vehicles and personnel protection may be at the primary development stage. Metal matrix composites, as a new class of these materials, are formed through combining the advantages of metal (good toughness, ductility, formability, and high strength) with the advantages of ceramics (high hardness, ablation resistance, and light-weight). These materials not only overcome the brittleness of ceramics and a lack of anti-projectile multi-hitting ability, but also make up for the metal's hardness and heaviness shortcomings. In addition, they have excellent bulletproof properties. Depending on their requirement, people can fabricate metal matrix composites with almost infinitely varied components of metals and ceramics. In most metal matrix composites, the ceramics are usually selected as the reinforcements, and their volume fraction is usually less than 30%. In some composites, the ceramic volume fraction can reach 80%. For example, the bulletproof armor of the US Air Force C-130 aircraft was manufactured from aluminum/boron carbide composites, in which the volume fraction of aluminum was about 25–30%, and the boron carbide content was about 70–75%. The armor density of only 2.6 g/cm² can reduce the weight of each C-130 aircraft by about 1365 kg. To date, the armor's bulletproof performance has been higher than that of the Al/SiC and Al/Al₂O₃ composite armor.

3.5.3 Metal Matrix Composite Applications in Transport Facilities

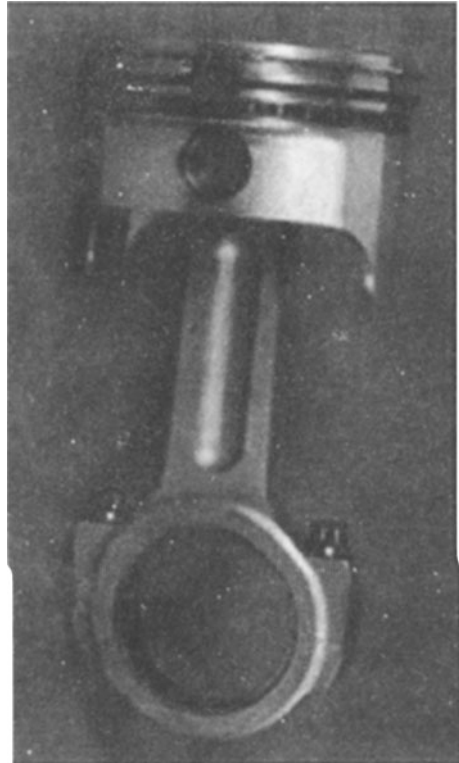
Transport facilities are always one of the most important civilian fields for metal matrix composites. However, this field, and especially the automobile industry, is extremely cost-sensitive, so the competition is very intense. Therefore, continuous fiber-reinforced metal matrix composites and discontinuous (such as whisker) reinforced metal matrix composites with their higher costs are excluded from the applications in this field. So, cheap particle- and short fiber-reinforced aluminum and magnesium matrix composites have the chance to be widely applied.

The earliest example of the successful application of composites in a transport facility is in Japan, where, since 1983, the Toyota Motor Corporation has substituted 5% alumina short fiber-reinforced aluminum composites for nickel cast iron and manufactured the materials into diesel engine pistons. Consequently, the piston weight decreased by 10%, the thermal conductivity increased by four times, and the thermal fatigue life was also significantly prolonged. Aluminum matrix composites were partially used to produce the pistons, and the annual output was more than one million pieces. Since 1990, the Suzuki Corporation of Japan has manufactured the piston tops of its marine engines from 20% SiC_w/A390 composites and has conducted industrial production. In 1999, the Russian Centre for Materials Research Institute presented AlB reinforced aluminum alloy plate structures. Compared with

aluminum alloy standard spacings, the compression bearing capacity of the structures trebled and the fatigue limit increased by 3–12 times. Under full-size intervals for the prototype moment of a ship obeying a dynamic maintenance principle, the carrying capacity of static cantilever bending is 1.2 times as that of an aluminum alloy standard spacing. This is an important technology for solution of the advanced ship strength problem with the dynamic maintenance principle. Since the mid-1980s, the Luoyang Ship Material Research Institute has developed aluminum/steel composite plates, and they had their first successful application in the aluminum superstructure and the steel ship deck transition connecting the Qiongzhou Straits “Gull 3” passenger catamaran in 1992. They have since successively and successfully been applied in the missile corvettes and civilian ships.

In addition, since the 1990s, automobile drive shafts, connecting rods, engine cylinders, and high-speed train and car brake pads, all of which were manufactured from silicon carbide or alumina particle-reinforced aluminum matrix composites, have emerged one by one. For example, the drive shaft was manufactured from 20% aluminum oxide particle-reinforced 6061Al composites, and its top speed was significantly increased because it had much greater stiffness than steels and aluminum alloys. In addition, the engine pistons manufactured from silicon carbide particle-reinforced aluminum matrix composite forgings were successfully applied in Ferrari Formula One racing cars (Fig. 3.79). The Honda Company manufactured and tested aluminum cylinders with aluminum matrix composite washers. The 16 valves and 2-L cylinders of the “Prelude” engine were cast from an Al–Si hyper-eutectic alloy, where alumina and carbon fibers were introduced into the blank pieces. The test results showed that the performance of this composite engine was significantly improved relative to engines using cast iron cylinder washers. The Textron and Dow Chemical Companies in America manufactured SiC_p/Mg composites that went into the strengthened internal cylinders. Dow also made the $\text{Al}_2\text{O}_{3p}/\text{Mg}$ and SiC_p/Mg composites that went into the pulleys, oil pump cover, and other wear-resistant parts. In particular, the pump was prepared entirely from $\text{Al}_2\text{O}_{3p}/\text{Mg}$ composites. Since 1992, Britain’s Magnesium Elektron Company has focused on Melram magnesium-based composites and has developed and designed a series of discontinuously reinforced magnesium matrix composites according to the special requirements for low-cost, recovery, and different applications. This company developed pipes made from $\text{SiC}_p/\text{Mg–Zn–Cu–Mn}$ (Melram 072) composites, which is known as one of the lightest metal matrix composites in the world. In addition, this company is developing their materials for applications in the defense and car industries. Germany’s Clausthal University of Technology manufactured Al_2O_{3p} and SiC_p/Mg composites into automotive parts, such as bearings, pistons, and cylinders. Canada’s Magnesium Institute of Technology successfully developed SiC_p/Mg composites using stirring casting and squeeze casting, and manufactured car parts using these composites for low density, wear resistance, and high stiffness, including the disk impeller used in cars, piston grooves, gears, gearbox bearings, differential bearings, shifting yokes, connecting rods, rocker arms, and other components.

Fig. 3.79 SiC_p/Al composite pistons used in Formula One racing



Metal matrix composites are particularly suitable for fabricating wear-resistant brake parts for automobiles and motorcycles, such as disc brakes. At present, all automobile and motorcycle disc brakes are fabricated using cast iron. However, cast iron is not very suitable for these applications for reasons including its thermal conductivity, friction coefficient, and weight. Since the 1980s, America, Japan, and other developed countries have begun to research applications of aluminum metal composites in automotive parts and have produced a great deal of results. Compared with cast iron, the aluminum matrix composites have many advantages, including lightweight, high thermal conductivity, good wear resistance, and high friction coefficients. Therefore, the application of aluminum matrix composites in disc brakes can reduce the weight by 50–60% relative to the original cast iron. Also, during the braking process, a larger amount of heat is transmitted more quickly because of the increased thermal conductivity. Therefore, the thermal shock resistance can be improved and the brake temperature can be reduced. For example, under repeat braking conditions, the surface temperature can remain at 450 °C for the composite brakes, but reaches 700 °C for cast iron brakes. In addition, these composites have better wear resistance and more stable friction coefficients than cast iron. With increasing initial speeds, the friction coefficient of the composite brake changes little. However, the friction coefficient decreases significantly when

the initial speed of cast iron brakes is above 120 km/h. Motorcycle hub test results showed that the brake hub weight decreased by 50–60%, the friction coefficient increased by 10–15%, the power distance increased by 16.7%, and the decay rate decreased by 56%. These characteristics shortened the braking distance, inducing the stable braking performance. Silicon carbide particle-reinforced aluminum matrix composites are particularly suitable for fabrication of the disc brakes (brake pads) of automobiles and trains. The composite disc brake not only exhibits good wear resistance, but also has lower density and better thermal conductivity when compared with traditional cast iron brakes. The weight decreased by about 50–60%, and the vehicle braking distance was shorter. Therefore, since 1995, the Ford and Toyota Motor Corporations have begun to partially make 20% SiC_p/Al -10%Si composites cast by the Alcan Company into their disc brakes (Fig. 3.80). In 1995, America's Lanxide Company fabricated SiC particle-reinforced Al-10% Si composites using a combination of methods of pressureless infiltration casting and forming, in which the material weight is 4 kg after mold casting and 2.7 kg after forming. Its highest working temperature can reach 500 °C. At the Frankfurt Motor Show in 1995, the Lotus Company showed the Elise sports roadster in two rows, in which SiC_p/Al disc brakes produced by the Lanxide Company were used in the four wheels of the roadster (Fig. 3.81). As a result of the use of these lightweight aluminum composites, the empty car weight is only 700 kg, allowing the 108 L, four-cylinder car to accelerate to 100 km/h in only 5.9 s. In 1996, SiC_p/Al

Fig. 3.80 SiC_p/Al composite brakes

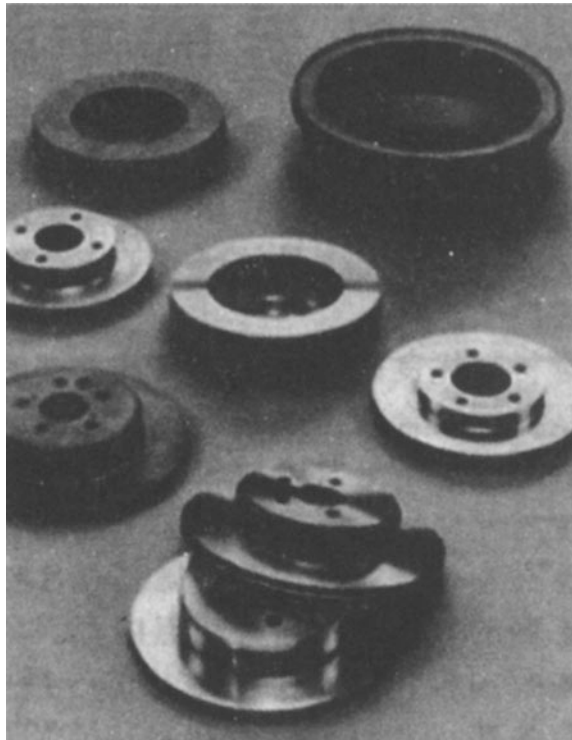


Fig. 3.81 Lotus Elise roadster



composite disc brakes produced by the Lanxide Company were put into mass production, and their daily output reached 1000 pieces. In addition, Germany has successfully applied SiC_p/Al disc brakes in high-speed trains with speeds of up to 160 km/h, where the weight of the suspension system decreased by more than 50%.

3.6 New Progress and Development Trends of Metal Matrix Composites

On the basis of consulting and investigating a great deal of domestic and overseas information on metal matrix composite research, a report on the research status and development direction of metal matrix composites has been written. The main contents of this research report include the metal matrix composite research status at home and abroad, the background requirements in China, the main contents and general objectives of further research in China, and proposed policies and measures [4, 6, 8, 15, 16, 81–83].

3.6.1 Research Status of Metal Matrix Composites

Metal matrix composites are a class of multi-phase materials fabricated by combining one or more reinforcement phases with metal alloys, in which the reinforcement materials generally have high strength, hardness, modulus, wear resistance, and heat resistance, but poor plasticity; the metal matrix materials usually have better plasticity, but lower strength and modulus. Metal matrix composites can fully use the performance advantages of both the reinforcement phases and the metal matrix materials, consequently exhibiting excellent all-round properties. Therefore, these composites have drawn widespread attention at home

and abroad. In the nearly 40 years of development of and research into such composites, considerable progress has been made in the basic theory research and application research. Meanwhile, these composites have been gaining increasing numbers of applications in aerospace, aviation, defense, sports, automotive, medical equipment, and other fields.

Depending on the reinforcement types, metal matrix composites can be divided into continuously (long fibers) reinforced metal matrix composites and discontinuously (short fibers, whiskers and particles) reinforced metal matrix composites. Although continuously reinforced metal matrix composites show high performances along the fiber reinforcement direction, their development, research, and applications are significantly limited by the high costs of the raw materials and of the composite manufacturing, their anisotropy properties, and the difficulties in forming processing. Therefore, over the past ten years, the focus of metal matrix composite research has concentrated on discontinuously reinforced metal matrix composites.

The main preparation methods for discontinuously reinforced metal matrix composites include powder metallurgy, squeeze casting, and stirring casting. The composite preparation methods have gained great attention worldwide, because the composite performances primarily depend on the manufacturing level. Discontinuously reinforced metal matrix composites prepared by powder metallurgy not only exhibit good all-round performance but also make it easy to design and control the composite components; they do have some disadvantages, such as the high cost of both raw materials and composite manufacturing, and the requirement for secondary plastic processing to enhance the composite density. America and Japan have taken leading positions in the research on metal matrix composites prepared by powder metallurgy. In China, the Institute of Metal Research, the Chinese Academy of Sciences, Harbin Institute of Technology, Northwestern Polytechnical University, and other units have also carried out different degrees of research on metal matrix composites produced by powder metallurgy. The metal matrix composites prepared by squeeze casting have advantages including simple fabrication technology, excellent performance, and enhanced density without secondary plastic deformation. However, the squeeze casting technique significantly restricts both reinforcement types and contents. At present, Japan has taken a leading position in the research on metal matrix composites made by squeeze casting. Harbin Institute of Technology and Southeast University in China have also investigated this aspect in depth. The stirring casting technique offers simple preparation technology, low-cost composite manufacturing, and easy implementation of mass production, but it markedly limits the control of composite performances and the choice of reinforcement types and contents. Worldwide, Britain and Canada have maintained leading positions in stirring casting technique research. Meanwhile, Shanghai JiaoTong University and the Beijing Institute of Aeronautical Materials have also investigated this technique and have formed a good working basis. In addition, the research into in situ synthesized metal matrix composites by the reaction synthesis method is also providing one of the most attractive research focuses at home and abroad. During the preparation process of

metal matrix composites by powder metallurgy and casting techniques, in situ reinforcements are synthesized through a chemical reaction between the raw materials. However, in situ synthesized metal matrix composites show strong interface binding and excellent performances. At present in Europe, Britain, Germany, and France have established a joint scientific research plan, implemented this plan, and have fully investigated the preparation technology and relevant basic theory, as along with applications for in situ metal matrix composites produced by reaction synthesis technology. America, Japan, India, and China have also conducted considerable research in this area and have obtained new research results; however, the development momentum is very rapid.

The comprehensive properties of the metal matrix composites are closely related to their microstructures, and the interface bond state plays a particularly important role. The research into composite interfacial bonding has great significance in the design of such composites, optimization of the preparation parameters, improving the material service performance and processing performance, and promoting the wider application of these composites. Therefore, research on the metal matrix composite interface is an immutable focus for basic theoretical research. The main research contents of the metal matrix composite interface include the following: (1) the reinforcement choices and surface treatments; (2) the alloying of the matrix alloys; (3) the interface bonding mechanism; (4) the interface residual stress; (5) the relationship between interface bonding and the composite properties; and (6) the interface behavior and its influence during the processes of composite plastic working and machining. The interface research as part of the basic theoretical research into metal matrix composites has been widely reported internationally. America, Japan, China, Britain, and several other countries have maintained leading positions in the world research fields.

To promote the wider application of metal matrix composites, countries around the world have paid great attention to the composite applications and basic theory research. The research content mainly includes the following: (1) plastic forming technology research; (2) machining technology research; (3) process research on strengthening heat treatments and size stabilization treatments; (4) surface treatment technology research; and (5) connection technology research. At present, the metal matrix composite research on both plastic forming and heat treatment has been widely reported. Through research into high-temperature extrusion deformation, rolling deformation, and isothermal forging deformation, the near-net-shape forming ability of complex composite components can be improved further; through research into the processes of strengthening heat treatment and size stabilization treatment, the composite performance potential can be brought further into play, and the all-round performance of the composites can be further enhanced. The research on machining technology, surface treatment technology, and connection technology will be important during the evolution of composite applications. However, little of this research has been conducted and further development will be required. For metal matrix composites, the basic research on applications still shows a large disparity with the basic research. Depending on the overall development trends and demand conditions, this basic application research will

have great development potential and prospects. Recently, America, Japan, and China have maintained leading positions in this area.

Discontinuously reinforced metal matrix composites have excellent comprehensive properties. Their main performance advantages are as follows: high specific strength and specific stiffness, good heat resistance and wear resistance, high anti-fatigue performance and high-temperature creep properties, small thermal expansion coefficient adjusted over a certain range, good damping performance, anti-radiation performance and anti-aging properties, suitability for use in both vacuum and space environments, ability to use conventional metal forming and processing methods that are applicable for the composite components, and practicable connections between these materials and other materials. The composite performance disadvantages include the following: lower plasticity at room temperature, more difficult machining than conventional metal materials, and higher material costs. The performance levels of discontinuously reinforced metal matrix composites are related to both the composite system selection and their preparation methods. In the current international reports, several typical discontinuously reinforced metal matrix composites have reached the performance index, as shown in Table 3.68. The table shows that the various discontinuously reinforced metal matrix composites have different characteristics. Therefore, these composites can be applied in different situations according to the needs of the applications.

Discontinuously reinforced metal matrix composites have broad application prospects in many areas because of the excellent performances shown in Table 3.68. Their applications in the aerospace field include not only aeroengine components such as modules, blades, exhaust nozzle joints, blade pans and hollow shaft

Table 3.68 Properties of typical discontinuously reinforced metal matrix composites

Reinforcements	Matrix alloys	Fraction volume (%)	Preparation methods	Properties			
				Tensile strength (MPa)	Elastic modulus (GPa)	Elongation (%)	Coefficient of thermal expansion ($\times 10^{-6} \text{ K}^{-1}$)
SiC particles	LD2 aluminum alloy	20	Powder metallurgy	550	110	1.8	13.5
		20	Stirring casting	450	110	1.5	14.1
		40	Squeeze casting	500	130	1.0	12.2
SiC whiskers	LD2 aluminum alloy	20	Powder metallurgy	560	120	2.0	13.0
		20	Squeeze casting	580	120	3.0	13.0
SiC whiskers	AZ91 magnesium alloy	20	Squeeze casting	320	90	2.5	14.0
TiC and TiB	TC4 titanium	10	Reactive hot-pressed sintering	1300	130	1.8	7.0

structures, but also spacecraft parts such as guidance system components, support structures, and truss structures. Their applications in the military defense field include guidance system components, imaging system components, mirror holders, armored track shoes, electronic equipment frames on aircraft, printed circuit boards, multi-core modules, oriented system shells, and many others. Their applications in the automotive sector include engine pistons, connecting rods, cylinders, cylinder liners, disc brakes, and drive shafts. Their applications in other industries include bike frames, high-speed train brake parts, motorcycle brake hoops, and numerous others. In summary, discontinuously reinforced metal matrix composites have wide applications, mainly in the aerospace field in the USA, as well as the automobile and transportation fields of Japan and some European countries.

3.6.2 Metal Matrix Composite Demand Background in China

Metal matrix composites are widely in demand in the aviation, aerospace, defense, automotive, and other industrial fields. However, China lags behind America and Japan in the application research of metal matrix composites. For nearly 30 years, metal matrix composites have been investigated in China, gradually reducing the difference between China and the rest of the world in both the basic research and the application research, in which certain researchers have reached the world's most advanced levels. Therefore, China has a good basis and conditions for the extensive application of metal matrix composites. However, the current applications in China are limited to the aerospace field, because the cost problem has not yet been resolved. For example, silicon carbide whisker-reinforced aluminum composites were successfully manufactured into the antenna screw for a certain model of Chinese satellite. Current application researches in China include the following: the applications of discontinuously reinforced aluminum matrix composites in the inertial platform components of rocket and missile guidance systems, the frame structures of aerospace propeller systems and space station systems, various pipe joint and connection components, electronic packaging components, car engine pistons and disc brakes, bike frames, and motorcycle brake hoops; the applications of discontinuously reinforced titanium matrix composites in aeroengine cores, leaves, and exhaust nozzle joints, and in car engine exhausts; and the applications of discontinuously reinforced magnesium matrix composites in aerospace pipe joint parts.

Although discontinuously reinforced metal matrix composites have not yet achieved large-scale application, they offer advantages including good high-temperature resistance, good abrasion resistance, high thermal conductivity, higher mechanical properties than the matrix metals, smaller thermal expansion coefficients than the matrix metals, and designability for all performances within certain ranges. Therefore, there must be several application fields where the advantages of composites can be brought into full play.

Whisker-reinforced aluminum matrix composites with not only comprehensive material performances but also better processing performances have predominance in applications in structural parts that require high performance and size precision. However, their main problems that still need to be solved are the research and development of both the whiskers and whisker-reinforced aluminum matrix composites with high performances and low costs, along with batch production methods for such materials.

Particle-reinforced aluminum composites have good wear resistance. Composites with low coefficients of thermal expansion and high thermal conductivity can be obtained by selecting the correct particle types and increasing the particle content. Therefore, these composites exhibit the required advantages and potential for application to wear-resistant parts and electronic packaging components. Their main problems that still must be solved are the composite preparation process and improvements in product quality stability.

In situ discontinuously reinforced titanium matrix composites have higher strength, higher modulus, and better wear resistance and heat resistance relative to titanium alloys. Therefore, such composites are expected to replace steels and cast iron on some occasions, consequently reducing the component and system weights. Titanium matrix composites have been applied in jet turbine engines, and increasing numbers of titanium matrix composite components have application in new turbine engines.

Discontinuously reinforced magnesium matrix composites with low proportions and good mechanical properties have greater potential applications in components and systems that require strict weight conditions. In the past, only magnesium alloys with the lowest density were used, and the number of applications was small because of their flammability during magnesium casting and their poor processing performance, as well as less than ideal mechanical properties. Existing research results show that magnesium matrix composites will easily find suitable application situations when their mechanical properties can be significantly improved. China is a country with large magnesium reserves, and this means that the development of magnesium matrix composites has important and practical significance.

Compared with aluminum matrix composites, the research bases for titanium and magnesium matrix composites in China are still poor, and there is greater distance from practical applications. Therefore, it is necessary to conduct further basic research and application research for both titanium and magnesium matrix composites.

3.6.3 The Main Aims of Further Research on Metal Matrix Composites

Based on the status of domestic and foreign research and the development trends of metal matrix composites, the research bases in China in particular and the application requirements background of metal matrix composites, and the distance

between China and the top level in the world, we suggest further support and investigation of discontinuously reinforced metal matrix composites in several areas, as detailed in the following.

(1) Perfecting discontinuously reinforced metal matrix composite systems

For discontinuously reinforced metal matrix composites, the reinforcements include various particles, whiskers, short fibers, and in situ synthesized phases; the main matrix materials are aluminum, titanium, and magnesium alloys. Various different single- or multi-phase-reinforced matrix alloy composites have different performance characteristics. In addition, the composite performances also vary with the reinforcement content. Therefore, discontinuously reinforced metal matrix composites exhibit excellent performance designability. Perfecting discontinuously reinforced metal matrix composite systems can not only sufficiently realize their potential and produce excellent composite performances, but will also enable us to freely design various composite performances, and consequently meet the composite properties requirements for different application environments. Therefore, improvement of the composite systems is the basis of and the prerequisite for expanding the application research of discontinuously reinforced metal matrix composites and must gain sufficient attention.

(2) The importance of development of discontinuously reinforced metal matrix composites with high performance and low cost

While discontinuously reinforced metal matrix composites are novel high-performance materials, their high costs significantly limit their widespread application, especially in civilian fields. This contradiction is becoming increasingly prominent. Therefore, research and development of discontinuously reinforced metal matrix composites with high performance and low cost are of great significance. The main reasons for the high costs of these composites include: 1) the high costs of the raw materials; 2) the complexity of preparation and expensive equipment requirements; 3) the lower quality stability of the composites; and 4) the higher costs of forming processing of composite components.

To reduce the composite costs and their component costs, research work must be conducted in the following areas: 1) the development of low-cost and large-output reinforcements suitable for metal matrix composites, including particles, whiskers, and short fibers; 2) research on the methods of manufacturing metal matrix composites from low-cost reinforcements or multi-phase hybrid reinforcements to obtain high-performance and low-cost composites; 3) optimizing composite preparation and improving composite stability; 4) research on high-temperature plastic deformation and the high-strain-rate superplasticity of the composites. The high-temperature plastic forming process can achieve near-net-shape forming of complex composite components, which can reduce the amount of raw materials used and the amount of machining of complex composite components; 5) research on composite machining and the development of processing methods and tools suitable for discontinuously reinforced metal matrix composites.

- (3) Research on the scientific basis of preparation and the preparation techniques of discontinuously reinforced metal matrix composites

Composite preparation methods directly affect the composite performances and costs. The in-depth development of the basic science research of discontinuously reinforced metal matrix composites is a basis for optimizing composite preparation. Research on the preparation techniques of composites will include the following contents: 1) new preparation methods and new preparation technology development for the composites; 2) optimization of the composite preparation parameters; and 3) the development of composite preparation equipment.

- (4) Research on heat treatment technology of discontinuously reinforced metal matrix composites

The performances of discontinuously reinforced metal matrix composites depend not only on the reinforcement types and contents, but also on the matrix performances and the composite interfaces. The performances of matrix alloys are related to the alloy types and the heat treatment. Adopting special heat treatments that are suitable for metal matrix composites can achieve the best matrix alloy performance levels, improve the composite interface, and give full play to the performance potential of metal matrix composites. Therefore, further study of heat treatment technology for discontinuously reinforced metal matrix composites is necessary.

- (5) Research on high-temperature plastic deformation and high-strain-rate superplasticity of discontinuously reinforced metal matrix composites

The research on high-temperature compressive deformation, hot extrusion, hot rolling, isothermal forging deformation, semisolid forming, and the high-speed superplasticity of discontinuously reinforced metal matrix composites not only provides a basis for achieving near-net-shape of complex components for the composites, but also provides important channels for reducing the costs of the composite components. It is essential to pay sufficient attention to this research.

- (6) Research into discontinuously reinforced metal matrix composite machining

Turning, milling, drilling, tapping, electric sparking, and other special processing methods for discontinuously reinforced metal matrix composites will be investigated to develop the processing parameters and tool materials required for metal matrix composites. This is a necessary research content to achieve the applications of discontinuously reinforced metal composites.

- (7) Research on the behavior of discontinuously reinforced metal matrix composites under different circumstances

Discontinuously reinforced metal matrix composites are suitable for use in various different environments, and particularly in space environments. Therefore, research on the microstructures and properties of discontinuously reinforced metal

matrix composites under various environmental conditions are important for expansion of their application range.

(8) Research on connection technology for discontinuously reinforced metal matrix composites

Connection methods that are suitable for metal matrix composites will be developed, the connection process parameters will be optimized, and high-performance connections between the composites themselves and between such composites and other materials will be achieved to satisfy the special needs of practical applications.

(Translated by Geng Lin, Kun Wu, Aibin Li, Xiaoshi Hu, and Guojian Cao.)

References

1. Guan M, Chang Z (2010) Development on preparation process for metal matrix composite. *Mater Heat Treat* 39(16):93–95 (in Chinese)
2. Clyne TW, Withers PJ(1993) An introduction to metal matrix composites. Paperback Pub. in 1994 ed. Cambridge University Press, Cambridge
3. da Costa CE, Lopez FV (2000) Castello JMT. Metal matrix composites. Part 1. Types, properties, applications. *Revista De Metalurgia* 36(3):179–192
4. Zhang X-N, Wang H, Hu J-H, Wu Z-F (2006) Review and prospect of the research on metal matrix composites. *Yunnan Metallurgy* 35(5):53–58 (in Chinese)
5. Torralba JM, da Costa CE, Velasco F (2003) P/M aluminum matrix composites: an overview. *J Mater Process Technol* 133(1–2):203–206
6. Hunt WH (2000) Aluminum metal matrix composites today. *Mater Sci Forum* 331–3:71–83
7. Dong T-S, Cui C-X, Liu S-J, Xue H-T (2006) Advancement of fiber-reinforced aluminum matrix composites. *Hot work technol* 35(6):49–55 (in Chinese)
8. Zhang H-X, Hu S-B, Tu J-P (2005) Development of Cu based composites reinforced by particles. *Mater Sci Technol* 13(4):357–364 (in Chinese)
9. Guang M, Yi W, Yin'e L, Hong W, Jing Z, Zhihuan J, Ting J (2007) Progress in research for Cu/C matrix composites. *Rare Met Lett* 26(12):6–10 (in Chinese)
10. Tjong SC, Mai Y-W (2008) Processing-structure-property aspects of particulate- and whisker-reinforced titanium matrix composites. *Compos Sci Technol* 68:583–601
11. Godfrey TMT, Goodwin PS, Ward-Close CM (2000) Titanium particulate metal matrix composites—Reinforcement, production methods, and mechanical properties. *Adv Eng Mater* 2(3):85–92
12. Leyens C, Hausmann J, Kumpfert J (2003) Continuous fiber reinforced titanium matrix composites: fabrication, properties and applications. *Adv Eng Mater* 5(6):399–410
13. Ye HZ, Liu XY (2004) Review of recent studies in magnesium matrix composites. *J Mater Sci* 39(20):6153–6171
14. Wu YF, Du WB, Nie ZR, Cao LF, Zuo TY (2007) Research status of particulate reinforced magnesium matrix composites. *Rare Met Mater Eng* 36(1):184–188 (in Chinese)
15. Yunsun Z, Shenrong Y (1997) Review and prospects for Zn based composites. *Journal of Kunming University of Science and Technology*. 22(1):129–134 (in Chinese)
16. Xiaocong PU, Jinhui LIN, Miao HE (2009) Research progress of high temperature metal-base composite. *Hot working technol* 38(10):118–121 (in Chinese)
17. Wo D (2000) *Cyclopedia of composites*. Chemical industry Publishing House, 469–523 (in Chinese)

18. Ibrahim IA, Mohamed FA, Lavernia EJ (1991) Particulate reinforced metal matrix composites—A review. *J Mater Sci* 26:1137–1156
19. Slipenyuk V, Kuprin Yu, Milman V, Goncharuk J Eckert (2006) Properties of P/M processed particle reinforced metal matrix composites specified by reinforcement concentration and matrix-to-reinforcement particle size ratio. *Acta Mater* 54:157–166
20. Geng L, Zhang HW, Li HZ, Guan LN, Huang LJ (2010) Effects of Mg content on microstructure and mechanical properties of SiCp/Al-Mg composites fabricated by semi-solid stirring technique. *Trans Nonferrous Met Soc China* 20(10):1851–1855
21. Sahin Y, Acilar M (2003) Production and properties of SiCp-reinforced aluminium alloy composites. *Composites* 34:709–718
22. Chawla N, Shen YL (2001) Mechanical behavior of particle reinforced metal matrix composites. *Adv Eng Mater* 3(6):357–370
23. Srivatsan TS, Sudarshan TS, Lavernia EJ (1995) Processing of discontinuously-reinforced metal matrix composites by rapid solidification. *Prog Mater Sci* 39:317–409
24. Deng KK, Wu K, Wang XJ, Wu YW, Hu XS, Zheng MY, Gan WM, Brokmeier HG (2009) Microstructure evolution and mechanical properties of a particulate reinforced magnesium matrix composite forged at elevated temperatures. *Mater Sci Eng A* 527(6):1630–1635
25. Wu K, Deng K, Nie K, Wu Y, Wang X, Hu X, Zheng M (2010) Microstructure and mechanical properties of SiCp/AZ91 composite deformed through a combination of forging and extrusion process. *Mater Des* 31(8):3929–3932
26. Yuan H, Tijin C, Ying M (1997) Fabrication technique and mechanical properties of SiCp/ZA27 composites. *Tezhong Zhuzao Ji Youse Hejin/Spec Cast Nonferrous Alloys* 2:25–28
27. Bi J, Ma Z, Lv Y, Shen H, Gao M (1992) Study Of SiCw/2124Al composites. *China Nonferrous Met* 2(2):63–66 (In Chinese)
28. Wang GS, Zhang J, Geng L, Wang DZ, Yao CK (2001) Microstructure and properties of SiCw/6061Al composites after compression at temperatures around the solidus of the matrix. *Mater Sci Technol* 17:632–926
29. Geng L, Wang DZ, Yao CK (1994) Effect of Matrix on Tensile Strength of SiCw/Al Composites. *Journal of Harbin Institute of Technology*. 1(2):56–60 (In Chinese)
30. Hong SH, Chung KH (1995) Effects of vacuum hot pressing parameters on the tensile properties and microstructures of SiC-2124 Al composites. *Mater Sci Eng A* A194:165–170
31. Zheng M, Wu K, Kamado S, Kojima Y (2002) Microstructure and mechanical properties of aluminum borate whisker reinforced magnesium matrix composites. *Mater Lett* 57(3):558–564
32. Zheng M (1999) Interface and fracture behavior of SiCw/AZ91 composites. Harbin Institute of Technology Dissertation for the Doctoral Degree in Engineering (in Chinese)
33. Zheng MY, Wu K, Yao CK (2001) Effect of interfacial reaction on mechanical behavior of SiCw/AZ91 magnesium matrix composites. *Mater Sci Eng A* 318(1–2):50–56
34. Evans AG (1991) The mechanical properties of reinforced ceramic, metal and intermetallic matrix composites. *Mater Sci Eng A* 143(1–2):63–76
35. Yi B, Feng J, Tao J, Zhang J (1996) Properties of Zn Al/Al₂O₃ short fiber composite. *Aerosp Mater Technol* 3:36–40 (in Chinese)
36. Maruyama Benji (2000) Continuously reinforced MMCs. *Compr compos mater* 3:717–739
37. Sebo P, Stefanik P (2003) Copper matrix-carbon fibre composites. *Int J Mater Prod Technol* 18(1–3):141–159
38. Ward-Close CM, Minor R, Doorbar PJ (1996) Doorbar. *Intermetallic-matrix composites—A review*. *Intermetallics* 4:217–229
39. Tjong SC, Ma ZY (2000) Microstructural and mechanical characteristics of in situ metal matrix composites. *Mater Sci Eng R- Reports* 29(3–4):49–113
40. Ni DR, Geng L, Zhang J, Zheng ZZ (2008) Fabrication and tensile properties of in situ TiBw and TiCp hybrid-reinforced titanium matrix composites based on Ti-B4C-C. *Mater Sci Eng A*. 8 478(1–2):291–296

41. Zhang XN, Geng L, Wang GS (2003) Microstructure and tensile properties of Al hybrid composites reinforced with SiC whiskers and SiC nanoparticles. *Key Eng Mater* 249:277–281
42. Lin G, Zhang X-N, Zheng Z-Z, Bin X (2006) Effect of aging treatment on the mechanical properties of (SiCw + SiCp)/2024Al hybrid nanocomposites. *Trans Nonferrous Met Soc China* 16:387–391
43. XU J-H, XU Z-F, Yu H (2010) Progress in research on fabrication of continuous Fiber reinforced aluminum matrix composites. *Foundry Technol* 31(12):670–1667 (in Chinese)
44. Li Y, Xu Y (2007) Development of preparation of SiC fibers reinforced composites. *Mater Rev* 21:434–437 (in Chinese)
45. da Costa CE, Lopez FV, Castello JMT (2000) Metal matrix composites. Part 2. Processing and consolidation techniques for particle reinforced MMCs. *Revista De Metalurgia*. 36 (3):193–197
46. Badini C, Fino P, Musso M, Dinardo P (2000) Thermal fatigue behaviour of a 2014/Al2O3-SiO2 composite processed by squeeze casting. *Mater Chem Phys* 64:247–255
47. Hashim J, Looney L, Hashmi MSJ (2002) Particle distribution in cast metal matrix composites —Part I. *J Mater Process Technol* 123:251–257
48. Qu SJ, Geng L, Han JC (2007) SiCp/Al composites fabricated by modified squeeze casting technique. *J Mater Sci Technol* 23(5):641–644
49. Huang LJ, Geng L, Xu HY, Peng HX (2011) In situ TiC particles reinforced Ti6Al4 V matrix composite with a network reinforcement architecture. *Mater Sci Eng A* 528(6):2859–2862
50. Feng YC, Geng L, Li AB, Zheng ZZ (2010) Fabrication and characteristics of in situ Al12 W particles reinforced aluminum matrix composites by reaction sintering. *Mater Des* 31(2):965–967
51. Zhang S, Zhang E (1996) Development of metal matrix composites formed by spray codeposition. *Aerosp Mater Technol* 4:1–7
52. Yanqiang L, Jianzhong F, Jimei S, Likai S (2010) Development of metal matrix composites by powder-metallurgy processing. *Mater Rev* 24(12):18–23
53. Gupta M et al (1997) Effect of particulate type on the microstructure and heat treatment response of Al-Cu based metal-matrix composites. *J Mater Proc Tec* 65(1–3):245–251
54. Geng L, Xu HY, Yu K, Wang HL (2007) Aging behavior of Al2O3 short fiber reinforced Al-Cu alloy composites. *Trans Nonferrous Met Soc China* 17(5):1018–1021
55. Geng L, Feng YC, Zheng ZZ, Zhang J, Wang QW (2009) Effects of heat-treatment on microstructures and mechanical properties of WO3 particle and Al18B4O33 whisker hybrid reinforced Al matrix composites by squeeze casting. *Mater Sci Eng A* 506(1–2):34–38
56. Zheng MY, Wu K, Kamado S, Kojima Y (2003) Aging behavior of squeeze cast SiCw/AZ91 magnesium matrix composite. *Mater Sci Eng A* 348:67–75
57. Gu M, Wu Z, Jin Y, Kocak M (1999) Effects of reinforcements on the aging response of a ZK60-based hybrid composite. *Mater Sci Eng A* 272:257–263
58. Wu K (1995) Interface structure and aging behavior of SiCw/AZ91 composites. Harbin Institute of Technology Dissertation for the Doctoral Degree in Engineering (in Chinese)
59. Ni D-R, Jin X-O, Geng L, Wang G-S (2007) Research on heat treatment of discontinuously reinforced titanium matrix composites. *Mater Sci Technol* 15 (1 2):173–176
60. Ranganath S (1997) A review on particulate-reinforced titanium matrix composites. *J mater sci* 32(1):1–16
61. Zhang XX, Deng CF, Wang DZ, Geng L (2005) Synthesis and thermal stability of multiwall carbon nanotubes reinforced aluminum metal matrix composites. *Trans Nonferrous Met Soc China* 15:240–244
62. Wu J, Li W, Xie Y (2011) Mechanical and experimental analyses of microyield behavior of metal matrix composites. *J Mater Sci Eng* 4 29(4):536–540
63. Li AB, Geng L, Zhang J, Zheng ZZ, Yao CK (2004) The effect of whisker misalignment on the hot compressive deformation behavior of a SiCw/6061Al Composite at 500 °C. *Mater Chem Phys* 84:29–32

64. Feng AH, Geng L, Zhang J, Yao CK (2003) Hot compressive deformation behavior of a eutectic Al-Si alloy based composite reinforced with a-Si₃N₄ whisker. *Mater Chem Phys* 82 (3):618–621
65. Qu SJ, Geng L, Meng QC (2005) Effects of hot rolling on microstructure and properties of a 20 vol. % SiCp/Al composite. *Rare Met* 24(1):95–99
66. Geng L, Guan LN (2009) Effect of hot extrusion on microstructure and properties of (ABO_w + SiCp)/ 6061Al composites fabricated by semi-solid stirring technique. *J Wuhan Univ Technol* 24:13–16
67. Geng L, Qu SJ, Lei TQ (2003) Hot extrusion and its effect on microstructure and properties of squeeze casting SiCp/Al composites with lower volume fraction of reinforcement. *Key Eng Mater* 249:233–238
68. Ma ZY, Tjong SC (2001) Creep deformation characteristics of discontinuously reinforced aluminium- matrix composites. *Compos Sci Technol* 61(5):771–786
69. Tian J, Li W, Han L, Peng J (2010) Research and development of creep of metal matrix composites. *Mater Rev* 24(3):119–123 (In Chinese)
70. Tochigi I, Imai T, Geng L (2000) High strain rate superplasticity of a Beta-Si₃N₄ whisker reinforced pure aluminum composite. *Key Eng Mater* 171–1:369–375
71. Geng L, Imai T, Mao JF, Takagi M, Yao CK (2001) Microstructure and high strain rate superplasticity of an in situ composite synthesized from Al and nano ZrO₂ particles by powder metallurgy. *Mater Science Technol* 17(2):187–194
72. Geng L, Wang GS, Meng QC, Wang DZ, YAO ZK, LEI TQ (2001). Investigation of coordination mechanism in superplastic deformation of SiCw/LD2AL composite. *Mater Sci Technol* 9(3):225–228
73. Hu H-E, Zhen L, Lei T-Q, Imai T (2003) High-strain-rate superplasticity of metal matrix composites. *Mater Science Techno* 11(4):406–409
74. Geng L, Yuan Z, Yao Z (1993) Turning of discontinuously reinforced metal matrix composites. *Aerosp Mater Technol* 2:13–16
75. Geng L, Yuan Z, Y Hui, Yao Z (1994) Effects of whisker orientation on the quality of cutting surface of the SiCw/Al composite. *J Mater Eng* 2:6–8
76. Shue B, Moreira A, Flowers G (2010) Review of recent developments in composite material for aerospace applications. *Proceeding of the ASME International Design Engineering Technical Conferences and Computers and Computers and Information in Engineering Conference* 1:811–819
77. Miracle DB (2005) Metal matrix composites—From science to technological significance. *Compos Sci Technol* 65(15–16):2526–2540
78. Wang YX, Yu Z, Yan PF, Yan B (2010) Development of aluminum matrix composites. *Shanghai Nonferrous Met* 31(4):194–198 (in Chinese)
79. Zhang X, Wang D, Yao Z (2002) Commercialization of discontinuously reinforced metal-matrix composites. *Aeronaut Manufact Technol* 5:35–38
80. Wu R (1997) The present condition and prospects on metal matrix composites. *Acta Metall Sin* 33(1):78–84
81. Zhang DI, Zhang G, Li Z (2010) The current state and trend of metal matrix composites. *Mater China* 129(14):1–6 (in Chinese)
82. Hao B, Duan X, Cui H, Yang B, Zhang J (2005) Present status and expectation of metal matrix composites. *Mater Rev* 19(7):64–68 (in Chinese)
83. Harris B (1991) A perspective view of composite materials development. *Mater Des* 12 (5):259–272

Chapter 4

Cement-Based Composite Materials

Keru Wu and Dong Zhang

Cement-based composite materials consist of hardened cement paste as a base, which is formed by hydration between cement and water, and a mixture of various inorganic, metallic, and polymeric materials. The mixture can comprise two or all three types of the above-mentioned materials. Conventional concrete, produced from portland cement, water, sand, and aggregate, has been extensively used in the construction industry since the beginning of last century. However, with the modernization of cities, urbanization of rural areas, and development of marine and underground structures, the performance of conventional cement concrete, as characterized by its low tensile strength, cracking, and brittle failure nature, cannot meet the requirements of the modern civil engineering work. Therefore, for several decades, researchers in various countries have done plenty of work on modifying the properties and developing the new potential of concrete. Great progress on the research and application of cement-based composite materials has been achieved.

4.1 Polymer-Based Cement Composite Materials

Polymer-based cement composite materials are produced by introducing an organic polymer into cement-based materials by various different methods. In the early 1940s, there were reports on this type of material, and further research and development was extensively done in the late 1960s, which reached its peak in the '70 s. Polymer cement concrete and polymer-impregnated concrete were successively developed. The high mechanical properties of this type of material were realized through plasticization, toughening, pore filling, and solidification of the polymer in the cement paste.

K. Wu (✉) · D. Zhang
Tongji University, Shanghai 200092, China
e-mail: keruwu@mail.tongji.edu.cn

4.1.1 Polymer Cement Concrete (PCC)

Polymer cement concrete is a type of cement-based composite material, in which a polymer is used to replace part of the cement and acts as a binding agent. According to the form of polymer used, the polymer cement concrete can be classified as polymer latex cement concrete, redispersible polymer powder cement concrete, water-soluble polymer cement concrete, and liquid resin cement concrete [1–4].

Besides cement, sand, aggregate, and water, the main components of polymer latex cement concrete are polymer latex and other additives such as defoamers and stabilizers. The types of polymer latexes are diverse; however, they can be divided into two groups: rubber latex and resin latex. Figure 4.1 exemplifies commercial polymer latexes. Currently, the most used polymer latexes are styrene-butadiene rubber (SBR), polyacrylic ester (PAE), and poly ethylene-vinyl Acetate (EVA).

Polymer latex (or emulsion) is a water suspension system consisting of polymer colloids with a particle size range of 0.05–5 μm. It is prepared by emulsification and polymerization of the polymer monomer in water. The solid content is generally in the range of 40–50%.

The properties of polymer latex cement mortar mainly depend on the type and content of the polymer. The polymer/binder ratio (weight ratio of the polymer solid to cement) is one of the main factors influencing the formulation of the polymer latex cement mortar. The addition of polymer latex also provides certain water-reducing effect; hence, the water/cement ratio of the polymer latex cement mortar can be reduced to achieve the same workability. Generally, if the polymer/binder ratio is 5–20%, the water content can be reduced to ~20–35%. Based on existing studies, the content range of the different components of polymer latex cement mortar is cement:fine aggregate = 1:(2–3); polymer/binder ratio: 5–20%; water/cement ratio: 30–60%. Table 4.1 presents the component mix ratios of polymer latex cement mortar according to different applications.

Generally, the polymer/cement ratio of the latex-modified concrete ranges from 5 to 15% and the water/cement ratio ranges from 30 to 50%. Table 4.2 gives the

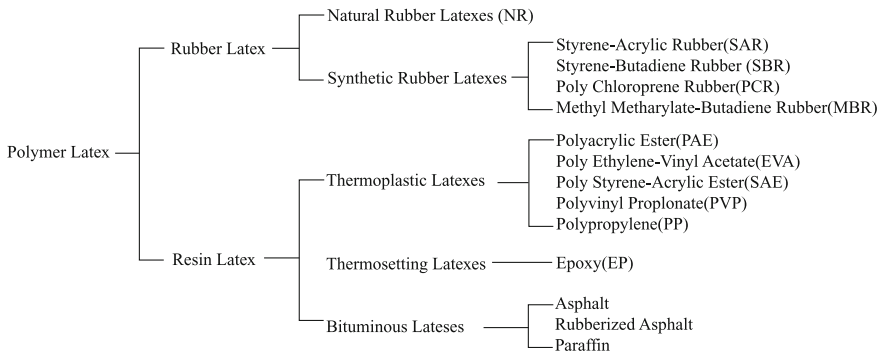


Fig. 4.1 Commercially available polymer latexes

Table 4.1 Application and mixing design of polymer latex cement mortar

Application	Example	Mixing ratio (by weight)			Thickness /mm
		Cement	Sand	Latex	
Paving materials	Floor for general houses, warehouses, offices, shops, toilets	1	3	0.2–0.3	5–10
Floorings	Passages, stairs, chemical plants, railway platforms, roads, garages	1	3	0.3–0.5	10–15
Waterproofing materials	Concrete roof decks, mortar and concrete block walls, water tanks, swimming pools, septic tanks, silos	1	2–3	0.3–0.5	5–20
Adhesives	Adhesives for flooring materials, walls materials, heat insulating materials within concrete floors and walls	1	0–3	0.2–0.5	–
	New to old concrete and new to old mortar joints	1	0–1	>0.2	–
	Crack repairs	1	0–3	>0.2	–
Anti-corrosive linings	Effluent drains, chemical factory floors, grouting for acid-proof tiles, septic tanks, foundations for machinery plants, floors for chemical laboratories, pharmaceutical warehouses	1	2–3	0.4–0.6	10–15
Deck coverings (ship decks, bridge decks)	Undercoats	1	2–3	0.9–1.0	1–2
	Mid-coats	1	3	0.4–0.6	5–6
	Topcoats	1	3	0.5–0.6	3–4

Table 4.2 ACI proposed guidelines for composition of latex-modified concrete for patching applications

Material	Weight/kg
Portland cement	94
Aggregate (blend of coarse and fine)	300
Polymer (wet basis—liquid with 50% total solid)	29–38
Polymer (dry basis—total solid)	14–19
Total water	4–25

American Concrete Institute (ACI) proposed guidelines for the composition of latex-modified concrete as a patching and repair material.

The processing technology of latex-modified cement concrete is comparable to that of conventional cement concrete. The following points should be noted: (1) because polymer latexes easily entrap air, suitable anti-foaming agents should be used; the speed and time of mixing should also be controlled (the mixing and casting must be completed within 1 h); (2) because the adhesion of polymer latex materials is very strong, a highly efficient de-molding agent should be used, and the

equipments must be immediately cleaned after casting; (3) the processing temperature must be controlled between 5 and 30 °C; (4) alternative dry and wet curing methods should be used. Wet curing should be used for the first three or seven days prior to dry curing to enhance the film formation of the polymer latex materials.

In latex-modified concrete, the polymer particles fill up the bigger pores in concrete. Hence, the pore volume, associated with pores that are larger than 200 nm, is reduced and that associated with pores that are smaller than 75 nm is increased when compared with the pore volume of conventional concrete. However, the total porosity decreases with increasing polymer/cement ratios. The resistance to water, gas, and chloride ion diffusion, and anti-carbonation properties are significantly improved. Table 4.3 lists the diffusion coefficients of chloride ions in latex-modified cement mortar.

In general, latex-modified mortar and concrete show noticeable improved tensile and flexural strength properties however, no such improvement in the compressive strength when compared with that of conventional cement mortar and concrete. The increased strength is due to the high tensile strength characteristic of the polymer and the overall improvement in the cement–aggregate bonding. Table 4.4 shows the strength properties of typical latex-modified cement mortar materials.

The elastic modulus of latex-modified cement concrete or mortar ($\sim 10\text{--}30 \times 10^3$ MPa) is lower than that of conventional concrete or mortar. However, the deformation behavior of the latex-modified materials is significantly improved (Fig. 4.2). The addition of latex has no notable effect on the Poisson's ratio.

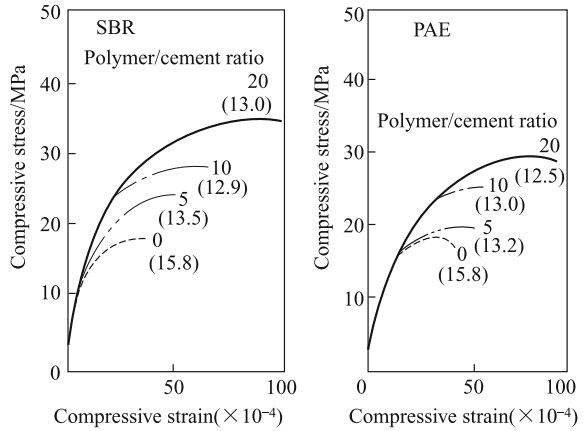
Table 4.3 Chloride ion diffusion coefficient of latex-modified cement mortar

Type of latex	Control	SBR	SBR	PCR	PCR
Polymer/cement/%	0	2.5	5.0	2.5	7.5
Diffusion coefficient/(cm ² /s)	9.34×10^{-9}	6.66×10^{-9}	4.34×10^{-9}	1.81×10^{-9}	0.94×10^{-9}

Table 4.4 Strength of latex-modified mortar

Latex	Polymer/cement/%	Flexural strength/MPa	Compressive strength/MPa
Control	0	3–5	18–20
NR	10	4–6	15–17
	20	2–3	4–5
PCR	10	5–6	18–19
	20	9–10	31–34
SBR	10	6–9	15–29
	20	7–12	17–32
PAE	10	6–8	16–18
	20	6–9	14–20
EVA	10	6–9	18–29
	20	6–11	19–32

Fig. 4.2 Compressive stress–strain curves for latex-modified mortars. Numbers in brackets indicate the elastic modulus ($\times 10^3$ MPa)



In contrast to conventional concrete, the adhesion bonding strength between latex-modified cement concrete and various substrates, such as old concrete, stone, ceramics, metal, timber, and brick, is higher. Figure 4.3 shows the experimental findings for the latex-modified cement concrete comprising SBR and PAE.

In addition, owing to the reduced porosity, latex-modified mortar and concrete have improved resistance to freezing and thawing, i.e., frost attack, when compared with that of conventional mortar and concrete. Figure 4.4 shows comparative weight loss of SAR-modified cement mortars, prepared by conventional and by pre-enveloping methods (whereby the sand particles are pre-coated by the polymer), following 100 freezing–thawing cycles. As deduced from the findings in

Fig. 4.3 Flexural bonding strength characteristics of latex-modified cement mortar and normal mortar. M—substrate damage; A—interface damage; and P—latex-modified mortar damage

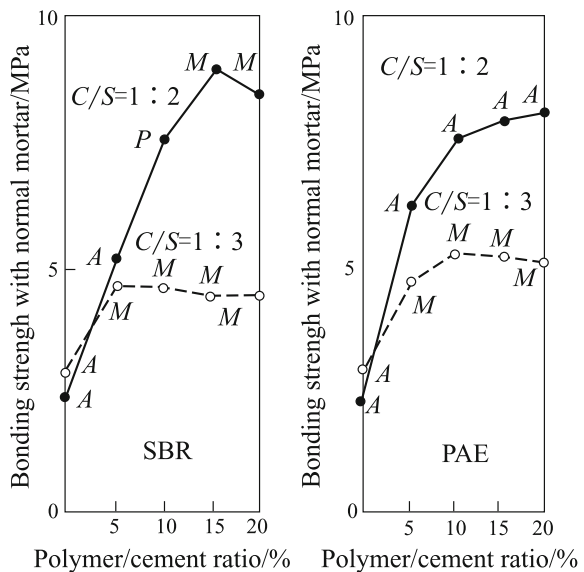


Fig. 4.4 Resistance to freezing and thawing property of SAR-modified mortars

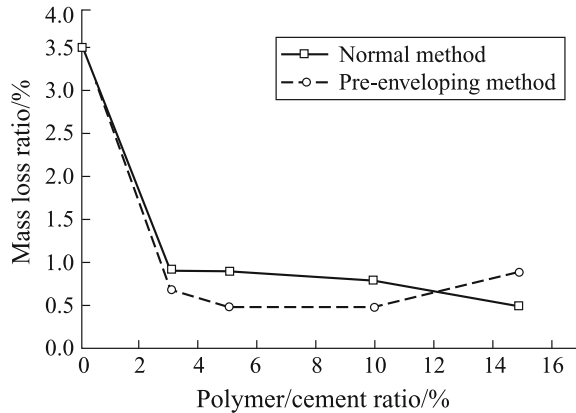


Fig. 4.4, the latex-modified cement concrete displays excellent abrasion resistance properties.

The chemical resistance of latex-modified mortar and concrete is dependent on the nature of the added polymers, polymer/cement ratio, and the chemicals. Most latex-modified mortar and concrete materials suffer from inorganic or organic acids and especially sulfate attacks. They also display poor chemical resistance to organic solvents.

Latex-modified mortar and concrete materials feature a rapid reduction in strength at increasing temperatures. This trend is more pronounced at temperatures above the glass transition temperature of the polymers. Most thermoplastic polymers in latex materials have a glass transition temperature of 80–100 °C.

The processing methodology of redispersible polymer powder-modified mortar and concrete is similar to that used for latex-modified systems except for the addition of the redispersible polymer powders. In general, the redispersible polymer powders are dry-mixed with cement and aggregates, followed by wet mixing with water. During the wet mixing, the redispersible polymer powders are redispersed or re-emulsified, thereby bearing similar functionalities to polymer latex in cement concrete. Examples of current commercially available redispersible polymer powders are poly ethylene-vinyl acetate (EVA) and poly vinyl acetate–vinyl versate (VA/VeoVa). The general advantage of redispersible polymer powders is their easy application. However, their performance is inferior to that of latex.

Water-soluble polymer-modified mortar and concrete materials are generally prepared at very low polymer/cement ratios and contain a small dosage of water-soluble polymer powder or water solution. This can afford improved matrix workability, prevention of matrix dry-out, and superior adhesion to porous substrates such as ceramic tiles, mortars, and concrete. The setting of the modified systems can be delayed to a certain extent. Examples of water-soluble polymers are methyl cellulose (MC) and polyvinyl alcohol (PVA).

4.1.2 *Polymer-Impregnated Concrete*

Polymer-impregnated concrete (PIC) was first developed by American scientists. Conventional preparation and curing methods produce numerous capillary pores in the cement paste even if the cement concrete is very well cured. The preparation of polymer-impregnated concrete is based on the removal of water from the capillary pores by replacement with appropriate solid materials. This affords enhanced properties owing to the significant reduction in pore volume. Through monomer impregnation, polymerization treatment to the hardened cement concrete, the pores in concrete are filled with polymer. Therefore, the porosity of the materials is not only reduced, but also the interfacial bonding between the cement and aggregate is also enhanced, resulting in improved strength, and resistance to abrasion, chemical, and freezing and thawing. Many different types of monomers have been successfully used to produce polymer-impregnated concrete. The requirements for the monomers are as follows: low viscosity, high boiling point, low thixotropy, easy polymerization, and low cost. Typical monomers, possessing a vinyl constituent that features a low viscosity, are methyl methacrylate (MMA), styrene (S), butyl acrylate (BA), and methyl acrylate (MA). These monomers may be used either on their own or in mixtures. The monomer impregnation solution consists of additives or modifiers such as cross-linking agents, plasticizers, initiators, promoters, retarders, and acceptors. However, owing to the nature of the components of the impregnation solution, the latter is generally toxic, combustible, and volatile. Thus, attention should be paid to safety measures [5].

There are two types of manufacturing processes: impregnation of precast concrete components and impregnation of onsite cement concrete. Both processes involve the following steps: (1) drying of the concrete, (2) monomer impregnation, and (3) polymerization of the monomer. The purpose of drying is to remove water from the concrete. For instance, the concrete can be dried via heated air or infrared radiation. The recommended drying temperature is 150 °C. The application of vacuum and pressure can improve the speed and effectiveness of the impregnation process. Polymerization of the monomer can be initiated by radiation, chemical, and heating methods. The latter method is the most common because of its simplicity. Figures 4.5 and 4.6 show the flowcharts of the impregnation processes of precast mortar or concrete, and onsite concrete, respectively.

Polymer impregnation greatly improves the mechanical, durability, and chemical resistance properties of conventional cement concrete. Table 4.5 shows the properties of concrete impregnated with polystyrene and polymethyl methacrylate. The compressive, flexural, and tensile strength properties of impregnated concrete are 2–4 times higher than those of non-impregnated concrete. However, the polymer-impregnated concrete behaves more like a brittle material. The stress–strain curve remains linear below a maximum loading of 75% (Fig. 4.7). The threshold energy for fracture and toughness is higher when compared with that of non-impregnated concrete. Polymer impregnation also enhances the bonding between the cement and aggregate. Fracture appears to run through the aggregate.

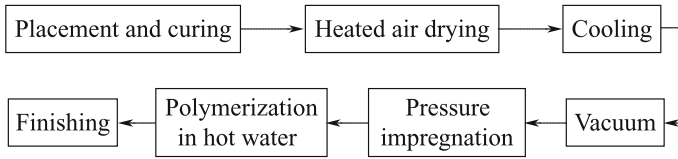


Fig. 4.5 Impregnation process of precast concrete

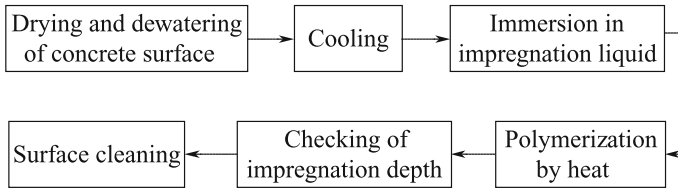


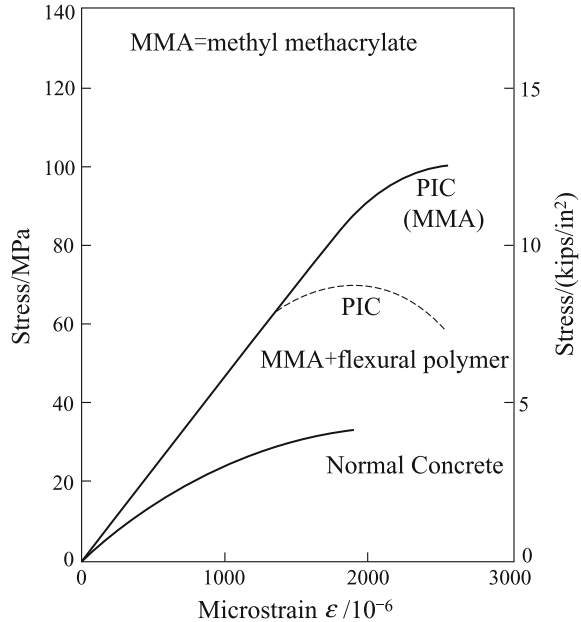
Fig. 4.6 Impregnation process of onsite cement concrete

Table 4.5 Properties of polymer-impregnated concrete

	Non-impregnated	Styrene	MMA
Compressive strength/MPa	37	70	127
E-Modulus/ $\times 10^4$ MPa	2.5	5.2	4.3
Tensile strength/MPa	2.9	5.9	10.6
Flexural strength/MPa	5.2	8.2	16.1
Water adsorption/%	14	6	4
Abrasion resistance/mm	1.26	0.93	0.37
Cavitation resistance/mm	8.13	0.23	0.51
Water permeability/(mm/a)	0.16	0.04	0.04
Thermal conductivity (23 °C)/[kJ/(m·h·°C)]	1.98×4	1.94×4	1.88×4
Thermal expansion ($\times 10^{-6}$ cm/cm·°C)	7.25	9.00	9.48
Freezing and thawing resistance (No. of cycles, weight loss/%)	490, 25.0	620, 0.5	750, 0.5
Sulfate acid resistance (300 days, expansion/%)	0.144	0	0

Because of incomplete impregnation or polymerization processes, and the onset of shrinkage during the reaction, the impregnated concrete also features some porosity. The strength and the Young's modulus (*E*-modulus) of the impregnated concrete are dependent on the porosity. The strength of polymer-impregnated concrete, prepared by radiation methods, is higher than that prepared by heating methods. The reaction by radiation methods is more complete than that by heating methods, especially when monomers that are difficult to polymerize are involved such as styrene. However, the strength of polymer-impregnated concrete is considerably reduced with increasing temperatures that instigate the softening of the

Fig. 4.7 Stress–strain curves of PIC and normal concrete



polymer. This behavior can be reduced by introducing cross-linking agents. For instance, polystyrene-impregnated concrete, comprising a cross-linking agent, can be safely used up to a temperature of 180 °C (355 °F).

The creep of polymer-impregnated concrete is very low, only about 1/10 of that of normal concrete. This is because, prior to impregnation, the concrete is fully dried. Consequently, no drying shrinkage is expected. Under high temperature conditions, the tendency toward deformation increases as the polymer starts to soften.

Polymer-impregnated concrete has the potential of improving the durability of concrete without the need of increasing the mechanical properties. The remarkable improved durability following impregnation (Table 4.5) is mainly credited to the reduced permeability of the matrix. Because the capillary pores are filled up with the polymer, the corrosive agent can only attack the outer surface of concrete, and thus, it is not able to diffuse into the concrete. In addition, a polymer “shell” forms at the outer surface of the concrete. Partial polymer impregnation can also result in comparable improved durability properties, as caused by the effective sealing of the concrete surface despite the small contribution toward the mechanical properties. However, particular attention should be paid to the formation of a uniform impregnation layer when performing partial impregnation. The drying process prior to impregnation also contributes to the improved durability properties; because of the absence of free water molecules for freezing, the resistance to freezing and thawing is improved.

Polymer materials are combustible; however, when polymers are distributed into the concrete, they do not support combustion. Even so, the polymer can produce harmful smoke and carbon upon combustion. This problem can be solved by using a flame retardant. The most important problem is that the mechanical properties of polymer-impregnated concrete could be reduced when exposed to high temperatures, thereby limiting its application under high temperature conditions.

Because of the complex production process and associated high costs, the application of polymer-impregnated concrete is limited. Polymer-impregnated concrete is mostly used in view of its high durability. The application areas of precast products of polymer-impregnated concrete include concrete drainage pipes, tunnel support-lining systems, underground supporting systems for mining, railway sleepers, piers, and precast piles for seawalls. In situ impregnation processes have a very promising future in the bridge decking and corrosion-resistant flooring industries.

4.1.3 Macro-Defect-Free Cement (MDF)

In the early 1980s, Birchall from the United Kingdom Imperial Chemical Company and his partners developed a new type of polymer-modified cement-based material, named macro-defect-free (MDF) cement, and fabricated the first cement-based spring in the world using this material. It caused great impact in the field of cement-based materials, and this was recognized as one of the great breakthroughs in the research and development of cement-based materials [6–9].

MDF cement materials are composed of ordinary portland cement or high alumina cement, water-soluble high molecular polymers (e.g., PVA and HPMC). The fabrication process is described as follows: Cement, PVA, and water (weight ratio of 100:7:11) are mixed in a bowl-type mixer to form a crumb paste. The resulting mixture is then fed onto a twin-roll mill. After thorough mixing at a very high shear rate ($\approx 100 \text{ s}^{-1}$) for 30 s, a plastic mixture with a very low yield stress, almost similar to the real plastic material (putty), is formed. The mixture is sheared to form a sheet that is then cured at 80 °C and a suitable pressure (5 MPa) for 10 min to remove entrapped air. The sheet is cut accordingly into different sizes and shapes. The mixture can also be extruded to form complex shapes. To achieve optimum strength development, the specimens are dry-cured at 80 °C for 25 h to remove excess solvent and complete the cross-linking of the polymers.

The most important features of MDF cement are as follows: very tiny pores ($<15 \text{ }\mu\text{m}$), very low porosity (generally below 1%), and high strength (flexural strength can be higher than 250 MPa). The engineering properties of MDF cement are listed below:

Compressive strength	>500 MPa
Flexural strength	250 MPa
<i>E</i> -Modulus	50 GPa

Fracture toughness	$3 \text{ MPa}\cdot\text{m}^{-1/2}$
Density	$2400 \text{ kg}\cdot\text{m}^3$
Thermal expansion	$10^{-6} \text{ }^\circ\text{C}^{-1}$

Based on the fracture theory of Griffith, the inventors of MDF cement suggested that the very high strength of MDF is due to the removal of large pores that control the strength in conventional cement paste. In recent years, further studies on the function of polymers in MDF cement showed that the removal of large pores is a contributor for the high strength property. It is now agreed that both the chemical and physical action achieve the high performance. The polymers in MDF cement serve as plasticizers, reducing the friction between the particles, and reaction with the hydrated products of cement. There is a complex structure similar to ceramic that forms between the cement and polymer. Therefore, many scientists suggested “organic cement” as a more appropriate name.

Initially, MDF cement suffered from moisture sensitivity, i.e., the mechanical properties drop dramatically under a high humidity environment. For example, the flexural strength after soaking in water for seven days drops to only about 30% of the original strength. After drying, the strength can be partially recovered, but it is not as high as the original value. The reasons for the MDF cement water sensitivity are as follows: Water-soluble polymers soften after absorbing water; loss of hydrated cement particles at the surface; rehydration of dehydrated cement particles causes interfacial damage; and the degradation of polymer in the high alkaline conditions caused by the hydration of cement. Obviously, the water solubility of the polymer is the main cause of the MDF moisture sensitivity. Using water-insoluble polymers is the best method to overcome this problem. By using high alumina cement, phenolic aldehyde monomer, and a plasticizer as main raw materials to produce MDF cement, there is no need to add water during processing. The water for the hydration of cement comes from condensation of the phenolic aldehyde. The materials produced this way do not contain any water-soluble polymer phases. Thus, the moisture sensitivity of MDF cement with PVA or PAM can be fundamentally solved, and the water resistance can be greatly improved. The typical composition is shown in Table 4.6.

Table 4.6 Composition of phenolic aldehyde–high alumina MDF cement

Material	Ratio by weight	Wt/%
High alumina cement	100.00	79.8
Phenolic aldehyde resin	13.06	10.4
Methanol	8.24	6.6
N-Methoxymethyl 6-nylon	1.70	1.4
Glycerin	2.30	1.8

N-Methoxymethyl 6-nylon for improved workability; glycerin used as a plasticizer

The equipments and methods for the fabrication of the material are the same as those used for conventional MDF materials. However, depending on the targeted performance, the hot-press program may be adjusted. For example, a flexural strength of 120 MPa can be achieved by curing at 200 °C for 18 h. If hot-press curing is performed at 80 °C and 6 MPa, the flexural strength can be doubled. To achieve optimal flexural strength, the heating rate must be slow and the temperature should be maintained at ≥ 65 °C for more than 30 min. Table 4.7 lists the typical properties of phenolic aldehyde–high alumina MDF cement.

As shown in Fig. 4.8, MDF materials derived from phenolic aldehyde–high alumina cement were subjected to outdoor conditions or water for one year. The *E*-modulus of the materials remains unchanged, and the flexural strength only dropped slightly. The moisture sensitivity issue was thus solved. A concrete company from Japan assessed the application of MDF cement, derived from phenolic aldehyde–high alumina cement, in various areas. Figure 4.9 shows a thermal insulation sheet machine component, fabricated from this MDF cement. MDF cement is especially suitable for lightweight shell structures, and lining layers used inside buildings. However, because it is still a new type of material, it has not been commercially applied yet.

Table 4.7 Typical properties of phenolic aldehyde–high alumina MDF cement

Property	Data	Property	Data
Flexural strength/MPa	120–220	Density	2.2
Flexural E-modulus/GPa	32–45	Thermal expansion rate/ $10^{-6} \text{ }^\circ\text{C}^{-1}$	17.8
Compressive strength/MPa	300	Thermal conductivity/[W/(m·K)]	0.8
Critical stress intensity factor/ $\text{MPa}\cdot\text{m}^{1/2}$	1.8	Electric resistance/ $\Omega\cdot\text{cm}$	$10^{13}\text{--}10^{14}$

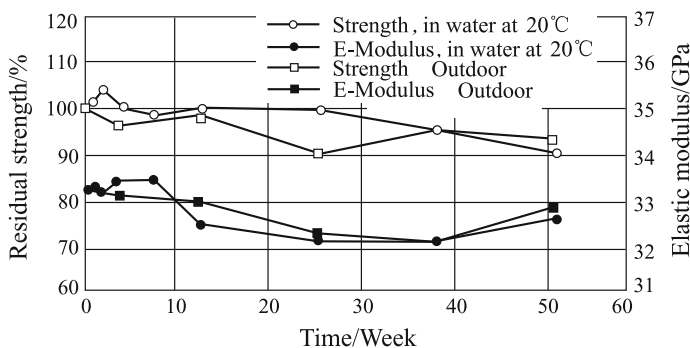
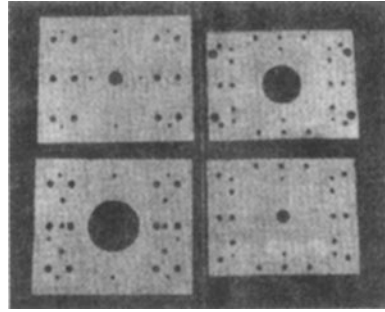


Fig. 4.8 MDF materials derived from phenolic aldehyde–high alumina cement

Fig. 4.9 MDF-based thermal insulation sheet



4.2 Fiber-Reinforced Cement-Based Composites

Fiber-reinforced cement-based composites consist of cement-based materials (e.g., hardened cement stone, mortar, and concrete) as the matrix, and metal fibers, inorganic fibers, or organic fibers as the reinforcing phase. The composite materials can overcome the limitations of cement-based materials such as low tensile strength, high brittleness, low cracking resistance, and low ultimate tensile strain.

The fibers for fiber-reinforced cement-based composites can be classified according to the materials properties: metallic fibers (steel and stainless steel fibers), inorganic fibers (including natural mineral fibers such as asbestos, alkali-resistant glass, alkali-resistant mineral, carbon, and other artificial mineral fibers), and organic fibers (including polyethylene, polypropylene, nylon, aromatic polyimide, artificial, and natural vegetable fibers such as sisal). They can also be classified according to the E -modulus of the fibers: high-modulus fibers (whereby the E -modulus is greater than that of cement-based materials such as steel, carbon, and glass fibers) and low-modulus fibers (such as polypropylene and some vegetable fibers). Also, there are non-continuous short fibers and continuous long fibers.

Currently, in the civil and construction industries, only steel fiber- and glass fiber-reinforced cement-based composites find the most application. Steel fiber- and glass fiber-reinforced cement-based composites and some high-performance fiber-reinforced cement-based composites developed in recent years are introduced in the following section.

4.2.1 Glass Fiber-Reinforced Cement-Based Composites (GRC)

The alkaline nature of cement hydrates causes the corrosion of glass fibers that damages the SiO_2 network, thereby dramatically reducing the strength of the glass fibers in cement paste. Therefore, necessary selection and treatment of the cement paste and glass fibers must be performed for the application of glass fiber-reinforced

cement-based composites. For example, the use of low-alkaline high alumina cement (pH of this liquid phase is in the range of 11.8–12.05, total amount of alkali is 0.15–0.20%, and during hydration, calcium hydroxide does not appear), or the use of pozzolan materials such as fly ash or partially fine sand-substituted cement. Fly ash and fine sand will absorb calcium hydroxide, released from the hydration of cement to produce hydrated calcium silicate, thereby improving the corrosion resistance of the glass fibers and the durability of the glass fiber-reinforced cement-based composites. During the manufacturing of glass fiber-reinforced cement-based composites, glass fibers with good alkaline resistance, such as A glass, E glass, and zirconia glass, should be selected. Zirconia glass has a higher alkaline resistance than the other two types of glass matrices. Generally, the content of glass fiber in glass fiber-reinforced cement-based composites is around 5% by weight of cement (in the range of 3–6%) [10–13].

4.2.1.1 Production Technology of Glass Fiber-Reinforced Cement-Based Composites

The performance of glass fiber-reinforced cement-based composites greatly depends on the fabrication methods. The production method for GRC was initially based on that used for glass fiber-reinforced plastics. Gradually, methods suitable for cement-based materials were developed, and described as follows:

1. Gravity molding: The premix, containing the glass fibers, is poured into the opening molds or two-side molds. The attached vibrators ensure even distribution of the premix in the molds. This method is similar to the one used for conventional precast concrete, and the advantage of this method is that very thin cross-sectional products can be prepared.
2. Compression molding: The premix is pressed in the mold to improve the density and surface finish. This method is mainly used to produce thin materials with a simple shape and decorative finish.
3. Injection molding: The premix, containing the thickening agent and glass fibers, is injected using a pump into the airtight molds to produce window frames, fence poles, hollow columns, and other products. The disadvantage of this method is the occurrence of glass fibers' damage during injection, forming pinholes on the surface.
4. Extrusion molding: Materials with complex shapes can be produced, as assisted by vibration that ensures premix flow and even distribution in the molds. By adjusting the vibration and extrusion parameters, the fibers can be arranged into specific orientations.
5. Spray-up process: This includes spray-suction and direct spraying methods that have the same working principles. In the spray-suction method, the continuous fibers are drawn to the spray gun by compressed air, and are cut into sections with a length of 10–50 mm. The chopped fibers and cement mortar are simultaneously deposited from the spray gun onto a prepared mold surface. The

excess water is then removed by vacuum suction. This method can be fully automated.

6. Winding-up method: This process is mainly used for the production of GRC pipes. The continuous fibers are immersed in the tank, containing the cement paste, and then wound to the roll according to the prescribed angle and distance. During the process, the chopped fibers and cement paste will be simultaneously sprayed into the roll. The product is then pressed by a press machine to remove excess water and cement paste. Because the products fabricated by the winding-up method have a very high glass fiber content, up to 15% by volume, the products possess high strength.
7. Layers-press method: The continuous fibers, glass fiber felts, or continuous fiber fabrics, following immersion, are poured into molds. Impregnation is enhanced by vibration or press.

4.2.1.2 Properties of Glass Fiber-Reinforced Cement Composites

1. Mechanical properties

The various strength properties of glass fiber-reinforced cement composites are improved to different degrees compared with those of cement base materials where the improvement in tensile, flexural, and impact strength, and fracture toughness is very obvious. Furthermore, the improvement depends on the composite fabrication conditions such as volume content of fibers, length of fibers, and the properties of the cement base materials.

At a given water/cement ratio, the tensile strength of the cement base material is at most 5 MPa; however, through the addition of glass fibers, the tensile strength of the composites linearly increases with increasing content. However, above a specific concentration, the properties of the composites do not improve further, but rather decrease, as shown in Fig. 4.10. The reason for this phenomenon is as follows: At a high concentration of glass fibers, the workability of the mix is greatly reduced. The workability can only be improved by adding water. Also, a large amount of air is introduced into the mix if excess fibers are added. This increases the porosity of the composites and decreases the bonding at the interfaces, therefore causing a drop in the properties of the composites. The addition of glass fibers clearly improves the impact and fracture performance of the composites. The studies showed that the impact resistance of glass fiber cement composites increased linearly with the volume content of glass fibers. However, if the glass fiber content is below 5%, improvement of the compressive, torsional, and shear strength between layers, and the E -modulus is not obvious.

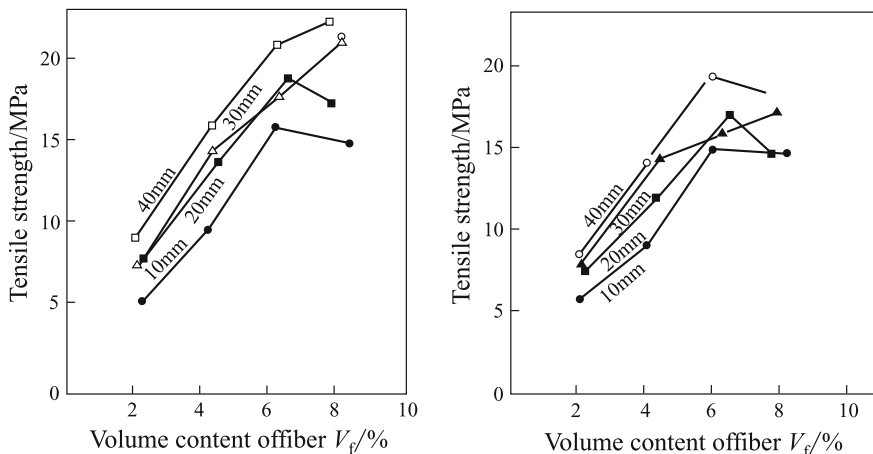


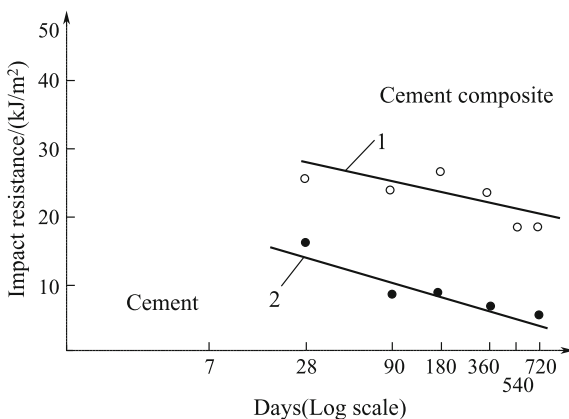
Fig. 4.10 Relationship between the tensile strength and volume content of fiber of glass fiber-reinforced cement composites, assessed over 28 days

2. Durability

Although low-alkaline cement and alkali-resistant glass fibers are used for cement-based composites, corrosion of the cement base phase will still occur in the long term. Therefore, the various properties (especially the impact resistance and tensile strength) of the glass fiber-reinforced cement-based composites will decrease with time. Increasing the alkali resistance of glass fibers is proposed as one of the most effective ways to improve the durability of GRC. Figure 4.11 shows the change of the impact resistance of glass fiber-reinforced high alumina cement-based composite with time.

To improve the durability of GRC, modification to the glass fiber was carried out: Alkali-resistant glass fiber containing ZrO_2 was developed. After immersion of

Fig. 4.11 Change of the impact resistance of glass fiber-reinforced high alumina cement-based composite with time



the modified glass fiber in an alkaline solution of cement paste, the tensile strength initially decreased dramatically. However after 180 days, the tensile strength remained unchanged. Furthermore, the E -modulus did not change notably. Coating of various resins on the normal glass fiber is also used to improve the durability.

4.2.1.3 Application of Glass Fiber-Reinforced Cement-Based Composites

With the advantages of lightweight and high strength, glass fiber-reinforced cement-based composites can be used as cladding panels. The trend of GRC cladding is thinning and upsizing. Cladding panels with a size of $5.5 \text{ m} \times 2.5 \text{ m}$ and thickness of 5–10 mm are now available on the market. Sandwich structures, composed of GRC panels, thermal insulation, or shield materials, can be used for lightweight and thermal insulation products for high-rise buildings. Another application of GRC is to fabricate molds that include square-shaped molds for in situ concrete floor casting and molds for bridge construction purposes. GRC can also be used in the construction of floating wharfs, docks, and boat scaffolds. Experts stipulate that with the development of technology it would be possible to use GRC pipes, with a diameter of 1 m, as a replacement for heavy steel concrete pipes.

4.2.2 Steel Fiber-Reinforced Cement-Based Composites

Among the various fiber-reinforced cement composites, steel fiber is the most effective for improving the properties of cement-based materials. The early studies on fiber-reinforced cement composites involved steel fiber-reinforced cement-based composites that achieved the most abundant results. Hence, steel fiber-reinforced cement-based composites found extensive application in the road pavement, runway, bridge deck, roof waterproofing, floor, hydraulic engineering, port, marine engineering, tunnel, culvert, building scaffolding, earthquake proofing construction, framework joint, anti-detonation engineering, and ballistic trajectory industries. Owing to their excellent technical and economic advantages, steel fiber-reinforced cement-based composites are currently recognized worldwide as one of the best cement-based composites [14–19].

4.2.2.1 Properties and Types of Steel Fiber

The parameters defining steel fibers include length of fiber (l_f), diameter of fiber (d_f), length/diameter ratio (l_f/d_f), shape of fiber, and strength and E -modulus of fiber. In most applications, the strength and E -modulus of steel fibers are always much higher than those of cement materials. Hence, the effect of these two

parameters on the performance of steel fiber-reinforced cement-based composites is not distinct. However, the size and shape of the fibers are closely related to the performance of the composite materials.

The most common dimensions of circular steel fibers are $d_f = 0.4\text{--}0.8$ mm and $l_f = 25\text{--}60$ mm. A short fiber length will affect the strength of the fiber. However, it is difficult to achieve an even distribution of fibers in cement materials, potentially causing caking, if long fibers are used. This would compromise the performance of the composite materials. Furthermore, if the fiber is too long and longer than its critical length (l_{fcr}), the failure mode of the steel fiber will change from “pull-off” to “broken,” and this will be unbeneficial to the toughening effect. The length/diameter ratio (l_f/d_f) is another important parameter affecting the strength of the steel fibers. Within a certain range, higher l_f/d_f values produce stronger steel fibers. The length/diameter ratio is typically smaller than 100; the most common value is 40–80. For non-circular fibers, d_f is denoted as the equivalent diameter d_{fe} . A. E. Naaman proposed that for most non-circular fibers, a fiber intrinsic efficiency ratio (FIER) should be used as a substitute to the length/diameter ratio. The fiber intrinsic efficiency ratio can be defined as the ratio of the surface area of the side bonded face to the cross-sectional area:

$$\text{FIER} = \frac{\psi L}{A}. \tag{4.1}$$

Figure 4.12 illustrates the relative FIER values of a circle, square, triangle, and rectangle. At a given cross-sectional area, the triangle can improve the effect by 28% when compared with the circle and square that give a 12% improvement. For the same fiber usage, the higher the FIER value of the fiber, the better performance the composite materials will have; or for the same performance requirement, the fiber usage can be reduced.

In fact, there are unlimited combinations of fiber geometry parameters such as cross-sectional shape, length, diameter or equivalent diameter, and surface shape. The cross-sectional shape can be a circle, square, rhombus, rectangle, triangle, polygon, or rough polygon. To improve the bond between the fiber and base material, the fiber can be roughened along the length or mechanically deformed. Therefore, fibers can be smooth, indented, round with end paddles, round with end buttons, round with hooked ends, or crimped. The typical profiles of steel fibers

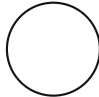

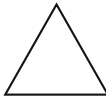

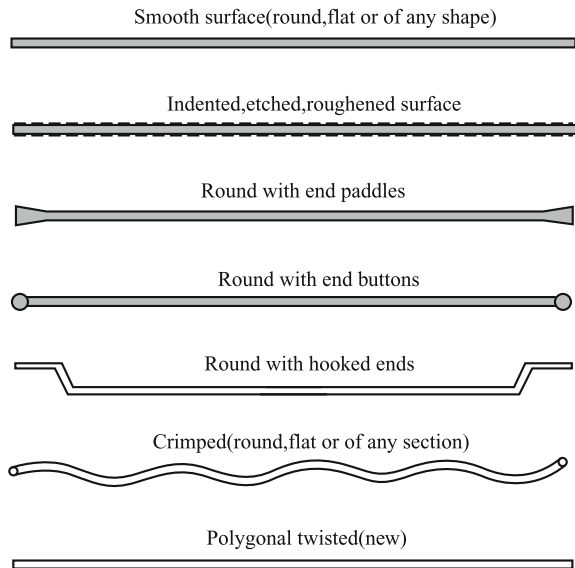
Section Shape				
Relative FIER	1	1.12	1.28	> 1.28

Fig. 4.12 Possible fibers’ sections and corresponding FIER values

Fig. 4.13 Typical profiles of steel fibers commonly used in concrete



commonly used in concrete are shown in Fig. 4.13; the polygon-based twisted fiber is the most recent fiber, developed by Prof. A. E. Naaman.

Based on diverse experimental research and engineering practice, steel fibers with hooked ends provide the best strengthening, toughening, and cracking resistant properties to concrete whereas fibers with a rectangular straight shape provide minimal improvement. The hooked ends of the steel fibers can not only enhance the binding between the steel fiber and cement base, but also increase the interfacial bonding between the fiber and cement. Furthermore, the angle between the fiber base and the hooked ends (normally 120°) can reduce the stress-concentration dependency, and will not cause local damage in the cement base when the composite is under loading. Compared with the rectangular straight fiber, under the same fiber usage conditions, fibers with hooked ends can improve the tensile strength of fiber-reinforced composites by 15–20%. The recently developed polygonal twisted fiber is very effective for improving the mechanical bonding. This is done by twisting the fiber to achieve a profile similar to that of a screw. To achieve twisting, fibers must have a polygonal cross section, capable of developing ribs along the fiber length. Round fibers cannot develop ribs during twisting, and flat fibers form tubelike tunnels that act as sites to stress concentration, thereby impeding diffusion by the matrix. Polygonal fibers have a higher surface-to-area ratio that improves the frictional and component adhesive bonding (Fig. 4.3). Additionally, they can be twisted, resulting in a very effective mechanical anchorage or mechanical bond. The results indicated that improvement in bonding between the fiber and matrix by twisting is much greater than that obtained by other mechanical-based deforming methods.

4.2.2.2 Production Technology of Steel Fiber-Reinforced Cement-Based Composites

The production technology of steel fiber-reinforced cement-based composites is very similar to that of conventional concrete. However, there are specific requirements on the production control: The most important requirement is to ensure that the fibers are evenly distributed in the matrix without caking. Only uniformly distributed steel fibers can improve the strengthening, toughening, and crack-resistant properties of the cement matrix. The production of steel fiber-reinforced cement-based composites typically consists of three phases that are dosing/mixing, transporting, and casting. The dosing/mixing and transportation steps have the most effect on the quality of composites produced.

There are three main mixing methods for preparing steel fiber-reinforced cement-based composites: (1) dry–wet mixing: All the solid components such as the steel fiber, coarse aggregate, fine aggregate, and cement are first premixed in the dry state. Water is then added for wet mixing. This method affords homogeneous distribution of the fibers in the cement matrix while avoiding caking of the steel fibers; (2) wet mixing: The coarse aggregate, fine aggregate, and cement are premixed in the dry form, and water is then added. During the wet mixing process, the steel fibers are evenly added, using a steel fiber distribution machine. Mixing is continued for a while. The use of the steel fiber distribution machine for the wet mixing method is essential to preventing caking; (3) gradual addition and mixing: 50% of the coarse and fine aggregate is mixed with the fibers under dry conditions. The remaining coarse and fine aggregate is then added to cement and water for wet mixing. This method requires longer mixing time.

For casting and finishing, vibration and shotcreting are the most commonly used technologies. The vibration method is similar to that used for preparing normal concrete. The equipments used should be table-type vibrators. If plug-type vibrators are used, the angle of the vibrator to the plane must be less than 30°, and the vibration period cannot be too long. In the shotcreting technology, the mixture of steel fibers and cement matrix is sprayed, by compressed air, over a designated spot. Shotcreting is suitable for structure scaffolding, strengthening, and repairing. Other methods for preparing specific steel fiber-reinforced cement composites include extrusion, grouting, and immersion.

4.2.2.3 Properties of Steel Fiber-Reinforced Cement Composites

1. Mechanical properties

Steel fiber can greatly improve the axial tensile strength of cement matrices. For example, for Grade C50 concrete, with the addition of 2% steel fiber by volume, the initial cracking strength can be increased by 135% (for rectangular straight fibers)

or 166% (for hooked-end fibers); the ultimate tensile strength can be increased by 182% (rectangular straight fiber) or 220% (hooked-end fibers); and the ultimate tensile strain can be improved by a factor of two or more.

Behavior under bending is the most important aspect for steel fiber-reinforced cement-based composites. Hence, research on the flexural properties of the composites is very extensive. The flexural properties of steel fiber-reinforced cement-based composites include flexural initial cracking strength, ultimate flexural strength, flexural toughness, and E -modulus. The above parameters can be obtained from the load–deflection curve. Depending on the properties of fibers (shape, size, and strength), for typical concrete, with the addition of 2% steel fiber, the flexural initial cracking strength can be increased by 75–100% and the ultimate flexural strength by 120–180%. For Grade C40 concrete, comprising 2% steel fiber, the toughness (according to the JCI simplified method) can be increased by a factor of 15 (for rectangular straight fibers) and 22.5 (for hooked-end fibers). However, the effect on the E -modulus is negligible at the low fiber dosage.

Steel fibers have little effect on the total strength of cement-based materials when compared with the influence on the tensile and flexural properties. For example, by adding 2% steel fiber, the total strength of cement-based materials with a W/C ratio of 0.40 can only be increased by $\sim 5\%$.

Steel fibers have a very distinct strengthening effect on the impact properties of cement-based materials. For example, according to the method proposed by the ACI Committee 544, with the addition of 2% fiber by volume, the initial cracking impacting number of steel fiber concrete can be increased by a factor of 12 ($l_f/d_f = 46$) and 14 ($l_f/d_f = 58$); the failure impacting number can be increased by a factor of 11 ($l_f/d_f = 46$) and 13 ($l_f/d_f = 58$); and the impact toughness can be increased by a factor of 10 and 14, respectively.

2. Durability

Frost resistance is one important property of cement-based composites. Steel fibers can improve the frost resistance of cement-based composites. After 300 freeze–thaw cycles, the relative dynamic E -modulus of cement-based composites, with a water/cement ratio of 0.51 and steel fiber volume dosage of 1%, only decreased by 7%. Contrarily, under the same conditions, the dynamic E -modulus of non-modified cement-based composites decreased by 50%. The general principle of improvement of frost resistance of cement-based composites by steel fiber is as follows: The cracking resistant steel fibers can effectively restrain the expansion during freezing; the steel fibers can also improve the pore structure of the cement-based composites. These two aspects can enhance and complement each other and hence achieve a double effect of “cracking resistance” and “buffering.” Therefore, frost damage of cement-based composites can be reduced and delayed.

Resistance to chloride corrosion is another important durability factor of steel fiber-reinforced cement-based composites. Owing to the small diameter and high specific surface area of steel fibers, the onset of corrosion causes a negative effect on the properties and life span of steel fiber-reinforced cement composites. This not

only compromises the strengthening and toughening effect of steel fiber, but also reduces the loading capacity and life span, and changes the failure model. The vast experimental research on the corrosion properties of steel fiber-reinforced composites in the UK, USA, Japan, and Australia showed that intact low-permeable steel fiber-reinforced cement-based composites have a good corrosion resistance under marine conditions. Contrarily, for high-strength steel fiber-reinforced cement-based composites, owing to the dense structure, the resistance to chloride corrosion can be improved further. The general proposed mechanism for the improved chloride corrosion resistance of steel fiber-reinforced composites is as such: The steel fibers can reduce the crack width of cement-based composites. The crack width in plays an important role toward the permeability of chloride ions in the cement-based composites. When the crack width is less than 0.2 mm, chloride ion diffusion is negligible.

4.2.2.4 Application of Steel Fiber-Reinforced Cement Composites

The application of steel fiber-reinforced cement-based composites is very wide. Steel fibers can be used in almost all industries. Steel fiber-reinforced cement composites play a key role for all structures and building products, which are subjected to high flexural–tensile loading, impact and fatigue loading, such as road pavements, airport runways, bridge decks, rooftops, industry floors, structures with rebar, structures without rebar, slabs, plates, columns, quake proof nodes, railway sleepers, and piles.

Road pavements are mainly subjected to static bending loading, dynamic fatigue loading, and thermal stress under heat expansion and cold shrinkage. Because conventional concrete pavements have a high brittleness, the tensile and flexural strength, and the crack resistance properties are very low. Pavements designed according to these properties have a high thickness and a short joint distance and life span. To overcome these problems, steel fiber-reinforced cement-based composites have been used for road pavements overseas since the 1970s and in China since the 1980s. In comparison with conventional concrete pavements, pavements constructed from steel fiber-reinforced cement-based composites (steel fiber volume dosage of 1–2%) have a reduced thickness of 40–50%; the joint distance can be increased by a factor of 8–10, and the fatigue number can also be an order of magnitude higher.

By adding 1–2% (by volume) steel fibers in the pre-stressed concrete sleeper, the latter matrix can not only withstand complex stress situations under dynamic loading, but the total loading capacity can also be greatly improved. Compared with normal concrete sleeper, the loading capacity of the steel fiber concrete sleeper can meet and exceed the requirements.

4.2.3 High-Performance Fiber-Reinforced Cement-Based Composites

Based on the proposal by the first international workshop on “High Performance Fiber Reinforced Cement Composites” that was held in Mainz, Germany, in June 1991, high-performance fiber-reinforced cement composites must not only have high strength and toughness, but also optimum combinations of workability, moldability, toughness, durability, impermeability, frost resistance, appearance, and stability. The materials described below can be considered as high-performance fiber-reinforced cement-based composites. [20]

4.2.3.1 Compact Reinforced Concrete (CRC)

Compact reinforced concrete (CRC) is a type of high-performance fiber-reinforced cement-based composite, containing steel fibers in the matrix of a densified system with ultrafine particles. [21–23]

1. Densified system with ultrafine particles (DSP)

The Aalborg Portland cement company (Netherlands) developed a new type of cement matrix called densified system with ultrafine particles. The binding materials of DSP are composed of portland cement, silica fume, and a superplasticizer.

Silica fume comprises spherical particles with a size in the range of 0.005–0.5 μm and average diameter of 0.1 μm . They are half the size of cement particles (0.5–100 μm). Therefore, silica fume is an ideal filling material for forming dense structures. Furthermore, owing to the amorphous structure of silica fume, the particles can react with the alkaline hydration products in the pores of the cement paste. To achieve a high density, a superplasticizer is used to disperse the cement and silica fume particles so that these particles can move easily during mixing and casting to avoid non-favorable effects on the workability.

The typical DSP binding material comprises 10–50% silica fume by weight of cement, 1–4% (solid content) of superplasticizer (surfactant), and a water/solid ratio (cement + silica fume) of 0.12–0.22.

In addition to filling the pores between cement particles and reacting with the ions in the alkaline solution in the pores, silica fume can block the capillary pores between cement particles to reduce the migration speed of liquid, in order to increase the cohesion of the DSP binding materials to the matrix (mortar, concrete). The bleeding behavior in the fresh state can be improved greatly. Hence, this type of material is very suitable for underwater casting and extrusion, and impression. DSP materials are more durable than normal cement paste. Owing to the blockage of capillary pores, chloride diffusion can be remarkably reduced. Studies showed that the chloride diffusion coefficient of DSP materials was an order of magnitude lower than that of normal cement paste. Even at temperatures below $-35\text{ }^{\circ}\text{C}$, freezing was not observed. Under rigorous freezing and thawing conditions, DSP

materials can last for nine months whereas high-quality concrete with a superplasticizer and a water/cement ratio of 0.25 will fail within two weeks. DSP materials thus have a very good frost resistance.

There is no doubt that DSP-based composites possess a high compressive strength. It can reach 130 MPa with normal aggregates, whereas with robust aggregates (e.g., calcined copiapite), the strength can be as high as 270 MPa (Fig. 4.14). DSP materials are very brittle: The higher the strength is, the more brittle they are. The brittleness is significantly higher than that of normal cement paste.

2. Compact reinforced concrete (CRC)

Compact reinforced concrete is produced by adding steel fibers to the DSP matrix to improve the mechanical properties, especially fracture performance (Table 4.8). When the volume dosage of steel fibers in DSP cement matrix reaches 4–6%, the composite will experience strain hardening.

Figure 4.15 shows the loading–deflection curve of CRC under a four-point bending loading and the loading–tensile strain profile, as measured by a strain meter.

The composition of this type of composite material is as follows:

1. Coarse quartz sand ($d = 4$ mm): 44.6%;
2. DSP binding material: 49.6% (cement: 47.6%; silica fume: 16.1%; water: 33.7%; and superplasticizer: 2.8%);
3. Steel fibers (6×0.15 mm): 3–12%.

The strengthening effect of fibers in CRC is enhanced because of the increased contact areas between the fibers and the surrounding matrix; the DSP matrix has a very dense microstructure in CRC. This was confirmed by pull-off tests performed on plain steel bars of 6 mm diameter, embedded 60 mm deep into the DSP cement mortar and

Fig. 4.14 Stress–strain curves of DSP and normal high-strength concrete

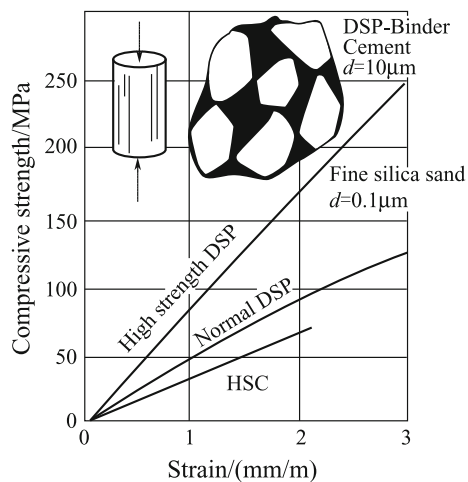


Table 4.8 Comparison of fracture properties of DSP paste, DSP mortar, FRDSP, cement paste, and concrete

Materials	Young's modulus/GPa	Tensile strength/MPa	Fracture energy/(N/m)	Crack zone deformation (CMOD)/ μm	Characteristic length/m	Critical stress intensity factor (K_{IC})/ $\text{MN}\cdot\text{m}^{-3/2}$
Cement paste	0.7	4	20	5	0.01	0.4
DSP paste	15	20	20 ^a	1 ^a	0.0008 ^a	0.5 ^a
Concrete	30	3	60	20	0.2	1.3
DSP mortar	50	20	100	5	0.0125	2.2
FRDSP (DSP mortar + steel fiber $V_f = 6\%$)	60	40	16000	400	0.60	31

^aEstimated data

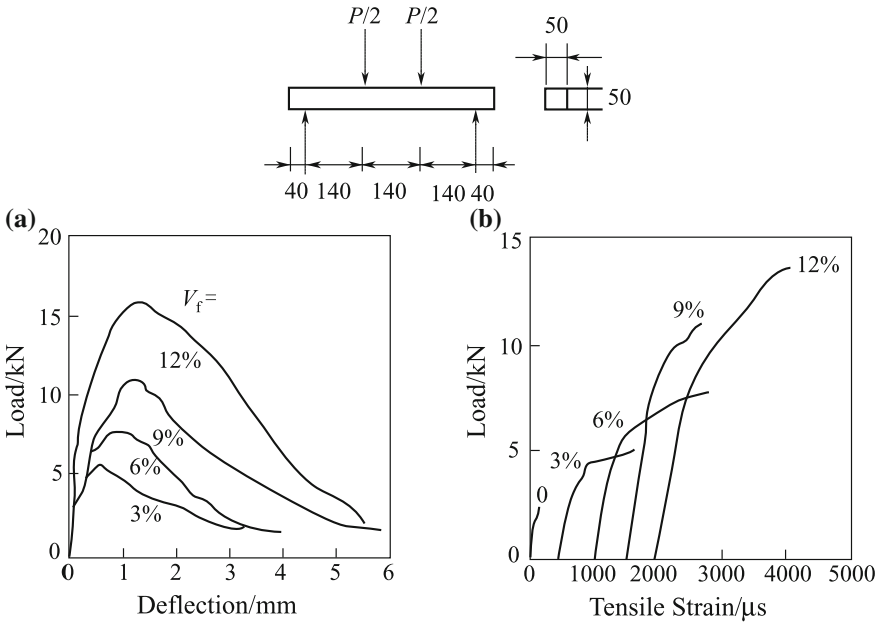
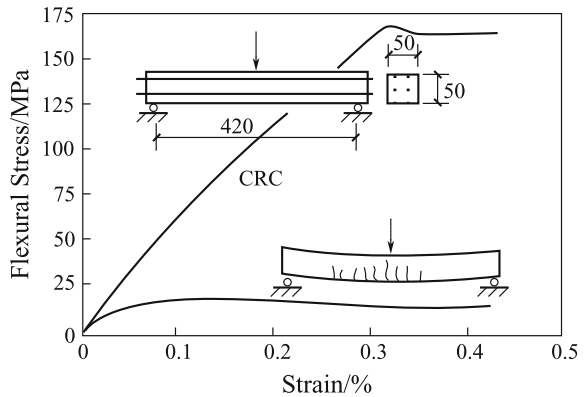


Fig. 4.15 (a) Loading–deflection curves of DSP materials with steel fiber under four-point bending. (b) Tensile strain, measured by a strain meter, with increasing loading

normal cement mortar. The ultimate tensile strain of CRC, with 6% steel fiber by volume (20% by weight) with length of 6 mm and diameter of 0.15 mm, is almost similar to the yield strain of soft steel. Even under the loading that would cause strain on the steel bars, the matrix will not crack. Bache reported the application of CRC bending products with addition of normal steel bar of 23% by the cross-sectional area. Figure 4.16 shows flexural stress–strain curve of a CRC beam containing normal steel bars. For comparison purposes, the curve of normal steel concrete beam is also shown.

Fig. 4.16 Flexural stress–strain curve of a CRC steel beam under a three-point loading. The load–deflection was recorded (maximum load is 31 kN), and the stress–strain was calculated according to the elastic beam theory. The stress–strain curve of normal steel concrete beam is also shown for comparison purposes



The flexural strength of the CRC beam is an order of magnitude higher than that of the normal steel concrete beam, comparable to that of steel structures. It should be emphasized that there are no surface cracks even under such a high strain. The details of the composition and rebar of the experimental CRC beam are as follows: quartz sand ($d = 4 \text{ mm}$): 44.6%; DSP binding material: 49.6% (cement: 47.6%, silica fume: 16.1%, water: 33.7%, superplasticizer: 2.8%); steel fiber ($6 \times 0.15 \text{ mm}$): 5.8%; longitudinal rebar: 5% deformed steel bars with a diameter of 8 mm. The longitudinal rebar occupied 10% of the cross-sectional area ($\rho \approx 0.1$).

Initially, CRC was only used as a concrete surface layer subject to a corrosive environment, and later used to replace rubber and steel as a lining material for containers and reactors. It was also used to produce molds and tools. It is expected that in the future, CRC will find wide application in the areas of low-temperature materials, tools, molds, rapid repair materials for building and roads, impact-proof materials, radiation shielding, fireproof, corrosion-resistant materials, treatment of dangerous wastes, and marine concrete structures. Because of high costs, the use of steel CRC as a replacement for normal steel concrete products is limited. Future research direction would include the development of structures near seacoasts, bridges, buildings in earthquake prone areas, and the defense engineering.

4.2.3.2 Reactive Powder Concrete (RPC)

Recently, P. Richard from Canada and M. H. Cheyrezy from France successfully developed a new high-performance steel fiber-reinforced cement-based composite called reactive powder concrete (RPC) that has a compressive strength of 200–800 MPa and fracture energy of 1200–40 000 J/m^2 . [24–27] The basic principle is to add steel fibers to improve the cement matrix, and the details are as follows:

1. Using ground fine quartz sand with a size of $<600 \mu\text{m}$ to replace the coarse aggregate and traditional sand, and adding silica fume with smaller particles than cement particles to improve the uniformity;
2. Optimizing the particle size grading (Fig. 4.17) and applying a press process before and during the setting of fresh concrete to increase the density;

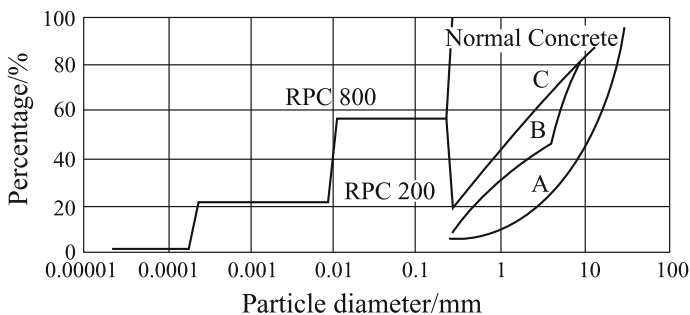


Fig. 4.17 RPC particle size grading curve

3. Applying a heat treatment after setting to improve the microstructure of concrete;
4. Adding steel fibers to make concrete ductile.

High-strength cement mortar can be produced based on the first three principles; however, the toughness is not better than that of normal cement mortar. With the addition of steel fibers, the tensile strength is increased and the required toughness is also achieved. The fracture energy of RPC greatly depends on the dosage of the steel fibers. Figure 4.18 shows the effect of volume dosage of steel fibers on the fracture energy. Straight carbon steel fibers with a diameter between 0.15 and 0.75 mm, and a length of 13 mm were used.

The composition and main mechanical properties of typical RPC200 and RPC800 are listed in Tables 4.9, 4.10, 4.11. A lower compressive strength (170 MPa) is achieved by curing at room temperature for 28 days, whereas a higher compressive strength (230 MPa) is achieved by curing in air for two days followed by heat curing. For RPC800, steel fibers with a length of 3 mm were used to replace the steel fibers with a length of 12 mm in RPC200. All other components were the same. After remolding, the specimens were pretreated by heating at 250–400 °C, and pressed at 50 MPa before and during setting. The fracture energy of RPC is 1200–20 000 J/m², which is ten times higher than that of normal concrete. If steel powder is used to replace quartz sand, the compressive strength can be as high as 800 MPa. Compared with normal mortar, RPC not only has a very high strength, but also a high flexure strain and good ductile properties.

Bouygues from France announced the development of RPC at the ACI spring meeting in San Francisco in 1994 for the first time. Currently, low compressive strength RPC is mainly used for the fabrication of structure components. High-strength RPC has been used as an anchor head of pre-stressed steel strands. The protection shield can withstand the impact of a bomb.

In normal situations, because of the high strength, high toughness, high density, and high durability, RPC can be used as a structure material without steel bars' reinforcement. When RPC is used as a structure element subject to bending (such as beams and slabs) or tension (such as girders), the pre-stressed technology can be applied to solve the unbalance problem associated with the compression and tension

Fig. 4.18 Effect of volume dosage of steel fibers on the fracture energy of RPC200

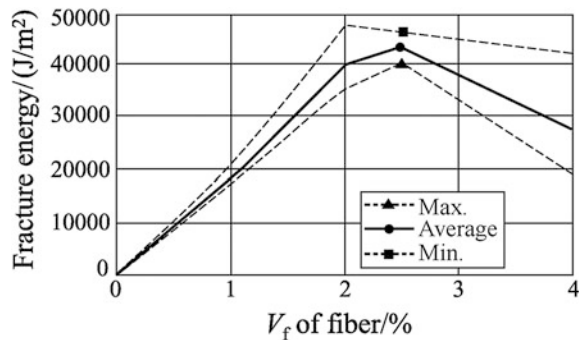


Table 4.9 Typical composition of RPC (by weight)

Material	RPC200				RPC800	
	No fiber		With fiber		Silica aggregate	Steel aggregate
Normal cement	1	1	1	1	1	1
Silica fume	0.25	0.23	0.25	0.23	0.23	0.23
Sand 150–600 μm	1.1	1.1	1.1	1.1	0.5	–
Crushed silica sand d ₅₀ = 10 μm	–	0.39	–	0.39	0.39	0.39
Superplasticizer	0.016	0.019	0.016	0.019	0.019	0.019
Steel fiber L = 12 mm	–	–	0.175	0.175	–	–
Steel fiber L = 3 mm	–	–	–	–	0.63	0.63
Steel aggregate d < 800 μm	–	–	–	–	–	1.49
Water	0.15	0.17	0.17	0.19	0.19	0.19
Casting pressure/MPa	–	–	–	–	50	50
Heat treatment temperature/°C	20	90	20	90	250–400	250–400

Table 4.10 Mechanical properties of RPC200 with active fine aggregate

Property	Index
Cylinder compressive strength	170–230 MPa
Flexural strength	30–60 MPa
Fractural energy	20 000–40 000 J/m ²
Young’s modulus	54–60 GPa
Failure strain	(5000–7000) × 10 ⁻⁶ mm ⁻¹

Table 4.11 Mechanical properties of RPC800 with active fine aggregate

Property		Index
Compressive strength	Silica aggregate	490–680 MPa
	Steel aggregate	650–810 MPa
Flexural strength		45–141 MPa
Fracture energy		1200–20 000 J/m ²
Young’s modulus		65–75 GPa

of RPC. In this case, the pre-stressed steel wires will withstand the main tensile stress whereas RPC will withstand the secondary tensile stress and all compressive loading. Figure 4.19 and Table 4.12 present the comparison of I-beams fabricated from RPC, steel, pre-stressed concrete, and reinforced concrete, respectively, with the same loading capacity. The cross-sectional size and mass per unit length of the RPC beam are all lower than those of the pre-stressed concrete beam and reinforced

concrete beam, and slightly higher those that of steel beam. The cost of RPC beams is higher than that of pre-stressed concrete beams and reinforced concrete beams, but lower than that of steel beams.

In Canada, Sherbmoke built an overbridge for pedestrians and bicycles using RPC. The bridge is single span with a length of 60 m, deck width of 4.2 m, and deck area of 202 m². The trusswork was made of RPC200 steel pipe concrete: stainless steel pipes with a diameter of 150 mm, wall thickness of 3 mm, and filled with RPC200. The lower camber is made of two RPC beams. The thickness of the RPC bridge deck is 30 mm; reinforced ribs, 70 mm high, were produced from normal concrete precast technology, and located at an interval distance of 1.7 m. Every precast segment is 10 m long and 3 m high, and is installed by a post-tension method after being transported to the site. The composition (weight) of RPC employed for the construction of the bridge is cement: 1; silica fume: 0.33; fine ground quartz powder: 0.3; quartz sand: 1.43; steel fiber: 0.2; superplasticizer: 0.03; water: 0.2; and water/binder ratio: 0.15.

Table 4.13 lists the raw materials' content used for the fabrication of RPC200, high-performance concrete (HPC60), and normal concrete (NC30), employed for the same project. The content can be greatly reduced by using RPC.

Three companies from France: Bouygues, Lafarge, and Rhodia partnered to develop RPC. Based on their patent, the trade mark "Ductal" was registered worldwide. Besides steel fibers, vinylon and polypropylene fibers are used as reinforcing materials. In recent years, a new type of fireproof fiber, DuctaAF, was developed. In May 2002, France published a report entitled "Design recommendation and application guideline for ultra high strength fiber-reinforced concrete."

Fig. 4.19 Cross section of I-beams made from RPC, steel, pre-stressed concrete, and steel concrete

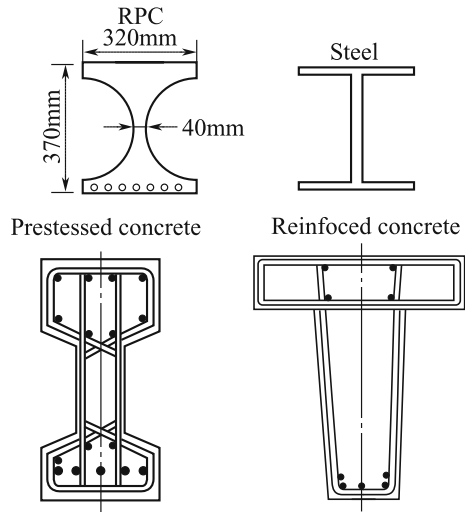


Table 4.12 Properties of I-beams made from RPC, steel, pre-stressed concrete, and steel concrete beam

Items		RPC	Steel	Pre-stressed concrete	Steel concrete
Section Shape/mm	Height	370	350	700	700
	Width	320	300	350	600
Mass/(kg/m)		140	112	467	530
Relative price per meter		450	500	390	400

Table 4.13 Raw materials' content in three concrete materials

Items	NC30	HPC60	RPC200
Effective section thickness/mm	500	400	150
Concrete volume/m ³	126	100	33
Binder consumption/(kg/m ³)	350	400	705
Total cement amount/t	44	40	27
Total aggregate amount/t	230	170	60

4.2.3.3 Slurry-Infiltrated Fiber Concrete

Conventional steel fiber-reinforced concrete composites comprise steel fibers and various components of normal concrete. If the length/diameter ratio of the steel fiber and the fiber volume fraction are too high, mixing and placing become difficult and caking will occur. Generally, the fiber volume fraction is limited to <2% for normal steel fiber-reinforced concrete [28–33].

To increase the fiber volume fraction in concrete for producing thin wall elements, a casting method using a pre-placing technique in which fibers are placed in a mold and infiltrated with a cement-based slurry was first published by Haynes in 1968. Since 1978, Lankard and co-workers have conducted a systematic and comprehensive research on this casting method, and managed to increase the steel fiber volume fraction to at most 20%. A fiber-reinforced cement-based composite with a high strength and ductility was developed and called SIFCON. Because of the pre-placing technique, SIFCON has a higher fiber volume fraction, high length/diameter ratio, optimum fiber orientation, and better bonding strength by selection of the matrix, translating to unique mechanical properties.

SIFCON does not contain coarse aggregate in the cement matrix; it normally consists of a slurry of cement and silica fume or fly ash or fine sand. The addition of silica fume (around 10% of the cement weight) benefits toward the improvement of strength. The addition of fly ash can improve the workability of the slurry. The fine sand used in the slurry (particle size smaller than 125 μm) can reduce the shrinkage; generally, the binder/sand ratio is around 1:1–1:1.5. In most cases, high-range water-reducing admixtures are used in order to improve the flowability of the slurry. The water/binder ratio of the slurry is generally around 0.30–0.35. Both flowability and strength should be considered when developing the matrix (slurry) composition.

The fabrication technique of SIFCON is as follows: Steel fibers are placed manually or by machine in the mold or on a substratum. The volume fraction of the steel fibers in the molds depends greatly on the geometry of the steel fibers and the placing method; it is normally in the range of 5–20%, and occasionally can be up to 27%. The mixed slurry is then infiltrated into the molds or fiber nests. To achieve complete filling of the fiber nests, vibration can be applied to the molds. When the fiber volume fraction and the infiltration ratio are high, the injection method should be used. The orientation of the fibers in SIFCON depends on the shape and size of the elements, length of fibers, and the placing method. In the fabrication of precast elements with a thickness of less than 25 mm, the fibers tend to orient themselves randomly in a two-dimensional (2D) configuration. The shorter the fibers, the higher the tendency for the fibers to adopt a three-dimensional orientation. For plate elements, if the fibers are manually placed, they will trend to adopt a 2D orientation. The fiber density at the edges of the mold is lower than that at other locations. In some places, there are either no fibers or the fibers are vertically oriented. This phenomenon, referred as the “fringe effect,” can be solved by inserting the mold, containing the fibers, in a magnetic field at a certain intensity.

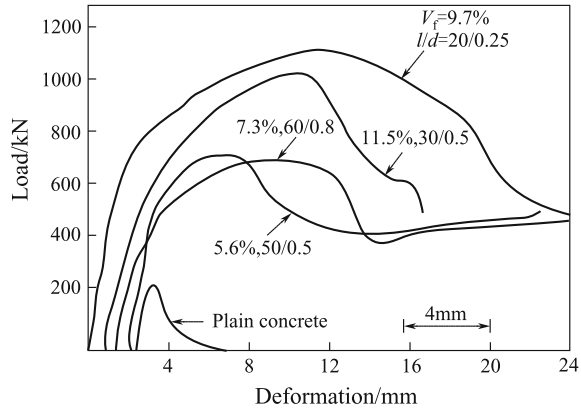
The main factors affecting the mechanical properties of SIFCON include matrix properties, fiber volume fraction, fiber orientation, and fiber geometry.

Matrix properties, especially the bonding strength to the steel fibers, have a great effect on the mechanical properties of SIFCON. Hence, by using high-strength cement, low water/binder ratio, low fly ash content, and adding adequate silica fume, all benefit to the improvement of the mechanical properties of SIFCON.

The fiber volume fraction of normal steel fiber-reinforced concrete cannot typically exceed 2%, and has no obvious effect on the compressive strength. The steel fiber fraction in SIFCON is very high, so that the compressive strength can be greatly improved. By varying the fiber fraction, the compressive strength can be increased by a factor of 2–3. The orientation of the fiber also has an important effect on the compressive strength of SIFCON. The compressive strength is higher when fibers are oriented perpendicular to the loading axis. Fiber geometries also have an effect, to some extent, on the compressive strength of SIFCON. The SIFCON specimens prepared in the laboratory by Lankard can reach a 63–190-MPa compressive strength at 28 days, and can be as high as 210 MPa. Figure 4.20 shows the typical load–deformation curve of a SIFCON specimen during compression. SIFCON not only has a very high compressive strength, but also a large strain capacity and ductility. The energy absorption is one to two orders of magnitude higher than that of a plain matrix. SIFCON specimens can better sustain micro-cracking before reaching the peak load and the onset of the strain-hardening phenomena. Lankard measured the elastic modulus of SIFCON that was in the range of 14–25 GPa under compression, which was higher than the matrix modulus.

Table 4.14 presents the effect of fiber geometry, volume fraction, and orientation, and bonding strength between the fiber and cement matrix on the tensile strength of SIFCON. Under the same conditions, the SIFCON specimens, with hooked-end fibers, have a higher tensile strength than those with straight fibers. The tensile strength is greater at the higher fiber volume fraction. Generally, with

Fig. 4.20 Load–deflection profiles during compression. The cylinder SIFCON specimens (10.2×17.8 cm, 28 days fog curing) contain 5.6 to 11.5% volume hooked-end steel fibers



ill-shaped fibers and a volume fraction of more than 10%, the tensile strength of the specimens is higher than 14 MPa, around twice as that of cement matrix, even when the fibers adopt a 2D configuration.

Figure 4.21 presents results for specimens made using a plain cement matrix ($w/c = 0.45$) and three different types of fibers. It can be seen that at a given volume fraction, the energy absorption and ductility of SIFCON specimens with hooked-end fibers are higher than those with surface-deformed fibers and deformed-end fibers. The energy absorption and ductility of materials increase with higher hooked-end fibers' volume fractions.

Balagum and Kendzulak investigated the effect of fiber length and volume fraction, and the matrix constituents on the flexural strength of SIFCON. The flexural strength of SIFCON is an order of magnitude higher than that of normal steel fiber concrete. For the same type of steel fiber, the flexural strength of SIFCON increases, only up to a certain limit, with increasing fiber volume fractions. After a certain limit, the flexural strength of SIFCON either does not increase further or decreases. The optimum fiber content is in the range of 8–10%. The optimum fiber volume seems to decrease with an increase in the fiber length. At a given fiber volume, longer fibers provide a slight increase in the flexural strength. The use of silica fume in the cement matrix substantially increases the flexural strength. Sand can be added to cement, up to a cement/sand ratio of 1:1.5, without adversely affecting the flexural strength properties.

Figure 4.22 shows the load–deflection curves of SIFCON beams with hooked-end fibers of different sizes and volume fractions, and normal steel fiber concrete beams. The matrix comprises cement and fly ash. As observed, the flexural strength, ductility, and deflection are all higher than that of normal steel fiber concrete; the toughness index can be ten times higher than the latter. SIFCON has a very strong resistance to the development of cracking.

Table 4.14 Tensile strength of SIFCON

Sample No	Matrix constituents/%	Water/Cement ratio	Fiber type	Length/Diameter L/dt	V _f /%	Tensile strength/MPa	Remarks
1	Cement90 + SF10	0.3	HE	50/0.5	5	13.6	Thickness: 19 mm
2	Cement90 + SF10	0.3	HE	50/0.5	8	15.7	
3	Cement100	0.45	DF	30/0.5	8.5	7.0	Thickness: 35 mm
4	Cement100	0.45	ST	25/0.4	8.5	4.0	
5	Cement100	0.45	HE	30/0.5	8.5	9.2	
6	Cement100	0.45	HE	30/0.5	13.5	14.1	
7	Cement100	0.35	HE	60/0.8	7.4	6.7	
8	Cement100	0.35	HE	25/0.5	9.9	7.8	Thickness: 35 mm
9	Cement100	0.35	HE + EE	50/0.8 + 25+ 0.5	6.5 + 4.0	6.9	
10	Cement100	0.45	HE + EE	60/0.8 + 25+ 0.5	6.1 + 4.2	10.7	
11	Cement80 + FA20	0.35	HE	30/0.5	11.7	15.6	Thickness: 37 mm
12	Cement80 + FA20	0.35	DF	30/0.5	12.6	10.9	
13	Cement80 + FA20	0.26	HE3	30/0.5	12.1	15.7	
14	Cement80 + FA20	0.26	DF	30/0.5	13.8	16.1	

NOTE: Types of steel fiber: HE—hooked end; DF—deformed; ST—straight; EE—deformed end

Fig. 4.21 Stress–displacement curves of various mixes with a w/c ratio of 0.45

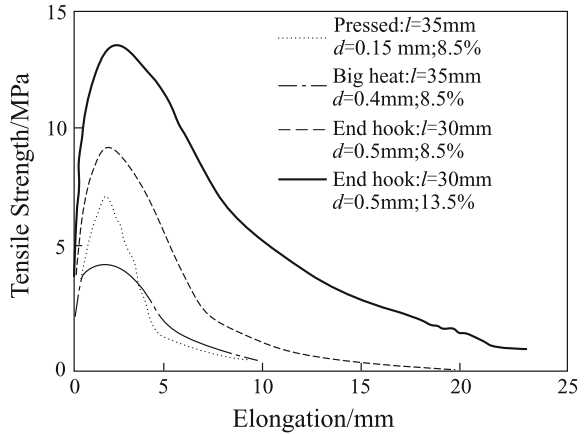
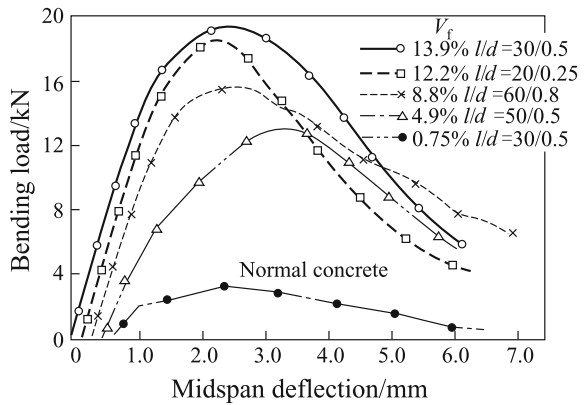


Fig. 4.22 Typical load–deflection behavior in of SIFCON



According to ASTM C1018, the toughness index is determined by dividing the area under the load–deflection curve, up to a specified deflection criterion, by the area, up to the deflection at the onset of the first crack. However, for SIFCON, it is difficult to find the point of first crack from the load–deflection curve. Therefore, Naaman suggested using the toughness of the matrix of SIFCON at the point of failure as the control toughness for determination of the SIFCON toughness index. Table 4.15 lists the toughness indices of SIFCON, with hooked-end fibers of 17% volume content and 30 mm in length, as measured by the above two methods.

Table 4.15 Determination of toughness indices of SIFCON by two methods (hooked-end fibers, $v_f = 17\%$)

Toughness	ASTM C1018 method	Naaman method
H_{m1}	1	1
H_{m5}	6.7	8.4
H_{m10}	12.2	200
H_{m30}	27.2	–

The results showed that the fiber length has a very little influence on both the strength and ductility of SIFCON. The average shear strength is 30.9 MPa, about five times the shear strength of plain concrete. The peak load was reached at about 1 mm of slip over a contact length of 50 mm, indicative of the good ductility of SIFCON under shear. The fiber volume fraction has a certain influence on the shear toughness of SIFCON (Fig. 4.23).

The matrix composition is cement:fine sand:silica fume = 1:1:0.15, water/cement ratio = 0.35, superplasticizer = 1.5% by cement weight. The shear strength is 14.8 MPa. The properties of the steel fibers are as follows: straight, rectangular cross section, length = 35 mm, effective diameter = 0.56 mm. The dimensions of the shear specimen are 100 mm × 100 mm × 400 mm, and orientation of fiber is 2D.

Lankard compared the shrinkage behaviors of SIFCON and plain slurry in air (Fig. 4.24). The shrinkage of SIFCON stops after about 28 days, whereas the shrinkage of the plain slurry continues up to 160 days. The magnitude of the SIFCON shrinkage strain, which ranges from 0.005 to 0.0125 mm/m, is slightly lower than that reported for typical normal-weight concrete.

SIFCON has a great energy-absorbing capacity under impact and blast loading. Its performance is also better than reinforced concrete for missile loads.

Fig. 4.23 Load–deflection curves of four different shear specimens

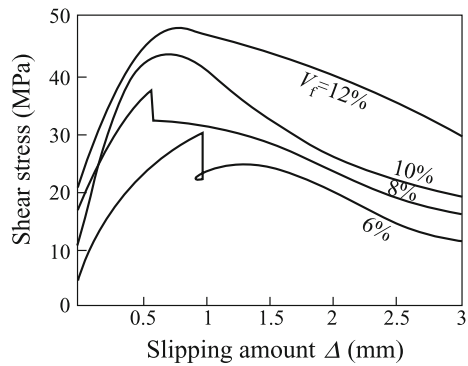
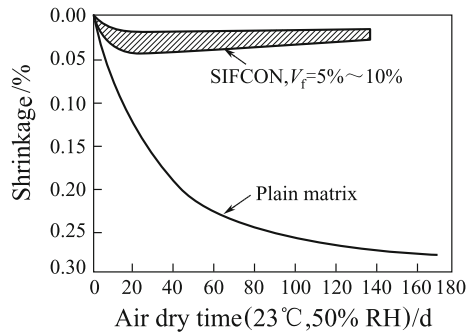


Fig. 4.24 Shrinkage of SIFCON and plain slurry



SIFCON belongs to the high-performance fiber-reinforced cement-based composites. Many properties are better than those of normal steel fiber concrete. However, because of the high fiber volume content, the cost is very high. The following lists some of the successful applications:

1. Explosive-resistant containers for storing materials that could accidentally explode;
2. Security vaults that need protection against blasting, drilling, and fire (torching);
3. Repair of structural components such as damaged pre-stressed concrete beams;
4. Pavement and bridge deck rehabilitation;
5. Abrasive-resistant surfaces in places such as a scrapyard.

SIFCON can also be used to strengthen bending elements for higher flexural strength and toughness. The inclusion of SIFCON in the tensile zones of concrete and steel concrete beams can increase the ultimate loading capacity.

4.2.3.4 Engineered Cementitious Composites (ECC)

Despite the addition of a high volume fraction of fibers into the cement matrix to achieve high performance, their application may be hindered by specific processing requirements because of the high fiber volume fractions and the use of precast components. To this effect, the Advanced Civil Engineering Materials Research Laboratory (ACE-MRL) of Michigan University, USA, developed a new type of high-performance fiber-reinforced cement-based composite. These composites were based on a micromechanics approach to engineer a high-performance fiber-reinforced cement-based composite that shows a pseudo-strain-hardening property, despite the relatively low fiber volume fraction and the use of typical mixing and casting techniques. They termed this class of materials as engineered cementitious composites (ECC) [34].

1. Easy fabrication: can be precast and applied onsite, without specific machineries.
2. Moderate fiber volume fraction (2% or less): for easy fabrication, low cost, and weight.
3. Homogeneous: There will be no weak plane under multi-axial loading for the entire structure.
4. High performance, strength, ductility, and fracture toughness, and shows a pseudo-strain-hardening behavior.

ECC can be prepared with a variety of fibers, including polymeric, steel, and carbon. The matrices used are mostly cement and mortar. To date, most studies have been conducted with high-modulus polyethylene fibers in a cement matrix. The typical material composition is given in Table 4.16; fiber volume fraction is 2%. For comparison purposes, the properties of a typical FRC, containing 1% steel fibers, are also shown. The ECC fabrication procedure is as follows: The

polyethylene fibers are supplied by the manufacturer in a bundle-like form. Prior to mixing, the fibers are dispersed using air pressure for approximately one minute. Then, the amount of fibers needed for the mix is weighed. After measuring the masses of all the constituents, the cement is poured into a three-speed mixer (Hobart) with a planetary rotating blade, and mixed. Silica fume is slowly added to the cement. Water and the superplasticizer are mixed together and slowly added to the mixture. When all of the water and superplasticizer are added, and the cement paste mix becomes uniform, the dispersed fibers are slowly added by hand to the mix. The total mixing time was between 15 and 30 min depending on the batch size and the amount of fibers used (fiber volume fraction). When the mix is ready, the specimens are cast under a high-frequency vibration (150 Hz) in pre-greased Plexiglas molds. Subsequently, they are covered with a polyethylene sheet and the mixture is allowed to harden at room temperature for one day prior to de-molding. The specimens are placed in a water curing tank for four weeks following the de-molding process, and then removed from water and prepared for testing.

The mechanical properties of ECC, obtained to date, are listed in Table 4.17. For comparison purposes, the experimental data obtained for FRC, tested under similar conditions, are also included. Figures 4.25, 4.26, 4.27 show the stress–strain curves of the two specimens, recorded under flexural, uniaxial tension, and compression conditions, respectively. ECC with a 2% volume fiber fraction shows a distinct pseudo-strain-hardening behavior with an average strain of 6%. The compressive strength is within the range of values of typical high-performance concrete (about 68.5 MPa), and the fracture energy is higher than that of normal fiber-reinforced concrete (up to 27 kJ/m²). Under flexural and shear loading, ECC beams showed great ductile behavior before and after peak loading.

Because of the processing flexibility and unique properties of ECCs, the materials can be used for precast or cast-in-place structures, and broad classes of applications such as those that require structural ductility, energy absorption, and crack width control under high strain conditions.

This chapter was translated by Jin Ping Lu.

Table 4.16 Composition of ECC and FRC

Materials	Cement	Silica fume	Superplasticizer	W/C	Aggregates FA/CA
ECC	1.0	0.10–0.20	0.01–0.03	0.30–0.32	–
FRC	1.0	–	–	0.45	1.73/1.73

Table 4.17 Properties of ECC and FRC

Material	Tensile				Compressive		Stiffness	Flexural	Fracture
	σ_{fc} /MPa	ε_{fc} /%	σ_{ct} /MPa	ε_{ct} /%	f_c '/MPa	ε_c '/%	E/GPa	MOR/MPa	J/(kJ/m ²)
ECC	2.5	0.021	4.6	5.6	68.5	0.67	22	25	27
FRC	4.3	0.035	4.3	0.035	55	0.48	32.5	10.9	4.9

Fig. 4.25 Stress–deflection curves of ECC and FRC under flexural loading

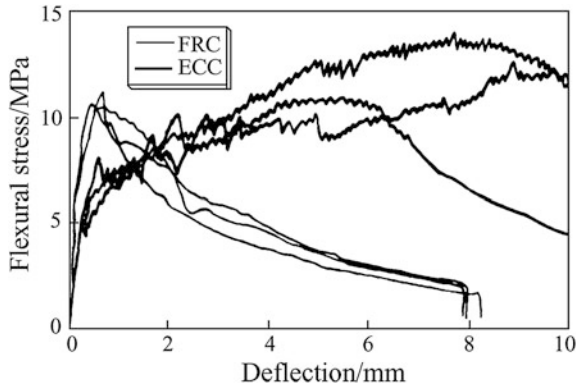


Fig. 4.26 Stress–strain curves of ECC and FRC under tension

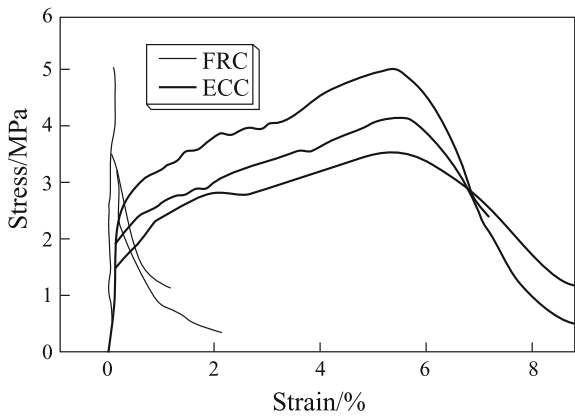
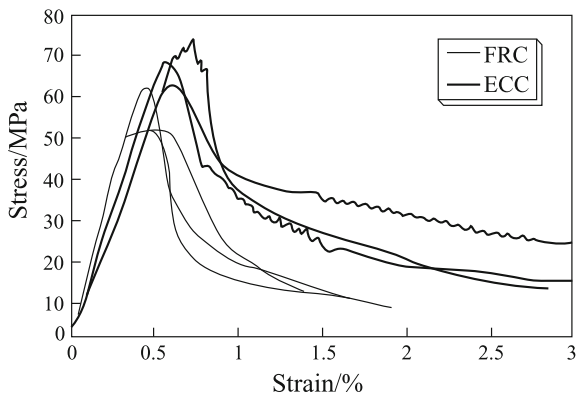


Fig. 4.27 Stress–strain curves of ECC and FRC under compression



References

1. ACI Committee 544 (2001) Fiber reinforced concrete, ACI 544.1R-96, ACI Manual of concrete practice Part 5, American concrete institute, Farmington Hills, MI
2. ACI Committee 548 (2001) "Guide for the Use of Polymers in Concrete, 548.1R-93", ACI Manual of Concrete Practice, Part 5, American Concrete Institute, Farmington Hills, MI
3. Auskin A, Horn W (1973) Polymers in concrete, International Symposium SP-40, Detroit
4. Bache HH (1981) Densified cement/ultrafine particle-based materials. In: Malhotra VM (ed) The second international conference on superplasticizers in concrete. CANIMET, Canada
5. Bache HH (1989) Fracture mechanics in integrated design of new, ultra-strong materials and structures. In: Elfgren L (ed) Fracture mechanics of concrete structures: from theory to applications. Chapman & Hall, London
6. Bache HH (1992) Principles of similitude in design of reinforced brittle matrix composites. In: Reinhardt HW, Naaman AE (eds) High performance fiber reinforced cement composites. E & FN Spon, London
7. Balaguru PN, Shah SP (1992) Fiber reinforced cement composites. McGraw-Hill, New York
8. Balaguru P, Endzulak JK (1986) Flexural behavior of slurry infiltrated fiber concrete (SIFCON) made using condensed silica fume. In: Malhotra VM (ed) Fly ash, silica fume, slag and natural pozzolans in concrete, SP-60. ACI, Michigan
9. Balaguru P, Kendzulak J (1997) Mechanical properties of slurry infiltrated fiber concrete (SIFCON). In: Shah SP, Batson GB (eds) Fiber reinforced concrete, properties and applications, SP-105. ACI, Detroit
10. Bentur A, Mindess S (1990) Fiber reinforced cementitious composites. Elsevier Applied Science, London and New York
11. Cement institute of construction engineering (1958) Ministry, Glass fiber concrete. Publishing House of Chinese Construction Industry, Beijing (in Chinese)
12. Chandra S, Ohama Y (1994) Polymers in concrete. CRC Press, Boca Raton
13. Cheng GQ (1999) Steel fiber reinforced concrete, theory and Application. Publishing House of Chinese Railway Industry, Beijing (in Chinese)
14. Cheyrez M, Daniel JI et al (1996) Specific production and manufacturing issues. In: Naaman AE, Reinhardt HW (eds) High performance fiber reinforced cement composites, 2nd edn. E & FN Spon, London
15. Haynes H (1969) Investigation of fiber reinforcement methods for thin shell concrete. Naval civil engineering laboratory, Port Hueneme, CA. N-979.Sep
16. Wu K, Zhang D, Song J (2002) Properties of polymer modified cement mortar using pre-enveloping method. *Cem Concr Res* 32(3):425–429 (in chinese)
17. Lankard DR, Newell JK (1984) Preparation of highly reinforced steel fiber reinforced concrete composites, In: Hoff GC (ed) Fiber reinforced concrete, International Symposium, SP-81, ACI
18. Li VC, Mishra DK, Wu HC (1995) Matrix design for pseudo strain-hardening fiber reinforced cementitious composites. *Mater Struct* 28(10):586–595
19. Lu JP, Xu LP, Wu XL (1990) Diffusion of chloride ions in polymer modified cement paste, Proceedings of the 6th ICPIC, Shanghai (in Chinese)
20. Maeda N (1996) Proc.of Maeta workshop on high flexural polymer-cement composites, Sakata, Japan
21. Majumdar AJ, Ryder JF (1968) Glass fiber reinforcement for cement products. *Glass Technol* 9:78–84
22. Naaman AE (2000) Optimized geometries of fiber reinforcements of cement, ceramic and polymeric based composites, U.S. Patent No.5989713 (1999). Divisional: U.S Patent No.6060163
23. Naaman AE (2003) Engineered steel fibers with optimal properties for reinforcement of cement composites. *J adv concr technol* 1(3):241–252

24. Qu FJ, Huang CK, Zhao GF (1996) Shearing performance of high performance fiber reinforced concrete (SIFCON), The 6th National Conference on fiber reinforce cement and Concrete (in Chinese)
25. Reinhardt HW, Naaman AE (eds) (1992) High performance fiber reinforced cement composites, Proc. of the International RILEM/ACI Workshop. London, E & FN Spon
26. Richard P, Cheyrezy M Reactive powder concretes with high ductility and 200–800 MPa compressive strength, Concrete technology: Past, Present and Future. SP-144, ACI
27. Richard P, Cheyrezy M (1995) Composition of reactive powder concrete. Cem Concr Res 25(7):1501–1511
28. Romualdi JP, Baston GB (1963) Mechanics of crack arrest in concrete. Proceedings, ASCE. 89(EM3)
29. Shen YX (1996) International trend of GRC Industry. New Building Materials (1) (in Chinese)
30. Tan MH, Ji CP, Zhang W (1983) Introduction to MDF, a kind of cement paste with high flexural strength. Concrete and reinforced concrete 6 (in Chinese)
31. Walraven J (1999) The evolution of concrete. Structural concrete (1)
32. Wang YM (ed) (2000) Glass fiber reinforced glass in China. Publishing House of Chinese Construction Industry, Beijing (in Chinese)
33. Yi C, Shen SZ (1998) Flexural performance of partial high density fiber beam. Industry Buildings 28(8) (in Chinese)
34. Young JF, Berg M (1993) Macro-Defect-Free Cement: a novel organoceramic material, in “Better Ceramics through Chemistry V”, Symp. Proc. Vol 271. Materials Research Society, Pittsburgh, PA

Chapter 5

Carbon Composites

Shouyang Zhang, Yulei Zhang, Aijun Li, Qiang Chen, Xiaohong Shi,
Jianfeng Huang and Zhibiao Hu

Carbon/carbon (C/C) composites with a carbon matrix reinforced by carbon fibers were an accidental discovery. In 1958, a laboratory technician from the Chance Vought Aircraft, Inc., made an operational mistake when measuring the fiber content in phenolic based composites. The phenolic matrix were not oxidized, but decomposed to form a carbon at high temperature. The as-obtained composites showed desirable structure and properties, so a new composite was born: C/C composites [1, 2].

C/C composite preparation techniques developed slowly during their first decade. Up to the late 1960 s, the composites were seen as new engineering materials. Since the 1970 s, they have been developed extensively in Europe and America. Many techniques to produce C/C composites were developed, such as fiber multidirectional weaving, high-pressure liquid infiltration, and chemical vapor infiltration (CVI). With these techniques, high-density C/C composites can be prepared effectively, which expanded the preparation, batch quantity production, and applications of these composites. Since the 1980 s, research on C/C composites has been very active. Research in this advanced field was also conducted in the Soviet Union and Japan, where great progress in improving properties, rapid densification, and application broadening was made. C/C composites have become important materials in the twenty-first century [1–4].

C/C composites possess not only the characteristics of other composites, but also had some unique traits [2]:

1. The whole system is composed of carbon. Therefore, C/C composites exhibit excellent stability at both low and high temperature because of the very strong affinity among carbon atoms. Meanwhile, the high melting point of the carbon materials endows these composites with excellent heat resistance up to 2000 °C.

S. Zhang (✉) · Y. Zhang · A. Li · Q. Chen · X. Shi · J. Huang · Z. Hu
Northwestern Polytechnical University, 710072 Xi'an, Shaanxi, China
e-mail: zhangshouyang@nwpu.edu.cn

It has been reported that C/C composites exhibit their best mechanical properties at high temperature under inert atmosphere [2]. Moreover, the strength of C/C composites increases with rising temperature, which has not been observed for other structures.

2. The density of C/C composites is low (less than 2.0 g/cm^3); it is a quarter that of nickel-based high-temperature alloys and half that of ceramic materials.
3. The ablation resistance of C/C composites is excellent and the ablation is uniform, so they can endure temperatures higher than $3000 \text{ }^\circ\text{C}$. C/C composites show incomparable advantages in short-time ablation environments, such as rockets' motor nozzles and throat inserts.
4. Because of their excellent frictional and wear properties, and low friction coefficient, C/C composites are suited for many frictional wear-resistant components.

These unique characteristics of C/C composites mean that they have received great attention in the aeronautic, astronautic, nuclear, and civil industries, and have been rapidly developed and widely applied during the last few decades.

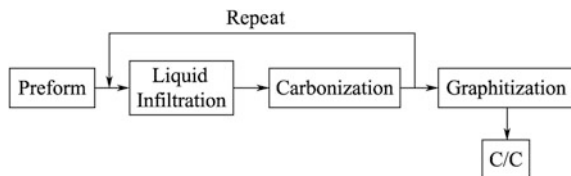
5.1 Preparation of C/C Composites

The preparation of C/C composites can be divided into two steps: preform preparation and densification. The first step involves preparing a carbon fiber preform, and the second involves filling the pores in the preform with a carbon matrix. Many materials can be used to make these preforms, including one-dimensional carbon fiber bundles, two-dimensional carbon fabrics, carbon felts, and carbon fiber woven preforms. There are two main filling methods: liquid infiltration carbonization and CVI. According to different precursors, liquid infiltration carbonization can be further divided into resin and pitch infiltration carbonization [1, 2, 5].

5.1.1 Liquid Infiltration Carbonization

Liquid infiltration carbonization is the traditional method used to prepare graphite materials and has become an important technique to prepare C/C composites. A flowchart of this process is shown in Fig. 5.1. Through repeated infiltration,

Fig. 5.1 Liquid infiltration process



carbonization, and graphitization, the density of composites can reach the required level. Liquid infiltration carbonization can be divided into resin and pitch infiltration carbonization depending on the precursor, and into ordinary pressure (0.1 MPa), high pressure (several tens of MPa), and super high pressure (higher than 100 MPa) depending on infiltration pressure.

5.1.1.1 Resin Infiltration Carbonization

The resin used in liquid infiltration carbonization must be selected carefully. The resin must meet the following conditions [1, 6]:

1. Appropriate viscosity, good flowability, and easily infiltrates into the preform;
2. High carbon yields after carbonization to increase infiltration efficiency and gives high bulk density;
3. Low volume shrinkage during infiltration, solidification, and carbonization processes to decrease damage to fibers.

Staple thermoplastic resins used to prepare C/C composites are polyetheretherketone (PEEK) and polyetherimide (PEI). Although using these resins can efficiently decrease the number of infiltration times, pressure is needed to increase the efficiency during solidification.

Most resins used in this industry are thermosetting ones, such as phenolic, ethoxyline, furan, furyl ketone, acetylenic, and polyimide. Most thermosetting resins readily cross-link at relatively low temperature to form thermosetting, infusible, and vitreous solids. The resin carbon after carbonization is difficult to graphitize; however, resin carbon can also be graphitized under stress at high temperature and pressure.

The process of resin infiltration carbonization is as follows: First, the preform is put into a vessel, and infiltration is carried out with the selected resin under vacuum. Then, gas is added to increase pressure to infiltrate the preform as much as possible. Finally, carbonization is carried out under Ar or N₂ atmosphere. During carbonization, resins decompose into carbon residues with weight loss and size change, leaving numerous micropores. Therefore, repeated infiltration and carbonization steps are needed to decrease the pore volume and densify the composite. Some typical resins are as follows:

Phenolic resins: First-generation thermosetting resins with high coke yield rate (57%–65%) are used to prepare C/C composites. The coke yield rate of some recent modified phenolic resins containing groups such as isocyanate, benzoxazine, and propargyl ether can reach 70%.

Acetylenic resins: These resins have been successfully used to prepare C/C composites abroad. At present, studies on these resins have been started in China, mainly involving polyarylacetylene (PAA) and propargyl substituted cyclopentadienyl resin. PAA is a highly bridged aromatic polymer that is easy to machine, and has a low carbonization shrinkage rate and high coke yield (800 °C, 80%–90%). In

the mid-1990 s, America developed PCP resin that was easy to isolate and prepare, and had a low resin viscosity and high coke yield (almost 95%), and therefore showed great potential in C/C composites [7, 8].

Other resins used for repeated infiltration include furan resin with a coke yield of 58% at 800 °C, and phthalocyanine resin containing phthalic nitrile with a coke yield higher than 93% at 800 °C [1, 8–10].

5.1.1.2 Pitch Infiltration Carbonization

The process of pitch infiltration carbonization is described in Fig. 5.2. The most important steps are vacuum-pressure infiltration and carbonization. During infiltration, vacuum and pressure are both applied to infiltrate the preform as much as possible.

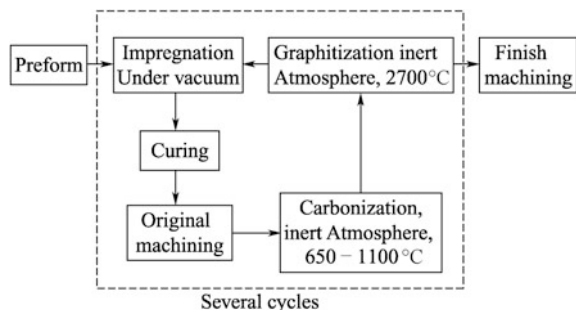
(1) Mechanism of Pitch Infiltration Carbonization

Pitch carbonization can be divided into several reaction processes as follows [11]:

1. C–H and C–C bonds breaking to form free radicals with chemical reactivity;
2. Molecular rearrangement;
3. Thermal polymerization;
4. Densification of aromatic rings;
5. Desorption of lateral chain and hydrogen.

These reactions usually occur simultaneously. The aromatic rings are easily transformed into free radicals, of which the two main types are σ and π radicals, through desorption of the lateral chain and hydrogen during heating. The σ radicals are produced by the dissociation of aromatic C–H bonds. The dissociation energy is high at about 420 kJ/mol. The π radicals are created by the dissociation of a methyl group and are more stable than σ radicals, with a dissociation energy of approximately 325 kJ/mol. The radicals are active and tend to coalesce into larger molecules. They become more active with increasing temperature, so ultimately the pitch transforms into semicoke. The formation of radicals is required for the

Fig. 5.2 Process of the pitch-based C/C composites



carbonization of pitch. The carbonization is accompanied with changes of the radicals, which can be divided into three stages according to the concentration of radicals.

The first stage (room temperature (RT) to 300 °C): Water and compounds with low molecular weight are desorbed from the pitch. The unstable lightweight components, mainly the γ components, volatilize readily. The concentration of radicals is very low, about 8%–12%. With the escape of the volatilized compounds, the lateral C–C chains in pitch break to form various structures, such as σ radicals, which are very unstable and quickly form polymers. As the content of the QI (α components) increases, the isolated duplets change into π radicals. The activation energy at this stage is 42–71 kJ/mol.

The second stage (300–550°C): This stage is the main process because of the great change of pitch components. The pitch decomposes considerably above 300 °C, the volatilized components escape as the temperature increases, and the maximum rate of weight loss is reached at 350 °C. Unstable chemical bonds are cleaved to form many radicals (mainly σ radicals). As a result, lots of low-molecular-weight compounds escape, and there is polycondensation of the residual products. The content of QI (α components) increases rapidly with the increased number of radicals. Between 350 and 450 °C, the radicals polymerize and aromatic hydrocarbons form through van der Waals forces. The content of QI increases rapidly and the radical concentration decreases. Above 450 °C, the incorporation of microcrystals increases the size of crystals and induces molecular structure rearrangement. The d_{002} increases because the degree of order of the crystals decreases. At about 550 °C, pitch pyrolysis is accompanied with an exothermic effect. Dehydrogenation is the main reaction at this temperature, and the concentration of stable radicals increases continually. The content of α components increases rapidly, while that of β and γ components decreases once β reaches a certain content. As a result, the semicoke formed initially and α component reached as high as 90%. The activation energy of this process is 335–785 kJ/mol.

The third stage (above 550 °C): Planar condensed arenes grow through polymerization of radical molecules as the temperature increases. The numbers of hydrogen and methyl radicals decrease rapidly and the microcrystals grow continually, as shown in Fig. 5.3. The coke structure is turbostratic as the temperature reaches 1000 °C. Actually, stable semicoke with numerous non-carbon elements such as O and H forms at 600 °C. These components escape as gas as the

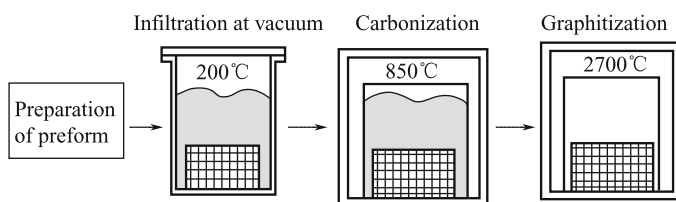


Fig. 5.3 Schematic diagram of impregnation and carbonization under atmospheric pressure

temperature increases, which causes the d_{002} to decrease and interlaminar bonding to strengthen.

Pyrolysis of pitch involves transformation of arene molecules into three-dimensional ordered graphite structures. However, it is a complicated process because polymerization not only occurred between the congeneric elements but also between heterogeneities due to the numerous types of pitch molecules present. The polymerization modes can also differ. Lewis [11] found that 11 products formed through the coalescence of anthracene, which could only be differentiated by the location of polymerization. The number of possible structures increases in series as the relative molecular mass increases. The thickening proceeds smoothly with increasing time and temperature. Because only some of the polymers cause thickening, the thickened materials are further polymerized and then change into graphite-like materials through dehydrogenation. Other materials are difficult to thicken, so they change into vitreous carbon structures. As a result, it is difficult to clarify the mechanism of the molecular reactions in the carbonization of pitch.

(2) Formation process of the mesophase

1. Formation of the mesophase. Liquid pitch usually carbonizes below 500 °C. It is pyrolyzed into low-molecular-weight compounds, and at the same time, aromatization and condensation polymerization also occur. Condensation is promoted by increasing temperature until all of the pitch is solidified. During this process, a liquid crystal substance known as a mesophase, which is composed of condensed nuclei, forms. The mesophase promotes ordered stacking of the lamellar carbon, which is ultimately transformed into three-dimensionally ordered carbon through graphitization. However, the presence of additives, such as oxygen, hydrogen, sulfur, promotes transformation into amorphous carbon, which is difficult to graphitize because of acute oxidation and cross-linking during mesophase formation. Therefore, it is important to study the formation and properties of the mesophases of carbon materials [12–14].

Mesophase spherules are nematic liquid crystals, so they possess the following properties:

- (a) Molecules in the mesophase spherules with dipole moments and aliphatic lateral chains with various lengths adopt a planar orientation;
- (b) Spherules can be incorporated into larger spheres;
- (c) High optical anisotropism is observed; anisotropic stripes can be seen under optical microscope;
- (d) Anisotropic permeability, where the planes orient along the magnetic force in a magnetic field, is observed;
- (e) Planar molecules can be aligned along the surface of a tangent solid;
- (f) During the first stage of mesophase formation, the formation and disappearance of spherules is reversible [15].

The formation of a mesophase has two requirements [16]: The planar arene molecule needs to be large enough to ensure strong interaction forces between

them, and the viscosity of the reaction system needs to allow free motion of molecules, which is an external condition.

The formation process of a mesophase is as follows: Various pitch components decompose and polymerize above 350 °C under inert atmosphere. When held at 400–430 °C for several seconds, the relative molecular mass of condensed arene nuclei might reach 1000–1500, and these nuclei approach each other through thermal motion. The molecules arrange in parallel through van der Waals forces and the molecular forces generated by dipole moments. Interfacial forces cause the aggregated molecules to adopt a spherical shape. Based on dynamics, the reaction process of mesophase formation can be summarized as follows [16]:

- ① The generation of free radicals



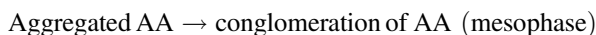
- ② The coalescence of free radicals



- ③ Molecular aggregation



- ④ The conglomeration of molecules



This is a homogeneous nucleation process. The formed spheres are stable in quinoline; they increased in size at constant temperature over a long period or when heated slowly. When their size reached above 100 μm, the spheres could be seen under polarization microscope [17]. The mesophase was equivalent to a mesh of carbon planes; the conglomerated system depended on the orientation of its equator, so a globe formed. The equatorial plane of the mesophase was perpendicular to the spherical face.

2. Carbonization of the mesophase. After formation of the mesophase, the system fluidity increases as the temperature rises; meanwhile, the activity of molecules increases, which will promote molecular coalescence. The spheres grow through absorption of condensed nuclei from the surrounding isotropic fluid. The condensed nuclei insert or bind to the edges of the planes. Meanwhile, the molecules at in the surface travel to the inside of the sphere. Time and temperature are the main factors that affect the nucleation and growth velocity of the spheres. Normally, the number of spheres decreases and growth velocity increases as the carbonization velocity decreases. This phenomenon facilitates mesophase formation. Then, the spheres coalesce and disintegrate as they grow, and are ultimately transformed into solid semicoke.

5.1.1.3 Conventional Impregnation Carbonization Method

(1) Impregnation and carbonization under atmospheric pressure

This method is widely used. As shown in Fig. 5.3 [18], preforms made of carbon fibers are first embedded in liquid pitch and impregnated by sorption at negative pressure. The preforms are then carbonized under normal inert atmosphere and ultimately transformed into C/C composite. Normally, many cycles are needed to produce C/C composites with an acceptable density.

Carbonization should be performed under N_2 atmosphere to prevent pitch oxidation at high temperature. A suitable heating rate is required, or the pitch will flow away from the preform, which leads to low density. Excessive volatilization of pitch components without action results in a low coke yield.

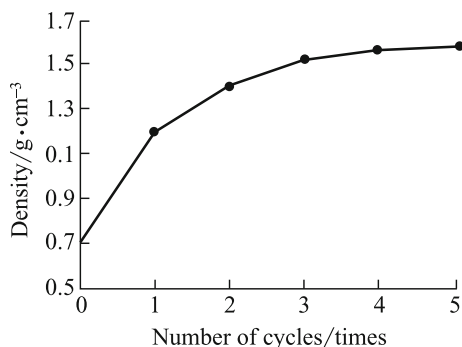
Many pores form on the surfaces of samples after the first cycle because pitch inevitably flows away from the preform at high temperature, and pitch volume contraction occurs after carbonization. To reach a high density, a number of cycles are needed or high-temperature treatment can be used to close the open pores.

As the number of cycles increases, the volume of open pores and the impregnation effect decrease. About 4–5 cycles are generally suitable. A typical density variation curve is shown in Fig. 5.4, which shows that densification rate decreases with increasing cycle number. The first two cycles were the most important, and the density increased little after four cycles.

The advantages of using atmosphere pressure for this process include the simplicity of the procedure and easy operation. The disadvantages are low coke yield (normally 50%) and the decrease in density when pyrolytic gas is released. The density of samples prepared by this process is usually below 1.60 g/cm^3 . Some measures have been developed to resolve this problem [19]:

1. Introducing carbon black into pitch can prevent volume expansion of mesophase pitch during carbonization and decrease the initial temperature of pyrolysis, which is equivalent to increasing the pyrolysis temperature range [15]. Therefore, rapid expansion caused by violent pyrolysis in a narrow temperature range and substantial loss of gas could be avoided. The pyrolytic gas could be

Fig. 5.4 Typical density variation curve during impregnation and carbonization cycles of pitch



lost smoothly. The addition of carbon black can improve the coke yield of pitch, but its effect on the fluidity of pitch below 400 °C is negligible. Carbon black also inhibits the coalescence of mesophase spheres and leads to formation of small particles and isotropic texture; thereby, the graphitizing properties of the matrix were decreased.

- Pre-oxidation treatment of pitch with oxygen or iodine [20]. The purpose of such treatment is to decrease expansion and improve coke yield, like addition of carbon black. White and Sheaffer [20] found that pre-oxidation of mesophase pitch prevented expansion in their study of two-dimensional pitch-based C/C composites. The expansion of mesophase pitch during carbonization was because pyrolytic gases could not escape from high-viscosity mesophase. After pre-oxidation, mesophase pitch was transformed into a cross-linked polymer with partially laminated structure that resulted in an increase of vitrification point and coke yield (to 90%). The volatile products were mainly CO₂ and CO, and the contents of CH₂ and H₂ were low compared with that of the untreated sample. The coke yield was increased from 73% to 93% after iodine pretreatment, and the texture of the composite was transformed from streamline to amosaic.

(2) Impregnation and carbonization at high pressure

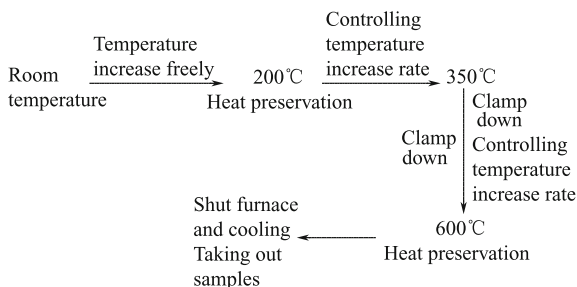
The coke yield of impregnation and carbonization under atmospheric pressure is low. Although it can be increased after various treatments, these procedures are unstable and time consuming. As a result, the high-pressure process is widely used, in which the coke yield can reach above 90%.

Carbonization under high-pressure conditions is usually carried out industrially using a hot isostatic press, which contains a complex gas pressurization system [21].

Generally, high-pressure impregnation and carbonization includes carbonization under high pressure and atmospheric pressure. The typical operating process was established according to the chemical composition, physical properties, and carbonization features of pitch, which is shown in Fig. 5.5.

Below 100 °C, a free heating state is used because of the low volatilization of the molecular components of pitch. However, above 100 °C, the heating rate should be controlled. The point at which to apply pressure is important. If pressure

Fig. 5.5 Typical process of impregnation and carbonization under high pressure



is applied when the temperature was too low, it was hard to impregnate pitch into the preform because of its high viscosity. In contrast, the pitch would flow backward because of volatilization of low-molecular-weight components and the viscosity of pitch increased as it changed when pressure is applied when the temperature is too high. Even if pressure was increased, pitch could not be impregnated into the preform again. Normally, the correct time to apply pressure is when the temperature is 1.5–2.0 times the softening point of pitch [22]. Above 350 °C, the heating rate should be slow because pitch at this stage reacts rapidly and the formation of mesophases and the other anisotropic processes is slow. Semicoke production occurs until 600 °C, but further high-temperature treatment under atmosphere pressure was needed because of the presence of non-carbon elements such as H, O, and N in the matrix. The required density could be reached after a number of cycles.

The important technical factors affecting this process are [23]:

1. Control of temperature. This includes heating, cooling, confirmation of heat preservation point, and ratio of heating and cooling.
2. Control of pressure, which is relevant to the hot isostatic pressing (HIP) equipment and impregnant and should match the temperature curve.
3. Choice of impregnant.

(3) Hot isostatic pressing (HIP)

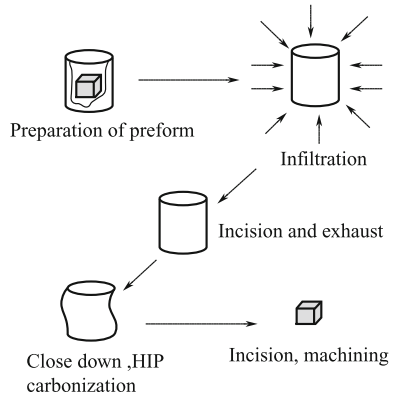
In this process, a preform is under isotropic gas pressure during heating, so it is densified under high temperature and pressure simultaneously. HIP was first developed in the USA to bond nuclear fuel elements. Beryllium was the first material produced by HIP. In the 1970 s, HIP was industrialized. In 1975, the first industrial production line of HIP to produce precision parts was established by Howmet Corporation in the USA. HIP equipment was enlarged and the temperature improved to 1700–2000 °C using a graphitic heating unit. In the 1980 s, this technique became widespread and sophisticated.

The advantages of HIP are as follows:

1. Products with complex shape are homogeneous in density and properties;
2. Materials availability was improved from 20% to 50%, so production costs decreased. Products with precise shape and dimension can be manufactured;
3. The porosity can be decreased from 0.05%–0.2% to 0.0001% or 0, which approaches the theoretical limit of HIP;
4. Fine texture and isotropic properties could be obtained;
5. Provides new processing methods to eliminate pores and reduce casting voids, improves the properties of casts, restores fatigue creep damage, and can be used to connect similar composites, and heterostructural materials.

The disadvantages of HIP are its high cost, long preparation period, and complicated canning technique.

Fig. 5.6 Schematic diagram of the HIPIC process



The preparation of C/C composites by hot isostatic pressure impregnation carbonization (HIPIC) is shown in Fig. 5.6. C/C composites with large dimensions, bulk, slab, and thick-wall axial symmetry are usually fabricated by this process.

Typical products are an orthogonally intersected three-dimensional C/C fabric with dimensions of 150 mm × 150 mm × 300 mm and braided C/C composites, which are used for throat inserts and diffusers. To make these products, first, carbon fiber fabric was impregnated with pitch using vacuum-pressure impregnation and carbonized under atmospheric pressure. Then, the sclerotized product was put in an enclosed stainless steel container filled with pitch, which was placed in a HIP. The ultimate temperature and pressure were 650–700 °C and 7–100 MPa, respectively.

After impregnation and carbonization, the surface of the preform was removed by rough machining and was then graphitized at 2500–2700 °C under argon atmosphere to complete one cycle. To obtain a density of 1.9–2.0 g/cm³, 4–5 cycles were needed. The pitch-based carbon was easy to graphitize and could transform into graphitic lamellar with highly oriented structure when it was heated to 2400–2600 °C. To obtain high-quality C/C composites, parameters such as temperature and pressure must be strictly controlled. The carbonization time was very long, one or even two days. Therefore, the parameters are normally controlled through a computer. If graphitization is needed, the product needs to be heated to 2500–2700 °C under argon atmosphere after impregnation and carbonization.

(4) Extra-high-pressure impregnation and carbonization procedure

This procedure is an improvement of high-pressure impregnation and carbonization made by researchers from Northwestern Polytechnical University (NPU) in 1995, and was applied for patent in the same year. Because the carbonization pressure could reach above 100 MPa, the densification efficiency, coke yield, and densities of composites were all improved substantially. At the same time, the costs were decreased considerably.

5.1.1.4 Effects of Pressure on Carbonization

Pressure can increase coke yield and density (Fig. 5.7 and 5.8, respectively) and decrease pore size and rate (Fig. 5.9) in carbonization from a macroscopic viewpoint.

From a microscopic viewpoint, pressure affects the active process and microstructure. The changes of inert molecular structure of pyrolytic production were observed as the alteration of interlayer spacing d_{002} . Figure 5.10 shows that the interlayer spacing decreases at all temperatures with increasing pressure. For carbon, d_{002} (0.3440 nm) is the criterion for distinction of graphite structure and turbostratic stacking. Figure 5.10 reveals that graphitic structure formed in the pyrolytic product, but only in small domains. Therefore, it was only a turbostratic stacking structure for the whole body. This was because the formation rate of mesophase spheres was larger than the coalescence and growth rates.

Compounds with low molecular weight, such as CO, CH₄, and C₂H₂, remained inside the bulk material involved in the polycondensation reaction when pitch was carbonized under high pressure. Meanwhile, the viscosity of reaction system

Fig. 5.7 Relationship between coke yield and pressure

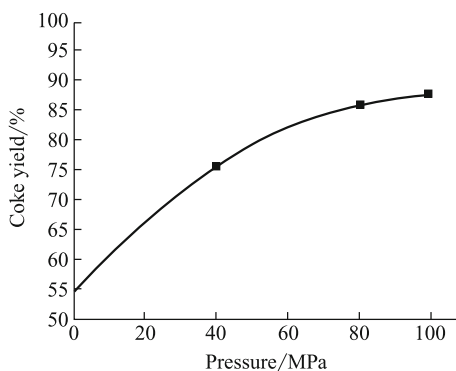


Fig. 5.8 Density change with number of cycles at different pressures

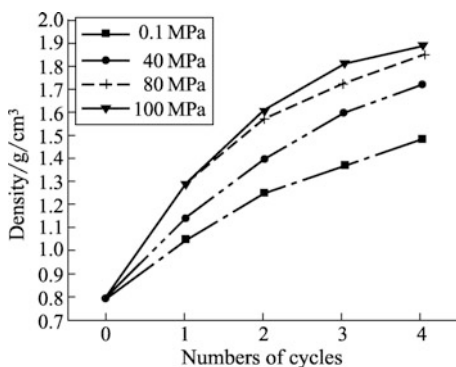


Fig. 5.9 Change of pore size after carbonization at different pressures

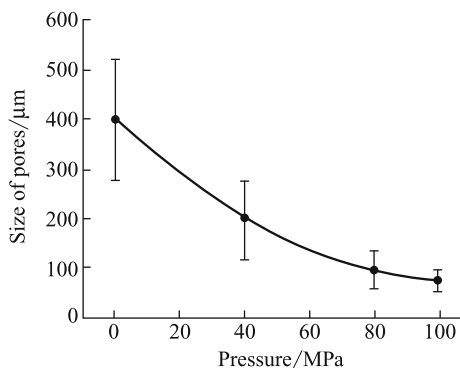
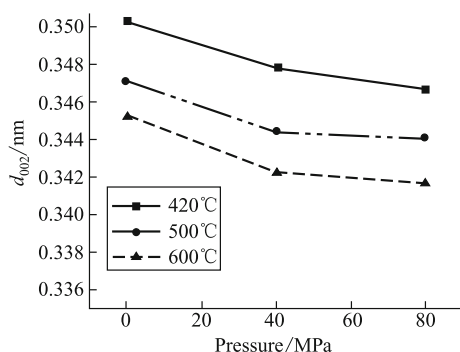


Fig. 5.10 Changes in the interlayer spacing of pitch with increasing of temperature



decreased because of the participation of the low-molecular-weight compounds, which promoted the motion and coalescence of large molecules and formation of a mesophase.

5.1.2 Chemical Vapor Infiltration (CVI)

CVI is a special type of chemical vapor deposition (CVD) technique that involves a multiphase chemical reaction at a gas–solid interface. The preforms used in CVI are porous low-density materials to allow deposition inside the fibers; however, CVD occurs directly on the surface of the substrate to deposit a coating. To produce C/C composites, a carbon fiber preform with specific shape is first put into a deposition furnace. Then, gaseous hydrocarbon is diffused into the preform, and then pyrolyzed to produce pyrolytic carbon as a coating on the surface of the fibers at a given temperature. The pyrolytic carbon grows, and the thickness of the coating increases with deposition time. The size of the voids between fibers decreases, and the coatings ultimately change into a continuous phase, that is, a carbon matrix.

The pyrolysis and deposition process can be described as follows [24]:

1. Gases infiltrate into the preform through diffusion and mass transfer;
2. Gases are adsorbed onto the surface of fibers;
3. Adsorbates are transformed into pyrolytic carbon through chemical reaction near or on the surface of the fibers;
4. By-products are desorbed from the surface of fibers;
5. Gaseous by-products are discharged from the preform by mass transfer.

These steps occur in an orderly fashion, and deposition rate is controlled by the slowest process. Steps 1 and 5 are transfer dominated and involve gas transmission, *i.e.*, gas transfer between the main gas flow and deposition surface. Steps 2, 3, and 4 are related to surface reactions, so they are called “chemical reaction-dominated.” Deposition is controlled by chemical reactions at low temperature, where the gas transfer rate is higher than the reaction rate. With increasing temperature, accelerated chemical reactions cause gas transmission to become the limiting factor of total rate. Therefore, the deposition process is mainly controlled by gas transmission at high temperature. The purpose of CVI is to obtain C/C composites with homogeneous density and complete structure. Therefore, gases transmission and reaction temperature should be adjusted to achieve effective deposition. Because of the dynamic densification process, the deposition control cannot be described by equilibrium thermodynamics at present.

Because of the competition between gas transmission and deposition reaction, a high deposition rate would result in a density gradient in the preform and a low deposition rate would prolong densification time. The main purpose of various CVI techniques is to increase the deposition rate while keeping homogenous density.

The advantages of CVI techniques are their simplicity, good matrix properties, controllable degree of densification, and better comprehensive properties compared with liquid infiltration method. By adjusting the parameters of CVI, C/C composites with different microstructures and properties can be obtained. CVI can also be used together with other methods to prepare C/C composites. The main disadvantages of CVI are the long preparation period and low production efficiency.

During the liquid infiltration process, volume shrinkage of precursors requiring repeated carbonization and graphitization cycles results in damage of the fibers and weak interface bonding between fibers and matrix, which affects the properties of the resulting materials. However, pyrolytic carbon can be deposited on the surface of fibers. This densification method increases the comprehensive properties of C/C composites because the emission of volatiles and volume shrinkage of organic materials during the liquid infiltration process are avoided. CVI techniques can also be used together with infiltration methods to increase densification efficiency and improve the properties of C/C composites. McAllister’s research indicated that the strength of phenolic-based C/C composites increased greatly after CVI-assisted densification[50–51]. The main reason of the increase was that CVI process filled residual micropores and decreased the stress concentration in materials.

Although many CVI techniques have been developed, the most traditional and widely applied is isothermal CVI, owing to its simple devices and ability to deposit complicated shaped and multiple parts. Nevertheless, because of the restrictions of diffusion transmission and preform permeability, C/C composites had to be deposited at low gas concentration and low temperature, which led to longer densification period and increased cost.

Some methods have been developed to improve the gas transmission efficiency and deposition rate, decrease the number of densification cycles, and improve the uniformity of density. These include four CVI techniques: isothermal pressure-gradient CVI, thermal-gradient CVI, pressure-pulsed CVI, and forced-flow CVI, which aim to control gas transfer and preform temperature distribution.

5.1.2.1 CVI Techniques

1. Isothermal CVI (ICVI)

According to the difference of the pressure in the deposition furnace, ICVI can be divided into atmospheric and negative pressure deposition processes. The advantages of atmospheric pressure ICVI are that a longer residence time, and higher concentration of the reactant gas can be obtained, which results in high densification rate. However, it is difficult to prepare high-density C/C composites without carbon black under atmospheric pressure, which affects the mechanical properties of C/C composites. Conversely, the negative pressure process gave low densification rate. However, the negative pressure process could prepare C/C composites with high density. Therefore, negative pressure ICVI is suitable for mass production and is used more widely than atmospheric pressure ICVI. Negative pressure ICVI is main method used to fabricate airplane brake disks. Generally, "ICVI" refers to the negative pressure process.

Because of the homogeneous distribution of temperature during the ICVI process and the lack of forced gas flow in the preform, the flow of precursor and by-products mainly depends on diffusion. The much higher transmission of gases at the surface region than internally means that carbon substrates can be preferentially deposited on the outer regions of a preform. This results in the premature formation of many closed micropores at the preform surface, which might block the inner gas transmission channels and result in inhomogeneity of the density of the material. To prevent the formation of closed micropores, lower temperature and gas concentration are used to slow the deposition rate. However, a large density gradient still appeared ultimately. Mechanical machining and graphitization treatment can be used to open closed micropores, allowing further deposition. However, this led to longer densification periods (several hundred to a thousand hours). As a result, ICVI is suitable to prepare thin-walled and irregular parts because of its stability. When a large deposition furnace is employed to prepare many carbon-based composite parts by ICVI, the cost of each component is decreased. Therefore, commercial C/C composites are mainly prepared by ICVI at present.

In 2001, reports by Huttinger et al. [25–27] changed opinions of CVI, especially atmospheric ICVI. Their results indicated that the residence time of precursor at the outer surface of a preform greatly affected the densification process. When residence time was short, high diffusion velocity made the gases diffuse into the inside of the preform and could improve deposition rate and decrease the number of closed micropores. Conversely, pyrolysis gas with larger residence time deposited preferentially on the outer region of the preform, which could close the micropores for gas diffusion.

C/C composites with a density of 1.9 g/cm^3 were deposited using methane for 120 h based on above-mentioned ICVI theory. This new ICVI technique could prepare C/C composites with rough laminar microstructures without high-temperature heat treatment or mechanical machining during the deposition process, and thus shows great potential for composite production.

2. Pressure-pulsed CVI

Pressure-pulsed CVI is another type of ICVI technique. Repeated oscillations in chamber pressure between a set pressure and vacuum occur during the deposition, allowing rapid introduction and excretion of reaction gases. The process of pressure-pulsed CVI is illustrated in Fig. 5.11 [28, 29]. Operation of a vacuum pump helped to eliminate reactant by-products and reduce the density gradient of the composites. The disadvantages of pressure-pulsed CVI are the high cost of its equipment and low precursor utilization ratio. Although pressure-pulsed CVI has not been applied widely, some simulation calculations have indicated that this technique can be to increase densification rate.

3. Thermal-gradient CVI

Thermal-gradient CVI was developed by changing the preform temperature during atmospheric ICVI through special heating and cooling methods [30]. Typical equipment used in thermal-gradient CVI is shown in Fig. 5.12. During this process, precursor gases diffuse from low to higher temperature. As the gases are

Fig. 5.11 Process of pressure-pulsed CVI

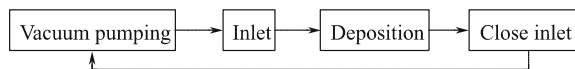
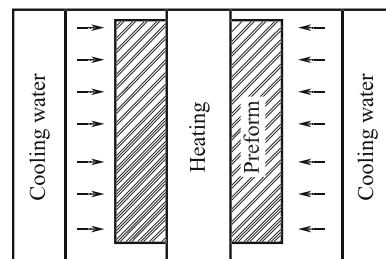


Fig. 5.12 Typical equipment used in thermal-gradient CVI



deposited, the porosity of the preform decreases gradually and thermal conductivity increases. The movement of the deposition region along the radial direction of the chamber from inner to outer results in densification of the whole preform. The gradual movement of the deposition region can also avoid the closure of micropores and extend the short densification time to obtain high density. However, C/C composites prepared by thermal-gradient CVI possess an inhomogeneous microstructure and morphology, and thermal-gradient CVI requires more complex equipment than ICVI.

Induced thermal-gradient CVI is a rapid densification technique proposed by AlliedSignal [31]. By vaporizing liquid cyclopentane, disk preforms with dimensions of 10.8 cm (inner diameter) \times 4.8 cm (external diameter) \times 3.0 cm (height) could be densified from 0.41 to 1.541 g/cm³ in 26 h, with an average densification rate of 0.044 g/(cm³·h). C/C composites prepared by induced thermal-gradient CVI exhibited RL microstructures, and the compressive strength of such C/C composites with a density of 1.79 g/cm³ was up to 268 MPa. Because the deposition temperature is higher than that of ICVI (about 200 °C), many advantages are observed for induced thermal-gradient CVI, such as high densification ratio, homogeneous density, and high conversion (20%–30%). In this process, no carbon and only little tar are formed. A suitable technique should be employed to meet product requirements, such as to produce preforms of various shape and size.

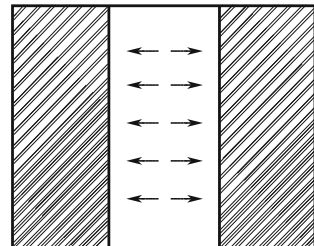
4. Isothermal pressure-gradient CVI

Isothermal pressure-gradient CVI is an ICVI technique with gradient pressure in the reactor. Its characteristics include homogeneous temperature distribution in the preform, forced flow of precursor through the preform, high efficiency of gas mass transfer, low gas concentration gradient, and high homogeneous density [2]. However, because the precursor concentration of the surface region is higher than that of the preform inner, closed micropores form on the surface of the preform, which affect further densification. Isothermal pressure-gradient CVI is suitable to prepare cylinder-shaped parts, as illustrated in Fig. 5.13. Parts with other shapes could also be prepared by this technique with the assistance of a mold.

5. Forced-flow CVI (FCVI)

Forced-flow CVI was first developed to fabricate SiC matrix composites by ORNL Laboratory (USA) and Georgia Institute of Technology in the mid-1980 s.

Fig. 5.13 Schematic diagram of isothermal pressure-gradient CVI



Later, the FCVI technique was used to fabricate C/C composites by Georgia Institute of Technology [32]. During deposition, two symmetrical planes of a preform were heated or cooled to produce a dramatic temperature gradient of about 200–500 °C. The introduction of precursor gases under pressure from the cooler side led to a pressure gradient in the preform. Precursor was first deposited at the hotter side of the preform, and then the deposition region moved to the cooler side. When appropriate conditions are employed, homogenous densification can be obtained by FCVI. FCVI can operate at higher temperature compared with ICVI, which might result in higher deposition rate [33–35]. C/C composites with flexural strength of 98.5–113 MPa and modulus of 14.95–16.26 GPa were prepared by FCVI at the Georgia Institute of Technology. The precursor of 50% hydrogen and 50% propylene was used to produce a deposition rate of 2.9–3.0 $\mu\text{m/h}$, which was 10–30 times that of ICVI.

With the combined advantages of thermal-gradient CVI and isothermal pressure-gradient CVI, FCVI could complete the densification process in one step in a short time. It is suitable for fabricating simple-shaped C/C composite parts with thick walls. The shortcomings of FCVI are that it is not suitable for mass production and preparing parts with complex shape. In addition, C/C composites prepared by FCVI possess different microstructures, which might limit the applications of this technique [32–35].

6. Limited temperature forced-flow CVI (LTCVI)

Limited temperature forced-flow CVI was proposed by NPU. Combined with the advantages of FCVI, TCVI, and isothermal pressure-gradient CVI, the temperature of the deposition region could be controlled by limiting the heated area. This technique gives high densification. The deposition first occurs at the upper surface of the preform; then, the deposition region is gradually moved down by adjusting the parameters to realize a top-down densification process. C/C composites with homogeneous microstructures, thickness of 10 mm, and density of 1.7 g/cm^3 can be fabricated within 80 h by LTCVI, so LTCVI shows enormous potential for the rapid preparation of C/C composites.

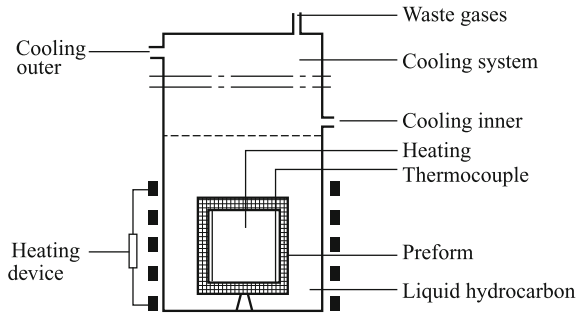
7. Heaterless chemical vapor infiltration (HCVI)

In 1999, Liu (Chinese Academy of Sciences) proposed a new type of chemical vapor infiltration technique, HCVI, which activated the intermediate to increase the deposition rate by applying alternating magnetic fields during the TCVI process [36]. C/C composites with a size of 200 mm \times 100 mm \times 25 mm and density of 1.7 g/cm^3 could be prepared within 20 h. HCVI operates at atmospheric pressure and uses precursors such as liquefied petroleum gas and other hydrocarbon gases.

8. Chemical liquid-vaporized infiltration (CLVI)

CLVI was developed by Houdayer et al. [37] and can be employed to prepare C/C composites with a density of 1.75 g/cm^3 in 3 h. The densification rate can be up to 1.5–2.0 mm/h, which is an increase of two orders of magnitude compared with

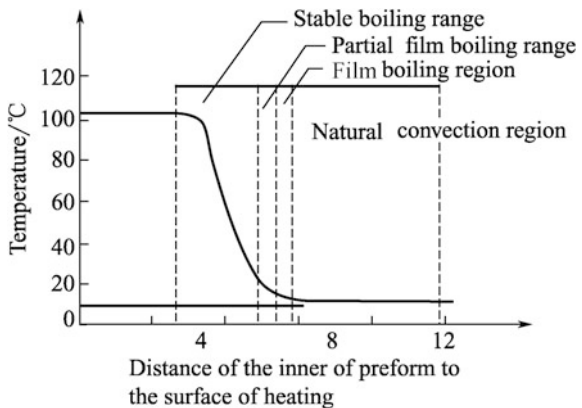
Fig. 5.14 Schematic diagram of CLVI equipment



that of traditional ICVI techniques. This patented technique shows high potential and has been a research focus in this field. A schematic diagram of CLVI is shown in Fig. 5.14. A preform is impregnated with liquid hydrocarbon by induced heating in a furnace. The vaporized hydrocarbon decomposes at the high-temperature side of the preform to form pyrolytic carbon. With time, the densification front moves gradually from inner to outer. This unique deposition method means CLVI is simple, allows quick densification and easy co-deposition with antioxidation additives. However, CLVI is unsuited for complex-shaped C/C composites. Flammable liquid hydrocarbons also increase the operation risk [38].

Because of convective mass transfer, the mass transfer efficiency of CLVI is increased greatly compared with that of traditional CVI. During the deposition, four regions exist in the preform, which are the natural convection region, film boiling region, partial film boiling region, and stable boiling region, as shown in Fig. 5.15. During deposition, the four regions move gradually to the outer side of the preform. A dramatic temperature gradient exists in the gas-liquid coexistence zone.

Fig. 5.15 Four boiling regions present in a preform during deposition by CLVI [38]



5.1.2.2 Computer Simulation of CVI

The above-mentioned CVI techniques could increase densification rate, shorten preparation period, and decrease preparation cost. However, because CVI techniques are very complex, processing parameters such as temperature, pressure, flow of reaction gases, and volume fraction of fibers in the preform affect densification, so the study of CVI techniques and their optimization is very difficult. Computer simulation of CVI may deepen our understanding of these processes and allow prediction of system behavior. In addition, some experiments are attractive to simulate because of their high cost and limitations of experimental conditions [39–41].

To simulate CVI processes, the following factors must be understood well: (1) mass transfer from gaseous precursor to fabric preform, (2) deposition mechanism of the matrix, (3) microstructural changes of the preform, which include the change of pore structure in the preforms and its surface.

Based on data from deposition mechanism simulations, understanding of factors 1 and 2 is easily achieved. However, factor 3 is difficult to simulate because of the complex shape of micropores. A suitable hypothesis needs to be proposed to simplify this problem.

When cylindrical pores are used to represent the real pores in a preform, it is usually called the single pore model. In this model, diameter variation is a function of time and position according to mass conservation and deposition mechanism equations [42]. Under the hypothesis that the transfer rate in preform pores was larger than the rate of pore size change, the results obtained by the model differed considerably from experimental results. This hypothesis was first proposed by Petersen to describe the carburizing process. Fitzer and coworkers [42] then predicted the deposition depth of SiC and optimized conditions for homogeneous deposition. In the simulation, the Thiele modulus was used to describe the deposition depth and the Damkohler number was defined. Van den Brekel proposed that the diameters of pores were not a function of time and extended the single pore model to a two-dimensional one. They thought that the reaction was first order and diffusion was mainly Fickian-type during the CVI process [43]. Rossignol et al. [44] estimated the ICVI process of TiC in preforms using van den Brekel's analysis results. They found that the densification time predicted by the model was one order of magnitude shorter than practical experimental densification time. This indicates that although van den Brekel's model reflects the dynamic process of CVI to some extent, extended practical application of the model was still needed. Moene et al. [45], Lin [46, 47], and Fedou et al. [48] all proposed cylindrical pore models that contained variable pore sizes. Comparison with experimental results revealed that these models were effective to describe first-order reactions. The error between experiment and simulation results was considered by Moene et al. as inconformity of actual deposition mechanism with that of ideal conditions. In fact, the representativeness of the geometric model of the preform might have an important effect on the accuracy of such simulations.

Solid growth rather than the changes of micropores during deposition was estimated in another model. Carrier [49] proposed a random overlap model of fiber

bundles during the infiltration process, in which fiber distribution was spatially random when observed from a cross section. Coatings grew only along the radial direction, which was favorable to understand the deposition among fiber bundles. Transitional porous structures were described by Gupte using a Bethe network in which the open, partially filled, and filled pores were also considered [52]. McAllister and Wolf [50, 51] suggested that the microstructure of pores did not affect the simulation results after they simulated an ICVI process using propylene as the precursor.

McAllister and Wolf [50, 51] proposed a CVI mathematical model and calculation formula of simultaneous densifications of multiple preforms. By analyzing the effects of process parameters on densification, they found that temperature greatly influenced the uniformity and time of densification. With the increasing furnace temperature, densification uniformity decreased and the closure time of micropores was shortened, which decreased rate of weight increase. Deposition time could be shortened by increasing gas concentration. However, the gas concentration had no effect on the degree of densification. Gas velocity influenced the degree of densification of a preform in the vertical direction but not the final degree of deposition or time. Low velocity led to deposition near the entrance of the precursor and high velocity to deposition at the middle of the preform. When the number of preforms in the furnace was decreased, densification rate increased because of the relative concentration rise. However, the degree of densification is independent of preform number. Initial and terminal stages of simulation were in accord with experimental results, but the middle stage was not. Middleman simulated the process of ICVI and analyzed the effect of pore distribution on composites. He thought the gas diffusion in a porous preform could be described using Fick's law. However, this hypothesis was inaccurate at the late stage because of the equivalent size of micropores and mean free path of molecules. As the size of the micropores decreased, the gas diffusion changed from molecular to Knudsen diffusion, in which mole flux contained not only molecular, Knudsen, and transition diffusion, but also viscous flow caused by the pressure gradient in the system.

Gupte and Ta [52] modeled a preform as cylindrical pores. Diffusion reaction only occurred in micropores until their closure. They also simulated the CVI process and found that the filling effect could be described as a non-isothermal process.

Tai and Chou [53] proposed a parallel fiber model for simulating the deposition process of matrix materials in preforms. They considered preforms as fiber constructions in which each fiber is parallel and their distribution is uniform. Tai and Chou simulated the processes of ICVI and FCVI using the parallel model and obtained excellent results. Starr [54] from Oak Ridge National Laboratory (USA) simulated the CVI process of SiC and carbon matrix composites systematically. He described preforms constructed from short-cut fibers with a staggered distribution of cylindrical pores. He also established the parallel fiber construction model using the Monte Carlo method. However, above-mentioned model is not suitable to describe fiber cloth-overlapped preforms usually used in CVI techniques. To characterize the preform structure well, Starr simulated fiber cloth-overlapped preforms using the node percolation model. In this model, the geometry, transfer

equation, and reaction kinetics of a preform are integrated to predict the densification time for various deposition conditions. The predictions agreed with experimental results. This model has been extended from two- to three-dimensional preforms and applied to SiC deposition processes. The main shortcoming of this model is the need to know transfer behavior beforehand. For example, conduction and deposition properties need to be described as functions of preform density. The absence of this data and the relationship between preform surface area and density currently restrict the application of this model in other materials systems.

The above-mentioned simulations mainly focused on SiC-CVI systems. Simulations of other CVI techniques for preparing C/C composites have seldom been reported.

Currently, the common simulation methods include the finite difference method, finite element method, manual network, and inheritance arithmetic. CVI techniques including ICVI, TCVI, FCVI, and LTCVI have been simulated.

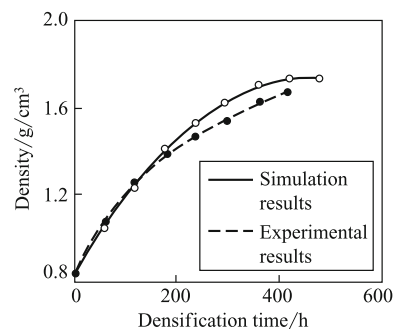
1. ICVI simulation

Many attempts to simulate ICVI have been carried out in China. The ICVI finite difference model for unilateral C/C composites was first established by Hou et al. [55], and simulated the densification process with excellent results (Fig. 5.16). Li [56] used the finite element method to describe the ICVI process and analyzed the effects of deposition temperature, fiber volume fraction, and preform size on the ICVI process (Fig. 5.17). Li et al. [56] used manual network to realize the fuzzy control and fuzzy optimal control of deposition conditions (Fig. 5.18). Gu et al. [57] achieved visual output of simulated results based on finite element simulation of ICVI, which reflected the relationship between deposition conditions and densification results.

2. TCVI simulation

Jiang simulated TCVI techniques using the finite difference method [58, 59]. The established model was specifically suitable for TCVI and gave calculation results that were close to experimental values (Fig. 5.19).

Fig. 5.16 Experimental and simulation results using the finite difference method



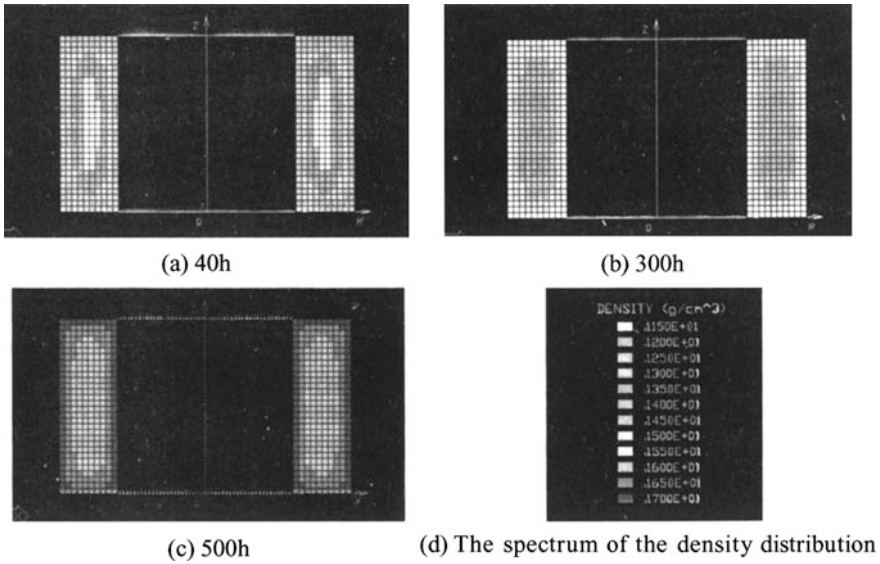


Fig. 5.17 Preform density distribution during deposition simulated by the finite element method

Fig. 5.18 Change of preform density with propylene pressure and time

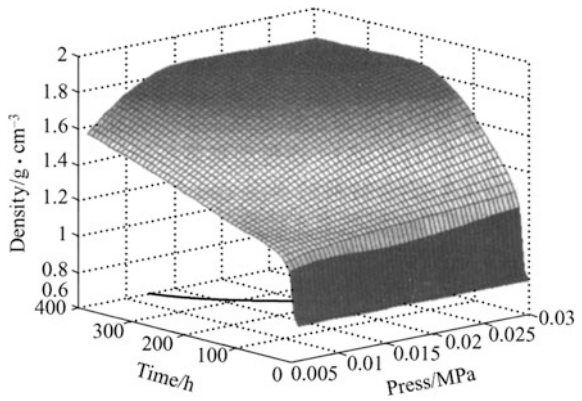
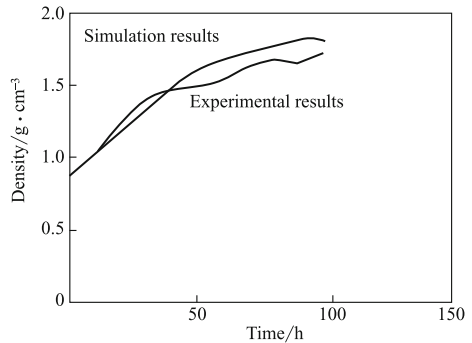


Fig. 5.19 Experimental and simulation results for thermal-gradient CVI



3. FCVI model and simulation

Great progress on the simulation of FCVI was made by Lackey et al. [60]. They proposed a one-dimensional finite element model, which incorporated gases transfer, heat conduction, and deposition dynamics. The model was successfully used to predict optimized deposition conditions and densification time. However, the calculated time was less than that needed experimentally because of the complexity of the CVI process. Although the two-dimensional finite element model proposed by Starr et al. simulates composites with complicated shapes, its cell plot and mathematical calculations are more complex.

Effective medium model has also been employed by Gupte et al. [61, 62] to describe the microstructure of preform columnar pores as Bethe networks for FCVI simulation. This model could be used to estimate transfer coefficients and investigate the effects of temperature, pressure, and pore distribution on densification. The simulation results indicated that the distribution of preform pores had an important influence on the structural characteristics of the preform, gas transfer, and on the whole densification process.

The model proposed by Lewis and Lackey [63] can calculate the microstructures of pyrolyzed carbon well. They considered that the residence time affected the formed microstructures of composites. Therefore, residence time should be included in models.

4. LCVI simulation

Solid disk-shaped C/C composites were modeled to establish mass and heat transfer continuous equations and velocity field equations using the pore model developed Jiang et al. [64]. The simulation results calculated by the finite difference method indicated that advance and process of densification in the preform was determined by the temperature distribution of LCVI. Pressure gradient also greatly influenced the densification process. The above simulation model readily described the LCVI deposit process when compared with experimental results.

5. CLVI simulation

Rovillian and coworkers from the Montesquieu-Bordeaux University in France [65] carried out elementary research on CLVI simulations. They proposed that the balance between mass and heat transfer in the non-densification region and local chemical reactions at the densification front controlled the densification process. Primary simulation and calculation using this model indicated that the main mass transfer mode was molecular diffusion.

5.2 Microstructure and Properties of C/C Composites

5.2.1 Room-Temperature Properties of C/C Composites

5.2.1.1 Strength of C/C Composites

The strength of C/C composites is mainly controlled by the strength and volume fraction of carbon fiber along the direction of load. To utilize the strength of carbon fiber most effectively, the interfacial bond between the carbon fiber and matrix must be adjusted. Therefore, the fracture strength of C/C composites can be interpreted with the Cook-Gordon theory, which is suitable for brittle matrixes. The strength and toughness of brittle matrixes increases significantly if the ratio of interfacial strength to solid effective strength changes within a suitable range. In addition, many factors directly affect the utilization of the strength of carbon fibers in C/C composites [66–69]. For example,

1. The decreased mechanical properties of carbon fiber during processing;
2. Residual stresses among the matrixes or carbon fibers caused by their mismatch of thermal expansion;
3. Stress concentration induced by matrix microcracks formed during the cooling period of the carbonization process;
4. Defects and micropores can result in delamination of the composites;
5. Poor interfacial bonding between carbon fiber and matrixes.

Previous studies showed that the direction of the carbon fiber affected the strength of C/C composites. The tensile strength of unidirectional C/C composites was the highest along the carbon fiber, but that along the transverse direction of the carbon fiber was low. Therefore, orthogonal reinforcement could reduce the difference between the transverse and longitudinal strength of the fibers.

5.2.1.2 Moduli of C/C Composites

The moduli of C/C composites were higher than calculated values. To some extent, this results from the change of crystal structure of carbon fibers induced by the thermal stress and thermal cycles during the process, which was determined by the initial elastic modulus of the carbon fiber and their interaction with the matrixes. The properties of the carbon matrixes would change during the initial heat treatment process, which results in a large variety of microstructures. The properties of carbon fibers with low modulus and graphitized matrixes change more than those of carbon fibers with high modulus.

Because of the difference of the moduli between carbon fiber and matrixes, the contribution of the matrixes to the moduli of C/C composites has usually been neglected. However, if the matrixes possess a highly crystalline structure where the

crystal lattice plane of graphite is parallel to the carbon fibers, the matrixes greatly affect the moduli of C/C composites.

5.2.1.3 Fracture Toughness of C/C Composites

In view of structure, fracture toughness is an important criterion determining the properties of composites alongside strength and hardness. Carbon materials with block or fabric structure are brittle and show weak fracture toughness. However, if the interfacial bond between carbon fibers and matrixes is sufficiently strong, the composites possess high fracture toughness and fracture energy. If the interfacial bond is weak, cracks form at the interface when the load exceeds the fracture strain of the matrixes. Therefore, the matrixes debond from the carbon fibers, which results in a pseudo-plastic fracture mode. The direction of the carbon fiber layer, the precursor, and the interfacial bond of carbon fibers and matrixes directly influences the fracture toughness of C/C composites [70, 71].

The factors influencing the toughness of C/C composites include: matrix rupture, debonding between carbon fibers and matrixes, fiber fracture, stress rebound, the friction at the interface between fiber and matrix, the bridging effect, and fiber pullout. Generally, the fracture energy of three-dimensional C/C composites is the highest, and that of carbon felt-based C/C composites is the lowest. The fracture toughness of two-dimensional C/C composites with carbon cloth or random carbon fibers lies between [70, 71].

5.2.1.4 Fatigue and Creep Behaviors of C/C Composites

C/C composites can exhibit excellent fatigue and creep performance. The tension-tension fatigue limits of three-dimensional C/C composites can reach 90% [72–75].

The fatigue process of C/C composites involves a series of changes. The volume of matrix cracks increases during the cycles, so the load might partly exceed the fracture strength of the matrixes, which leads to the formation of small particles. Then, the matrix dissociates from the small particles through local fracture [76, 77].

5.2.1.5 Friction and Wear Performance of C/C Composites

The carbon fiber in C/C composites possesses a turbostratic structure, which has a friction coefficient higher than that of graphite. Therefore, carbon fiber could not only act as reinforcement, but also improve the friction coefficient of composites. Because of its layer-like structure, graphite possesses high solid lubrication ability and can reduce the friction coefficient of brake disks. C/C composites with moderate friction coefficient and sufficient strength can be obtained by adjusting the graphitization degree of the carbon matrix.

Fig. 5.20 Effect of braking pressure on friction coefficient [78]

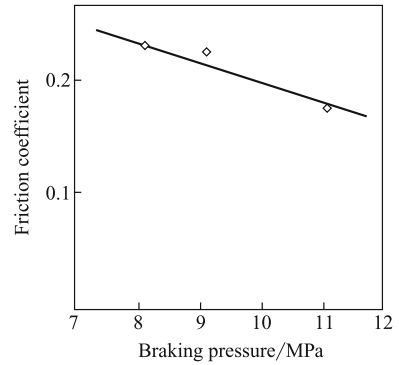
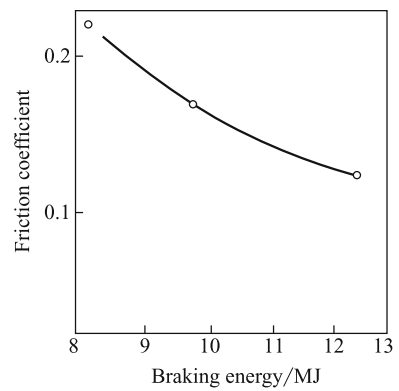


Fig. 5.21 Effect of braking energy on friction coefficient [78]



The braking behavior of C/C composites under wet conditions was studied by NPU [78]. The results showed that the cleavage plane of turbostratic graphite was a surface with low energy. However, the edge of graphite possesses high activity, and readily reacted with oxygen and water vapor to form different oxidative groups. As a result, the turbostratic graphite in C/C composites consisted of a low-energy cleavage plane and edge surface with low surface energy under wet conditions, which resulted in a small friction force between different crystal planes and low friction coefficient. Figures 5.20 and 5.21 show the effects of braking pressure and braking energy on the friction coefficient of C/C composites under wet conditions. With increased braking pressure, the friction coefficient exhibited a small linear decrease when braking energy was kept constant. When braking pressure was constant, friction coefficient decreased considerably as the braking energy increases. Therefore, C/C composites should be useful as damp-proof brake disks.

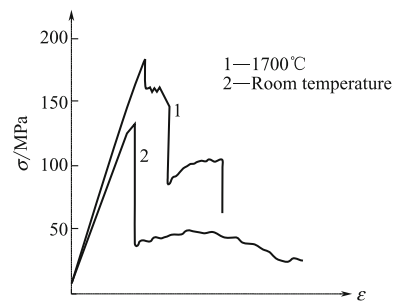
5.2.2 High-Temperature Performance of C/C Composites

Because of the unique mechanical properties and excellent thermal performance of carbon materials, high strength maintenance at high temperature, creep resistance, and thermal shock resistance, C/C composites are excellent high-temperature thermal-structure materials under inert atmosphere. A unique characteristic of C/C composites is that their mechanical properties at 2000 °C are as good or better than those at room temperature.

The improvement of the mechanical properties of C/C composites with increasing temperature could be attributed to the structural variation with temperature, which not only influences the stress conduction mechanism, but also changes the failure mechanism. The structural variation with increasing temperature includes healing of big defects, and the closure of stress cracks induced by the thermal expansion of carbon fiber and matrix. The former results in the improved mechanical properties, whereas the latter changes the failure mechanism of the composites. A study of high-temperature damage of C/C composites showed that the fracture toughness (crack propagation energy) increased with increasing testing temperature. The reason for this was that the resistance to damage or crack propagation increased through the increased strength of the interfacial bonding between fiber/matrix and matrix/matrix, and the closure of defects and cracks [66–69]. Figures 5.22 and 5.23 show stress-strain curves measured for two- and three-dimensional C/C composites, respectively, at different testing temperatures [79]. Obviously, the brittleness increased at high temperature and the failure mode changed. The failure mode variation of three-dimensional C/C composites is also attributed to the closure of cross-cracks by the thermal expansion of the fiber/matrix.

Figures 5.24, 5.25, and 5.26 present fracture-surface SEM micrographs of two- and three-dimensional C/C composites at different testing temperatures, which reveal the interface variation of the composites [79]. Compared with other structural materials, C/C composites exhibit high specific strength above 1000 °C.

Fig. 5.22 Flexural failure behaviors of two-dimensional C/C composites at room and high temperature [79]



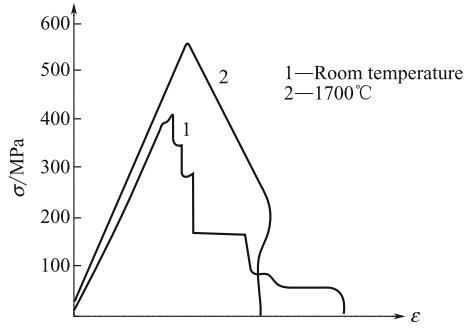


Fig. 5.23 Flexural failure behaviors of three-dimensional C/C composites at room and high temperature [79]

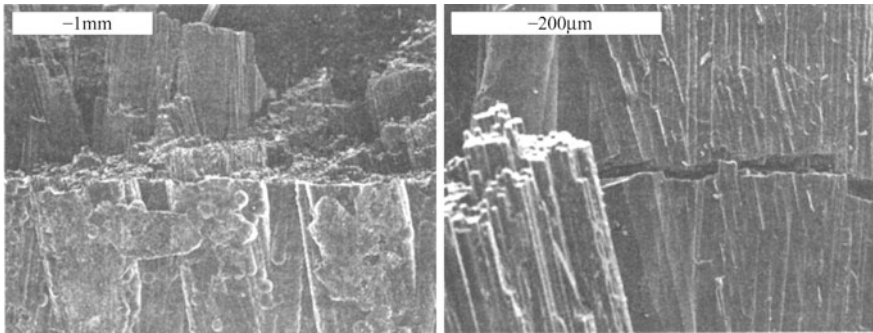


Fig. 5.24 SEM micrographs of the fracture surfaces of three-dimensional C/C composites at 1700 °C

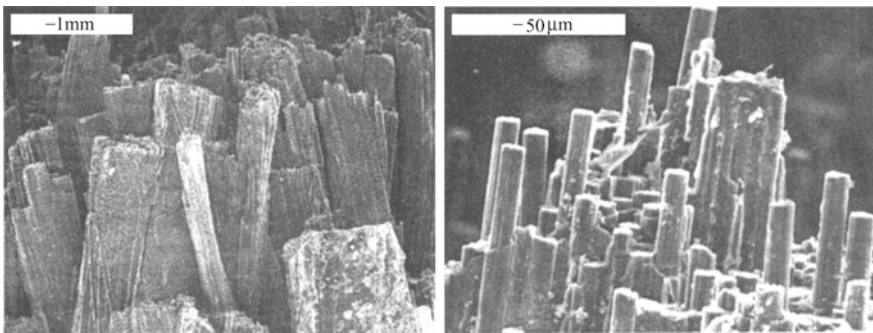


Fig. 5.25 SEM micrographs of the fracture surface of three-dimensional C/C composites at room temperature

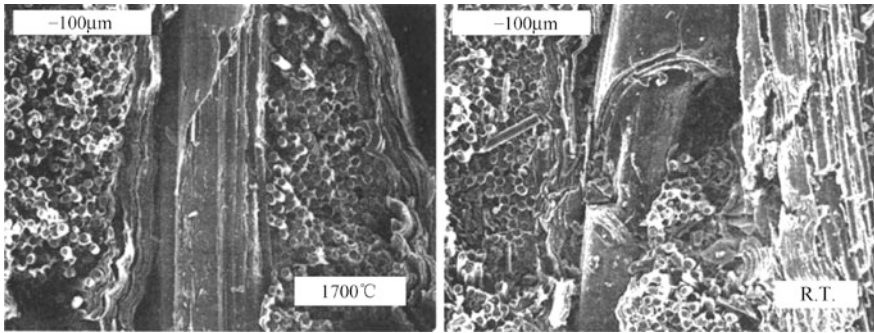


Fig. 5.26 SEM micrographs of the fracture surfaces of two-dimensional C/C composites at room and high temperature

5.2.3 Thermal Properties of C/C Composites

5.2.3.1 Thermal Conductivity of C/C Composites

Because of the different precursors and densification processes used to produce C/C composites, the carbon fiber and carbon matrix can possess different microstructures, which affects the thermal properties of the composite. Meanwhile, the shape, dimensions, and porosity of C/C composites can also be changed by composition and process conditions. As a result, the thermal conductivity mechanism of C/C composites is complex [68, 80, 81].

Generally, C/C composites are prepared by the pyrolysis of polymers and CVI. Because the carbon matrix grows along the layer plane of the carbon fiber, the thermal conductivity parallel to the carbon fiber can be estimated using the mixture rule:

$$K_c = K_f V_f + K_m (1 - V_f - V_p) \quad (5.1)$$

where K_f and K_m are the thermal conductivities of fiber and matrix, respectively, and V_f and V_p are volume fractions of fiber and pores, respectively.

In contrast, the thermal conductivity perpendicular to the carbon fiber is difficult to predict because the thermal fluxes do not take a single path. The fiber and pores interrupt the thermal fluxes and reduce the thermal conductivity. In addition, pitch and PAN-based carbon fiber introduce more parameters because of the multiphase microstructure along different cross sections. Some mathematical models used to predict the transverse thermal conductivity of two-phase polymers or carbon materials are not suitable for different fibers and matrixes, especially for those with random or multidirectional carbon fiber reinforcement [68, 80].

In summary, the thermal conductivity of C/C composites depends on the volume fraction of the fiber, matrix, and various defects. The absolute thermal conductivity is determined by the thermal transmission of the components. The thermal properties of C/C composites directly determine their applications, but systematic

studies of the relationship between these properties and various factors have seldom been reported. Reported data of thermal conductivity is related to specific products rather than systematic calculations.

5.2.3.2 Thermal Expansion of C/C Composites

The dimensional stability of C/C composites at high temperature depends on their thermal expansion properties and coefficient of thermal expansion (CTE). An important characteristic of graphite is its low or even negative CTE. Like its mechanical properties, the CTE of graphite exhibits anisotropy. Along the plane direction, the CTE of graphite is low or even negative, but it is positive in the vertical direction. The absolute value of the CTE depends on the carbon precursor, heat treatment temperature, process conditions, and the degree of matrix graphitization [82]. The CTE of carbon fiber also depends on the precursor and heat treatment temperature.

In C/C composites, the CTE along the reinforced direction is controlled by the nature of the reinforcement. However, the content and porosity of the matrix play important roles in the CTE perpendicular to the fiber [83]. The volume fraction of carbon fiber affects the CTE and anisotropy of the composites. Increasing the fiber volume fraction increases the CTE in both directions. The CTE perpendicular to the fiber is mainly affected by the porosity and crack shrinkage of the matrix, which could be compensated for pore shrinkage. Therefore, composites with high fiber volume fraction and low porosity show high CTE in the vertical direction. The CTE of three-dimensional C/C composites is lower than that of unidirectional and two-dimensional C/C composites.

5.2.4 Microstructure of C/C Composites

5.2.4.1 Polarized Light Microscopy of Pitch-Based C/C Composites

Different classifications are used by various research groups to distinguish the optical microstructure of carbon materials from pitch carbonization. In general, the microstructure of C/C composites can be classified into three categories: mosaic, flowline, and domain structure.

Mosaic structure includes very fine, fine, medium, coarse, and super mosaic. Under a polarized light microscope, mosaic structure is observed as a random distribution of bright particles surrounded by black regions. The luminance of the bright particles changes when the object stage is rotated, which indicates that mosaic structures are optically anisotropic and aligned randomly. Flowline structure includes medium, coarse, and acicular flow. Flow, small, and broad domains all belong to domain structure. Mosaic, flowline, and domain structure are obtained from mesophases via different procedures [84–87].

5.2.4.2 Polarized Light Microscopy of C/C Composites Fabricated by CVD

Initially, the theory of fluidized beds was used as a reference to research the structure and properties of C/C composites. The interrelated conclusions were also used to investigate the relationship between structure and process. From this, attention was gradually focused on the particulate nature of pyrocarbon. The shape of the particles that were coated in the fluidized bed was simple and the correlation between the thermodynamics and hydrodynamics was explicit, so a specific deposition mechanism would be dominant in the fluidized bed for fixed deposition parameters. Because many micropores are distributed in carbon fiber preforms and the gas concentration and temperature change continuously, different pyrocarbons form at different deposition times and positions in the same preform because of the heterogeneous distribution of the deposition parameters over a preform. The complexity of deposition is exemplified by the CVI densification of porous preforms [88–95].

Classification of the microstructure of pyrocarbon is still incomplete, with different standards used. According to the features of pyrocarbon under a polarized light microscope, Bokros classified pyrocarbon deposited in fluidized bed reactors into four categories: columnar, granular, laminar, and isotropic [91].

Pierson and Lieberman performed a comprehensive study of the pyrocarbon deposited on carbon fiber felts and distinguished three typically observed matrix microstructures:

1. Smooth Laminar (SL): The cross-light extinction of this microstructure is regular under polarized light. This microstructure is obtained at low temperature (<1300 °C using methane as precursor), medium hydrocarbon concentration and gas pressure, and large substrate surface area. Planar complexes are thought to form in the gas phase and deposit on the substrate, resulting in a surface of nucleated pyrocarbon with growth cones, which often emerge radially from the substrate surface. The SL microstructure is turbostratic.
2. Rough Laminar (RL): This microstructure possesses irregular cross light extinction under polarized light. This microstructure is deposited at low pressure and low temperature or at very high temperature.
3. Isotropic (ISO): There is no cross light extinction in this microstructure under polarized light. Isotropic pyrocarbon always forms in the range of 1400–1900 °C and at higher gas pressure and hydrocarbon concentrations, but with low gas flow rate. Under these conditions, carbon particles are considered to form in the gas phase and deposit on the substrate, resulting in a porous isotropic pyrocarbon.

The orientation of microstructures was quantified by Diefendorf and Tokarsky according to their extinction angle, A_e , which was extracted from polarized light micrographs [90]. The values of the extinction angles are presented in Table 5.1. They also defined a dark laminar pyrocarbon. Describing the orientation of

Table 5.1 Extinction angles of pyrocarbon microstructures [90]

Pyrocarbon	Rough lamellar	Smooth lamellar	Dark lamellar	Isotropic
A_e	$>18^\circ$	$12^\circ-18^\circ$	$4^\circ-12^\circ$	$<4^\circ$

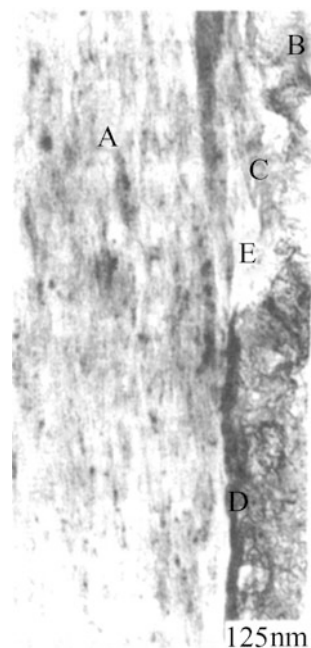
microstructures and quantifying the pyrocarbon species with the help of extinction angle helped to progress research in this area.

The method proposed by Pierson and Liberman to classify pyrocarbon into three categories, RL, SL, and ISO, has been approved by scholars and is still used to analyze the microstructure of pyrocarbons [89–93].

However, there were discrepancies in the properties of different types of pyrocarbons: The anisotropy of SL was large and cracks existed at the interface and laminae; the density of ISO was low, the bonding strength with carbon fibers was strong, and there were no cracks at interface; RL possessed better comprehensive properties and its graphitization rate was twice that of SL. This disparity is ascribed to the match of different pyrocarbons. For example, the strength and stiffness are high for RL/ISO, whereas the fracture toughness is very good for SL/RL.

RL, SL, and ISO are the most common microstructures in C/C composite and are depicted in Fig. 5.27. The regularities of RL and SL are on different scales, and so they cannot coexist. The regularity of SL and RL depends on the type of microscopy used to view the structure. Both SL and RL show growth cones. The cross light extinction of RL is strongly disrupted by growth cones, but it is regular and complete in SL.

Fig. 5.27 Pinning structures at the interface of fiber and matrix A: carbon fiber; B: pyrocarbon; C: polluted surface of fibers; D: polluted area of the fiber surface; E: clearance of interface



To control the microstructure of pyrocarbon, the relationship between CVI parameters and microstructure was investigated by scholars. However, the results showed that RL, SL, or ISO was always deposited as a matrix in the CVI process of C/C composites. SL and ISO are common in C/C composites. RL, which is the ideal microstructure because it has the highest graphitization degree, can be obtained when the deposition parameters are carefully controlled.

5.2.5 Interfaces of C/C Composites

The interfaces in C/C composites are an important microstructure that greatly influence both the macro- and microproperties of the composites. The bond strength between carbon fibers and the matrix has to transmit load in high-performance composites. In C/C composites, load cannot be transmitted when there is low-interface bonding strength, but high bonding strength can make the composites brittle. If the bonding strength is moderate, cracks deflect at interfaces and composites fracture nonlinearly. Therefore, ideal interface microstructure is very important to optimize design and realize the full scope of C/C composites. A way to obtain ideal interfaces in C/C composite is needed to fabricate composites that achieve high performance.

The interfaces of C/C composites depend on the materials and preparation conditions. Although reinforcement fibers and matrix are both carbon, they differ greatly in structure and properties. Carbon fiber is anisotropic and pyrocarbon is turbostratic and isotropic, so a distinct reinforcement fiber/matrix interface and coefficient of expansion mismatch exist. Some examples of the work on this topic are included below.

1. Surface treatment of carbon fiber

Deng et al. [96] prepared carbon fibers using a two-fluid surface treatment process with expandable graphite as a modified matrix. The tensile stretch of the pitch-based C/C composite was increased by 0.85% to 55%. Bahl et al. [97] investigated pyrocarbon coatings deposited on the surface of T800 carbon fibers. The results showed that the high- and low-temperature properties of the C/C composite coated with pyrocarbon were improved greatly. Iwashita [98] prepared coatings using silicon and titanate acid ester coupling agents on high-modulus carbon fibers. The interface of coated fiber/matrix was weak, but the tensile strength was improved. Meanwhile, Zhang et al. [99] studied the influence of treated carbon fiber surfaces on C/C composite strength and discussed the change of fracture mechanism. They thought that moderate oxidation of the carbon fiber could improve the interface of fiber/matrix and obtain good utilization of the carbon fiber tensile strength.

2. Measurement of interface strength

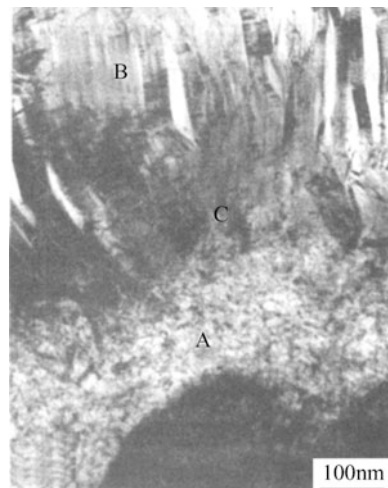
Much research has been carried out to measure interface strength using methods including: short beam cut, pullout, and push out [100, 101].

3. Observation of interface features

Zeng and Peng [102] investigated the interface features of C/C composites by TEM and SEM observation and proposed that pinning and induced structures existed at the interfaces of carbon fiber/pyrocarbon or pitch carbon. When carbon was deposited by CVD as the interface of matrix carbon and carbon fibers, the pores and defects on the surface of the carbon fibers would be filled and result in a pinning structure. Figure 5.27 shows the interface features of pyrocarbon and pitch carbon. Rong [103, 104] from NPU observed the interface of pyrocarbon with the help of HR-TEM to observe the induced structure (Fig. 5.28). Hou studied the fracture surface of samples prepared by different CVI processes and found that carbon fibers that had been pulled out were homogeneously covered by pyrocarbon [105]. This shows that the contraction and expansion of cracks and debonding of the interface occurred inside the laminar pyrocarbon. This discovery differs from the weak interface between carbon fibers and matrix, and a regenerative interface was proposed. The interface area was bigger than that of carbon fiber/matrix, so it could improve the comprehensive properties of the composite if debonding and pulling out occurred under the same conditions. Reznik and coworkers [106] have extensively researched the interfaces in C/C composites by means of TEM.

In general, the study of the interfaces in C/C composites has a long way to go compared with that of resin- and ceramic-based composites. There is still much work on applications to perform, for example, the effect of process parameters on the complex state of interfaces and the optimization, design, and control of interfaces.

Fig. 5.28 Microstructure of pyrocarbon, pitch carbon, and transition region A: pyrocarbon; B: pitch carbon; C: transition region



5.3 Oxidation Protection of C/C Composites

C/C composites possess outstanding properties such as low density, high thermal conductivity, low thermal expansion coefficient, good thermal shock resistance, and high strength and modulus [107, 108]. However, this composite exhibits poor antioxidation ability in oxidizing atmosphere at high temperature. It has been indicated that C/C composites begin to oxidize from 370 °C, and the oxidation rate increases rapidly with increasing temperature. This could damage the materials and greatly restricts their application as thermal-structure materials [109–111]. As a result, it is important to prevent oxidation of the composites to expand their application fields.

5.3.1 Oxidation Process and Characteristics of C/C Composites

Above 370 °C under an oxygenic atmosphere, the carbon in C/C composites can react with oxygen, generating CO and CO₂ (Eq. (5.2) and (5.3)). Even with very low oxygen partial pressure, there is also a large Gibbs free energy difference that drives the reactions. The oxidation rate is directly proportional to the oxygen partial pressure [112].



Shemet et al. [113] divided the oxidation process of carbon materials into three types according to the control process at certain temperatures: At low temperatures, the reaction between oxygen and the active carbon on the surface of the material controls the oxidation process. With increasing temperature, the process becomes controlled by the migration rate of oxygen in the materials. At high temperatures, the oxidation rate is mainly determined by the diffusion speed of oxygen in the concentration boundary region at the material surface. Wu et al. [114] verified the difference of the three oxidation types and obtained their activation energies of 178.07, 86.94 and 20.9 kJ/mol.

Oxidation of C/C composites is affected by the types of fibers and matrix, braiding method, heat-treatment temperature, content of impurities and graphitization degree. C/C composites prepared by different methods have different oxidation characteristics. The oxidation process of C/C composites can be described as follows:

1. Reaction gas is transferred to the material surface;
2. The reaction gas is adsorbed by the surface of the C/C composite;

3. Oxidation reaction on the surface;
4. Gas generated during the oxidation process desorbs;
5. Gas is transferred in the opposite direction.

Because of the porous characteristic nature of C/C composites, the unreacted gas could diffuse into the material and react with carbon atoms at walls of pores while diffusing. At low temperatures, diffusion is quicker than the reaction in the pores, so the whole bulk reacts homogeneously. As the temperature increases, the reaction rate accelerates, so less gas reacts inside the pores of C/C composites because more oxygen is consumed on the surface of the composite. At even higher temperature, almost no reaction happens inside C/C composites. In other words, pores and the high-energy active region at the interface between fibers and matrix oxidize first, and then generated ablation cracks enlarge and stretch toward the center of the materials. After that, the oxidation regions are the fiber axis surface, fiber ends, and finally the isotropic and anisotropic carbon substrates sandwiched between the fiber layers. Oxidation of C/C composites can weaken the interface of the matrix and fibers and decrease the strength of fibers; finally, the structure of C/C composite is destroyed.

There are two main technologies to protect C/C composites from oxidation: modification methods including fiber modification and matrix modification, and coating technology.

5.3.2 *Modification Technologies*

The oxidation resistance of C/C composites can be improved using the modification method. Fiber modification is preparing the coating on the surface of carbon fibers, whereas matrix modification involves changing substrate components to improve the oxidation resistance of C/C composites. There has not been a breakthrough in modification technology research; the protecting temperature is under 1000 °C, so this method can only be used for oxidation protection at low temperatures.

5.3.2.1 Fiber Modification

Oxidation mostly occurs at the interface between fibers and matrix, so preparing an isolating layer at the surface between fibers and matrix to prevent the oxygen from diffusing inside the materials can protect the composites from oxidation to some degree.

At present, the most common fiber modification method is CVD method fiber coating technology by CVD. In this process, a hot-wall reactor or current heating method is used to make the gas react and deposit on the fiber surface. The factors affecting the CVD process include the reaction temperature, gas concentration, and diffusion rate of the vapor on the fibers' surface. Therefore, the temperature distribution in the reactor, reactant concentration and distribution, gas transfer rate distribution, reactor geometry, fiber feeding speed, gas reaction dynamics,

Table 5.2 Coatings on the surface of carbon fibers and their preparation methods

Coating technology	Coating material	Coating thickness/ μ m
Chemical vapor deposition	TiB, TiC, TiN, SiC, BN, Si, B ₄ C, Ta, C	0.1–1.0
Sputtering	SiC	0.05–0.5
Spraying	Al	2.5–4.0
Electric plating	Ni, Co, Cu	0.2–0.6
Solgel	SiO ₂	0.07–0.15
Liquid metal transformation	Nb ₂ C, Ta ₂ C, TiC-Ti ₄ SN ₂ C ₂ , ZrC-Zr ₄ SN ₂ C ₂	0.05–2.0

thermodynamics of the reactants and products, and gas transfer rate (diffusion coefficient and viscosity) all influence the coating of the fibers.

Labruquere et al. [115] deposited B₄C, Si, and SiC coatings by CVD, and then densified the fibers using CVI. Experiment results indicated that B₄C was oxidized before carbon, and a B₂O₃ layer was generated. The B₂O₃ layer isolated carbon from oxygen and efficiently decreased surface oxidation. The oxidation resistance was better with coatings thicker than 100 μ m. It was concluded that coatings should be oxidized prior to carbon, a certain coating thickness is required, the coating should not react with the fibers, and the oxidation of the coating should generate a stable oxide.

Coatings can protect fibers from oxidation, change the fiber/matrix interface characteristics, and improve their antioxidation ability. However, it is very difficult to prepare coatings on the surface of a single fiber or inside a material. In addition, microcracks can be generated because of the mismatch of the thermal expansion coefficients between the coating and fiber. The main shortcomings are that coatings can decrease the strength of fibers, and affect fiber flexibility and waviness. Meanwhile, the antioxidation lifetime of fiber modification materials is limited because the matrix is not protected. Table 5.2 lists some coatings and their common preparation methods.

5.3.2.2 Matrix Modification

Matrix modification method involves the following process: When preparing C/C composites, antioxidants are added to the carbon precursor, so the antioxidants co-deposit with the carbon substrate on the carbon fibers to give composites with oxidation resistance. The antioxidants used for matrix modification should satisfy the following requirements:

1. Good physical and chemical compatibility with carbon matrix;
2. Low oxygen permeability;
3. Not catalyze oxidation;
4. Not affect the mechanical properties of C/C composites.

There are three main kinds of matrix modification technology: liquid impregnation, solid phase composition, and CVI.

1. Liquid impregnation technology

Liquid impregnation involves introducing antioxidants into the matrix as precursors after preparing C/C composites and then heating the bulk to obtain the antioxidants. The antioxidants might be oxide glass or non-oxide particles. Precursors of oxide glass include boric acid, borate, phosphate, and orthosilicate ethyl ester. The precursors of non-oxide particles are mainly organic metal alkanes. Glass antioxidants mainly depend on filling the pores in the fibers to prevent the C/C composites from oxidation, so the glass viscosity and wettability with the C/C composites play important roles [116, 117]. There are three antioxidants commonly used in impregnation: borate glass, phosphate glass, and silicate glass. Borate glass has ideal viscosity and wettability, and good oxidation resistance over a wide temperature range; however, it absorbs moisture easily and exhibits poor corrosion resistance. Because of its high vapor pressure, the oxidation protection temperature of borate glass is mainly below 1000 °C. Phosphate glass has better oxidation resistance, but with a lower protection temperature of below 600 °C. Silicate glass has poor flow behavior and wettability but better corrosion resistance than borate glass and its protection temperature is higher than 1500 °C.

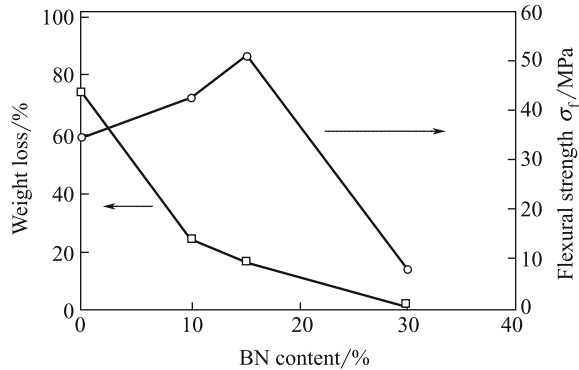
2. Solid phase composition

Solid phase composition introduces antioxidants into C/C composites as solid particles. The antioxidants might be simple substances such as Si, Ti, B, carbides including B₄C, TaC and SiC, borides such as TiB₂ and ZrB₂, silicides like TiSi₃, MoSi₂, and polyorganic boron silane [117]. The antioxidation mechanism of these antioxidants is that carbon reacts with these compounds to generate carbides. These oxides formed from oxidation of the carbides and the added compounds do not only react with oxygen, but also could prevent oxygen from diffusion. Therefore, the modified materials show good oxidation resistance.

C/C composites containing different antioxidants show different oxidation resistance, mainly because the carbides or added compounds possess different properties and crystal structure. If the carbides have high activity with high activation energy ΔG , they readily react with oxygen. However, during preparation, if some carbide has an incomplete crystal structure, it would be easily oxidized. If the generated oxides have a loose structure, then they do not prevent oxygen from diffusion, which results in poor oxidation resistance.

In an oxidizing atmosphere under 1150 °C, boron and borides are the best antioxidants owing to their ability to decrease the driving force of the reaction between carbon and oxygen [118]. Borides can be oxidized to B₂O₃ glass in air at 580 °C with 250% volume expansion [119]. B₂O₃ glass has low viscosity, so it fills the holes and cracks and covers the active points in the matrix. Song et al. [120] used BN to modify C/C composites. Modified composites with 15% BN exhibited the best mechanic and antioxidation properties, as shown in Fig. 5.29.

Fig. 5.29 Influence of BN content on the oxidation resistance and flexural strength (800 °C) of C/C composites



Zhu et al. [121] from NPU used metals such as Ti, W, Zr, and Ta as additives to form metal carbides, resulting in an inner multilayer gradient system. The oxidation resistance of C/C composites was improved greatly. The oxidation ablation rate was decreased by 75% after modification, and the oxidation starting temperature increased by 200 °C.

Liu et al. [122] impregnated carbon matrixes with B_4C and SiC as antioxidants. Then, C/C composites were prepared through matrix modification using oil coke as carbon precursor without binder. The weight loss of the as-prepared modified composites was less than 2% after oxidation for 2 h at 1200 °C. Under an air flow rate of 50 mL/min, the weight loss of samples increased after oxidation for 10 h with increasing oxidation temperature; however, less than 1% was lost below 1100 °C.

Adding modifiers to composites is always accompanied with a decrease of material strength. Meanwhile, ceramic grains impregnated in the composites easily break at high temperature. Modification with nanoceramic grains could solve this problem. Yang et al. [123] dispersed SiC in a carbon precursor. At a certain temperature, they began to bind together accompanied with the generation of microcarbon globes. Finally, a matrix material composed of nano-SiC grains reinforcing a carbon globules was obtained. Because of the strong bonding between carbon and Si, the composites showed good oxidation resistance.

The artificial nerve networks were introduced into C/C composites by ablation to build a net model of ablation rate *versus* composite additives [124]. The results indicated that the model could describe the relation between additive and ablation rate successfully. The experiment ablation rate had an aberration of less than 0.32% with the corresponding predicted value. Using the optimal additive indicated by the above model for modification, the composite ablation rate was decreased by 49.3%.

C/C composites doped with zirconium carbide were prepared with zirconium oxychloride solution as a precursor by Shen et al. [125, 126]. The ablation properties of the composites were tested using an oxyacetylene torch. The results showed that the linear and mass ablation rates of the composites after doping with 4.14 wt% zirconium carbide decreased by 83.0% and 77.0%, respectively.

3. CVI

CVI could realize the co-infiltration of carbon and antioxidants to improve the antioxidation properties of composites. Presently, co-infiltrating C and SiC to form double-matrix composites has mostly been studied. C- and SiC-co-infiltrated composites made using modern CVI technology include nano-matrix, gradient-matrix, and double-matrix composites. Their outstanding thermal physical and chemical properties indicate that they will be thermal materials with wide-ranging applications.

Liu et al. [127] prepared C-SiC double-matrix composites using a two-step CVI. First, preforms were infiltrated with a little pyrolytic carbon, and then with SiC until compaction. The characteristics of C-SiC double-matrix composites include two different matrixes from inner core to outer core: an inner layer of pyrolytic carbon with a rough layer structure, and an outer layer of isotropic SiC. There was no interface between carbon and SiC, and no microcracks were found in the composites. The fiber and carbon layer and C and SiC layer both had good cohesion. Fractured samples revealed that the weakest interface was not between C and SiC, but between the fibers and carbon. C/C and C-SiC composites of the same size were oxidized for 30 min at 1000 °C in air. The relative weight loss of C/C was 85% whereas that of C-SiC was 55%, and their oxidation starting temperatures were 500 and 600 °C, respectively.

5.3.3 Coatings Technology

Because the above modification methods cannot sufficiently isolate the C/C composites from oxygen, the antioxidation temperature and lifetime of modified C/C composites are limited and can only be used below 1000 °C in air. Above 1000 °C, the antioxidation of C/C composites relies on coatings technology.

5.3.3.1 Development of Antioxidation Technology of C/C Composites

Extensive research on the antioxidation of graphite has been performed since 1934, and it became the foundation for finding ways to prevent C/C composites against oxidation. From the 1970 s, the antioxidation of C/C composites used as thermal protection and friction materials began being studied. Many oxidation resistance problems such as the short antioxidation lifetime of nose cones and the leading edges of aerospace craft (the oxidation protection time was no more than 30 h below 1650 °C) and airplane brake disks (service life was 3000 landings and takeoffs below 1100 °C) have been successfully solved. As high-temperature thermal-structure materials, the investigation of C/C composites used in high-performance aero-engines and reusable space vehicles has been the main focus

of carbon materials since the 1980s. Research of C/C composites has recently focused on high-temperature, long-lived antioxidation coatings.

5.3.3.2 Essential Requirements for Oxidation-Resistant Coatings

Certain factors must be considered for the coatings prepared on the surface of C/C composites, including coating volatility and flaws, the interface bonding strength and chemical-mechanical compatibility between the coating and C/C composite matrix, and oxygen and carbon diffusion. These requirements determine the structure of antioxidation coatings of C/C composites. Specific requirements can be summarized as follows [128]:

1. Low oxygen diffusion coefficient;
2. Self-healing property;
3. Low vapor pressure in the service temperature range;
4. Matching thermal expansion coefficients of the coating and matrix;
5. Chemical-mechanical compatibility between the coating and matrix.

5.3.3.3 Oxidation Behavior of Coated C/C Composites

The oxidation behavior of C/C composites with coatings is obviously different from that of uncoated C/C composites. This can be explained using the characteristic oxidation temperature of the coatings, which is shown in Fig. 5.30. Research performed at NPU [128] indicated that the threshold oxidation temperature (T_T) of coated C/C composites was the same as the oxidation starting temperature of C/C composites, which was 370 °C. In general, coatings were prepared at high temperature, which was called the preparation temperature of coatings (T_F).

Furthermore, the service temperature limit of coatings (T_L) was not only related to the properties of the coating materials, but also to their lifetime. Below the preparation temperature of the coatings, cracks were formed by the mismatch of thermal expansion coefficient between the coatings and C/C composites, so this temperature was called the formation temperature of cracks (T_C). The temperature range from T_C to T_L was termed the intrinsic antioxidation temperature range. Within this range, the oxidation behavior of coated C/C composites was consistent

Fig. 5.30 General oxidation behavior of coated C/C composites [128]

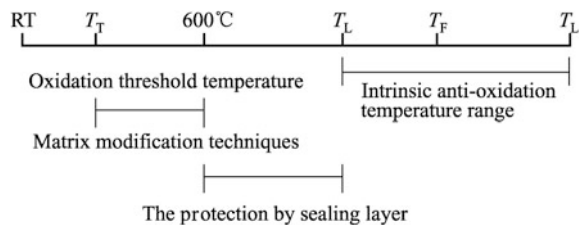
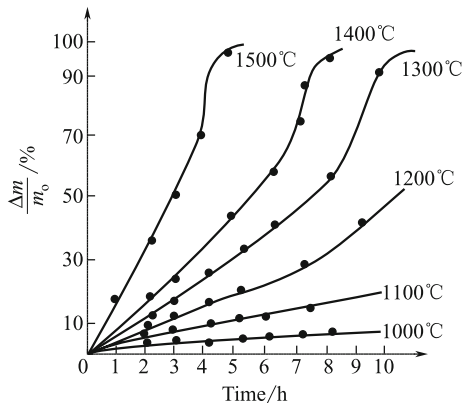


Fig. 5.31 Relationship between weight loss and Oxidation time of SiC-coated C/C composites [112]



with that of the coatings. From T_T to T_C , there was no essential difference of the oxidation behavior of coated and uncoated C/C composites.

For coated C/C composites, the oxidation process generally involves three stages, as shown in Fig. 5.31 [112]. In the initial low-temperature oxidation stage, the oxidation rates of the coated C/C composites are proportional to the oxidation time (the weight loss is below 20%):

$$\Delta m/m_0 = k_{21}t$$

In the mid-high-temperature oxidation stage, the oxidation rates of the coated C/C composites are proportional to the oxidation time (the weight loss is in the range from 20% to 70%):

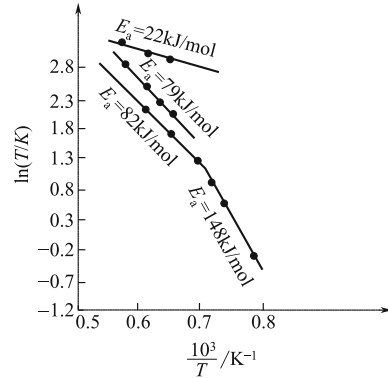
$$\Delta m/m_0 = k_{22}t \quad k_{22} > k_{21}$$

In the high-temperature oxidation stage, the oxidation law of the coated C/C composites shows log-type behavior (the weight loss is above 70%):

$$\Delta m/m_0 = 1 - e^{-k_{23}t}$$

where Δm is the weight loss, m_0 is the initial weight, t is the oxidation time, and k_{11} , k_{22} , k_{12} , k_{22} , k_{23} are all constants. By calculating the oxidation rate constant and plotting the Arrhenius curve (Fig. 5.32), it could be found that the first stage (at low temperature) of the curves was composed of two broken lines with different activation energies. The activation energy changed with increasing temperature, showing that the oxidation mechanism changed. The activation energy was higher for the low-temperature stage. In this case, because the diffusion rate of oxygen is higher than the reaction rate, there was no oxygen concentration gradient in the diffusion channels, so the oxidation of the sample was uniform and the oxidation rate was mainly controlled by the oxidation reaction rate. In the linear oxidation region above the transition temperature (the second stage), with the increase of

Fig. 5.32 Arrhenius curves of SiC-coated C/C composites [112]



reaction temperature, the gas-solid reaction rate accelerates and can even exceed the diffusion rate. In this case, the oxidation not only depends on the oxidation reaction, but also on the diffusion of oxygen through the coating and matrix. During the final stage of oxidation, the oxidation of the coated materials obeys the logarithmic law. In contrast, the uncoated materials showed linear behavior, and the oxidation rate increased significantly. This situation occurs at high temperature, when many ablation cavities have formed and the rates of interface reaction and diffusion are very high, so the reaction is controlled by the diffusion of reactants and products through the matrix or coating.

5.3.3.4 Structure of Coatings

According to their antioxidation temperature, coatings can be divided into low-temperature coatings (less than 1100 °C) and high-temperature coatings (1100–1800 °C). The former includes B_2O_3 , while examples of the latter are SiC, $MoSi_2$, and other high-temperature ceramics [129]. Coatings can also be divided according to their structure into single and multilayer coatings. Single coatings are mainly used for low temperature and short-term antioxidation. Multilayer coatings are mainly used for long-term, high-temperature antioxidation. The different structures of multilayer coatings play different roles; they are categorized as follows:

1. Corrosion-resistant layer

C/C composite parts are generally used in high-speed airflow environments, so the erosion of the coating by high-speed airflow and self-evaporation are important factors that affect the lifetime of the coating. In addition, the coating is rapidly oxidized if its outer surface is not dense. As a result, corrosion-resistant layers are usually dense oxide ceramic materials with low surface vapor pressure.

Using the Langmuir theory, the maximum allowable surface vapor pressure of oxides can be calculated. Sheehan's calculation results showed that the maximum allowable surface vapor pressure usually was 133.322×10^{-3} Pa [107]. Even in a

high-speed mobile environment, the allowable vapor pressure was still close to the calculated value because of the presence of a surface boundary layer. Considering surface vapor pressure, most oxides could be used as corrosion-resistant materials below 1700 °C. However, most oxides simultaneously possess other properties that make them unsuitable for use as corrosion-resistant coating materials. For example, CaO and BeO are very sensitive to humidity, BeO is highly toxic, ThO₂ is radioactive, and TiO₂ is sensitive to the oxygen concentration of the environment. Although the cracking tendency of HfO₂ is slower than those of Y₂O₃, HfO₂, and ZrO₂, it must undergo crystal stabilization treatment to avoid destructive phase transformation during thermal cycling [107, 130, 131].

2. Oxygen barrier layer

Preventing oxygen in the external environment from permeating into the matrix is the key requirement to the oxidation resistance of coatings. Even if a dense and crack-free coating can be prepared, the oxygen penetration caused by solid diffusion is also an important problem.

Thermodynamic calculations have shown that dense, high-purity Si₃N₄ and SiC coatings can provide oxidation protection for C/C composites under strongly oxidizing atmospheres in the temperature range of 1700–1800 °C. The durability of Si₃N₄ and SiC depends on the formation of an SiO₂ protective film, which is an excellent oxygen barrier layer because of its very low oxygen permeability (10^{-13} g·cm⁻¹·s⁻¹ at 1200 °C, and 10^{-11} g·cm⁻¹·s⁻¹ at 2200 °C) [107, 130–132]. Oxygen cannot quickly penetrate through an integrated SiO₂ layer to attack the underlying matrix material. The service temperature of Si₃N₄ and SiC is determined by the purity of the materials, the components used, and environmental conditions.

The oxygen penetration rate of HfO₂, ZrO₂, and ThO₂ reaches up to 10^{-9} g·cm⁻¹·s⁻¹ in the temperature range of 1300–1400 °C, so the oxidation resistance of such coatings at high temperatures is poor. However, the oxygen penetration rate of Al₂O₃ is lower than 10^{-9} g·cm⁻¹·s⁻¹ at 1800 °C. In addition, iridium has a high melting point (2240 °C) and low oxygen penetration rate of less than 10^{-14} g·cm⁻¹·s⁻¹ at 1800 °C. Based on the above analysis, HfO₂, ZrO₂, and ThO₂ are not suitable for an oxygen barrier, but could be considered as a corrosion layer. Although iridium and Al₂O₃ provide low oxygen permeability, iridium is a noble metal, and its thermal expansion coefficient mismatches with that of carbon. Furthermore, iridium generates volatile IrO₃ in oxidizing environments. The oxygen penetration rate of Al₂O₃ is higher than that of SiO₂, and Al₂O₃ reacts with carbon at high temperature. Synthetically, considering the requirements of corrosion and oxygen barriers, SiC and Si₃N₄ show the best comprehensive performance below 1800 °C [107, 118, 130–132].

3. Sealing layer

Carbon fiber has an extremely low CTE; for example, T300 with an axial CTE is $-0.72\text{--}0.932 \times 10^{-6}$ K⁻¹, and radial is 8.85×10^{-6} K⁻¹. The linear expansion coefficient of C/C composites using high-modulus carbon fiber as reinforcement is in

the range of $0-1 \times 10^{-6} \text{ K}^{-1}$. In this regard, the linear expansion coefficient of SiO_2 is similar to that of C/C composites. However, at high temperature, SiO_2 reacts with carbon and produces CO in the interface, which results in the formation of bubbles or pores in SiO_2 glass. Thus, SiO_2 cannot be used directly on the surface of C/C composites. The linear expansion coefficients of Si_3N_4 and SiC are the next best with SiO_2 , but are still 5–10 times that of C/C composites. In particular, parallel to the fiber direction, when materials cool from a high temperature, a pulling stress is produced on the surface of coating, which causes the coating to crack. Because the oxidation starting temperature of carbon materials is 370°C , and although it can be improved to 600°C by modification, it is still far from the self-sealing temperature of cracks. To prevent oxygen from oxidizing the matrix through the cracks between the oxidation starting temperature of carbon materials and the self-sealing temperature of cracks, it is necessary to add a vitreous sealing layer inside the outer coating layer. Currently, there are three categories of glass used to fill cracks: borate, phosphate, and silicate glass. However, phosphate glass has a low service temperature, silicate glass is poor at filling, and borate glass is deliquescent. Therefore, the composition of the glass needs to be optimized. For example, the introduction of SiO_2 could improve the sealing temperature, while adding alkaline earth metal oxides and B_2O_3 could improve sealing at low temperature.

4. Transition layer

The major roles of a transition layer are to reduce the mismatch of linear expansion coefficient between the coating and substrate, improve the internal structures of coatings, and prevent chemical reaction between the sealing layer and substrate to improve the physical and chemical compatibility of interfaces. The cracks caused by mismatch of the linear expansion coefficient are another important factor influencing the antioxidation behavior of coatings. Under the erosion caused by high-speed airflow, these cracks not only promote oxygen permeability, but also cause the coating to spall. Therefore, the linear expansion coefficient of transition layer should be as close to that of the substrate materials as possible. Usually, an SiC or Si_3N_4 layer is prepared by CVD on the substrate surface as a transition layer.

5.3.3.5 Preparation Methods of Oxidation-Resistant Coatings for C/C Composites

The methods used to prepare oxidation-resistant coatings depend on the application of the composites. The main methods to fabricate oxidation-resistant coatings of C/C composites are listed as follows:

1. Pack cementation

In this process, C/C composites are encapsulated with several kinds of mixed powders, and then heat treated at high temperature. The mixed powders react with the surface of the C/C samples to form coatings.

Compared with other methods, the advantages of pack cementation are:

1. Dense, crack-free coatings can be obtained by a single, simple preparation process;
2. The change of sample size is very small;
3. It is applicable to any fiber-reinforced composite;
4. A composition gradient can be formed at the interface of the coating and C/C matrix, and the bonding between the coating and C/C matrix is excellent.

However, there are some disadvantages that limit the wide application of pack cementation. For example, the fibers can be damaged by reaction with the powders at high temperatures, which could affect the mechanical properties of the C/C composite. In addition, it is very difficult to control the uniformity of coatings; the upper and lower surfaces of the coatings are uneven because of gravity.

2. CVD

CVD is an important method for preparing oxidation-resistant coatings for C/C composites. The coating materials, generally compounds, are introduced into a CVD furnace. A series of processes including decomposition, synthesis, diffusion, adsorption, and desorption are performed at certain temperature and pressure to form solid films on the surface of C/C composites. Because the coatings formed by CVD are very dense and pure, their microstructure, morphology, and composition can be controlled. The deposition rate can also be controlled, so overall CVD has attracted considerable attention.

CVD is a common technique, and uniform classification standards are available. According to the deposition pressure, CVD can be divided into atmospheric, low-pressure, and pulsed CVD. According to the deposition temperature, CVD can be divided into isothermal and temperature-gradient CVD. Other methods such as laser-assisted CVD (LACVD) and plasma-assisted CVD (PAVCD) have also been developed.

The main advantages of CVD are that coatings containing several elements and compounds can be deposited at low temperature, defects and damage of the C/C composites resulting from heating at high temperature can be avoided, and complete, high-purity crystalline coatings can be obtained. The composition and structure of the coatings prepared by CVD can be controlled.

However, fine control of the CVD process is difficult and requires vacuum or a protective atmosphere. Because the gas phase is used to form the coating, and there are several reactions during the CVD process, solid particles may be involved in the gas phase. The flow of the mixed phases lies between those of the gas phase and solid particles during the deposition process, making the kinematics viscosity difficult to control. In addition, the effects of deposition temperature, diffusion, convection in the boundary layer, reaction thermodynamics, kinetics, preferential orientation of crystals have important effects on the coating [133]. Therefore, it is very difficult to build a quantitative mathematical model to describe the CVD process.

At present, the coatings prepared by CVD on the surface of C/C composites mainly include SiC, Si₃N₄, BN, ZrC, TiC, and MoSi₂. SiC and Si₃N₄ silicides are the most common coatings.

3. Gaseous permeation

Taking permeation of Si as an example, the principle of gaseous permeation is as follows: Si becomes Si vapor at high temperature. The Si gas diffuses into the surface and inside the C/C matrix, and then reacts with carbon in the C/C matrix to form a SiC coating. The advantages of this method are that the atmosphere is easy to homogenize, and the reaction rate and thickness of the coating are uniform. Gaseous permeation is simple, easy to operate, and the thickness of the coating can be controlled by changing vapor pressure and deposition time. The disadvantages of this method are that the setting position of the sample affects deposition, and the thickness of the coating is not uniform because Si vapor pressure in the furnace cannot be uniform in theory.

4. Liquid method

The liquid method involves the porous C/C composite matrix being impregnated with a solution of organometallic compounds, alkoxy metal compounds, metal salt, or colloid, and then decomposed or reacted to form coatings by drying or reaction. The yield of liquid phase transforming into coating material is low, so multiple impregnations are needed. Debrunner and Clements [134], Wilson [135], and Stratre [136] described the preparation of oxidation-resistant coatings by this method in their patents. The selection of raw materials, the preparation temperature, and the process control were considered. This method is suitable not only for preparing special ceramics such as SiC, MoSi₂, and WSi₂, but also glass materials such as B₂O₃ and SO₂.

The selection of raw materials for liquid impregnation requires consideration of the following factors: First, it needs to prevent the diffusion of oxygen inside the matrix; second, the raw materials must have low volatility and excellent bonding with the matrix; third, the coating needs to prevent the outward diffusion of carbon to prohibit the carbothermal reduction reaction; finally, the chemical compatibility and match of expansion coefficients between the materials and C/C composite matrix need to be good.

Yi et al. [137, 138] from the Central South University of China impregnated the surface of C/C composites, brushed the coating, and then carried out solidification treatment to form coatings with excellent oxidation resistance. The oxidation starting temperature of the composites by pre-impregnation was increased by about 200 °C, and the weight loss of C/C composites prepared by pre-impregnating phosphoric acid or a mixture of phosphoric acid and boric acid was 0.40% and 0.33%, respectively, after oxidation for 2 h at 900 °C.

The liquid reaction-formation method was proposed by Cheng et al. [139, 140] from NPU to prepare oxidation-resistant coatings. The as-prepared oxidation-

resistant coatings were dense and uniform. The oxidation-resistant Si-Mo coatings prepared by this method could protect C/C composites for 10 h at 1650 °C.

The advantages of the liquid method are as follows: The preparation temperature is low, there is little effect on the matrix strength, the bonding strength is high, and the self-sealing property of the as-prepared coatings is excellent. The disadvantages are that the composition of coatings is affected by the impregnation liquid and diffusion in the matrix, and a large amount of protective gas is required. In addition, the liquid materials and matrix were wet. The wetting angle needs to be below 60° to ensure high bonding strength between the coating and C/C matrix.

5. Slurry method

The slurry method involves mixing the coating materials with bonding agent to form a slurry, which are brushed on the surface of matrix to obtain the required coating thickness and then solidified at a certain temperature. As-prepared samples are then heat treated at elevated temperature under an inert atmosphere to obtain the coating. This method possesses advantages such as being a simple process and easy control of the coating thickness. However, the bonding strength between coating and matrix is poor. As a result, the thermal shock resistance of the coating is not good. In addition, the uniformity of the coating is difficult to control.

6. Plasma spray method

The plasma spray method was developed following the flame and arc spray methods. In this method, powders are heated and accelerated using plasma produced by a spray gun. The molten or near-molten plasma is sprayed onto the surface of a matrix to form a coating. The temperature produced by plasma electric arc is up to 16000 °C, and the speed of the spray is up to 300–400 m/s. As a result, this approach can be used to spray various coatings with high melting point, friction resistance, and heat resistance. The coatings prepared by this method show comparatively high bonding strength, few impurities, and good controllability of coating thickness. The plasma spray method has been used to prepare ceramic coatings such as Al₂O₃ and ZrO₂. If using inert gases as the medium, the oxidation during the course of plasma flight could be reduced. However, because of the mismatch of thermal expansion coefficient between coatings and matrix and the presence of some remnant gases such as N₂ or Ar, cracks and holes readily form in the coatings during spraying. Huang et al. [141, 142] used the plasma spray method to prepare gradient yttrium silicate multi-composition coatings on the surface of SiC-coated carbon/carbon composites. The obtained coatings showed excellent oxidation protection ability and could protect C/C composites from oxidation in air at 1500 °C for a long time.

7. Sol-gel technique

The solgel technique is mainly used to prepare glass, glass ceramics, ceramics, and other inorganic materials using metal alkoxides as precursors. Under mild conditions, by the hydrolysis, polycondensation, and other reactions of the raw

materials, the sol forms a gel, which is then sintered at low temperature to form an inorganic material. The sol-gel technique involves dissolving the metal alkoxide in organic solvent, adding other reagents to form a uniform solution. At a certain temperature, the solution is converted into a sol, and then into a gel. Finally, the gel is changed into glass, ceramic, or other inorganic materials by drying, heat treatment, and sintering.

The uniformity of coatings prepared by this method is easy to control at the beginning of preparation. However, unsintered coatings readily crack or spall during drying because of shrinkage of the gel, which reduces the service life of such coatings. Research by Huang et al. [143] showed that spalling of the coating could be reduced by pre-decomposition after immersion in the sol. The resulting Sol-gel gradient ZrO_2 - SiO_2 coatings improved the oxidation resistance of C/C composites.

In recent years, to meet different requirements, some special preparation methods have been developed. Besides the above-mentioned seven methods, supercritical fluid technology is also a feasible approach to prepare coatings on carbon/carbon composites.

Supercritical fluid technology, which originally was patented in the USA [144], uses supercritical fluid as solvent and carrier to fill the internal defects of C/C composites. The supercritical fluid helps the precursor to impregnate the C/C composite and form an oxidation-resistant coating through thermolysis. It is well known that as the temperature and pressure of a chemical system exceed certain critical conditions, it forms a state where it is present as both liquid and vapor, namely a supercritical fluid, which has some special physical characteristics. On the one hand, supercritical fluids exhibit high solubility and can dissolve some high-molecular-weight polymers that are considered insoluble under normal conditions. The solubility of materials in supercritical fluids largely depends on the temperature and pressure, which are easy to control. On the other hand, supercritical fluids possess low viscosity, high diffusivity, and lack surface tension, which improve transport properties and allow penetration of submicron-size pores. The inventor of this patent used the advantages of supercritical liquids to design the following technical process: First, the precursor is placed in a container. The C/C composites are wrapped by fiber glass weaves to avoid direct contact with precursor and then placed in the container. After pressurization, the container is filled with gas precursor in supercritical liquid. The pressure and temperature are increased until a supercritical liquid that can dissolve the precursor is formed. These conditions are maintained for a long period to allow adequate permeation of the C/C composite, and then the pressure and temperature are reduced at a constant rate to deposit the precursor in the porous body. Thereafter, the body is pyrolyzed under an inert atmosphere. A supercritical liquid was obtained using propane in the supercritical state. Typical oxidation-resistant precursors are polycarbosilane and polysilicon methane to prepare SiC coating, and N-hexylcarborane as a precursor for B_4C coatings. The most important advantage of supercritical liquid technology is its favorable transport properties, not only an oxidation-resistant coating is formed on the outer layer of the composite, but also the precursor penetrates into the interior and fills up holes and defects. This improves the oxidation protective ability of the

coating from inner to outer layers. In the patent, polycarbosilane was dissolved in propane to prepare an oxidation-resistant coating. The supercritical liquid propane was formed at 160 °C at a pressure of 40 MPa, and the precursor was dissolved completely and then maintained under these conditions for one hour to achieve immersion. Then, the pressure was reduced and the temperature decreased to deposit the coating. Finally, pyrolysis was conducted at 1000 °C.

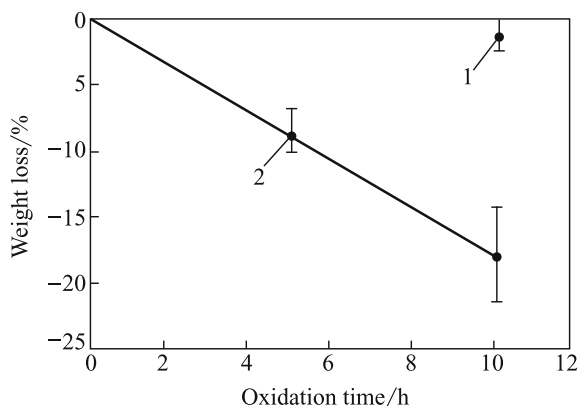
5.3.3.6 Oxidation-Resistant Coating Systems

(1) Si-based ceramic coatings

Si-based ceramic coatings are the most deeply investigated among all oxidation protective coating systems. These coatings are prepared by synthesizing Si-based ceramic composites on the surface of carbon matrix. The Si-based ceramic reacts with oxygen to form a silica oxidation protective coating on the surface of the coatings.

1. Si-based single layer coatings. At present, SiC and Si₃N₄ coatings, commonly prepared by CVD, are widely applied as oxidation-resistant coatings. Because of the long-term preparation cycle of CVD, some other methods have been developed in recent years. Wu [114] and Huang [145] used the diffusion reaction of liquid Si and C to prepare SiC coatings by pack cementation. Chen et al. [146] used reaction sintering technology to brush Si and epoxy on the surface of C/C composites to form a pre-coating, which was then sintered at 1800 °C to obtain an SiC coating. Other silicides such as WSi₂, MoSi₂, and HfSi₂ can react with oxygen at high temperature to generate silica, but the thermal linear coefficient of silicides is larger than that of C/C composites, which indicates that these silicides are not suitable to prepare directly on the surface of C/C composite. Therefore, they need to be combined with other ceramic materials with similar CTE to that of C/C composite to form an oxidation protective coating. Si–Hf–Cr, Si–Zr–Cr, and Si–Ti coatings formed by the slurry method can improve the oxidation-resistant temperature of C/C composites up to 1600 °C [147]. In this method, Si and high-purity metals were mixed in certain proportions. Inorganic agents were added to get a slurry, and the viscosity of the slurry was adjusted by changing the ratio of inorganic components. The C/C samples were dipped in the slurry, and the thickness of the coating was controlled by changing the dipping speed. The coated samples were heat treated at 1300–1400 °C under vacuum to form alloy coatings on the surface of the matrix. SiC particles were dispersed equally throughout the integrated oxidation-resistant coating. To ensure the integration of the coating and increase density, the whole process was repeated. The produced coating had a homogeneous composition that showed improved oxidation resistance.

Fig. 5.33 Oxidation time versus weight loss of SiC-coated C/C composites prepared by CVD (Samples were heated at 1700 °C in N₂-CO₂-H₂O mixed gas under isothermal oxidation) 1: composites without fiber interlayers; 2: composites with interlayer



- Si-based double ceramic coatings. The first SiC fiber composite coating was reported by Etesaikao and Cheng in *Electric Carbon* in 2002 [148]. First, SiC fiber felt was used to cover the surface of a three-dimensional C/C substrate. This was dipped into a slurry containing a uniform distribution of C and Si particles, and then SiC was deposited by CVD to form a compact coating on the surface of the composite. The prepared SiC fiber composite coating was composed of a double-layer structure: The inner layer was a porous SiC/SiC fiber layer and the outer layer was dense SiC layer. The total thickness of the SiC fiber composite coating was about 300 μm . Because the linear expansion coefficient of the SiC/SiC fiber layer was between that of C/C composite and SiC coating formed by CVD, spalling of the coating caused by thermal stress due to the mismatch of linear expansion coefficient could be reduced to a minimum using the SiC/SiC interlayer as a buffer. Figure 5.33 [149] shows the isothermal oxidation curves of the coated C/C samples in air at 1700 °C. Oxidation-resistant coatings for C/C composites such as Si/MoSi₂ and SiC/MoSi₂ have been developed [149–154]. These coatings have an excellent antioxidation ability at 1500 °C and do little damage to the underlying matrix. At 1500 °C, the oxidation weight loss rate of Si/MoSi₂-coated composites stabilized at $2.43 \times 10^{-5} \text{ g}/(\text{m}^2 \cdot \text{s})$, and the weight loss after 242 h of oxidation was just 0.57% due to the evaporation of glass phases, as shown in Fig. 5.34. The composites with SiC/MoSi₂ coatings were oxidized for 50 h at 1700 °C. Under such conditions, their weight loss was less than 2%, as shown in Fig. 5.35. Meanwhile, both the coatings show good self-sealing and thermal shock resistance properties [155–158].
- Multilayer silica-based ceramic coatings. Zhu et al. [159] prepared (SiC/Si₃N₄)/C functional gradient coatings using silicon infiltration technology. The weight loss of the coated composites after 20 h at 1500 °C was just 0.25%. First, the silicon-packed C/C composites were heated in a vertical carbon furnace under NH₃ atmosphere. When the temperature exceeded the fusion point of Si, it

Fig. 5.34 Isothermal weight loss curve of uncoated and Si/MoSi₂-coated C/C composites at 1500 °C

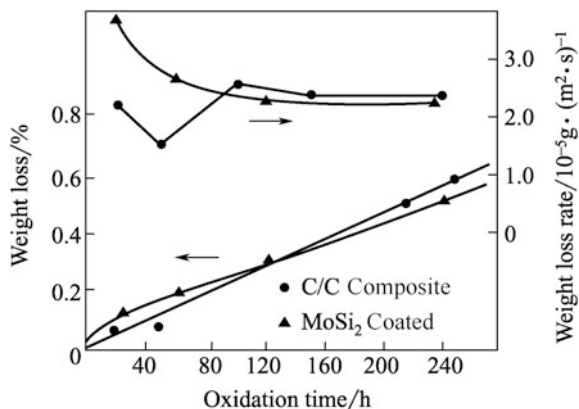
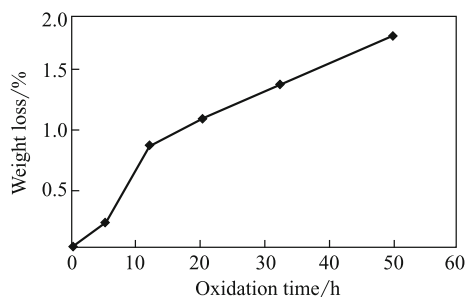


Fig. 5.35 Weight loss curve of SiC/MoSi₂-coated C/C composites at 1700 °C



reacted with NH₃ and C to form the (SiC/Si₃N₄)/C functional gradient coating. Because the thermal resistance of Si₃N₄ is almost equivalent to that of SiC, but its expansion coefficient is smaller, this structure nicely solved the problem of mismatch between the C/C composite and coating and improved oxidation resistance.

Cheng et al. [160, 161] used the liquid method to prepare multilayer gradient coatings on C/C composites that exhibited good oxidation resistance at 1650 °C. The system was composed of: SiC transition coating/CVD-formed SiC barrier layer/liquid thermal glass sealing coating. The coating with this structure could work for more than 168 h at 1600 °C (Fig. 5.36) [161].

Huang et al. [162, 163] prepared an Al₂O₃-mullite-SiC-Al₄SiC₄ coating using pack cementation. The coating exhibited outstanding oxidation resistance (Fig. 5.37), with a weight loss of 1.41% at 1500 °C after oxidation for 41 h. The coating was prepared using SiO₂, Al₂O₃, Si, and C powders in the first pack cementation cycle. In the second pack cementation cycle, Si, C, SiC, SiO₂, and Al₂O₃ were used to form the Al₂O₃-mullite-SiC coating. The weight loss of the coated C/C composites was 1.86% after oxidation for 45 h at 1600 °C (Figs. 5.38, 5.39, and 5.40) [164].

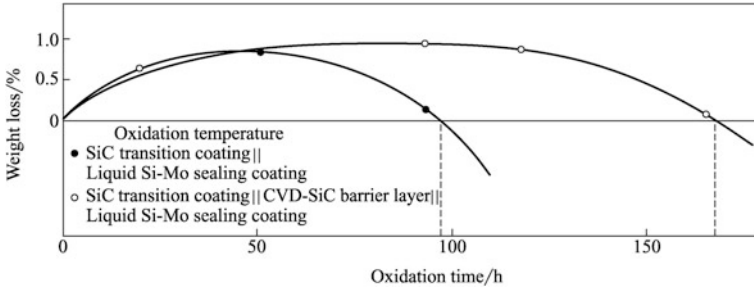


Fig. 5.36 Weight loss of SiC/SiC/Si-Mo-coated C/C composites over time [157]

Fig. 5.37 Weight loss of Al₂O₃-mullite-SiC-Al₄SiC₄-coated C/C composite at 1500 °C [162]

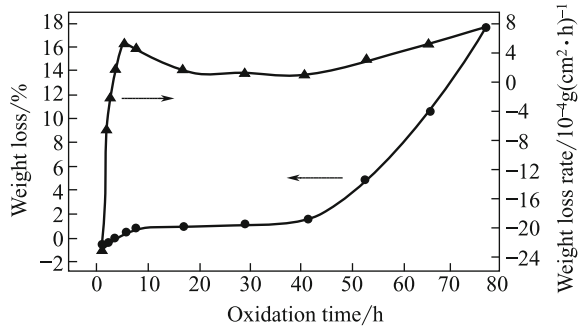
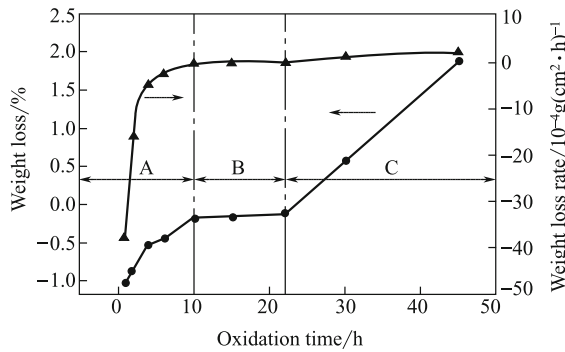


Fig. 5.38 Relation between weight loss and oxidation time at 1600 °C for C/C composites coated with an Al₂O₃-mullite-SiC multilayer coating



Huang and coworkers [165, 166] have successfully obtained SiC/yttrium silicate coatings. The coating had a dense structure and could provide 200 h of protection for C/C composites at 1600 °C with a weight loss of less than 1% [167–174].

(2) Glass coatings

At high temperatures, microcracks are form in coatings because of the mismatch of thermal expansion coefficient between ceramic coatings and C/C composites.

Fig. 5.39 Microstructure of the cross section of an SiC/yttrium silicate/glass multilayer coating

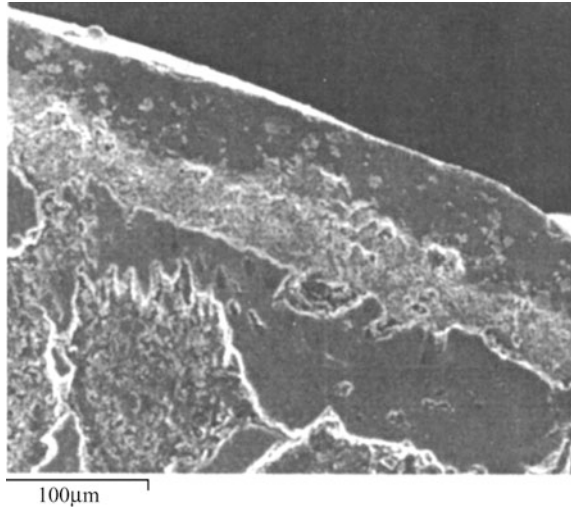
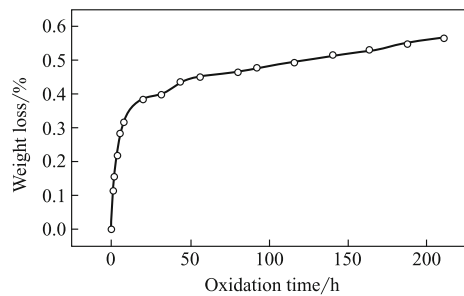


Fig. 5.40 Relation between weight loss and oxidation time at 1600 °C for C/C composites coated with an SiC/yttrium silicate/glass multilayer coating [164]



Because of the diffusion of oxygen, the antioxidation ability of a coating degrades and eventually fails. Glass coatings can efficiently heal microcracks within them at high temperature [175].

1. Borate glass coatings. Borate glass melts are mainly composed of B_2O_3 , but the properties of B_2O_3 such as its high sensitivity to moist environments at room temperature, volatility, and decreasing wettability with increasing temperature limit the oxidation resistance of such coatings, so they are not suitable for oxidation protection above 1000 °C. To improve the oxidation resistance of B_2O_3 coatings, researchers have modified their treatment. SiC coatings were first deposited on the surface of C/C composites by CVD. A sealing layer was then prepared with metal oxides (such as Na_2O , K_2O , Al_2O_3 , and CaO) and boron carbides, which reacted with each other at high temperature to form metal borides. The antioxidation temperature of the resulting material is up to 1100 °C.

The stable binary phase system of B_2O_3 - SiO_2 is formed by the reaction of B_4C and SiC with oxygen at high temperature. In this system, microcracks in the inner

coatings can be sealed through the mobility of B_2O_3 with SiO_2 , and a stable, dense oxygen barrier layer can be formed to cover the oxidation-active centers on the C/C composite surface. The binary phase system exhibited dual antioxidation effects and could protect C/C composites up to 1200 °C.

A double-layer borate glass coating was prepared on SiC-coated C/C composites by Smeacetto et al. [176, 177]. The oxidation resistance of the composites was improved greatly by the multilayer coatings. After oxidation for 150 h at 1300 °C, the weight loss of the coated samples was less than 1%.

2. Phosphate glass coating. As a novel inorganic adhesive, phosphate glass received attention because it is nontoxic, odorless, nonpolluting, and shows good high-temperature performance. Aluminum phosphate, calcium phosphate, barium phosphate, zinc phosphate, and strontium phosphate are all good glass-forming substances. Glass with the required properties can be formed by reacting the above phosphate glasses with each other. The structure of phosphate glass is based on the network of $[PO_4]$ and possibly contains $[PO_2]$ circles. Aluminum phosphate is the main component of stable phosphate glass, but the gel formation mechanism of aluminum phosphate adhesive that involves losing water is very complex, and the adhesion mechanism is not very clear, so both need further study. Aluminum phosphate is an acidic compound consisting of aluminum diacid phosphate, water, and phosphonic acid. It then loses water sequentially to form the adhesives $Al_2(HPO_4)_3$ and $AlPO_4 \cdot 2H_2O$. $AlPO_4$ forms at about 700 °C, which has a special network that shows excellent strength [178].

Coatings formed through adhesion of phosphonic acid and phosphates possess strong adhesive properties, allowing solidification of the powders of coatings with the substrate. There are two generally accepted adherence theories of phosphonic acid and phosphates. The first is the film adherence theory, which is that the film envelops the surrounding particles when the acid phosphates are heated. The second is inorganic polymerization theory; the polymeric catenulate molecules become vitrescent at higher temperature to agglutinate the particles when the phosphates are heated.

The raw materials of such phosphate coatings are inexpensive, and the brush process is very simple. These coatings are suitable for C/C composite plane brakes and have been paid much attention as aircraft antioxidation C/C composite brakes for the reverse of frictional surfaces.

Phosphates have good wettability for C/C composites, which could allow the coating slurry to fully spread over the surface of substrates to seal the holes and other defects on the surface. It could also reduce the number of oxidation-active centers and the mismatch of CTE between the substrate and coating. In addition, phosphonic acid transforms to phosphorous acid by water loss, then to pyrophosphoric acid, and finally P_4O_{10} upon heating. P_4O_{10} has a network frame of phosphorous cross-linked with oxygen, which can form thin inner coatings when attached to the inner surface of holes in C/C composites. The network of P-O blocks

oxygen from diffusing through the outer coating or cracks in the coating, and prevents the C/C composite from oxidation. Energy-dispersive X-ray analysis of the coating surface showed that there was considerable phosphorous on the coating surface, indicating that P_4O_{10} moved to the surface of the coating in the opposite direction to oxygen diffusion at a certain temperature and reacted with oxides on the surface of the coating. The reaction of P_4O_{10} to form oxides would protect the C/C composites from oxidation. In addition, the phosphate coatings were dense and bonded strongly with the C/C matrix. The oxidation resistance and thermal shock resistance of these coatings are excellent.

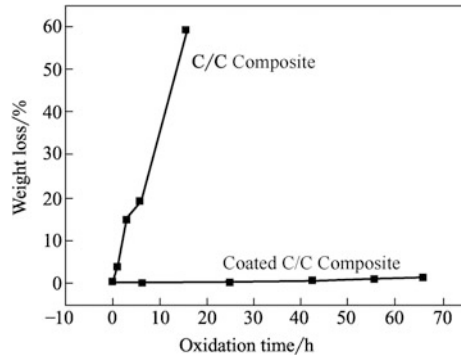
At present, some research institutes in China have invested heavily in investigating the antioxidation of C/C composite brakes and made great progress on corresponding theories and experiments of phosphate coatings [179–181].

Yang et al. [182] of Huaxing Aircraft Wheel Corporation used the solgel method to prepare coatings on the surface of C/C composites. The raw materials were mainly phosphorous acid and metal phosphate, as well as boric acid and acid-soluble metal oxides and some phosphate modifier. C/C composite samples covered with the above coatings were oxidized for 24 h in a double-pipe stove at 710 °C and air flow of 200 mL/min; the weight loss was 4.7. Coated samples were oxidized at 710 °C for 2 min and then placed at room temperature for 3 min fifty times, held at 850 °C for 2 min and at room temperature for 3 min five times, and then at 1100 °C for 2 min and at room temperature for 3 min three times. After these cycles, the weight loss of the coated samples was 0.58%.

Liu et al. [183] from Central South University prepared multi-composition ceramic-compound coatings that were mainly composed of silicides and borides, with phosphonic acid, phosphates, SiC, SiO_2 , B_4C , and boracic compounds. After being oxidized at 900 °C for 10 h, the weight loss of the coated C/C composite samples was 10.37%. When the coated samples were oxidized in air at 900 °C for 3 min and then held at room temperature for 2 min 100 times, their weight loss was 8.41%.

Phosphate coatings have also been studied extensively by the Materials Research Center of C/C Composites, National Key Laboratory of Thermostructural Composites, NPU. Two kinds of phosphate coatings were prepared using different materials. Phosphate coating I was composed of alumina, boric oxide, aluminum phosphate, and some acid oxides. The weight loss of coated samples was only 1.2% after oxidation in air at 650 °C for 30 h, and 7.07% after 8 h at 800 °C. Phosphate coating II was composed of boric oxide, silicon oxide, and some phosphates. The weight loss of the coated samples was 1.11% after oxidation in air at 700 °C for 66 h (Fig. 5.41). When the samples were oxidized in air at 900 °C for 3 min and then held at room temperature for 2 min 100 times over 10 h, the weight loss was 1.6%. During the oxidation test, phosphate coating II adhered to the substrate well kept intact and no peeling was observed. This shows that the coating was suited as an antioxidation coating of C/C composite brakes because of its resistance to high temperature and good thermal stability.

Fig. 5.41 Isothermal oxidation curves of phosphate-coated C/C composites at 700 °C [184]



5.3.4 Prospects

The oxidation resistance of C/C composites is an important and very difficult topic. This field has been developed greatly in the previous three decades, and they were applied in many fields such as plane brakes, and the nose and wing tips of space shuttles, because of their ability to resist high temperature during reentry to the atmosphere. However, long-lived coatings used at temperatures of 1650–1800 °C and above 1800 °C are still not available. Many coatings have been developed, but none has been employed in practice. Much work should be done to improve the oxidation resistance of these coatings. The emphasis of study on the oxidation resistance of C/C composites has the following four directions:

1. Up to now, most coatings were prepared on the surface of small samples, so research on coatings was based on small samples. The stability, uniformity, and practicability of coatings for large components should be investigated.
2. The effects of coatings on the properties of C/C composites should be investigated. The properties of C/C composites should not be decreased greatly after coating.
3. The specific demands of coating applications should be investigated. Because C/C composite components cooperate with other components in many situations, the wear resistance or adhesion to other components should be determined.
4. The oxidation resistance of coatings in different atmospheres and resistance to scouring under high-speed flow should be investigated. Under high-speed flow, the sealing layer on the coating surface might be removed from the surface of components, so the oxidation resistance of the coating would be decreased. Therefore, the oxidation resistance of C/C composites needs further research to meet the demands of practical applications.

5.4 Applications and Prospects of C/C Composites

C/C composites have been used in the aeronautic, astronautic, and military fields because of their excellent unique properties. With the development of technology and the reduction of cost, C/C composites have gradually emerged in many civilian areas. In this section, the applications of C/C composites in the aeronautic, astronautic, military, and biomedical materials industries are introduced briefly.

5.4.1 Application of C/C Composites as High Speed Braking Materials

Aircraft brakes are the largest application field of C/C composites. In 1976, C/C composite aircraft brakes were used successfully in Concord supersonic aircraft by British Airways. Gradually, C/C composite brakes were included in high-speed military aircraft and large civil aircraft. The weight of “B-1” bombers was reduced from 1406 to 725 kg using C/C composite brakes [185, 186]. After their development in the 1970s and 1980s, the market for C/C composite brakes became relatively mature in the 1990s. The market for aircraft brakes reaches nearly 800 million dollars each year. Aircraft brakes made from C/C composites instead of steel have become increasingly popular: 25% of brakes was carbon before 2000, but this reached 50% by 2000 [187–189].

C/C composite brakes have a number of important advantages [190–194].

1. **Lightweight.** The density of C/C composites is 1.80 g/cm^3 , whereas that of steel is 7.8 g/cm^3 . This means that the weight of C/C composite brakes is approximately 23% that of steel brakes of the same size. In a typical jumbo jet aircraft, flying with an extra 1 kg load will consume an extra 0.070 kg fuel. If fuel costs US\$1.20 per gallon, the hourly cost of flying would increase by US\$0.032 for each additional 1 kg load. The flying time of long-range airliners is approximately 3500 h each year, and the weight saving of large passenger aircraft with C/C composite brakes could reach to 600 kg. Therefore, a long-range airliner with C/C composite brakes could save US\$67200 dollars every year. Airlines with many large passenger aircraft could save millions of dollars each year using C/C composite brakes.
2. **Long life.** The lifetime of C/C brakes is five times that of steel brakes. Calculated as the number of landings, the lifetime of steel brakes is around 150–200 times, whereas the lifetime of C/C brakes is about 1000 times. Dunlop Aviation compared C/C composite brakes with steel ones. The results showed that though the cost of C/C composite brakes was five times that of steel ones, because the lifetime of C/C brakes was five times that of steel brakes, the operating cost did not increase. Moreover, using C/C composite brakes could reduce weight, increase payload, and minimize fuel consumption. A comparison of C/C composite and steel brakes is shown in Table 5.3 [194].

Table 5.3 Comparison of C/C composite and steel brakes [194]

Item	C/C composite brake	Steel brake
Maximum takeoff weight of airplane/kg	11000	10500
Normal landing weight of airplane/kg	7600	6600
Weight saving using C/C composite brakes/kg	92	
Increase of payload using C/C composite brakes/kg	592	
Estimated useful life/landings	1000	150–200
Operation costs	The total operating cost of C/C composite and steel brakes are the same	

- Desirable properties. Compared with steel, C/C composite brakes have a number of advantages, such as better high-temperature strength, higher thermal conductivity, larger specific heat capacity, smaller linear expansion coefficient, less flight wear, and higher service temperature. The tensile strength of steel is only 14 MPa at 1000 °C, whereas the tensile strength of C/C composites is 80–380 MPa under the same conditions. Because the thermal conductivity of C/C composites is higher than that of steel, the heat dissipation of C/C composite brakes is faster than that of metal brakes; the heat loss rate of the former is 30% higher than that of the latter, which is very important for aircraft with short grounded times. At room temperature, the specific heat capacity of C/C composites is 150% that of steel. When the temperature reaches 1000 °C, the specific heat of C/C composites is more than twice that of steel. From room temperature to 500 °C, the linear expansion coefficient of C/C composites is only a quarter that of steel. The flight wear of C/C composite brakes per use is 0.0015 mm/(surface•time brake), while that of metal brakes is 0.050 mm/(surface•time brake), so the flight wear of metal brakes is three times higher than that of C/C composite brakes. The used temperature of metal is usually below 900 °C, whereas C/C composites can be used at 3000 °C. As mentioned above, one very important characteristic of C/C composites is that their mechanical and thermal properties can improve with the increase of temperature. Tensile, compression, and bending properties as well as heat conductivity and specific heat capacity can be improved with the increase of temperature. In contrast, the mechanical properties of metals, such as steel, iron, or titanium, decrease significantly with increasing temperature [194].
- Use in overloading. C/C composite brakes, besides possessing advantages such as lightweight, long lifetime, high performance, and low cost, have another important feature, which is that C/C composite brakes can be used in overloading in emergency situations. In August 1981, a Concord plane took off from New York's John F Kennedy Airport, but a tire of the plane was damaged. While taxiing to take off, the tire next to the damaged tire was also damaged, so the plane had to brake immediately from a speed of 164 nautical miles per hour using the remaining six brakes. Luckily, the braking of the plane was successful.

The temperature of each brake reached 1650 °C during braking. Testing showed that part of the titanium torque had melted, but the C/C composite brakes withstood the test and avoided an accident. Another proof that C/C composite brakes can withstand large energy came from Dunlop Aviation, who tested the C/C composite brakes of AV8B produced by McDonald Douglas Corporation. Generally, the designed interrupted takeoff load is 2.5×10^6 J/kg. To ensure the ultimate ability of C/C composite brakes, the test energy was increased continuously. At 3.5×10^6 J/kg, the C/C composite brakes could still interrupt takeoff successfully, which revealed the total overloading operating capacity of C/C composite brakes. In contrast, when metal brakes are used rapidly under overloading interrupted takeoff, the brake disks tend to melt together, and even lose their function as brakes.

1. A brief introduction to the international application situation and market for C/C composites

The international market of C/C composites is monopolized by a few developed countries. In the military area, solid rocket nozzles, manned space thermal protection components, and engine parts are still unavailable in the open market because of confidentiality. In civilian areas, mainly brakes, there is fierce national competition. In the USA, many companies produce C/C composite brakes, such as Hitco, Bendix affiliated with AlliedSignal Aerospace, ABS, B.F. Goodrich, and Union Carbide Corporation, among which the sales of Hitco and Bendix are the biggest. In France, the companies that produce C/C composite brakes include SEP, Messier-Bugatti, and Aerospatiale. SEPCARB from SEP has been used in Mirage 2000, Mirage 4000, and Mirage F1. Messier-Bugatti mainly provides C/C composite brakes for Airbus aircraft. In Germany, the major manufacturer producing C/C composite brake materials is SGL Carbon. In the UK, C/C composite brakes are mainly produced by Dunlop, which started to produce C/C composite brakes earlier than other companies. However, the companies enjoying the largest market share at present are Hitco in the USA, Messier-Bugatti in France, SGL Carbon in Germany, and Dunlop in the UK, which are introduced further below [196, 197].

1. Hitco. Hitco produces basic raw materials, such as carbon fiber, carbon felt, carbon fabric, silica fabric, acupuncture carpet, and flexible graphite, and is currently the largest joint venture in the world producing C/C composites. This company has declared that they have been leading the global industry of C/C composites for the past 30 years. They first used two-dimensional C/C composites in the exit cone of high-performance solid rocket nozzle, which sparked the use of C/C composites in aircraft friction applications, and also were the first to use antioxidation C/C composites in aviation engines. The material properties, design, and manufacturing methods they use match their intended applications well. Years of research and development at Hitco have paved the use of carbon matrix composites in industrial applications.
2. Messier-Bugatti. Messier-Bugatti is a transnational united corporation affiliated with SNECMA, which mainly undertook the tasks of national strategic defense

systems. Besides France, they have also done business in other countries including the USA, Britain, Canada, and Singapore. In 1968, they started using carbon brakes in commercial and military aircraft, which opened up a new area of carbon brakes. Since then, the carbon brakes of Messier-Bugatti have been used in Mirage 1, Mirage 2000, Falcon 900, and Falcon 2000. In 1985, carbon brakes were used in Airbus A310, 300, and A300-600. Also in 1985, SEP and Alstom affiliated with SNECMA co-founded a new enterprise named “Carbone Industrie,” which was merged into Messier-Bugatti in 1997. Messier-Bugatti has become the main supplier of carbon brakes globally. On May 16, 2000, Messier-Bugatti announced that a new brake factory had been set up in Walton, Kentucky of the USA. This factory covers 36 hectares, so it is surprising that the factory was built so fast; the total time from buying land to beginning production was only one and a half years. The project investment for the first stage was 30 million US dollars, and the output is 100t per year. The factory covered the preparation of preforms, antioxidation coatings, carbonation, densification, heat treatment, and processing. In the beginning of 21st century, Messier brakes have 30% of the international market. There are 1300 jetliners and 145 airlines using their products. The total number of landings a day is about 16000, which is once every 5s. Their service nets are global, and the number of employees is around 1500. The development of Messier carbon brakes is shown in Table 5.4 [195].

3. SGL Carbon. SGL Carbon is a transnational corporation situated in Germany. On July 22, 1997, the corporation announced in Wiesbaden, Germany, that they

Table 5.4 Development of Messier-Bugatti brakes in the international market [195]

Civilian aircraft			
Aircraft manufacturer	Aircraft type	Trademark of carbon brake material	Year developed
Airbus	A300	SA3D	1985
		SEPCARB Plus	1999
	A310	SA3D	1985
	A319/A320	Sepcarb	1996
	A319/A320	Sepcarb Plus	1999
	A321	SepcarbTM	1993
	A330	SepcarbTM	1994
	A340	SepcarbTM	1995
Civilian aircraft			
Aircraft manufacturer	Aircraft type	Trademark of carbon brake material	Year developed
Boeing	767-300/200	Sepcarb	1999
Military aircraft			
MIR 2000		Carbon brake	December, 9, 1982
Rafale		Carbon brake	First flight May, 1991
Rafale		Carbon brake	First flight December, 1991

had bought Hitco from the USA. The combination of Hitco and SGL Carbon greatly strengthened the market position of SGL Carbon in the field of carbon composites in the USA. In 1977, the sales made by SGL Carbon totaled nearly 80 million German marks. Their products cover a wide range of fields including aviation, automotive, energy, chemical, and semiconductor. SGL Carbon owns more than 25 factories, and sales and service outlets in more than 90 countries around the world. America, Britain, and Germany are their major investors. Although the leading products of SGL Carbon are carbon and graphite, they also occupy a pivotal position in composite materials. They received production licenses for both military and civilian aircraft brakes. They also became the largest independent manufacturer of solid rocket nozzles in the USA based on their 35 years of experience. Their products have been successfully used in the Delta II, III, IV series, Titan IV, Trident D-5, Militia, and other solid rocket thruster systems of Lockheed Martin. In addition, there are another five major brand-name products for users to choose, which are "SIGRABOND" (C/C), "SEMI-CARB" (C/C), "CERACARB" (SiC/C), "SIGRASIC" (C/SiC), and "GLISCARB" (C/C). These products with different performances are widely used in the metallurgical, chemical, aerospace, nuclear energy, semiconductor, and automotive fields.

4. Dunlop [194]. The research of C/C composites performed by Dunlop began in the early 1970s. The density of C/C composite brakes produced by CVI was more than 1.8 g/cm^3 . Research on C/C composites mainly focused on aircraft brakes. The development of Concord aircraft brakes is described below.

In 1971, the first C/C composite brakes for Concord were presented.

In 1972, C/C composite brakes simulated the safety requirements of interrupted takeoff for Concord successfully.

In 1972, C/C composite brakes were tested successfully for the first time in Toulouse.

In 1973, C/C composite brakes were used in a Super VC10 aircraft for the first time.

In 1975, a factory to produce C/C composites by CVI began production.

In 1976, a supersonic Concord aircraft with Dunlop C/C composite brakes was put on a flight course.

In 1981, a BAe146 aircraft with C/C composite brakes accomplished its first flight.

In 1982, Delta airlines used Dunlop C/C composite brakes in Boeing 757 aircraft.

In 1983, Dunlop C/C composite brakes were used in Agile Combat Aircraft (AGA) fighter aircraft.

In 1984, a Boeing 757 aircraft with Dunlop C/C composite brakes accomplished its first flight.

In 1986, C/C composite brakes were used in Aerospiale/Aeritalia ATR 72 by Dunlop.

In 1986, BAe ATP and EAP aircraft with Dunlop C/C composite brakes accomplished their first flights.

To meet the increasing requirements of military and civilian aircraft, the performance of C/C brakes has been continuously improved by Dunlop. The density of C/C composites has been raised to 1.80 g/cm^3 , tensile strength is more than 70 MPa, compressive strength is more than 120 MPa, and shear strength exceeds 10 MPa. The required thermal conductivity is 8–20 W/(m·K) before heat treatment, and the thermal expansion is 0.2% and 1.5% in the parallel and vertical directions, respectively [194].

Dunlop used natural gas in the CVI process to prepare C/C composites. The deposition temperature was about 1000 °C, and the pressure was 50 Tuo (1 Tuo = 133.32 Pa). To overcome the shortcomings of CVI, such as long production period, a large-capacity induction furnace and a large-quantities input method were used by Dunlop. In this method, 2000 C/C brake roughcasts were put into a large CVI induction furnace with a diameter of 2.74 m. Once the density of C/C brake roughcasts was increased to a certain extent by CVD, they were machined. This process was repeated for a specific number of cycles depending on the target and requirements. The number of deposition/processing cycles of C/C brakes in Concord aircraft was six, while that of AV8B from McDonnell Douglas was only three. When the required density of the C/C composite brakes was obtained, they were graphitized to adjust their structure performance. After graphitization, the thermal conductivity of C/C composites increased. Before graphitization, the thermal conductivity of C/C composites is 8–20 W/(m·K), and after graphitization, it increases to 30–120 W/(m·K). However, their mechanical properties were reduced by 30%; for example, bending strength was about 120 MPa before graphitization and reduced to 85 MPa after graphitization. The graphitization temperature used by Dunlop to produce C/C composites is 2500–2700 °C.

According to different requirements, C/C composites produced by Dunlop include CA7, CA8, CB6, GB7, CC3, and CD4 [194].

2. Domestic application situation and market for C/C composites in China

The first unit engaged in the research of air brakes in China is Huaxing Aviation Aircraft Company. In 1972, Lanzhou Carbon Factory and Shaanxi Huaxing Aviation Wheel & Brake System Co., Ltd cooperated to research aircraft brakes. In 1977, they performed simulated brake tests of carbon disk samples in a large inertia station with fan-shaped structure [195] for the first time in China. In 1983, they finished the simulated brake tests with the overall structure of carbon disk samples. In 1986, the development of carbon brake wheels was classified as a National “7th five year” Science and Technology Key Tackling Project. From 2000 to now, more and more scientific research units have started to develop and produce C/C composite brakes [198]. During the 1990 s, advances in the technology of domestic carbon brakes allowed carbon brakes to be installed in major military aircraft. At present, Shaanxi Huaxing Aviation Wheel & Brake System Co., Ltd has installed C/C composite brakes in multiple types of aircraft and overhauled the carbon brakes in A300 and A310 aircraft. Central South University started to invest in the

mass production of C/C aircraft brakes in 1998. In addition, Xi'an Aerospace Composite Materials Research Institute, China Academy of Launch Vehicle Technology, NPU, and the Yantai Institute of Metallurgy and New Materials also have strong research and production capacity [199].

5.4.2 Application of C/C Composites as High-Temperature Structural Components of Aero-Engines

The application of C/C composites as high-temperature structural materials for long-term use, especially as hot-end components of aero-engines, has become a focus of C/C composite research. With the increase of thrust-weight ratio, the temperature of the turbine front inlet increases; when the thrust-weight ratio of an aero-engine reaches 15–20, the temperature of the hot end is as high as 2000 °C, which requires materials with a specific strength five times higher than the strength of the current materials [196]. Only C/C composite materials can satisfy these requirements under such harsh conditions. In addition, because of the low specific gravity of C/C composites [196], the weight of an engine could be decreased greatly, and the thrust-weight ratio would be increased. Moreover, because of the consumption of cooling air, the engine efficiency would also be increased. Therefore, C/C composites are considered important high-temperature materials for the next generation of aero-engines with high thrust-weight ratio. If a country can completely resolve the problems of C/C composites, then it will likely become dominant in the development of high-performance engines.

According to reported information, Hitco manufactures scales, LTV manufactures turbine blades and other turbine parts, and performed ground ultra-turn tests at 1760 °C. The General Electric Company used C/C composite materials to produce turbine blades and other turbine parts for low-pressure turbines in JID verification machines. The operating temperature was 1649 °C, which was 555 °C higher than that of the general turbine, and the test was successful without gas cooling. Rohr (USA) and Garret Engine Branch Company from AlliedSignal researched the materials and technology of low-price C/C composite turbine rotor blades, as well as engine tests. However, the rotors have not yet been used in practical applications. The components being used and tested in this research are as follows:

1. Fire plates [200]

Small turbine jet engines are mainly used in military training aircraft, target aircraft, unmanned aircraft, and missiles because burning metal cans cannot stop gas from entering into neighboring regions. As a result, they cannot be used in turbine jet engines. Therefore, a kind of insulating protection sleeve material is needed to be developed for engine burning cans. This material should be able to maintain gas burning for 2 min to allow the pilot to stop the engine. C/C composite materials have good thermal properties, so they could be used as sleeve materials.

In 1970, C/C composites were used in the burning cans of turbine jet engines for the first time.

2. Exhaust systems [197, 200]

Future military aircraft requires higher thrust-weight ratio, with a depression and elevation thrust vector control device, and good stealth performance. The use of C/C composites as coatings in gas turbine engines could also meet the requirements of fighters. As early as 1978, the USA began to prepare nozzle plates, gaskets, and lining physical models with C/C composites. In 1983, they started to design materials, prepare full-size components, and perform tests. Experiments were carried out in American F100 engines. By 1991, the test time of C/C composite-coated nozzle plates had exceeded 1300 h with 5100 afterburner cycles, which was the same as 2100 h of flying time. The best parts were two-dimensional carbon fiber-reinforced pitch or resin matrix composites with a SiC or SiN coating. A two-dimensional C/C composite flap liner with a SiC coating was used in the axisymmetric nozzle of F-100, and it was 38% lighter than the traditional flap liner.

3. Combustion chambers [197]

If propellant burns under conditions close to the ideal ratio, then the thrust per unit flow would reach its maximum, and supersonic flight could be achieved without afterburning, so the persistence of supersonic flight could be improved by increasing thrust and reducing weight. C/C composite combustion chambers can withstand high burning temperature and minimize the required amount of cooling gases. C/C composite combustion chamber components with a SiC coating were designed and produced in 1984. In 1986, the total working time of coated C/C combustion chamber components exceeded 163 min at a gas temperature of 1343 °C, and their performance was satisfactory.

4. Self-lubricating bearings [197]

In 1996, researchers from the USA prepared C/C composite bearing sleeves containing ball bearings with a diameter of 30 mm. The C/C composite bearing sleeves was operated at a speed of 35 rev/min for 32 h, the working temperature was 399–510 °C, and the thrust load was 46–182 kgf. This was the first example of ball bearings showing stable performance in such a harsh working environment.

5. Blades [195, 197]

Because the inlet temperature of future engines was expected to reach up to 1700–1800 °C, the best materials for future engine blades are C/C composites. Many countries have researched this topic, but publicly reported progress has been limited. In 1993, the Japanese Institute of Space and Astronautical Science tested C/C composite turbine blades of an aero-stamping air breathing engine. These C/C turbine blades were prepared by pressing infiltration of specially designed preforms and were tested under actual load and speed. NPU also prepared two- and three-dimensional C/C composite turbine blade samples.

6. Revolving door commutator [187, 194, 197]

In 1981, Hurel-Dubois proposed the thrust commutator, which is also known as the revolving door commutator. Compared with a general commutator, the revolving door commutator is easy to use and lightweight. In 1991, Jouan researched the applications of revolving door commutator in engines, which was then used in MD11 and Airbus A330 aircraft. In 1992, Matera and Merola from the CEC Joint Research Center researched the high-temperature performance of C/C composite commutators.

In China, NPU has also researched these materials and has made great progress. Their products include blade samples, four-dimensional woven micro-engine jet nozzles, inner cones, high-temperature protective casings, and adjustment sheets. The bending strength of their two-dimensional C/C composites is up to 393 MPa at room temperature, and up to 592 MPa at 1700 °C. The protective ability of C/C composites with an oxidation protective coating reached 200 h at 1650 °C in air, and the oxidation protective ability of C/C composites in gas erosion at 1300 and 1500 °C exceeded 30 h.

5.4.3 Application of C/C Composites as Anti-Ablation Materials for Solid Rocket Motors

1. Use of C/C composites as throats

The nozzle of solid rocket motors can reach temperatures as high as 3500 °C, which induces erosion by liquid and solid particles, and chemical corrosion by high-temperature gas. Therefore, these nozzles need to serve under very harsh conditions. Because there is no cooling system, the nozzle needs to tolerate gas at high temperature. In particular, the throat must endure the harshest working environments, and its size should not be changed by ablation or erosion [196, 201, 202]. This is because pressure is reduced when the throat radius increases, which would reduce the thrust.

In the 1950s, the throat material for the first-generation nozzles was mainly high-strength graphite. In the 1960s, the throat materials used for military missiles were mainly W-Cu and W-Ag. C/C composites have low density (1.75–1.90 g/cm³), which is just 1/8–1/10 that of W-Cu. If C/C composites are designed according to different requirements, their fracture factors can be 10–20 times that of graphite. The linear expansion coefficient of C/C composites is only $(4-5) \times 10^{-6}/\text{°C}$ at 2000–2400 °C. In addition, C/C composites can endure high temperatures of 3000 °C with adjustable thermal conductivity, and they can resist erosion by H₂, CO, and CO₂. A C/C composite throat showed uniform ablation in a star-hole charging engine without corrosion steps and notches. Importantly, its strength increased with temperature below 2500 °C. Since the 1970s, countries researching and manufacturing solid rocket motors have gradually started using C/C composite throats. As a result, the thrust to mass ratio and reliability have been advanced greatly. At the same time,

the size of throats has been increased. Initially, the diameter of C/C composite throats was only $\varnothing 60\text{--}80$ mm, and mainly used in miniature engines. This was later increased to $\varnothing 100\text{--}200$ mm. By the 1990 s, the size of C/C composite throats of the French Ariane 5 solid rocket nozzle reached $\varnothing 900$ mm in inner diameter, and $\varnothing 1060$ mm in outer diameter. In Russia, inner and outer diameters of $\varnothing 800$ mm and $\varnothing 1000$ mm, respectively, were achieved [192, 196].

Many processes are used to prepare C/C composite throats, such as whole carbon felts, laminated acupuncture of carbon cloth pre-oxidized felts, three-dimensional braiding, four-dimensional mixed braiding, four-dimensional soft braiding, and four-dimensional hard braiding. The density of braiding is $0.6\text{--}0.9$ g/cm³, and that of carbon felt is $0.12\text{--}0.15$ g/cm³. According to different requirements, the content of all directions of fibers in weaving could be pre-designed. The multiple processes used to form C/C composite throats include liquid resin pitch infiltration, carbonization, and CVI, and the high-temperature treatment methods include graphitization under vacuum and with protective gas. These methods could be used across and circularly to achieve the expected performances of thermal physics, mechanical, and dynamic ablation [187, 194, 202, 203].

C/C composite throat materials were first developed successfully in 1963, and their application has experienced three generations. The first generation of C/C composite throat materials was made of two- or three-dimensional fabric, and the main production companies were Thilkol, SEP, and FMI. The second generation of C/C composite throat materials was made of three- or four-dimensional fabrics, and the main production companies were GE, SETP, and AVCO. The third generation of C/C composite throat materials was made of four-dimensional fabrics, and the main production companies were Morton, SEP, and Tholkol. At present, the fourth generation of C/C throats is being researched and is mainly produced by AVCO and SEP. AVCO fabricates three-dimensional C/C composites with a density of $1.87\text{--}1.92$ g/cm³ and tensile strength of $50.7\text{--}76.8$ MPa. GE sells four-dimensional C/C composites with a density of 1.92 g/cm³ and tensile strength of 220.9 MPa. Meanwhile, SEP produces four-dimensional C/C composites with a density of $1.85\text{--}1.95$ g/cm³ and tensile strength of 115 MPa. C/C composite throat materials have been used in engines such as STAR30E SRM, IVS SRM-1 and Delta boosters from the USA, mAGE-II SRM, M4 SRM, and Ariane-5 boosters from France, and SEP/CSD SRM from France and the USA [202, 203].

In the aerospace field, three- and four-dimensional C/C composite throat materials have been widely used in solid rocket motor (SRM) at all levels, surface-to-surface strategic missile SRM, Submarine to ground strategic missile SRM, advanced tactical missile SRM, and large-scale carrier rocket boosters. The weights of these SRM range from several hundred grams to 1820 kg. The diameter of the throat materials made by three-dimensional mixed weaving with carbon fiber and axial carbon rods has reached 2438.4 mm, which make them the biggest C/C composite throat materials in the world.

2. The applications of C/C composite nozzle diffusers

The main function of a nozzle diffuser is to control the expansion of gas and send the highest thrust to engines. A nozzle diffuser should be able to resist erosion and corrosion by high-temperature gas. To reduce weight, the wall thickness of the nozzle diffuser is limited; the thickest area is 8–15 mm, and the thickness of the exit is 1.5–4.0 mm. The minimum wall thickness of C/C composite nozzle exits produced by China in 1989 was only 0.9 mm. In the 1990s, C/C composite diffusers were widely used in advanced missile solid rocket motors. The main reason for the application of C/C diffusers was that they could reduce the weight of level 2 rockets by 35% and level 3 rockets by 35%–60%. The technology of C/C composite diffusers is important technology to produce nozzles with high thrust-weight ratio. In America, Russia, France, and Germany, C/C composite diffusers have been used in strategic missiles, satellite apogee engines, and inertia top engines [203].

The United States was the first country to study C/C composite diffusers. In the 1970s, AVCO and the Fiber Materials Corporation started studying C/C composite diffusers. Then FMI, GE, and Union Carbide Corporation also began research on C/C composite diffusers. The successful ignition of SEP-CSD composite engines marked the C/C composite nozzle as a good step. By 1979, SEP-CSD-extended nozzles were ignited successfully at Edwards Air Force Base, California, USA. In 1981, SEP-CSD cooperated again with the approval of the US State Department, and developed extension cone nozzles with four-dimensional throats and an exit thickness of only 1.5 mm. Because high specific thrust and high-temperature propellants HTPB and FEFO were used in the MX, a C/P exit cone could not meet the requirements. After a series of technical improvements, the exit cone SEP-CSD was used in the level 3 MX. The weight of the level 3 extension cone of MX including the expanding components was 67.65 kg, the expansion ratio of the nozzle increased from 24.10 to 67.46, and the specific thrust increased by 5.6%, which is equivalent to about 16 s. The extension efficiency was 0.2275 s/kg, which saved a length of 962.7 mm. Later, the extension cone technology of C/C composite diffusers was used in level 2 and 3 Dwarf missiles [203].

The former Soviet Union began to study C/C composite-extended cones in the 1970 s. By the mid-1980s, C/C composite extension cones were being used in the missiles of SS-24 and SS-25. The largest diameter of the exit was $\varnothing 2200$ mm, and the thickness of the exit was 3–5 mm. SEP (France) started to develop two-dimensional diffusers in the 1970 s, and their products include two-dimensional petal-shaped ply C/C composite diffusers, three-dimensional Sepcarb T22, Sepcarb T24, Sepcarb T30, and T60 woven materials. From the 1980 s, they began to develop the exit cone materials NOVOLTEX, which had a small internal cavity and the merits of both two- and three-dimensional materials. Compared with the two-dimensional C/C composites used in MAGE-II, the thickness of NOVOLTEX was 2 mm without stratification, and the size of NOVOLTEX composites could be up to $\varnothing 2500$ mm \times 3000 mm. NOVOLTEX composites have been used in Sepcarb solid rocket motors. In addition, the French Aerospace Company developed BK900 and BK2000 bar-inserted knitting machines that could manufacture fabrics with a

size of up to $\varnothing 2150 \text{ mm} \times 1500 \text{ mm}$. Former West German company Feist-Incon developed mixed weaved 500 mm knitting machines that could produce large-scale C/C composite thin-walled materials used for diffusers and extended cones with a size of $\varnothing 1500 \text{ mm} \times 2000 \text{ mm}$ [187, 194, 203].

3. The application of C/C composite throats in China [203–205]

At present, the institutions engaged in the research and production of ablation-resistant C/C composites in China include Xi'an Aerospace Composite Materials Research Institute, China Academy of Launch Vehicle Technology, NPU, Central South University, and Shanghai University. In 1971, China proposed a development plan of C/C composite throat materials. Then, the Metal Research Institute of the Chinese Academy of Sciences was commissioned to study the CVI densification technology, and Xi'an Aerospace Composite Materials Research Institute began to develop technology to densify laminated carbon cloth impregnated with resin. In 1972, C/C composite throat materials were first tested in engines in China.

From 1973 to 1975, after hard work by the Metal Research Institute, Lanzhou Carbon Factory, Taiyuan Institute of Coal Chemistry, Jilin Carbon Factory, Shanghai Carbon Factory and General Research Institute for Nonferrous Metals, C/C composite throats with a density of 1.82 g/cm^3 , and central inserts were developed successfully and tested 20 times.

In 1976, laminated flat carpet C/C composite throats, which were densified by CVD to a density of 1.77 g/cm^3 , for use in apogee engines were developed and tested in apogee engines successfully. By 1978, the highest density of these throat materials had reached 1.89 g/cm^3 (densification by CVD and PIC), and a production line of this throat material with a diameter of $\varnothing 700 \text{ mm}$ was completed in 1981.

In 1984, the first communication satellite of China with an apogee engine containing flat carpet C/C throat liners was launched successfully, which signified that China's C/C composite throat materials had entered a practical stage.

In the early 1980s, the overall performance and reliability of C/C composite throat materials were improved by successful application of second-generation multi-woven C/C composite throat materials.

Third-generation C/C composite throat materials with a density of 1.98 g/cm^3 were developed in the early 1990s, These C/C composite throat materials made the major breakthroughs of low erosion rate and high strength.

Over the past 30 years, Xi'an Aerospace Composite Materials Research Institute, China Academy of Launch Vehicle Technology, NPU, Central South University, and Shanghai University have developed a series of C/C composite throat components for various types of solid rocket motors. The performances of some C/C composite throat materials have reached advanced international levels (Table 5.5).

In 2001, Central South University began to research and develop C/C composite throat materials. The maximum size of the samples that they could prepare was

Table 5.5 Mechanical and thermal properties of C/C composite throat liner materials produced by Xi'an Aerospace Composite Materials Research Institute [203]

Parameters	Type	Carbon fiber felt	4D fine weaving C/C	4D axial rod C/C	Needle-punched carbon cloth C/C
Density/g·cm ⁻³		1.75–1.89	1.90	1.95	1.85
Tensile strength/MPa	∥	35	264.5	33.3	79.1
	⊥	15	91.6	94.6	
Bending strength/MPa	∥	60.5	105.7	82.2	150.3
	⊥	25.1	58.9	101.8	
Compressive strength/MPa	∥	99.0	268.4	93.0	159.0
	⊥	113.0	146.6	156.6	239.0
Shear strength/MPa	⊥	13.1	48.3	28.7	16.1
Thermal conductivity/W·(m·K) ⁻¹	∥	105.2	23.1	70.1	138.6
	⊥	79.1	38.5	49.9	68.4
Linear expansion coefficient/10 ⁻⁶ K ⁻¹	∥	0.45	0.97	-0.31	0.32
	⊥	0.81	0.43	-0.25	

400 mm in diameter and 200 mm in thickness. The performance of these C/C composite liner materials is shown in Table 5.6 [205].

NPU began to research and develop C/C composite throat materials prepared by quick CVI technology in 1996, including two- and three-dimensional and carpet substrate throats. The maximum size of the samples they could prepare was 500 mm in diameter and 400 mm in thickness, and some of these throats have been used in applications.

Table 5.6 Properties of C/C throat materials produced by Central South University of China [205]

Parameters	Type	Carbon fiber felt	3D C/C
Density/g·cm ⁻³		1.80–1.85	1.80–1.87
Tensile strength/MPa	∥	47–120	132–160
	⊥	15–62	59–86
Compressive strength/MPa	∥	85–130	110–135
	⊥	260–320	271–320
Shear strength/MPa	∥	53–70.4	62–85
	⊥	32–65	35–72
Thermal conductivity/W·(m·K) ⁻¹	∥	47–70	45–78
	⊥	26–59.4	24–60
Linear expansion coefficient/10 ⁻⁶ K ⁻¹	∥	0.5–0.8	0.6–0.8
	⊥	1.2–1.5	1.1–1.4

5.4.4 Application of C/C Composites as Thermal Structural Materials of Reentry Spacecraft

When a space shuttle returns into the atmosphere, the nose temperature can be as high as 1463 °C, and the wing leading edge temperature is more than 1000 °C [206]. As high-temperature ablation-resistant materials and high-temperature thermal structural materials, C/C composites have been used as thermal-resistant components, such as the wing leading edges and nose cones of the American Space Shuttle, National Aeronautics and Space Shuttle (NASP), Japanese HOPE Space Shuttle, French Hermes Space Shuttle, Russian Buran Space Shuttle, German Sanger Space Shuttle. The applications of thermal structural composite materials in spacecraft manufactured in different countries are shown in Table 5.7.

In China, NPU prepared the C/C composite nose cones and wing leading edges of spacecraft successfully in 2003.

Table 5.7 Selection of thermal protective system structures and materials used in advanced spacecraft [206]

Type	Model	Layout of thermal protective system and selection of structure materials		
		Highest temperature areas	Higher temperature areas	Lower temperature areas
Space Shuttle	Shuttle (American)	Oxidation-resistant C/C shell thermal structure	Oxidation-resistant C/C composites instead of rigid ceramic thermal protective tiles in some regions of nose cone	Flexible ceramic thermal protective felts
	Buran (Russian)	Oxidation-resistant C/C shell and oxidation-resistant thermal protective tile	Rigid ceramic thermal protective tiles	Flexible ceramic thermal protective felts
	Hermes (French)	Oxidation-resistant C/C shell thermal structure	C/SiC cover boards + thermal protective tiles	Flexible ceramic thermal protective felts
	HOPE (Japan)	Oxidation-resistant C/C shell thermal structure	Oxidation-resistant C/C support panels, thermal protective layers, and light ceramic tiles	Ti alloy multilayer wall and flexible ceramic thermal protective felts
Type	Model	Layout of thermal protective system and selection of structure materials		
		Highest temperature areas	Higher temperature areas	Lower temperature areas

(continued)

Table 5.7 (continued)

Type	Model	Layout of thermal protective system and selection of structure materials		
		Highest temperature areas	Higher temperature areas	Lower temperature areas
Space Shuttle	National Aeronautics and Space Shuttle (NASP), and other advanced hypersonic aircraft (American)	Oxidation-resistant C/C and refractory metal thin-walled thermal structure	Ti or Al compounds and their metal-matrix composites (or oxidation-resistant C/C) panels + thermal protective layers	Ti alloys and their metal-matrix composites + thermal protective layers
Space Shuttle	Hotol (British)	C/SiC and oxidation-resistant C/C shell thermal structure	Foreside: oxidation-resistant C/C (or C/ceramic) + thermal protective layers Central and rear section: BC/Ti panel + thermal protective layers	Ti alloys and Ti-based composites panels + thermal protective layers
	Sanger (Germany)	SiC/SiC shell thermal structure (level 1)	Nickel-based alloys multilayer wall + thermal protective layers	Ti alloys multilayer wall + thermal protective layers
	HIMIS (Japan)		Rigid ceramic thermal protective tiles and fiber-reinforced metal-matrix composites (FRM) (SiC/C/Ti)	Ti alloys (Ti-6Al +4 V) and rapid solidified Ti alloys (Ti-6Al +4 V-1B)

5.4.5 Biomedical Applications of C/C Composites

Carbon materials have been used for heart valves, ligaments, and sinews because of their excellent biocompatibility. However, the strength and fragility of C/C composites restrict their extensive use in medical applications. C/C composites that are composed of carbon fibers and carbon matrixes are considered the most promising biomedical materials. They combine the biocompatibility of carbon materials and

the mechanical properties of fiber-reinforced materials and have shown viable applications in the reconstruction of bone [207, 208].

The merits of biomedical C/C composites are as follows [209–213]:

1. Good biocompatibility. The overall structure is composed of carbon, and body tissues can adapt themselves well to C/C composites.
2. Corrosion resistance. No ion release and character degeneration of implants were found in the surrounding tissue, which were better results than obtained for metal materials.
3. Good biomechanical properties. The elastic modulus of C/C composites is similar to that of human bone, which could help to avoid stress shielding and sequent bone absorption.
4. The high strength, outstanding fatigue, and high toughness of C/C composites could be adjusted to satisfy the specific mechanical demands.

Globally, researchers have paid special attention to the biomedical applications of C/C composites.

1. Biocompatibility of C/C composites

C/C composites consist of carbon fibers embedded in a carbon matrix. The carbon fibers are composed of glass carbon, and the carbon matrix is made up of pyrolytic carbon or glass carbon. C/C composites are considered the most promising artificial materials for orthopaedics owing to their remarkable mechanical strength and toughness properties. Therefore, the initial problem for C/C composites used in orthopaedics was their hard tissue compatibility [214, 215].

Adams and Williams [215] reported that C/C composites showed excellent hard tissue biocompatibility when they were implanted into the mouse femoral bone. No transitional soft tissues and inflammation were found between the C/C composite and bone. The shear strength of the C/C composite bone was significantly greater than that of a titanium-bone system. No bad responses were found, indicating the good appency between the C/C composite and bone. Microstructure analyses showed that bone tissue readily connected to the C/C composite, and the bone tissues grew along the groove of the C/C materials. Bone tissue can grow into materials with holes of 50–300 μm . However, the holes in the C/C composites in this study were less than 10 μm , which provided a mechanically embedded function [216].

It is obvious that C/C composites and carbon fiber-reinforced materials exhibit high joining strength. It has also been demonstrated that the size and number of holes in the carbon materials decrease after implantation for one month [216]. The reason for this might be that the cells grow into the implanted materials.

C/C composites show particular biocompatibility because of their excellent tissue response. Previous studies showed that skins grew along C/C composite rods when they were inserted into soft tissue [215, 217]. The soft tissue closely adhered to the surface of the C/C materials. In contrast, when a metal rod made of stainless steel or Co-Cr alloy was used in the same experiment, fiber films formed on the

surface of the materials that separated the tissue and metal rods. The skin could not grow along the materials. The skin grew along the carbon materials because of the good compatibility between soft tissue and the holes on the surface of the carbon materials. This characteristic could be used to fix implants, which is crucial for C/C composites used for orthopaedics.

Baquesy et al. [217] studied the blood compatibility of C/C composites using radio tracing methods. Platelets adhered to the materials when in contact with blood for 1 h. However, erythrocyte and fibrinogen adhesion were not found. The microstructure of the materials plays an important role in the adhesion of platelets, but the mechanism was not clear [218].

Carbon materials are also useful anti-thrombosis materials. Numerous studies have shown that the surfaces of carbon materials are modified when contacted with blood. For example, the surface energy of LTLC decreased quickly when in contact with blood for 2 h. The albumins promoted the adhesion of the platelets onto the carbon materials. The roughness of C/C composites affects their anti-thrombosis properties. Blood aggregates formed easily on rough surfaces, and also, the rough surface held up the flow of blood. As a result, the rough surface showed poorer anti-thrombosis properties than the smooth surface. That is, C/C composites should be pretreated before use in anti-thrombosis applications.

When C/C composites were used in a living body, the interactions of the materials with the blood, soft tissue, and bone were complicated. The biocompatibility of C/C composites was affected by the microstructure, matrixes, surface conditions, and morphology [219–221]. To produce biomedical C/C composites suitable for specific conditions, attention should be paid to the effective control of the microstructure and surface conditions of the composites. A major problem is understanding the relationship between the biocompatibility and microstructure of C/C composites.

2. Current research state of biomedical C/C composites

Because of their excellent biocompatibility and latent mechanical properties, C/C composites show very good application prospects in the biomedical field. Pelvises, bone splints, and spicules made of C/C composites have been used in clinical applications, and artificial heart valves and middle ear repair materials made of C/C have also been reported. Moreover, C/C artificial tooth roots showed good clinical results [219, 222, 223]. Christel et al. [228] studied the feasibility of several kinds of C/C composite materials used for artificial hip joints and analyzed the effect of various kinds of C/C composite materials on the bone cerebral cortex. They found that the carbon-based composites obtained by CVI were more suitable for hip joint replacement than other kinds of carbon-based composites. This material possessed the biocompatibility and biomechanical stability needed by the physiological environment in joint replacement [224–230].

Japanese researchers have developed C/C artificial tooth roots. They found that the implants should satisfy several properties to connect suitably with the biological tissue, which are discussed below [208, 209, 217, 222, 230].

1. Good cell adhesion. The character of the material should be similar to that of the bone.
2. Implant surface should be porous and the pores must be big enough for cells to grow in them and to provide sufficient oxygen and nutrition.
3. Three-dimensional interweaves should be formed between the porous surface and the newborn bone collagen fibers; the resulting material structure should be porous and stable.

Tooth root-form fine rahmen surface (FRS) dental implants were made by Japanese researchers. The C/C composite core was wrapped with nonwoven carbon fabric, and the resulting substrate was treated by thermal-gradient CVI. Pyrolytic carbon joined the C/C composite core and carbon fabric, and formed a hard coating on the surface of the materials. FRS is a special kind of C/C composite with large holes on the surface and dense structure in the core. The FRS dental implants are perfect artificial bone materials and might be used for other parts of the human body.

3. Application prospects

Compared with metallic materials, biomedical C/C composite materials have only been studied in recent years, and there are several problems that need to be resolved.

1. Mechanical analysis, structure design, microstructure control, and surface coating and modification with consideration of biomedical applications rather than aerospace uses;
2. Compared with metallic materials, the performance evaluation criteria of composite materials are not clear, and the response is more complex when composites are used in the human body. There is not a clear criterion for the analysis of biocompatibility and mechanical compatibility of composite materials at present.

The appearance of C/C composite materials has improved the strength and toughness of carbon materials fundamentally, and the elastic modulus mismatches have been solved. C/C composite materials show viable future application in the reconstruction of bone, although there are few clinical examples at present. Considerable research in this field has been undertaken abroad. However, few studies have been completed in China. Therefore, there is still a lot of work to do on the materials science, clinical research, and basic theory to promote the development of C/C composites.

5.4.6 Application Prospects of C/C Composites

Although C/C composites exhibit excellent performance and broad applications, their applications have been limited by their high price. As a result, C/C composites

have mainly been used in aerospace and military fields, especially for aircraft brakes. To broaden the application of C/C composites in civilian areas, further work should be done in the following areas.

1. Developing efficient and low-cost techniques. In recent years, though a variety of new techniques have been developed, such as FCVI, RDT, and EHV, all of these technologies have problems with practicability and adaptability. For example, FCVI, LTCVI, and low-cost hot pressing technology can only be used to produce specific parts. Compared with these technologies, RDT has a broader adaptability, but it is still not like ICVI technology, which can adapt to all types of parts, and different shapes of parts can be deposited in the same reactor. Only when we solve these problems will the use of C/C composites be expanded, and developed to civilian areas.
2. Developing effective oxidation-resistant coatings for C/C composites used at temperature of more than 1700 °C. Although many researchers have studied high-temperature oxidation-resistant coatings for C/C composites, high-temperature oxidation-resistant coatings that work at 1600–1800 °C have not been achieved. Therefore, research on high-temperature oxidation-resistant coatings is needed to further develop C/C composites. The stability and adaptability of coating processes in different environments are also important problems.
3. Integration of the design, structure, and manufacture of C/C composites. Unlike metal materials, C/C composites cannot be made as square spindle materials or flat materials first and then be processed by machine because it would seriously affect the performance of parts and increase their cost. Therefore, to ensure that parts make full use of their excellent performance, and to reduce the cost of preparation, the design, structure, and manufacture of C/C composite must be integrated to obtain components with satisfactory structure, performance, and cost.
4. Diversification of C/C composites. In addition to developing high-performance and high-density C/C composites, low-density C/C composites suitable for insulation and packing, ablation-resistant C/C composites, high thermal conductivity high-density C/C, and short fiber-reinforced C/C composites should also be developed for different applications.
5. Solving the stability problem of material performance and technology. At present, the preparation of C/C composites mainly relies on the experience of the operator. Because of many factors, it is difficult to ensure the reliability and repeatability of processing. Therefore, it is important to research computer simulation, advanced systems, and intelligent control to lay the foundation for the robust engineering of C/C composites.

References

1. Huahui C, Haijin D, Ming, L et al (1998) Advanced composite material. China Substances Press: Beijing (in Chinese)
2. Hejun L (2001) Carbon-Carbon Composites. *New Carbon Mater* 16(2):79–80 (in Chinese)
3. Fitzer E, Manocha L. M (1998) Carbon reinforcements and carbon/carbon composites. Springer-Verlag, Berlin
4. Thomas C. R (1993) Essentials of carbon-carbon composites. Royal Society of Chemistry, Cambridge
5. Jiecai H, Xiaodong H, Shanyi D (1994) Research and application of carbon-carbon composites I. *Aerosp mater technol* 24(4):1–5 (in Chinese)
6. Yi L, Junshan W (2000) Development of Carbon matrix precursors for Carbon-Carbon Composite Materials. *Aerosp mater technol* 5:6–9 (in Chinese)
7. Torsten W, Gordon B (1997) Carbon-carbon composites: a summary of recent developments and applications. *Mater Des* 18(1):11–15
8. Economy J, Jung H, Gogeva T (1992) A one-step process for fabrication of carbon-carbon composites. *Carbon* 30(1):81–85
9. Chung DDL (1994) Carbon fiber composites. Butterworth-heinemann, Newton
10. Savage G (1993) Carbon-Carbon composites. Chapman & Hall, London
11. Lewis IC (1980) Thermal polymerization of aromatic hydrocarbons. *Carbon* 18(3):191–196
12. Ryuji F, Takashi K, Koichi K (1993) Evaluation of naphthalene-derived mesophase pitches as a binder for carbon-carbon composites. *Carbon* 31(1):97–102
13. Bhatla G, Fitzer E, Kompalik D (1986) Mesophase formation in defined mixtures of coal tar pitch fractions. *Carbon* 24(4):489–494
14. Kanno K, Fernandez JJ, Fortin F et al (1997) Modifications to carbonization of mesophase pitch by addition of carbon blacks. *Carbon* 35(10–11):1627–1637
15. Shenghua L, Wenjie L, Yajie Z (1993) Progress in the carbonaceous mesophase research (II). Nematic Liquid Crystals and the carbonaceous mesophase. *Carbon* 3:7–12 (in Chinese)
16. Marsh H, Escandell MM (1999) Reinoso F R. Semicokes from pitch pyrolysis: mechanisms and kinetics. *Carbon* 37(3):363–390
17. Lemin S, Hejun L (2000) The process and microstructure of pitch based Carbon – Carbon Composites by LPIC. *Mech Sci Technol Aerosp Eng* 19(2):278–280 (in Chinese)
18. Palmer K R, Marx D T (1996) Carbon and Carbonaceous Composite. *Materials World Scientific*, London, p 409
19. Fernandez JJ, Figueiras A, Granda M et al (1995) Modification of coal-tar pitch by air-blowing: I. Variation of pitch composition and properties. *Carbon* 33(3):295–307
20. White JL, Sheaffer PM (1989) Pitch-based processing of carbon–carbon composites. *Carbon* 27(5):697–707
21. Kostikov V I (1995) Ceramic-and carbon-matrix composites. Chapman & Hall, London, p 305
22. Hejun L, Lemin S (2000) Research on carbonization mechanism of coal-tar pitch under high pressure. 1st World Conference on Carbon. Berlin, German, July
23. Linyuan L, Kangli W (1991) Some questions of Carbon-Carbon Composites in research, production and usage. *J Solid Rocket Technol* 3:99–104 (in Chinese)
24. Kaae JL (1985) The mechanism of the deposition of pyrolytic carbons. *Carbon* 23(6):665–673
25. Wei-gang Z, Hüttinger KJ (2001) Chemical vapor infiltration of Carbon - Revised Part II: experimental result. *Carbon* 39(7):1023–1032
26. Hu Z, Schoch G, Hüttinger KJ (2000) Chemistry and kinetics of chemical vapor infiltration of pyrocarbon: VII: infiltration of capillaries of equal size. *Carbon* 38(7):1059–1065
27. Zijun H, Klaus J (2001) Hüttinger Chemistry and kinetics of chemical vapor deposition of pyrocarbon: VIII. Carbon deposition from methane at low pressures. *Carbon* 39(3):433–441

28. Hee-Dong P, Hyeok-Je J, Young-Min C et al (1994) Processing parameters of pulse CVI in C/C composites. *Ceram Trans* 46:155–163
29. Jeong HJ, Park HD, Lee JD (1996) Densification of Carbon-Carbon Composites by Pulse Chemical Vapor Infiltration. *Carbon* 34(3):417–421
30. Glocki, RCM (1995) Rapid densification of carbon- carbon by thermal-gradient chemical vapor Infiltration. *Ceram Eng Sci Proc* 16(4):315–322
31. Golecki I, Morris RC, Narasimhan D (1994) Method of rapidly densifying a porous structure. P. US Patent: 5348774
32. Sundar V, Lackey WJ, Garth BF, Pradeep KA, Matthew DL (1995) Fabrication of carbon-carbon composites by forced flow-thermal gradient chemical vapor infiltration. *J Mater Res* 10(6):1469–1477
33. Vaidyaraman S, Lackey WJ, Agrawal PK, Garth B (1995) Freeman. Forced flow-thermal gradient chemical vapor infiltration for fabrication of carbon/carbon. *Carbon* 33(9):1211–1215
34. Lewis JS, Lackey WJ, Vaidyaraman S (1997) Model for prediction of matrix microstructure for carbon/carbon composites prepared by forced flow-thermal gradient CVI. *Carbon* 35 (1):103–112
35. Bertrand S, Lavaud JF, Hadi RE, Vignoles G, Pailler R (1998) The thermal gradient-pulse flow CVI process: A new chemical vapor infiltration technique for the densification of fibre performs. *J Eur Ceram Soc* 18(7):857–870
36. Wenchuan L, Jingyi, D, Haifeng, D, Fang, L (1999) A rapid fabrication process of C/C composites. P. Chinese Patent:99122649.6
37. Houdayer M, Spitz J, Tran-Van D (1984) Process for the densification of a porous structure. P. US Patent: 4472454
38. Wanchang S, Hejun L, Shouyang Z et al (2002) Progress in rapid liquid-vaporized densification processing for fabricating C/C Composites. *J Chin Ceram Soc* 30(4):513–516 (in Chinese)
39. Li K, Li H, Jiang K, Hou X (2000) Numerical simulation of isothermal chemical vapor infiltration process in fabrication of carbon-carbon composites by finite element method. *Sci China Ser E: Technol Sci* 43(1):77–85
40. Zhang W, Hüttinge KJ (2001) Chemical vapor infiltration of carbon – revised: Part I: Model simulations. *Carbon* 39(7):1013–1022
41. Dekker JP, Moene R, Schoonman J (1996) The influence of surface kinetics in modelling chemical vapour deposition processes in porous performs. *J Mater Sci* 31:3021–3033
42. Fitzer E, Hegen D (1979) Chemical vapor deposition of Silicon Carbide and Silicon Nitride —Chemistry's contribution to modern Silicon Ceramics. *Angew Chem, Int Ed Engl* 18 (4):295–304
43. Brekel C.H.J. van den, Fonville R M M, Straten P J M Van Der, Verspui G (1981) In: Blocher J M Jr and Vuitlard G E (eds) *Proceedings of the 8th International Conference on Chemical Vapour Deposition*. (The Electrochemical Society, Pennington) 81–7, 412
44. Rossignol JY, Langlais F, Naslain R (1984) In: Robinson, M (ed) *Proceedings of the 9th International Conference on Chemical Vapour Deposition*, Seattle, USA, 1984. (The Electrochemical Society, Pennington) 84–7 596
45. Moene R, Dekker JP, Makkee M, Schoonman J, Moulijn JA (1994) Evaluation of isothermal chemical vapor infiltration with Langmuir-Hinshelwood type kinetics. *J Electrochem Soc* 141(1):282–290
46. Lin YS, Burggraaf AF (1991) Modelling and analysis of CVD processes in porous media for ceramic composite preparation. *Chem Eng Sci* 46(12):3067–3080
47. Lin YS (1990) In: Spear KE, Cullen GW (eds), *Proceedings of the 11th International Conference on Chemical Vapour Deposition*, Seattle, USA, 1990, (The Electrochemical Society, Pennington) 90–12, 532
48. Fedou R, Ais FL, Naslain R (1990) In: Spear KE, Cullen GW (eds) *Proceedings of the 11th International Conference on Chemical Vapour Deposition*, Seattle, USA, 1990, (The Electrochemical Society, Pennington) 90–12, 513

49. Currier RP (1990) Overlap model for chemical vapor infiltration of fibrous yarn. *J Am Ceram Soc* 73(8):2274–2280
50. Mcallister P, Wolf EE (1991) Modeling of chemical vapor infiltration of Carbon in porous carbon substrates. *Carbon* 29(3):387–396
51. Mcallister P, Wolf EE (1993) Simulation of a multiple substrate reactor for chemical vapor infiltration of pyrolytic Carbon with Carbon-Carbon Composites. *AIChE J* 39(7):1196–1209
52. Gupte SM, Tsamopoulos JA (1989) Tsamopoulos. Densification of porous materials by chemical vapor infiltration. *J Electrochem Soc* 136(2):555–561
53. Tai NH, Chou TW (1989) Analytical modeling of chemical vapor infiltration in fabrication of Ceramic Composites. *J Am Ceram Soc* 72(3):414–420
54. Starr TL (1995) Gas transport model for Chemical Vapor Infiltration. *J Mater Res* 10(9):2360–2366
55. Hou X, Li H, Chen Y, Li K (1999) Modeling of Chemical Vapor Infiltration process for fabrication of Carbon -Carbon Composites by Finite Element Method. *Carbon* 34(4):699–671
56. Aijun Li, Hejun Li, Kezhi Li et al (2003) Modeling of CVI process in fabrication of carbon/carbon composites by an artificial neural network. *Sci China (Series E)* 33(3):209–216 (in Chinese)
57. Zhengbin G, Hejun Li, Kezhi Li et al (2003) Simulation and visualization of isothermal CVI processes of Carbon/Carbon Composites. *J Northwest Polytechnical Univ* 21(3):360–363 (in Chinese)
58. Kaiyu J, Hejun Li, Kezhi Li et al (2000) Numerical simulation of thermal-gradient CVI process for C/C Composites. *Acta Materiae Compositae Sinica* 17(4):84–87 (in Chinese)
59. Kaiyu J, Hejun Li, Minjie W (2002) The numerical simulation of thermal-gradient CVI process on positive pressure condition. *Mater Lett* 54:419–423
60. Vaidyaramana S, Lackey WJ, Agrawal PK, Starr TL (1996) 1-D model for forced flow-thermal gradient chemical vapor infiltration process for carbon/carbon composites. *Carbon* 34(9):1123–1133
61. Gupte SM, Tsamopoulos JA (1990) An Effective Medium Approach for Modeling Chemical Vapor Infiltration of Porous Ceramic Materials. *J Electrochem Soc* 137(5):1626–1638
62. Gupte SM, Tsamopoulos JA (1990) Forced-flow chemical vapor infiltration of porous ceramic materials. *J Electrochem Soc* 137(11):3675–3682
63. Lewis JS, Lackey WJ (1997) Model for prediction of matrix microstructure for carbon-carbon composites prepared by forced flow-thermal gradient CVI. *Carbon* 35(1):103–112
64. Kaiyu J, Hejun L (1999) Mathematical model of numerical simulation of CVI process for carbon and ceramic matrix Composites. *Aerosp Mater Technol* 3:42–45 (in Chinese)
65. Rominillain D, Trinquescoste M, Derre A et al (2000) Abstract and programme oral presentations, Eurocarbon 2000, 245–246, 1st World Conference on Carbon 9–13, Vol 1. July, Berlin
66. Fitzer E, Manocha LM (1998) Carbon reinforcements and Carbon-Carbon Composites. Springer – Verlag, Heidelberg
67. Fitzer E, Huttner W (1981) Structure and strength of carbon/carbon composites. *J Phys D Appl Phys* 14:347–371
68. LM MANOCHA. High performance carbon-carbon composites. *Sadhana*, 28 (Parts 1 & 2) : 349–358
69. Hatta H, Goto K, Aoki T (2005) Strengths of C/C composites under tensile, shear, and compressive loading: Role of interfacial shear strength. *Compos Sci Technol* 65:2550–2562
70. Guess TR, Hoover WR (1973) Fracture toughness of Carbon-Carbon Composites. *J Compos Mater* 7(1):2–20
71. Moet A, Minick J (1991) Fracture Toughness of Carbon/Carbon Composites. ADA240200 Final rept. 1 Apr 89-30 Jun
72. Savage G (1993) Carbon-Carbon composites. Chapman & Hall, London

73. Hatta H, Kogo Y, Tanimoto T, Morii T(1995). Static and fatigue fracture behavior of C/C composites. In: Proc of fourth Japan Int SAMPE Symposium, p. 368–73
74. Allaron C, Roubly D, Reynaud P, Fantozzi G (1999) Improvement of cyclic fatigue analysis by the use of a tensile master curve in carbon/carbon composites *Key Eng Mater* (164–165), pp. 329–332
75. Ozturk A, Moore RE (1992) Tensile fatigue behavior of tightly woven carbon–carbon composites. *Composites* 23:39–46
76. Han HM, Li HJ, Wei JF et al (2003) Micro-pleating in Carbon-Carbon Composites under a cyclic load. *Science In China (Series E)* 33(7):614–618 (in Chinese)
77. Liao L, Li J, Xu F, Kzh L (2008) Effects of tensile fatigue loads on flexural behavior of 3D braided C/C composites. *Compos Sci Technol* 68(2):333–336
78. Luo RY, Li HJ, Yang Zh et al (1995) Brake properties in damp condition of C/C Composites aeroplane brake discs. *Carbon Techn* 5:25 (in Chinese)
79. Han HM, Zhang XL, Li HJ et al (2003) Mechanical Behaviors of Carbon -Carbon Composites under the High-temperature. *New Carbon Mater* 18(1):20–24 (in Chinese)
80. Chen J, Long Y, Xiong Xi, Xiao P (2012) Microstructure and thermal conductivity of carbon/carbon composites made with different kinds of carbon fibers. *J. Cent. South Univ.* 19:1780–1784
81. Luo Y, Liu T, Li JS, Zhang B, Chen Zhijun, Tian Guanglai (2004) Thermophysical properties of carbon/carbon composites and physical mechanism of thermal expansion and thermal conductivity. *Carbon* 42(14):2887–2895
82. Pierson HO (1993) *Handbook of Carbon, Graphite, Diamond and Fullerenes*. Noyes Publication, New Jersey
83. Bowers DA, Davis JW, Dinwiddie RB (1994) Development of 1-D carbon composites for plasma-facing components. *J. Nucl Mater* 212–215, Part 2: 1163–1167
84. Hao L, Li KZH, Li HJ, Lu JH, Zhai YQ (2007) Microstructure and mechanical properties of mesophase pitch-based C/C Composites. *Rare Met Mater Eng* 39(S3):331–334
85. Liu H, Li KZH, Li HJ, Lu JH, Zhai YQ (2008) Microstructure and mechanical properties of C/C Composites with a mesophase pitch transition layer. *J Inorg Mater* 23(3):486–490
86. Chollon G, Siron O, Takahashi J, Yamauchi H, Maeda K, Kosaka K (2001) Microstructure and mechanical properties of coal tar pitch-based 2D-C/C composites with a filler addition. *Carbon* 39:2065–2075
87. Matzinos PD, Patrick JW, Walker A (1996) Coal-tar pitch as a matrix precursor for 2D-C/C composites. *Carbon* 34:639–644
88. Reznik B, Gerthsen D (2003) Microscopic study of failure mechanisms in infiltrated carbon fiber Felts. *Carbon* 41:57–69
89. Reznik B, Huttinger KJ (2002) On the terminology for pyrolytic carbon. *Carbon* 40(4):620–624
90. Diefendorf RJ, Tokarsky EW (1971) The relationships of structure to properties in graphite fibers. Air Force Report, AF33 (615)-70-C-1530
91. Bokros JC (1969) Deposition, structure, and properties of pyrolytic carbon. In Walker PL Jr. *Chemistry and physics of carbon*, Vol 5, New-York: Marcel Dekker:1–118
92. Oberlin A (2002) Pyrocarbons. *Carbon* 40:7–24
93. Bourrat X, Trouvat B, Limousin G, Vignoles G (2000) Pyrocarbon anisotropy as measured by electron diffraction and polarized light. *J Mater Res* 5:92–101
94. Bortchagovsky EG (2004) Reflection polarized light microscopy and its application to pyrolytic carbon deposits. *J Appl Phys* 95:5192
95. Bourrat X (2001) Structure in carbons and different artifacts. In: Marsh H, F Rogriguez-Reinoso (eds) *Sciences of carbon materials*, Publicaciones de la Universidad de Alicante, p. 1–98
96. Deng HB, Cui WL, Ma BX et al (1997) On optimal procedure for improving properties of Carbon Fiber. *Journal Northwest Polytechnical Univ* 15(2):325–326 (in Chinese)

97. Bahl OP, Mathre RB, Dhimi TL et al (1999) Carbon -Carbon composites with pyrolytic carbon coated carbon fibers, Carbon' 99, Extended Abstracts and Program, Vol 1, 42–43, Charleston, South Carolina
98. Iwashita N, Psomiadou E, Sawada Y (1998) Effect of coupling treatment of carbon fiber surface on mechanical properties of carbon fiber reinforced carbon composites. *Compos A* 29(8):965–972
99. Zhang XL, Xu ZH, Li HJ (2003) Effect of fiber surface pretreatment on the tensile strength of unidirectional Carbon-Carbon Composites. *Mech, Sci Technol* 22(3):484–486 (in Chinese)
100. Domnanovich A, Peterlik H, Kromp K (1996) Determination of interface parameters for carbon-carbon composites by the fibre-bundle pull-out test. *Compos Sci Technol* 56 (9):1017–1029
101. Han JC, Huang YD, He XD et al (1995) Characteristics of interfaces in 3D fine weave Carbon-Carbon Composites. *Acta Materiae Compositae Sinica* 12(4):72–78 (in Chinese)
102. Peng WZH, Yu Q, Pu TY, Zeng HM (1987) A study of interface structure of 3D carbon-carbon composites. *J Astronaut* 4:66–72
103. Shi R, Hu GX, Li HJ et al (1998) Interfacial microstructures of intrabundle in as-received Carbon-Carbon Composites prepared by CVI. *Carbon* 36(9):1331–1335
104. Shi R (1997) Research on the microstructures and mechanical properties of carbon/carbon composites with pyrolytic carbon matrix. Ph.D. thesis, Northwestern Polytechnical University, Xi'an, People's Republic of China
105. Hou XH, Li HJ, Zhang SY et al (2001) Interface-like fracture mechanism in pyrolytic Carbon-Carbon Composites. *Mater Lett* 48(2):117–120
106. Reznik B, Gerthsen D, Guellali M, et al (2001) Structure and properties of interfaces in infiltrated carbon fiber felts, *Carbon* 01(July):15–19, Lexington, USA
107. Sheehan JE, Buesking KW, Sullivan BJ (1994) Carbon- Carbon Composites. *Annu Rev Mater Sci* 24:19–44
108. Westwood ME, Webster JD, Day RJ, Hayes FH, Taylor R (1996) Oxidation protection for Carbon Fiber Composites. *J Mater Sci* 31:1389–1397
109. Jacobson NS, Roth DJ, Rauser RW, Cawley JD, Curry DM (2008) Oxidation through coating cracks of SiC-Protected Carbon/Carbon. *Surf Coat Technol* 203:372–383
110. Smeacetto F, Ferraris M, Salvo M (2003) Multilayer coating with self-sealing properties for Carbon-Carbon Composites. *Carbon* 41:2105–2111
111. Ho CT, Chung DDL (1990) Inhibition of the Oxidation of Carbon-Carbon Composites by Bromination. *Carbon* 28:815–824
112. Li HJ, Zeng XR, Zhu XQ, Xu ZH (1999) On the Oxidation Resistance of Carbon-Carbon Composites. *Carbon* 3:2–7 (in Chinese)
113. Shemet VZh, Pomytkin AP, Neshpor VS (1993) High-temperature oxidation behaviour of Carbon Materials in air. *Carbon* 31:1–6
114. Wu TM, Wei WC, Hsu SE (1993) Temperature dependence of the oxidation resistance of SiC coated Carbon/Carbon Composite. *Mater Chem Phys* 33:208–213
115. Labrquere S, Blanchard H, Pailler R, Naslain R (2002) Enhancement of the oxidation resistance of interfacial area in C/C Composites. Part II: oxidation resistance of B-C, Si-B-C and Si-C coated Carbon performs densified with Carbon. *J Eur Ceram Soc* 22:1011–1021
116. Yang ZSH, Wang Y (2001) Development of Aircraft C/C Composite Brake Material. *Aeronaut Sci Technol* 1:28–30 (in Chinese)
117. Cui H, Su JM, Li RZH et al (2000) On improving anti ablation property of multi matrix C/C to withstand 3700K. *J Northwest Polytechnical Univ* 18(4):669–673 (in Chinese)
118. Savage G (1993) Carbon-Carbon Composites. Chapman&Hall, London, pp 198–209
119. Sheehan JE (1989) Oxidation protection for carbon Fiber Composites. *Carbon* 27(5):709–715
120. Song YZH, Zai GT, Jinren S (2001) Study on Oxidation Behavior of Carbon Substrates Internally Modified by BN Additives. *Aerosp Mater Technol* 6:31–33 (in Chinese)

121. Zhu XQ, Yang Zh, Kang MK et al (1994) Effect of matrix modification on the oxidation resistance of Carbon-Carbon Composites. *Acta Mater Compos Sinica* 11:107–111 (in Chinese)
122. Liu QCH, Zhou SL, Xu XW (2002) Anti-oxidation mechanism of bindless Carbon-Carbon Composites. *J Chem Ind Eng* 53(11):1188–1192 (in Chinese)
123. Yang ZSH, Lu GR, Qu DQ (2001) Anti-oxidation of Phosphate and Boron contained coatings for C/C composites brake material. *Mater Prot* 34(3):12–13 (in Chinese)
124. Chen Q, Li HJ, Li KZH et al (2003) Neural network simulation on effect of burning rate of modified Carbon-Carbon Composites. *J Xi'an Jiaotong Univ* 37(3):249–251 (in Chinese)
125. Shen XT, Li KZ, Li HJ, Du HY, Cao W-F, Lan F-T (2010) Microstructure and ablation properties of Zirconium Carbide doped Carbon/Carbon Composites. *Carbon* 48:344–351
126. Shen XT, Li KZ, Li HJ, Fu QG, Li SP, Deng F (2011) The effect of Zirconium Carbide on ablation of Carbon/Carbon Composites under an Oxyacetylene flame. *Corros Sci* 53(1):105–112
127. Liu WCH, Deng JY, Du HF et al (1998) Microcosmic fabric character of C/C, C/C-SiC grads radix, Nanometer radix, Unit doublet radix C/C Composites. *Sci China B* 28(5):471–490 (in Chinese)
128. Cheng LF, Zhang LT, Han JT (1992) Development and status of oxidation protection coatings for C/C composites. *High Technology Letters*, 10 (in Chinese)
129. Dhani TL, Bahl OP, Awasthy BR (1995) Oxidation-resistant Carbon-Carbon Composites up to 1700 °C. *Carbon* 33(4):479–490
130. Deal BE, Grove AS (1965) General relationship for the Thermal Oxidation of Silicon. *J Appl Phys* 36(12):3770–3778
131. STRIFE JR, SHEEHAN JE (1988) Ceramic coating for Carbon-Carbon Composites. *American Ceramic Society Bulletin* 67(2):369–374
132. Jian-feng H, He-jun L, Xie-rong Z, Xin-bo X, Ye-Wei FU (2005) Progress on the oxidation protective coating of Carbon-Carbon Composites. *J New Carbon Mater* 20:373–379
133. Zhihuai X, Hejun L (2000) Orthogonal analysis of CVD SiC coating processing. *Ordnance Mater Sci Eng* 23(5):35–40 (in Chinese)
134. Debrunner RE, Clements PC (1973) Method of protecting carbonaceous material from oxidation at high temperature. United States Patent 3713882. Jan 30
135. Strater HH (1970) Oxidation resistant Carbon-Carbon Composites. United States Patent 3510347. May 5
136. Wilson WF (1974) Oxidation retardant for graphite. United States Patent 4439491. Mar 29
137. Yi M zh, Ge Yichg, Peng Ch L et al (2002) Effect of pre-impregnation on anti-oxidation of Carbon/Carbon Composite for Airplane Brake Disc. *Chin J Nonferrous Met* 12(2):260–263 (in Chinese)
138. Liu B, Yi MZH, Xiong X et al (2000) Preparation of oxidation resistant coatings for Carbon/Carbon Composites Aircraft Brake Pairs. *Chin J Nonferrous Met* 10(6):864–867 (in Chinese)
139. Cheng LF, Zhang LT (1996) Investigation of liquid spreading out in the preparation of oxidation protection coating for C/C by Liquid Reaction-Formation Method. *Acta Aeronautic Et Astronautic Sinica* 17(4):508–510 (in Chinese)
140. Cheng LF, Zhang LT (1992) New technology of anti-oxidation coating preparation for C/C Composites: Fluid generation method. *Chin High Technol Lett* 2(9):4–7 (in Chinese)
141. Huang JF, Li HJ, Zeng XR, Li KZH, Xiong XB, Huang M et al (2004) A New SiC/Yttrium Silicate/Glass Multi-layer oxidation protective coating for Carbon/Carbon Composites. *Carbon* 42(11):2356–2359
142. Huang JF, Zeng XR, Li HJ, Xiong XB, Fu YW, Huang M (2004) SiC/yttrium silicate multi-layer coating for oxidation protection of Carbon/Carbon Composites. *J Mater Sci* 39(24):7383–7385
143. Huang JF, Zeng XR, Li HJ et al (2003) ZrO₂- SiO₂ Gradient anti-oxidation coating for SiC Coated Carbon-Carbon Composites by the solgel process *Carbon* 3(July): 6–10 Oviedo, Spain

144. Philip L. Berneburg et al (1991) Processing of Carbon/Carbon Composites using supercritical fluid technology. United States Patent 5035921. Jul 30
145. Huang JF, Zeng XR, Li HJ Xinbo, Fu et al (2004) Influence of the preparing temperature on phase, microstructure and anti-oxidation property of SiC coating for C/C Composites. Carbon 42(8-9):1517-1521
146. Chen MM (1996) Microstructure and oxidation resistance of SiC coated Carbon-Carbon Composites via pressless reaction sintering. J Mater Sci 31:649-654
147. Joshi A, Lee JS (1995) Coating with particulate dispersions for high temperature oxidation protection of Carbon and C/C Composites. Composites (Part A) (4):181-189
148. Etesaikao A, Jie C (2002) Enhancing the anti-oxidation performance of C/C composites using CVD-SiC coating on the SiC blanket. Dian Tan 2:17-22 (in Chinese)
149. Zeng XR, Li HJ, Li L, Li AL (2002) Dynamic anti-oxidation behavior of MoSi₂-SiC coating system for Carbon-Carbon Composites. Acta Materiae Compositae Sinica 19(6):43-46 (in Chinese)
150. Zeng XR, Li HJ, Yang Zh (1999) Effect of microstructure and component of MoSi₂-SiC multilayer ceramic coating on oxidation resistance. J Chin Ceram Soci 27(1):8-15 (in Chinese)
151. Zeng XR, Li HJ, Yang Zh, Kang MK (2000) Investigation of microstructure for oxidation protection coated C/C composites. transactions of materials and heat treatment 21(2):64-67 (in Chinese)
152. Zeng XR, Li HJ, Zhang G et al (2000) Effect of microstructure and component on oxidation resistance of MoSi₂-SiC multilayer ceramic coating. Acta Materiae Compositae Sinica. 17 (2):42-45 (in Chinese)
153. Zeng XR, Zheng CQ, Li HJ, Changqing Z (1997) Investigation of oxidation protection system of MoSi₂-SiC coating for Carbon-Carbon composites. Acta Aeronautic Et Astronautic Sinica 18(4):427-432 (in Chinese)
154. Zeng XR, Zheng CQ, Li HJ, Yang Zh (1997) Properties of oxidation resistant MoSi₂ coating of Carbon/Carbon composites. Acta Materiae Compositae Sinica 114(3):37-40 (in Chinese)
155. ZHANG Yu-lei, LI He-jun, FU Qian-gang, LI Ke-zhi, WEI Jian, WANG Peng-yun (2006) A C/SiC gradient oxidation protective coating for Carbon/Carbon composites. Surf Coat Technol 201:3491-3495
156. Hou D, Li K, Li H, QiangangFu YZ (2008) SiC/Si-W-Mo coating for protection of C/C composites at 1873 K. Journal of University of Science and Technology Beijing, Mineral, Metallurgy, Material. 15(6):822-826
157. Fu QG, Li HJ, Shi XH, Liao XL, Li KZ, Huang M (2006) Microstructure and anti-oxidation property of CrSi₂-SiC coating for Carbon/Carbon composites. Appl Surf Sci 252, p. 3475
158. Li H, Xue H, Wang Y-J et al (2007) A MoSi₂-SiC-Si oxidation protective coating for Carbon/Carbon composites. Surf Coat Technol 201(24):9444-9447
159. Zhu YC, Ohtani S, Sato Y et al (1998) The improvement in oxidation resistance of CVD-SiC coated C/C composites by Silicon infiltration pretreatment. Carbon 36(7-8):929-935
160. Cheng LF, Zhang LT (1996) Preparation of gradient composite coating for high temperature and long life oxidation protection of Carbon-Carbon composites. Chin High Technol Lett 5:16-18 (in Chinese)
161. Cheng LF, Zhang LT, Xu YD (1997) Structure of the oxide film on the Si-W coating for C/C composites prepared by liquid reaction formation method. J Chin Ceram Soci 25(5):537-541 (in Chinese)
162. Huang Ji F, Zeng XR, Li HJ, Xiong XB, Huang M (2004) Al₂O₃-Mullite-SiC-Al₄SiC₄ multi-composition coating for Carbon/Carbon composites. Mater Lett 58:2627-2630
163. Huang JF, Zeng XR, Li HJ, Xiong XB, Min H (2003) Mullite-Al₂O₃-SiC oxidation protective coating for Carbon-Carbon composites. Carbon 41(14):2825-2829
164. Huang JF, Li HJ, Zeng XR et al (2006) Preparation and oxidation kinetics mechanism of three-layer multi-layer-coatings-coated Carbon/Carbon composites. Surf Coat Technol 200 (18-19):5379-5385

165. Zhangg YL, Li HJ, Fu QG, Zh Li K, Sh Hou D, Fei J (2007) A Si-Mo oxidation protective coating for C/SiC coated Carbon/Carbon composites. *J Carbon* 45(5):1130–1133
166. Zhang YL, Li HJ, Fu QG et al (2008) An oxidation protective Si-Mo-Cr coating for C/SiC coated Carbon/Carbon composites. *J Carbon* 46(1):179–182
167. Feng T, Li HJ, Fu QG et al (2010) Microstructure and oxidation of multi-layer MoSi₂-CrSi₂-Si coatings for SiC coated carbon/carbon composites. *Corros Sci* 52(9):3011–3017
168. Li HJ, Feng T, Fu Q G et al (2010) Oxidation and erosion resistance of MoSi₂- CrSi₂-Si/SiC coated C/C composites in static and aerodynamic oxidation environment. *Carbon* 48 (5):1636–1642
169. Fu QG, Li HJ, Shi XH, Li et al (2007) A SiC whisker-toughened SiC-CrSi₂ oxidation protective coating for Carbon/Carbon composites. *Appl Surf Sci* 253(8):3757–3760
170. Li HJ, Fu QG, Shi XH, Li KZ, Hu ZB (2006) SiC whisker-toughened SiC oxidation protective coating for Carbon/Carbon composites. *Carbon* 44:602–605
171. Fu QG, Li HJ, Zhang ZZ, Zeng XR, Li KZ (2010) SiC nanowire-toughened MoSi₂-SiC coating to protect Carbon/Carbon composites against oxidation. *Corros Sci* 52:1879–1882
172. Chu YH, Fu QG, Cao CW, Li HJ, Li et. al (2010) SiC nanowire-toughened SiC-MoSi₂-CrSi₂ oxidation protective coating for carbon/carbon composites. *Surf Coat Technol* 205 (2):413–418
173. Chu YH, Li HJ, Fu QG et al (2012) Toughening by SiC Nanowires in a Dense SiC-Si Ceramic coating for oxidation protection of C/C Composites. *J Am Ceram Soc* 95(11):3691–3697
174. Chu YH, Fu QG, Li HJ et al (2010) Influence of SiC nanowires on the properties of SiC coating for C/C composites between room temperature and 1500 °C. *Surf Coat Technol* 205 (2):413
175. Buchanan FJ, Little JA (1993) Glass sealants for Carbon-Carbon composites. *J Mater Sci* 28:2324–2330
176. Smeacetto F, Ferraris M, Salvo M (2003) Multilayer coating with self-sealing properties for Carbon-Carbon composites. *Carbon* 41(11):2105–2111
177. Smeacetto F, Salvo M, Ferraris M (2002) Oxidation protective multilayer coatings for Carbon-Carbon composites. *Carbon* 40(4):583–587
178. Xiao ZH (1999) Experiment on Ceramic flat filter binded by Aluminium Phosphate colloid for Cast Steel. *Foundry Technol* 2:22–24 (in Chinese)
179. Li HJ, Luo RY, Yang Zh (1997) The status and future on research and application about Carbon/Carbon composites in the Aeronautical area. *J Mater Eng* 8:8–10 (in Chinese)
180. Liu YQ, Li RL (2001) Status in Carbonaceous Brake on Civil Aircraft and Development of its prefabrication. *Civ Aircr Des Res* 3:27–30 (in Chinese)
181. Liu W Ch, Deng JY (2001) C/C composite market research. *Mater Rev* 11(2):13–16 (in Chinese)
182. Yang ZSh, Lu GR, Qu DQ (2001) Anti- oxidation of Phosphate and Boron contained coatings for C/C composites brake material. *Mater Prot* 34(3):12–13 (in Chinese)
183. Liu B, Zh YM, Xiong X, Jiang Ch, Huang BY (2000) Preparation of oxidation resistant coatings for Carbon-Carbon composites Aircraft brake pairs. *Chin J Nonferrous Met* 10 (6):864–867
184. Fu QG, Li HJ, Huang JF, Shi XH et al (2005) Anti-Oxidation of phosphate contained coatings for C/C composites. *Mater Prot* 3:52–54
185. Fitzer E, Manocha LM (1998) Carbon reinforcements and Carbon-Carbon composites. *Spirmger –Verlag, Heidelberg*
186. Chen HH, Deng HJ, Li M et al (1998) Advanced composite material. *China Substances Press, Beijing* (in Chinese)
187. Li HJ (2001) Carbon-Carbon Composites. *New Carbon Mater* 16(2):79–80 (in Chinese)
188. Zheng G, Jiexiang Z (1995) Study and devolvement of Carbon/Carbon composites. *Aerosp Mater Technol* 7(5):25–28
189. Cao JM, Sakai M (1996) The crack-face fiber bridging of a 2D-C/C composite. *Carbon* 34 (3):387–395

190. Loboiondo NE, Jones LE, Clare AG (1995) Halogenated glass system for the protection of structural Car-bon-Carbon composites. *Carbon* 33(4):499–508
191. Li HJ, Zeng XR, Zh LK et al (2001) Research and application of Carbon-Carbon composites in China. *Carbon* 4:8–13 (in Chinese)
192. Hyeok JJ, Hee DP (1996) Densification of Carbon - Carbon composites by pulse chemical vapor infiltration. *Carbon* 34(3):417–421
193. Anada K, Gupta V, Dartford D (1994) Failure mechanisms of laminated Carbon-Carbon composites– II. Under shear loads. *Carbon* 42(3):797–809
194. Zhao JX (1989) Carbon/Carbon composites in Aerospace department of Dunlop. *New Carbon Mater* 2:10–17
195. Liu WC, Deng JY (2001) C/C composite market research. *Mater Rev* 11(2):13–16 (in Chinese)
196. Li HJ, Luo RY, Yang Z (1997) The status and future on research and application about Carbon/Carbon composites in the aeronautical area. *J Mater Eng* 8:8–10 (in Chinese)
197. Liu YQ, Li RL (2001) Status in carbonaceous brake on civil Aircraft and development of its prefabrication. *Civ Aircr Des Res* 3:27–30 (in Chinese)
198. Yang S, Wang Y (2001) Development of Aircraft C/C composite brake material. *Aeronautical, Science and Technology* 1:28–30 (in Chinese)
199. Ji YX, Tian ZX (2000) Research future of carbonaceous brake block on the warcraft in China. *Aircr Des* 1:49–51 (in Chinese)
200. Song Y, Ren M, Sun JL (2000) The Application of Carbon-Carbon composites in the propulsion system. *Technical Textiles* 18(16):39–42 (in Chinese)
201. Ren XY, Ma FK (1996) The developing prospect of Carbon/Carbon Composites. *Mater Rev* 8(2):72–76 (in Chinese)
202. Huo XY, Liu HL, Zeng XM et al (2000) Applications of Carbon fiber composites on SRM. *Hi-tech Fiber Appl* 25(3):1–7 (in Chinese)
203. Su JM (2001) Development and research of C/C Composites on throat insert material. *Carbon Techniq* 11(1):6–11 (in Chinese)
204. Yu Q, Chen WJ, Luo Y (1999) About some important aspects in research trend of composite material. *Aerosp Mater Technol* 12(1):12–15
205. Zuo JL, Zhang HB, Xiong X et al (2003) Evolve of a research of C/C Composites used for nozzle throat. *Carbon* 2:7–10 (in Chinese)
206. Liu WC (1994) Preparation and application of thermostructural composites. *Mater Rev* 2:62–66 (in Chinese)
207. Evans SL, Gregson PJ (1998) Composite technology in load-bearing orthopaedic implants. *Biomaterials* 19(15):1329–1342
208. Hou XH, Chen Q, Yu CH et al (2000) Biocompatibility and medical application of Carbon - Carbon Composites. *J Funct Mater* 31(5):460–463 (in Chinese)
209. Pesakova V, Klezl Z, Balik K, Adam M (2000) Biomechanical and biological properties of the implant material carbon-carbon composite covered with pyrolytic carbon. *J Mater Sci Mater Med* 11(12):793–798
210. Wang GH, Yu S, Zhu SH, Gao CQ, Liu Y, Miu YL, Huang BY (2009) Biological properties of Carbon/Carbon implant composites with unique manufacturing processes. *J Mater Sci: Mater Med* 20(2):2487–2492
211. Fu T, He LP, Han Y, Xu KW, Mai YW (2003) Induction of bonelike apatite on Carbon-Carbon composite by sodium silicate. *Mater Lett* 57(22–23):3500–3503
212. Zhang LL, Li HJ, Li KZ, Li XT, Zhai YQ, Zhang YL (2008) Effect of surface roughness of Carbon/Carbon composites on osteoblasts growth behaviour. *J Inorg Mater* 23(2):341–345
213. Zhai YQ, Li KZ, Li HJ, Wang C, Liu H (2007) Influence of NaF concentration on fluorine-containing hydroxyapatite coating on Carbon/Carbon composites. *Mater Chem Phys* 106(1):22–26
214. Lewandoswska-Szumie M, Komender J, Gorecki A, Kowalski M (1997) Fixation of Carbon fibre-reinforced Carbon composite implanted into bone. *J Mater Sci Mater Med* 8(2):485–488

215. Adams D, Williams DF (1984) The response of bone to Carbon-Carbon Composites. *Biomaterials* 5:59–64
216. Fu H, Maozhang W (1995) Carbon fiber and its composites. Science Press, Beijing, pp 251–257 (in Chinese)
217. Baquey C, Bordenave L, More N (1989) Biocompatibility of Carbon-Carbon materials: Blood tolerability. *Biomaterials* 10(7):435–440
218. Jenkins GM, Carvalho FX (1977) Biomedical applications of Carbon fibre reinforced carbon in implanted prostheses. *Carbon* 15(1):33–37
219. More N, Baquey C, Barthe X et al (1988) Biocompatibility of Carbon-Carbon materials: in vivo study of their erosion using 14 carbon labelled samples. *Biomaterials* 9(4):328–334
220. Zhang LL, Li HJ, Li KZh et al (2008) Effect of surface roughness on the MG 63 cell behavior. *J Inorg Mater* 23(2):341–345
221. Gu HQ, Xu GF (1993) Biomedical materials. Science and translation Press, Tianjin, pp 433–447 (in Chinese)
222. Williams KR, Blayney AW (1986) An optical and electron microscopy study of materials implanted in the rat middle ear: I. Carbon. *Biomaterials* 7(4):283–286
223. Fizter E, Huüttmr W, Claes L (1980) Torsional strength of Carbon fiber reinforced composites for the application as internal bone plates. *Carbon* 12(6):383–387
224. Buckley JD (1988) Carbon-Carbon: an overview. *Ceram Bull* 67(2):1169–1180
225. Sui JL, Li MS, Lu YP (2004) Plasma-sprayed hydroxyapatite coatings on Carbon/Carbon Composites. *Surf Coat Technol* 176(2):188–192
226. Walker PL (1990) Carbon: an old but new material revisited. *Carbon* 28(2–3):261–279
227. Bokros JC (1977) Carbon Biomedical Devices. *Carbon* 15(6):355–371
228. Christel P, Meunier A, Leclercq S et al (1987) Development of a Carbon-Carbon hip prosthesis. *J Biomed Mater Res* 21(2):191–218
229. Bruckmann H, Keuscher G, Huttinger K (1980) Carbon, a promising material in endoprosthetics, Part 2: tribological properties. *Biomaterials* 1(2):73–81
230. Howling GI, Sakoda H, Antonarurajah A (2003) Biological response to wear debris generated in carbon based composites as potential bearing surfaces for artificial hip joints. *J Biomed Mater Res B* 67B(2):758–763